Vol. 57, No.1 / 2019

e: ISSN 2068 – 2239
p: ISSN 2068 – 4215

INMATEH – AGRICULTURAL ENGINEERING

JANUARY - APRIL

Editorial

The National Institute of Research-Development for Machines and Installations designed to Agriculture and Food Industry - INMA Bucharest has the oldest and most prestigious research activity in the field of agricultural machinery and mechanizing technologies in Romania.

Short History

- In 1927, the first research **Center for Agricultural Machinery** in Agricultural Research Institute of Romania - ICAR (Establishing Law was published in O.D. no. 97/05.05.1927) was established;
- In 1930, was founded **The Testing Department of Agricultural Machinery and Tools** by transforming Agricultural Research Centre of ICAR - that founded the science of methodologies and experimental techniques in the field (Decision no. 2000/1930 of ICAR Manager - GHEORGHE IONESCU ŞIŞEŞTI);
- In 1952, was established the Research Institute for Mechanization and Electrification of Agriculture - ICMA Bănеasa, by transforming the Department of Agricultural Machines and Tools Testing;
- In 1979, the Research Institute of Scientific and Technological Engineering for Agricultural Machinery and Tools – ICSITMUA was founded - subordinated to Ministry of Machine Building Industry - MICM, by unifying ICMA subordinated to MAA with ICPMA subordinated to MICM;
- In 1996 the National Institute of Research-Development for Machines and Installations designed to Agriculture and Food Industry – INMA was founded – according to G.D. no.1308/25.11.1996, by reorganizing ICSITMUA, G.D no. 1308/1996 coordinated by the Ministry of Education and Research G.D. no. 823/2004;
- In 2008 INMA has been accredited to carry out research and developing activities financed from public funds under G.D. no. 551/2007, Decision of the National Authority for Scientific Research - ANCSno. 9634/2008.

As a result of widening the spectrum of communication, dissemination and implementation of scientific research results, in 2000 was founded the institute magazine, issued under the name of SCIENTIFIC PAPERS **(INMATEH)**, ISSN 1583 – 1019.

Starting with volume 30, no. 1/2010, the magazine changed its name to **INMATEH - Agricultural Engineering**, appearing both in print format (ISSN 2068 - 4215), and online (ISSN online: 2068 - 2239). The magazine is bilingual, abstract being published in native language and English, with a rhythm of three issues / year: January-April, May-August, September-December and is recognized by CNCSIS – with B^+ category. Published articles are from the field of AGRICULTURAL ENGINEERING: technologies and technical equipment for agriculture and food industry, renewable energy, machinery testing, environment, transport in agriculture etc. and are evaluated by specialists inside the country and abroad, in mentioned domains.

Technical level and performance processes, technology and machinery for agriculture and food industry increasing, according to national requirements and European and international regulations, as well as exploitation of renewable resources in terms of efficiency, life, health and environment protection represent referential elements for the magazine „**INMATEH - Agricultural Engineering**".

We are thankful to all readers, publishers and assessors.

Editor in chief,

Ph. D. Eng. **Vladut Nicolae-Valentin**

In the present, *INMATEH - Agricultural Engineering* journal is indexed in the next international databases:
ELSEVIER /SciVerse SCOPUS, CLARIVATE ANALYTICS' WEB OF SCIENCE- Emerging Sources Citation Index (ESCI), ULRICHS Web: Global Serials Directory, CABI, SCIPIO, Index COPERNICUS International, EBSCO Publishing, Elektronische Zeitschriftenbibliothek

INMATEH - Agricultural Engineering
vol. 57, no.1 / 2019
NATIONAL INSTITUTE OF RESEARCH-DEVELOPMENT FOR MACHINES AND INSTALLATIONS DESIGNED TO AGRICULTURE AND FOOD INDUSTRY - INMA Bucharest
6 Ion Ionescu de la Brad Blvd., sector 1, Bucharest

Three issues per year,
e-ISSN: 2068 – 2239
p ISSN: 2068 – 4215

Edited by: INMA Bucharest

CONTENT

RESULTS OF LABORATORY INVESTIGATIONS OF SOIL SCREENING ABILITY OF A CHAIN DIGGER WITH ASYMMETRIC VIBRATOR ARRANGEMENT

/

РЕЗУЛЬТАТЫ ЛАБОРАТОРНЫХ ИССЛЕДОВАНИЙ ПРОСЕВАЕМОСТИ ПОЧВЫ НА ПРУТКОВОМ ЭЛЕВАТОРЕ С АСИММЕТРИЧНЫМ РАСПОЛОЖЕНИЕМ ВСТРЯХИВАТЕЛЕЙ

PhD. Eng. Sc. Sibirev A.V., PhD. Eng. Sc. Aksenov A.G., Prof. PhD. Eng. Sc. Dorokhov. A.S.
FSBSI "Federal Scientific Agronomic and Engineering Centre VIM"/ Russian
Telephone: 89645843518; E-mail: sibirev2011@yandex.ru

Keywords: *chain digger, asymmetric arrangement, vibrator, laboratory installation*

ABSTRACT

The increased yield of onion sets through the use of high-yielding hybrids as seed material entails an increase in weight and number of onion bulbs per one running meter. Consequently, the onion set heap supply from the surface of modern harvesters digging over the separating working parts is also increased. However, these harvesters do not ensure complete removal of soil impurities during onion set harvesting in the traditional onion set production conditions. In this regard, it is necessary to carry out investigations to identify areas on the surface of a chain digger with asymmetric vibrator arrangement and minimum value of soil screening, as well as to develop recommendations and proposals for their improvement.

The paper describes a procedure and results of laboratory tests of a chain digger with asymmetric vibrator arrangement to determine soil screening ability on its surface. It was found out that the greatest value of the screened soil mass, regardless of the supply of soil impurities, was observed at the wave length attenuation section of the loaded strand in the chain digger due to elliptical vibrator impact relevant to the length of the chain digger L_{EL} =1020 mm.

The paper provides the results of laboratory tests of a chain digger with asymmetric vibrator arrangement and determines the length-width soil screening relationship.

РЕЗЮМЕ

В связи с увеличением урожайности лука-севка, в результате использования в качестве семенного материала высокоурожайных гибридов происходит увеличения массы и количества луковиц лука-севка на одном погонном метре. Следовательно, увеличивается подача вороха лука-севка с поверхности подкапывающих на сепарирующие рабочие органы современных лукоуборочных машин, которые не обеспечивают полноту выделения почвенных примесей при уборке лука-севка в современных условиях производства лука-севка. В связи с этим, необходимо проведение исследований по выявлению участков на поверхности пруткового элеватора с асимметричным расположением встряхивателей с минимальной величиной просеивания почвы и разработка рекомендаций и предложений по их повышению.

Описана методика проведения и результаты лабораторных исследований пруткового элеватора с асимметричным расположением встряхивателей по определению просеваемости почвы на его поверхности.

Определено, что наибольшее значение массы просеянной почвы вне зависимости от значения подачи почвенных примесей наблюдается на участке затухания длины волны рабочей ветви пруткового элеватора от воздействия эллиптического встряхивателя соответствующей длине пруткового элеватора L_{EL} =1020 мм.

В статье приведены результаты лабораторных исследований пруткового элеватора с асимметричным расположением встряхивателей и определена зависимость просеивания почвы по длине и ширине.

INTRODUCTION

The continuing extensive investigations in the field of mechanized production technology of onion sets *(Aksenov A.G., Sibirev A.V., Emelianov P.A., 2018)* do not solve the problems associated with poor design of digging and separating parts of onion harvesters, as evidenced by the contents of the soil lumps commensurable with bulbs in the heap being separated *(Sibirev A.V., Aksenov A.G., Dorokhov A.S., 2018).*
To intensify separation of the onion set heap, the separating surface of the chain digger *(Tauseef Asghar M., Abdul Ghafoor, Anjum Munir, Muhammad Iqbal, Manzoor Ahmad, 2014)* is made with rods *2* located on chains *1* (Fig 1).

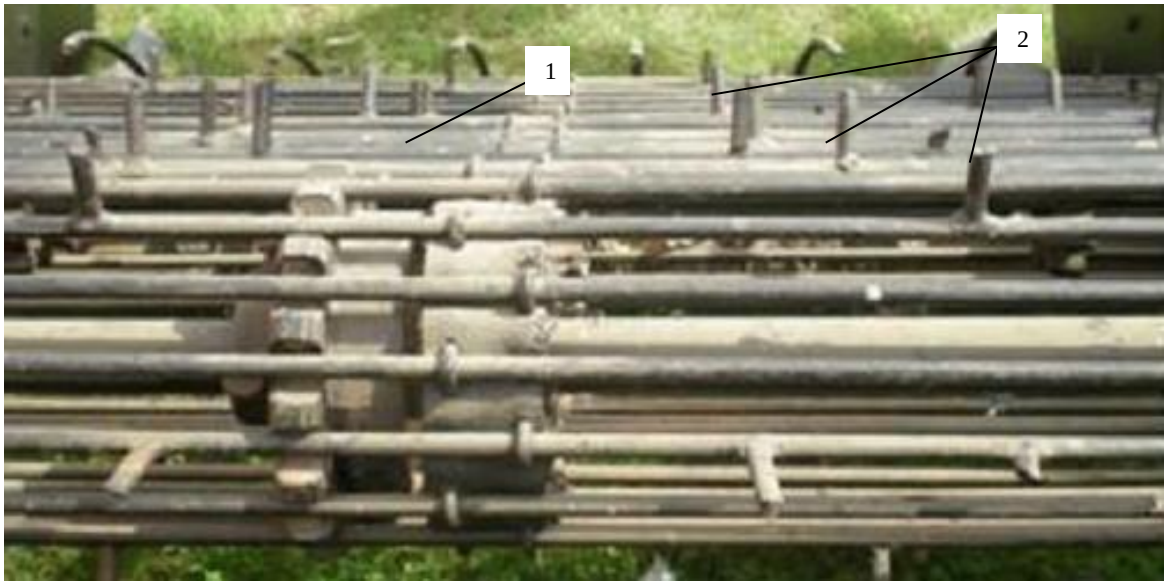

Fig. 1 – Separating chain digger
1 – chain; 2 – rod

The main purpose of rods *2* located on chains *1* is the destruction of soil lumps coming from the digging part of the harvester. However, in addition to the process of destruction of the soil lumps themselves, intensive force action of rods *2* on the root crops occurs, which increases the damage to the separated products.

There is a known design of separating chain digger (Fig. 2), wherein a passive two-plate vibrator *4* located under the upper strand of the chain digger apron *3* intensifies the separation process (*Natenadze N., 2016)*.

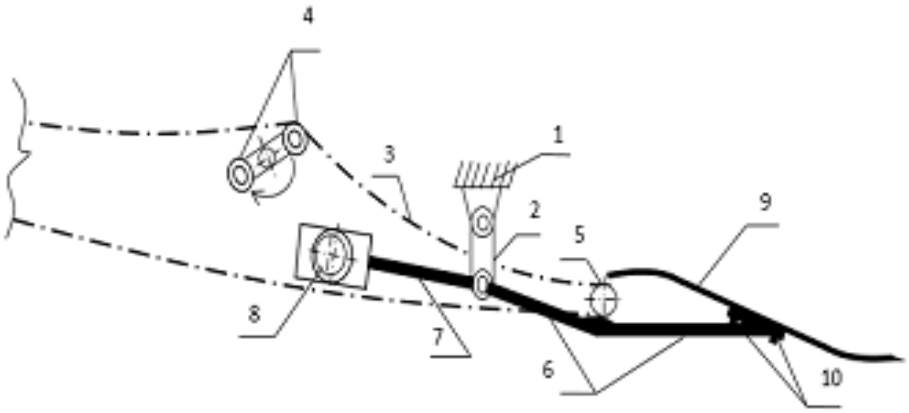

Fig. 2 – Separating chain digger
1 – frame; 2 – draft; 3 – chain digger; 4 – two-plate vibrator; 5 – supporting roller; 6 – mounting bracket; 7 – intermediate bracket; 8 – wobbler shaft; 9 – digging shovel; 10 – shovel bracket

In addition, the front part of the chain digger apron from the side of digging shovel *9* oscillates in the vertical plane when bracket *6* of digging shovel *9* acts on supporting roller *5*, which provides additional force to the soil layer, and thereby intensifies the process of separation of soil-vegetative impurities.

The disadvantages of this known design of the chain digger include increased damage to root crops during the transition from one cascade to another, and also the impossibility of dispersing a heap of onion sets along the entire width of the conveyor.

Analysis of the mechanized harvest machinery suggests that the operating elements of the harvester with different types of separation intensifiers do not provide quality indicators of root crops harvesting on such indicators as the completeness of separation and damage to root crops *(Aniket U. Dongre, Rahul Battase, Sarthak Dudhale, Vipul R. Patil, Deepak Chavan, 2017).*

This is because after digging the soil layer together with the bulbs, a significant amount of soil lumps enters the separating working parts, which are difficult to separate on the working parts and are not always subjected to dynamic destruction under the influence of different types of separation intensifiers *(Farhadi R., Sakenian N., Azizi P., 2012).* As a result, it causes damage to the bulbs due to the interaction with soil lumps during transportation of the onion heap to post-harvest processing *(Sibirev A.V., Aksenov A.G., Mosyakov M.A., 2018).* This circumstance is caused by unsatisfactory process of soil impurities screening on the most widespread working part of primary separation – the chain digger *(Natenadze N., 2016).*

In this regard, it is necessary to conduct investigations to identify areas with a minimum value of soil screening on the chain digger surface with an asymmetric vibrator arrangement, and to develop recommendations and proposals for their improvement. The outcome of the research will make it possible to design working parts of the devices for both primary and secondary separation at the known values of the release of the onion heap from digging and separating working parts, as well as at known values of the separation rate of the chain digger and its translational speed.

MATERIALS AND METHODS

Determination of the regularity of the soil impurities separation on a chain digger with an asymmetrically installed elliptical digger and supporting roller, as in *Patent No. 2638190 Russia, IPC A01 D33/00. (Sibirev A.V., Aksenov A.G., Kolchin N.N., Ponomarev A.G., 2017)* was performed on a laboratory installation (Fig. 3, 4).

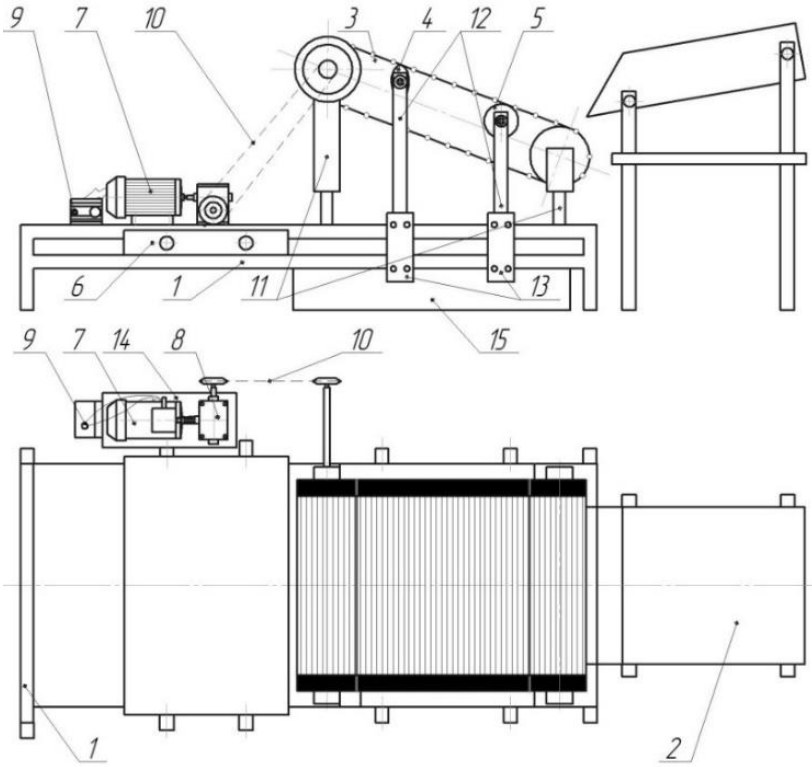

Fig. 3 – Laboratory installation for determining the impact of the process parameters of the chain digger on the quality of onion set heap separation

1 – frame; 2 – container for preliminary heap placement; 3 – chain digger; 4 – elliptical vibrator; 5— cylindrical roller; 6 – tarpaulin of separated products; 7 – electric motor; 8 – single-stage gearbox; 9 – frequency converter; 10 – chain transmission; 11 – support posts; 12 – vibrator and support roller posts; 13 – connecting bracket; 14 – support plate; 15 – impurity collector

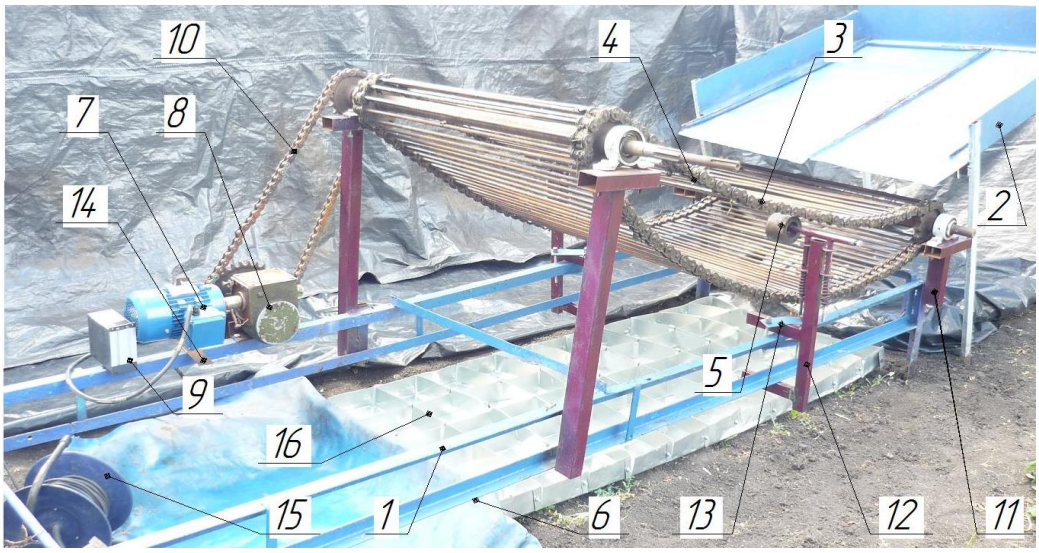

Fig. 4 – Laboratory installation for determining the impact of the process parameters of the separating chain digger on the quality of onion set heap separation

1 – frame; 2 – container for preliminary heap placement; 3 – chain digger; 4 – elliptical vibrator; 5 – supporting roller; 6 – tarpaulin of separated products; 7 – electric motor; 8 – single-stage gearbox; 9 – frequency converter; 10 – chain transmission; 11 – support posts; 12 – vibrator posts; 13 – connecting bracket; 14 – support plate; 15 – impurity collector

The laboratory installation consists of a container *2* for the preliminary placement of a heap, a separating chain digger *3* (working length 1.9 m and width 0.94 m) installed on support posts *11* of frame *1 (Sibirev A.V., Aksenov A.G., Mosyakov M.A., 2018).*

Under chain digger apron *2*, there are passive elliptical vibrators *4* and supporting rollers *5* with the possibility of moving along frame *1* on the posts *12* by fixing the position of bracket *13* on frame *1* with the bolted connection. The electric drive of chain digger *3* is carried out from the electric motor *7* of asynchronous brand 4A180U3 GOST 1050-88 (N = 0.6 kW, n = 920/1,200 rpm) and frequency converter *9* Tecorp Group (N = 0.75 kW; $U_{EN} = 220$ V, $U_{OUT} = 220$ V) through single-stage gearbox *8* (models 1-TsU-160-2-23) which are installed on base plate *14*.

To determine the amount of soil screened through the slots of chain digger *2*, under its surface, there is an impurity collector *16*, the diagram of which is presented in Figure 3.

The impurity collector (Fig. 5) represents a metal tray 1 with a length L_y and width B_y exceeding the length L_{EL} and width B_{EL} of the chain digger. This involves: L_y =2040 mm, B_y =1020 mm.

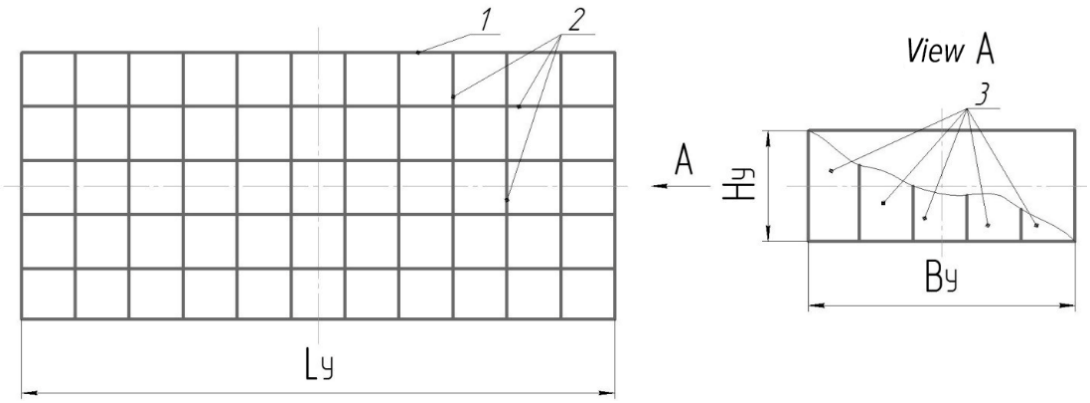

Fig. 5 – General view of the impurity collector

1 – metal tray; 2 – partition; 3 – cell

The surface of metal tray *1* is divided by partitions *2* along the length and width, forming cells *3* in height H_y, with dimensions of 170 × 170 × 100 (mm).

Each cell that determines the location of soil screening on the chain digger surface has its own serial number. The investigations to determine the regularity of the soil impurities separation *(Sibirev A.V., Aksenov A.G., Dorokhov A.S., 2018)* on a chain digger with an asymmetric digger arrangement were carried out with

a minimum feed of onion sets Q_{Vp} = 10 kg/s, with an increase in the limit value Q_{Vp} = 50 kg/s and a variation interval of 10 kg/s for different values of the translational v_{EL} speed of the chain digger and the interaxial S_5 distance between passive elliptical vibrator *4* and supporting roller *5*. The lower limit of the range of translational speed variation v_{EL} was 1.4 m/s and then changed in 0.2 m/s increments to a limiting value of 1.8 m/s. An elliptical vibrator was installed at a distance of 350 mm from the rotation axis of the chain digger barrel. Interaxial S_5 distance between the passive elliptical vibrator and the supporting roller was set equal to 0.4 m in accordance with the results of the laboratory tests, ensuring, at a given quantitative value of the process parameter, the maximum separation completeness. The procedure of investigations was as follows.

A soil sample with a certain weight and moisture was placed on the surface of container *2* for the preliminary heap placement. The required soil moisture for the investigations was provided by superficial watering of the soil sample, then, it was maintained for several hours to achieve the required humidity in accordance with the research plan. An impurity collector was installed under the apron of chain digger *3*.

The optimal values of the translational v_{EL} speed of the chain digger and the interaxial S_5 distance between passive elliptical vibrator *4* and supporting roll *5* were set, in accordance with the results of the laboratory tests.

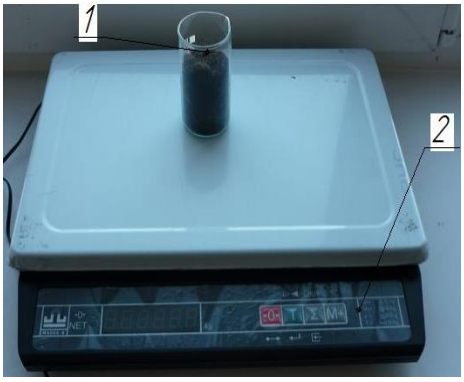

Fig. 6 – Electronic desktop scales MK-15.2-A21

1 – a glass bulb; 2 – electronic table scales

Then, frequency converter *9* and electric motor *7* were successively turned on.

In the steady regime of the apron movement of chain digger *3*, a soil impurity sample was fed from container *2* for the preliminary heap placement. After soil impurities passing through the separating surface of chain digger *2*, electric motor *7* was switched off at the investigated value of the Q_{Vp} supply of soil impurities.

Further from each cell of impurity collector *16*, soil was extracted and weighed on scales of the MK-15.2-A21 model (Fig. 6).

Based on the results of weighing the screened soil taken from each cell of the impurity collector that passed through the slit openings of the chain digger, the dependence of the mass of the screened soil impurities of soil K_P along the length L_{EL} and width B_{EL} of the chain digger was determined, i.e.:

$$f(K_p) = Q_{Vp}, v_{EL} = const;\ S_5 = const. \quad (1)$$

In addition, the separation coefficient K_C of soil impurities was determined on the chain digger with an asymmetric vibrator arrangement along its length $L_{EL}$and width B_{EL}:

$$K_C = \frac{m_P}{m_{CONST}} \cdot 100\% \quad (2)$$

where m_P – is the mass of screened soil impurities (in the impurity collector), kg;

m_{CONST} – is the mass of incoming soil impurities, kg.

The research results were recorded in the observation log.

Further, the studied factors were changed and the experiment was repeated in accordance with the chosen research plan.

The experiments repetition during the research of the influence of the chain digger process parameters with an asymmetric vibrator arrangement on the size of the soil screening ability is fivefold.

RESULTS

The results of the conducted research were recorded in the observations log and are presented in Tables 1-4.

Table 1

Results of research to determine the mass of screened soil impurities of soil K_P along the chain digger surface at Q_{Vp} =10 kg/s, v_{EL} =1.6 m/s, S_5 =0.4 m

Chain Digger Width V_{EL}, mm	Chain Digger Length L_{EL}, mm												Total, kg
	170	340	510	680	850	1,020	1,190	1,360	1,530	1,700	1,870	2,040	
170	0.03	0.04	0.13	0.15	0.13	0.16	0.06	0.07	0.08	0.09	0.1	0.08	9.93
340	0.05	0.07	0.15	0.18	0.15	0.17	0.07	0.07	0.07	0.06	0.06	0.05	
510	0.06	0.07	0.24	0.25	0.32	0.28	0.16	0.15	0.14	0.14	0.13	0.12	
680	0.07	0.08	0.26	0.28	0.33	0.29	0.16	0.15	0.13	0.12	0.11	0.09	
850	0.06	0.08	0.25	0.27	0.33	0.29	0.15	0.14	0.13	0.12	0.11	0.1	
1020	0.05	0.06	0.18	0.2	0.21	0.2	0.13	0.12	0.11	0.09	0.08	0.07	

Table 2

Results of research to determine the mass of screened soil impurities of soil K_P along the chain digger surface at Q_{Vp} =20 kg/s, v_{EL} =1.6 m/s, S_5 =0.4 m

Chain Digger Width V_{EL}, mm	Chain Digger Length L_{EL}, mm												Total, kg
	170	340	510	680	850	1,020	1,190	1,360	1,530	1,700	1,870	2,040	
170	0.08	0.11	0.23	0.35	0.43	0.36	0.09	0.11	0.11	0.12	0.1	0.09	19.68
340	0.08	0.1	0.23	0.36	0.42	0.37	0.12	0.13	0.12	0.11	0.09	0.09	
510	0.11	0.15	0.38	0.59	0.68	0.64	0.28	0.26	0.23	0.21	0.18	0.15	
680	0.11	0.15	0.41	0.64	0.71	0.75	0.3	0.27	0.24	0.22	0.21	0.17	
850	0.12	0.14	0.48	0.57	0.68	0.69	0.28	0.26	0.21	0.19	0.18	0.16	
1,020	0.11	0.15	0.38	0.43	0.52	0.54	0.24	0.23	0.21	0.22	0.13	0.12	

Table 3

Results of research to determine the mass of screened soil impurities of soil K_P along the chain digger surface at Q_{Vp} =30 kg/s, v_{EL} =1.6 m/s, S_5 =0.4 m

Chain Digger Width V_{EL}, mm	Chain Digger Length L_{EL}, mm												Total, kg
	170	340	510	680	850	1,020	1,190	1,360	1,530	1,700	1,870	2,040	
170	0.09	0.11	0.46	0.57	0.68	0.75	0.21	0.18	0.15	0.11	0.12	0.1	29.16
340	0.09	0.12	0.58	0.65	0.71	0.84	0.28	0.25	0.22	0.15	0.14	0.12	
510	0.11	0.12	0.71	0.78	0.83	0.93	0.31	0.27	0.24	0.17	0.16	0.15	
680	0.11	0.15	0.78	0.88	0.97	0.92	0.46	0.39	0.38	0.36	0.32	0.26	
850	0.1	0.14	0.79	0.87	0.94	0.92	0.45	0.37	0.35	0.33	0.32	0.28	
1,020	0.1	0.11	0.76	0.79	0.88	0.96	0.31	0.28	0.23	0.16	0.15	0.13	

Table 4

Results of research to determine the mass of screened soil impurities of soil K_P along the chain digger surface at Q_{Vp} =40 kg/s, v_{EL} =1.6 m/s, S_5 =0.4 m

Chain Digger Width V_{EL}, mm	Chain Digger Length L_{EL}, mm												Total, kg
	170	340	510	680	850	1,020	1,190	1,360	1,530	1,700	1,870	2,040	
170	0.11	0.12	0.87	0.96	0.98	1.58	0.29	0.25	0.23	0.19	0.17	0.12	38.56
340	0.11	0.13	0.89	0.94	1.02	1.43	0.31	0.28	0.25	0.21	0.18	0.13	
510	0.12	0.14	0.88	0.98	1.32	1.76	0.37	0.35	0.28	0.26	0.23	0.15	
680	0.12	0.14	0.96	1.12	1.38	1.68	0.38	0.37	0.29	0.28	0.24	0.16	
850	0.12	0.14	0.87	1.07	1.37	1.64	0.36	0.36	0.27	0.25	0.25	0.17	
1,020	0.11	0.13	0.88	0.94	0.92	1.21	0.43	0.38	0.32	0.28	0.21	0.17	

Graphical display of the investigation results to determine the pattern of soil impurities separation is shown in Figures 7-10.

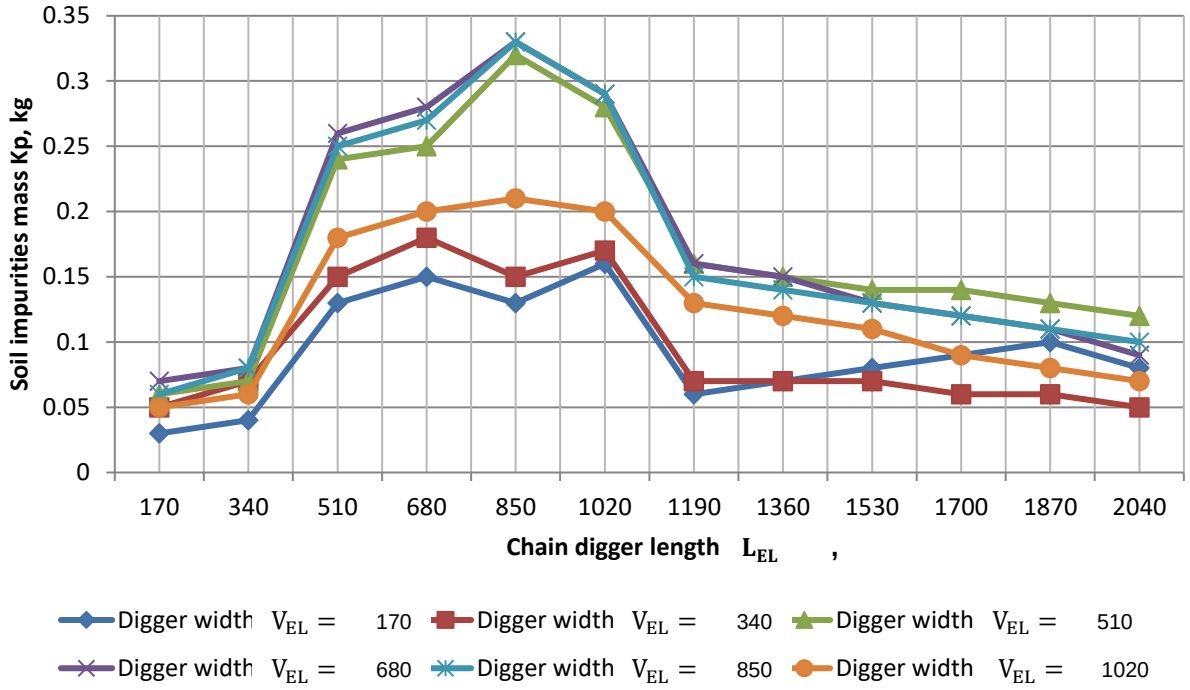

Fig. 7 – Dependence of soil screening along the length and width of the chain digger with an asymmetric vibrator arrangement at Q_{Vp} =10 kg/s, v_{EL} =1.6 m/s, S_5 =0.4 m

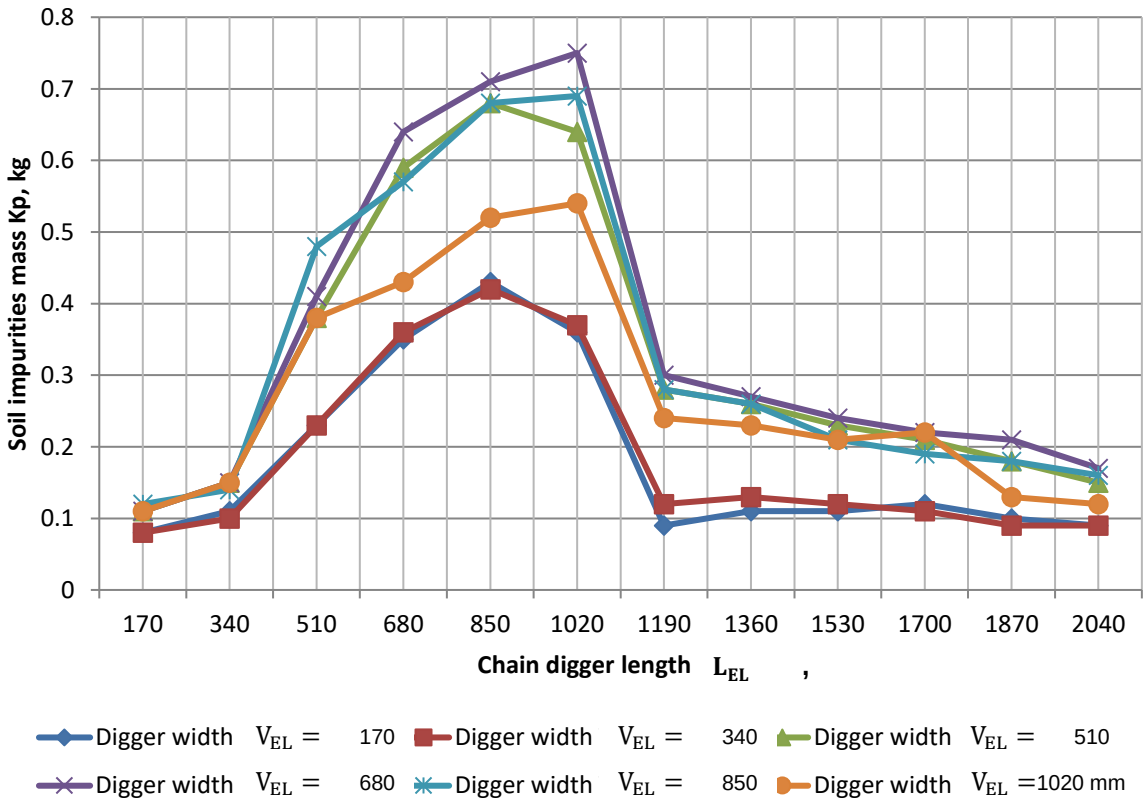

Fig. 8 – Dependence of soil screening along the length and width of the chain digger with an asymmetric vibrator arrangement at Q_{Vp} =20 kg/s, v_{EL} =1.6 m/s, S_5 =0.4 m

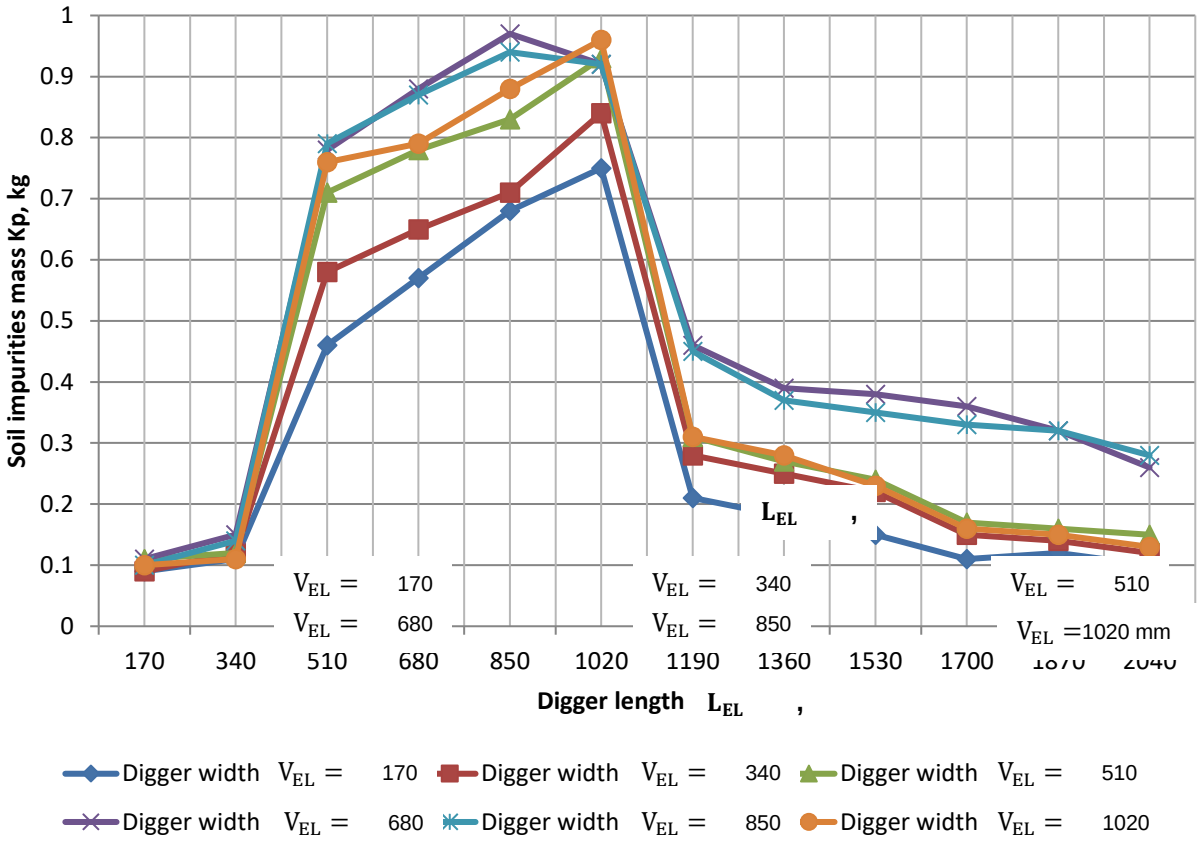

Fig. 9 – Dependence of soil screening along the length and width of the chain digger with an asymmetric vibrator arrangement at Q_{Vp} =30 kg/s, v_{EL} =1.6 m/s, S_5 =0.4 m

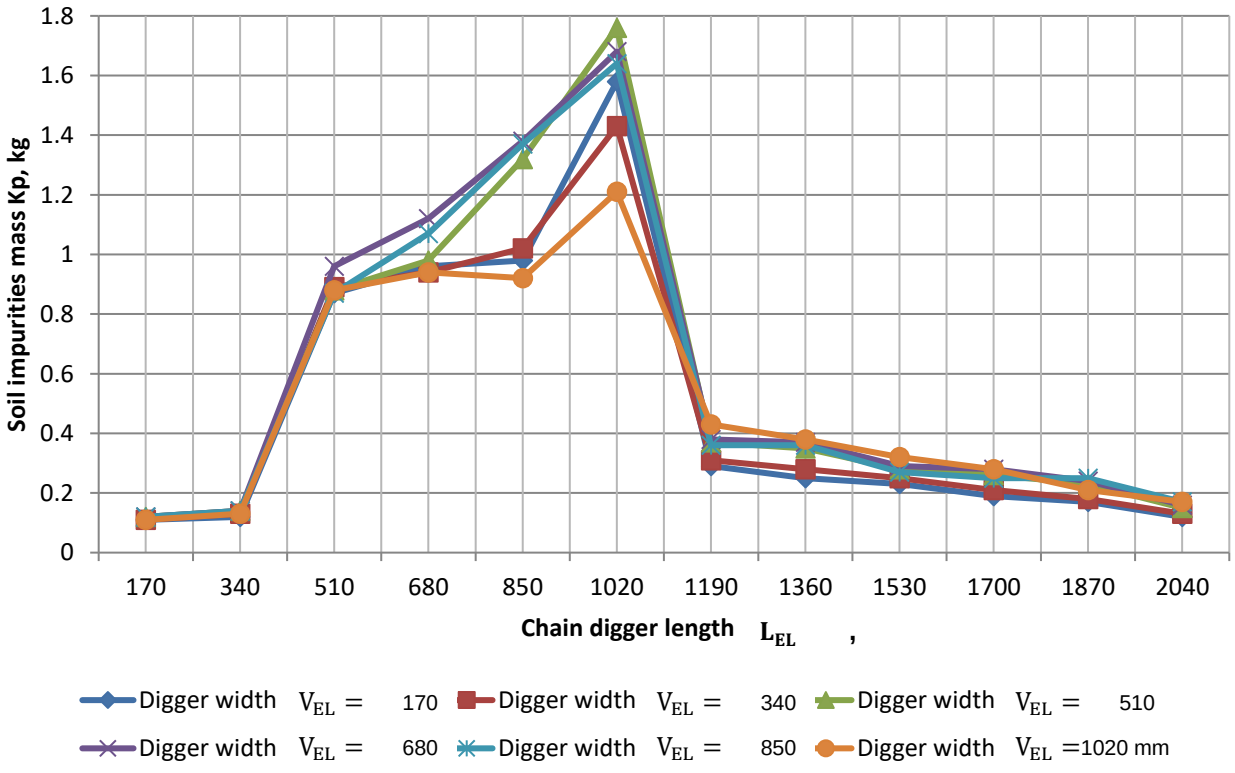

Fig. 10 – Dependence of soil screening along the length and width of the chain digger with an asymmetric vibrator arrangement at Q_{Vp} =40 kg/s, v_{EL} =1.6 m/s, S_5 =0.4 m

Using the presented graphical dependencies, it is possible to determine the mass of screened soil impurities through the slots of the chain digger with the asymmetric vibrator arrangement during feed change of $Q_{Bп}$ soil impurities with constant values of process parameters $v_{EL} = const$; $S_5 = const$.

For this, after determining the appropriate area along the length of the chain digger, it is necessary to draw a straight line parallel to the y-axis, before crossing with the graph.

The variable length of the chain digger is indicated along the x-axis, along the y-axis—the mass of screened soil impurities.

The presented graphical dependencies show that the soil screening intensity on the chain digger with an asymmetric vibrator arrangement is provided with an increase in the soil impurities supply from 10 to 40 kg/s.

This circumstance is explained by the fact that when a soil impurities mass moves along the chain digger surface, there occurs the process of wedging of large particles in the soil mass.

Since in the soil sample of a larger mass there is a content of large soil particles exceeding their presence in a sample of a lesser mass, the soil particles screening occurs more intensively with an increase in the soil impurities supply to the chain digger surface.

And the greatest value of the K_P screened soil mass, regardless of the supply of soil impurities, is observed at the attenuation section of the wave length of the chain digger loaded strand from the action of an elliptical vibrator corresponding to the chain digger length L_{EL} =1020 mm.

With further movement of the soil mass along the chain digger length, there is a decrease in the intensity of soil impurities screening as a result of the attenuation of the wave length of the chain digger loaded strand from the action of an elliptical vibrator.

CONCLUSIONS

The investigation results show that most of the soil impurities are screened at the section of vibrators forming the vibrating wavelength, which during the research was established in the range of values S_5 = 0.4 m.

The results obtained will allow an intensified separation of root crops and bulbs from soil impurities by the optimal vibrator arrangement along the chain digger length at known values of maximum soil impurity penetration.

The results of the experiments indicate a high intensity of soil screening in the area of the chain digger with the vibrator arrangement.

REFERENCES

[1] Aksenov A.G., Sibirev A.V., Emelianov P.A., (2018), Oriented Bulbs Planting with Forked-Roller Planting Apparatus, *Vestnik of Mordovia University*, Issue number 1, pp. 20-24, Saransk/Russia;

[2] Aniket U. Dongre, Rahul Battase, Sarthak Dudhale, Vipul R. Patil, Deepak Chavan, (2017), Development of Potato Harvesting Model, *International Research Journal of Engineering and Technology (IRJET),* Issue number 4, pp. 1567-1570, Tamil Nadu/India;

[3] Farhadi R., Sakenian N., Azizi P., (2012), Design and construction of rotary potato grader, Bulgarian Journal of Agricultural Science, Issue number 2, pp. 304-314, Sofia / Bulgaria;

[4] Mayer V., Vejchar D., Pastorková L., (2017), Measurement of potato tubers resistance against mechanical loading, Research in Agricultural Engineering, Issue number 2, pp. 22-31, Prague/Czech Republic;

[5] Natenadze N., (2016), The design and theoretical justification of a vibratory digger shovel, *Scientific technical union of mechanical engineering Bulgarian association of mechanization in agriculture*, Issue number 5, pp. 9-12, Sofia/Bulgaria;

[6] Sibirev A.V., Aksenov A.G., Dorokhov A.S., (2018), Refined calculation of the separating surface of onion harvester, *Agricultural machines and technologies*, Issue number 3, pp. 20-24, Moscow/Russia;

[7] Sibirev A.V., Aksenov A.G., Mosyakov M.A., (2018), Justification of constructive and process parameters of a separating chain conveyor with asymmetric arrangement of elliptical vibrator and supporting roller, *Bulletin of the Federal State Educational Institution of Higher Professional Education Moscow State Agro-Engineering University named after V.P. Goryachkina*, Issue number 3, pp. 20-24, Moscow/Russia;

[8] Sibirev A.V., Aksenov A.G., Kolchin N.N., Ponomarev A.G., (2017), Patent No. 2638190 Russia, IPC A01 D33/00. *Separating conveyor of the root crop harvester*, No. 2017107814; Application dated 10 March 2017; published 12 December 2017, Bulletin No. 35;

[9] Sibirev A.V., (2017), Theoretical definition of the amount of inflow of onion set heap on the digging shovel, *Agrarian Scientific Journal*, Issue number 5, pp. 75-78, Saratov/Russia;

[10] Tauseef Asghar M., Abdul Ghafoor, Anjum Munir, Muhammad Iqbal, Manzoor Ahmad, (2014), Design modification and field testing of groundnut digger*, Asian Journal of Science and Technology,* Issue number 5, pp. 389-394, Islamabad/Pakistan.

INFLUENCE OF TYPES OF TRACTOR RUNNING GEARS ON THE VALUE OF HOP GARDEN ROW SPACING COMPACTION

/

ВЛИЯНИЕ ТИПОВ ДВИЖИТЕЛЕЙ ТРАКТОРОВ НА ВЕЛИЧИНУ УПЛОТНЕНИЯ ПОЧВЫ В МЕЖДУРЯДЬЯХ ХМЕЛЬНИКОВ

As. PhD. Eng. Smirnov P.A.[1)], As. PhD. Ec. Makushev A.E. [1)], Prof. Ph.D. Eng. Kazakov Y. F. [1)], Prof. Ph.D. Eng. Medvedev V.I. [1)], As. PhD. Eng. Vasilyev A.O. [1)*], As. PhD. Eng. Andreev R.V. [1)]

[1)]Chuvash State Agricultural Academy / Russia

**Tel: +79373777222; E-mail: 3777222@bk.ru*

Keywords: *soil, compaction, density, hop, deformation*

ABSTRACT

Based on experimental research, a method of comparing areas of compaction by tractor running gears in field conditions and in hop garden row spacing was suggested. Zones of inefficient and intensive use of hop garden row spacing area were determined. Also, a solution to the row spacing zone optimization problem was given. The results of experimental research on soil density in case of compaction by track and wheel tractors were presented.

АННОТАЦИЯ

По экспериментальным исследованиям предложена методика сравнения площадей уплотнения движителями трактора в полевых условиях и в междурядье хмельника. Определены зоны неэффективного и интенсивного использования площади междурядья хмельника. Также приведено решение задачи оптимизации зон междурядья. Приведены результаты экспериментальных исследований плотности сложения почвы при уплотнении гусеничного и колесного тракторов.

INTRODUCTION

A negative factor of the solution to modern problems of energy saving through a sharp increase in the power-to-weight ratio of tractors and maximum operating width of the machine-tractor aggregate (MTA), which is provided by the required weight of the tractor itself, is high soil compaction under its running gear (Alatyrev et al., 2018; Vasiliev, 2013). Unfortunately, such a trend can be observed in fields of crop farming with multiple interrow tillage too. A high power-to-weight ratio enables performing unique operations of deep soil loosening; however, this operation is not always possible in perennial hop gardens.

In the present paper a method of calculating areas of compaction by tractor running gear in field conditions and in hop garden row spacing was suggested, zones of inefficient and intensive use of hop garden row spacing area were determined based on experimental measurements in the territory of hop gardens of the Chuvash Republic and Mari-El Republic, calculations of intensive use zone of hop garden row spacing were made.

To compare the area of compaction by running gears of the machine-tractor aggregate (MTA) based on known constants of the running gear width, it is feasible to introduce the parameter of relative area of compaction by running gears. We assume that main soil compaction takes place under tractor wheels (tracks) and we take the rear, wider wheel width as the track width. At the same time, in modern hop growing technologies in use up to 12...14 passes on row spacing are provided for *(Vasiliev A.O. et al, 2017; Zakharov et al., 2016; Zakharov et al., 2017).*

The most acceptable theoretical and empirical explanations of shear deformations as a result of compaction by tractor wheels are given in the works of (*Medvedev et al., 2017*) and also in *(Niziolomski et al., 2016; Obour et al., 2017; Peng et al., 2012; Silva et al., 2018; Szatanik-Kloc et al., 2018)*. Here is the description of the research.

In research of shear deformations impact on destruction of weeds roots similar confirming indicators were obtained *(Schnaitter et al., 2016*). The relationship of the deformation from the elongation was drawn based on the obtained data (*Medvedev et al., 2017*).

Similar negative impact of soil compaction, for example, for potatoes was analyzed in (*Rees et al., 2015*). Even presence of small compaction sites with 6 cm thickness influenced growth and yield of the crop.

MATERIALS AND METHODS

The relative compaction area is determined in the following way:
for a track tractor in hop garden row spacing

$$v_к = \frac{2b_g}{b_n}100 \ [\%], \tag{1}$$

where: b_g is track width [m] ;
$b_1, b_2 \ldots b_n$ is hop garden row spacing width [m].

For a track tractor in field conditions

$$v_к = \frac{2b_g}{b_m}100 \ [\%], \tag{2}$$

where: b_m is MTA operating width in field conditions [m].

For a wheel tractor in the hop garden row spacing

$$v_к = \frac{2b_к}{b_n}100 \ [\%], \tag{3}$$

where: b_k is rear wheel width [m].

For a wheel tractor in field conditions

$$v_к = \frac{2b_к}{b_m}100 \ [\%]. \tag{4}$$

The accepted initial data: b_K = 0.4 m (MTZ-921 tractor), b_g = 0.3 m (T-54V tractor), hop garden row spacing b_1=2.25 m, b_2 =2.5 m, b_3 - 3.3 m and the operating width of the field MTA b_m=6.0 m (harrowing aggregate), b_m=3.6 m (KRG-3,6 cultivator).

The above mentioned explains absence of any hop roots under running gear tracks and in gauge area of row spacing at the plow layer depth established by visual inspection during sampling and soil crossovers in hop gardens of the Chuvash Republic.

Consequently, the problem requires more thorough study and optimization.

On the whole, light-grey forest soils are also present in hop gardens of the Chuvash Republic; according to mechanical composition, there are middle and heavy loamy soils (northern regions of the Chuvash Republic). Based on agrochemical analysis data, there is 2.1...2.5 % humus content in the fertile layer. The mean fertile layer depth is 23.5…28 cm. The soil reaction is medium acid. There is no or little, within 1.5...5% range, hop garden slope.

On both sides of the tractor track or wheel pit, two trenches *I* and *II* (Figure 1) are dug and flexible steel strips *1* with cross-section of 0.2x10 mm^2 are laid from the first trench towards the other one. The number of flexible elements is selected depending on the soil deformation analysis depth, for example, in 0.1 m along the vertical line. Circular cross-section guide bushings with 4...6 mm diameter are used to lay them. It was experimentally proven that in this case natural soil texture at the given moment of the research and its monolithic nature do not change as the rod diameter is small comparing to the steel strip width.

The steel strip end is attached to the rod end in deepening *II* and is laid through the soil fragment under analysis to trench *I*. Strip ends in trench *I* are rigidly fixed in special clamp *2*, the opposite ends in trench *II* are in free state.

After the passage of the machine-tractor aggregate a transverse soil crossover is undertaken along the vertical line of steel strip laying and deformation value Δh on each strip is determined. Also, length reduction Δl of the free strip end in trench II is measured and the soil deformation value under the drive unit track is determined based on this reduction.

Thus, it was established that under the impact of vertical loads upper soil layers undergo much bigger deformations. It was noted that deformations get less with deepening. However, the steel strip bending nature remains the same for all layers under analysis (Figure 1).

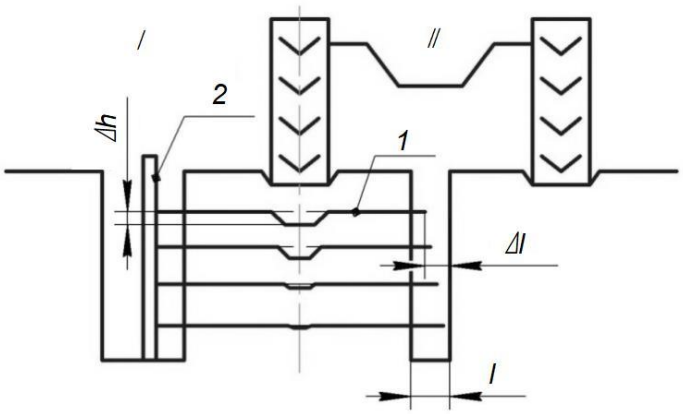

Fig. 1 - Soil deformation determination scheme
1-strip; 2 – clamp; I and II – trenches;

Taking into account a high number of MTA passes in case of the traditional hop growing technology (up to 14 passes), with inter-row cultivation unable to ensure sufficient treatment depth, compacted strips under tractor tracks in hop garden row spacing are permanent. Correspondingly, quantitative reduction of the blocked hop garden row spacing area is required for improvement of hop growing conditions. To solve the problem, the function $b_z = f(b_m, b_k)$ was analyzed (Figure 2).

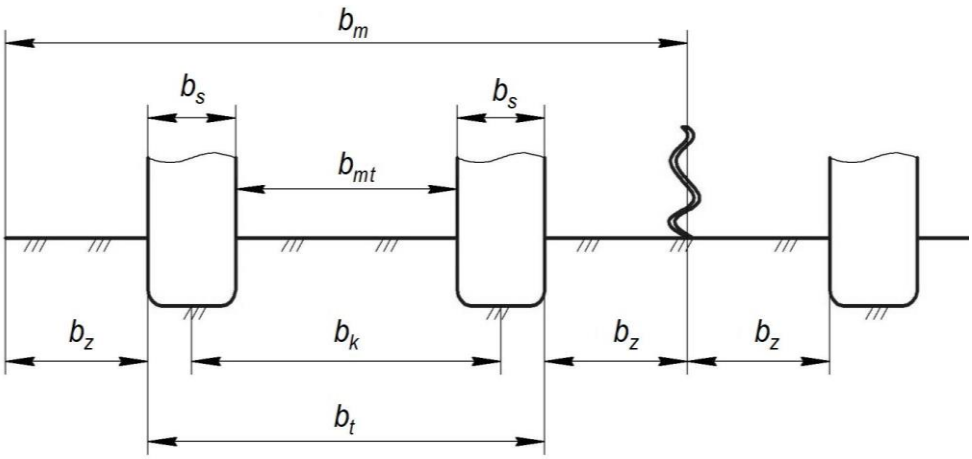

Fig. 2 - Scheme of initial data for calculation of efficient row spacing use
(notation in the text)

The following data were selected as initial data:

1) tractor width by rear wheels (track) $b_t = b_k + b_s$ [m];

2) row spacing width $b_m = b_t + 2b_z$ [m];

3) rear wheel tire (track) width b_s=0.4 m for MTZ tractors; b_s= 0.3 m for LTZ tractors; b_s=0.23 m for T-30A, "Agromash-30TK" tractors;

4) minimum tractor track – b_k :b_k =1.4 m for MTZ; b_k =1.2 m for LTZ tractor [5]; b_k =1.1 m and 1.2 m for T-30A and “Agromash-30TK”; b_k =0.98 m for T-54V tractor;

5) plant protective area width b_k [m];

6) width of the inter-wheel area under the tractor b_{mt} [m].

Relative indicators are calculated using the following expressions:

1) compacted area under tractor wheels:

$$\delta_g = \frac{2b_s}{b_m} 100 \quad [\%] \tag{9}$$

2) inter-wheel area under the tractor:

$$\delta_{mt} = \frac{b_{mt}}{b_m} 100 \quad [\%] \tag{10}$$

3) zone of inefficient row spacing use:

$$\delta_m = \frac{2b_s + b_{mt}}{b_m} 100 \quad [\%] \tag{11}$$

4) zone of intensive row spacing use:

$$\delta_i = \frac{2b_z}{b_m} 100 \quad [\%] \tag{12}$$

RESULTS

The obtained calculation data are given in Tables 1-3.

Table 1

Relative area of compaction by running gears of MTZ-921 and T-54V tractors in hop garden row spacing of different width

Hop garden row spacing width, [m]	Relative area of compaction of hop garden row spacing, [%]	
	by MTZ-921 tractor wheels	by T-54V tractor tracks
2.25	35.56	26.67
2.50	32.00	24.00
3.30	24.40	18.02

Experimental research was conducted in hop gardens of "Agrokhmel" LLC of Vurnary region of the Chuvash Republic, where primarily T-54V track tractors are used, and "Leninskaya Iskra" Pilot Research Collective Farm of Yadrin region of the Chuvash Republic.

There MTZ-921 wheel tractors are used. Soils of hop gardens of "Agrokhmel" LLC are primarily dark-grey forest soils with the mean humus content of 4.1%, at the depth up to 0.2 m (with 2.4...3.1% humus content), those of "Leninskaya Iskra" Pilot Research Collective Farm are grey forest soils with humus content of 2.9% at the depth of 0.2 m.

Table 2

Relative area of compaction by running gears of MTZ-921 and T-54V tractors in field conditions

Field MTA operating width [m]	Relative area of compaction of hop garden row spacing [%]	
	by MTZ-921 tractor wheels [%]	by T-54V tractor tracks [%]
6.0 m (harrowing aggregate)	13.3	10.0
3.6 m (KRG-3,6 cultivator)	22.2	16.67

Table 3

Comparison of field MTAs for different hop garden row spacings by compaction area

Hop garden row spacing width [m]	The ratio of area of compaction by tractor running gears in hop garden row spacing to field MTA compaction area			
	harrowing		cultivator	
	MTZ-921	T-54V	MTZ-921	T-54V
2.25	2.6676	2.67	1.6003	1.5998
2.5	2.4006	2.4	1.4401	1.4397
3.3	1.8184	1.82	1.0909	1.0905

As it can be seen from tables 1-3, due to the limitedness of hop garden row spacing, as is the case with row spacings of similar crops (vineyards and horticultural crops), soil compaction by tractor running gears comparing to field MTA for tractors under consideration (harrowing and cultivation) is 1.1-2.67 times as high.

The soil density was obtained on the basis of the ratio of dried mass of cylinder-shape soil sample obtained by pressing a hollow thin cylinder in soil at the depth of 0...30 cm to its volume.

The results obtained during the experiments show that the soil in hop gardens where track tractors are used has a higher density than in areas where wheel tractors are used (Figures 3, 4). The obtained results conform to the research data of tractor running gears impact on grey forest soil in maize cultivation.

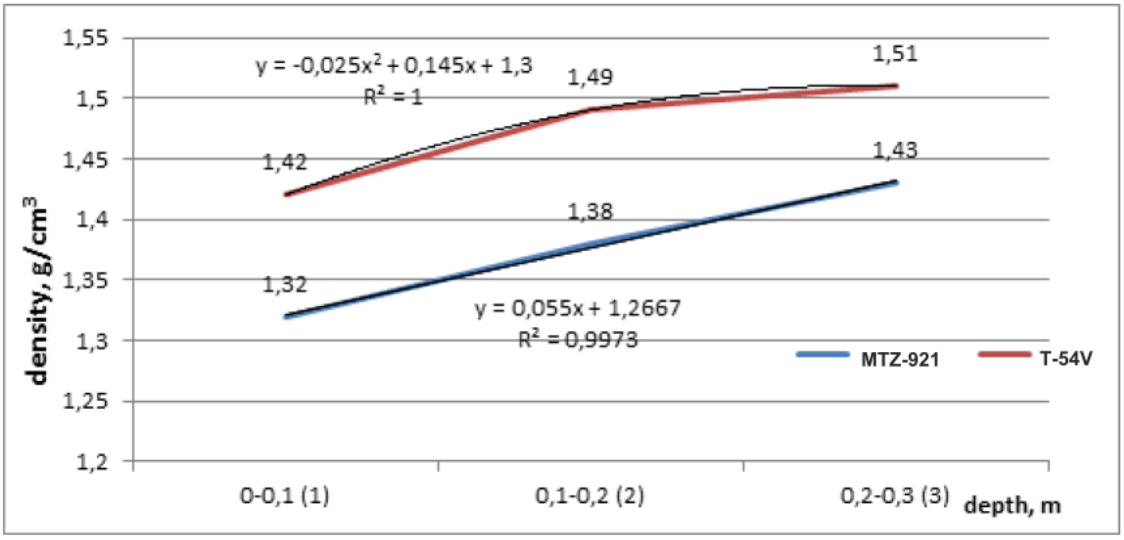

Fig. 3 - Diagram of soil density under tractor support running gears *(based on 27 measurements)*

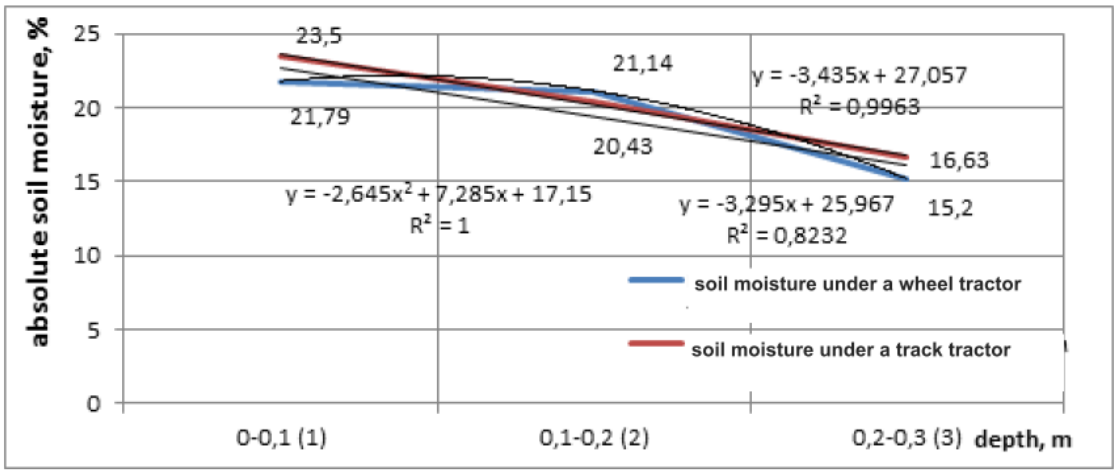

Fig. 4 - Absolute soil moisture under tractor support running gears at the plow layer depth *(based on 27 measurements)*

As a result of experimental data processing, the relations between soil density and soil moisture and the depth of the layer under consideration in parametric form were obtained:

- For compaction by T-54V tractor tracks:

$$\begin{cases} \omega_a = -3.435x + 27.05 \\ \gamma = -0.025x^2 + 0.145x + 1.3 \end{cases}, \quad (5)$$

where: ω_a is the soil moisture [%];

γ is the soil density [kg/m^2];

x is depth of the layer [m].

- For compaction by MTZ-921 tractor wheels:

$$\begin{cases} \omega_a = -3.292x + 25.96 \\ \gamma = 0.055x + 1.266 \end{cases}, \quad (6)$$

By solving parametric equations 5 and 6, the explicit equations were obtained:

- For T-54V tractor:

$$\gamma = 0.0021\omega_a^2 - 0.182\omega_a + 4.06 \quad (7)$$

- For MTZ-921 tractor:

$$\gamma = -0.0171\omega_a + 1.702. \quad (8)$$

The graphical expression of equations 7 and 8 is given in Figure 5.

The conclusion based on ratios 7 and 8 and diagrams (Figure 5) is the following. Soil density and soil moisture are in a linear relationship, and soil density under MTZ-921 tractor tracks is less subjected to changes with moisture growth (or reduction). If we imagine an opposite picture of moisture content dependence on compacted condition of soil, we get a rather low moisture-holding capacity of the compacted area. In case of the experiment a minimum quantity of hop roots was observed under the tractor running gear tracks.

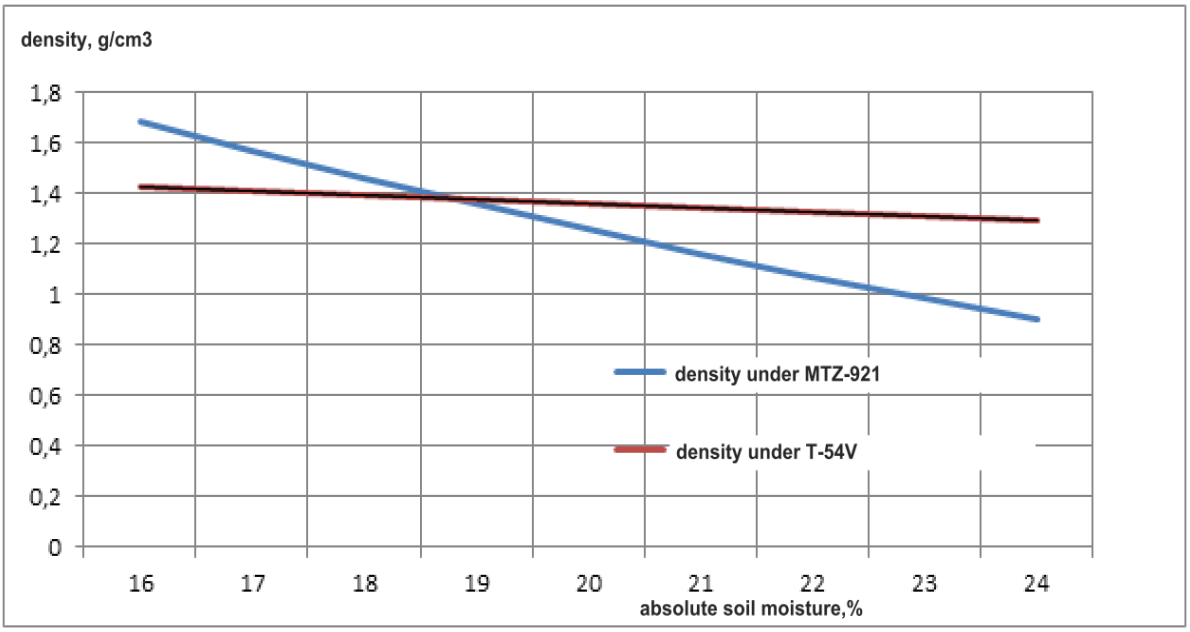

Fig. 5 - The ratio soil density and soil moisture in the compacted area under tractor running gear tracks in hop garden row spacing

Based on the above described experiment, we drew the following diagrams that characterize vertical shear processes on both sides of the running gear track (Figure 6).

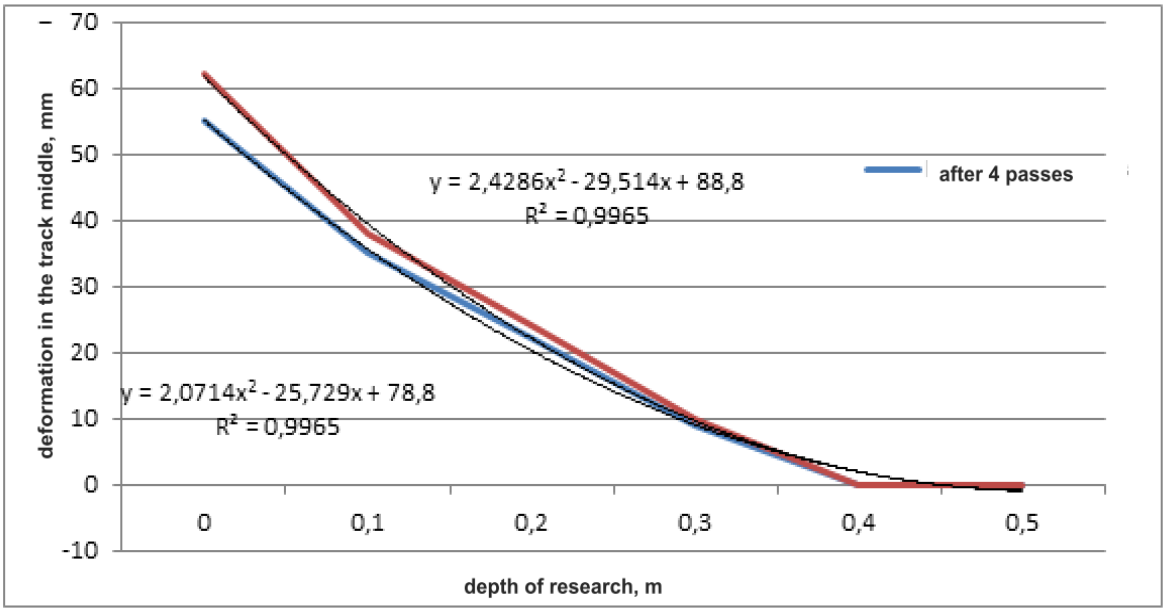

Fig. 6 - Shear vertical deformation along the wheel track (mm) by depth, m

In hop gardens the negative impact of power means running gears spreads on the whole gauge area. During soil crossovers for soil sampling (54 measurements) it was established that at the plow layer depth of 0...0.3 m there are no ("Leninskaya Iskra" Pilot Research Collective Farm) or few ("Agrokhmel" LLC) hop roots between tractor tracks.

The analysis of shear vertical deformation along the wheel track and its spread by depth (Figure 7) shows that after a triple passage over the same track there is almost no soil layer displacement.

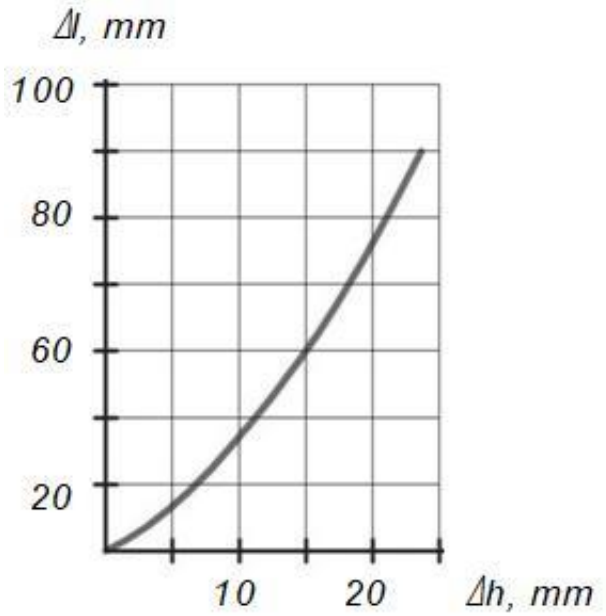

Fig. 7 - Relation of the deformation and the elongation

However, for our case the reverse diagram is of interest (Figure 7). In case of deformation 10 mm elongation reaches up to 30 mm, in case of Δh=20 mm elongation is up to 90 mm, that is such absolute elongation destroys any root system.

A detailed examination of the process of increased soil compaction with tracked tractor thrusters revealed the following. It occurs incrementally, under the front of the track, the value of the distributed load is less than under the rear. Also under the track roller, there is also an instantaneous vertical force more than in between the rollers. Thus, the caterpillar loads the bearing surface cyclically according to the principle "track roller - intermediate zone" with increasing vertical force from the first track roller to the last. It is the repeated cyclic compaction that is the basis of soil compaction.

Also, tracked tractors have increased vibration transmission to the ground. The wheeled tractor transmits minimal vibrations to the porous surface due to the elasticity of the pneumatic tires and the presence of air in the chambers. Despite the presence of a torsion bar suspension on a crawler tractor T-54B, transverse and longitudinal vibrations are fully transferred to the soil, which greatly enhances its compaction.

The results of the analysis of function $b_z = f(b_m, b_k)$ are presented in tables 4 and 5.

Table 4

Structure of inefficient and intensive hop row spacing use zones with different parameters b_k and b_m for b_m = 2.25 and 2.5 m

No.	Tractor	δ_g,%	δ_{mt},%	δ_m, %	δ_i, %	δ_g,%	δ_{mt},%	δ_m, %	δ_i, %
		$b_m = 2.25$ [m]				$b_m = 2.5$ [m]			
1	MTZ-80/82 (b_k=1.4 m)	35.6	44.4	80	20	32	40	72	28
2	LTZ (b_k=1.2 m)	26.7	40	66.7	33.3	24	36	60	40
3	T-25A (b_k=1.1 m)	20.4	38.7	59.1	40.9	18.4	34.8	53.2	46.8
4	30TK (b_k=1.2 m)	20.4	30.2	56.9	36.5	18.4	38.8	57.2	42.8
5	T-54V (b_k=0.98 m)	26.7	30.2	56.9	43.1	24	27.2	51.2	48.8

Table 5

Structure of inefficient and intensive hop row spacing use zones with different parameters b_k and b_m for b_m = 3.0 and 3.33 m

No.	Tractor	δ_g,%	δ_{mt},%	δ_m, %	δ_i, %	δ_g,%	δ_{mt},%	δ_m, %	δ_i, %
		$b_m = 3.0$ [m]				$b_m = 3.33$ [m]			
1	MTZ-80/82 (b_k=1.4 m)	26.7	3.33	60	40	24	30	54	46
2	LTZ (b_k=1.2 m)	20	30	50	50	18	28	45	35
3	T-25A (b_k=1.1 m)	15.3	29	44.3	55.7	13.8	26.1	39.9	60.1
4	30TK (b_k=1.2 m)	15.3	32.3	47.6	52.4	13.8	29.1	42.9	57.1
5	T-54V (b_k=0.98 m)	20	22.7	42.7	57.3	18	20.4	38.4	61.6

Here the following equation is valid:

$$\delta_m = \delta_g + \delta_m \text{ [\%]}. \quad (13)$$

The calculation data (Tables 4, 5) were used for drawing diagrams of intensive use of hop garden row spacing with different planting width (Figures 8, 9).

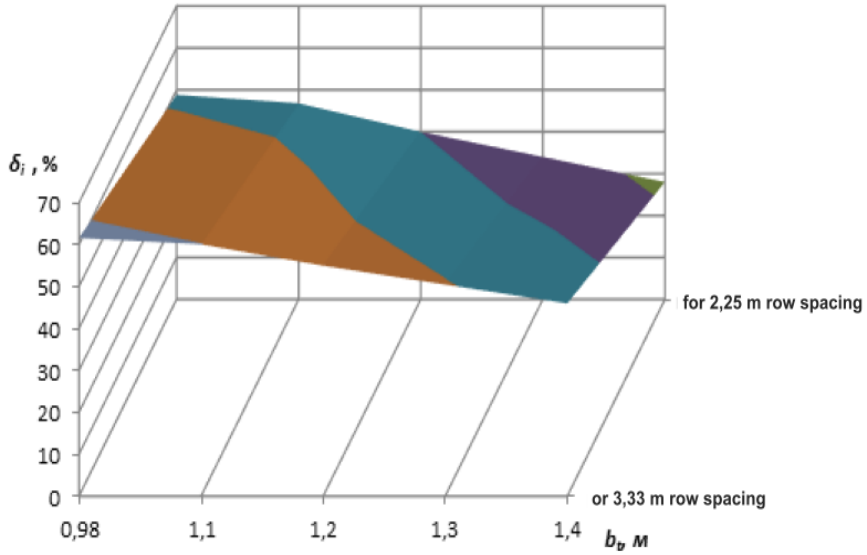

Fig. 8 - The relation between the zone of intensive use of hop garden row spacing δ_i and tractor track width b_k and hop garden row spacing b_m.

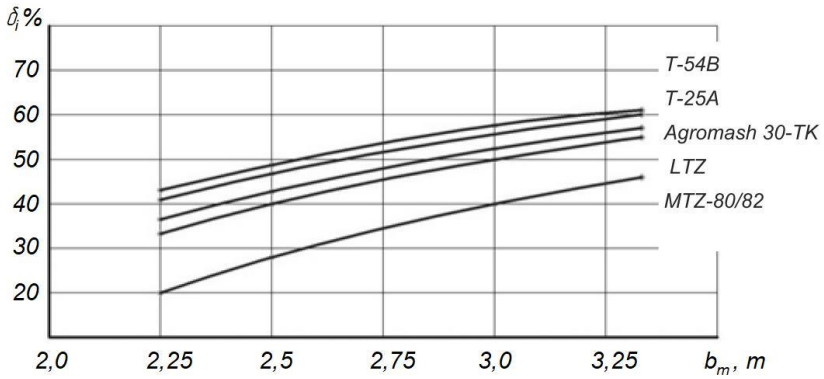

Fig. 9 - Diagrams of the zone of intensive use of hop garden row spacing with different planting width b_m

CONCLUSIONS

1. A method of calculating areas of compaction by tractor running gears in field conditions and in hop garden row spacing was suggested. The given method can also be used in vineyards and on berry bush grounds in gardens. An increase in the area of compaction in hop gardens comparing to field conditions, primarily, due to limited nature of row spacing was revealed.

2. The results of experimental research of soil density in hop gardens of the Chuvash Republic were presented. The relation between soil density and its moisture was given. Despite the opinion of small soil compaction by track tractors, soil density under T-54V tracks is greater comparing to MTZ-921 wheel tractor (Figure 1).

3. The value of the zone of intensive hop garden row spacing use increases with introduction of prospective high-yield hop varieties. The given analytical solutions show that the zone of intensive hop garden row spacing use of over 60% is achieved with the use of T-54V and T-25A tractors with the minimum track during planting of a hop garden with row spacing of 3.33 m.

REFERENCES

[1] Alatyrev S. S., Andreev R. V., Vasiliev A. O., Pushkarenko N. N., Grigoryev A. O., Tikhonov S. V., (2018), Influence of the parameters of support wheels on the amount of the device of the trailer from the tracking course, *IOP Conference Series: Materials Science and Engineering*, vol. 457, 012002, Moscow, Russian Federation;

[2] Lozhkin A. G., Makushev A. E., Pushkarenko N. N., Kornilova L. M., Stepanova V. V., Fedorova O. N., (2017), Revival of hop-production in the Chuvash Republic: problems, challenges and opportunities, *30th IBIMA Conference*, pp. 5295-5299, Madrid, Spain;

[3] Medvedev V. I., Kazakov Y. F., Pushkarenko N. N., Smirnov P. A., Vasiliev A. O., (2017), The current level of hop cultivation mechanization in Chuvash Republic: problems and directions of development (Современный уровень механизации возделывания хмеля в Чувашской Республике: проблемы и направления развития), *Bulletin of the International Academy of Agrarian Education,* no. 37, pp. 27-31, Russia;

[4] Niziolomski J. C., Simmons R. W., Rickson, R. J., & Hann, M. J., (2016), Tine options for alleviating compaction in wheelings, *Soil and Tillage Research*, Elsevier, no.161, pp. 47-52;

[5] Obour P. B., Schjønning P., Peng Y., Munkholm L. J., (2017), Subsoil compaction assessed by visual evaluation and laboratory methods. *Soil and Tillage Research*, Elsevier, no. 173, pp. 4-14;

[6] Peng X., Zhang Z. B., Wang L. L., Gan L., (2012), Does soil compaction change soil shrinkage behaviour, *Soil and Tillage Research*, Elsevier, no. 125, pp. 89-95;

[7] Rees H. W., Chow T. L., Xing Z., Li S., Monteith J. O., Stevens L., (2015), Depth to compact subsoil effects on soil properties and barley–potato yields on a loamy soil in New Brunswick, *Canadian Journal of Soil Science*, no. 95(3), pp. 203-218;

[8] Schnaitter M., Wimmer A., Kollmannsberger H., Gastl M., Becker T., (2016), Influence of hop harvest date of the 'Mandarina Bavaria' hop variety on the sensory evaluation of dry-hopped top-fermented beer. *Journal of the Institute of Brewing*, no. 122(4), pp. 661-669, U.K;

[9] Silva R. P., Rolim M. M., Gomes I. F., Pedrosa E. M. R., Tavares U. E., Santos A. N., (2018), Numerical modeling of soil compaction in a sugarcane crop using the finite element method, *Soil and Tillage Research*, Elsevier, no. 181, pp. 1-10;

[10] Szatanik-Kloc A., Horn R., Lipiec J., Siczek A., Szerement J., (2018), Soil compaction-induced changes of physicochemical properties of cereal roots, *Soil and Tillage Research*, Elsevier, no. 175, pp. 226-233;

[11] Vasiliev A. O., Andreev R. V., Pushkarenko N. N., Smirnov P. A. & Ivanov E. A., (2017), Modern ways of improving the mechanization of hop cultivation. *30th IBIMA Conference*, 5294-5289. Madrid, Spain;

[12] Vasiliev A. O., (2013), *Improving the quality indicators of the cabbage harvesting machine by improving its support-trailer system (Улучшение качественных показателей работы капустоуборочной машины путем совершенствования ее опорно-прицепной системы)*, PhD dissertation, Chuvash State Agricultural Academy, Cheboksary/Russia;

[13] Zakharov A.I., Evgrafov O.V., Zakharov D.A., Ivanova E.V., Tolstova M.L., Tsaregorodtsev E.I., (2016), Factors of intensification in the hops cluster of Chuvashia, *International Journal of Environmental and Science Education*, vol. 11, iss. 17, pp. 10651-10659, Russia;

[14] Zakharov A., Makushev A., Evgrafov O., Zakharov D. & Tsaregorodtsev E., (2017), Formation of the hop-growing cluster in the Chuvash Republic. *30th IBIMA Conference*, pp. 4802-4810. Madrid / Spain.

THE OPTIMAL CHOICE OF THE CHARACTERISTIC WAVELENGTHS IN SPECTRAL IMAGING FOR CUCUMBER DOWNY MILDEW
/
黄瓜霜霉病光谱图像特征波长优化选取

As. Prof. PhD.Eng. Geng C.X.[1)], Ms. Stud. Eng. Wang P.[1)], As. Prof. PhD.Eng. Qin P.L.[2)], Eng. Zhang W.B.[3)], As. Prof. PhD.Eng. Wang P.B.[*1)]

[1)]Robotics and Microsystems Centre，Soochow University，Suzhou/China;
[2)] Wisdom Agriculture College, Suzhou Polytechnic Institute of Agriculture, Suzhou/China;
[3)]Suzhou Agricultural Machinery Technology Promotion Station, Suzhou/China;
Tel:+8618662299887; E-mail: pbwang@suda.edu.cn

Keywords: *cucumber Downy Mildew; spectral image; characteristic wavelength; sensitive waveband*

ABSTRACT

Aiming at the spectral image acquisition of cucumber downy mildew, the study proposed the optimal selection method of spectral imaging characteristic wavelengths combining the mean-variance analysis and analysis of variance. In this study, the variation degree and range of reflection spectrum was quantitatively measured for both healthy leaves and disease spots in cucumber plants. The analysis showed that the three sensitive wavebands (493 - 533 nm, 561 - 653 nm, and 689 - 698 nm) could properly reflect the inter class difference in spectral reflectance between the dorsal part of lesion and healthy leaves. When the selected combination of spectrum was used as the reference for disease spectral imaging acquisition, it showed that the choice of sensitive wavebands can better reflect the difference in the characteristics between lesion and healthy leaves. It has laid the foundation for obtaining the effective spectral images of disease and simplifying the algorithm for image identification.

摘要

针对黄瓜霜霉病的光谱图像获取，提出了基于均值方差法和方差差异分析相结合的光谱图像特征波长优化选取方法，定量衡量了黄瓜作物健康叶片和病斑的反射光谱差异程度及差异范围，提取了 493 nm – 533 nm、561 nm – 653 nm、689 nm – 698 nm 三个敏感波段，分析表明上述波段能较好反映病斑与健康叶片正面的类间光谱反射差异，并将选定的光谱组合作为病害光谱图像获取的参考依据，表明敏感波段的选择能较好地反映病斑与叶片间的特性差异，为获取病害有效光谱图像和简化图像识别算法奠定了基础。

INTRODUCTION

The characteristics of the reflectance spectrum of any plant vary under the influence of disease and biological stress; however, there are rules for the variation (*Manjunath et al., 2014; Shi et al., 2016; Bandaru et al., 2016*). There have been many studies for detecting plant diseases and biological stress from the perspective of spectral analysis and spectral imaging at home and abroad. For instance, (*Wei et al., 2014*) used three wavelengths (518, 711 and 980 nm) to differentiate the maturity in persimmons into four stages: immature, early mature, fully mature and over mature; and the accuracy can be as high as 95.3%. (*Sirisomboon et al., 2013*) used near-infrared spectroscopy (NIRS) to detect rice mould infections and found that the error rate could be reduced to 18.723%, and the deviation to 4.613%. (*Mahlein et al., 2013*) studied the waveband between 450 and 950nm and developed a specific spectral disease index (SDIS) for crop disease detections, and the result showed that the index is highly accurate and sensitive. (*Min et al., 2005*) found the wavelengths related to chlorophyll are 450, 550, 660 and 719 nm, and those related to protein are 2054 and 2180 nm. (*Kong et al., 2013*) used the spectroscopic analysis together with image processing and stoichiometric methods, established a least squares support vector machine (LSSVM) model for the early diagnosis of grey mould in stems of tomatoes. The result suggested that using the hyperspectral imaging technology to diagnose the grey mould disease of tomato stems at early stage is feasible. (Jiang et al., 2013) used three sensitive wavelengths (532, 610 and 700nm) to measure chlorophyll content in tomato leaves and acquired outstanding results.

The unique reflectance characteristics at different wavelengths in a plant's spectrum can be effectively transformed into the expression of target information and detection information of spectral imaging via analyses (*Sun et al., 2016; Ma et al., 2016; Story et al., 2010*). For efficient spectral imaging of plant diseases in complex environments, it requires analyses of their spectral properties and selection of characteristic wavebands (*Ye et al., 2016; Polat et al., 2014*). The aim of this study was to use spectral analysis methods to determine the optimal spectral wavebands that could diagnose the downy mildew disease, to increase the grey scale contrast of the corresponding spectral image object and background, and to provide a useful basis for the subsequent image processing.

MATERIAL AND METHODS

- **Experiment Materials**

The cucumber for experiment was the cultivar "Zhongke 958", grown with a trailing method. Spectral data collection was conducted in the solar greenhouse at Shang-Zhuang Experimental Station of China Agricultural University in November 2015. Owing to the need for supportive materials in trailing cultivation, such as bamboo poles, nylon slings and clamps, there were a considerable amount of background information in the spectral imaging acquisition results. In order to study the cucumber downy mildew and the spectral characteristics in cucumbers, leaves and complex background, 11 types of samples, including the dorsal and ventral sides of leaves with lesions caused by downy mildew, the dorsal and ventral sides of the healthy leaves, cucumbers, dried leaves, bamboo poles, green nylon slings, black clamps, dry soil and wet soil, were selected as the main objects for spectral data collection.

- **Choice of Instrument**

The spectral reflectance data was collected using the FieldSpec Pro VNIR handheld spectrometer (Analytical Spectral Devices, Inc., USA). The spectrometer measures wavelengths ranging between 325 nm and 1075 nm, and the spectral resolution is at 1 nm. Prior to data collection, the standard whiteboard was used to calibrate and eliminate systematic errors. After the calibration, the spectral reflectance was measured in the 11 types of samples. The sensor probe was vertically pinned and the sampling height was 20 mm. The measured object was at the same level as the standard white board in measurement. 20 probe points were randomly selected on each sample, with each point being tested for 5 times. The mean of the 5 measurements was then used as the final measurement for each testing point. The raw spectral reflectance data of each measured point was acquired at the waveband between 325 nm and 1075 nm. The measurements were saved in Microsoft EXCEL format and further analyzed using Matlab.

- **Data processing method**
- **Spectral reflectance analysis**

A highly consistent spectra and an identical trend of reflectance was observed in the dorsal and ventral sides of lesion and healthy leaves. In the meantime, the distribution of healthy and lesion parts was spatially intersected. Here, a mean-variance analysis was used for an emphasis on analysing the volatility of the spectra for the dorsal and ventral sides of lesion and healthy leaves. The method was described as follows:

By defining the estimated value for the mean reflectivity of sample x is:

$$\hat{\mu}_x = \frac{1}{n}\sum_{m=1}^{n} x_m \tag{1}$$

where $\hat{\mu}_x$ - is the estimated value for the mean reflectivity of sample x; n - number of sampling points;

X_m - the reflectivity of the sampled wavelength for the m-th sampling point of sample x.

One could prove the estimate $\hat{\mu}_x$ is unbiased. Thus:

$$E(\hat{\mu}_x) = \mu_x \tag{2}$$

Where μ_x- the true value of the mean reflectivity of sample x.

When the samples are uncorrelated and the estimates are consistent, then:

$$\lim_{n\to\infty} E\mu_x - \hat{\mu}_x = 0 \tag{3}$$

When the true value of the mean reflectivity of a given sample is known, its variance can be estimated by the following equation:

$$\delta_x^2 = \frac{1}{n}\sum_{m=1}^{n}(x_m - \mu_x)^2 \quad (4)$$

Where δ_x^2 - the variance of sample x.

Here, the estimate is unbiased and consistent. However, if the true value of the mean is unknown, then $\hat{\mu}_x$ should be used to replace μ_x in the estimation, and the estimation would be biased.

Nevertheless, an unbiased variance can be estimated with the following formula:

$$\delta_x^2 = \frac{1}{n-1}\sum_{m=1}^{n}(x_m - \mu_x)^2 \quad (5)$$

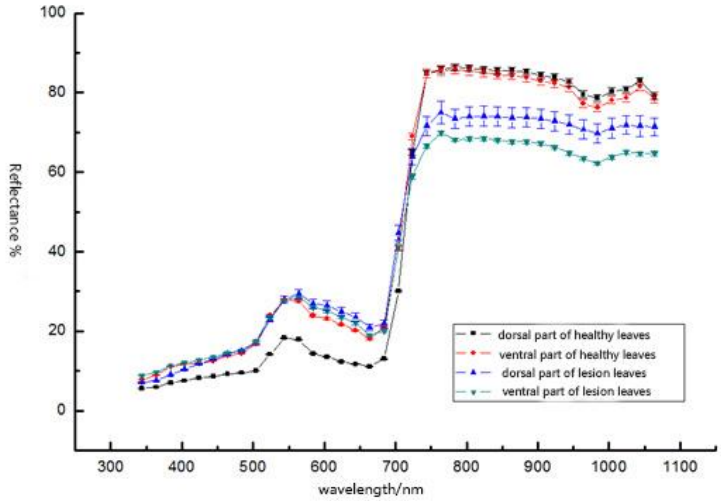

Fig. 1 - The spectral fluctuate characteristic of double sides of the disease and the healthy leaves

When the Savitzky-Golay smoothing (SG) (*Li et al., 2015*) was used to eliminate random noises, as shown in Fig. 1, the fluctuation of sample data was smaller and the sample variance was also smaller; thus, the reflectance curves of the four types of sample could be distinguished with ease. In the visible band, the maximum spectral reflectance for the dorsal and ventral sides of healthy leaves was found at 760 nm (94.35% and 93.03%, respectively). The maximum reflectance for the dorsal and ventral sides of lesion leaves was at 763 nm (75.51% and 70.30%, respectively). In near infrared band, the minimum spectral reflectance at the near infrared band for the dorsal and ventral sides of healthy leaves was at 988 nm (77.77% and 75.22%, respectively). For the dorsal and ventral sides of lesion leaves, the minimum reflectance was at 974 nm (68.91% and 61.58%, respectively). The maximum spectral reflectance for the dorsal part of the lesion leaves was 75.22% at 1068 nm, and for the ventral part was 68.96% at 823 nm. The result from the qualitative analysis showed that the differentiation was more obvious at near infrared band than at the visible light band, although the spectral reflectance was less distinguishable between them according to the extreme values of their spectral reflectance.

- **Selection on the characteristic sensitive wavebands**

Based on the results from the qualitative analysis, this study used a wavelength selection method based on the analysis of variance to quantitatively analyse the level and range of differences of the reflectance spectra in healthy and lesion leaves in cucumbers, and to confirm the ideal characteristic sensitive wavebands that may diagnose the cucumber downy mildew (*Camargo et al., 2008; Yao et al., 2013*). Here, M was defined as the number of categories. For clarification, Formula (1) was reformatted as Formula (6):

$$\bar{x}_j = \frac{1}{n_j}\sum_{i=1}^{n_j} x_{ij} \quad (6)$$

where $\bar{x}_j$- the mean reflectivity of the spectra in *j* category; n_j - the number of samples in *j* category;

x_{ij}- the reflectivity of the spectra of the *i*-th sample in *j* category.

The mean reflectivity for all samples can be expressed by:

$$\bar{x} = \frac{1}{Mn_j}\sum_{i=1}^{M}\sum_{j=1}^{n_j} x_{ij} \tag{7}$$

where $\bar{x}$ - the mean reflectivity for all samples; M - the number of categories.

The error sum of squares S_E represents the variation in spectral reflectance of different categories and is expressed by Formula (8). As shown in Fig. 2, the error sum of squares S_E for the spectrum of the four samples was of relatively high spectral reflectance at the bands of 500 nm and above, which was the most obvious on the dorsal part of lesion leaves.

$$S_E = \sum_{i=1}^{M}\sum_{j=1}^{n_j}(x_{ij} - \bar{x}_j)^2 \tag{8}$$

where S_E - the error sum of squares.

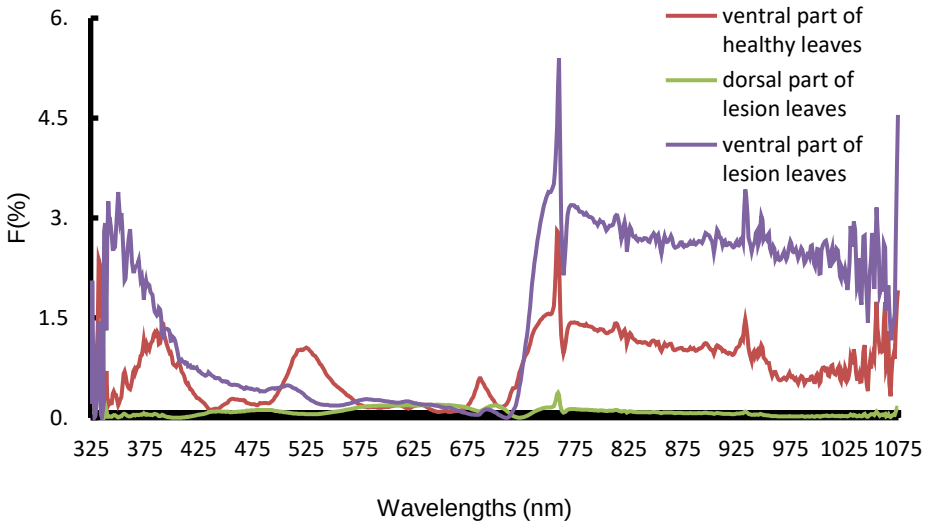

Fig. 2 - The error sum of squares SE of reflectance spectrum for the double sides of healthy cucumber leaf and disease area

Here, $S_A$was defined as the efficacy sum of squares, representing the difference of spectral reflectance among different categories, expressed by Formula (9).

The curves of the efficacy sum of squares S_A were shown in Fig. 3, where a consistency of the reflectance trend among the four samples can be seen.

$$S_A = \sum_{i=1}^{M}\sum_{j=1}^{n_j}(\bar{x}_j - \bar{x})^2 \tag{9}$$

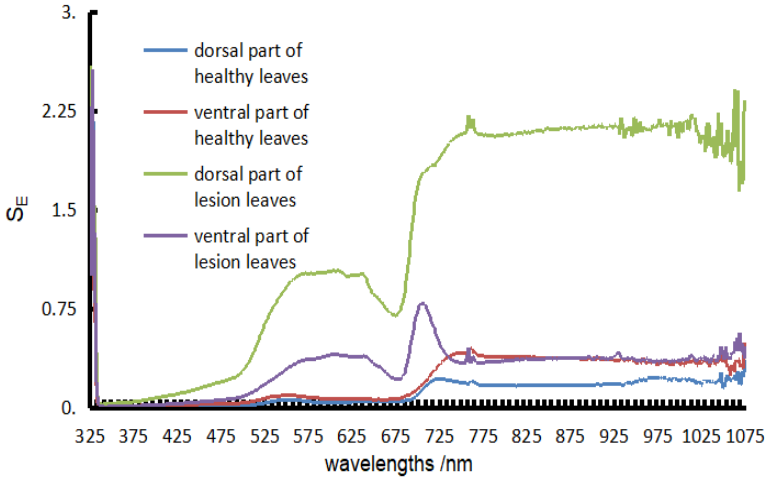

Fig. 3 - The efficacy sum of squares SA of reflectance spectrum for the double sides of healthy cucumber leaf and disease area

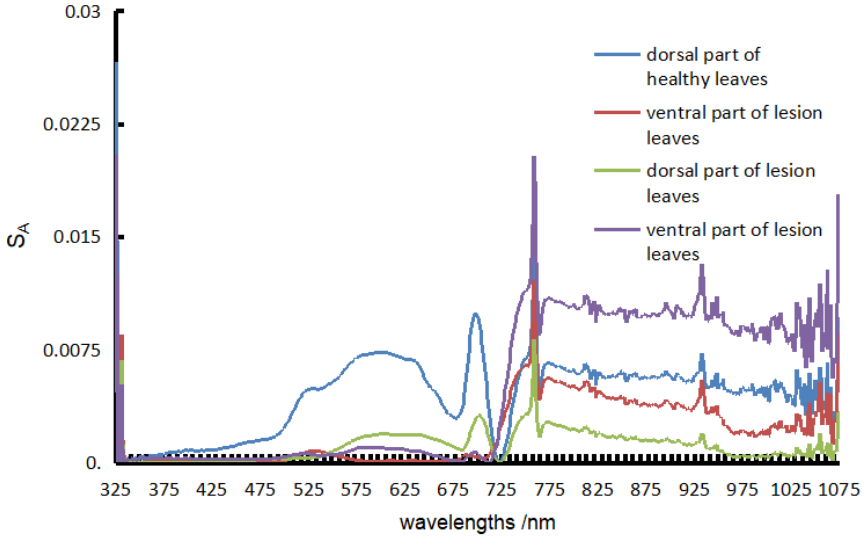

Fig.4 - The curve of F value of reflectance spectrum for the double sides of healthy cucumber leaf and disease area

Hence, for a given wavelength, the distinctiveness of the reflectance spectrum (F) in a sample can be shown as:

$$F = \frac{S_A}{S_E} \times 100\% \tag{10}$$

Where F is the distinctiveness of the reflectance spectrum.

The F value represents a relative value for the classification error and the random error.

The greater value means the greater difference in spectral reflectance between the categories.

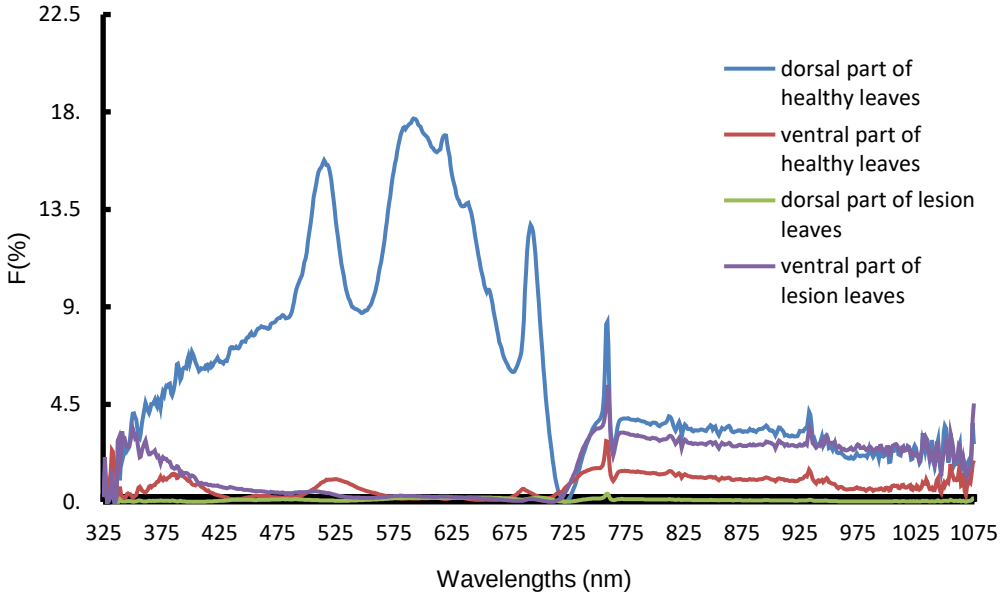

Fig. 5 - The curve of F value of reflectance spectrum for the back side of healthy cucumber leaf and the double sides of disease area

The raw spectral data was analyzed using the analysis of variance, and the curves for the F value variation among the reflection spectra of both ventral and dorsal parts of healthy and lesion leaves were shown in Fig. 4. By and large, the greatest difference was found in the spectral reflection in the dorsal part of healthy leaves, the ventral part of healthy leaves, and both dorsal and ventral parts of lesion leaves. In particular, the most obvious difference in spectral reflectance was within the visible light band; the curve for the F value variation showed a certain degree of characteristics and distinctiveness.

The most significant differentiation was seen at the waveband of 378 nm - 705 nm, with a minimum F value of 5.17%. The peak value was at 592 nm and the F value was at its maximum, 17.70%. The wavebands with the F value >10 were: 493 nm - 533 nm, 561 nm - 653 nm, and 689nm - 698 nm; the analyses suggested these wavebands can better reflect the difference of spectral reflection between the lesion and healthy leaves, and they can be regarded as the sensitive wavebands for the raw spectral data. However, as shown in Fig. 5, the characteristics of spectral reflectance in the ventral part of healthy leaves and the lesion leaves was unobvious in those above three wavebands

REASULTS

Spectrum Capture

The curves for the reflection spectra of all the 11 types of samples are shown in Fig. 6. The spectral reflectance of each sample was calculated as the mean of the spectral reflectance of all the pixels in the samples, overcoming the limitation of using partial observation to represent the whole picture in the traditional spectrum method. Using the measured spectral reflectance of the 11 samples and based on the general experience in division of wavebands in spectroscopy, the selected spectral detection region was firstly divided into two empirical sub-bands: the visible spectrum (380 - 780 nm) and the near-infrared spectrum (780 - 1025 nm). The rhythm of the spectral curves was remarkable (Fig. 6); a typical green-plant spectral curve could be found in every cucumber organ; that is, a strong reflection peak of chlorophyll around 550 nm, a trough around 680 nm, that is mainly caused by strong absorption of chlorophyll, and a high reflection plateau at 700 - 900 nm. The reflectance curves for non-plant samples were significantly different, indicating a great disparity.

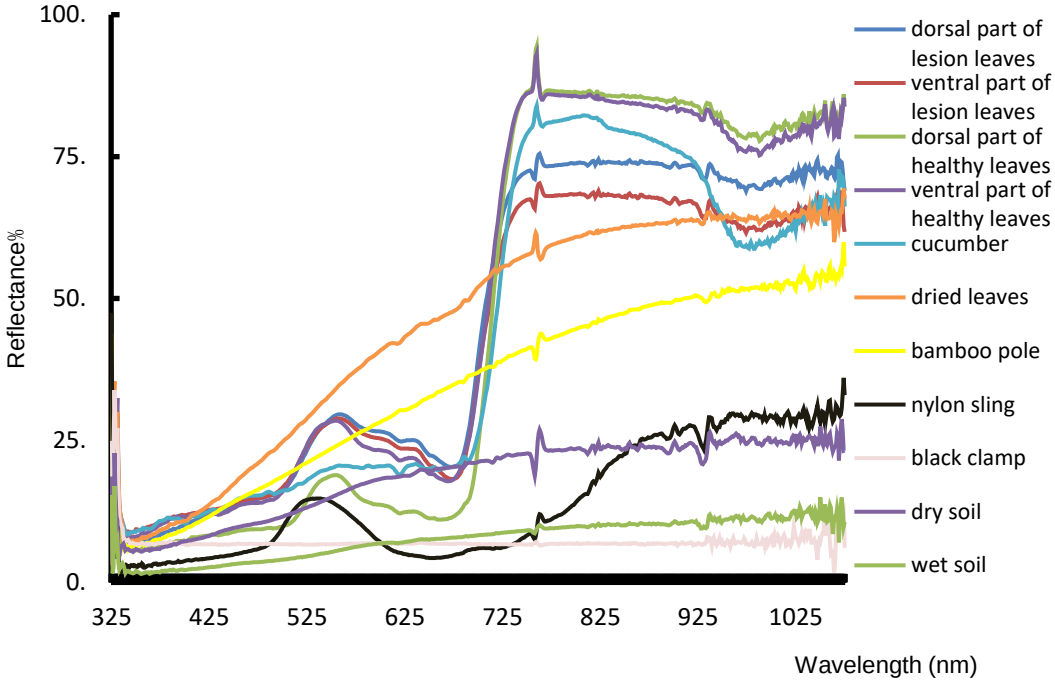

Fig. 6 - Spectral reflection curves of the 11 kinds of samples

Characteristic spectral imaging

Owing to the limitation of the greenhouse environment and the establishment of image acquisition system, the main object for the image detection was the dorsal part of the leaf. From the section "Selection on the characteristic sensitive wavebands", we can see that the wavebands with the F value >10 were: 493 nm - 533 nm, 561 nm - 653 nm, and 689nm - 698 nm; the analyses suggested these wavebands can better reflect the difference of spectral reflection between the lesion and healthy leaves, and they can be regarded as the sensitive wavebands for the raw spectral data. The above three main bands were selected as the main spectral band for the disease information acquisition (*Singh et al., 2012*).

The spectral imaging was constructed through a black and white camera with light filters, and the filter types were one with a central wavelength of 506 nm, half-bandwidth of 35 nm and a maximum transmittance of 90%; the other with a central wavelength of 625 nm, half-bandwidth of 20 nm and a maximum transmittance of 80%; and the third with a central wavelength of 680nm, half-bandwidth of 20 nm and a

maximum transmittance of 80%. The collected images were shown in Fig. 7. The differences between lesion and healthy leaves were demonstrated clearly in the images and the use of grayscale images at characteristic wavebands as the raw images for disease extraction greatly simplified the algorithm for disease extraction and reduced computing amount, and thus improved the timeliness of image processing for the spray robot operation to make decisions on-site.

A.Spectral image at 506 nm B.Spectral image at 625 nm C.Spectral image at 680

Fig. 7 - The spectral image of cucumber leaves

CONCLUSIONS

- By establishing the optimal detection waveband for healthy and lesion cucumber leaves, this study qualitatively analysed the differentiation of both in the visible light and near infrared wavebands. The result showed that the difference was more distinct in the near-infrared band than in the visible light band, but less distinct in the spectral reflectance, from the perspective of the extremums of spectral reflectance.
- The F value for the distinctiveness of the reflectance spectrum in samples was calculated through the analysis of variance. The three wavebands with the F value >10 (i.e., 493-533 nm, 561-653 nm and 689-698 nm) were selected, and the result suggested these wavebands can properly reflect the difference in the spectral reflection between the lesion and healthy leaves, and they can be regarded as the sensitive wavebands for the raw spectral data.
- In the examination of the spectral imaging for the cucumber plants in the three wavebands via the method of using a black and white camera with light filters, the result showed that the selected sensitive bands can properly reflect the differences in the inner components and external features in the healthy and lesion cucumber leaves and highlight the obvious differences in spectral imaging, hence simplify the complexity of the algorithm for image processing, and improve the timeliness of the algorithm.

ACKNOWLEDGEMENT

The study was supported by two National Key Research and Development Program of China (No. 2016YFD0700600)(No. 2017YFD0701500), and 2017 high-end training program for professional leaders of teachers in higher vocational colleges in Jiangsu Province(NO. 2017GRFX044).

REFERENCES

[1] Bandaru V, Daughtry C.S., Codling E.E. et al., (2016), Evaluating leaf and canopy reflectance of stressed rice plants to monitor arsenic contamination, *International Journal of Environmental Research and Public Health*, Vol.13, pp.606-609, Pubmed, Beltsville/U.S.A.;

[2] Camargo A，Smith J.S., (2008), An image-processing based algorithm to automatically identify plant disease visual symptoms, *Biosystems Engineering*, Vol.102, pp.9-21, Academic Press INC Elsevier Science, San Diego/U.S.A.;

[3] Jiang W.J., Sun M, (2011), Research on predicting modeling for chlorophyll contents of greenhouse tomato leaves based on multi-spectral imaging, *Spectroscopy and Spectral Analysis*, Vol.31, pp.758-761, The Chinese Optical Society, Beijing/China;

[4] Kong W.W., Yu J.J., Liu F. et al., (2013), Early diagnosis of gray mold on tomato stalks based on hyperspectral data, *Spectroscopy and Spectral Analysis*, Vol.33, pp.733-736, The Chinese Optical Society, Beijing/China;

[5] Li X.L., Yi S.L., Zheng Y.Q., et al., (2015), Analysis of phylogenetic relationships of main citrus germplasms based on FT-IR spectra of petals, *Intelligent Automation & Soft Computing*, Vol.21, pp.295-304, Taylor & Francis INC., Philadelphia/U.S.A.;

[6] Ma W, Wang X, Qi L.J., (2016), Study on spectrum recognition of leaf spot disease based on visible-near infrared spectroscopy, *Spectroscopy and Spectral Analysis*, Vol.36, pp.121-123, The Chinese Optical Society, Beijing/China;

[7] Mahlein A.K., Rumpf T, Welke P, et al., (2013), Development of spectral indices for detecting and identifying plant diseases, *Remote Sensing of Environment*, Vol.128, pp.21-30, Elsevier Inc., Malden/U.S.A.;

[8] Manjunath K.R., Kumar A, Meenakshi M. et al., (2014), Developing spectral library of major plant species of Western Himalayas using ground observations, *Journal of the Indian Society of Remote Sensing*, Vol.42, pp.201-216, Springer (India) Private Ltd., Ahmedabad/India;

[9] Min M, Lee W.S., (2005), Determination of significant wavelengths and prediction of nitrogen content for orange, *Transactions of the ASABE*, Vol.48(2), pp.455-461, American society of Agricultural and Biological Engineers, Michigan/U.S.A.;

[10] Polat I，Baysal O，Mercati F, (2014), Characterization of pseudoperonospora cubensis isolates from Europe and Asia using ISSR and SRAP molecular markers, *European Journal of Plant Pathology*, Vol.139, pp.641-653, Springer, Dordrecht/Netherlands;

[11] Shi T.Z., Wang J.J., Chen Y.Y., et al., (2016), Improving the prediction of arsenic contents in agricultural soils by combining the reflectance spectroscopy of soils and rice plants, *International Journal of Applied Earth Observations and Geoinformation*, Vol.52, pp.95-103, Elsevier B.V., Wageningen/Netherlands;

[12] Singh C.B., Jayas D.S., Paliwal J, et al., (2012), Fungal damage detection in wheat using short-wave near-infrared hyperspectral and digital colour imaging, *International Journal of Food Properties*, Vol.15, pp.11-24, Taylor & Francis INC., Philadelphia/U.S.A.;

[13] Sirisomboon C.D., Putthang R, Sirisomboon P, (2013), Application of near infrared spectroscopy to detect aflatoxigenic fungal contamination in rice, *Food Control*, Vol.33, pp.207-214, Elsevier Science Ltd., London/U.K.;

[14] Story D, Kacira M, Kubota C. et al., (2010), Lettuce calcium deficiency detection with machine vision computed plant features in controlled environments, *Computers and Electronics in Agriculture*, Vol.74, pp.238-243, Elsevier Science B.V., Wellington/Netherlands;

[15] Sun J, Lu X. Z., Zhang X.D. et al., (2016), Identification of red bean variety with probabilistic GA-PNN based on hyperspectral imaging, *Transactions of the Chinese Society for Agricultural Machinery*, Vol.47, pp.215-211, Chinese Society for Agricultural machinery, Beijing/China;

[16] Wei X, Liu F, Qiu Z.J. et al., (2014), Ripeness Classification of Astringent Persimmon Using Hyperspectral Imaging Technique, *Food and Bioprocess Technology*, Vol.7, pp.1371-1380, Springer, Newyork/U.S.A.;

[17] Yao H.B., Hruska Z, Kincaid R, et al., (2013), Detecting maize inoculated with toxigenic and atoxigenic fungal strains with fluorescence hyperspectral imagery, *Biosystems Engineering*, Vol.115, pp.125-135, Academic Press INC Elsevier Science, San Diego/U.S.A.;

[18] Ye H.J., Lang R, Liu C.Q., et al., (2016), Recognition of cucumber downy mildew disease based on visual saliency map, *Transactions of the Chinese Society for Agricultural Machinery*, Vol.47(5), pp.270-274, Chinese Society for Agricultural machinery, Beijing/China;

RESEARCH ON THE BLOCK-PORTION SEPARATOR PARAMETERS INFLUENCE ON THE ADJUSTMENT RANGE OF OPERATING ELEMENTS SPEED

/

ДОСЛІДЖЕННЯ ВПЛИВУ ПАРАМЕТРІВ СИСТЕМИ ГІДРОПРИВОДІВ БЛОЧНО-ПОРЦІЙНОГО ВІДОКРЕМЛЮВАЧА НА ДІАПАЗОН РЕГУЛЮВАННЯ ШВИДКОСТІ РОБОЧИХ ОРГАНІВ

Ph.D. Ivanov M.I.[1)], Ph.D. Rutkevych V.S.[1)], Ph.D. Kolisnyk O.M.[1)], Ph.D. Lisovoy I.O.[2)]
[1)]Vinnytsia National Agrarian University / Ukraine; [2)]Uman National University of Horticulture
Tel:+380962700443; E-mail: v_rut@ukr.net

Keywords: *hydraulic drive, design, pump, processes, speed*

ABSTRACT

The article focuses on solving the problem of reducing the energy intensity of the separating ensilage fodder process from trench silo with the block-portion method by developing and substantiating the parameters and operating modes of the hydraulic drives system of the block-portion separator. This allows adjusting the operating modes of the cutting mechanism drive and the vertical feed drive of the П-shaped frame. The system allows adjusting the feed of the П-shaped frame in accordance with the change in the cutting effort that makes an effect on the cutting mechanism. As a result, we get stabilization of energy consumption in the process of separating an ensilage fodder block portion if the parameters that determine the cutting process characteristics fluctuate. It was proven that the expansion of the actuating hydro-motors speed adjustment range and, accordingly, the hydraulic drive system responsiveness increase is possible by the appropriate choice of the slide valve parameters. The most effective of the speed range adjustment expansion of the cutting mechanism hydraulic motor and the hydraulic cylinder of the П-shaped frame drive is provided by reducing the width of the slide valve working edges. The influence of the hydraulic system parameters of the ensilage fodder block-portion separator on the speed adjustment range of the operating elements has been studied. The hydraulic drives system parameters which have the greatest influence on the expansion of the hydraulic drives operating modes adjustment range were established. This allows increasing the responsiveness and efficiency of the proposed block-portion separator of ensilage fodder hydraulic drives system by identifying the rational values of these parameters. Recommendations on the design parameters choice are given.

РЕЗЮМЕ

Стаття присвячена розв'язанню проблеми зменшення енергоємності процесу відокремлення консервованих кормів з траншейних сховищ блочно-порційним методом шляхом розробки та обґрунтування параметрів і режимів роботи системи гідравлічних приводів блочно-порційного відокремлювача, яка дозволяє узгодити режими роботи двох приводів – привода різального механізму та привода вертикальної подачі П–подібної рамки. Система передбачає регулювання подачі П–подібної рамки відповідно зміни зусилля різання, яке діє на різальний механізм, в результаті чого відбувається стабілізація енерговитрат на відокремлення блок-порції консервованого корму при умові коливання параметрів, які визначають характеристики процесу різання. Встановлено, що розширення діапазону регулювання швидкостей виконавчих гідродвигунів та, відповідно підвищення чутливості системи гідроприводів можливе шляхом відповідного вибору параметрів золотникового роздільника. Найбільш ефективно розширення діапазона регулювання швидкостей гідромотора різального механізму та гідроциліндра привода П–подібної рамки забезпечується шляхом зменшення ширини робочих кромок золотника. Досліджено вплив параметрів системи гідроприводів блочно-порційного відокремлювача консервованого корму на діапазон регулювання швидкості робочих органів. Встановлено параметри системи гідроприводів, що мають найбільший вплив на розширення діапазону регулювання режимів роботи системи гідроприводів, що дозволяє шляхом визначення раціональних значень даних параметрів підвищити чутливість та ефективність запропонованої системи гідроприводів блочно-порційного відокремлювача консервованих кормів. Дано рекомендації з вибору конструктивних параметрів.

INTRODUCTION

Recent development of agricultural machinery involves further increase in hydraulic drives operating elements development level. They are aimed at increasing their productivity, power, as well as reducing energy consumption and improving dynamic characteristics (*Andrenko P.N., Lurye Z. Ya., 2016*).

According to the Strategy for the agrarian economic sector development for the period until 2020, the national agricultural machinery must reach a fundamentally new level of development. In order to achieve the set goals it is necessary to solve a number of actual problems. The problems in the engineering industry include the lack of innovative potential and weak development of the Ukrainian agricultural machinery. This results in the increase of the industry dependence on technologies and equipment import (*Privalov F.I., 2017*). A significant increase in the number of hydraulic developments for the machines and equipment is the trend in modern agricultural machinery. The hydraulic drive is demanded to carry out several operations simultaneously. It is conditioned by both economic and functional requirements for hydraulic machines and equipment (*Shylo I.N., Tolochko N.K., Romanyuk N.N., Nukeshev S.O., 2016*). There are many machines and technological equipment such as harvesters, loaders, manipulators. Their work mainly requires simultaneous operation of several operating elements. Besides, such systems always require precise speed control adjustment during operation, for example, to maintain the assigned kinematics of their movement. The adjustment accuracy should be ensured even under variable loadings on the operating elements (*Andrenko P.N., Lurye Z. Ya., 2016; Galukhin N.A., 2014*).

Therefore, the research on the influence of the block-portion separator hydraulic drives parameters on the speed range of the operating elements adjustment is an actual scientific problem for the country's agricultural and industrial complex. The solution to the problem will increase the mechanization level in loading and unloading operations, the quality of technological operation while separating fodder and reducing the agricultural products cost price.

The block-portion separators of ensilage fodder which are now used at the Ukrainian enterprises, as well as other national agricultural machines are equipped with hydraulic drives of fixed flow control valve which do not meet modern requirements for speed, reliability and power consumption related to these machines (*Ivanov M.I., Hrytsun A.V., Podolyanyn I.M., Rutkevych V.S., 2010*). The main disadvantages of the drives are significant power losses when it is necessary to perform precise movements or to regulate the flow of hydraulic oil used in operating elements (hydraulic motors). Some unconnected hydraulic motors of the separator's cutting mechanism drive and the hydraulic cylinder of the feeding drives lead to applying hydraulic motors with increased capacity (*Ivanov N., Shargorodskiy S., Rutkevych V., 2013; Ivanov M.I. et al., 2013*). As a result, the power of each of these machine's drives increases to 25 kW under condition of identifying the maximum required power of the cutting mechanism drive within the separator in the range of 4.5-6.0 kW, and the drive of the feeder – up to 0.8 kW by using calculation and experimental method (*Rutkevych V.S., 2017*). That is why the world's leading hydraulic equipment manufacturers from Parker Hannifin, Bosch Rexroth, Bucher Hydraullics, Hunger Hydraulik, Turbo, Moog and others pay much attention to the "intellectual drives" development and the existing drives redesigning and upgrading (*Kozlov L.G., 2013*). As a rule, the main problem that arises in the independent simultaneous adjustment of several operating elements speeds of the hydraulic drive is the energy losses excessive level and unacceptably low efficiency coefficient of the hydraulic system (*Sidorenko V.S.et al., 2017*).

MATERIALS AND METHODS

The experimental part of the work was carried out at the laboratory stands within the "Machinery and equipment for agricultural production" department at Vinnytsia National Agrarian University. The experimental research was intended to prove the development effectiveness of the hydraulic drives system in the block-portion separator of ensilage fodder and the reasonableness in the choice of the determined drive to ensure the compliance of the two drives operation – the cutting mechanism drive and the П-shaped frame vertical feeding drive. During the theoretical studies of the hydraulic drives system in the block-portion separator, recommendations were made for the choice of its parameters. The parameter values should ensure the absence of unstable (oscillatory) processes and the precise operation of the controlled signal by the slide valve for the flow with increasing torque on the hydraulic motor. The adequacy of the theoretical analysis results to the real performance of the developed system in hydraulic drives of the block-portion separator was verified by studying the system operation on an experimental stand. Mathematical modelling results and experimental studies of the physical model comparison make it possible to prove the results reliability.

Theoretical analysis of the processes that determine the characteristics and the quality of the block-portion separator hydraulic drives system was carried applying the mathematical modelling methods, using the fundamental laws of hydraulics, hydromechanics and theoretical mechanics with the use of differential calculus. A numerical experiment based on the mathematical model was performed applying modern software packages Mathcad and Delphi.

For experimental research we used modern measuring and recording equipment. On the basis of the analogue-digital converter of m-DAQ 12 model a recording equipment set was created. That allowed accumulating and processing an array of measurement results. The experimental data processing was performed by regression analysis methods. Algorithmic computing was conducted using modern packages of applications Mathcad 17, Microsoft Excel 2003, Delphi. To simulate the laboratory installation design and the processes under study we used modern software packages SolidWorks, T-Flex. The reliability of the theoretical statements, scientific and practical results presented in the work, was confirmed experimentally under laboratory conditions.

RESULTS

The objective of the study is to set the block-portion separator for ensilage fodder hydraulic drives parameters which will allow expanding the speed adjustment of operating elements range with variable loading.

The system of hydraulic drives in block-portion separator was elaborated within the department of machines and equipment of agricultural production at Vinnytsia National Agrarian University. The system provides the adaptation of actuating hydraulic motors to the technological surface condition (*Rutkevych V.S., 2017*). The schematic diagram of the hydraulic drive system in the block-portion separator for ensilage fodder is shown in Fig. 1.

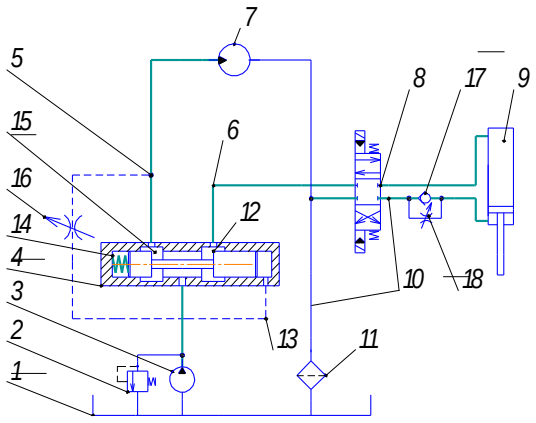

Fig. 1 - Hydraulic circuit in the hydraulic system of a block-portion separator for ensilage fodder

The system operation principle involves adjusting the feeding of the П-shaped frame according to the changes of the cutting effort that affects the cutting mechanism (*Ivanov M.I. et al., 2013*), which results in the energy consumption stabilization of the ensilage fodder block portion separator under the condition of fluctuating parameters that determine the cutting process characteristics.

The ensilage fodder block-portion separator drives system includes a hydraulic tank *1*, a safety valve *2*, a hydraulic pump *3*, a slide valve separator of the flow *4* with a control line *13*, a controlled slide valve *12*, a hydraulic motor *7*, pressure gauges *5,6*, a four-line three-positioned distributor with electrohydraulic control *8*, a hydraulic cylinder *9*, drain hose lines *10*, filter *11*, check valve *17*, chokes *16,18* and a spring *14* (Fig. 1). The suggested use of the flow divider *4* between the actuating hydraulic motor of the cutting mechanism 7 and the hydraulic feeding cylinder *9* (Fig. 1) allows co-ordinating the reduction of its feeding when the load on the cutting mechanism increases, which in turn, leads to a reduction in the cutting force. At the same time, hydraulic oil supply to the hydraulic motor of cutting mechanism drive increases, which also contributes to the reduction of the cutting force and the required power of the cutting mechanism hydraulic drive.

The study of the operation processes of hydraulic drives system in the ensilage fodder block-portion separator was carried out by means of a computational experiment. As a result of solving the problem on the PC, the transient processes that arise during the operation of the hydraulic system in the block-portion separator for ensilage fodder were determined.

The algorithm for determining transients in the specified system takes into account the variable load on the output elements of the actuating hydro-motors, which is actually the cause of the transient processes.

The operation of hydraulic drives system of ensilage fodder block-portion separator starts at zero load on the actuating hydraulic drives, which in general corresponds to the process of moving the П-shaped frame to the surface of the ensilage fodder monolith when the load on the output elements of the actuating hydraulic motors is minimal or absent.

At 400 ms from the operation beginning, occurs the increase in the load on the output elements of the actuating hydro-motors to the value that corresponds to the real value of the loading moment on the hydro-motor shaft M_{gm}=100 Nm and the force $F_{cutting}$ = 1200 N on the hydraulic cylinder rod. In further study of the process of hydraulic drives system operation the moment from the forces of cutting silage monolith and the effort to overcome the resistance strength when feeding the П-shaped frame corresponded to the value determined experimentally in the study of the block-portion fodder separating process from the silage monolith.

Fig. 2 shows the calculating transient processes (as a result of a numerical experiment) in the hydraulic drive system of the block-portion separator caused by the change of the loading on the drive hydraulic motors actuating segments.

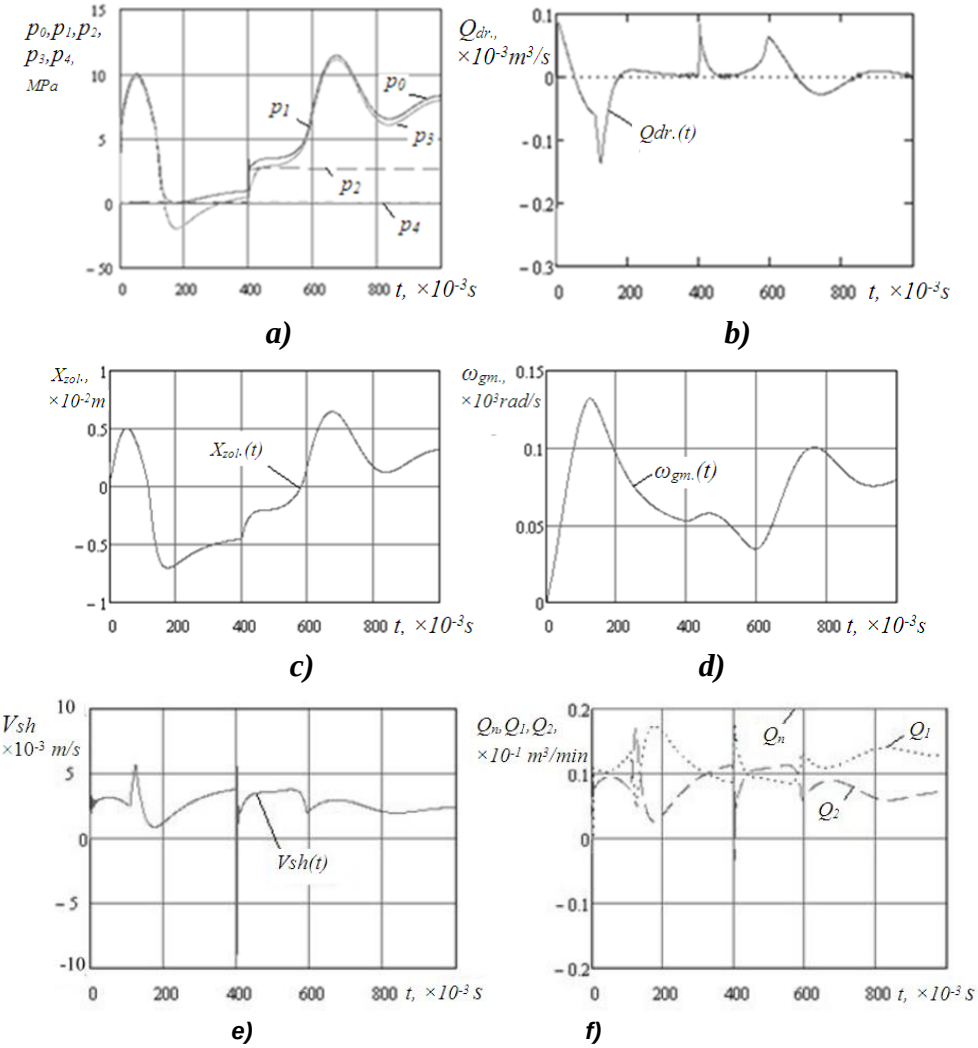

Fig. 2 - Transitional process in the hydraulic drive system of the block-portion separator at initial parameters values

a) change of pressure in the housings of the hydro-system; b) the flow of oil through the throttle; c) the displacement of the slide valve of the flow separator; d) the angular speed of the hydraulic motor shaft; e) the speed of the hydraulic cylinder supply; f) the flow of liquid consumed by the hydraulic motor (Q_1) and the hydraulic cylinder (Q_2).

The transient processes shown in Fig. 2 were calculated at the following initial values of the hydraulic system parameters in the block-portion separator: the volume supply of the pump $Q_n = 2.38 \cdot 10^{-4}$ m³/s, which corresponds to the volumetric supply of a gear pump in the НШ-10 type with the power of the pump drive at five kW; the working edges width of the separator slide valve for the flow is

a=1mm; the initial working windows opening value in the slide valve of the flow separator l_1=6 mm, l_2=2 mm; flow rate of the hydraulic oil through throttle openings is μ=0.62; nominal pressure in the hydraulic system p_0=10.0 MPa; hydraulic oil density ρ=850 kg/m^3; the coefficient of the housing compliance of the hydraulic drive system, filled with the hydraulic oil is K=0.6·10^{-9} m^2/N, the diameter of the separator flow nozzle slide valve d_{zol}=25 mm; the moment of inertia in the rotating parts, which are connected to the shaft of the hydraulic motor I=100 kg·m^2; the mass of the ensilage fodder separator moving parts m_{mp}=45 kg is reduced to the Π-shaped frame; the coefficient of viscous friction β=2.5·10^3 N·s; the diameter of the actuating hydraulic cylinder supplying the Π-shaped frame D_z=63 mm; the volume of hydro-line that connects the actuating hydrostatic motors with a flow separator W_1= W_2= W_4= 100 cm^3; the volume of the hydro-line connecting the throttle with the torsion housing of the flow separator W_3=25 cm^3; the value of the flow separator slide valve displacement to the left of the stop b_1=1 mm; the value of the flow separator slide valve displacement to the right of the stop b_2=2 mm; stiffness of the spring installed in the interstitial housing of the flow separator slide valve C_{pr}=0.5 N/mm.

Fig. 2 shows the block-portion separator parameters change – the oil flow, the displacement of the flow slide valve, the angular speed of the hydraulic motor and the speed of the hydraulic cylinder rod which occur during the transition process that is caused by changes in the loads on the actuating hydraulic drives. The change in the rotation speed of the hydraulic motor shaft and the Π-shaped frame feeding speed arose as a result of the flow slide valve displacement at 3 mm to the opening of the first working window connecting the pump with the hydraulic motor and reducing the opening of the second working window, respectively, the oil in the corresponding housings of the hydraulic motor and the hydraulic cylinder (Fig. 2, f). The oil volume supply Q_1, consumed by the hydraulic motor increases from 0.088×10^{-1} m^3/min to 0.136×10^{-1} m^3/min which corresponds to the increase in the rate of cutting of silage monolith by 57 %. At the same time, oil supply Q_2, consumed by the hydraulic cylinder decreases from 0.113×10^{-1} m^3/min to 0.075×10^{-1} m^3/min which corresponds to the decrease in the feed rate of the Π-shaped frame by 43%.

Therefore, the oscilloscopes shown in Fig. 2 indicate that the proposed system of hydraulic drives for the block-portion separator works in a steady mode while providing a wide range in speed control of actuators. It allows stabilizing the cutting forces while changing the conditions of cutting and, thus, applying the reserves for reducing the power of the hydraulic drives used.

At the same time, it was found that certain parameters of the hydraulic system have a greater impact on the expansion of the hydraulic system operation adjustment range, which allows identifying rational values of the parameters and increasing responsiveness and efficiency of the proposed ensilage fodder block-portion separator hydraulic drives system.

The objective criterion for the efficiency of adjusting speed of the hydraulic motor shaft according to the change in feeding the hydraulic cylinder rod is the dependence of those parameters on the cutting tool load during the separation of the ensilage fodder bale. Thus, Fig. 2 shows the transition process in the hydraulic drive for the fodder block-portion separator calculated on the condition that the loading moment on the hydraulic motor shaft increases to the value of M_{gm}=100 N·m from the initial zero value. This process corresponds to the process of cutting into the monolith of ensilage fodder. According to the results, the feed of the rod decreases, as the supply of the oil (oil flow rate Q_2) to the hydraulic cylinder decreases. At the same time, the hydraulic motor shaft rotation speed increases, affecting the decrease of the cutting force.

Fig. 3 shows the dependences on the change in the volume flow of the hydraulic oil to the actuating hydraulic motors, that is the cutting mechanism drive hydraulic motor and the Π-shaped frame drive hydraulic cylinder. Q_1 and Q_2 show the dependence on the value of the load moment in the hydraulic motor M_{gm}. In the initial state, without loading on the drives of the operating elements in the cutting mechanism, the flow rate from the pumping station is evenly distributed between the hydraulic motors Q_1 = Q_2=0.10 ×10^1 m^3/min (Graph 1). Increasing the loading at the moment of cutting on a hydraulic motor shaft according to the predetermined algorithm for the operation of the hydraulic system leads to an increase in the flow (flow rate) Q_1 to the hydraulic motor of the cutting mechanism drive (Graph 2) and to the reduced supply of the oil Q_2 to the cylinder of the Π-shaped frame drive (Graph 3). So, with the increase of the loading moment to the value M_{gm}=50 N·m, the oil flow Q_1 at the inlet of the hydraulic motor of the cutting mechanism increases from 0.10×10^{-1} m^3/min in the initial state to 0.115×10^1 m^3/min, i.e. increases by 15%. Accordingly, there is a decrease in the oil flow rate Q_2 at the inlet of the hydraulic cylinder of the Π-shaped frame. If there is an increase of loading on the hydraulic motor to M_{gm}=50 N·m, the flow rate Q_2 decreases accordingly to 0.085×10^{-1} m^3/min, i.e. decreases by 15%. In case of further increase of the loading moment to M_{gm}=100 N·m, the flow rate Q_1 increases to 0.13×10^{-1} m^3/min, that is, the growth of flow rate is 30% of the initial value.

In this case, the flow rate of the oil Q_2 decreases to 0.07×10^{-1} m³/min which means a 30% decrease in the Q_2 rate and, accordingly, a decrease in the feed speed of the П-shaped frame that unloads cutting mechanism and provides the total power of the drives at the level which does not exceed 5 kW.

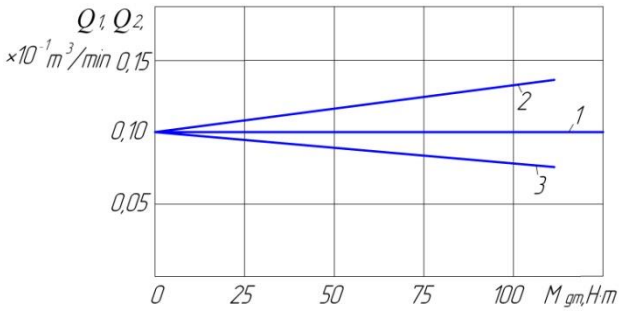

Fig. 3 - The influence of the cutting mechanism drive hydraulic motor load moment on the change of the oil flow Q_1 at the input of the hydraulic motor and Q_2 at the input of the hydraulic cylinder

1- flow rates Q_1 and Q_2 without loading, 2 - dependence of the flow rate Q_1 on the loading moment M_{gm}, 3 - dependence of the flow rate Q_2 on the loading moment M_{gm}

Further increase in the loading moment on the hydraulic motor of the cutting mechanism drive at the value M_{gm}=150 N·m increases the pressure in the injection line to a value exceeding the value of the pressure in setting the safety valve, which is 16 MPa. In this case, the periodic opening of the safety valve leads to the self-sustained wave process, which is unacceptable in terms of the agricultural machine performance. In this case, other hydraulic drives system parameters of the ensilage fodder block-portion separator were of initial values.

Fig. 4 presents the dependence graphs of the oil volume flow change (flow rates) to the actuating hydraulic motors – the hydraulic motor drive of the cutting mechanism and the hydraulic cylinder drive of the П-shaped frame; the dependence of Q_1 and Q_2 on the surface f_{dr} of the throttle, through which the treated housing of the flow slide valve is connected with hydraulic line of the oil supply to the hydraulic motor. Fig. 4a shows the dependencies of the indicated flow rates on the throttle area, identified at different operating modes of the actuating hydraulic motors with and without loading.

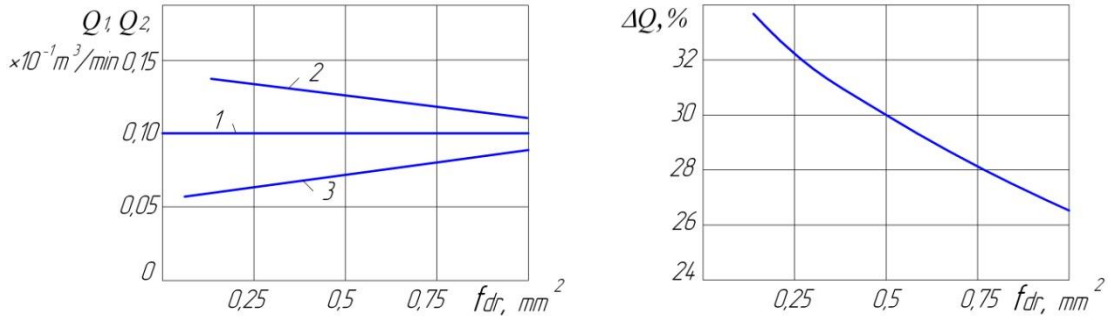

a) ***b)***

Fig. 4 - Assessment of the influence of the throttle $f_{др}$ flow section area size on the change in the oil flow rate at the hydraulic motor Q_1 inlet and the hydraulic cylinder Q_2 inlet

a) dependence of the flow rate Q_1 and Q_2 on the size of the area of the throttle f_{dr} (1 – the values of the flow rates Q_1 and Q_2 without loading, 2 - dependence of the flow rate Q_1 on the area of the throttle with loading, 3 - dependence of the flow rate Q_2 on the area of the throttle with loading), b) relative change in the flow rates Q_1 and Q_2 in case of changing the size of the throttle area f_{dr}.

Dependence 1 corresponds to the flow rate Q_1 and Q_2 in the process of the hydraulic drives system operation without loading. In fact, changing the size of the throttle surface does not affect the balance of the specified flow rates and their value, in this range of change of the throttle area, remains unchanged Q_1=Q_2=0.10×10^{-1} m³/min. At the simultaneous feeding on the shaft of the hydraulic motor the loading moment M_{gm}=100 N·m and on the hydraulic cylinder rod with the force F_{rez}=1200 N, which occurs at 400th millisecond (0.4 s), there is a predicted change in oil flow rates because of the pressure of the block-portion separator hydraulic system.

The flow rate Q_1 with the value of the throttle area f_{dr}=1 mm^2 increases to Q_1=0.127×10^1 m^3/min. (Graph 2), and the flow rate Q_2 decreases to Q_2=0.073×10^{-1}m^3/min. (Graph 3). With further decreasing the throttle area to the value f_{dr}=0.15 mm^2, there is an increase in the difference between the rates Q_1 and Q_2. The flow rate Q_1 increases to a value of Q_1=0.134×10^{-1} m^3/min, that is, increases in accordance with the original value by 33.6%, and the flow rate Q_2 decreases to Q_2=0.066 ×10^{-1} m^3/min (the decreases is 33.6%), namely, it becomes almost twice lower than the rate Q_1. The speed of the output parts of the hydraulic motors varies accordingly, which should reduce the cutting force and the torque on the hydraulic motor shaft. The responsiveness of the hydraulic drive system to the changes of the loading on the operating elements allows adjusting the loading on the cutting mechanism at a wider range. This is also facilitated by the range expansion of adjusting the feeding speed in the Π-shaped frame.

Fig. 5 presents the graphs of the dependence of the volume feeds variation (rates) on the actuating hydraulic motors, particularly the cutting mechanism drive hydraulic motor and the Π-shaped frame drive hydraulic cylinder; dependence of Q_1 and Q_2 on the width ***a*** of the slide valve operating edges.

The graphs of dependencies are plotted on the conditions that the parameters of the hydraulic system in the block-portion separator correspond to the initial values, and the value of the loading moment at the 400th ms of the hydraulic motor of the cutting mechanism drive is M_{gm}=100 N·m.

According to the graphs (Fig. 5) that show reducing the width of the flow slide valve edges considerably extends the range of feeding adjustments of Q_1 and Q_2. If at the initial value of the width of the flow slide valve edges ***a***=1mm at the loading moment on the hydraulic motor of the cutting mechanism, the flow rate at the input of the hydraulic motor increases to Q_1=0.13×10^{-1} m^3/min, and at the cylinder inlet in the drive of the Π-shaped frame decreases to 0.07×10^1 m^3/min, then, with reducing the width of the operating edge of the slide valve to the value of ***a***=0.5mm, the flow rate Q_1 increases to Q_1=0.16×10^{-1} m^3/min (Graph 2), and the flow rate Q_1 decreases to Q_2=0.04×10^{-1} m^3/min (Graph 3). As a result, the range of adjustment of the oil flow rates increases, which goes to the actuating hydraulic motors hydraulic drive system of the block-portion separator. As a result the responsiveness of the drives to the loading considerably expands. The accuracy in the analysis of the control corresponding signals of the hydraulic drive system operating mode improves.

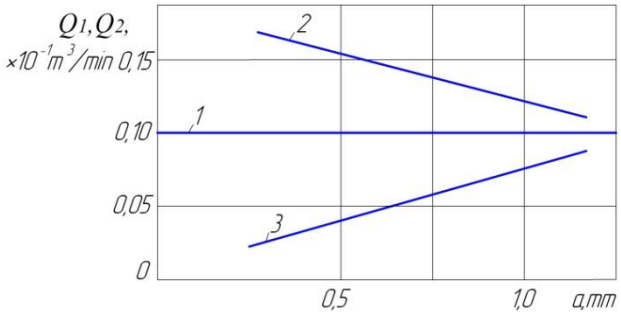

Fig. 5 - Influence of the width a of the flow separator slide valve edge on the oil flow rate change at the hydraulic motor Q_1 inlet and at the hydraulic cylinder Q_2 inlet

1- the value of flow rates Q_1 and Q_2 without loading, 2 - dependence of the flow rate Q_1 on the width of the slide valve edge of the flow separator under loading, 3 - dependence of the flow rate Q_2 on the width of the slide valve edge of the flow separator under loading.

The analysis of the influence of other block-portion separator hydraulic system parameters on the width of the volume control range of the flow rates in the hydraulic lines that provide the oil flow rate by the cutting mechanism drive hydraulic motor and the Π-shaped frame drive hydraulic cylinder showed that the change in these parameters values in a wide range does not significantly affect the expanding speed adjustment range of the hydraulic motor and the hydraulic cylinder. At the same time, in this case there are unstable modes of operation of the hydraulic system and, as a result, it loses efficiency.

As a result of the study, it was found that by changing the operating widths of the separator slide valve in the direction of reduction, there is a significant increase in the responsiveness of the hydraulic drive system in the block-portion separator to the changes in the loading on the cutting tool. As a result, the adjustment range of the hydraulic cylinder feeding of the Π-shaped frame, which increases the efficiency of stabilizing the separation process from the monolith of block-portion for ensilage fodder with a minimum power of the hydraulic drive system, is substantially expanded.

CONCLUSIONS

The results of the mathematical modelling prove the principle possibility to provide the given algorithm for the operation of the block-portion separator hydraulic drive system in the process of the proposed system in hydraulic drives, which must provide the speed control of the actuating hydro-motors in this hydraulic system in accordance with the load of the cutting mechanism. So, with increasing the load of the cutting mechanism, the supply of the hydraulic cylinder of the П-shaped frame decreases at the same time as the proportional increase in the rotation speed of the drive hydro-motor in the cutting mechanism.

The studies of the mathematical model showed the possibility to adjust the range of changes in the hydraulic motor speed and the feeding of the rod by the appropriate choice of rational values for a number of parameters of the hydraulic system in the block-portion separator. In the largest degree, the increase of the adjustment range is possible by reducing the width of the operating edges of the separator slide valve to the value a=0.5 mm, and the area of the throttle adjustment to the value f_{dr}=1 mm^2. The specified values of the parameters correspond to stable operating modes of the hydraulic system in the block-portion separator. Changing the values of other parameters of the hydraulic system in the block-portion separator does not cause a noticeable expansion of the speed adjustment range of the system in hydraulic drives of the block-portion separator.

REFERENCES

[1] Andrenko P.N., Lurye Z. Ya., (2016), Trends in development of fluid power drive, *Industrial hydraulics and pneumatics (Промислова гідравліка і пневматика)*, №2 (52), pp. 3–14, Ukraine;

[2] Galukhin N.A., (2014), Research on the influence of pump flow saturation on the flow sharing efficiency coefficient, *Industrial hydraulics and pneumatics*, №1(43), pp.55–63, Ukraine;

[3] Ivanov M.I., Hrytsun A.V., Podolyanyn I.M., Rutkevych V.S., (2010), Dependence of the cutting efforts on physical and mechanical features of ensilage fodders (Залежність зусиль різання від фізико-механічних властивостей консервованих кормів), *Vibrations in technical devices and technologies (Вібрації в техніці та технологіях)*, №4 (60), pp. 106–110, Ukraine;

[4] Ivanov N., Shargorodskiy S., Rutkevych V.,(2013), Mathematical model of the hydraulic drive of ensilage fodder block-batch separator (Математическая модель гидропривода блочно-порционного отделителя консервированных кормов), *MOTROL*, №5, pp.83–91, Ukraine;

[5] Ivanov M.I., Pereyaslavskyi O.M., Rutkevych V.S., Zinev M.V., Sharyi A.I., (2013), *Hydraulic drive of a block-batch separator of ensilage fodder (Гідравлічний привод блочно-порційного відокремлювача консервованих кормів)*, Patent № 80958, UA;

[6] Rutkevych V.S., (2017), Adaptive hydraulic drive of ensilage fodder block-batch separator (Адаптивний гідравлічний привод блочно-порційного відокремлювача консервованого корму), *Machines, power production, transport of agro-industrial complex (Техніка, енергетика, транспорт АПК)*, №4(99), pp. 108-113, Ukraine;

[7] Kozlov L.G. (2013), Reducing power losses in the hydraulic system of a mobile operating machine (Зменшення втрат потужності в гідросистемі мобільної робочої машини), *Bulletin KhNU (Вісник ХНУ)*, № 4, pp. 24-30, Ukraine;

[8] Privalov F.I., (2017), Fodder production development strategy until 2020 (Стратегия развития кормопроизводства до 2020 года), *Farming and plant protection (Земледелие и защита растений),* № 1, pp. 15-21, Ukraine;

[9] Sidorenko V.S., Grischenko V.I., Rakulenko S.V., Poleshkin M.S., (2017), Adaptive hydraulic drive with volumetric flow control of the technological machine (Адаптивный гидропривод с объемным регулированием подачи инструмента технологической машины), *Bulletin of Don State Technical University (Вестник Донского государственного технического университета)*, № 2, pp. 88-98, Ukraine;

[10] Shylo I.N., Tolochko N.K., Romanyuk N.N., Nukeshev S.O., (2016), *Intellectual technologies in agro-industrial complex (Интеллектуальные технологии в агропромышленном комплексе)*. Minsk: BSATU, 336 pp.

EVALUATION OF IMPACT SYSTEMS NOISE LEVEL IN GRAIN PRODUCTION
/
ОЦЕНКА УРОВНЯ ШУМА УДАРНЫХ СИСТЕМ В ЗЕРНОПРОИЗВОДСТВЕ

Prof. Dr. Eng.Sc. Rodimtsev S.A., Prof. Dr. Eng.Sc. Kuznetsov Y.A.,
Prof. Dr. Eng.Sc.Kolomeichenko A.V., Assoc. Prof., PhD Eng. Sc. Goncharenko V.V.,
Senior Lecturer Patrin E.I., PhD. Phil. Sc., Assoc. Prof. Mikhaylova Y.L.
Orel State Agrarian University named after N.V. Parakhin / Russia
Tel: +79208289219; E-mail: kentury@rambler.ru

Keywords: *threshing and separating device, noise conditions, industrial disease, acoustic properties*

ABSTRACT

Threshing of grain mass in the threshing and separating devices is one of the most «noisy» operations. The main noise sources of a working thresher are the processes of impact interaction of grain with the threshing device cover. Based on the simulation of dynamic and acoustic processes, a formula for calculating the noise level generated by the dynamic contact of free grain with the details of the thresher design, which allows planning of the organizational and technical measures to reduce noise at workplaces, was obtained.

РЕЗЮМЕ

Обмолот хлебной массы в молотильно-сепарирующих устройствах является одной из наиболее «шумных» операций. Основными источниками шума работающей молотилки являются процессы ударного взаимодействия зерна с кожухом молотильного устройства. На основе моделирования динамико-акустических процессов получена формула для расчета уровня шума, создаваемого динамическим контактом свободного зерна с деталями конструкции молотилки, позволяющая спланировать организационно-технические мероприятия по снижению шума на рабочих местах.

INTRODUCTION

One of the most common harmful factors, the physiological effect of which causes damage to the acoustic apparatus and derangements in the central nervous system of a human being is noise. So, in the structure of industrial diseases, due to the impact of physical factors of the labour process, sensorineural hearing loss prevails and it represents about 55.9% of the number of all diseases. According to the same source, sensory neural hearing loss is at the level of 11.2% *(Pogonysheva I.A. et al, 2015; Zewdie Retta and Kic Pavel, 2017; Guida H.L. et al, 2010).* In the eyes of a number of researchers, this pathology in relation to various «noise» occupations can reach 70-77% *(Lie A. et al, 2016; Marlene E.B. et al, 2016)*. In *(Ilkaeva E.N. et al, 2008)* it is noted that working in an acoustic environment with a sound pressure level of 85.2 dB SPL, disorders of the nervous system and cardiovascular diseases are more common than of those who work at a sound pressure level of 42.5 dB SPL, on average, by 5% and 30% respectively.

Among the main occupational risks associated with industrial diseases, noise is ranked second after back pain *(Pogonysheva I.A. et al, 2015; Ilkaeva E.N. et al, 2008)*. In agricultural production, the share of noise, ultrasound air and infra sound, in the total amount of harmful and dangerous factors affecting workers, is more than 9.3% and is prevalent among the working environment factors *(Lie A. et al, 2016; Ilkaeva E.N. et al, 2008; Lashgari M. and Maleki A., 2015)*. Thus, industrial noise remains one of the main problems of work safety in agriculture.

The process of grain mass threshing in the threshing and separating devices (TSD) is one of the most «noisy» among the operations used in agriculture *(Li Y.M. and Sun P., 2014; Calvo A. et al, 2016; Rodimtsev S.A. et al, 2016)*. The equivalent sound level of an operating TSD of a combine harvester can reach 156 dB or more; stationary sheaf thresher used in the processes of selection and primary seed production is not less than 110 dB. At the same time, the maximum permissible sound level and the equivalent sound level for the workplaces of agricultural machines and equipment service personnel is 80 dB *(Li Y.M. and Sun P., 2014; Calvo A. et al, 2016; Jahanbakhshi A. et al, 2016; Rodimcev S.A. et al, 2014)*.

The analysis of the noise impact on the operator (fig. 1) *(Rodimtsev S.A. et al, 2016)*, using the example of the laboratory head thresher WINTERSTEIGER LD 180, showed that the main sources of noise with the maximum impact level are a working engine, moving structural elements (mainly mechanical energy transfer devices) and impact noise caused by the multiple interaction of grain with working bodies and the threshing device cover. The share of the latter in the overall structure of the acoustic impact is rather large and it even exceeds the noise of the electric motor, as well as the noise caused by dynamic processes in the kinematic pairs of the thresher drive.

It can be assumed that the main factors determining the noise level from the impact of free grain interaction with the details of the thresher construction are the impact speed, inertial parameters, state and properties of vegetable origin materials and construction details.

In this regard, the development of measures to reduce the level of noise at workplaces to acceptable values is relevant. The theoretical underpinning of interaction of the grain material with the structural elements of the process equipment is of particular interest.

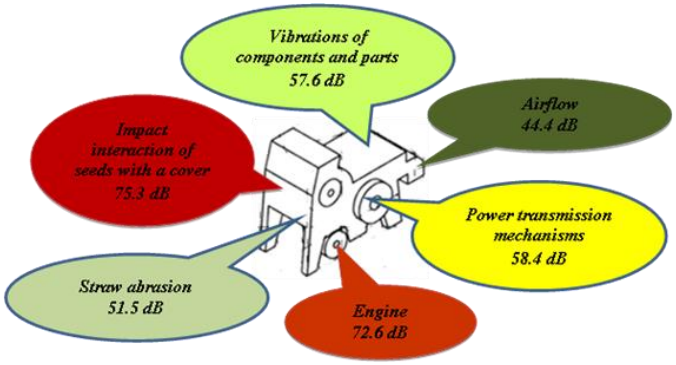

Fig. 1 - Sources of noise of the laboratory thresher «WINTERSTEIGER LD 180»

MATERIALS AND METHODS

The study of noise level influence on workers was carried out using the example of head thresher MK-1M (Russia). This thresher is used in the seed-breeding process for threshing individual heads and bunches of grain, leguminous plants and other crops with the release of light impurities. The main technical features of the thresher are given in table 1.

Table 1

Technical features of the thresher MK-1M

Features	Value
Productivity, ears per hour/h	320
Installed engine capacity, kW	0.25
Rotation frequency, min^{-1}: - **Drum** - **Ventilator**	 1000;1300;1600 3400
Drum diameter, mm	194
Quantity of renewal concaves, pcs.	3
Size of the concaves units, mm	6×32; 4×25; 3×20
Dimensional specifications, mm	570×330×485
Mass, kg	21.3

To study the dependence of the noise level on the distance outdoors an individual technique was developed.

The research on the noise impact of the head thrasher was carried out applying the orientative method for open platforms absolutely excluding any kind of barriers and reflection of sound waves. Regarding the noise source, eight axes were identified (fig. 2), in the direction of which measurements were made. Each axis was divided into ten points, in step size of one meter. The height from the floor level at each point was chosen to be 1560 mm, which roughly corresponds to the ordinate of the position of the adult's auditory analyzer, according to anthropometric indicators used in ergonomics.

The measurements were carried out at steady working state of the thresher. For threshing, prepared bunches of winter wheat «Moskovskaya 39» (Russia) were used. The drum rotation frequency was 1300 min^{-1}.

To compile a noise map and organize the empirical data into homogeneous groups, the cluster analysis method was used.

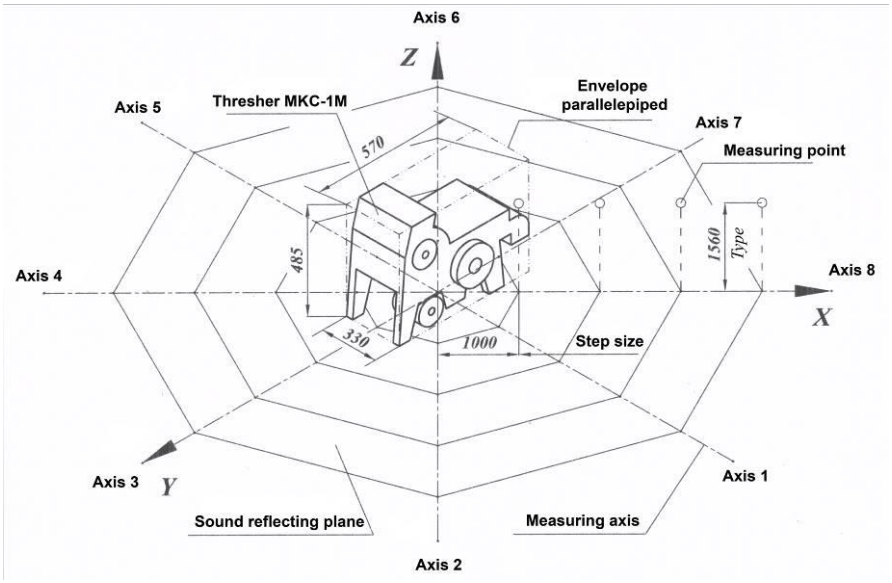

Fig. 2 - Measurement scheme

To convert natural values into coded units, a linear scaling index formula was used:

$$Index = \frac{x - x_{\min}}{x_{\max} - x_{\min}}, \quad (1)$$

where: x – the first value in the row;

x_{max}, x_{min} – the maximum and minimum values of the indicators.

To distribute the obtained values over the intervals of the numerical series, the number of groups was determined using the Sturges formula *(Boldin A.P. and Maksimov V.A., 2012)*:

$$n = 1 + 3.32 \lg N \quad (2)$$

where: N - the number of measurements.

The interval step size was determined by the formula:

$$h = \frac{x_{\max} - x_{\min}}{n} \quad (3)$$

where: x_{max}, x_{min} - the maximum and minimum values of the indicators;

n - the number of groups.

A special windproof device was developed to reduce the impact of wind gusts on the measurement accuracy as well as to capture sound waves in the direction of the measurement axis (fig. 3). It allows getting a sharply directional microphone sound level meter when assessing the noise level in extreme situations, under the conditions of ambient noise and to remote sound sources. The use of a windproof device reduces the influence of external noise by 75-80%.

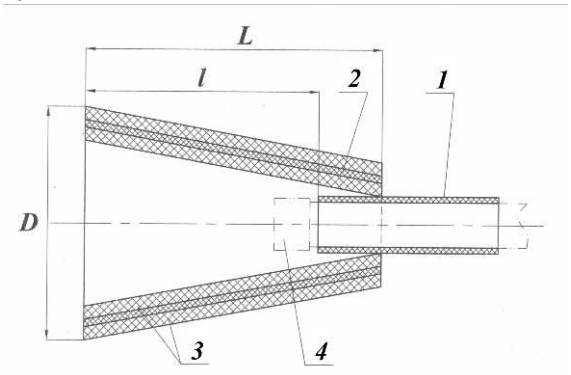

Fig. 3 - Windproof device

1 - carrier sleeve; 2 - protective housing; 3 – sound insulator (felt); 4 - sensor (microphone)

The simulation of the shock processes in the threshing chamber was carried out by dropping the same number of grains from a certain height onto the cantilever plate. The number of discarded grains in each portion was 10 pieces for each of the crops. The time interval between dropping grains was 1 sec. This was enough to fix the level of sound impact from each grain in one portion and calculate the arithmetic average value. For the experiment, a special device was used, allowing fixing height of dropping grains relative to the cantilever plate (Fig. 4). The studies were conducted with a technical method in the laboratory, with a free sound field above the sound reflecting plane.

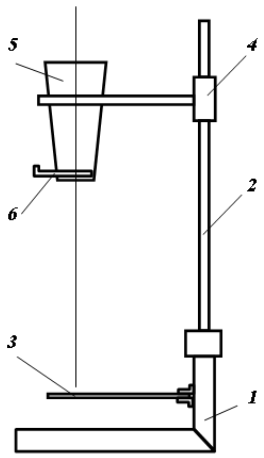

Fig. 4 - Scheme of the device for the study of shock-acoustic effect
1 - base; 2 - stand; 3 - replaceable cantilever plate; 4 - bracket; 5 – entry guide; 6 - valve

The following grain crops were used for the research: beans, peas, wheat, different in weight, shape and geometric dimensions. The mass of grains varied from 1.7 to 3.3%, relative to the arithmetic mean value (table 2).

Table 2

Grain weight of crops used in the research

Crop	Average weight of grain, g	Mean square deviation, σ, g	Coefficient of variation, K_v, %
Peas	0.12	0.002	1.7
Wheat	0.03	0.01	3.3
Beans	0.41	0.01	2.4

To assess the dependence of the noise level by the interaction of grains with the surfaces of various materials rubber, metal and wooden plates were used (table 3). The height of grain dropping was taken to be equal to 10, 310, 610, 910 and 1210 mm.

Table 3

Characteristics of the impact surfaces

Plate material	Dimensional specifications, mm: length width height	Modulus of elasticity Young, $E \times 10^{-5}$, MPa*
Tree (pine tree)	200×70×10	10000
Rubber (heat-and-acid-alkali resistant)	200×70×10	5
Steel (St.3)	200×70×10	200000

* Reference data *(Doronin F.A., 2018)*

The noise level was measured with a noise-level meter Octave-101 AM (Russia) *(Ivanov N.I., 2008)*. A microphone preamplifier «KMM 400» with a microphone capsule «VMK-205» was used. The microphone was mounted at the distance of 1.2 m from the noise source and at the height of 1 m.

RESULTS

During thresher operation, it was found that the greatest sound pressure of the equivalent noise level reaches 81.2 dBA, while the acceptable value of the equivalent sound levels for workplaces in laboratories with noisy equipment, according to *(GOST 12.1.003-2014)*, is not more than 75 dBA.

With increasing distance from the noise source, the sound pressure level decreases. As it can be seen from table 4, the maximum values of the noise level can correspond to both the measurement points closest to the noise source and immediately following them. This is explained both by the location in relation to the measuring point of the main sources of sound vibrations (motor, drive, fan) and the vibrating parts of the thresher that create additional noise. In addition, a slight decrease in the sound pressure level near the thresher may be caused by the shielding effect of the construction protruding elements.

Table 4

Values of the equivalent sound levels in control points during work of the threshing machine MKS-1M, dBA

Distance from the noise source	Measurement axis number							
	1	**2**	**3**	**4**	**5**	**6**	**7**	**8**
1	81.2	75.9	76.2	76.8	76.8	75.5	76.5	76.2
2	77.5	75.7	75.4	74.6	75.4	76	77.1	77.1
3	75.7	75.8	74.6	73.4	74.3	75.5	74.7	75.3
4	75.7	74.3	71.7	73.2	72.8	75.1	73.8	73
5	76.3	76.1	74	74.8	74.4	74.2	75.8	75.7
6	76	74.5	73.5	73.7	73.8	74.4	74.7	74.6
7	77.1	75.8	74.8	75	75.1	75.7	76	75.9
8	76	73.7	72.7	72.9	73	73.6	73.9	73.8
9	74	71.4	70.4	70.6	70.7	71.3	71.6	71.5
10	73	71	70	70.2	70.3	70.9	71.2	71.1

Experimental studies conducted under laboratory conditions concerned a comparative assessment of the equivalent sound level caused by the impact interaction of agricultural crop grains with a fixed surface.

It was established that regardless of the impact surface material, the level of the impact sound increased with increasing height of grain dropping (fig. 5). In general, for all the crops with an increase in the height of grain dropping from 10 to 1210 mm, the sound level rose 1.3 times.

We'll denote the dependence of the sound level on the height of grain dropping, as:

$$y = f(x) \tag{4}$$

where: y - the sound level, [dB];

x - height of grain dropping, [m].

Then, the nature of the change of dependence (4) obeys the law

$$y = a \cdot \ln(x) + b \tag{5}$$

where: a, b - free coefficients depending on the conditions of the experiment.

The mass of grains also influences significantly the sound level. It was established that the sound level when striking a metal surface of wheat grains, with an average weight of 0.03 g was 40.5; 57.3 and 63.8 dB, with a drop height of 10, 610 and 1210 mm, respectively. Beans, having an average mass of 0.41 g, when dropped from a similar height, generated a sound of 56.8; 68.1 and 72.4 dB, which, in general, was 1.2 times higher than the sound level from the impact interaction with the metal console of wheat grains.

The sound level when dropping peas onto a metal surface was 50.8; 64.1 and 68.3 dB with an average grain mass of 0.12 g and dropping height of 10; 610 and 1210 mm.

The sound level from the impact interaction of grains with the contact surface depends significantly on the material properties of this surface, which is confirmed by a number of studies *(Li Y.M. and Sun P., 2014; Jahanbakhshi A. et al, 2016; Krolczyk J.B. et al, 2014)*. From the graphs shown in figure 6 it can be seen that the most «noisy» is the process of contacting grains with a metal surface.

Thus, the sound level when dropping grains from the height 1210 mm was 63.8; 68.3 and 72.4 dB - for wheat, peas and beans, respectively. When dropping the grains of these crops on a wooden surface, the sound level was 58.4; 62.5 and 68.3 dB. The sound level at the contact of the grains with the surface of the rubber was minimal. So, for grains of wheat, peas and beans, when dropped from a height of 1210 mm, the

sound level values were 45.8; 48.6 and 54.2 dB. These values are 1.31 times lower than the corresponding sound level indicators for the same crops when dropped on a metal surface.

As it can be seen, the acoustic parameters of the process of grain interaction with an impact surface are determined by the dynamic characteristics of this process.

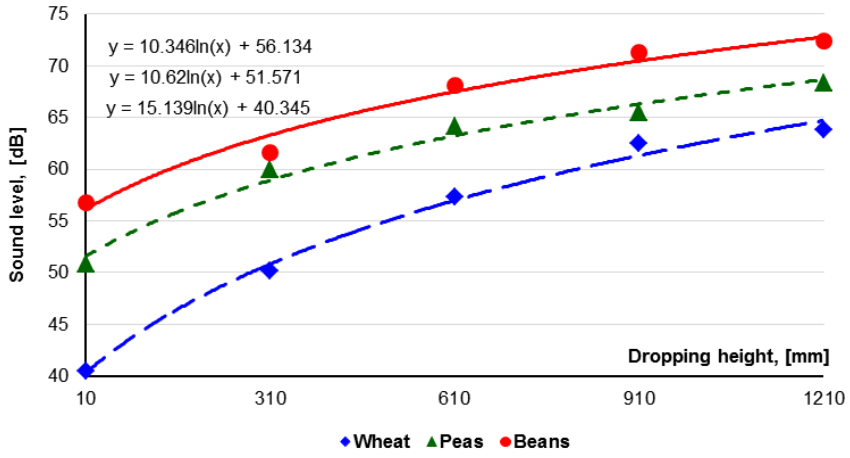

a)

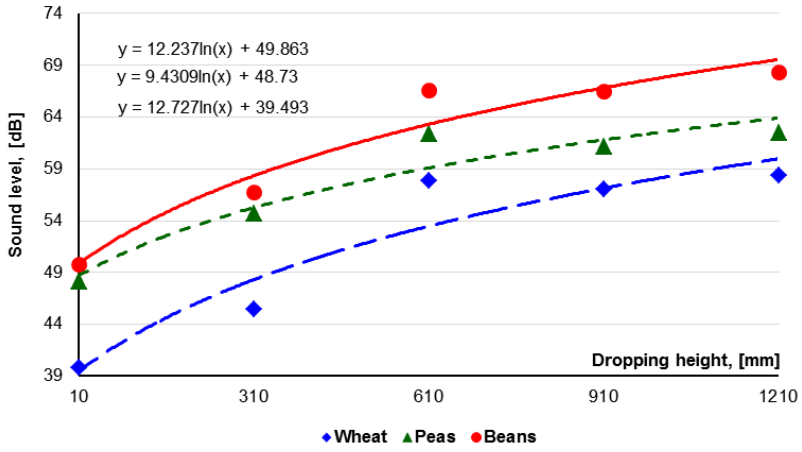

b)

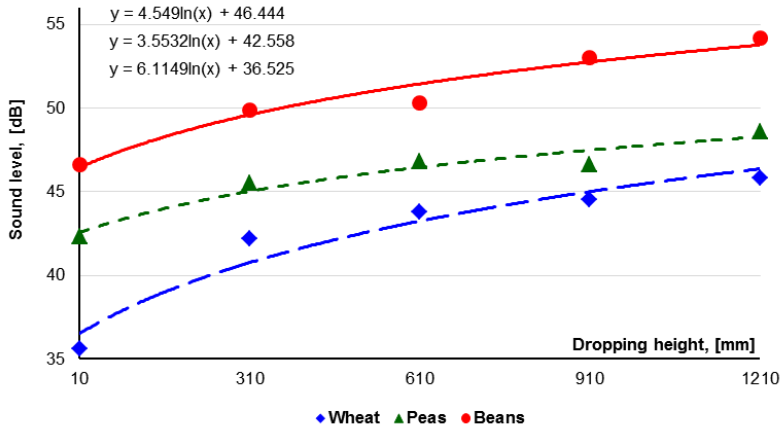

c)

Fig. 5 - Dependence of the sound level by the impact on the height of the grain dropping on the steel (a), wooden (b) and rubber (c) cantilever surfaces

For the mathematical description of the relation of acoustic and dynamic parameters of grain collision process with a fixed surface, a decimal logarithm of the ratio of two values of the force value, expressed in decibels, was used *(Ivanov N.I., 2008)*:

$$D = 20 \cdot \lg \frac{F_1}{F_0}, \text{ [dB]} \quad (6)$$

where: F_0; F_1 - the threshold (fiducial) and current values of the force value, respectively, [N].

Based on the law of similarity used in calculating the acoustic characteristics of sources *(GOST 12.2.028*), we proposed an expression for the analytical description of the dependence of the sound level LH created in the full-scale process of the "seed-casing system" impact interaction on the impact interaction force *(Rodimtsev S.A. et al, 2014)*:

$$L_H = L_M + (\psi \cdot \log \frac{F_H}{F_M}) \quad (7)$$

where: L_M - the sound level during impact interaction in the model process, [dB];

ψ - coefficient taking into account the conditions of natural dynamic process;

F_H, F_M - the force of the grain impact interaction with the contact surface, with the full-scale and model processes, [N].

In the formula (7), the numerical values of the force F_M and the corresponding sound level value L_M are determined in a specially conducted model experiment. The coefficient ψ depends on the similarity level of the natural process to the model process and can take numerical values from 0 to 1. In the research carried out by the authors, ψ, as a rule, took a value from 0.8 to 1.0.

Assuming that the undeformed state of the impacted bodies is not fully restored and the grain gravity centre after impact and before the impact moves at different speeds, we have the classic case of a central, not quite elastic impact. For a theoretical description of the quantity F_H entering the formula (7), we use the principle on the change of the momentum of a material point in the integral form, applied to instantaneous forces *(Doronin F.A., 2018)*:

$$mV_2 - mV_1 = \sum_{k=1}^{n} S(F_k) \quad (8)$$

or, in projection on the axis *n*:

$$mV_{2n} - mV_{1n} = \sum_{k=1}^{n} S_n(F_k) \quad (9)$$

where: *m* - body mass;

V - body speed;

S - body impulse;

F - force.

The right side of the equation (9) is the vector sum of impulses of instantaneous forces. In application to the problem in question, the only instantaneous force is the reaction of the plate F_n. Therefore, we can write:

$$\sum_{k=1}^{n} S_n(F_k) = \int_{t}^{t+\tau} F_n dt \quad (10)$$

where: *t* - the beginning of the impact;

τ - duration of the impact.

Based on the generalized mean-value theorem *(Yakovlev G.N. et al, 2009)*, if the functions *f(x)* and *g(x)* are integrable on the interval [a, b], and the function f(x) is continuous, then on this interval there will be such an «average» point $\bar{x}$, that

$$\int_a^b f(x)g(x)dx = f(\bar{x})\int_a^b g(x)dx \quad (11)$$

Using the property (11) to the right side of the equation (10), we write:

$$\int_{t}^{t+\tau} F_n dt = F_{ncp} \int_{t}^{t+\tau} dt \tag{12}$$

Here, F_{ncp} - average value of the plate reaction.

As

$$F_{ncp} \int_{t}^{t+\tau} dt = F_{ncp} \cdot t + F_{ncp} \cdot \tau - F_{ncp} \cdot t \tag{13}$$

then, the expression (12) will have the following form:

$$\int_{t}^{t+\tau} F_n dt = F_{ncp} \cdot \tau \tag{14}$$

Using (9) and taking into account the found equalities (10) and (14), after simple transformations, we obtain the initial dependence for determining the impact reaction of the plate.

$$F_{ncp} = \frac{m(V_{2n} - V_{1n})}{\tau} \tag{15}$$

The free movement of a body without an initial velocity ($V_0 = 0$) will be described by the following equations:

$$V_n = gt \text{ , [m s}^{-1}\text{]} \tag{16}$$

$$h = \frac{gt^2}{2} \text{ , [m]} \tag{17}$$

where: g - the gravitational acceleration, [m/s^2];

h - drop height, [m].

It follows from the formula (17):

$$t = \sqrt{\frac{2h}{g}} \text{ , [s]} \tag{18}$$

Therefore, the speed of the body V_1, at the beginning of the impact will be:

$$V_1 = \sqrt{2gh_1} \text{ , [m/s]} \tag{19}$$

After not a quite elastic impact on the plate, the grain begins to rise upward at a speed of V_2. At the highest lifting point h_2, the grain speed is zero. Consequently:

$$V_2 = \sqrt{2gh_2} \text{ , [m/s]} \tag{20}$$

To find the unknown value h_2, we use coefficient of restitution k.

The relation between the velocity modules of a grain gravity center at the beginning and at the end of the impact is the following:

$$V_1 = k \cdot V_2 \text{ , [m/s]} \tag{21}$$

where: k - coefficient of restitution of the body by the impact.

Substituting the values of V_1 and V_2 from (19) and (20) into the formula (21), we obtain:

$$k = \sqrt{\frac{h_2}{h_1}} \tag{22}$$

Then the unknown value of h_2 will be:

$$h_2 = k^2 h_1 \text{, [m]} \tag{23}$$

Using the found speeds of the body before and after the impact onto the surface of the plate, the formula (15) will be finally the following:

$$F_{ncp} = \frac{m \cdot \sqrt{2gh_1} \cdot (k-1)}{\tau}, \text{ [N]} \quad (24)$$

where: m - weight of one grain of an agricultural crop, [kg];
g - gravitational acceleration, [m/s^2];
h_1 - height of grain dropping, [m];
k - coefficient of restitution of grains by the impact;
τ - duration of impact, [s].

Based on the research data of a number of authors *(Shkodkin VN et al, 2017; Glebov LA, 1979)* the duration τ of the active interaction of a single grain with a steel working surface can be from (1.2-2.5)×10^{-5} to (4-5)×10^{-5} s.

Using (24) and taking $F_н$=$F_{пср}$, the formula (7) will be finally written in the form:

$$L_H = L_M + \left(\psi \cdot \log \frac{m \cdot \sqrt{2gh_1}(k-1)}{F_M \cdot \tau} \right), \text{ [dB]} \quad (25)$$

CONCLUSIONS

When the parameters of the impact force of the grains with the contact surface F_M and sound level L_M, were found in the model experiment, as well as the corresponding reference values, the obtained analytical dependence (25) allows us to calculate the expected sound level L_H when the grains interact with structural elements of various process equipment in the field.

The obtained results will allow planning organizational and technical measures to reduce the sound impact on a person at workplaces, in areas of processing crop products, depending on the conditions of the technological operations, as well as physical and mechanical properties and state of the processing object.

REFERENCES

[1] Boldin A.P., Maksimov V.A., (2012), Fundamentals of Scientific Research (Основы научных исследований), *Publishing Centre "Academy" (Издательский центр «Академия»)*, ISBN 978-5-7695-7171-8, 336 p., Moscow / Russia;

[2] Calvo A., Deboli R., Preti C., (2016), Operators' exposure to noise and vibration in the grass cut tasks: comparison between private and public yards, *Agricultural Engineering International: GIGR Journal*, Vol. 18, Issue 1, ISSN:1682-1130, pp.213-225, Beijing / China;

[3] Doronin F.A., (2018), Theoretical Mechanics, *LLC «Publishing House Lan» (ООО «Издательство Лань»)*, ISBN 978-5-8114-2585-3, 480 p., St. Petersburg / Russia;

[4] GOST (ГОСТ) 12.2.028. Occupational safety standards system. General-purpose ventilators. Methods of noise characteristics determination (Система стандартов безопасности труда. Вентиляторы общего назначения. Методы определения шумовых характеристик), 26 p., Moscow / Russia;

[5] Guida H.L., Morini R.G., Cardoso A.C.V., (2010), Audiological evaluation in workers exposed to noise and pesticide, *Brazilian Journal of Otorhinolaryngology (impr.)*, Vol.76, Issue 4, ISSN: 1808-8694, pp. 423-427, São Paulo / SP Brazil;

[6] Ilkaeva E.N., Volgareva A.D., Shaikhlislamova E.R., (2008), Assessment of the probability of the formation of hearing organs professional disorders by the workers exposed to industrial noise (Оценка вероятности формирования профессиональных нарушений органа слуха у работников, подвергающихся воздействию производственного шума), *Occupational medicine and industrial ecology (Медицина труда и промышленная экология)*. Issue number 9, ISSN: 1026-9428, pp.27-30, Moscow / Russia;

[7] Ivanov N.I., (2008), Engineering Acoustics. Theory and practice of noise control (Инженерная акустика. Теория и практика борьбы с шумом). *Publishing Group «Logos» (Издательская группа «Логос»)*, ISBN 978-5-98704-286-0, 423p., Moscow / Russia;

[8] Jahanbakhshi A., Ghamari B., Heidabeigi K., (2016), Effect of engine rotation speed and gear ratio on the acoustic emission of John Deere 1055I combine harvester, *Agricultural Engineering International: GIGR Journal*, Vol. 18, Issue 3, ISSN:1682-1130, pp.106-112, Beijing / China;

[9] Krolczyk J. B., Legutko S., Krolczyk G.M., (2014), Dynamic balancing of the threshing drum in combine harvesters-the process, Sources of imbalance and negative impact of mechanical vibrations, *Applied Mechanics and Materials*, vol. 69, Issue 3, ISSN: 1660-9336, pp.424–429, Zürich / Switzerland;

[10] Lashgari M., Maleki A., (2015), Comparison of sound pressure level of noise emitted by two conventional combines in Iran and assessment of related factors*, Iran Occupational Health Journal*, Issue number 12 (4), ISSN:1735-5133, pp.11-20, Tehran / Iran;

[11] Li Y.M., Sun P., (2014), Advanced Materials Research, Vols. 971-973, ISSN: 1662-8985, pp.324-328, Zürich / Switzerland;

[12] Lie A., Skogstad M., Johannessen H.A., Tynes T., Mehlum I.S., Nordby K.C., Engdahl B., Tambs K., (2016), Occupational noise exposure and hearing: a systematic review, *International archives of occupational and environmental health*, Vol.89, Issue 3, ISSN: 0340-0131, pp.351–372, Berlin / Germany;

[13] Marlene E.B., Andre L.L.S., Carlos A.C.P. de O., (2016), Analysis of the Hearing and Tinnitus in Workers Exposed to Occupational Noise, *International Journal of Tinnitus Journal*, Vol.20, Issue 2, ISSN: 0946-5448, pp.88-92, London / United Kingdom;

[14] Pogonysheva I.A., Pogonyshev D.A., Krylova A.A., (2015), The influence of noise on the psycho physiological parameters and the working capacity of the human body (Влияние шума на психофизиологические параметры и работоспособность организма человека). *Bulletin of the NVSU (Bulletin of the NVSU)*, Issue number 1, ISSN: 2311-1402, pp.87-93, Nizhnevartovsk / Russia;

[15] Rodimtsev S.A., Kuznetsov Yu..A., Goncharenko V., Patrin E., Kalashnikova LV, (2016), Investigation of noise parameters at head thresher operation and noise map development in free sound field, *Poljoprivredna tehnika*, ISSN:0554-5587, Vol. 41, Issue 4, pp.21-26, Belgrade / Serbia;

[16] Rodimtsev S.A., Patrin E.I., Kuznetsov Yu.A., Goncharenko V.V., Denisyev S.A., (2016) Investigation of noise parameters during the operation of a head thresher and development of a noise map in a free sound field (Исследование параметров шума при работе колосовой молотилки и разработка шумовой карты в свободном звуковом поле), *Machinery and equipment for the countryside (Техника и оборудование для села)*, Issue number 2 (225), ISSN: 2072-9642, pp. 20-24, Pravdinskiy / Russia;

[17] Rodimcev S.A., Timokhin O.V., Patrin E.I., Shapenkova A.A., Kulakova E.V., (2014), Improvement of labour conditions as a factor of agro-industrial complex development under the WTO conditions, *Bulletin of the Orel state agrarian university (Вестник Орловского государственного аграрного университета)*, Issue number 6(51), ISSN:1990-3618, pp. 87-95, Orel / Russia;

[18] Yakovlev G.N., Martynov N.N. Lukankin G.L., Shadrin G.A., (2009), Higher Mathematics (Высшая математика), *OJSC «Publishing House «Higher School» (ОАО «Издательство «Высшая школа»)*, ISBN 978-5-06-006144-4, 584 p., Moscow / Russia;

[19] Zewdie Retta, Kic Pavel, (2017), Noise pollutants in agricultural machinery drivers cabin, *16th International Scientific Conference «Engineering For Rural Development»*, Vol.16, ISSN 1691-5976, pp.425-430, Jelgava / Latvia;

[20] GOST (ГОСТ) R 12.1.003-2014. Occupational safety standards system. Noise. General safety requirements (Система стандартов безопасности труда. Шум. Общие требования безопасности), 13 p., Moscow / Russia;

[21] Shkondin V.N., Semenikhin A.M., Gurinenko L.A., (2017), Two-stage feed grain chopper (Двухступенчатый измельчитель кормового зерна), *Machinery and equipment for the countryside (Техника и оборудование для села)*, Issue number 1 (235), ISSN: 2072-9642, pp. 24-28, Pravdinskiy / Russia;

[22] Glebov L.A., (1979), The speed of impact of the complete grinding of grain in the production of animal feed (Скорость удара полного измельчения зерна при производстве комбикормов), *Flour-grain elevator and feed mill industry (Мукомольно-элеваторная и комбикормовая промышленность)*, Issue number 8, pp. 29-30, Moscow / Russia.

MATHEMATICAL MODELING AND NUMERICAL SIMULATION OF THE DRYING PROCESS OF SEEDS IN A PILOT PLANT

/

MODELAREA MATEMATICĂ ȘI SIMULAREA NUMERICĂ A PROCESULUI DE USCARE A SEMINȚELOR ÎNTR-O INSTALAȚIE PILOT

Assist. Ph.D. Eng. Arsenoaia V.N.*[1)], Ph.D. Eng. Vlăduț V.[2)], Prof. Ph.D. Eng. Țenu I.[1)], Ph.D. Eng. Voicea I.[2)], Lecturer Ph.D. Eng. Moiceanu G.[3)], Assoc. Prof. Ph.D. Eng. Cârlescu P. M.[1)]

[1)] University of Agricultural Sciences and Veterinary Medicine Iași / Romania

[2)]INMA Bucharest / Romania; [3)] Politehnica University of Bucharest / Romania

Tel: 0722508104; E-mail: vlad_arsenoaia@yahoo.com

Keywords: *mathematical modeling, numerical simulation, seed drying*

ABSTRACT

The artificial drying of grain seeds is widespread to ensure that they are preserved, as reducing the water content allows products to be stored for long periods of time without the need for complex storage facilities. The proposed drying installation is a low-capacity pilot one, which can change and monitor in real time a series of important parameters of the drying process. By means of the CFD simulation the construction of the cylindrical box and of the deflectors was optimized. This leads to reaching a uniform drying and to reducing the energy consumptions.

REZUMAT

Uscarea artificială a semințelor de cereale este larg răspândită pentru a asigura condiții de conservare a acestora, deoarece prin reducerea conținutului de apă se permite păstrarea produselor pe perioade lungi de timp fără a fi nevoie de instalații complexe de depozitare. Instalația de uscare propusă este una pilot, de capacitate mică, prin care se pot modifica și monitoriza în timp real o serie de parametri importanți ai procesului de uscare. Cu ajutorul simulării CFD a fost optimizată construcția casetei cilindrice și a deflectoarelor. Aceasta conduce la obținerea unei uniformități a uscării și la o reducere a consumurilor energetice.

INTRODUCTION

The experimental laboratory investigations of cereal seed drying precede the CFD simulation process, because the simulation involves the use of physical parameters (porosity, volume mass, specific heat, conductivity) for both the product and the air used as drying agent.

By CFD simulation of the cereal seed drying process, it is possible to graphically visualize the evolution of temperature and humidity fields at any point in the product layer. Calibration of the simulation is performed by comparison with the experimentally obtained data, measured in the median area of each product layer.

The degree of precision of the mathematical model, obtained by CFD simulation, is given by the differences in temperature and humidity of grain seeds determined under laboratory conditions. An important weight in these differences is also the simplifying assumptions on which the mathematical model of convective drying was built, considering that this process is complex by the large number of physical parameters, as dependent variables, which vary simultaneously over short time.

The use of the Computational Fluid Dynamics technology has made it possible to design and simulate a drying baffled unit for agricultural seed, to achieve uniform seed temperature distribution and to reduce the energy demand.

Franks believes that mathematical models are based on three rules: for physical processes, there must be a number of independent equations equal to the number of unknown sizes; from any equation, the solution leads to the value of an unknown; equations are systematized so that each one obtains one of the most significant quantities (*Franks, 1961*).

Many mathematical models have been developed to simulate the heat and the moisture transfer in the aerated bulk stored grains. A lot of them were obtained at low temperatures and low seed humidity.

Iguaz et al. (2004) developed a model for the storage of rough rice during periods with aeration. *Andra* (2001) and *Devilla* (2002) simulated the temperature changes in a wheat storage bin, but, without moisture changes.

Chang et al. (1993) and *Sinicio et al.* (1997) also developed a rigorous model to predict the temperature and the moisture content of wheat seeds during storage with aeration.

The aim of this paper is to propose the mathematical model of mass and heat transfer and to simulate the air flow in a cylindrical drying unit with deflectors, using the FLUENT software.

MATERIALS AND METHODS

CFD analyses can provide complex information on the drying phenomenon that cannot be obtained under experimental conditions. Table 1 presents the capability and limits of the experiment and the CFD numerical simulation by comparative analysis.

Table 1

Comparative analysis between experiment and simulation

Elements	Experiment	CFD Numerical Simulation
	Quantitative description of the drying phenomenon using measurements	**Quantitative prediction of the drying phenomenon using mathematical models and CFD simulation programs**
Model scale	normal	real
Number of analyzed problems	limited	unlimited
Conditions of deployment	laboratory	real conditions
Sources of errors	measurements errors	modeling, meshing, implementation

The mathematical model of the convective drying process is based on fluid dynamics, mass balance and energy dynamics theory.

The equations of the mathematical model of the air flow are: the differential equation of continuity, Navier – Stockes equations, mass transfer equation, heat transfer equation and moment transfer equation.

The system of the equations described above is the general mathematical model. This system is solved by numerical procedures, using solving algorithms. Numerical solving by CFD simulation of the equation system in the mathematical model is accomplished by the iterative method using the Gauss-Seidel model.

CFD simulation, based on the proposed mathematical model, involves the following steps:

- numerical meshing of the calculation area by the finite volume method (centered difference approximation) in the pre-processing stage;
- imposing boundary conditions to obtain a determined system of equations, which is done in the pre-processing stage for geometry;
- solving the system of equations in each domain node by the interactive method until obtaining the convergence in the processing stage;
- graphical representation of the solutions obtained at each node in the studied field, for parameters of speed, temperature, humidity and current lines, in the post-processing stage.

During the pre-processing stage are presented the numerical meshing techniques and the limit conditions for obtaining a determined system of equations.

Approximation by meshing is a fundamental concept based on several numerical methods such as finite difference method, finite volume method, finite element method and spectral method.

The numerical discretization of the computation domain in this simulation is done by the finite volume method (centric approximation). Control volume discretization applies to a three-dimensional domain divided into a finite number of adjacent volumes of parallelepipedal shape chosen to contain a single node of the network represented by the coordinates i, j, k and side faces intersecting the lines of the network in points located halfway between two neighbouring nodes (fig. 1).

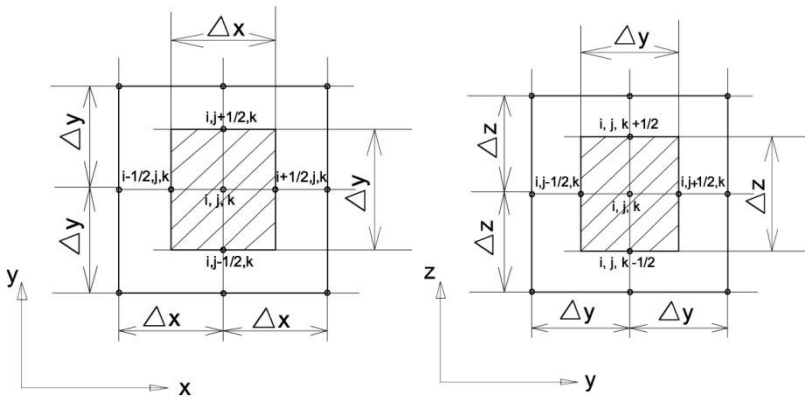

Fig. 1 - Defining the control volume

At the basis of this method are the solutions for the integration of an equation on each volume, by choosing a certain distribution law of *u* (*u* may be a function of temperature, humidity, displacement of a fluid or product) so that it can be evaluated integrally. The meshed form of the equation contains the function values for a group of nodes of the network, adjacent to the central node.

The areas of separation between the adjacent control volumes are in this case discontinuous surfaces. The values of the function *u* on these surfaces are considered equal to the arithmetic mean of the values corresponding to the volumes placed on one side and the other, being represented by the relations:

$$u_{i+\frac{1}{2},j.k} = \frac{u_{i+1,j,k} + u_{i,j,k}}{2} \; ; \; u_{i-\frac{1}{2},j.k} = \frac{u_{i,j,k} + u_{i-1,j,k}}{2} \tag{1}$$

$$u_{i,j+\frac{1}{2}.k} = \frac{u_{i,j+1,k} + u_{i,j,k}}{2} \; ; \; u_{i,j,-\frac{1}{2}.k} = \frac{u_{i,j,k} + u_{i,j-1,k}}{2} \tag{2}$$

$$u_{i,j,k+\frac{1}{2}} = \frac{u_{i,j,k+1} + u_{i,j,k}}{2} \; ; \; u_{i,j,k-\frac{1}{2}.} = \frac{u_{i,j,k} + u_{i,j,k-1}}{2} \tag{3}$$

where: *i*, *j*, *k* as the index represents the natural number.

By integrating the partial derivative equations on the finite control volume V (V=Δx·Δy·Δz), the first and second order integrals appear, which will take a discretised form respecting the values of the function in the neighbouring volumes. The discretized form on the three directions will be:

$$\int_{\Delta V}\left(\frac{\partial u}{\partial x}\right)dxdydz = \left(\frac{u_{i+1,j,k} - u_{i-1,j,k}}{2\Delta x}\right)\Delta V \tag{4}$$

$$\int_{\Delta V}\left(\frac{\partial u}{\partial y}\right)dxdydz = \left(\frac{u_{i,j+1,k} - u_{i,j-1,k}}{2\Delta y}\right)\Delta V \tag{5}$$

$$\int_{\Delta V}\left(\frac{\partial u}{\partial z}\right)dxdydz = \left(\frac{u_{i,j,k+1} - u_{i,j,k-1}}{2\Delta z}\right)\Delta V \tag{6}$$

where: V represents the volume.

The expressions of the integrals of the mixed derivatives can be obtained using the integration of second-order mixed derivatives:

$$\int_{\Delta V}\left(\frac{\partial^2 u}{\partial x \partial y}\right)dxdydz = \frac{u_{i+1,j+1,k} - u_{i+1,j-1,k} + u_{i-1.j-1,k} - u_{i-1,j+1,k}}{4\Delta x \cdot \Delta y} \tag{7}$$

Finite volume discretization involves an analysis of the working range that is volumetric represented by the cylindrical unit. It has the form of a cylinder that has three slots where the cereal seeds are introduced for drying. The hot air enters this cylindrical box through the central region, being guided by cylindrical tubing that connects to the dryer.

The geometry of the three-layer cylindrical unit is shown in fig. 2, and the mesh geometry is shown in fig.3.

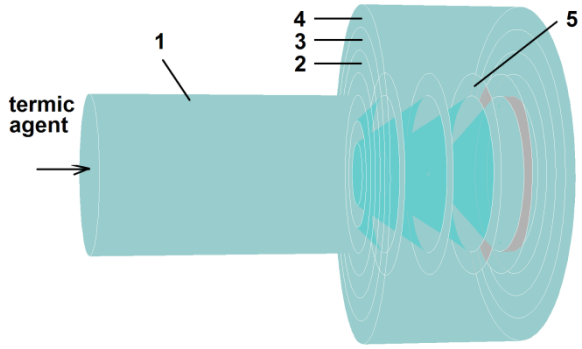

Fig. 2 - Defining the control volume

1 – heat duct, 2 – first seed layer, 3 – second layer, 4 – third layer, 5 – deflectors; thermal agent – heated air.

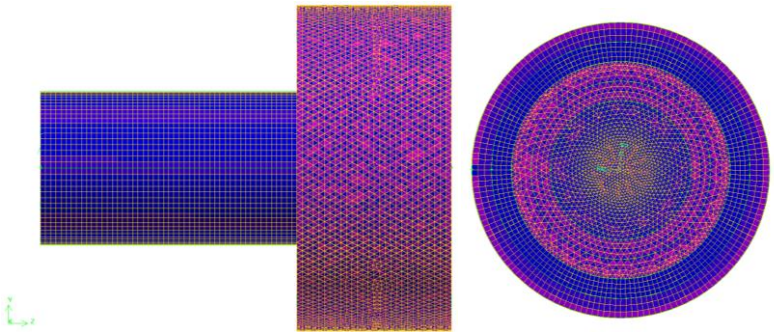

Fig. 3 - Cylindrical box meshing

The cylindrical unit geometry is hybridized. The mesh of the cylindrical introduction of the drying agent is structured, and in the region of the three slots where the seeds are introduced, the mesh is unstructured.

The air inlet and outlet area in the free volume and the four vertical surfaces define the free volume and are shown in table 2.

The processing imposed conditions for the drying agent were:

- for simulation version I – air velocity (2 m/s), inlet surface temperature and adiabatic wall temperature (313 K), air humidity (0.008 kg water vapour / kg dried air), air density (1.225 kg / m^3), exit pressure (0 Pa), specific heat (1011 J / kg K), thermal conductivity (0.0454 W / m K);
- for simulation version II – air velocity (2 m/s), inlet surface temperature and adiabatic wall temperature (343 K), air humidity (0.020 kg water vapour / kg dried air), air density (1.325 kg / m^3), exit pressure (0 Pa), specific heat (1001 J / kg K), thermal conductivity (0.0244 W / m K).

Table 2

Cylindrical unit imposed initial conditions

Cylindrical box areas	Contour conditions
Entry	Speed
Exit	Pressure
Surfaces	Wall
Volume	Fluid

At the discretization of the pressure and other conservation equations, the upwind mesh scheme of the first order was used (Ansys-Fluent-User Guide, 2012). The value of the velocity *u* is transported to the edge of the volume element relative to the local speed direction. A linear (first order) scheme was used to simulate the pressure equation in order to maintain the stability of the final solution. The quadratic scheme is more sensitive to pressure deformations, resulting in instability of the calculation, of the solution for the multiphase flow (air plus humidity) and of the density (of nodes) imposed by the mesh. All the simulations were unstated.

The initial conditions imposed for corn seed processing were: 25% relative humidity, 0.156 kg water vapour/kg dried product absolute humidity, 615 kg/m^3 product density, 1679 J/kg K specific heat, 0.158 W/m K thermal conductivity.

The porosity index was determined experimentally by scanning a determined volume (68.7 cm^3) of 78 corn seeds with a mass of 42.3 grams with a 3D SKYSCAN 1172 micro CT scanner at a resolution of 27.224 μm, resulting a porosity index of 34.5%.

For the stability of the calculation, the following coefficients of sub-relaxation were applied: pressure - 0.3; moment - 0.7; energy - 1. The convergence criteria used for all solution variables was set at 0.001. The total number of iterations for the processing stage was 180. The time step at which the simulation data was retrieved and recorded at the processing stage was 120 seconds.

The flow regime for simulation is tested to obtain a convergent equilibrium state in the evolution of residuals (fig. 4).

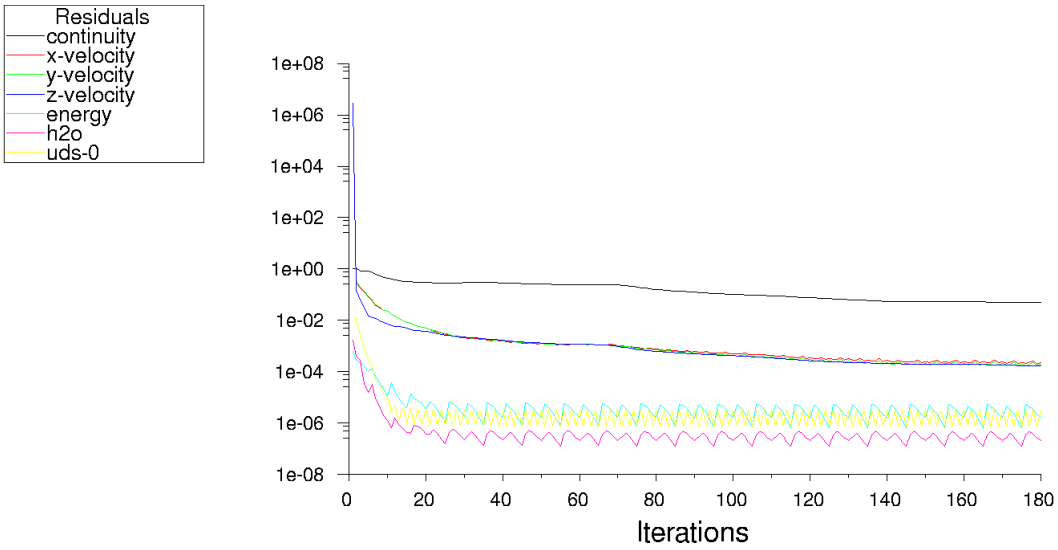

Fig. 4 – Convergence plot of the simulation

Following the mathematical modeling of the drying process, CFD simulations were made in two variants for the three-layer cylindrical unit with corn seeds from the DKC 4751 hybrid.

In the simulation, the residual was imposed at 1e-4 and the graph shows the trend of decreasing the speed on the three directions and the continuity, but the convergence check was also required and it was obtained after 180 iterations.

It can be said that the numerical solution converges when it tends towards the analytical solution, when the network step tends to zero. A numerical solution converges if the values of the variables in the computing domain nodes tend to approach the exact solution. Also, the numerical solution process is considered stable if errors in the discrete solution do not increase so much that the result becomes not real.

The post-processing step aims to present in colours the main parameters of interest in the process of drying the corn seeds. Parameters are rendered for each computational node in the form of temperature, humidity fields, or by showing the flow of air through current lines depending on its velocity and temperature. The post-processing was done for the three layers of corn seed following the distribution of temperature and humidity in the seed layers.

RESULTS

The field of the current lines obtained in the three-layered cylindrical unit has a laminar flow of the drying agent at the unit entrance, and in the region of the baffles, one can see a uniform distribution of the hot air over the entire surface of the corn seeds to be dried. In the simulation version I, with a thermal velocity of 2 m/s and its inlet temperature of 313 K (40°C), a speed increase of up to almost 8 m/s is observed in the deflector region as a result of the reduction of the section and afterwards it reaches uniformly again the value of 2 m/s on the surface of the first seed bed. Passing the three layers of corn seeds, the speed of the current lines drops to 0.3 m/s at the exit of the last layer (fig. 5). The surface temperature of the first seed coat is 313 K (40°C) with a uniform distribution of current lines, and in the seed layers the temperature decreases, yielding heat for drying and lowering to the last layer up to 300 K (27 °C).

In the CFD simulation variant II at an air velocity of 2 m/s and its inlet temperature of 343 K (70°C), the same speed increase in the deflector region is observed as a result of the section reduction, which will be uniformly reached again at 2 m/s on the surface of the first grain seed bed. Passing the three layers of corn seed, the current line speed drops to 0.3 m/s at the exit of the last layer. The distribution of air velocity in the three-layer cylindrical box is preserved as in variant I, with very small variations, as the geometry remains unchanged (fig. 6).

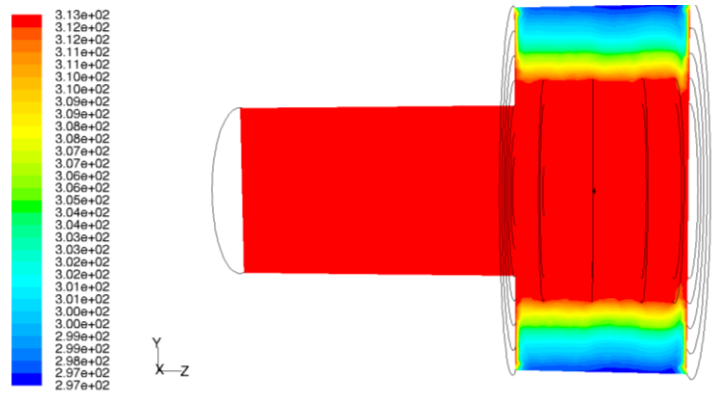

a)

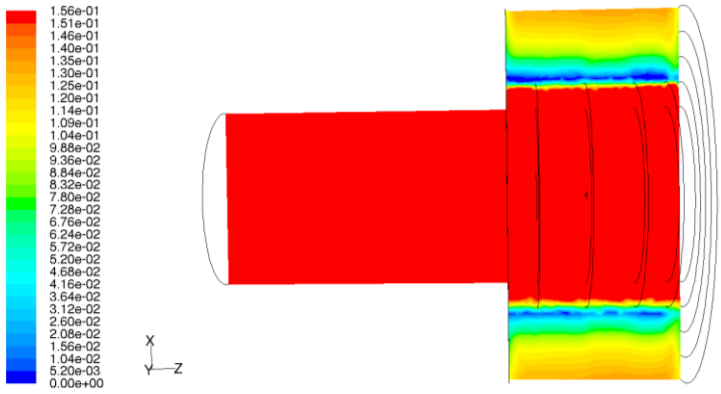

b)

Fig. 5 - The longitudinal section representation of the temperature field (K) and the absolute humidity field (kg water vapors/kg dry product) for the first version (temperature of 313 K = 40°C):
a – temperature; b – absolute humidity.

The temperature at the surface of the first seed bed is 343 K (70°C) with a uniform distribution of the current lines, and in the seed layers, the temperature decreases giving off their heat for drying and lowering to the last layer to 311 K (38°C). As shown in fig. 5 and fig. 6, regardless of the working regime of the drying unit, the same uniformity of the current lines is maintained over the whole surface of the first layer of seeds. In the design phase of the three-layer cylindrical unit, the distance between the baffles and sections was optimized by repeated CFD simulations to achieve this uniformity of spreading of the drying agent at the layers of corn seeds. In order to obtain the seed temperature and humidity parameters CFD simulation was performed at two different temperatures of the hot air.

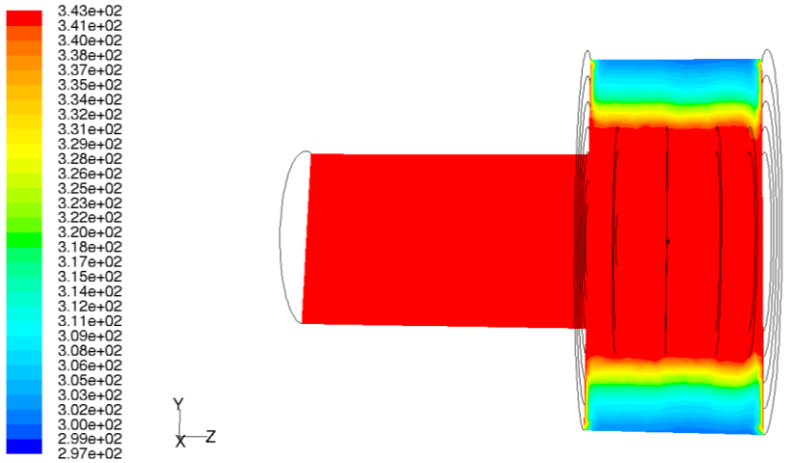

a)

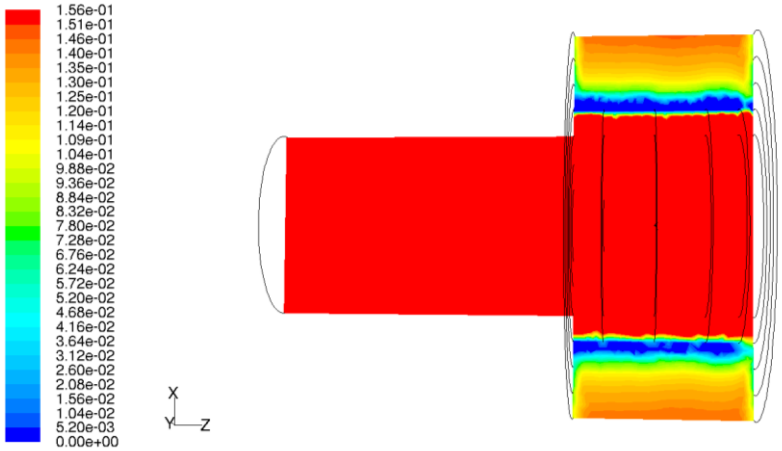

b)

Fig. 6 - The longitudinal section representation of the temperature field (K) and the absolute humidity field (kg water vapors/kg dry product) for the second version (temperature of 343 K = 70°C):
a – temperature; b – absolute humidity.

CONCLUSIONS

After the drying process mathematical modeling, CFD simulations have been made in two variants for the cylindrical box with three corn seeds layers.

The results regarding the distribution of the corn seed humidity, in the three layers of the cylindrical box in the second variant, had medium values that varied from the first to the last layer as it follows: the medium value reached was 11.5% in the first layer, 17% in the second and 21% in the third one.

By means of these CFD simulations calibrated with the experiment, one can make a sufficiently exact model, so that it could be used for other types of seeds too. The main condition is that the entry data introduced in the simulation and obtained experimentally should be as exact as possible. By means of the CFD simulation one can optimize the working process in the cereal seed drying.

Also, by means of the CFD simulation the construction of the cylindrical box and of the deflectors was optimized so that one could obtain a uniform distribution of the air currents and of the temperature fields in the three cereal seed layers. This leads to reaching a uniform drying and to reducing the energy demand.

REFERENCES

[1] Allen T., (2003), Particle size analysis by sieving. *Powder Sampling and Particle Size Determination*, Ed. Elsevier, London/U.K.;

[2] Andra de E.T., (2001), *Simulacao da variacao de temperatura em milho armazenado em silo metalico (Simulation of temperature variation in maize stored in silo – PhD Thesis)*. Tese de doutorado em Engenharia Agricola. Minas Gerais: Imprensa Universitaria, Universidade Federal de Vicosa, Brasil;

[3] Chang C.S., Converse H.H., Steele J.L., (1993), Modeling of temperature of rain during storage with aeration. *Trans. Am. Soc. Agric. Engrs*., 36, 2: 509-519;

[4] Devilla I.A., (2002), *Simulacao de deterioracao de distribuicao de temperatura umidade em uma massa de graos armazenados em silos com aeracao (Simulation of deterioration of temperature distribution moisture in a mass of grains stored in silos with aeration – PhD Thesis)*. Tese de doutorado em Engenharia Agricola. Minas Gerais: Imprensa Universitaria, Universidade Federal de Vicosa, Brasil;

[5] Dieter B., Karl S., (2006), *Heat and mass transfer*. Springer-Verlag, Berlin;

[6] Franks, F.G.E., (1961). *Mathematical Modeling in Chemical Engineering*. John Wiley and Sons. Wiley;

[7] Iguaz A., Arroqui C., Esnoz A., Virseda P., (2004), Modeling and simulation of heat transfer in stored rough rice with aeration. *Biosystems Engineering*, 89, 1: pp.69-77;

[8] Incopera D., Bergman T., (2007), *Fundamentals of heat and mass transfer*, John Wiley and Sons, New York;

[9] Incropera F.P., de Witt D.O., (1990), *Fundamentals of Heat and Mass Transfer*, Wiley;

[10] Jia C. C., Sun D.W., Cao, C.W., (2001), Computer simulation of temperature changes in a wheat storage bin. *J. Stored Prod. Res*., 37: pp.165-167;

[11] Jokiniemi T., Mikkola H., Rossner H., Talgre L., Lauringson E., Hovi M., Ahokas J., (2012), Energy savings in plant production, *Agronomy Research Biosystem Engineering,* Special Issue, 1, pp.85-96;

[12] Macovei V. M., (2000), Thermophysical characteristics collection for biotechnology and food industry (Romanian), *Alma*, Galați/Romania;

[13] Momenzadeh L., Zomorodian A., Mowla D., (2009), Experimental and theoretical investigation of shelled corn drying in a microwave-assisted fluidized bed dryer using Artificial Neural Network, *Food and Bio products processing*, 89, 15-21;

[14] Özahi E., Demir H., (2014), Drying performance analysis of a batch type fluidized bed drying process for corn and unshelled pistachio nut regarding to energetic and exergetic efficiencies, *Measurement*, 60, pp.85-96;

[15] Sinicio R., Muir W.E., Jayas D.S., (1997), Sensitivity analysis of a mathematical model to simulate aeration of wheat stored in Brazil. *Postharvest Biol. Technol*. 11: pp.107-122;

[16] Thorpe G.R., (2007), Heat and moisture transfer in porous hygroscopic media: two contrasting analyses. *Fifth International Conference on Heat Transfer, Fluid Mechanics and Thermodynamics*, Sun City, South Africa;

[17] Thorpe G.R., (2008). The application of computational fluid dynamics codes to simulate heat and moisture transfer in stored grains. *Journal of Stored Products Research* 44: 21-31;

[18] *** *Ansys-Fluent*. User Guide. 2012.

THE INFLUENCE OF BASIC PARAMETERS OF SEPARATING CONVEYOR OPERATION ON GRAIN CLEANING QUALITY

/

ВПЛИВ ОСНОВНИХ ПАРАМЕТРІВ РОБОТИ ТРАНСПОРТЕРА-СЕПАРАТОРА НА ЯКІСТЬ ОЧИЩЕННЯ ЗЕРНА

Prof. Ph.D. Eng. Vasylkovskyi Oleksii[1)], Lect. Ph.D. Eng. Vasylkovska Kateryna[1)], Lect. Ph.D. Eng. Moroz Serhii[1)], Prof. Dr. Eng. Sc. Sviren Mykola[1)], Dr. Agric. Sc. Storozhyk Larysa[2)]

[1)] Central Ukrainian National Technical University / Ukraine;

[2)] Institute of Bioenergy Crops and Sugar Beet National Academy of Agricultural Sciences of Ukraine / Ukraine

Tel: +380667103625; E-mail: vasilkovskakv@ukr.net

Keywords: *separating conveyor, research, sieve, separation fineness, impurities*

ABSTRACT

The rational succession of technological operations of all-purpose grain cleaning machines was substantiated at the Department of Agricultural Engineering at Central Ukrainian National Technical University. The original design of a separating conveyor used in the first stage of the proposed cleaning scheme was created. The experimental separating conveyor allows extracting large impurities before feeding the grain mass to aspiration, reducing the resistance of the system and creating optimal conditions for air cleaning.

The objective of our research was to identify rational parameters and operating modes of the suggested separating conveyor. The objective was achieved by studying the influence of the basic parameters of the conveyor: the inclination angle α, sieve hole diameter d, buckets velocity v, as well as the specific loading of the sieve width unit q_B on one of the most important qualitative indicators which is grain separation fineness. The fineness is characterised by the content of full-value grains in fodder waste.

The experimental device and methodology for laboratory research were developed to identify the most influential factors on the separation fineness. During the research, the matrix of the full factorial experiment of the 2^4 type was implemented. The basic level and intervals of factors variation were chosen based on the analysis of theoretical studies results and experimental research preliminary data.

The obtained regularities confirmed the efficiency of the suggested design and allowed identifying the rational parameters of the separating conveyor to ensure acceptable separation fineness of grain.

РЕЗЮМЕ

На кафедрі сільськогосподарського машинобудування Центральноукраїнського національного технічного університету було обґрунтовано раціональну послідовність технологічних операцій в зерноочисних машинах загального призначення і створено оригінальну конструкцію транспортера-сепаратора, що використовується на першому етапі запропонованої схеми очищення. Дослідний транспортер-сепаратор дозволяє виділити крупні домішки перед подачею зернової маси до аспірації, зменшуючи опір системи і створюючи оптимальні умови для повітряного очищення.

Метою наших досліджень було встановлення раціональних параметрів і режимів роботи запропонованого транспортера-сепаратора. Досягнення поставленої мети здійснювалося шляхом вивчення впливу його основних параметрів: кута нахилу α, діаметра твірних решета d, швидкості переміщення ковшів v, а також питомого завантаження одиниці ширини решета q_B, на один з найбільш важливих якісних показників – чіткість сепарації зерна, що характеризує вміст повноцінного зерна у фуражних відходах.

Для встановлення найбільш впливових факторів на чіткість сепарації було розроблено експериментальну установку і складено методику лабораторних досліджень. В ході проведення досліджень реалізовано матрицю повного факторного експерименту типу 2^4. Основний рівень та інтервали варіювання факторів обрані на основі аналізу результатів теоретичних досліджень та попередніх даних експериментальних досліджень.

Одержані закономірності дозволили підтвердити ефективність запропонованої конструкції і встановити раціональні параметри транспортера-сепаратора для забезпечення допустимої чіткості сепарації зерна.

INTRODUCTION

The market of agricultural machines constantly develops and is updated with new models of machines. The vast majority of the national manufacturers often copy best models of the well-known international brands. A small number of the Ukrainian machine builders develop their own designs, test them and eliminate failings. A smaller number of manufacturers create original designs of machines and mechanisms on the basis of scientific research. However, this category of manufacturers has long-term prospects for creating truly competitive products for the world market.

MATERIALS AND METHODS

Several designs of all-purpose grain-cleaning machines were created at the Department of Agricultural Engineering of Central Ukrainian National Technical University through the conduct of scientific research. One of the main operating elements of each design is a separating conveyor (*Moroz S. M., 2014; Moroz S. M., 2011*) which is installed at the beginning of the technological cycle of the machine and allows the grain to be cleaned from large impurities at the stage of loading.

The experimental device (Fig.1, 2) consists of the frame *1*, to which the housing of the separating conveyor *2* with the drive mechanism is fixed on the joint *10.* The sieve with circular longitudinal baffles *3* and upper (driving) and lower (driven) drums *4* and *5* on bearing spherical supports are fixed to the sides of the housing inside the separating conveyor. The grain comes from hopper *11*, equipped with dispenser *12* and slide gate *13* in the grain pipe *8*. Under the sieve, there is a receiver for grain fraction pass-through 7. The separating conveyor is actuated by the electric motor *14* with the help of a V-belt drive and the six-speed gearbox *15* that provides the change of the buckets velocity v from 0.5 to 2.83 m/s.

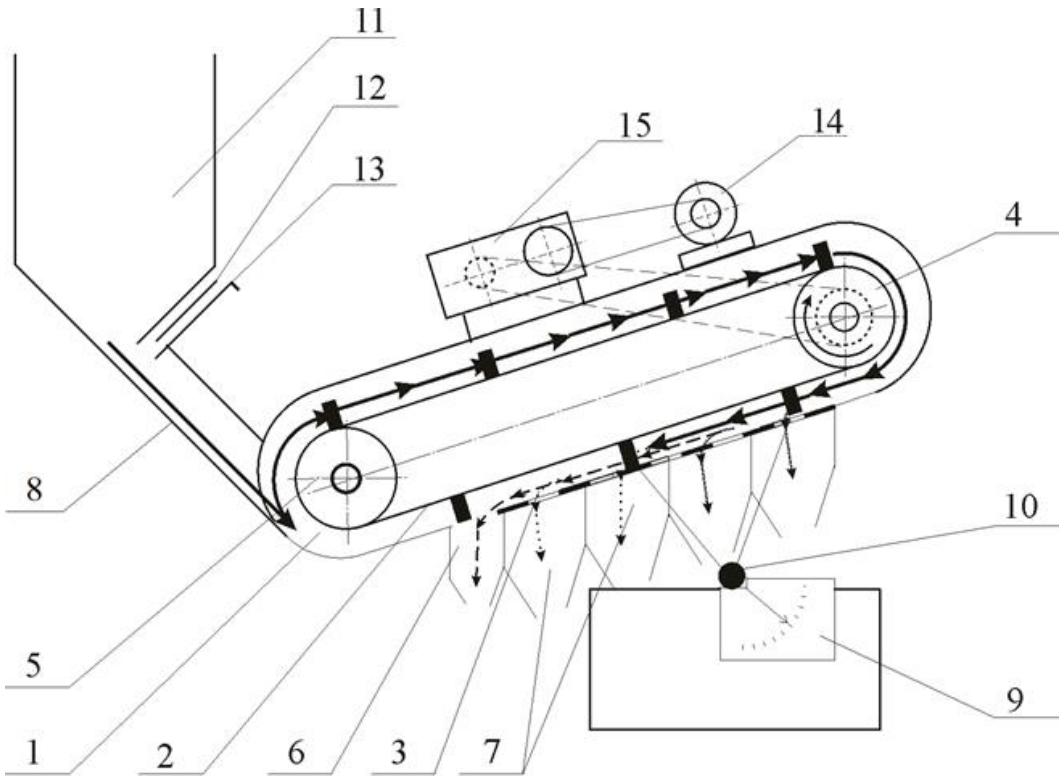

Fig. 1 - Schematic layout of the experimental device

The change of the housing inclination angle α of the separating conveyor relatively to the horizon was carried out by its rotation relatively to the joint *10* with the fixation in the required position. The control and measurement of the conveyor inclination angle relatively to the horizon was carried out using angle gauge *9*.

The sieves with longitudinal baffles of round shape with the diameters of 1.3 and 5 mm (Fig. 3, 4) serve as surfaces for the separation.

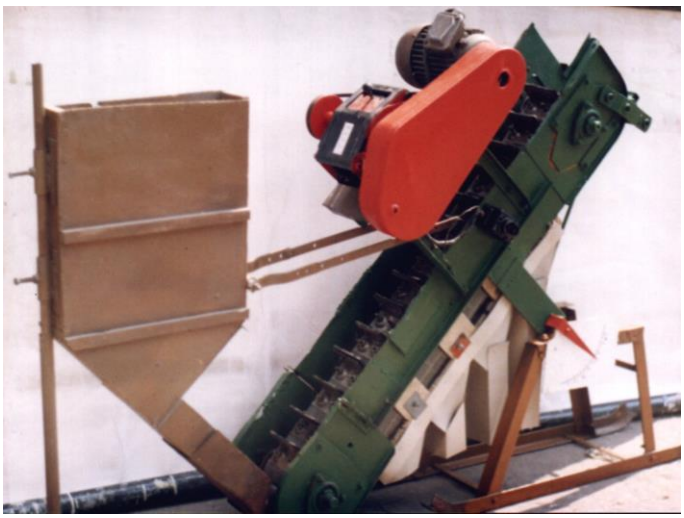

Fig 2 - General view illustration of the experimental device

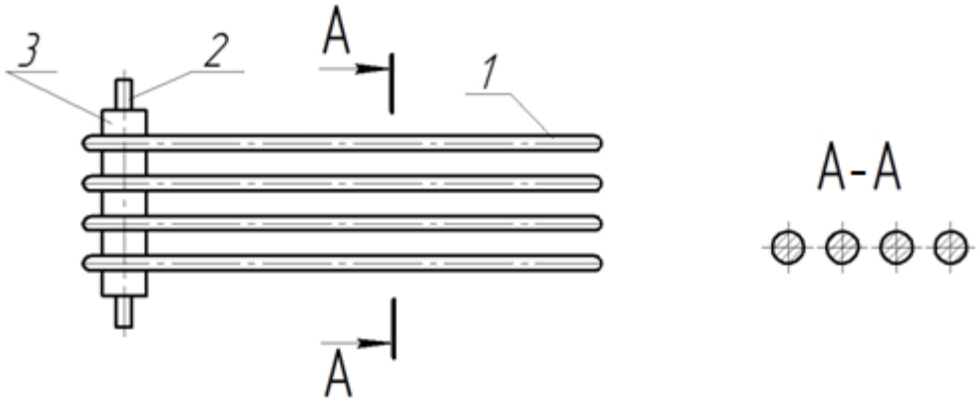

Fig 3 - Schematic view of the sieve

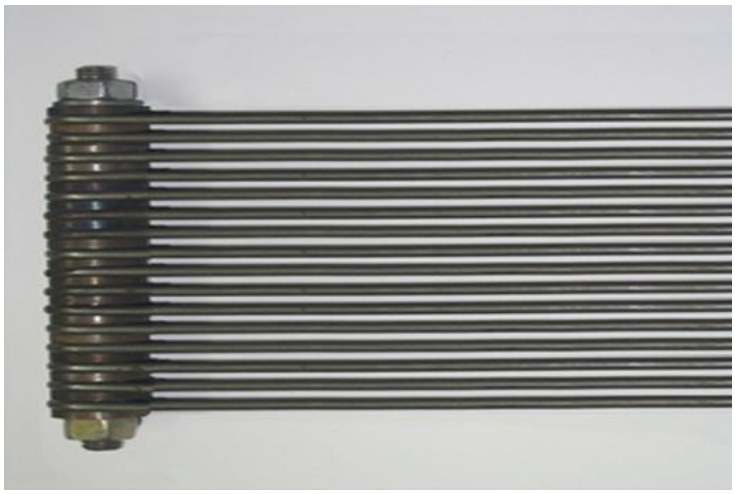

Fig 4 - General view of the sieve

During theoretical and experimental studies, the dependences of the influence of its constructive parameters values and operation modes on the grain separation completeness were established (*Dryncha VM, 2006; Kotov BI, 2017; Kroulik M., 2016; Levdanskiy EI, 2008; Piven M., 2015; Stepanenko S., 2017; Tishchenko L., 2014; Tishchenko L., 2016*). However, the separation fineness, which characterizes the content of the full-value grain in large impurities, has not been studied in details.

The objective of the research is to determine the influence of the design parameters and the operating mode of the suggested separating conveyor on the separation fineness. The research will give

grounds for identifying rational values on conditions that the agro-technical requirements regarding the content of the full-value grain in the fodder waste are provided.

Separation fineness *Y* – the relative content of full-value grain in the waste was determined by sieving and weighing. To identify the influence of the investigated factors on the separation fineness and to determine the direction of motion to the part of the response surface, where the conditions of the process were optimal, the matrix 2^4 was applied (*Borovikov V.P., 2003*). Independent variables, variation intervals, and planning matrix are presented in Table 1.

Table 1

Planning of the experiment while studying the separation process

Investigated factor	Angle of inclination of a sieve, α, deg.	Diameter of the cross-cut baffle of the sieve, d, mm	Speed of scrapers, v, m/c	Specific productivity, q_B, kg/(m×c)		
Basic level	**30**	**3**	**1**	**11**		
Variation interval	**±10**	**±2**	**±0,5**	**±3**		
Code designation	x_1	x_2	x_3	x_4	Y_u	S_u^2
Experiment 1	+	+	–	+	16.10	0.012
Experiment 2	+	–	+	–	3.91	0.012
Experiment 3	–	+	–	–	1.03	0.0031
Experiment 4	+	–	+	+	8.95	0.0052
Experiment 5	–	–	–	+	4.13	0.0031
Experiment 6	+	+	+	–	6.05	0.0043
Experiment 7	–	–	+	+	6.08	0.011
Experiment 8	+	+	+	+	20.10	0.280
Experiment 9	–	–	–	–	0.15	0.0019
Experiment 10	–	–	+	–	1.50	0.0013
Experiment 11	–	+	+	+	11.2	0.317
Experiment 12	–	+	+	–	4.90	0.210
Experiment 13	+	+	–	–	4.10	0.0077
Experiment 14	–	+	–	+	7.80	0.0067
Experiment 15	+	–	–	+	9.10	0.280
Experiment 16	+	–	–	–	1.85	0.0037

The basic level and intervals of factor variations were selected based on the analysis of theoretical studies results and experimental research preliminary data.

RESULTS

After conducting experiments, the regression equation was obtained. This equation describes the local area of the response surface, which characterizes the separation fineness:

$$Y = 6.864 + 2.08x_1 + 2.006x_2 + 1.152x_3 + 3.748x_4 + 0.592x_1x_2 - 0.169x_1x_3 + \\ + 1.044x_1x_4 + 0.501x_2x_3 + 1.142x_2x_4 - 0.002x_3x_4 \quad (1)$$

The verification of the obtained model adequacy (Table 1) was carried out according to Fisher's criterion (F-criterion). The calculated value of the *F*-criterion, which is *F*=0.211, is less than the value in the Table F_t=2.561 (selected for p=0.95; $f_{a\partial}$=11; f_y=32) (*Vasylkovskyi O., 2016*). Thus, the hypothesis of the linear equation adequacy is confirmed and can be used to describe the process.

The significance of the obtained coefficients was checked by Student's criterion (t-criterion) to ensure the reliability of the assessment – 0.95 and the number of degrees of freedom f_t=15. The analysis of the confidence interval shows that in the studied interval there are statistically insignificant regression coefficients b_1b_2, b_1b_3, b_2b_3 and b_3b_4.

The statistically significant coefficients include all the coefficients except for the coefficients b_1b_2, b_1b_3, b_2b_3 and b_3b_4.

The response surfaces and maps of lines of equal output (fig. 5-10) allow not only to reveal the coherent influence of factors on the separation fineness, but also to determine the direction of movement to rational design and technological parameters of the investigated operating element.

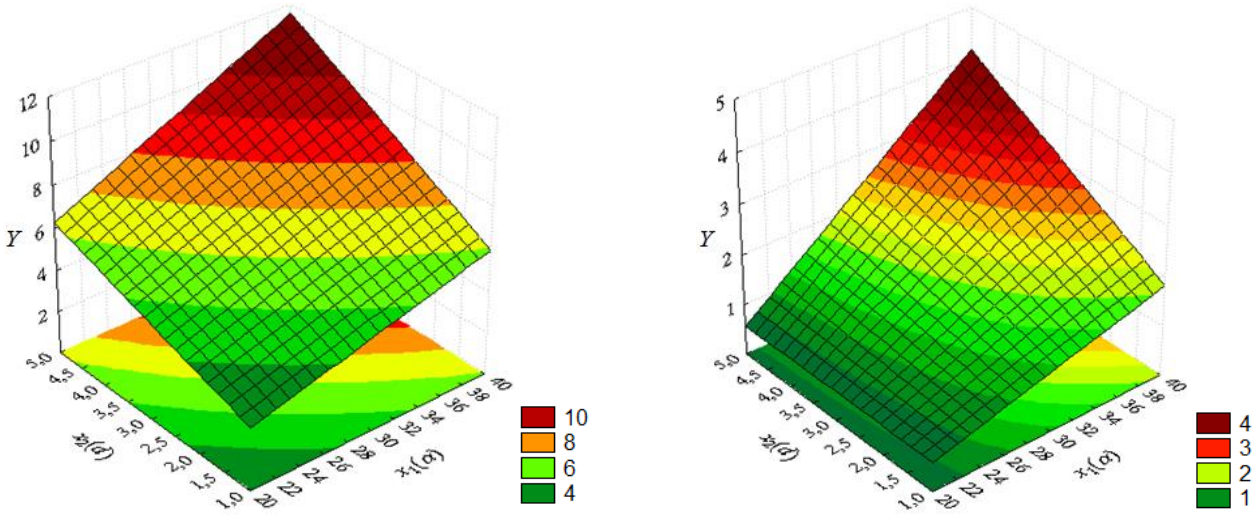

a) **b)**

Fig 3 - Dependence of the separation fineness on the sieve inclination angle and diameter of the sieve cross-cut baffle

a – basic level of factors; b – lower level of factors

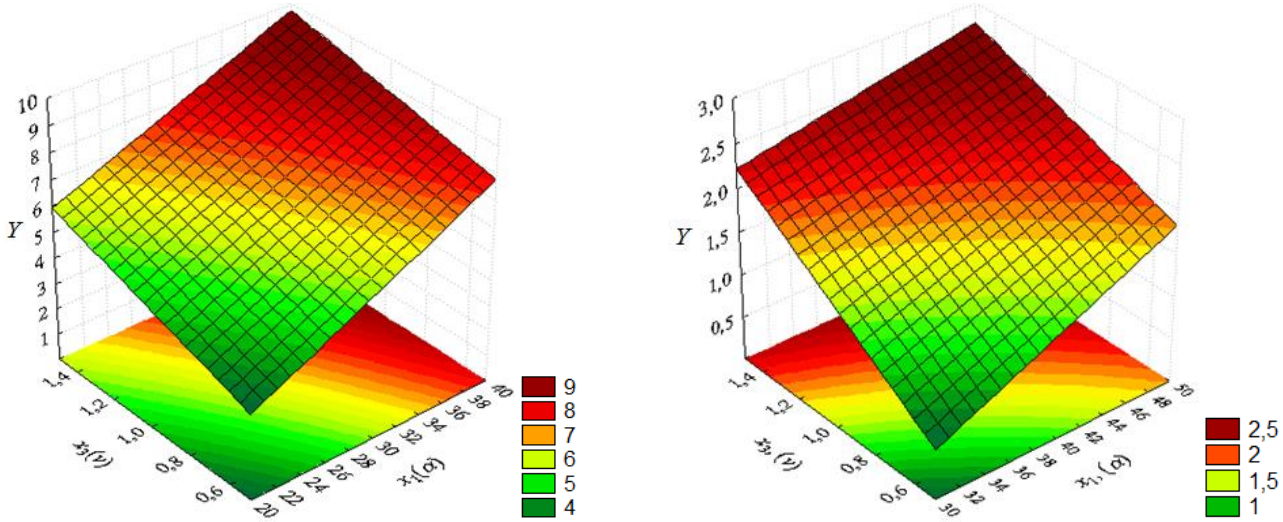

a) **b)**

Fig. 4 - Dependence of the separation fineness on the sieve inclination angle and the initial velocity of the material motion

a – basic level of factors; b – lower level of factors

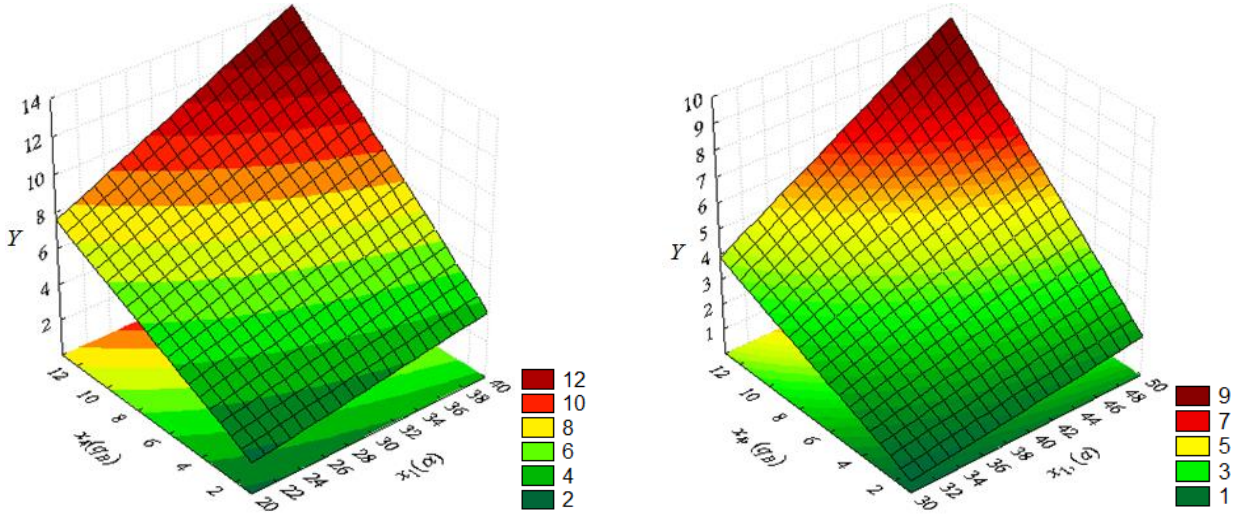

a) **b)**

Fig. 5 - Dependence of the separation fineness on the sieve inclination angle and material feeding

a – basic level of factors; b – lower level of factors

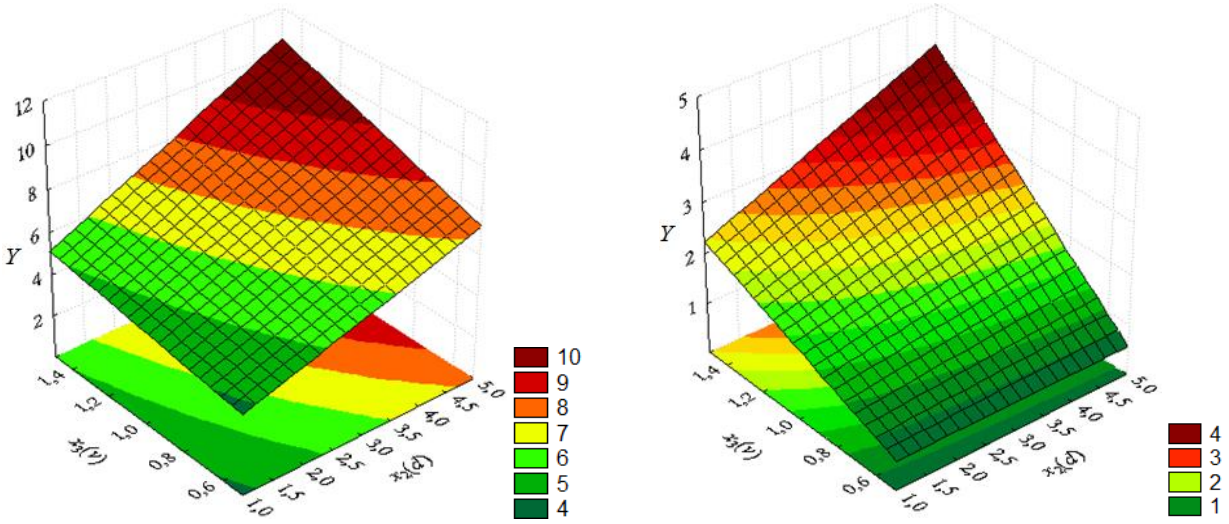

a) b)

Fig. 6 - Dependence of the separation fineness on the diameter of the sieve cross-cut baffle and the initial velocity of the material motion

a – basic level of factors; b – lower level of factors

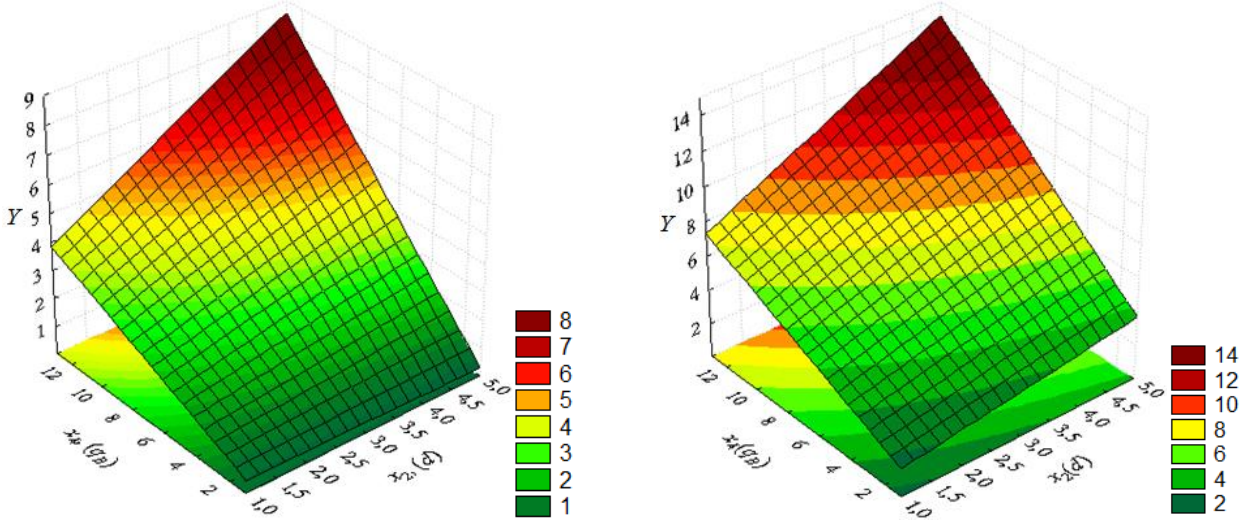

a) b)

Fig. 7 - Dependence of the separation fineness on the diameter of the sieve cross-cut baffle and material feeding

a – basic level of factors; b – lower level of factors

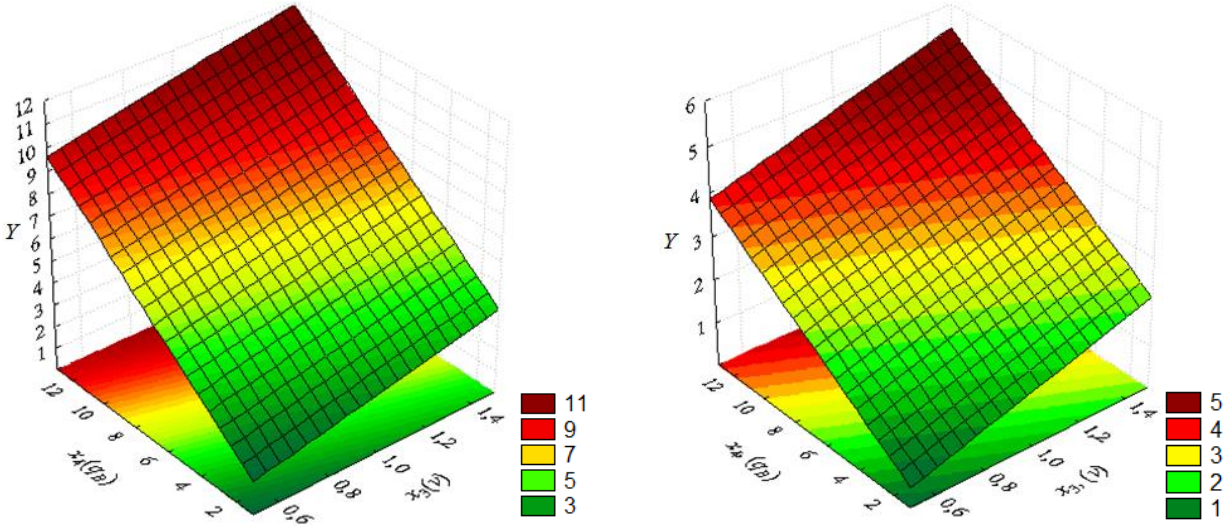

a) b)

Fig. 8 - Dependence of the separation fineness on the initial velocity of the material motion and material feeding

a – basic level of factors; b – lower level of factors

In the experiments, a natural heap of winter wheat with a moisture content of 14.6% and a total contamination of 12.2% was used.

The analysis of the results allows the following as a whole to be argued. The increase in the angle of inclination (x_1), the diameter of the sieve cross-cut baffle (x_2), the speed of the scraper (x_3) and the specific productivity (x_4) increase the degree of separation clarity. This is observed in experiments where the remaining factors are at the main level of variation (fig. 3a-8a). In the case where the remaining factors are at the lower level, the pattern is slightly different. In particular, it turns out that the diameter of the sieve transverse cross-sections does not affect the clarity of separation (fig. 3b, 6b). This pattern can be explained by the increased time on grain sifting as a result of a small specific feed and speed of movement.

After analyzing the Pareto-cards (fig. 11), we can conclude that all factors influence the separation fineness ε. In addition, the interaction of factors was also influential: the inclination angle and the feeding x_1x_4; diameter and feeding x_2x_4. The feeding x_4 has the greatest influence and the initial velocity of the chaff motion x_3 has the smallest influence.

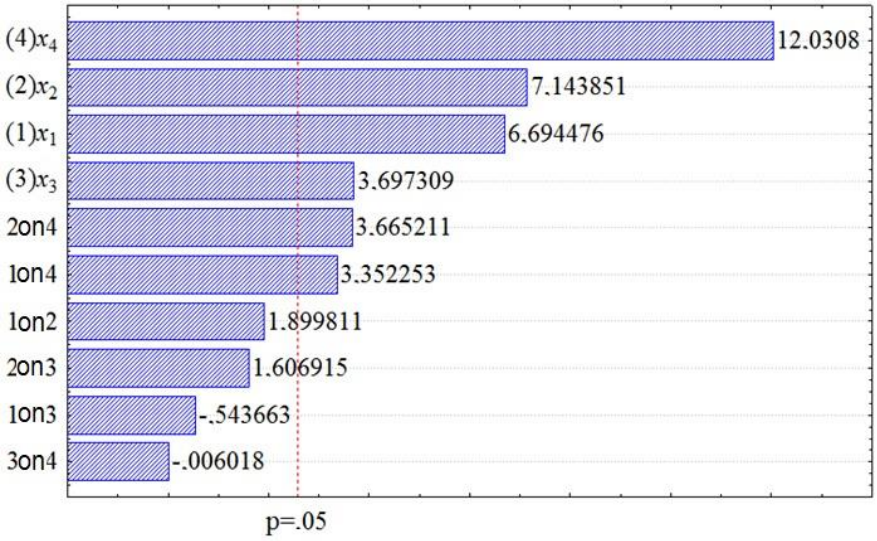

Fig. 11 - Standardised Pareto-card for separation fineness *Y*(ε)

CONCLUSIONS

The analysis of experimental data made it possible to identify the nature of the change of factors and to analyse their mutual influence on the optimization criterion. With an increase in the specific grain loading x_4 (*qB*), the separation fineness decreases proportionally. It was found that increasing the inclination angle of the sieve x_1 (α), the diameter of its baffles x_2 (*d*), and the initial velocity of the grain material motion x_3 (*v*) cause a decrease in separation fineness.

It has been identified that the specific grain loading x_4 (*qB*) should not exceed 7 kg/(m·s), the initial velocity of the grain material x_3 (*v*) is at the level of 0.5-1.2 m/s and the inclination angle of the sieve x_1 (α) ranges within 20-30º. According to the above-mentioned factors, the rational diameter of the sieve baffles x_2 (*d*) should not exceed 1-3 mm. By these parameters, it is possible to achieve separation fineness at the edge limit of 2%.

REFERENCES

[1] Borovikov V.P., (2003), *Statistica. The art of computer data analysis: for professionals*. 688 p., St. Petersburg/Russia;

[2] Dryncha V.M., (2006), *Research on grain separation and elaboration of machine technologies for their preparation*, Publishing house NPO «MODEK», 384 p., Voronezh/Russia;

[3] Kotov B. I., Kalinichenko R. A., Stepanenko S. P., Shvyda V. O., Lisetsky V. A., (2017), *Modelling of technological processes in typical objects of after-harvesting processing and storing of grain (separation, drying, active ventilation and cooling): monograph*. Publisher Private Entrepreneur Lysenko M. M. 552 p., Nizhyn/Ukraine;

[4] Kroulík M., Húla J., Rybka A., Honzík I., (2016), Pneumatic conveying characteristics of seeds in a vertical ascending airstream. *Research in Agricultural Engineering*, Vol.62, pp. 56-63, Prague/Czech Republic;

[5] Levdanskiy E.I., Levdanskiy A.E., Chyrkun D.I., Opymakh E.V., (2012), Design and research of grain cleaning machine with air separator. Scientific works of Odessa national academy of food technologies, Issue. 41(2), pp. 124-129, Odessa/Ukraine;

[6] Lukaszuk J., Molenda M., Horabik J., Szot B., Montross M.D., (2008) Airflow resistance of wheat bedding as influenced by the filling method. *Research in Agricultural Engineering*, Vol.54, pp. 50-57, Lublin/Poland;

[7] Moroz S.M., Vasylkovskyi O. M., Anisimov O. V., (2014), Technical means for simultaneous loading and separation of grain chaff according to the sizes. *Collection of Scientific Works of Kirovohrad National Technical University. Machines in agricultural production, branch engineering and automation*. *No. 27.* pp. 181-186. Kirovograd/Ukraine;

[8] Moroz S. M., Vasylkovskyi O. M., Goncharov V.V., (2011), Analysis of multi-layer grain motion on the fixed inclined working surface. *Design, production and operation of agricultural machines. A national interdepartmental scientific and technical collection of works,* Vol.41, Part.1, pp. 203–207, Kirovohrad/Ukraine;

[9] Piven M., (2015), Grain flow dynamics on vibrating flat sieve of finite width. *TEKA. Commission of motorization and energetics in agriculture.* Vol. 15, No. 3, pp. 113-119, Lublin/Poland

[10] Stepanenko S. P., Shvyda V. O., Popadyuk I. S., (2017), Analysis of the development of constructions of pneumatic separating systems of the separators. *Mechanization and electrification of agriculture*, Vol. 5, pp. 132-142, Glevakha/Ukraine;

[11] Tishchenko L. N., Piven M. V., Bredykhin V. V., (2014), The study of the inner-layer motion of the grain mixtures. *Journal of Kharkov National Technical University named after P. Vasylenko,* Vol.152, pp. 5-11, Kharkiv/Ukraine (DOI: 10.15587/1729-4061.2016.65920);

[12] Tishchenko L., Kharchenko S., Kharchenko F., Bredykhin V., Tsurkan O., (2016), Identification of a mixture of grain particle velocity through the holes of the vibrating sieves grain separators. *Eastern European Journal of latest technology,* Vol.2, No.7 (80), pp. 63-69, Kharkov/Ukraine;

[13] Vasylkovskyi O. M., Leshchenko S. M., Vasylkovska K. V., Petrenko D.I., (2016), The textbook of a researcher. Study guide for students of agro-technical specialties, 204 p., Kharkov/Ukraine.

DESIGN AND RESEARCH OF AUTOMATIC ALIGNMENT TEST DEVICE OF SEMI-FEEDING PEANUT COMBINE HARVESTER

/

半喂入式花生联合收获机自动对行试验装置的设计与研究

Prof. Ph.D. Eng. Lv X.L.[1, 3], R. Ph.D. Eng. Hu Z.L.*[2], R.A.M.S. Eng. Wang S.Y.[2], R.A.M.S. Eng. Yu Z.Y.[2]

[1] Ministry of Agriculture, Key Laboratory of Modern Agricultural Equipment/China

[2] Ministry of Agriculture, Nanjing Research Institute for Agricultural Mechanization /China

[3] Chuzhou University, College of Machinery and Automotive Engineering/China

Tel: 862584346246; E-mail: nfzhongzi@163.com

Keywords: *Peanut harvester; Automatic alignment; Detection mechanism; Control system; Performance test*

ABSTRACT

For the caused harvesting loss problem by inaccurate alignment of the semi-feeding peanut harvester, an automatic alignment system on the control core of the single chip microcomputer μPD78F0525 was designed. The system adopts a four-bar detection mechanism to transmit the offset to the controller through the sensor and to adjust the excavator in time. On this basis, a peanut automatic alignment test device is developed, which is composed of conveying platform, ridge ditch, hydraulic execution system, signal detection mechanism, signal processing and control system, etc. The influence effect of the main factors of the system is tested through the test bench. The results show: the reaction time increases with the increase of spring preload and deviation distance, gradually decreases and tends to remain unchanged with the increase of forward speed, and first decreases and then increases with the increase of hydraulic flow. The unqualified rate first decreases and then increases with the increase of spring preload, gradually increases with the increase of forward speed and deviation distance, and gradually decreases with the increase of hydraulic flow. The effectiveness and stability of the automatic alignment system can meet the operation requirements. It effectively solved the problem of automatic alignment of the semi-feeding peanut harvester and provided a technical reference for the research and development of the automatic alignment system for harvesting the fruits under the soil.

摘要

针对半喂入式花生收获机对行不准确造成收获损失的问题，设计了一种基于单片机μp78f0525 为控制核心的自动对行系统。系统采用四杆检测机构，通过传感器将补偿量传递给控制器，并及时调整挖掘铲。在此基础上，研制了由输送平台、垄沟、液压执行系统、信号检测机构、信号处理与控制系统等组成的花生自动对行试验装置。对该系统主要因素的影响效果进行了测试，结果表明：随着弹簧预紧力和偏位距离的增大，自动对齐反应时间增大，随着前进速度的增加，反应时间逐渐减小，并趋于不变，随着液压流量的增加，反应时间先减小后增大；不合格率随弹簧预紧力的增加先减小后增大，随着前进速度和偏离距离的增加而逐渐增大，随着液压流量的增加而逐渐减小；自动对行系统的有效性和稳定性均能够满足作业要求。该系统有效解决了半喂入式花生收获机的自动对行问题，为土下果实收获自动对行系统的研制提供了技术参考。

INTRODUCTION

In China, peanut is an important oil crop and high-quality protein resource; it is also the most competitive crop at international level. The overall level of peanut mechanized harvesting in our country is low. How to improve the level of peanut mechanized harvesting is a major problem (*Lv X L et al, 2012*). The ridge cultivation is the main method of peanut planting in China. Because the digging shovel cannot align with the peanut under soil, it will cause large loss and low efficiency. In order to improve the harvesting quality, it is necessary to adjust the digging shovel during operation, so the operator labour intensity is high and the accuracy of the alignment is greatly affected by man-made factors. At present, a great deal of research has been done on the agricultural machinery automatic operation in the country and abroad. The great progress has been obtained in the automatic control system of agricultural machinery (*Fernando A Auat Cheein et al, 2016; Perez-Ruiz Manuel et al, 2014; Ji Changying et al, 2014; Saeys W et al, 2008; Chen Man et al, 2016*), but little research has been done on the automatic alignment of the fruit under the soil. The research on automatic alignment of harvesting fruit under the soil in China is still in the initial stage.

Qingdao Agricultural University has made a preliminary study on the automatic alignment device of peanut combine harvester (*Yang Ranbing et al, 2011*), which adopted the structure of the moving chassis and moving shovel as a whole, and the research is still in the experimental stage. The automatic alignment system of beet harvester is studied by the Nanjing Research Institute for Agricultural Mechanization of the Agriculture Ministry (*Wang Shenying et al, 2014; Wu Huichang et al, 2013*) and the automatic alignment hydraulic rectification system of beet harvester is designed, which is in the experimental stage at present. This paper studies and designs the automatic alignment test device. It can effectively solve the existing technology problems in the automatic alignment of the semi-feeding peanut harvester in China and provide the technical conditions for promoting the development of the automation and intellectualization of peanut industry.

MATERIALS AND METHODS

- **Overall scheme and working principle**

As shown in Fig. 1, the designed automatic alignment test bench mainly includes: deviation detection mechanism, signal processing and control system, rectifying mechanism, signal feedback system, conveying platform, longmen rack and ridge ditch, etc.

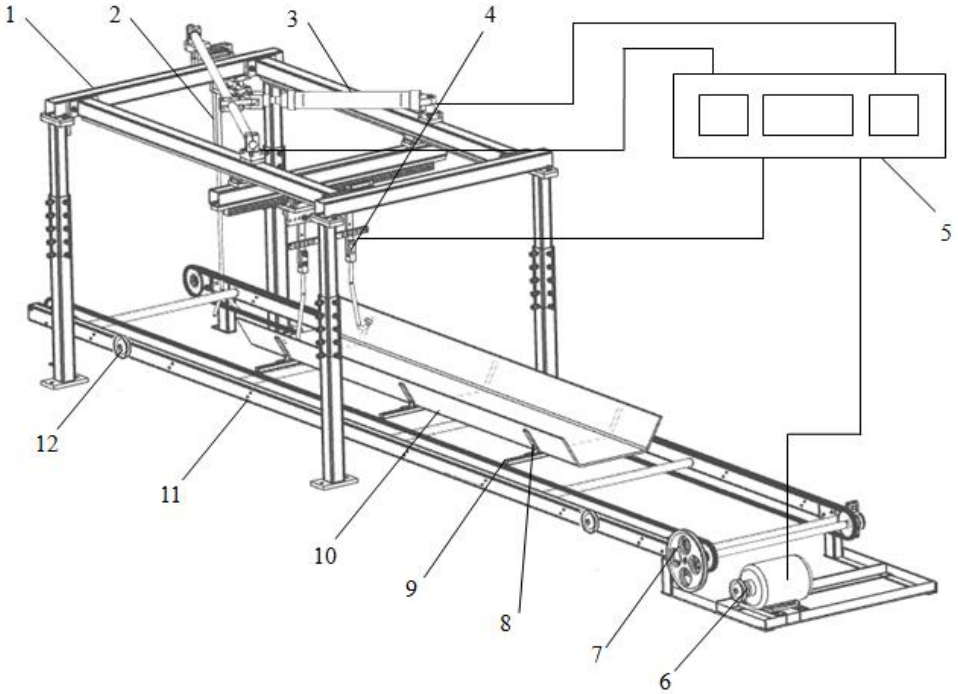

Fig. 1 - Structure diagram of automatic alignment test device

1- Longmen rack; 2- Rectifying rod; 3- Cylinder; 4- Detection mechanism; 5- Controller; 6- Motor; 7- Transmission system; 8- Clamping plate; 9- Adjusting slot; 10- Ridge ditch; 11- Conveying platform; 12- Control switch;

When the test bench is working, the motor drives the ridge ditch movement to imitate the machine driving in the field, and the moving direction and distance of the ridge ditch are controlled by the adjusting switch on the conveying platform. When the roller of the deviation detection mechanism contacted with the ridge ditch, the roller drives the detection rod to swing. The displacement signal is transformed into angle signal by the angle sensor and transmitted to the single chip microcomputer for calculation and processing. The hydraulic system of the rectifying mechanism adjusts the position of the rectifying rod to imitate the adjustment of the digging shovel during the machine working and, at the same time, the rotation angle of the pull rod on the cylinder is monitored in time. The rectifying situation is fed back to the signal processing and control system in time and the timely rectification is finished.

- **Design of automatic alignment system**

Deviation detection mechanism

As shown in Fig. 2, the deviation detection mechanism is mainly composed of the fixed frame, detection rod, roller, sensor and reset spring.

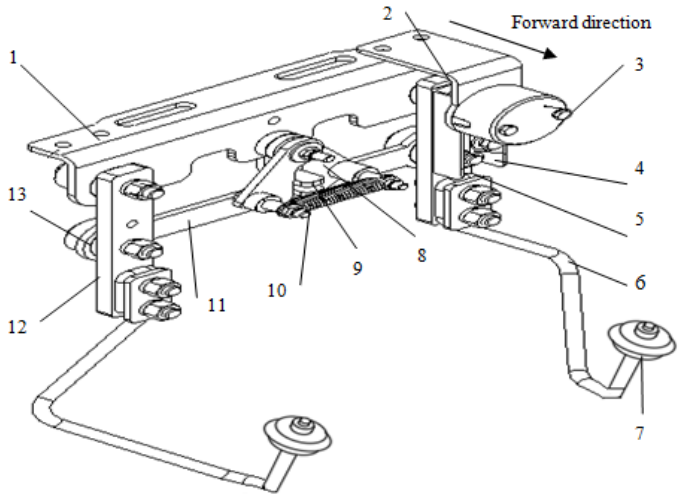

Fig. 2 - Structure diagram of detection mechanism

1- Fixing frame; 2- Mounting plate; 3- Sensor; 4- Connecting shaft; 5- Support plate; 6- Detection rod; 7- Roller; 8- Spring limit plate; 9- Block; 10- Replacing spring; 11- Connecting rod; 12- Swing arm; 13- Bearing

It is composed of the swing arm, connecting rod and frame formed four link mechanisms. The deviation situation of the digging shovel was detected by the roller on the detection rod. The connecting shaft of the sensor is connected with the supporting plate, which can drive the connecting shaft of the sensor to rotate, and the displacement signal is transformed into angle signal by the sensor and transmitted to the controller. The controller controls the rectifying mechanism to finish automatic alignment. The replacing device is composed of the spring limit plate, replacing spring and block. The two spring limit plates are located separately to the two sides of the block and the blade on the connecting rod, and are connected with the replacing spring. When the detection rod is forced to swing, the blade on the connecting rod pushes the spring limit plate on the opposite side to swing. When the force is greater than the spring preload, it drives the rotating shaft of the sensor to rotate. When the detection rod is not forced, it will be replaced in time under the combined action of spring preload and the block. According to experience and experimental measurement, the minimum preload of the replacing spring cannot be less than 30N. According to the requirement of the detection mechanism, the angle sensor selects the photoelectric incremental encoder VLH11 with three-phase square wave output of EPC Company in USA, its maximum revolution is 7500r/min, the starting torque is 1.5×10^{-5}N·m, the response frequency is 100kHz and the resolution ratio is 1024P/R. The angle sensor has the direction indication of angle change, the pulse output of the angle sensor are connected to the external interrupt input of the microprocessor, and the interrupt of the way touch edge is used to count pulse and determine direction.

- ***Rectifying execution system***

The system is mainly composed of hydraulic control system, cylinder, pull rod, signal feedback device and rectifying rod, as shown in Fig. 3.

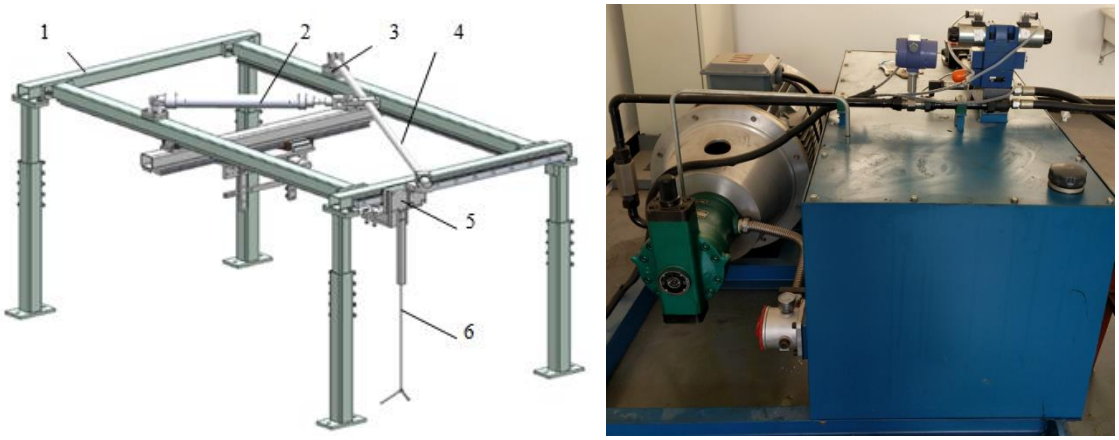

(a) Rectifying mechanism (b) Hydraulic control system

Fig. 3 - The rectifying execution system

1- Longmen rack; 2- Cylinder; 3- Signal feedback device; 4 - Pull rod; 5- Bracket; 6- Rectifying rod

The rectifying rod is connected with the longmen rack by the bracket and can move to the left and right along the beam by the pull rod driving. The signal feedback device mainly includes angle sensor and sensor mounting bracket. The actual rotation angle of the pull rod is transmitted to the control system by the angle sensor and the adjustment of the digging shovel is imitated by the cylinder adjusting the rectifying rod. As shown in Fig. 4, according to the processing result of the detection signal (*Zhang Hui et al, 2010; Chen Yazhou et al, 2012; Yu Yang et al, 2011*), the 2-position, 3-way solenoid valve *4* is first controlled by the controller, the high-pressure oil enters into the oil circuit and then the movement direction and flex value of the hydraulic cylinder are controlled by the 3-position, 4-way solenoid valve *8*. The high-pressure oil can be conveyed to the 3-position, 4-way solenoid valve *8* by controlling the 2-position 3-way solenoid valve *6* and adjusting throttle valve *7*, so that the hydraulic cylinder *9* moves smoothly and accurately.

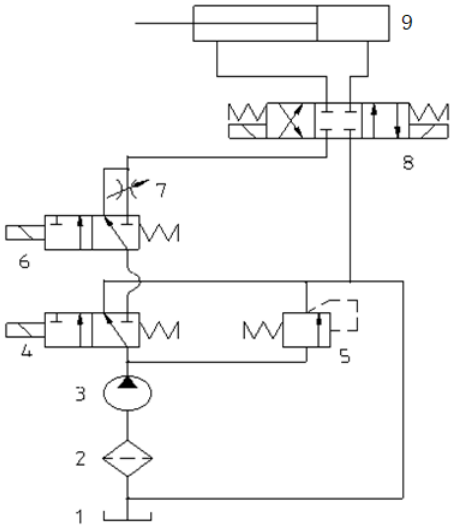

Fig. 4 - Schematic diagram of hydraulic system

1- Fuel tank; 2- Filter; 3- Hydraulic pump; 4, 6- 2-position, 3-way solenoid valve; 5- Relief valve; 7- Adjustable throttle valve; 8- 3-position, 4-way solenoid valve; 9- Cylinder

- ***Signal processing and control system***

The system mainly processes the detection information in time, and controls the execution parts to complete the rectification (*Feng Huimin et al, 2018; Wei Xinhua et al, 2009*). As shown in Fig. 5, the system takes the single-chip microcomputer as the control core, converts the offset into electrical signal by the angle sensor and transmits it to the controller. The speed sensor transmits the forward speed of the harvester to the controller. The controller judges rectifying value according to the angle sensor transmitted signal and finishes the rectification in time by controlling the hydraulic valve to adjust the flex value of the cylinder. The controller determines the adjusting time according to the speed sensor signal. The signal feedback sensor monitors the angle change of the pull rod in time and transmits to the controller to adjust the output control signal in time. The closed-loop control system is formed. According to the requirement, the speed sensor adopts KJT-J18GW-ZK proximity sensor of Nanjing kaijite Electric Co., Ltd, and the angle sensor uses the three-phase square wave output photoelectric incremental encoder VLH11 of USA EPC Co., Ltd.

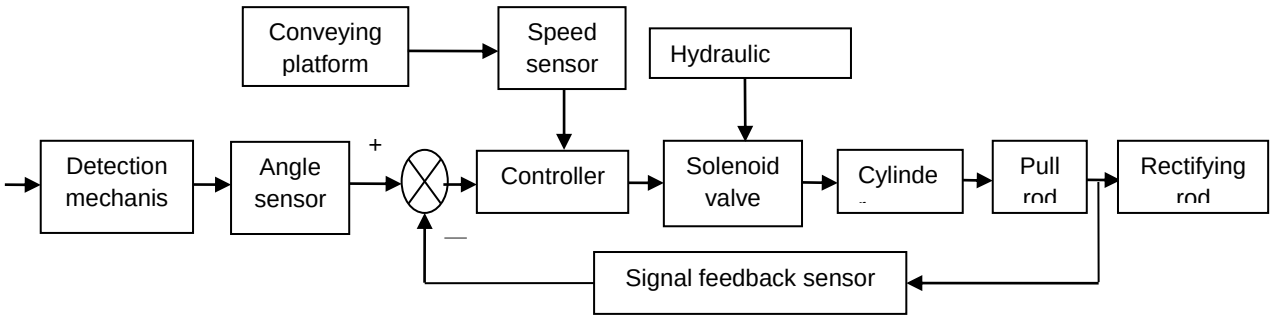

Fig. 5 - The schematic diagram of signal processing and control system

The system needs to finish complex logic judgment, so the digital-analog hybrid circuit is adopted on the single chip microcomputer. The overall structure is mainly composed of the smallest processor system, data storage, power supply, solenoid valve drive and clamp-limiting filtering circuit. The single chip microcomputer adopts μPD78F0525 (*Cai Guohua et al, 2011; Hu Lian et al, 2009*). As shown in Fig. 6, the minimal system mainly includes single chip microcomputer, crystal oscillator circuit and reset circuit. It mainly finishes the scanning and identification of the input information of angle sensor and speed sensor and processing of the internal program, and outputs the control signal of the electromagnetic valve driving circuit. As shown in Fig. 7, in order to improve the anti-interference ability of the interface, the clamp-limiting filtering circuit is added in the interface between the angle (speed) sensor and the single chip computer. As shown in Fig. 8, the drive circuit of solenoid valve is mainly composed of the opto coupler TLP817 and the field effect Transistor 2SK2931. In order to eliminate the reverse flow of solenoid valve coil, a diode stack 10GL2CZ47A is added.

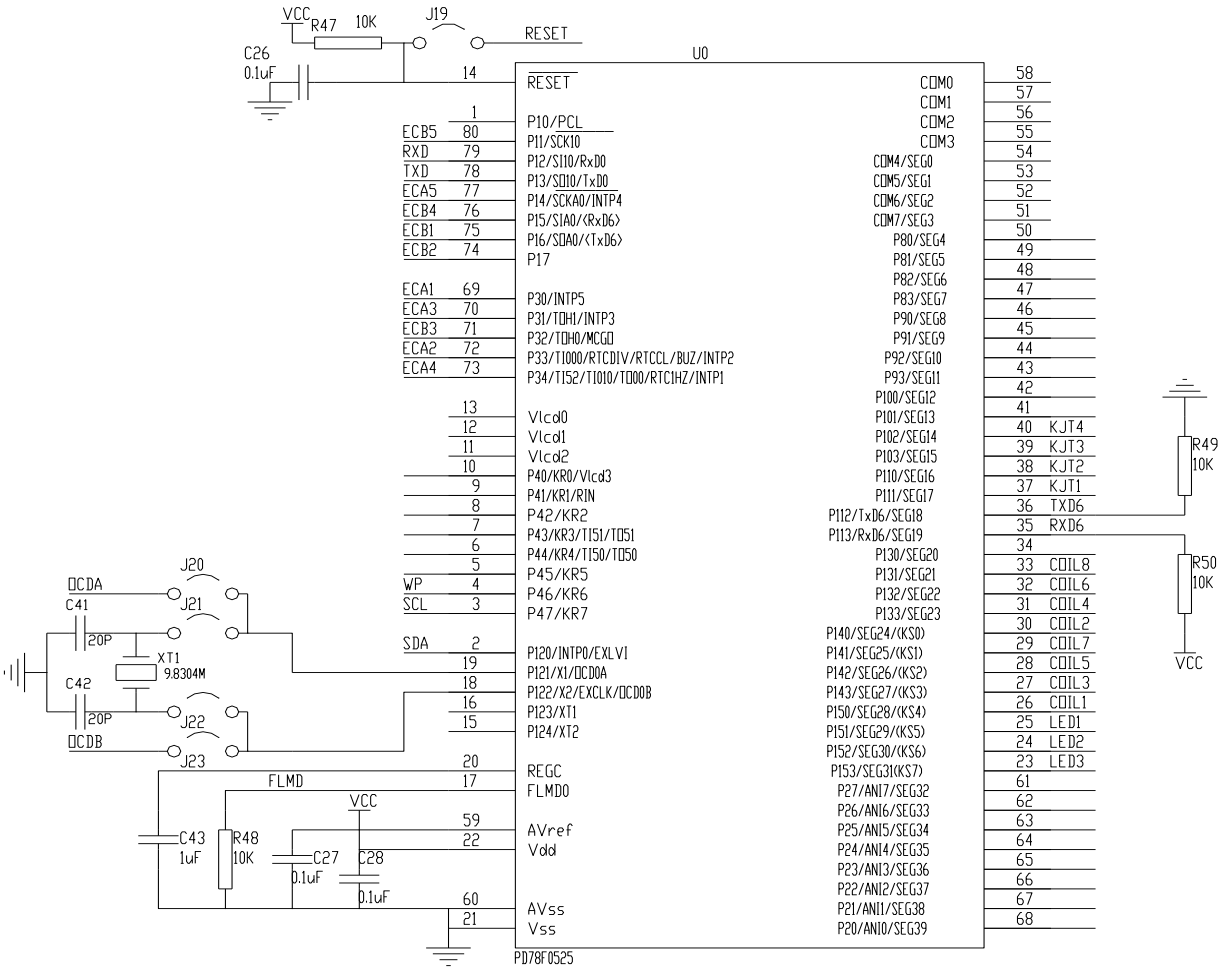

Fig. 6 - Minimum system circuit diagram of the single chip microcomputer

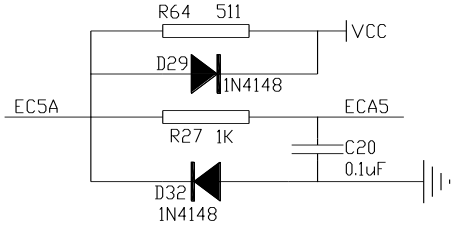

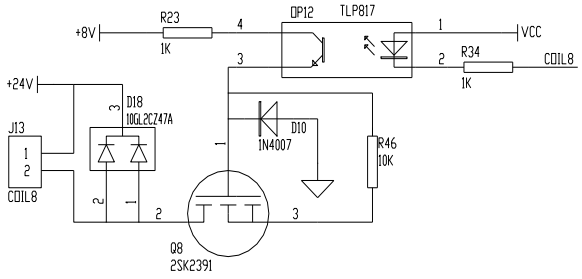

Fig. 7 - Diagram of clamp-limiting filtering circuit **Fig. 8 - Driving circuit diagram of the solenoid valve**

The main program flow chart of the detection and control system of the automatic alignment is shown in Fig. 9.

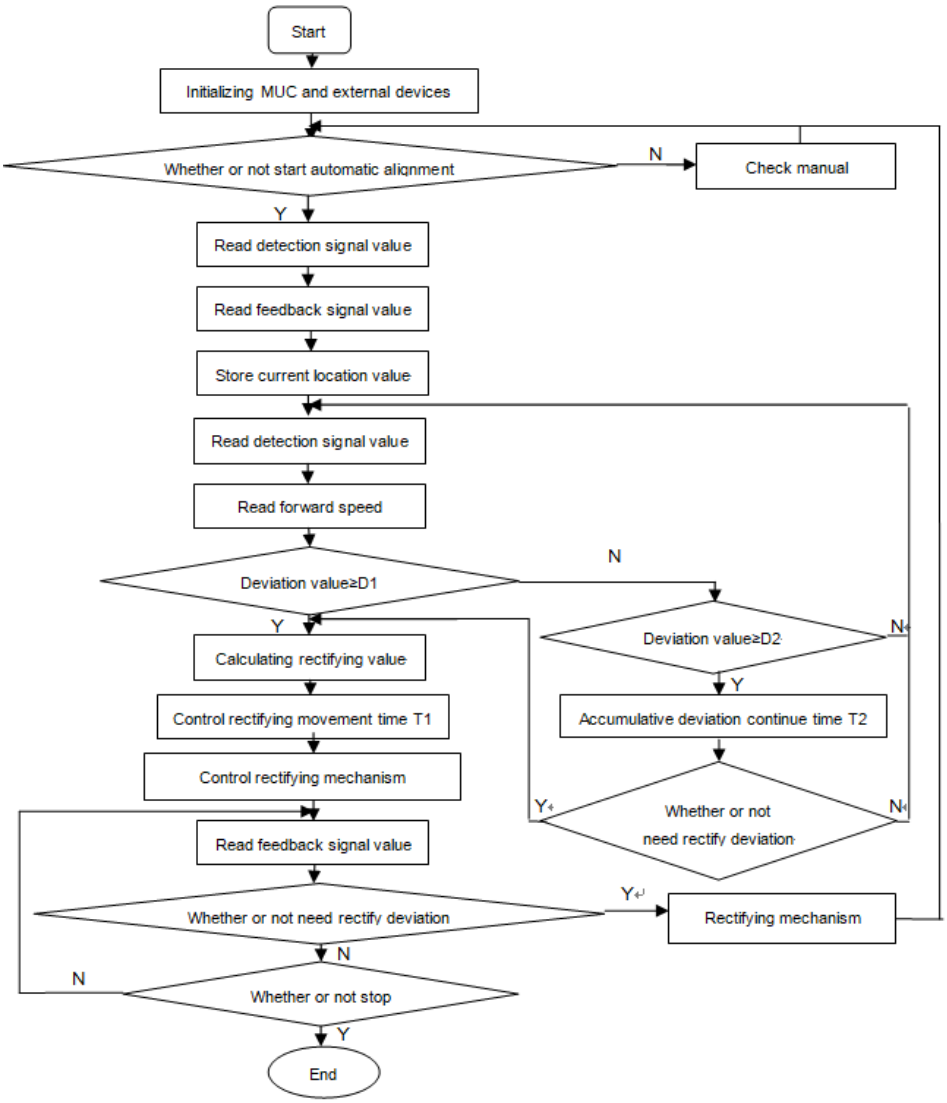

Fig. 9 - Flow chart of main program

The program first initializes and then processes the detection signal of the sensor in time. The main program first reads the angle values of the detection mechanism and the feedback mechanism, and stores the values in current position. Then, it extracts the forward speed of the harvester and the angle value of the detection mechanism and judges whether the angle value exceeds the range of the allowed value. When it does not exceed the allowed range, the controller will not send out the control signal, carrying on the trimming after the corresponding time according to the forward speed of the harvester. When it does exceed the allowed range, the controller calculates the rectifying value according to the deflection angle and calculates the rectifying adjustment time according to the harvester forward speed to adjust the flex value of the cylinder in time, then adjusts it properly according to the feedback signal. Until the rectification meets the requirements, the rectification mechanism replaces it and the system enters into the next adjustment or meets the stop conditions to stop work. In order to reduce the inertia of the hydraulic rectifying mechanism and improve the stability and accuracy of the adjustment, the throttle valve was started to carry on the trimming before the beginning and ending adjustment of the cylinder.

- **Performance test**

Test equipment and instruments

The automatic alignment test bench of semi-feeding peanut harvesting (As shown in Fig. 10), tape (range is 5m, accuracy is 1mm), tachometer (range is 1-19999r/min, accuracy is ± 0.02%), scientific calculator, oscilloscope (2 channels, bandwidth is 100MHz, vertical resolution is 8bit, maximum real-time sampling rate 1.25GS/s, recording length of the per channel is 27500 points)), BM902 multimeter.

Fig. 10 - The automatic alignment test bench of semi-feeding peanut combine harvester

Contents and methods of the test

The influence of the main factors on performance of the automatic alignment system are tested (*Zhai Changyuan et al, 2009; Zuo Xingjian et al, 2016*) and the influence law is analyzed. The spring preload, forward speed, deviation distance and flow were selected as the test factors, and the rectifying unqualified rate and system reaction time were selected as the test indexes. The levels of each factor were as shown in Table 1. In the test, the moving speed of conveyor platform is used to imitate the forward speed of the harvester. The moving speed of the test bench is adjusted by the frequency converter, and the speed is measured by the tachometer. The position status of the digging shovel is imitated by the moving track of the rectifying rod at the bottom of the ridge ditch. The value of the rectifying rod deviating from centreline of ditch bottom is selected as the deviation value of the digging shovel. When the value exceeds the deviation range, it is unqualified. In order to measure the reaction time of the system, the detection sensor and the feedback sensor are connected to the oscilloscope respectively to measure the reaction time of the automatic alignment system. In the test, single factor test was done. Each factor level was repeated three times and the average value was taken as the test result.

Table 1

Factor and level table

Levels	Factors			
	Spring preload /N	Forward speed /m.s^{-1}	Deviation distance /cm	Flow /L.min^{-1}
1	53	0.4	3	15
2	125	0.8	6	20
3	198	1.2	9	25
4	272	1.6	12	30
5	346	2.0	15	35

RESULTS

As shown in Fig. 11, the test results and analysis illustrate that: (1) the preload of the spring has greater effect to the reaction time, but smaller effect to the unqualified rate. With the increase of spring preload, the reaction time increases, while the unqualified rate first decreases and then increases. The preload force of the replaced spring increases, the swing resistance force of the detection rod increases, so that the signal extracting time of the detection system increases. (2) The forward speed has much great effect to the reaction time and the unqualified rate. With the increase of the forward speed, the reaction time gradually decreases and tends to remain unchanged, and the unqualified rate gradually increases. With the increase of the forward speed, the signal extraction time of the detection system decreases. When the speed is greater than a certain value, the reaction time of each link of the system reaches "saturation" state, and the reaction time does not change. With the increase of the forward speed, the reaction time of the system

decreases, so that the digging shovel cannot be adjusted to location in reaction time. It makes the unqualified rate improve. (3) The departure distance has greater effect on the reaction time and the unqualified rate. With the increase of the departure distance, the reaction time and unqualified rate increase gradually. The longer the deviation distance is, the larger the swing angle of the detection rod is and the longer the signal extraction time of the detection system is. It makes the adjustment quantity of the hydraulic cylinder increases, so that the action time of the rectification execution system increases. The longer the deviation distance, the longer the rectification time, so that the digging shovel cannot be adjusted to location in time. It makes the unqualified rate improve. (4) The flow has greater effect on the reaction time, but smaller effect on the unqualified rate. With the increase of the flow, the reaction time decreases first and then increases, and the unqualified rate gradually decreases. With the increase of the flow, the movement time of hydraulic cylinder decreases, so that the automatic alignment speed increases and the reaction time and the unqualified rate decrease. When the flow exceeds the demand value, the too fast hydraulic cylinder movement causes the overshoot of the rectification execution mechanism. It causes reciprocating vibration of the rectification execution mechanism, and the reaction time decreases first and then increases.

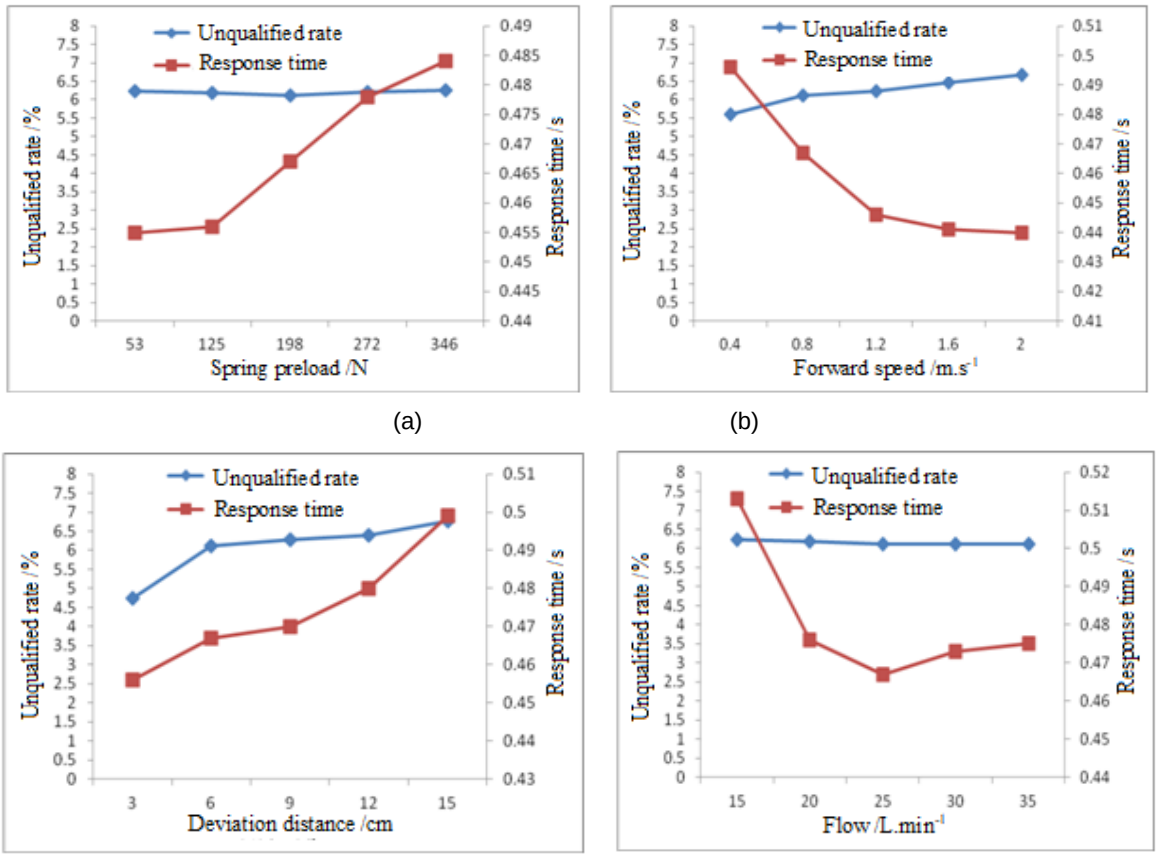

Fig. 11 - The influence of the factors to automatic alignment performance

CONCLUSIONS

The automatic alignment system of the semi-feeding peanut harvester was designed. The system is mainly composed of the deviation detection mechanism, signal processing and control system, rectifying execution mechanism, signal feedback system, etc. The core of the signal processing and control system adopts the single chip microcomputerμPD78F0525. By the angle sensor, the deviation signal is transformed into an angle signal and processed in time. On this basis, the test bench of the automatic alignment system of the peanut harvester is designed. The test bench is mainly composed of the conveying platform, ridge ditch, hydraulic execution system, signal detection mechanism, signal processing and control system. The working performance of the automatic alignment system and the influence effect of the main factors are tested. The test results show that: the spring preload, forward speed of the peanut harvester, deviation distance of the digging shovel and flow of the hydraulic system rate have significant effects on the response time of the system. With the increase of the spring preload and deviation distance, the reaction time

increases. With the increase of the forward speed, the reaction time gradually decreases and tends to remain unchanged. With the increase of the flow, the reaction time decreases first and then increases. The spring preload and flow of the hydraulic system have smaller effects on the unqualified rate. The forward speed of the peanut harvester and deviation distance of the digging shovel have greater effects on the unqualified rate. With the increase of the spring preload, the unqualified rate decreases first and then increases. With the increase of the forward speed and deviation distance, the unqualified rate gradually increases. With the increase of the flow, the unqualified rate gradually decreases. The system has good real-time performance, stable operation performance and can better meet the requirement of the automatic alignment operation of the peanut harvester.

ACKNOWLEDGEMENT

The study was supported by the Key Laboratory of Modern Agricultural Equipment, Ministry of Agriculture, P.R. China (201602002), and the Natural Science Foundation for colleges and universities in Anhui Province of China (KJ2018A0423).

REFERENCES

[1] Cai Guohua, Li Hui, Li Hongwen et al, (2011), Design of test-bed for automatic depth of furrow opening control system based on ATmega128 single chip microcomputer, *Transactions of the Chinese Society of Agricultural Engineering*, Vol.27, Issue 10, pp.11-16, Beijing/ China;

[2] Chen Man, LU Wei, Wang Xiaochan et al, (2016), Design and experiment of optimization control system for variable fertilization in winter wheat field based on fuzzy PID, *Transactions of the Chinese Society for Agricultural Machinery*, Vol.47, Issue 2, pp.71-76, Beijing/ China;

[3] Chen Yazhou, Pi Jun, Zheng Tianyi, (2012), Electro-hydraulic proportional manipulation system of land leveller based on pilot oil distribution method, *Transactions of the Chinese Society of Agricultural Engineering*, Vol.28, Issue 2, pp.7-12, Beijing/ China;

[4] Feng Huimin, Gao Na'na, Meng Zhijun et al, (2018), Design and Experiment of Deep Fertilizer Applicator Based on Autonomous Navigation for Precise Row-following, *Transactions of the Chinese Society for Agricultural Machinery*, Vol.49, Issue 4, pp.60-67, Beijing/ China;

[5] Fernando A Auat Cheein, Gustavo Scaglia, Miguel Torres-Torriti et al, (2016), Algebraic path tracking to aid the manual harvesting of olives using an automated service unit, *Biosystems Engineering*, Vol.142, pp.117-132, England/ UK;

[6] Hu Lian, Luo Xiwen, Zhao Zuoxi et al, (2009), Design of electronic control device and control algorithm for rice transplanter, *Transactions of the Chinese Society of Agricultural Engineering*, Vol.25, Issue 4, pp.118-122, Beijing/ China;

[7] Ji Changying, Zhou Jun, (2014), Current situation of navigation technologies for agricultural machinery, *Transactions of the Chinese Society for Agricultural Machinery*, Vol.45, Issue 9, pp.44-54, Beijing/ China;

[8] Lv X.L., Wang H.O., Zhang H.J. et al, (2012), Present Situation and Analysis on Peanut Picking Technology and Equipment, Hubei Agricultural Sciences, Vol.51, Issue 18, pp.4116-4118, Wuhan/ China;

[9] Perez-Ruiz Manuel, Slaughter David C, Fathallah Fadi A, et al, (2014), Co-robotic intra -row weed control system, *Biosystems Engineering*, Vol.128, pp.45-55, England/ UK;

[10] Saeys W, Wallays C, Engelen K, et al, (2008), An automatic depth control system for shallow slurry injection, part 2: Control design and field validation, *Biosystems Engineering*, Vol.99, Issue 2, pp.161-170, England/ UK;

[11] Yang Ranbing, Shang Shuqi et al, (2011), Research on automatic alignment technology for harvesting machinery of rootstalk crops, *CSAE 2011*, pp.1-5, Beijing/ China;

[12] Yu Yang, Shi Boqiang, Hou Youshan, (2011), Analysis on stability of hydraulic servo systems affected by structure stiffness, *Transactions of the Chinese Society of Agricultural Engineering*, Vol.27, Issue Supp.2, pp.32-35, Beijing/ China;

[13] Wang Shenying, Hu Zhichao, Wu Huichang et al, (2014), Design simulation and test of auto-follow row control system employed in beet harvester based on Proteus, *Journal of Chinese Agricultural Mechanization*, Vol.35, Issue 3, pp.35-40, Beijing/ China;

[14] Wei Xinhua, Li Yaoming, Chen Jin et al, (2009), System integration of working process intelligent monitoring and controlling devices for combine harvester, *Transactions of the Chinese Society of Agricultural Engineering*, Vol.25, Issue Supp.2, pp.56-60, Beijing/ China;

[15] Wu Huichang, Hu Zhichao, Peng Baoliang et al, (2013), Development of auto-follow row system employed in pull-type beet combine harvester, *Transactions of the Chinese Society of Agricultural Engineering*, Vol.29, Issue 12, pp.17-24, Beijing/ China;

[16] Zhai Changyuan, Zhu Ruixiang, Sui Shuntao et al, (2009), Design and experiment of control system of variable pesticide application machine hauled by tractor, *Transactions of the Chinese Society of Agricultural Engineering*, Vol.25, Issue 8, pp.105-109, Beijing/ China;

[17] Zhang Hui, Li Shujun, Zhang Xiaochao et al, (2010), Development and performance of electro-hydraulic proportion control system of variable rate fertilizer, *Transactions of the Chinese Society of Agricultural Engineering*, Vol.26, Issue Supp.2, pp.218-222, Beijing/ China;

[18] Zuo Xingjian, Wu Guangweiu Weiqiang et al, (2016), Design and experiment on air-blast rice side deep precision fertilization device, *Transactions of the Chinese Society of Agricultural Engineering*, Vol.32, Issue 3, pp.14-21, Beijing/ China.

DETERMINATION OF ROLLING RADIUS OF SELF-PROPELLED MACHINES' WHEELS

/

ВИЗНАЧЕННЯ ДІЙСНОГО РАДІУСУ КОЧЕННЯ ТА ОЦІНКА КОВЗАННЯ КОЛІС САМОХІДНИХ МАШИН

Prof.PhD.Eng. Golub G.A., Ph.D. Eng. Chuba V.V., Ph.D. Eng. Marus O.A.
National University of Life and Environmental Sciences of Ukraine, Kyiv / Ukraine;
Tel:+380953115050, E-mail gagolub@ukr.net

Keywords: *wheel deformation, tire air pressure, wheel contact area, wheel slipping, pneumatic tires*

ABSTRACT

The obtained results allow calculating the actual rolling radius of the wheel and evaluate the slipping of the drive wheels of self-propelled machines in accordance with the air pressure in the tires and the parameters of interaction with the support surface.

On the basis of the developed model for determining the initial radius of the wheel and the length of the contact zone of the wheel with the support surface, the dependence for determining the actual radius of the wheel rolling was obtained.

The studies have confirmed an increase in the actual rolling radius and a decrease in wheel slip with an increase in air pressure in the tires. For example, for the rear wheel of a tractor John Deere 7130 with an increase in pressure from 0.6 to 2.6 atm, an increase in the rolling radius by 21 mm and a decrease in the slip coefficient from 1.94 to 0.83% were observed. For the front wheel, when the pressure changed from 1 to 2 atm, the rolling radius increased by 7 mm and the wheel slip coefficient decreased from 1.76 to 1.12 %. The determination index of calculated and experimental values of the real rolling radius is $\eta^2 = 0.98$ for the front and $\eta^2 = 0.99$ for the rear wheels, which indicates the adequacy of the calculated dependences.

РЕЗЮМЕ

Отримані результати дають змогу виконати розрахунок дійсного радіуса кочення колеса та оцінити ковзання приводних коліс самохідних машин відповідно до тиску повітря в шинах та параметрів взаємодії з опорною поверхнею.

На основі розробленої моделі для визначення початкового радіуса колеса та довжини зони контакту колеса з опорною поверхнею отримано залежність для визначення дійсного радіуса кочення колеса.

Виконані дослідження підтвердили збільшення дійсного радіуса кочення та зменшення ковзання колеса при збільшенні тиску повітря в шинах. Так, наприклад, для заднього колеса трактора John Deere 7130 при збільшенні тиску від 0,6 до 2,6 атм спостерігалося збільшення радіуса кочення на 21 мм та зменшення коефіцієнта ковзання від 1,94 до 0,83%. Для переднього колеса при зміні тиску від 1 до 2 атм спостерігалося збільшення радіуса кочення на 7 мм та зменшення коефіцієнта ковзання коліс від 1,76 до 1,12 %. Індекс детермінації розрахункових та експериментальних значень дійсного радіуса кочення становить $\eta^2 = 0,98$ для передніх та $\eta^2 = 0,99$ для задніх коліс, що свідчить про адекватність отриманих розрахункових залежностей.

INTRODUCTION

In most studies concerning the movement of wheel propellers, carried out in the middle of the last century, it was considered a static radius of rolling wheels *(Bekker, 1956; Dwyer et al., 1974)*. However, this approach is valid only for wheels that are not subjected to deformation.

Modern studies of the mechanics of interaction between the drive wheel and the support surface are aimed at improving the technical means and control systems of optimal modes of self-propelled machines movement *(Gray et al., 2016; Taghavifar and Mardani, 2015)*. Such systems require precise measurements and the minimum errors in the calculations. The rolling radius of the wheel is an important parameter because it determines the interaction of the wheel with the support surface when converting engine power

into traction. At present, there is no single approach to determining the actual rolling radius of pneumatic wheels during the movement of self-propelled machines.

In the study (*Upadhyaya et al, 1998)*, while testing of agricultural power units traction properties in terms of tires interaction with the soil, it was noted that it was necessary to determine the actual rolling radius of the wheel. The authors consider the possibility of determining the actual rolling radius of the wheel on the basis of testing the rolling self-propelled machine on different soil background. It was found that there was a difference in the values of the wheel rolling radius depending on the presence of traction load and its absence.

It was also investigated the process of rolling the drive wheel with a pneumatic tire on the ground that is deformed (*Kiss P, 2003)*. Based on the conducted researches, three wheel rolling radii are allocated, namely: kinematic radius which arises as a result of existence of slipping (sliding) of a wheel; kinetic radius which is calculated with a ratio of a torque and the reduced movement resistance force of a wheel and geometrical radius – as a distance between the wheel centre and the bottom part of a tire. The author notes the discrepancy and interdependence of this radius.

In the study *(Hamersma et al, 2016)* theoretical approaches were considered and experimental studies were carried out to determine the kinematic and kinetic radii using modern measuring instruments. The discrepancy between the experimentally obtained radius and the static radius of the wheel was found. The authors presumed the possibility of using the static radius of the wheel to perform simulation of changes in the interaction of the wheel with the support surface.

Those highlighted in the methodological approaches of the works done by *Kiss P (2003); Hamersma et al (2016),* for determining the rolling radius of the wheel, allow solving the problems of interaction between the wheel and the ground with the corresponding errors, but for the widespread use these approaches require further improvement. Taking into account the nature of the relationship between the wheelset, wheel rotation and the formation of the traction force *(Golub et al, 2017)*, it was proposed to carry out calculations using one real wheel rolling radius.

To date, a certain number of studies based on empirical dependences obtained under different conditions of interaction between the drive wheel and the support surface have been carried out.

According to *Jazar (2017)*, the actual rolling radius of the wheel is proposed to be calculated as follows:

$$R_D = \frac{2}{3} R_u + \frac{1}{2} R_l \tag{1}$$

where R_D – the actual rolling radius of the wheel, m; R_u – the radius of the wheel without load, m; R_l – the radius of the loaded wheel, m.

In the work *(Pauwelussen et al., 2007)*, the actual rolling radius of the wheel is proposed to be determined by semi-empirical dependence:

$$R_D = R_U - \rho_0 \left[D \arctan\left(B \frac{\rho}{\rho_0} \right) + E \frac{\rho}{\rho_0} \right] \tag{2}$$

where ρ – the actual deflection of the tire, m; ρ_0 – the deflection of the tire at rated load, *B, D, E* – the design parameters of the tire, characterizing the parameters of the tire associated with the nature of deformation of the tire under load, relative units.

In the paper *(Wilson et al., 2011)*, to determine the actual rolling radius depending on the function of drive torque, load, and pressure, it was proposed the dependence based on empirical coefficients:

$$R_D = R_U - \lambda^* \left[1 - (1 - W / W^*) p / p^* \right] T \tag{3}$$

where W – vertical load on the wheel, N; p_W – wheel pressure, kPa; T – torque applied to the wheel, N m; λ^*, W^*, p^* – the empirical factors of the tire longitudinal elasticity, load, and pressure, respectively.

The use of these dependencies, as well as similar ones, make it possible to perform an approximate calculation of the change in the actual rolling radius of the wheel, but in practical use can lead to significant errors.

In their work, *Ryan and Bevly (2012)*, on the basis of application of modern GPS technologies, authors considered possibility of application of operational control of pressure in the tire on the basis of change of the actual rolling radius. The actual rolling radius is proposed to be determined on the basis of the ratio of the vehicle linear velocity and the wheel angular velocity. This approach makes it possible to record the change in radius only in the absence of a change in torque and the absence of wheel slip. In real conditions, there is

always a slip, variable deformation due to the reduced torque and wheel slip. Testing of the similar methodology for determining the actual rolling radius is provided in the paper *(Sabatini et al., 2017)*. In this case, the linear velocity was determined using the GPS sensor, and the angular velocity – with the help of the wheel rotation sensor. The analysis showed a high coincidence between the measured speed of movement with the help of GPS system and calculated based on measurements of the wheel angular speed at uniform motion. The results obtained allow us to assert the possibility of using the proposed method to estimate the change in the real radius of the wheel rolling at constant motion.

The study *(Taghavifar and Mardani, 2014)* provides theoretical and experimental aspects of occurrence of the drive wheels slipping when loading the vehicle. The authors conclude that there is a paradigm of wheel slipping control depending on its load and operating conditions. To control driving wheels slipping, it is substantiated the necessity of creating an algorithm for parallel control for an instant tire rolling radius and the angular velocity of the wheel.

Considering the relevance of determining the actual radius of the wheel, a number of methods for its experimental determination by measuring the wheel angular velocity of rotation were developed. Thus, in *(M'Sirdi et al, 2008)* ABS sensors were used to experimentally determine the wheel speed. At a given speed and when measured using a laser ruler of the wheel radius, it was determined the actual stiffness of the tire.

It was also provided the simulation of the wheel radius change at the vehicle speed in the range from 21 to 22 m/s *(Tannoury et al, 2011)* taking into account the angular velocity, which ranged from 70 to 81.48 rad/s. On the basis of this, the change in the actual wheel radius, which ranged from 30 to 27 cm depending on the ratio of the linear and angular wheel speed, was determined.

The application of a sensitive electronic system for determining the change in the position of the centre of mass is proposed *(Huang and Wang, 2013)*. This made it possible to fix the deformation of the wheel depending on the applied dynamic load. This approach makes it possible to determine the stiffness of the wheel on the basis of changes in the actual radius of the wheel.

The analysis of the studies *(M'Sirdi et al, 2008; Tannoury et al, 2011; Huang and Wang, 2013*) shows the potential application of different methods to determine the wheel slip, which allows to indirectly draw conclusions about the change in the actual rolling radius of the wheel. The practical value of the application of the analyzed methods can be obtained only in the case of determining the value of the real instantaneous rolling radius, but it is necessary to set the initial value of the real rolling radius.

Investigating the change in the kinematic and power characteristics of a pneumatic wheel in slipping motion *(Rubinstein et al., 2018)*, it is proposed to determine the instantaneous and average rolling radius on the basis of the covered distance and the number of the wheel turns. It is proposed to measure the covered distance using a separate additional measuring wheel. However, a significant drawback of the use of an additional measuring wheel is the need to take into account the slip during its movement, which will depend on the rolling speed and contact interaction with the support surface.

The method of determining the wheel slipping based on the ratio of the linear and angular velocities of the wheel is given in *(ASABE Standards, 2013)* but it does not provide the parameters of the initial rolling radius of the wheel. While studying the rolling radius of the wheel of an agricultural tire with different density of the soil, it was made the assumption of the existence of the wheel initial rolling radius, which corresponds to a certain initial value of the wheel slipping *(Rubinstein et al., 2018)*. The actual rolling radius of the wheel is determined from the wheel initial rolling radius and the inverse ratio of the initial and final slipping values. On the basis of theoretical and experimental studies it is concluded that the best criterion for determining the wheel initial rolling radius is the condition of the absence of traction force on the wheel.

The analysis of existing publications showed the absence of a unified approach and methodology in determining the actual radius of the wheel rolling during the interaction of the wheel with the support surface. It should also be noted the diverse influence of many parameters of the interaction of the wheel and the bearing surface on the actual radius of the wheel rolling. The inability to determine the actual rolling radius leads to significant errors in the interpretation of experimental and theoretical studies of wheel operation. Setting the actual rolling radius of the wheel will determine the pulling force and slipping of the wheel. Clarification of the method for determining the initial rolling radius of the pneumatic wheel, depending on its design parameters, is an urgent scientific task. The use of modern technological devices for measuring linear and angular velocity at a known initial rolling radius of the wheel will allow determining the instantaneous rolling radius with high accuracy.

The aim of the research is to substantiate the method of determining the actual rolling radius of pneumatic drive wheels of self-propelled machines and its experimental determination.

To achieve the goal, the following tasks were solved:

– to substantiate the conditions and methods for determining the initial radius of the wheel;

– to develop a method for calculating the actual rolling radius of the wheel when deformed by a vertically applied load;

– to perform an experimental determination of the change in the actual rolling radius of the drive wheels of self-propelled machines from changes in the air pressure inside the tire.

MATERIALS AND METHODS

When substantiating the method and determining the initial and actual rolling radius of the drive wheels, the geometric modeling of pneumatic wheel deformation was used. During the movement of wheeled tractors, cars and other self-propelled machines, the deformation of the wheel tires occurs due to the action of the reduced vertical load and the action of the wheel torque. The research was made under the condition of the wheel without applying drive torque. Due to the deformation of the wheel tires, the actual distance covered by the wheel is less than the one the wheel would have covered in the absence of tire deformation. Thus, wheel deformation contributes to the overall wheel slipping.

Most researchers consider the slipping phenomenon as the ratio of the difference between the linear and the real speed of the wheel to the linear one, or the ratio of the difference between the possible and the covered distance to the possible one:

$$\delta = \frac{\omega R_K - V_D}{\omega R_K} = \frac{2\pi R_K n - S_D}{2\pi R_K n} \quad (4)$$

where:

δ – the coefficient slipping, relative units;

V_D– the actual speed, m/s;

ω – the angular velocity of the drive wheel, rad/sec;

R_K – the driving wheel rolling radius, m;

n – the number of turns made by the wheel per unit of time, turns per second;

S_D – the actual distance covered by the wheel for a certain number of the wheel turns, m.

Pneumatic tire of the power unit wheel in contact with the support surface is subjected to the initial deformation from the action of vertical loads of the tractor weight. Since the vertical load on the pneumatic tire can be considered conditionally constant, this state of the deformed wheel can be considered as the initial and must be taken into account when determining the actual initial radius of the wheel rolling. According to the analysis of the literature, the distance from the wheel centre of rotation to the bearing surface of the loaded wheel is not the actual radius of rotation of the wheel and is not suitable for calculations. The actual radius of rotation of the deformed wheel was determined based on the assumption of the existence of the deformed wheel slipping relative to the free undeformed state.

Mathematically, slipping was determined as the difference between the arc length, which is limited by the central angle based on the deflection chord of the wheel tire, and the longest chord of the deflection of the wheel tire, as follows (Fig. 1):

$$\delta_G = \frac{2\pi}{\alpha}\left(\frac{\left(\alpha R - 2R\sin\frac{\alpha}{2}\right)}{\alpha R}\right) = \left(1 - \frac{2}{\alpha}\sin\frac{\alpha}{2}\right) = \left(1 - \frac{L}{\alpha R}\right) = \left(1 - \frac{R_D}{R}\right) \quad (5)$$

where:

δ_G – the wheel slipping, relative units;

R – the initial radius of the wheel rolling, m;

α – the central angle limiting the chord of the wheel tire deflection, rad.

L – the length of the chord formed by the deflection of the wheel tire, m, we obtain:

R_D – the actual radius of the deformed wheel rolling, m.

The actual radius of the deformed wheel was determined as follows:

$$R_D = \frac{L}{\alpha} = \frac{L}{2\arcsin\frac{L}{2R}} \quad (6)$$

The length of the chord in contact with the wheel bearing surface can be easily determined with the help of experimental measurements. It is more difficult to determine the initial radius of the wheel, as the shape and deformation of the wheel are set by design features of the wheel and tread.

Since the initial actual rolling radius is specified by the applied vertical load, the initial radius was considered as the state of the wheel when the tread deformation is caused by the wheel's own weight.

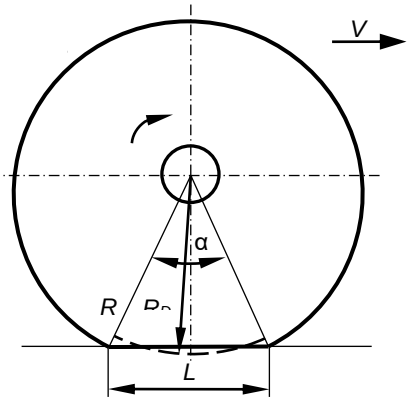

Fig. 1 - A simplified geometric interpretation of the deformation process of the wheel tire

When observing the wheel in the free state, it can be noticed that the cross-section radius is variable. The radius of the wheel in the free state decreases from the centre of the tread to the outer edge. When the wheel is loaded with its own weight, the tread is deformed in the spot of contact with the support surface. The nature of the tread deformation determines the rigidity of the pneumatic tire frame and the internal pressure in the tire.

In this case the change in the radius of the wheel caused by the load of its own weight was determined as follows:

$$\Delta r = \frac{(l_C - l_K)k_{DP}}{2\pi} \tag{7}$$

where:

Δr – reducing the wheel radius relative to the centre of the tread and its edge in cross section, m; l_C – the wheel length in the middle of the tread, m; l_K – the length of the wheel along the edge of the tread, m; k_{DP} – the coefficient of stiffness of the tire, which determines the deformation of the tire in the longitudinal and transverse directions, relative units.

Considering the equation (7), the initial radius of the wheel was defined as follows:

$$R = R_C - \Delta r = \frac{l_C}{2\pi} - \frac{(l_C - l_K)k_{DP}}{2\pi} = \frac{l_C(1-k_{DP}) + l_K k_{DP}}{2\pi} \tag{8}$$

where:

Rc – the radius of the middle of the wheel tread in the free state, m.

The actual radius of the deformed wheel was defined as follows:

$$R_D = \frac{L}{2\arcsin\dfrac{L\pi}{l_C(1-k_{DP}) + l_K k_{DP}}} \tag{9}$$

An experimental study of changes in the geometric parameters of the contact spot of John Deere series 7130 tractor tires due to changes in tire pressure was performed. In experimental studies, the tractor was equipped with front Goodyear Super Traction Radial 14.9 R24 and rear Firestone Radial 800 460/85 R38 tires.

The length of the tire circle in the centre and the edge of the tread was determined at a given tire pressure for the raised wheel (in the absence of load).

The chord of the wheel contact zone with the support surface under the load of the tractor weight was measured at different tire pressures.

To validate the reliability of the obtained theoretical dependences, an experimental verification of the change in the actual rolling radius of the tractor wheels was performed at the tire pressure changes and at moving along a horizontal concreted site. When determining the actual rolling radius, the necessary tire

pressure was set and the rolling was carried out at a distance of 10 complete turns of the wheel. During the rolling, it was recorded the distance traversed by the wheel during one turn and total covered distance.

After performing 10 turns, averaging of the distance covered by the wheel in one turn was performed. On the basis of the average distance covered in one turn of the wheel, it was determined the actual rolling radius of the wheel. Based on the obtained values of the real rolling radius and the initial radius of the wheel, slip coefficients at different tire pressures were calculated.

The reliability of the theoretically and experimentally obtained real rolling radius was provided by comparing the wheel slipping relative to the initial radius of the wheel.

RESULTS

To determine the actual rolling radius, the necessary parameters of the front and rear wheels were experimentally measured. A change in the tread lengths in the free state of the wheel with a change in pressure is obtained. At the accepted values of the tire stiffness coefficients, the initial radius of the wheel is calculated at the corresponding pressure in the wheel. The calculation of the actual rolling radius and the corresponding wheel slipping is also performed. Experimental and theoretical parameters when changing the front wheel pressure are performed in table 1, and for the rear wheel – in table 2.

Table 1

Experimental and theoretical parameters of the front wheel

The name and units of measurement	Symbol	Wheel pressure, atm					
		1	1.2	1.4	1.6	1.8	2
Length in the middle of the tread, m	l_C	3.875	3.88	3.88	3.885	3.885	3.89
Length at the protector edge, m	l_K	3.75	3.747	3.748	3.755	3.755	3.753
Stiffness coefficient, relative units	k_{DP}	0.92	0.91	0.9	0.89	0.865	0.845
Initial radius, m	R	0.5984	0.5982	0.5986	0.5999	0.6004	0.6006
Length of the contact zone chord, m	L	0.383	0.349	0.33	0.32	0.314	0.309
Calculated real rolling radius, m	R_D	0.5879	0.5896	0.5909	0.5926	0.5934	0.5939
Slipping, %	δ_G	1.759	1.454	1.295	1.21	1.162	1.124
Experimental real rolling radius, m	R_{DS}	0.588	0.59	0.591	0.593	0.593	0.594
Slipping, %	δ_{GS}	1.755	1.449	1.295	1.215	1.154	1.119

The dependences of the length of the wheel contact zone chord with the support surface formed by the deflection of the wheel tire on the air pressure in the tires were obtained (Fig. 2). The graph shows a tendency to reduce the length of the contact zone of the deformed wheel tire with increasing air pressure in the tires.

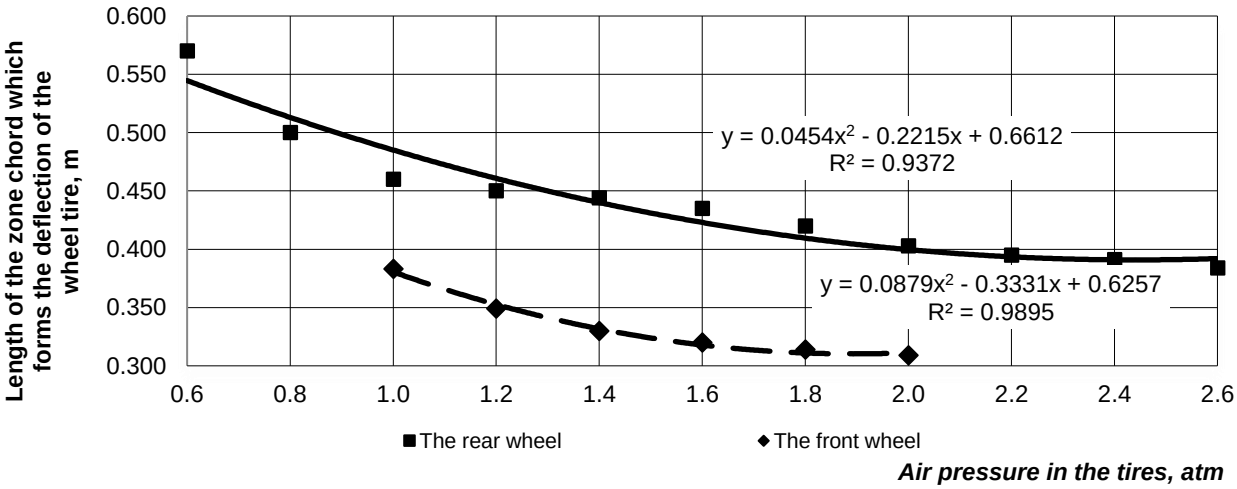

Fig. 2 - The dependence of the length of the zone chord (the length of the deformed wheel tire imprint), which forms the deflection of the wheel tire from the air pressure in the tires

Table 2

Experimental and theoretical parameters of the rear wheel

The name and units of measurement	Symbol	Wheel pressure, atm										
		0.6	0.8	1	1.2	1.4	1.6	1.8	2	2.2	2.4	2.6
Length in the middle of the tread, m	l_C	5.483	5.484	5.485	5.485	5.495	5.495	5.5	5.505	5.51	5.51	5.51
Length at the protector edge, m	l_K	5.253	5.253	5.253	5.253	5.254	5.254	5.255	5.254	5.255	5.26	5.26
Stiffness coefficient, relative units	k_{DP}	0.615	0.6	0.595	0.545	0.495	0.45	0.42	0.37	0.365	0.36	0.355
Initial radius, m	R	0.85	0.85	0.851	0.852	0.855	0.857	0.858	0.861	0.862	0.862	0.862
Length of the contact zone chord, m	L	0.57	0.5	0.46	0.45	0.444	0.435	0.42	0.403	0.395	0.391	0.384
Calculated real rolling radius, m	R_D	0.833	0.838	0.840	0.842	0.845	0.847	0.850	0.853	0.854	0.855	0.855
Slipping, %	δ_Γ	1.938	1.477	1.244	1.185	1.145	1.094	1.014	0.927	0.888	0.869	0.838
Real rolling radius, m	R_{DS}	0.833	0.837	0.839	0.842	0.845	0.847	0.849	0.853	0.854	0.854	0.855
Slipping, %	$\delta_{\Gamma\Sigma}$	1.945	1.463	1.268	1.173	1.144	1.083	1.017	0.949	0.899	0.872	0.839

The initial radius of the wheel depending on the air pressure in the tire, calculated by the equation 8, is shown in Fig.3. The graph shows that the initial radius of the wheel increases with increasing air pressure in the tire.

Fig.4 and Fig.5 demonstrate the results of calculation and experimental measurement of changes in the actual rolling radius of the front and rear wheels, respectively, depending on changes in air pressure in the tire. The calculated real rolling radius is determined based on the length of the wheel contact zone chord and the initial radius of the wheel according to the equation 9 for the corresponding tire pressure in the wheel.

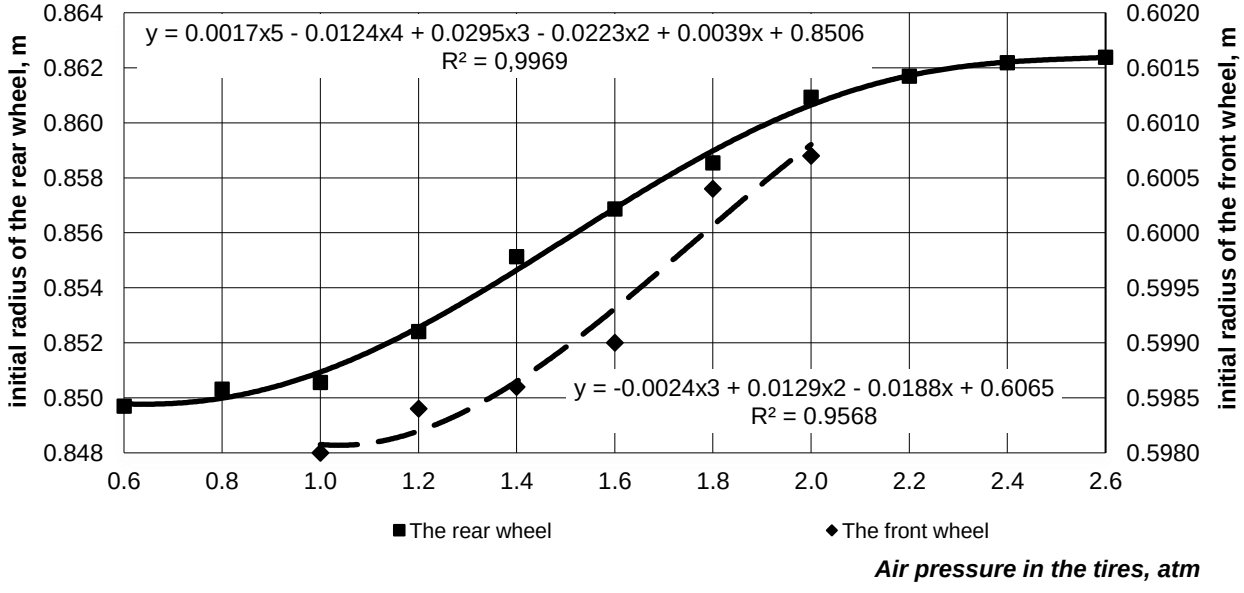

Fig. 3 - The dependence of the initial radius of the wheel, considering the deformation of the tread caused by its own weight

Analysis of the obtained dependences Fig. 4 and Fig. 5 indicates an increase in the real rolling radius with increasing air pressure in the tire. For the front wheels with an increase in pressure from 1 to 2 atm, the change in the actual rolling radius was about 7 mm for the rear wheel; the change in the actual radius was about 21 mm with a change in pressure from 0.6 to 2.6 atm. The determination index of the calculated and experimental data was $\eta^2 = 0.98$ for the front and $\eta^2 = 0.99$ for the rear wheels.

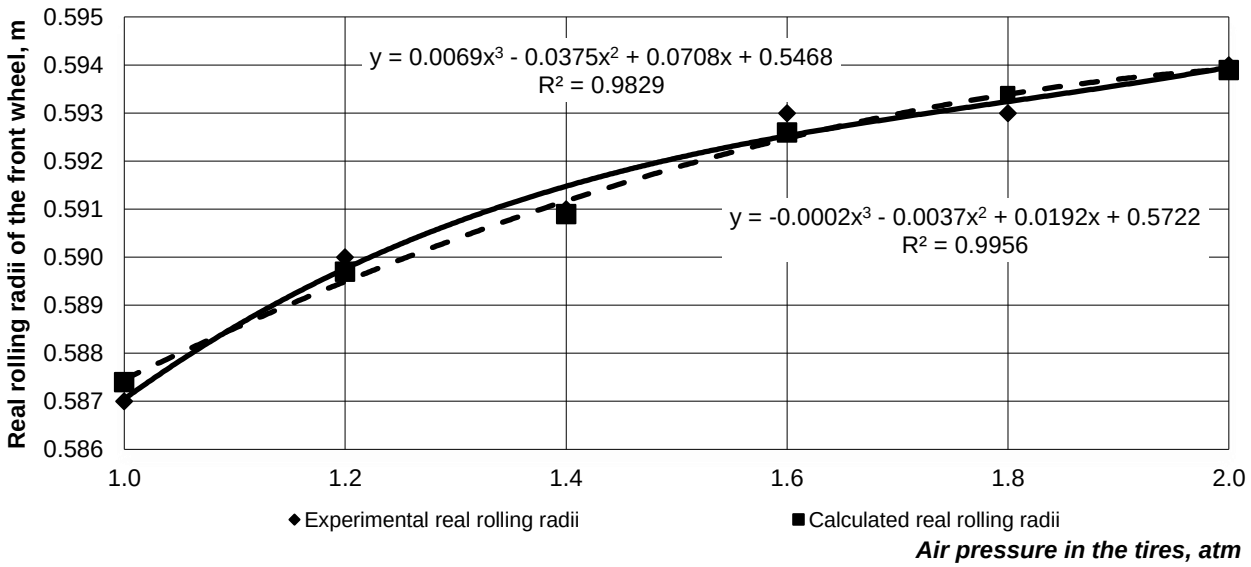

Fig. 4 - Dependences of the calculated and experimental real rolling radius of the front wheel on changes in tire air pressure

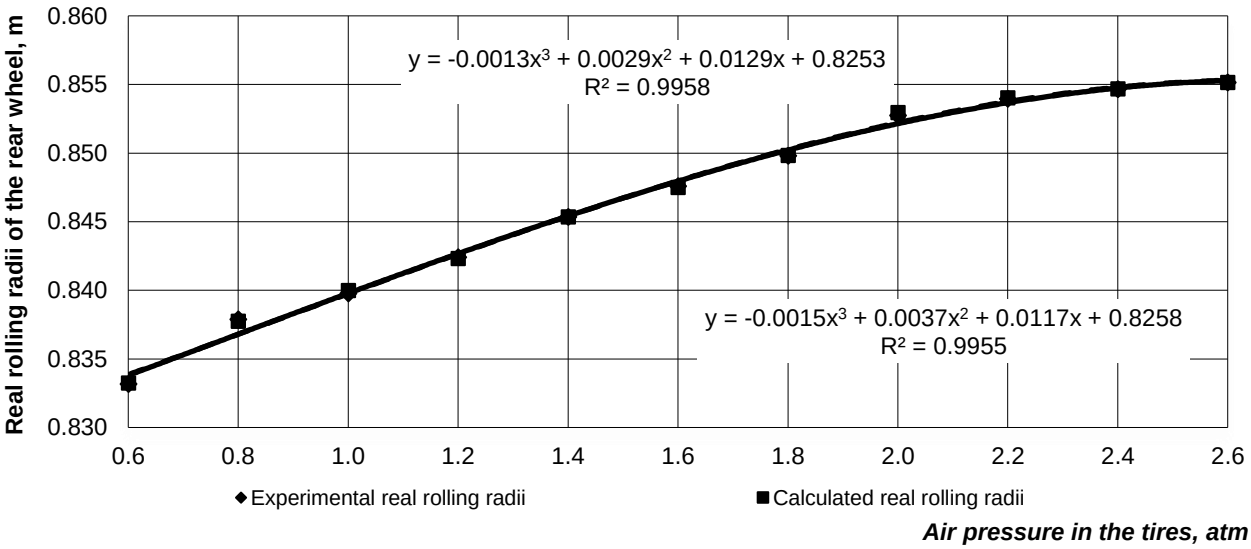

Fig. 5 - Dependences of the calculated and experimental real rolling radius of the rear wheel on changes in tire air pressure

It is also provided the calculation of the wheel slipping when changing the internal pressure of the tire (Fig. 6, 7).

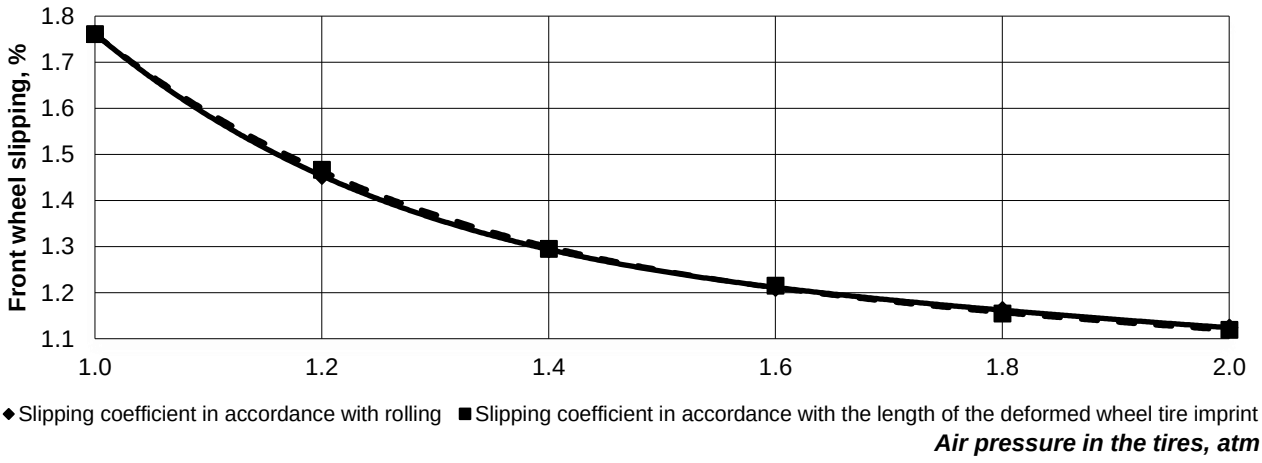

Fig. 6 - The dependence of the front wheel slipping on air pressure in tires

Thus, the calculated slipping has a value from 1.94 to 0.83% for the rear wheels, and from 1.12 to 1.76% for the front wheels. The value of the wheel slipping decreases as the air pressure in the tires increases, which is explained by a decrease in the length of the tire contact zone chord and an increase in the actual radius of rotation of the wheel relative to the initial one.

The high level of coincidence between the calculated and experimental dependences for determining the wheel slipping indicates the adequacy of the proposed method for determining the initial radius of the wheel and the actual rolling radius.

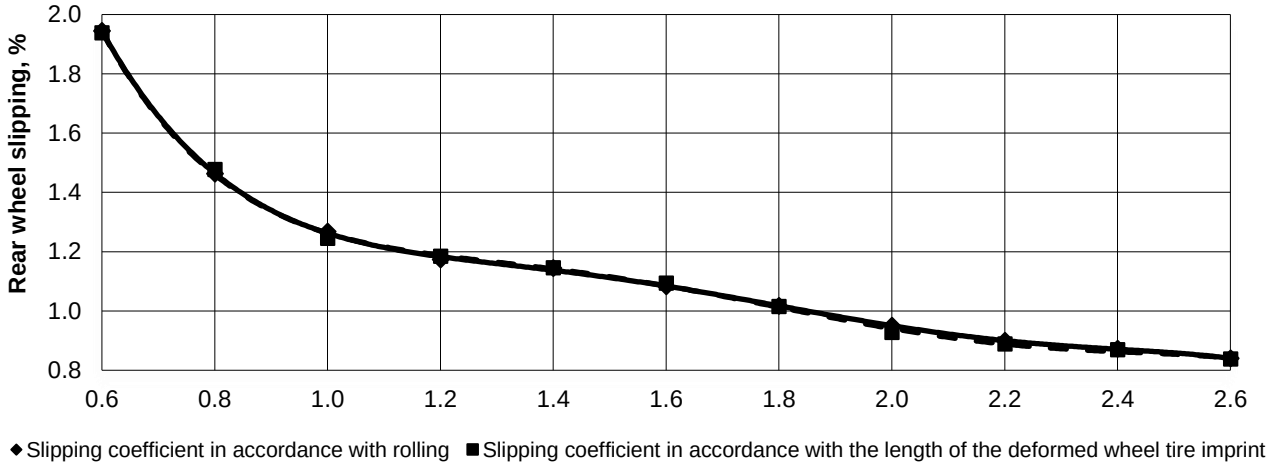

Fig. 7 - The dependence of the rear wheel slipping on air pressure in tires

As a result of the research, the principles of determining the initial radius of the wheel based on which it is possible to determine the actual radius of the wheel rolling are substantiated. The high level of coincidence between the calculated and experimental values of the actual wheel radius and wheel slipping indicates the adequacy of the developed methods and dependencies for practical application.

The obtained results allow estimating the effect of wheel deformation under the influence of vertical load (the weight of the power unit) on the actual wheel rolling radius and the wheel slipping. As long as the vertical load is constant, than the actual rolling radius and the slipping while wheel rolling can be taken for the initial state of the wheel. The initial state of the wheel allows evaluating the impact of other parameters on the wheel rolling performance, which creates the prerequisites for the development of a control system for the operation of wheel systems of self-propelled machines.

Further research is advisable to continue in the direction of determining the effect of torque on the change in wheel rolling and driving wheel slipping. The other important issue for further research is determining the nature of the stiffness coefficient of the pneumatic tire tread and determining the impact of the wheel tire design parameters on the deformation of the tread and the wheel frame.

CONCLUSIONS

1. Determining the initial radius of the wheel allows calculating the actual rolling radius of the wheel, taking into account the geometric parameters of wheel deformation in the area of contact with the support surface. The coincidence of the dependences of wheel slipping on the change of air pressure in the tire, obtained based on the calculated and experimentally determined real rolling radius, suggests that the proposed model for determining the initial radius of the wheel is adequate.

2. On the basis of the geometric parameters of the contact zone at the interaction between the wheel and the support surface, an expression for determining the actual radius of the wheel rolling is obtained. Comparison of the calculated and experimentally obtained real rolling radius of the wheel allows us to assert the adequacy of the applied technique and the obtained dependence for determining the actual rolling radius. The determination index of the calculated and experimental data is η^2 = 0.98 for the front and η^2 = 0.99 for the rear wheels.

3. The studies proved an increase in the actual rolling radius and a decrease in wheel slipping with increasing air pressure in the tire. Thus, for the rear wheel, at an increase in pressure from 0.6 to 2.6 atm, an increase in the rolling radius by 21 mm, and a decrease in the slipping from 1.94 to 0.83% are observed. For the front wheel, when the pressure changes from 1 to 2 atm, the rolling radius increases by 7 mm and the

wheel slipping decreases from 1.76 to 1.12 %. The obtained results allow evaluating the slipping of the drive wheels of power units in accordance with the air pressure in the tires and the parameters of interaction with the support surface.

REFERENCES

[1] Bekker M.G., (1956), *Theory of land locomotion: the mechanics of vehicle mobility*, Ann Arbor: The Univ. Michigan Press., 522 p., USA;

[2] Dwyer M.J., Comely D.R., Evernden D.W., (1974), The field performance of some tractor tyres related to soil mechanical properties, *Journal of Agricultural Engineering Research*, Vol. 19, ISSN: 00218634, pp. 35–50;

[3] Golub G., Chuba V., Kukharets S., (2017), Determining the magnitude of traction force on the axes of drive wheels of self-propelled machines, *Eastern European Journal of Enterprise Technologies*, Vol. 4 (7), ISSN: 17293774, pp. 50-56;

[4] Gray J.P., Vantsevich V.V., Paldan J., (2016), Agile tire slippage dynamics for radical enhancement of vehicle mobility, *Journal of Terramechanics*, Vol. 65, ISSN: 00224898, pp. 14-37;

[5] Hamersma H.A., Botha T.R., Schalk Els.P., (2016), The dynamic rolling radius of a pneumatic tyre on hard terrains, *18th International Conference of the ISTVS, International Journal of Vehicle Systems Modelling and Testing*, Vol 11 (3), ISSN: 17456436, pp. 234-251;

[6] Huang X., Wang J., (2013), Centre of gravity height real-time estimation for lightweight vehicles using tire instant effective radius, *Control Engineering Practice*, Vol. 21 (4), ISSN: 09670661, pp. 370-380;

[7] Jazar R. N., (2017), *Vehicle dynamics: Theory and application*, Springer, Cham, ISSN: 978-3-319-53440-4, 985 p, USA;

[8] Kiss P., (2003), Rolling Radii of a Pneumatic Tyre on Deformable Soil, *Biosystems Engineering*, Vol. 85, ISSN: 15375110, pp. 153-161;

[9] M'Sirdi N.K., Rabhi A., Fridman L., Davila J., Delanne Y., (2008), Second order sliding-mode observer for estimation of vehicle dynamic parameters, *International Journal of Vehicle Design,* Vol. 48, ISSN: 01433369, pp. 190-207;

[10] Pauwelussen J.P., Dalhuijsen W., Merts M., (2007), *Tyre dynamics, tyre as a vehicle component, Virtual Education in Rubber Technology (VERT)*. HAN University, http://laroverket.com/wp-content/uploads/2015/03/tyre_as_car_component.pdf;

[11] Rubinstein D., Shmulevich I., Frenckel N., (2018), Use of explicit finite-element formulation to predict the rolling radius and slip of an agricultural tire during travel over loose soil, *Journal of Terramechanics*, Vol. 80, ISSN: 00224898, pp. 1-9;

[12] Ryan J., Bevly D., (2012), Tire radius determination and pressure loss detection using GPS and vehicle stability control sensors, *IFAC Proceedings Volumes 8th IFAC Symposium on Fault Detection, Supervision and Safety of Technical Processes*, Vol 8 (1), ISSN: 14746670, pp. 1203-1208;

[13] Sabatini S., Formentin S., Panzani G., Santos J.D.-J.L., Savaresi S.M., (2017), Motorcycle tire rolling radius estimation for TPMS applications via GPS sensing, *1st Annual IEEE Conference on Control Technology and Applications,* ISBN: 978-150902182-6, pp. 1892-1897;

[14] Taghavifar H., Mardani A., (2014), Applying a supervised ANN (artificial neural network) approach to the prognostication of driven wheel energy efficiency indices, *Energy*, Vol. 68, ISSN: 03605442, pp. 651-657;

[15] Taghavifar H., Mardani A., (2015), Net traction of a driven wheel as affected by slippage, velocity and wheel load, *Journal of the Saudi Society of Agricultural Sciences*, Vol. 14, 167–171;

[16] Tannoury C. El., Plestan C., Moussaoui F., Romani N., (2011), Tyre effective radius and vehicle velocity estimation: A variable structure observer solution, *Eighth International Multi-Conference on Systems, Signals and Devices.*, ISBN: 978-1-4577-0413-0, pp. 1-6;

[17] Upadhyaya S., Chancellor W. Wulfsohn D., (1988), Sources of variability in traction data, *Journal of terramechanics*, Vol. 25 (4), ISSN: 00224898, pp. 249-272;

[18] Wilson T., Siero M., Kopchick C., Vantsevich V., (2011), Rotational Velocities and Tire Slippages, *SAE Technical Paper*, ISSN 0148-7191, 2011-01-2157;

[19] ***ASABE Standards, (2013) General Terminology for Traction of Agricultural Traction and Transport Devices and Vehicles. ASABE Standards s296.5.

MATHEMATICAL MODEL FOR THE EVOLUTION OF *Chlorella Algae*
/
MODEL MATEMATIC PENTRU EVOLUȚIA ALGELOR CHLORELLA

Mat. Cârdei P.[1)], Ph.D. Eng. Nedelcu A.[1)], Ph.D. Eng. Ciuperca R.[1)]
[1)] National Institute of Research-Development for Machines and Installations Designed to Agriculture and Food Industry - INMA Bucharest / Romania
Tel: +40726142837; E-mail: petru_cardei@yahoo.com

Keywords: *mathematical, model, evolution, algae, Chlorella*

ABSTRACT

The paper presents an example of a mathematical model for algal cultures. The model presented is based on an elementary growth equation (more generally, evolution or dynamic, because it includes the phenomenon of decreasing population), represented by a first-order differential equation, over which are grafted (according to the influence parameters model, for example used for the USLE modelling of soil erosion is used), as factors of influence, the parameters that influence the evolution of the algae. We have given some examples of simulation of algal evolution processes and the possible applications, advantages and disadvantages of the model are suggested. References are made and conclusions are drawn on the extremely important role played by experiments both in the construction and in the validation of the mathematical models of the living systems (bio-systems) evolution phenomena. The model is easy to transfer and generalize to crop plants, as well as other bio-systems.

REZUMAT

Lucrarea prezintă un exemplu de model matematic pentru culturile de alge. Modelul prezentat se bazează pe o ecuație elementară de creștere (mai general, evoluție sau dinamică, deoarece include fenomenul de scădere a populației), reprezentat de o ecuație diferențială de ordinul întâi, peste care sunt altoiți (conform modelului parametrilor de influență, folosit spre exemplu, in modelul USLE al eroziunii solului), ca factori de influență, parametrii care influențează evoluția algelor. S-au prezentat câteva exemple de simulare a proceselor de evoluție a algelor și s-au sugerat posibilele aplicații, avantaje și dezavantaje ale modelului. S-a făcut referire și s-au tras concluzii cu privire la rolul extrem de important pe care îl au experimentele atât în construcția, cât și în validarea modelelor matematice ale fenomenelor evoluției sistemelor vii (biosisteme). Modelul este ușor de transferat și generalizat la plantele de cultură, precum și la alte bio-sisteme.

INTRODUCTION

The mathematical modelling of algal growth process is generally approached very often in the literature. Under these conditions, it's both hard and easy to be original. It is very difficult to fundamentally modify a mathematical model or build a new one. It is easy to operate a simple change, thus obtaining a new model, starting from an old one. In both cases, validation is required. However, the most difficult experimental stage is the previous one, and simultaneously the mathematical model.

In the dynamic mathematical modelling of algal crops development, a fairly clear distinction can be made between models that work with a single differential equation of growth, (*Stemkovski et.al., 2016; Thornton et al. 2010; Yang JSh et al. 2011; Yang Zh et al., 2017*), the rest of the parameters being loads or control functions, and respectively, the models working with a system of differential equations, (*Concas et al., 2013; Davidson and Gurney, 1999; Mardlijah et.al., 2017*). In the latter case, some of the process's influence parameters, or all, become unknown functions of the differential equations system, but they also have charging and / or elimination components.

From an experimental point of view, it is simpler to construct and validate a mathematical model in the first category. When experimental possibilities are lower or at an early stage, a simple model from the first category is therefore more appropriate. For these reasons, the experimental model presented in this paper is part of the first category. The development can be done after validation, gradually, taking into account the large variety of mathematical models existing in the literature.

MATERIALS AND METHODS

The results presented in this article are based on hypotheses formulated using data and experimental conclusions by *Blinova et.al. (2015)* and *Nedelcu et.al. (2018 a, b)*.

1) General Algal Evolution Model

The mathematical model presented in this paper is an evolutionary model of the *Chlorella vulgaris* algae crop. We call it a model of evolution because it is not only a growth mathematical model; it is a model that can also describe the decline of the algae population, including the death of the algae colony.

The evolution of the algae population is described by a single ordinary differential equation *(Chen Sh et al., 2009; Surendhiran et.al., 2015 and Thornton et al., 2010)*:

$$\frac{dx}{dt} = \mu(t,x) - \delta(t,x) \tag{1}$$

Mathematical models of type (1) are frequent in the literature dedicated to the evolution of living matter and originate in the classical growth model that only shows the growth rate in the right side. If the growth rate is strictly positive, then the population grows monotonous. The origin of this model is found in (*Malthus, 1798*), in the finite form. The logistic form of growth is formulated by *Verhulst (1838)* and *McKendricka & Kesava (1912),* for example. Many contemporary mathematical models retain the fundamental forms of growth or modify them, more or less *Stemkovski et.al. (2016) and Thornton et al. (20100,* for example.
The names, meanings, and measurement units of all model parameters are given in Table 1.

Table 1

Notation, meanings and units of the mathematical model

Notation	Meanings	Units
x	algae concentration in solution	g/l
t	time	hours
x_0	initial value of algae concentration in solution	g/l
t_0	initial time	hours
μ	the growth rate of the algae population	1/hours=hours^{-1}
δ	the decline rate of the algae population	1/hours=hours^{-1}
μ_0	model parameter to be determined experimentally	1/hours=hours^{-1}
δ_0	model parameter to be determined experimentally	1/hours=hours^{-1}
θ	average temperature in the algae crop solution	Celsius degree
co2	time dependence in carbon dioxide concentration in the solution	%
ph	time dependence of pH in the solution	-
cflL	minimum degree of illumination	lux
cflLb	degree of illumination with blue light	lux
cflLr	degree of illumination with red light	lux
pl	wavelength of light	nm
s	time dependence of the solution salinity	g/l
Θ	the function of the temperature influence	-
CO_2	the function of influence of the dissolved carbon dioxide concentration in the solution	-
pH	the function of the algae crop solution pH	-
L	the function of the degree of illumination influence	lux
N	the function of the nutrient concentration in the algae crop solution	-
S	the function of the algae crop salinity influence	-
$\delta_{\lim}$	natural factor of algae growth moderation at reaching a limit concentration	-
$x_{\max}$	maximum algal concentration in solution	g/l
δ_1	model parameter to be determined experimentally	dimensionless

Obviously, the model (1) may become a growth and decrease model, even if only the growth rate is considered, assuming that it can move from negative values to positive values, and possibly return to positive values.

2) The modelling of the process influences by multiplication of separate influences

According to (*Blinova et.al., 2015 and Nedelcu et.al., 2018a, b*), is considered the *hypothesis* that the physical parameters which influenced the algal evolution, are the following: solution temperature variation, variation in the amount of dissolved carbon dioxide in the solution, pH variation of the solution, degree of crop illumination, the amount of nutrients introduced into the solution, the salinity of the solution.

A second *hypothesis* we introduce is the structure by of product, of the growth rate:

$$\mu(t,x) = \mu_0 \cdot x \cdot \Theta \cdot (1 - CO_2) \cdot pH \cdot L \cdot N \cdot S \tag{2}$$

and of the decrease rate:

$$\delta(t,x) = \delta_0 \cdot (1 - pH) \cdot x \cdot \delta_{\lim}(x) \tag{3}$$

where the form of the moderation factor, by ***hypothesis***, is the following:

$$\delta_{\lim}(x) = \begin{cases} 1, if\ x < x_{\max} \\ \delta_1 \cdot \dfrac{x - x_{\max}}{x_{\max}}, if\ x \geq x_{\max} \end{cases} \tag{4}$$

The parameters that influence and form the structure of the growth and decrease rates take values between 0 and 1. These functions, the influence parameters, are defined in the following subchapter.

3) Bump functions

The *bump functions* are functions of one or more real variables, with values in the set of real numbers, which is both smooth (in the sense of having continuous derivatives of all orders) and compactly supported, *Muthukumar, (2016); Thornton et al., (2010), Tu, (2008) and Fry and McManus, (2002),* for example.

In this paper we used *bump functions* to model the action of factors that influence the evolution of algae, particularly Chlorella. The parameterization of curves which is the graph of the bump functions (of a single variable) is given in Figure 1.

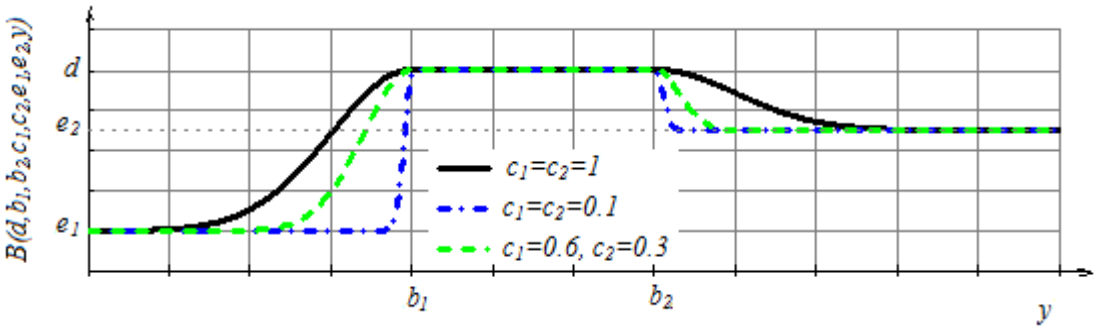

Fig. 1 - Parameterization of bump function, which is used to model the influence of factors involved in the algal evolution process

The phenomenological interpretation of a bump function consists of filtering an optimal zone of influence or, on the contrary, an area unfavourable to the phenomenon. This area is geometrically visible by the constant height *d*, bounded by the abscissa b_1 and b_2. The curve in Figure 1 corresponds to a bump function that models a parameter with only one optimal interval. The linear summation of such functions yields models for influence factors with several optimal ranges. Influence factors must not necessarily be annulled outside the optimum range. Influence factors modelled by *bump functions* can take non-zero values outside the optimum range. Outside of optimal interval, the *bump function*, asymptotically converge to the values e_1 and e_2 (can be, or not be zero).

To define the bump function, first define the Gaussian function:

$$G(p,q,r,s,y) = p \cdot \exp\left(\frac{-(y-q)^2}{2r^2}\right) + s \tag{5}$$

where *p*, *q*, *r* and *s* are parameters and *y* is the real variable. Using the Gaussian function (5), the function of the bump is defined by the formula (6):

$$B(d,b_1,b_2,c_1,c_2,e_1,e_2,y) = \begin{cases} G(d-e_1,b_1,c_1,e_1 y), if\ y < b_1 \\ d, if\ y \in [b_1,b_2] \\ G(d-e_2,b_2,c_2,e_2 y), if\ y > b_2 \end{cases} \tag{6}$$

The bump functions can be extended to forms that are not constant on the centre of optimal range.

4) The final description of the model

Taking into account the observations (in *Blinova et.al., 2015*) regarding the influence of temperature on algae evolution, the function of the temperature influence is defined by the following formula[1]:

$$\Theta(\theta) = B(1,16,27,2,3,0.005,0.05,\theta) \tag{7}$$

Experimental observations in *Blinova et.al., 2015*, lead to assumptions that result in the following influence functions for algae growth:

$$CO2(co2) = 1 - B(0.4,0.015,0.055,0.01,0.01,0.1,0.1,co2) \tag{8}$$

for the CO2 concentration influence function (see also *Mardlijah et.al., 2017; Singh SP and Singh P, 2014*),

$$pH(ph) = B(1,7,9,2,4,-0.5,-0.5,ph) \tag{9}$$

for the pH influence[2] function,

$$L(pl) = cfIL\left[cfILb \cdot B(1,400,500,1,1,0.5,0.5,pl) + cfILr \cdot B(1,600,700,1,1,0.5,0.5,pl)\right] \tag{10}$$

for the light influence[3] function,

$$S(s) = B(1,0.022,0.026,1,1,0.2,0.2,s) \tag{11}$$

for the salinity influence function,

$$N(\chi) = B(1,0.006,0.009,1,2,1,0.0,\chi) \tag{12}$$

for the nutrition influence function. Establishing the nutrient requirement for Chlorella culture requires two essential aspects: the amount of nutrients needed and the nutrient quality. The two aspects can be introduced into the influence function (12), as follows: the limits b_1 and b_2 denote the minimum and maximum values of the feed requirement per algal concentration in the solution, and the value of the constant ceiling d will be expressed according to the load with nutrients and the structure[4] of nutrients administered. The quantitative aspect also requires discussion. The amount of nutrients can be gradually added by progressive loading, depending on the evolution of the biomass concentration in the solution, or it can be discharged into the initial solution at the beginning, taking into account a limit value of the biomass concentration at the time of harvesting. Consideration should be given, in the latter case, to possibilities of nutrient degradation in interaction with the culture medium, and thus losses that can turn into biomass losses at harvest. Also, all these issues need to be discussed considering the use of algae crops (biofuels, food or medication). The final use of harvested biomass dictates the nutrition charge through the final filter of the content in useful substances of the crops. Numerous papers are dedicated to the content of valuable substances from algae, depending on the final use and the adopted cultivation technology, (*Yang JSh et al., 2011; Surendhiran et.al., 2015*).

RESULTS

The mathematical model of evolution of Chlorella algae proposed by the authors is described by equations (1) - (12). This model is complex in the sense that it includes command functions and filters, each with a number of parameters. The complete testing of such a model consumes a lot of time and the results, in detail, would be very bulky. For this reason, only some representative tests, performed on a simplified model, will be given in the results chapter. The simplicity that is made in the tests consists in considering a single rate of "growth", μ, which can be positive (and then the real growth rate) but also negative values, and in this case, the rate of decrease. Simplification can be synthesized by cancelling the parameter δ_0 in the formula (3). Due to this simplification, the asymptotic equilibrium phenomenon, given through the function $\delta_{\lim}$ is also lost.

1) The case of a growth regime with strictly controlled control parameters

[1] The numerical arguments of these filter functions applied by algae to physical fields in the environment or applied by culture technologies may vary depending on the environmental conditions of each of the other filter functions, or the age of the algae colony, for example. Clarifying such behaviours requires very laborious experiences.

[2] To model the influence of pH on algae growth, we recommend, for example, *Ma et.al., 2017*.

[3] For a more precise formulation of the light algae power filter function, results such as those in *Huesemann et.al., 2016*, should be taken into account in the future.

[4] For example, in *https://www.wikihow.com/Grow-Chlorella-for-a-Food-Supplement*, accessed 07.01.2018, a nutrient recipe is given by the authors as optimal. This refers to Chlorella algae grown for food. It is possible to elaborate a quality coefficient that takes maximum value for the optimal concentrations prescribed by the authors for each component.

A first elementary test of the simplified version of the mathematical model (1) - (12) consists in simulating a strictly controlled evolution regime: temperature, dissolved carbon dioxide concentration, pH and salinity, constants, and linear loading with nutrients, as it is specified in the commentary of Figure 2. Five constant illumination regimes, also specified in Figure 2, have been applied.

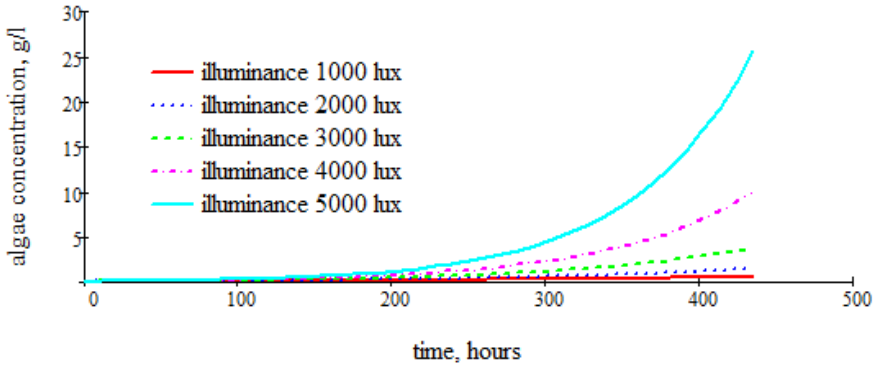

Fig. 2 - The evolution of algal concentration in the solution for a controlled regime: temperature 18 °C, CO_2 - 0.03, pH - 8, progressive loading with nutrients - 0.000001+0.7·t g/l, salinity - 0.023 g/l

It is noted that all the evolution curves of algal concentration in the solution are strictly increasing and preserve the same type of convexity. The curves in Figure 2 are common to growth phenomena, but most experimental results on algae show that their growth curves are closer to logistic growth than exponential growth. Logistic growth curves change the type of convexity in the course of evolution. The effect can also be obtained in model (1) - (12) considering a logistic factor function $\delta_{\lim}$, introduced in the definition of the growth rate, (4).

2) The effect of lowering the pH of the solution

Suppose there is an accidental loss of control of the pH of the solution containing the algae crop, either due to negligence or because of a pollution phenomenon, for example[5].

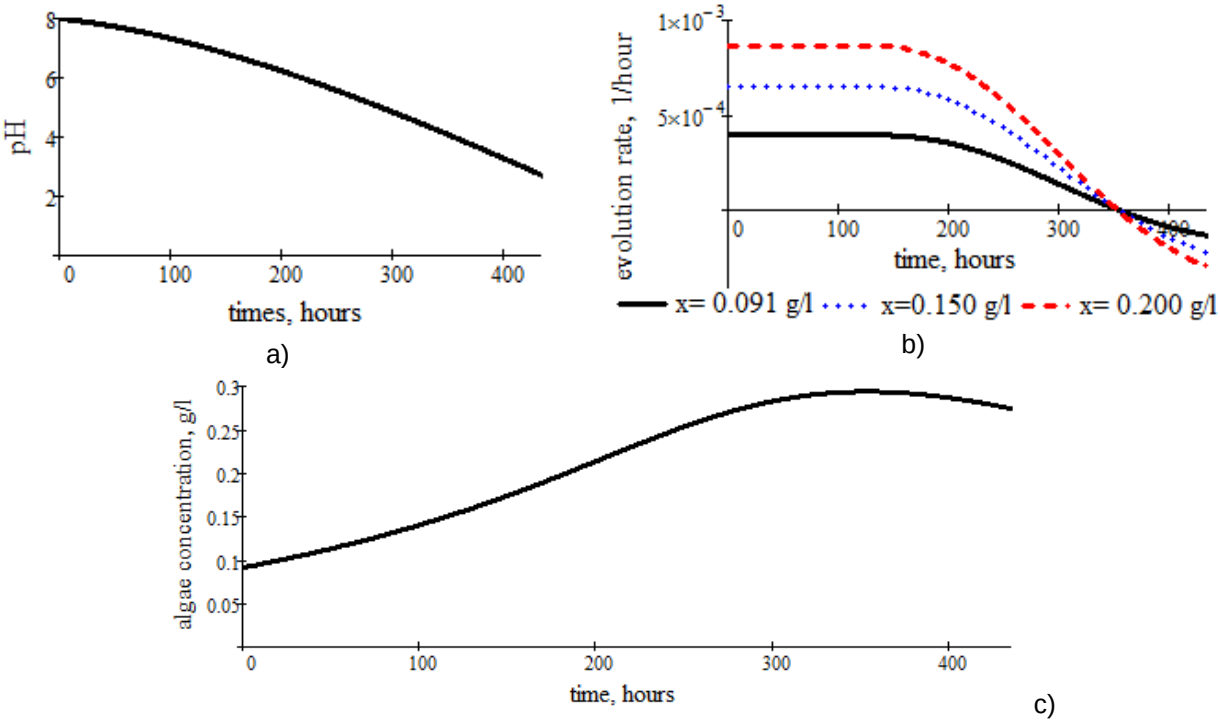

Fig. 3 - Effect of lethal, pH variation on algal concentration in solution

[5] There is also possible an intentional command of the operator, given in order to diminish the algae population, for various reasons: the supportability of the algae density or the qualitative structure of the crop. The problem is that in the case of such processes there are masses of dead algae that can produce positive (in the operator's interest) or negative effects, in which case the dead algal mass should be removed if possible.

The pH variation of the algae-containing solution is based on the scenario described in Figure 3 a). Under these conditions, the pH filter of the algae crop (8) implies the evolution rate of the variation in Figure 3, b). It is noted that there is a time value when the rate of evolution is cancelled regardless of algae concentration. This cancellation is due to the decrease of the pH below a lethal value (solution with unbearable acidity for the algae culture after going through zero, the evolution rate[6] becomes negative and the death process of some of the algae begins. This process is visible in Figure 3, c), in which, starting from the moment of the evolution rate cancellation, the algal concentration variation curve begins to decrease. With the exception of the pH of the algae solution and the illumination, kept constant at 1000 lux, the other control conditions of the process were maintained identical to those specified in the scenario of the first example, conditions specified in the comment in Figure 2.

3) The effect of the thermal variation

In this subchapter, an example of the influence of the thermal field large variations on the algal culture evolution is given. To achieve this aim, we have modified the thermal filter (7) to mark temperature limits beyond which algae may die. The modified thermal filter is given by the formula (13):

$$\Theta(\theta) = B(1,16,27,7,6,-0.5,-0.5,\theta) \tag{13}$$

The temperature dependence of the algae solution is given in Figure 4 a). The small amplitude and high frequency correspond to the variation of the diurnal temperature, and the component with high amplitude of the temperature time dependence corresponds to an accidental variation. This example is inspired by the experiences the processed results of which were exposed in *Nedelcu et.al., 2018b*. In these experiments the thermal control was minimal, applied only in order not to exceed the lethal limits of the algae crop.

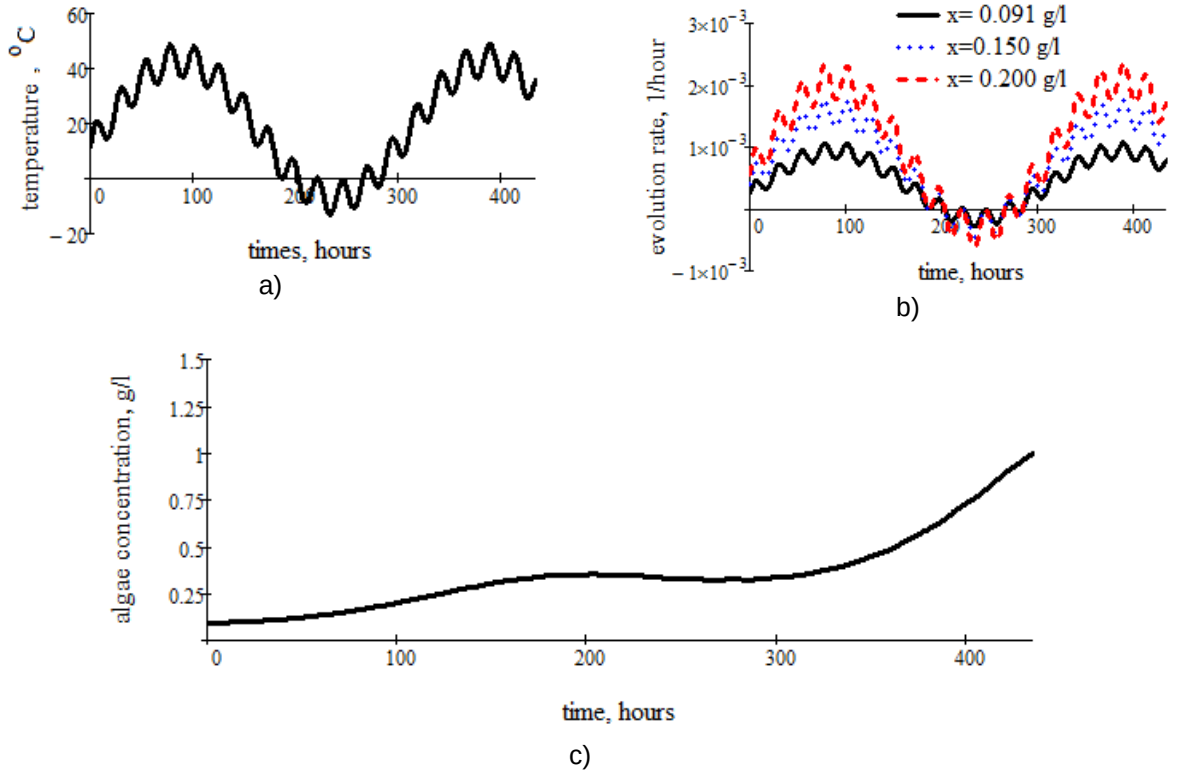

Fig. 4 - Effect of the thermal variation (with random component) on the algae crop biomass concentration

The evolution rate of algae crop varies according to temperature, copying both diurnal and random variation, as it can be seen in Figure 4, b). As we can see, variation in the evolution rate of algae cultures differs for different concentrations of the solution. More precisely, the higher the concentration is, the higher the rate of variation.

[6] In other words, the evolution rate goes from the (positive) state of the growth rate to the (negative) state of the decrease rate.

This topic also deserves an experimental exploration about the existence of a mechanism to limit the growth rate of algal evolution, taking into account the conditions of culture. The consequence of the heat field variation on algae culture can be seen in Figure 4 c).

The growth of the algae population is not monotonous however, even with the simulated accident in the scenario, culture continues to develop. After accidental temperature variation (around 220 hours), a decreasing portion appears immediately, but with a low intensity and after that population growth continues. The algae concentration in the solution at the end of the 435 hours of observation is 1.001 g/l.

To investigate in depth the behaviour of the model, let's see how the algae culture developed in the absence of accidental (random) thermal phenomenon. The normal heat regime for the algae crop remains, in this case, the one given by the daily variation (about 18 days), the temperature variation over time being shown in Figure 5, a). The evolution rate of the algae crop varies over time as in Figure 5, b). The algal concentration variation over the observation time frame is given in Figure 5, c).

It is observed that algae concentration in the solution increases monotonously, only with small growth oscillations due to the daily temperature variation. The result of this growth regime is interesting, at the end of the 435 hours of observation, the algal concentration being 0.597 g / l. This value is slightly more than half the value the crop, which suffered by the thermal accident, has reached.

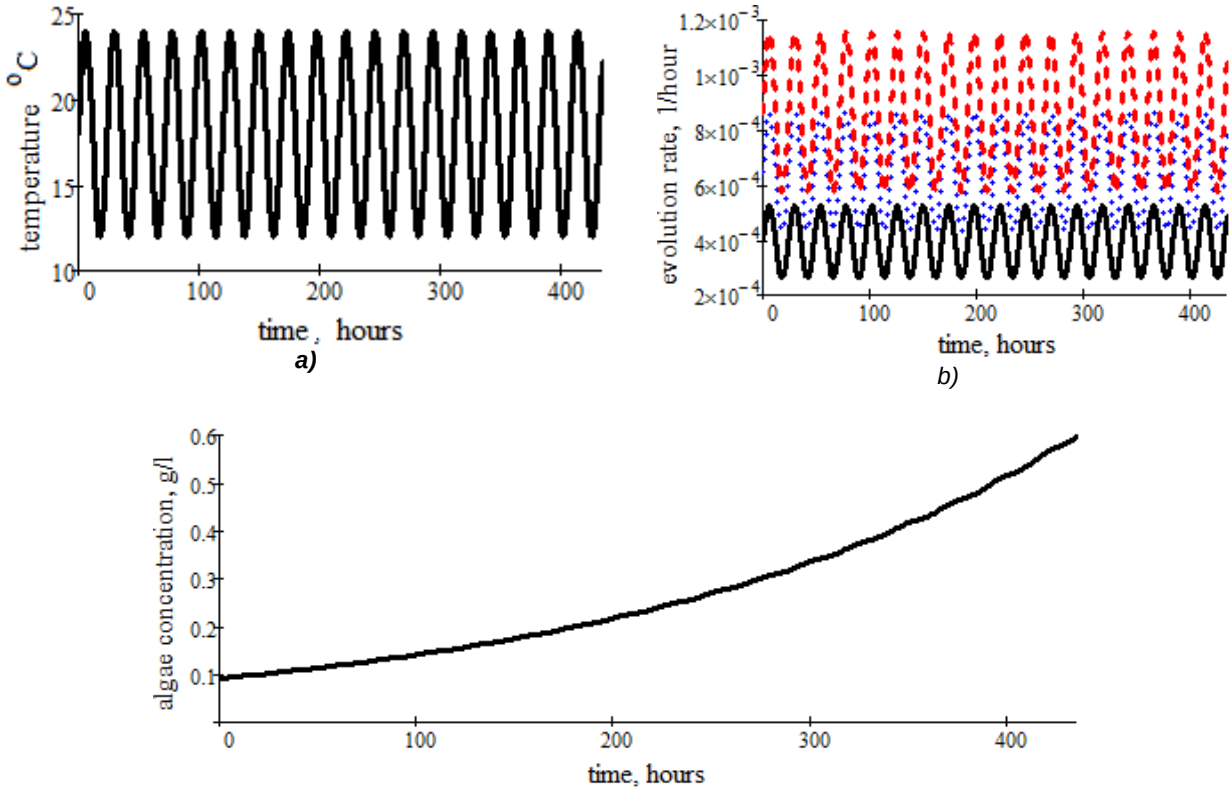

Fig. 5 - Effect of the thermal variation (without the random component) on the algae crop biomass concentration

One of the explanations of this phenomenon (a crop that suffers a thermal accident has a higher harvest than the same crop that would not have been subjected to this accident) is that the variation of the random thermal component increased the average evolution rate: from 0.001163 per hour, in the case without the random component, at 0.00209 per hour, if the random thermal component act, i.e. almost double. This example may explain some seemingly paradoxical phenomena in the cultivation of various algae or plants. For the average evolution rate of the crop algae, we used the following definition (14):

$$\bar{\mu} = \frac{1}{T - t_0} \int_{t_0}^{T} \mu(t, x(t)) dt \tag{14}$$

4) Simulation of a real evolution

When the first ideas about this model[7] arose, we considered the evolution of an algae crop, recorded in the experiments described in *Nedelcu et.al., 2018b*. Generally, in algae crops, we are accustomed to monotonous growth curves, comfortable in cultivation processes using optimized and partially or completely automated technologies, see Figure 5, c), (or *Blanken et.al., 2016; Huesemann et.al., 2016; Jamsa et.al., 2017; Stemkovski et.al., 2016 and Ma et.al., 2017*). There are also sources that indicate for algae crops, evolutionary curves that are not monotonous (*Dontu N., 2013; Jamsa et.al., 2017; Nedelcu, et.al., 2018,b*). The deviation from the monotonous growth regime of algae biomass draws attention due to several assumptions unfavourable to the cultivation process, which can be formulated: sudden variations of the thermal field or in the pH of the solution, dangerous variations in the carbon dioxide content in air or water, sudden or uncontrolled variations of algae illumination, dangerous variations in the salinity of the solution, and possible nutrient feeding errors. Other types of causes cannot also be excluded: diseases specific to algal cultures, penetration of culture system by the pests, measurement errors and monitoring. Over these causes, there is also the hypothesis that algae, individually or in the colony, develop mechanisms to reject forced growth (with too much growth rate) or even develop tempering functions. In this latter hypothesis we have also introduced the limitation of algal density (limit concentration), which was not used in these examples, however. Because the temperature of the solution, pH, salinity, illumination were well monitored (abstracted from possible errors), we focused on less well-monitored parameters. We have not been able to obtain the desired variations in the algal concentration using the carbon dioxide concentration variation within the limits prescribed (by *Blinova et.al., 2015*, for example).

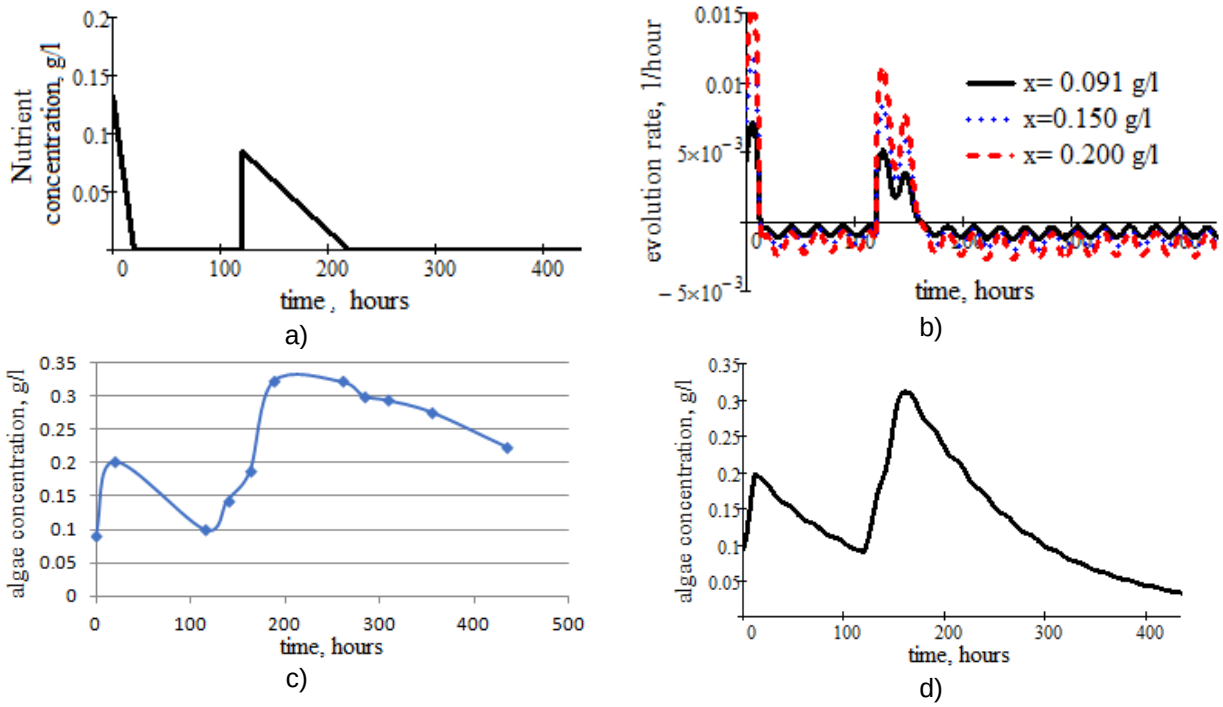

Fig. 6 - Simulation of a real evolution of a *Chlorella vulgaris* algae crop, recorded in the experiments described in *Nedelcu et.al., 2018 b*

a) Nutrient control function (based on nitrogen); b) Time dependence of the evolution rate of algae biomass in solution, at different concentrations; c) The evolution of algae concentration in solution, experimentally recorded; d) Evolution of algae concentration in solution, simulated using the mathematical model described in this article.

Then, from the set of parameters chosen for the influence of algal growth, there was still nutrient supply available.

Using the nitrogen nutrient load given in Figure 6, a) and a slightly modified nutrient filter function, formula (15), (after *Rowley W.M., 2010*), as:

$$N(\chi) = B(2.,0.069,0.137,0.01,0.01,-0.5,0.1,\chi) \tag{15}$$

[7] This model is neither the best, nor the nicest possible. It has advantages and disadvantages. Some of the advantages and disadvantages of this mathematical model will be discussed in the conclusions. But it can be the starting point for more performing models.

we obtained the algal concentration variation in Figure 6, d). How well approximates the prediction of the mathematical model (Figure 6, d), the experimental result (Figure 6, c), at least qualitatively, can be observed by comparing the two curves. The time dependences of the parameters that influenced the evolution of algae, for the example describe in this subchapter, are given graphically in Figure 7. Using these variations of process parameters, a theoretical response that satisfactorily approximates the actual response could be obtained. Due to experimental inaccuracies, however, nutrient loading monitoring cannot be used for comparison with theoretical load. Among these, first, it is important to monitor each parameter that influences the process at the resolution of the shortest (in time) process of significant and planned variation of any of the parameters.

In order to complement the image of the proposed mathematical model, we will give an example, exactly under the same conditions mentioned in this third case examined. The further simulated aspect is the action of the moderation factor, according to formula (16), on the simplified form.

$$\mu(t,x) = \mu_0 \cdot x \cdot \Theta \cdot (1 - CO_2) \cdot pH \cdot L \cdot N \cdot S \cdot \delta_{\lim}(x) \tag{16}$$

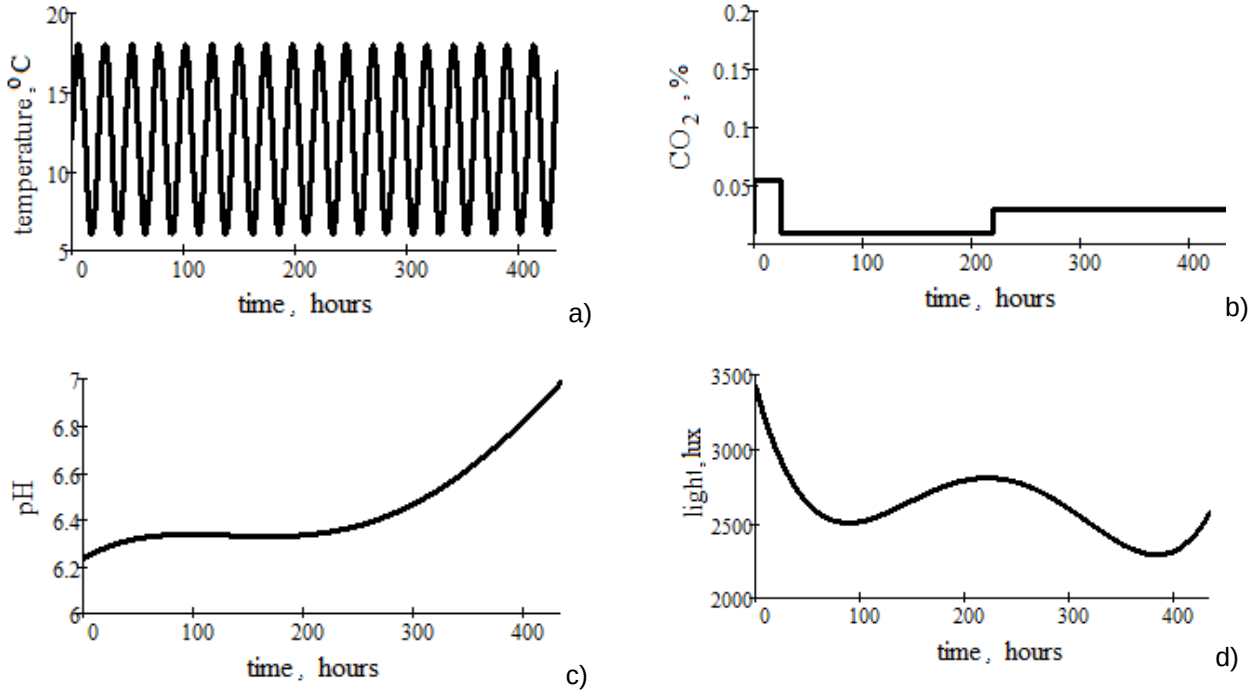

Fig. 7 - Time dependence of the process parameters considered. Salinity was considered to be constant, 0.023 g /l

The evolution of the algae culture under the conditions in which the moderating factor acts as in (16), and the parameters that influence the process behave as in Figures 6 and 7, is graphically represented in Figure 8.

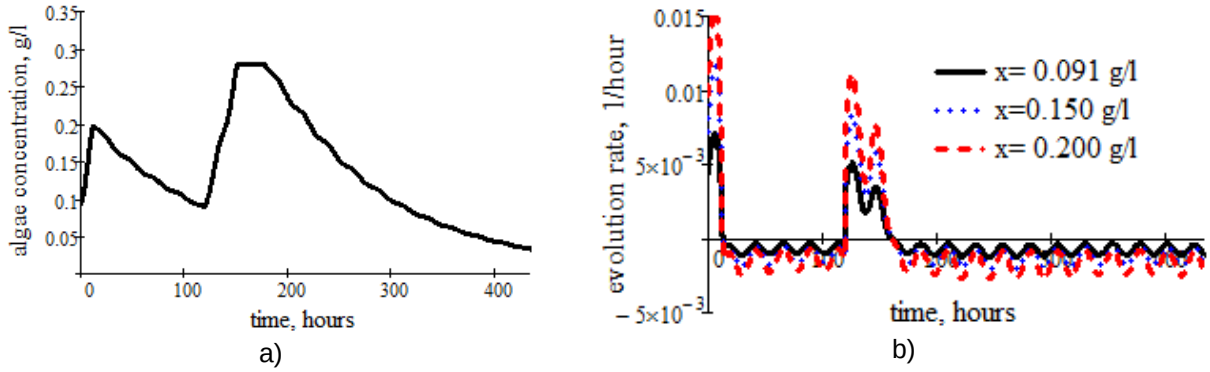

Fig. 8 - Time dependence of the process parameters considered, when the moderation factor (4) acting

Given that 0.28 g/l (chosen intentionally to highlight the consequences) was taken for the upper limit accepted by the culture, it is observed the cutting of the global peak, which is limited to a horizontal ceiling at the biomass limit value. The cut-off effect of growth at the given value corresponds to a population that "does not support excessive crowding", the high density of individuals. In the case of a culture with this type of behaviour, the optimal time of harvesting can be taken as the starting point of the horizontal ceiling. The response of the algae, dictated by the moderation factor, is similar to the behaviour of the mathematical models (*Davidson and Gurney, 1999*), in relation to yield-limited batch culture notion.

CONCLUSIONS

C1) Is recommend the increasing the resolution (in time) of the monitoring to the value of the smallest, planned, significant variation range for each of the process parameters.

C2) Is recommend the increasing the quality of monitoring through extended automation, avoiding as far as possible the laboratory analyses in which the human factor intervenes (labourers manipulating classical devices, typical of chemical laboratories).

C3) The mathematical modelling of algal evolution processes (generally of any plant or animal, of any life form), regardless of the purpose for which it is made, must include as many aspects of its life, meaning important moments: birth, growth, maturation, aging, death (natural or not), diseases, etc. Any measured parameter can give information, or it can be connected with other important parameters. That is why everything which can be measured must be measured and stored (regardless of resolution, given the extreme complexity of the experiences made with living matter).

C4) Deepening experimental research may include accumulation mathematical operators that, depending on feed and environmental parameters introduced, reflect the accumulation of valuable components for transformation into biofuels, food, or medication in algae. Such operators can be, for example, those introduced by *Cârdei P (2000)*, to model the phenomenon of materials fatigue. These operators are by integral type and transform the evolutionary equation of living matter into an integral-differential equation. For this kind of equations, numerical methods are more complex.

C5) The mathematical model considered is simple. The model of influence parameters of a process was used, in part, as in the mathematical model of soil erosion, called the Universal Soil Loss Equation (USLE), (*Wischmeier and Smith, 1960*). This type of model allows estimating the effect of parameters on process evolution, but not vice versa. For this reason, variance equations of each of the parameters that influence the process must be introduced into the model. Thus, the influence of biomass[8] growth on pH, carbon dioxide, temperature, etc. can be emphasized. Creating such mathematical models requires very complex experiences, the costs of which cannot be said to be justified, at least for now.

C6) The influence factors method can also be applied to complex mathematical models of evolution (dynamic, kinetic) defined by systems of differential equations or even equations and systems of partial derivative equations. To achieve this goal, it is sufficient to convert some of the constants or model parameters into a product by factor functions, which express the contribution of each parameter to the value of a particular model parameter.

C7) Mathematical models of crops' evolution, using influence factors, allow for detailed expertise of the losses of some crops, high probability to identifying, of the causes, and imagining real-time loss recovery scenarios.

As a conclusion to this modelling attempt in the field of algae growing (and generally living matter), we will set out some requirements for experiments to clarify the behaviour of algae and not only of them.

In order to better model the influence of physical fields (temperature, pH, concentrations of carbon dioxide, light, nutrients, radiation, etc.) on the studied biological entities, one should, for example, study the variation of the growth rate with the intensity of these fields between the extreme values, more precisely, those values at which the growth rate is cancelled and, if possible, determine the values at which the phenomenon of putrefaction occurs.

It is also necessary to know the extreme values of algal concentrations or their density: the minimum concentration from which development can begin (if any) and the maximum concentration at which the crop yet develops (if there is this limit, especially for crops bounded in space).

[8] Living or dead biomass can also influence the environmental status.

ACKNOWLEDGEMENT

The research work was funded by financing contract no. 8 N/2016 the project PN 16 24 04 04 „Researches regarding the development of an innovative technology for obtaining advanced biofuels from non-food bio-resources".

Also, this work was supported by a grant of the Romanian Research and Innovation Ministry, through Programme 1 – Development of the national research-development system, subprogramme 1.2 – Institutional performance – Projects for financing excellence in RDI, contract no. 16PFE.

REFERENCES

[1] Blanken W., Postma P.R., de Winter L., Wijffels R.H., Janssen M., (2016), Predicting microalgae growth. *Algal Research*, vol.14: pp. 28-38, Ed. Elsevier, London / U.K;

[2] Blinova L., Bartosova A., Gerulova K., (2015), Cultivation of microalgae *(Chlorella vulgaris)* for biodisel production. *Research Papers Faculty of Materials Science and Technology Slovak University of Technology*, Vol.23, No.36, pp. 87-95, Bratislava/Slovakia;

[3] Cârdei P., (2000), Models for bodies with unsteady quality, *Revue Roumaine des Sciences Techniques. Mecanique Appliquee*, tome 45 (1), pp.97-109, Bucharest / Romania.

[4] Chen Sh., Chen X., Peng Y., Peng K., (2009), A mathematical model of the effect of nitrogen and phosphorus on the growth of blue-green algae population. *Applied Mathematical Modelling*. Vol.33, no.2, pp.1097–1106, Ed. Elsevier, London / U.K;

[5] Concas A., Pisu M., Cao G., (2013), Mathematical Modelling of *Chlorella Vulgaris* Growth in Semi-batch Photobioreactors Fed with Pure CO_2, *AIDIC Conference* Series 11: 121-130 DOI: 10.3303/ACOS1311013.

[6] Davidson K., Gurney W.S.C., (1999), An investigation of non-steady-state algal growth. II. Mathematical modelling of co-nutrient-limited algal growth, *Journal of Plankton Research*, vol.21, no. 5, pp. 839-858, Oxford University Press;

[7] Dontu N., (2013), Cultivation of *Chlorella Vulgaris Beijer, Synechocystis Salina Wisl., Phromodium Foveolarum (Mont.) Gom.* and *Tribonema Viride Pasch*. Algae in Medium with urban waste water addition, *Studia Universitatis Moldaviae. Scientific Journal of State University in Moldova*, vol.6, no.66;

[8] Fry R., McManus S., (2002). Smooth bump functions and the geometry of banach spaces: A brief survey, *Expositiones Mathematicae*. Vol. 20, no. 2, pp. 143-183, Ed. Elsevier, London/U.K;.

[9] Huesemann M., Crowe B., Waller P., Chavis A., Hobbs S., Edmundson S., Wigmosta M., (2016), A validated model to predict microalgae growth in outdoor pond cultures subjected to fluctuating light intensities and water temperatures, *Algal Research*, vol.13, pp. 195-206, Ed. Elsevier, London/U.K;

[10] Jamsa M., Lynch F., Santana-S. A., Laaksonen P., Zaitsev G., Solovchenko A., Allahverdiyeva Y., (2017), Nutrient removal and biodiesel feedstock potential of green alga UHCC00027 grown in municipal wastewater under Nordic conditions. *Algal Research*, vol.26, pp. 65-73, Ed. Elsevier, London/U.K.

[11] Ma M., Yuan D., He Y., Park M., Gong Y., Hu Q., (2017), Effective control of *Poterioochromonas malhamensis* in pilot-scale culture of *Chlorella sorokiniana* GT-1 by maintaining CO2-mediated low culture pH. *Algal Research*, vol.26, pp. 436-444, Ed. Elsevier, London/U.K;

[12] Malthus T. R., (1798), An Essay on the Principle of Population. *Library of Economics and Liberty*, London. https://www.econlib.org/library/Malthus/malPop.html?chapter_num=1#book-reader.

[13] Mardlijah M., Jamil A., Hanafi L., Sanjaya S., (2017), Optimal control of algae growth by controlling CO2 and nutrition flow using Pontryagin Maximum Principle, *ICoAIMS 2017*, Journal of Physics Conference Series 890 (1): pp. 1-6, Kuantan, Pahang, Malaysia;

[14] McKendricka A.G., Kesava P.M. (1912), XLV.-The Rate of Multipliation of Micro-organisms: A Mathematical Study, *Proceedings of the Royal Society of Edinburgh*. Vol.31, pp. 649–653.

[15] Muthukumar T, (2016), Sobolev Spaces and Applications. accessed 19.09.2018 http://home.iitk.ac.in/~tmk/courses/mth656/main.pdf.

[16] Nedelcu A., Ciuperca R., Popa L., Gageanu I., Pruteanu A., (2018), Research on Algae Growing in Open System with Cascade-Type Installation, *Proceedings of The 17th International Scientific Conference Engineering for Rural Development.*, pp 412-418, Jelgava / Letonia;

[17] Nedelcu A., Cardei P., Ciuperca R., (2018), Researches on the cultivation of *Chlorella vulgaris* algae in a laboratory installation aimed at designing a real-scale installation. Accessed 20.09.2018. *https://www.researchgate.net/publication/322211066_Researches_on_the_cultivation_of_Chlorella_vulgaris_algae_in_a_laboratory_installation_in_aim_to_design_a_real-scale_installation?showFulltext=1&linkId=5a4bca7d0f7e9b8284c2e2ab*

[18] Rowley W.M., (2010), *Nitrogen and phosphorus biomass-kinetic model for chlorella vulgaris in a biofuel production scheme*, Thesis, Air Force Institute of Technology, Ohio.

[19] Singh S.P., Singh P., (2014), Effect of CO2 concentration on algal growth: A review, *Renewable and Sustainable Energy Reviews,* vol. 38, pp.172–179, Ed. Elsevier, London/U.K;

[20] Stemkovski M., Baraldi R., Flores K.B., Banks H.T, (2016), Validation of a Mathematical Model for *Green Algae* (Raphidocelis Subcapitata), Growth and Implications for a Coupled Dynamical System with Daphnia Magna. *Applied Science*, vol.6, no. 5: p.155. DOI:10.3390/app6050155.

[21] Surendhiran D, Vijay M, Sivaprakash B, Sirajunnisa A, (2015). Kinetic modeling of microalgal growth and lipid synthesis for biodiesel production. *3 Biotech*, vol.5, no.5, pp.663-669. Springer International Publishing;

[22] Thornton A.R., Weinhart T., Bokhove O., Zhang B., van der Sar D.M., Kumar K., Pisarenco M., Rudnaya M., Savcenco V, Rademacher J., Zijlstra J., Szabelska A., Zyprych J., van der Schacs M., Timperio V., Veerman F., (2010), Modeling and optimization of algae growth. *Proceedings of the 72nd European Study Group Mathematics with Industry*, pp. 54-85, Amsterdam: C.W.I;

[23] Tu L.W., (2008), An Introduction to Manifolds, Springer;

[24] Verhulst P.F., (1838), Notice sur la loi que la population suit dans son accroissement. *Correspondance mathematique et physique*, volume 10, pp. 113-121.

[25] Wischmeier W.H., Smith D.D., (1960), A universal soil-loss equation to guide conservation farm planning. *Transactions of the 7th International Congress of Soil Science,* vol.1: pp. 418-425;

[26] Yang J.Sh., Rasa E., Tantayotai P., Scow K.M., Yuan H., Hristova K.R., (2011), Mathematical model of Chlorella minutissima UTEX2341 growth and lipid production under photoheterotrophic fermentation conditions. *Bioresource Technology*, vol.102, pp. 3077-3082, Ed. Elsevier, London/U.K.;

[27] Yang Zh, Zhao Y, Liu Zh, Liu C, Hu Zh, Hou Y, (2017), A Mathematical Model of Neutral Lipid Content in terms of Initial Nitrogen Concentration and Validation in Coelastrum sp. HA-1 and Application in Chlorella sorokiniana, *BioMed Research International*, vol. 2017, Article ID 9253020, 10p. https://doi.org/10.1155/2017/9253020.

[28] ***https://www.wikihow.com/Grow-Chlorella-for-a-Food-Supplement, accessed 07.01.2018.

PARAMETER OPTIMISATION AND EXPERIMENT ON THE COMBING OF *Cerasus humilis*

/

钙果梳脱部件参数优化与试验

As. Ph.D. Stud. Eng. Xiaobin Du, Prof. Ph.D. Eng. Junlin He*, M.S. Stud. Eng. Yongqiang He, M.S. Stud. Eng. Dawei Fang

College of Engineering, Shanxi Agriculture University, Taigu/China;

Tel: +86-0354-6288400; E-mail:hejunlin26@126.com

Keywords: *Cerasus humilis, comb rod, threshing, removal, damage, optimisation*

ABSTRACT

In this paper, the mechanical injury evaluation standard of Cerasus humilis was established based on extrusion deformation energy and fruit storage days. The key factors affecting extrusion deformation were determined by analysing the contact force during combing. The single-factor test and three-factor, three-level quadratic regression orthogonal test were carried out by using the fruit removal rate and damage rate as the evaluation indices and the comb distance, combing speed and comb rod radius as the influencing factors. Results showed that the fruit removal rate decreased and the damage rate initially decreased and then increased with the increase in comb distance; with the increase in combing speed, the fruit removal rate remained unchanged and the damage rate increased; with the increase in comb rod radius, the fruit removal rate initially increased and then decreased, while the damage rate initially decreased and then increased. The order of influence on the fruit removal rate was comb rod radius > comb distance > combing speed. The order of influence on the damage rate was combing speed > comb distance > comb rod radius. Response surface methodology obtained the following optimal parameters: comb distance of 9 mm, combing speed of 340 mm/s and comb rod radius of 8 mm. A validation test was carried out on a combing test bench under the optimised parameters. The fruit removal rate was 96.89% and the damage rate was 6.36%. These values were consistent with the results of optimum parameters; thus, the regression model was reliable.

摘要

本文基于挤压变形能和果实存放天数，建立钙果机械损伤评价标准，分析钙果在梳脱过程中的接触受力，确定影响挤压变形的关键因素。以脱净率和损伤率为评价指标，以梳齿间距、梳脱速度和梳齿杆半径为影响因素分别进行单因素试验和三因素三水平二次回归正交试验，结果表明：当梳齿间距增大时，脱净率降低，损伤率先减小后增加；梳脱速度增加时，脱净率基本保持不变，损伤率逐渐增大；梳齿曲率半径增加时，脱净率先增加后减小，损伤率先减小后增加。对脱净率的影响显著顺序为：曲率半径>梳齿间距>梳脱速度；对损伤率的影响显著顺序为：梳脱速度>梳齿间距>曲率半径。基于响应面法进行参数优化，得到最佳组合参数：梳齿间距为9 mm，梳脱速度为340 mm/s，曲率半径为8 mm。以优化后的参数组合，在梳脱试验台上进行验证试验，其结果为：脱净率96.89 %，损伤率6.36 %，与优化参数结果基本吻合，回归模型可靠。

INTRODUCTION

Cerasus humilis is a unique fruit tree resource in China. It has high calcium content in pulp and a developed root system, so it has high development potential. *C. humilis* fruits are small and numerous, and their bushes are low and lodging. Fruits rot in 10–20 days after ripening if not harvested on time, result in serious economic losses. Large-scale planting bases need to employ a large number of manpower, which restricts large-scale development. Therefore, studies on the mechanised harvesting of *C. humilis* are necessary and the harvesting components are the primary research contents for designing *C. humilis* harvester.

Extensive research has been made on picking small berries. The vibration principle is mainly used in the literature. A vibration rod is used to knock fruit off or vibrate the trunk of the plant to cause fruit swing and loss *(Peterson et al., 1997; Peterson et al., 2003; Wang et al., 2009)*. *C. humilis* branches are soft and easy to lodge, which is not conducive to vibration transmission. Therefore, harvesting devices must be designed depending on the growth characteristics of *C. humilis*. The double-roller stripping device of *C. humilis* adopts the method of staged harvesting. Branches are cut off, collected and transported to the stripping device. The

fruit is stripped off by the impact of the pick roller. This harvesting method damages the branches and easily affects the quality of newly germinated basal shoots in the next year, thereby reducing yield *(Liu., 2014; Sun., 2016)*. Comb-type *C. humilis* harvester has a high removal rate and low damage rate, which indicates that the comb stripping method can meet the requirements of *C. humilis* harvesting *(Zhang et al., 2018)*. The comb structure is widely used in cutting tables and the threshing mechanism of rice, rape, camellia and other crops *(Yuan et al., 1998; Chen et al., 1999; Ji et al., 2016; Gao et al., 2013)*. The clearance of comb rod is larger than the stalk diameter but smaller than the fruit diameter. Fruits are picked by the impact force of the comb rod *(Zhang et al., 2014)*. Research on the root soil-removing device of knotweeds shows that it is effective in separating roots and soils by using the linear comb-type soil-removing roller finger *(Chen et al., 2015)*. In the field of edible chrysanthemum harvesting, combs can also be used to achieve differential harvesting *(Ji et al., 2016; Ji et al., 2017)*. Combs can apply vibration to improve the harvesting efficiency *(Xu et al., 2018)*. The comb does not directly act on branches during fruit removal, which can reduce damage to branches *(Li et al., 2015)*, but directly acts on fruits, which may increase the damage of *C. humilis* and lead to fruit leakage.

Considering that the comb stripping method meets the requirements of *C. humilis* harvesting, this study analysed the comb as the end-effector of *C. humilis* harvester. To improve the removal rate and reduce the damage rate of *C. humilis*, the combing parameters were optimised to provide reference for the design and optimisation of *C. humilis* harvesting machinery.

MATERIALS AND METHODS

Materials

Sampling was conducted on September 15, 2017. The sampling site was Juxin Modern Agriculture Base in Taigu County, Shanxi Province, China (E 112°29′, N 37°23′), and the variety was ‘Nongda 4’. At this time, *C. humilis* of this variety matured for 3–4 days and was in the stage of large-scale harvesting. The average diameter of roots was 6.78 mm, whereas the average diameter of fruits was 21.56 mm. The average damage force was 24.6 N, whereas the average fruit removal force was 8.82 N.

Instrument and device

The experiment was carried out on a self-made experiment bench to simulate the combing process with the simplest structure. The device is shown in Fig. 1. The setup included a frame, comb rod fixture, five sets of combing devices with different specifications (self-made) and branch traction device (self-made).

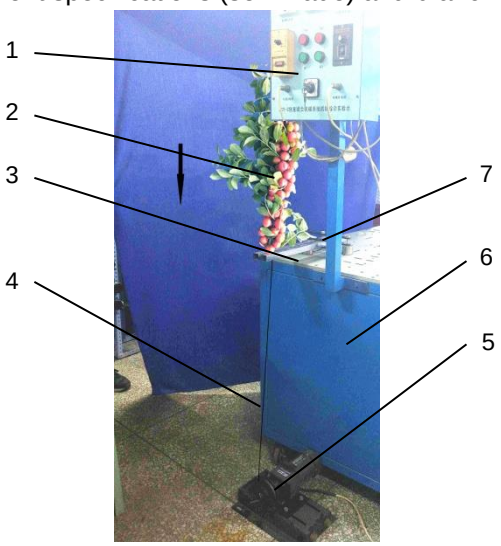

Fig. 1 - Experimental device of fruit comb threshing

1- Speed control panel; 2- Branch with fruits; 3- Comb rods; 4- Wire rope; 5- Gear motor; 6- Frame; 7- Comb rod fixture

The combing device was mainly composed of comb rods and their fixture. The comb rods were circular pipes and the fixture included the base, gap adjusting block and pressing plate. The base and pressing plate were fixed on the frame by bolts and two rods were placed horizontally in the middle. The gap adjusting block was placed between the rods. The structure was used to fix the rod and adjust the gap between the rods. The clamping diameter of the device was 0–30 mm, whereas the gap adjustment ranged from 0 mm to 40 mm.

The branch traction device mainly consisted of a winch, wire rope and speed reduction motor (90YYJ-60). The winch was fixed on the output shaft of the reducer motor and placed directly below the comb rods to ensure that the wire rope drew branches vertically through the clearance of the comb rods. Before the test, a circular groove was made at the root of the branch to prevent the branch from slipping, and the other end of the wire rope was connected with the winch. The speed range of the traction device was 0–800 mm/s.

Experimental factor

The clearance of comb rods was larger than the branch diameter but smaller than the diameter of *C. humilis*. When the comb rods moved relative to the branches, the calcium fruit branches were combed. Previous experiments found that the fruit was extruded under the force of comb rods, which resulted in the fruit being stuck in the crack of comb teeth, causing damage or leakage.

As shown in Fig. 2, the force of comb rod on fruit was *T*, and its vertical and horizontal components were as follows:

$$\begin{cases} T_y = T \cdot \sqrt{1-\left(\dfrac{D+2R_1}{d+2R_1}\right)^2} \\ T_x = T \cdot \dfrac{D+2R_1}{d+2R_1} \end{cases} \quad (1)$$

Where:

T is the force of comb rod on fruit, [N];

Ty is the vertical force of comb rod on fruit, [N];

Tx is the horizontal force of comb rod on fruit, [N];

d is *C. humilis* diameter, [mm];

D is Comb distance, [mm];

R_1 is Comb curvature radius, [mm].

In order to shed the fruit, it is necessary to satisfy the following requirements:

$$2T_y \geq F \quad (2)$$

Where: *F* is fruit removal force, [N].

So：

$$T \geq \frac{F}{2} \cdot \frac{1}{\sqrt{1-\left(\dfrac{D+2R_1}{d+2R_1}\right)^2}} \quad (3)$$

On the right side of the inequality is the critical force that the comb rods need to remove fruits, which is related to comb distance *D* and comb rod radius R_1. A large comb distance *D* and comb rod radius R_1 correspond to high critical force, which can easily damage fruits and is not conducive to the combing operation.

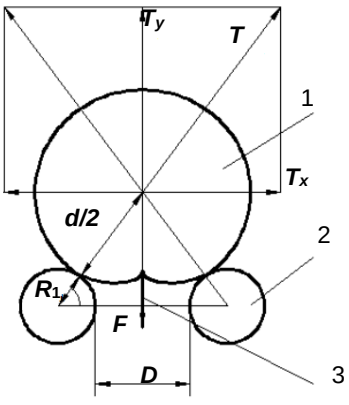

Fig. 2 - Forces on *C. humilis* fruit

1- C. humilis ; 2- Comb rods; 3- Stalk

With *C. humilis* as the research object, the following assumptions were made *(Bao et al., 2017)*: *C. humilis* was simplified into homogeneous and isotropic spheres. Its deformation was much smaller than its size, and its contact surface was continuous and uncoordinated. When the fruit came into contact with the comb rod, as shown in Fig. 3, deformation *δ* occurred in the two contact centres.

The force between them is T, and δ is as follows:

$$\delta = \left(\frac{9P^2}{16RE^{*2}} \right)^{1/3} \tag{4}$$

$$\frac{1}{R} = \frac{1}{R_1} + \frac{1}{R_2} \tag{5}$$

$$\frac{1}{E^*} = \frac{1-\mu_1^2}{E_1} + \frac{1-\mu_2^2}{E_2} \tag{6}$$

Where:

δ is extrusion deformation, [mm];
T is contact force between fruit and comb rod, [N];
R is equivalent radius, [mm];
E^* is equivalent modulus of elasticity, [MPa];
R_1 is comb rod radius, [mm];
R_2 is fruit radius, [mm];
μ_1 is Poisson ratio of fruits;
μ_2 is Poisson ratio of comb rod;
E_1 is Elastic modulus of fruit, [MPa];
E_2 is Elastic modulus of comb rod, [MPa].

To prevent the fruit from becoming stuck in the comb gap, it is necessary to make:

$$2\delta \frac{2R_1 + D}{2R_1 + d} \le d - D \tag{7}$$

So:

$$T \le \sqrt{\frac{16RE^{*2}(d-D)^3}{9\left(2\frac{D+2R_1}{d+2R_1}\right)^3}} \tag{8}$$

On the right side of the inequality is the critical force that does not produce leakage, which is related to D and R_1. A small D and R_1 correspond to high critical force. Fruit cannot easily become stuck in the comb clearance, which is conducive to the combing operation.

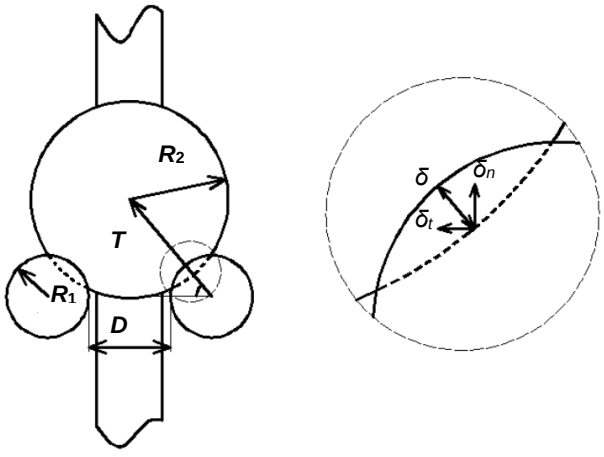

Fig. 3 - Extrusion force schematic of fruits and comb rods

The combing speed was found to affect extrusion between *C. humilis*. Therefore, the experimental factors selected in this paper were D, R_1 and combing speed.

Performance evaluation of combing

a. No compression deformation ***b. Causing compression deformation***

Fig. 4 - Schematic of C. humilis combing deformation

Apart from breaking, some fruits decay and deteriorate at 1–2 days after combing. This phenomenon is caused by damage of the internal structure of the fruit, and mechanical damage occurs before the fruit breaks down, as shown in Fig. 4. On the basis of the relationship between collision deformation energy and fruit collision damage, the work done by the compression force in the direction of compression deformation is transformed into fruit deformation energy. When fruit deformation accumulates a certain value, the fruit suffers from mechanical damage *(Bao et al., 2017)*.

C. humilis fruits were selected as samples and the quasi-static compression test was carried out by using a CMT-6104 computer-controlled electronic universal testing machine (Shenzhen New Sans Material Testing Co., Ltd., accuracy ±5% and resolution ±100 000 yards). The test fruits were placed on a plane and compressed using a flat-plate indenter. The loading rate was 20 mm/min and the maximum loading displacement was 10 mm. The deformation–force curve was obtained as shown in Fig. 5. Assuming that the deformation curve equation is $F=F(\Delta)$, then

$$E = \int_0^{\Delta} F(\Delta) d\Delta \tag{9}$$

Where: Δ is fruit deformation, [mm];

E is fruit deformation energy, [J];

F is a deformation curve equation.

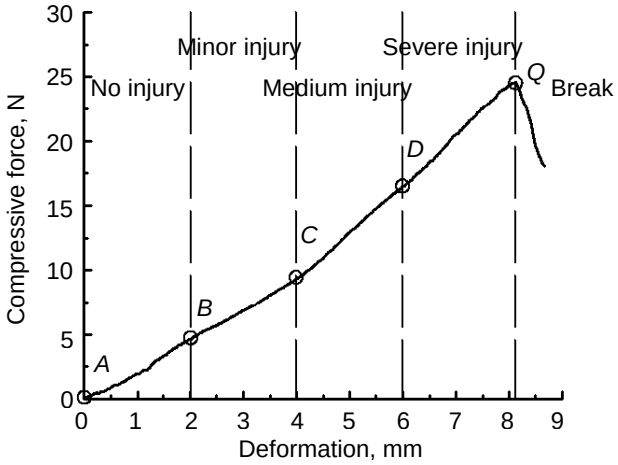

Fig. 5 - Deformation–force curve of *C. humilis*

After the samples were removed from the testing machine, the softening degree of the compressed part was assessed based on the deformation of each stage and the damage degree was determined. In curve *AB* segment, the storage deformation energy of fruit was low and the fruit was not damaged. Mechanical damage occurred when the sample was compressed to point *B*. In curve *BC* segment, the fruit softened slightly, resulting in minor damage. In curve *CD* segment, the fruit softened moderately, resulting in medium damage. In curve *DQ* segment, the fruit softened severely, resulting in severe damage. When compressing the sample to point *Q*, the fruit broke, fruit deformations increased, but stress decreased sharply. On the basis of fruit deformation energy and storage time after compression, the mechanical injury evaluation standard of *C. humilis* was obtained (Table 1).

Table 1

Mechanical injury evaluation standard of *C. humilis*

Position on curve	Deformation *Δ*	Deformation energy *E*	Injury evaluation	Storage time
	[mm]	[10^{-3}J]	[m/s]	[d]
AB	0~2	0~4.20	No injury	>10
BC	2~4	4.20~17.99	Minor injury	7~10
CD	4~6	17.99~43.75	Medium injury	3~4
DQ	6~8.1	43.75~87.81	Severe injury	0~1
Q	>8.1	>87.81	Break	0

C. humilis fruits with minor and severe injuries were selected and placed for 24 h for observation and comparison, as shown in Fig. 6. The fruit with minor injury was still bright in appearance. Beside the contact zone, the pulp could maintain its original firmness (Fig. 6a). After cutting the fruit, the boundary between the pulp and core was obvious (Fig. 6c). The colour of the subcutaneous pulp in the contact deformation area became dark. This finding indicated that the pulp in the extrusion area was damaged. The appearance of severely injured fruits became dark and soft, as shown in Fig. 6b. After cutting the fruit, as shown in Fig. 6d, no obvious boundary was observed between the pulp and core. This finding suggested that the fruit was close to deterioration at this time and it was likely to break up during transportation. This phenomenon was considered fruit damage.

a. Appearance of minor injury

b. Appearance of severe injury

c. Section of minor injury

d. Section of severe injury

Fig. 6 - Internal injury comparison of *C. humilis*

Therefore, in this experiment, the fruit removal rate *μ* and damage rate *η* were selected as the evaluation indices of combing performance.

$$\mu = \frac{N_1}{N} \tag{10}$$

$$\eta = \frac{N_2 + N_3}{N_1} \tag{11}$$

Where:

μ is the fruit removal rate, [%];
η is the damage rate, [%];
N is the total number of fruits on the branch before the experiment.
N_1 is the number of fruits removed;
N_2 is the number of fruits that have been broken;
N_3 is the number of deteriorated fruits after 24 hours.

Experiment design

Design of single factor experiment

To clarify the effects of comb distance, combing speed and comb rod radius on the fruit removal rate and damage rate, single-factor experiments were designed. The experimental factors and levels are shown in Table 2.

Table 2

Scheme of single factor experiment

Factors	1	2	3	4	5	6	7	8	9	10	11	12	13	14	15
Comb distance [mm]	8	9	10	11	12	10					10				
Combing speed [mm/s]	300					200	250	300	350	400	300				
Comb rod radius[mm]	8					8					4	6	8	10	12

Design of orthogonal experiment

To study the influences of interactive factors on the performance of combing, a three-factor, three-level orthogonal experiment was carried out based on the Box–Behnken centre combination method *(Golub et al., 2018)*. Comb distance, combing speed and comb rod radius were used as factors. Fruit removal rate and damage rate were utilised as indices. The experimental factors and levels are shown in Table 3.

Table 3

Coding schedule of experimental factors

Coded value	Comb distance	Combing speed	Comb rod radius
	[mm]	[mm/s]	[mm]
	X_1	X_2	X_3
Lower level (-1)	8	200	4
Middle level (0)	10	300	8
Upper level (1)	12	400	12

RESULTS

Results and analysis of single factor experiment

The results of the single-factor experiment are shown in Fig. 7. Fig. 7a shows the relationship between comb distance and the fruit removal rate and damage rate. As the comb distance increased, the fruit removal rate decreased from 98.36% to 94.94% and the damage rate decreased from 7.50% to 5.16% and then increased to 7.86%. Fig. 7b shows the relationship between combing speed and the fruit removal rate and damage rate. With the increase in combing speed, the variation trend of the fruit removal rate was not obvious, and the difference between the maximum and minimum values of the fruit removal rate was only 0.63%. The damage rate increased from 3.90% to 9.40%. Fig. 7c shows the relationship between comb rod radius and the fruit removal rate and damage rate. With the increase in comb rod radius, the fruit removal rate increased from 94.74% to 96.74% and then decreased to 95.30%, whereas the damage rate decreased from 5.84% to 5.16% and then increased to 6.58%.

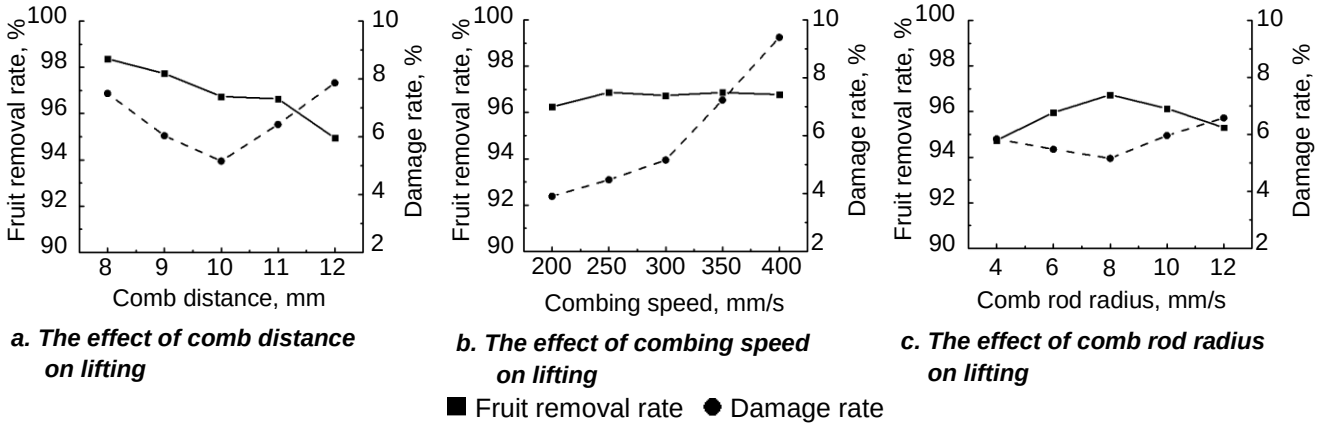

a. The effect of comb distance on lifting

b. The effect of combing speed on lifting

c. The effect of comb rod radius on lifting

Fig. 7 - Results of single-factor experiment

Results and analysis of orthogonal experiment

Orthogonal experiments were designed by Design Expert software based on the Box–Behnken centre combination method. The experimental results are shown in Table 4, and the findings of variance analysis are shown in Table 5. The quadratic regression models of the fruit removal rate μ and damage rate η were extremely significant, while the lack of fit was not significant. The determinant coefficients R^2 of the regression equation were 0.9475 and 0.9943. The predicted values of the regression model fitted well with the actual values. The regression model could be used to predict and analyse the effects of comb distance, combing speed and comb rod radius on the fruit removal rate and damage rate.

The quadratic polynomial regression models among the comb distance, combing speed, comb rod radius and fruit removal rate and damage rate were established. After eliminating the insignificant factors, the regression equation was obtained as follows:

$$\mu = 96.74 - 2.04X_1 + 0.42X_3 - 0.76X_1X_3 - 2.23X_3^2 \quad (12)$$

$$\eta = 5.16 + 2.84X_2 + 0.38X_3 - 0.24X_1X_2 - 0.23X_2X_3 + 2.21X_1^2 + 1.62X_2^2 + 1.14X_3^2 \quad (13)$$

Where:

X_1 is comb distance, [mm];
X_2 is combing speed, [mm/s];
X_3 is comb rod radius, [mm];
μ is the fruit removal rate, [%];
η is the damage rate, [%].

Table 4

The orthogonal experimental results

No.	Comb distance X_1	Combing speed X_2	Comb rod radius X_3	Fruit removal rate μ	Damage rate η
	[mm]	[mm/s]	[mm]	[%]	[%]
1	-1	-1	0	98.57	5.89
2	1	-1	0	95.15	6.18
3	-1	1	0	98.17	12.26
4	1	1	0	94.02	11.61
5	-1	0	-1	94.86	8.16
6	1	0	-1	91.98	8.21
7	-1	0	1	97.51	8.93
8	1	0	1	91.61	8.74
9	0	-1	-1	94.73	4.53
10	0	1	-1	94.26	10.44
11	0	-1	1	95.24	5.85
12	0	1	1	94.83	10.83
13	0	0	0	96.48	4.89
14	0	0	0	97.12	5.05
15	0	0	0	96.69	5.28
16	0	0	0	96.07	5.34
17	0	0	0	97.33	5.22

Table 5

ANOVA

Sources	DF	MS	*F* Value	*P* Value	Sources	DF	MS	*F* Value	*P* Value
Model 1	9	6.74	33.06	<0.0001**	**Model 2**	9	11.89	313.06	<0.0001**
X_1	1	33.42	163.88	<0.0001**	X_1	1	0.031	0.82	0.3945
X_2	1	0.73	3.56	0.1011	X_2	1	64.35	1694.21	<0.0001**
X_3	1	1.41	6.92	0.0339*	X_3	1	1.13	29.81	0.0009**
X_1X_2	1	0.31	0.65	0.4455	X_1X_2	1	0.22	5.82	0.0467*
X_1X_3	1	2.28	11.18	0.0124*	X_1X_3	1	0.014	0.38	0.5576
X_2X_3	1	0.0009	0.004	0.9489	X_2X_3	1	0.22	5.69	0.0485*
X_1^2	1	1.13	5.54	0.0509	X_1^2	1	20.63	542.98	<0.0001**
X_2^2	1	0.28	1.37	0.2807	X_2^2	1	10.99	289.38	<0.0001**
X_3^2	1	20.94	102.71	<0.0001**	X_3^2	1	5.48	144.25	<0.0001**

Sources	DF	MS	*F* Value	*P* Value	Sources	DF	MS	*F* Value	*P* Value
Residual	7	0.20			**Residual**	7	0.038		
Lack of Fit	3	0.14	0.55	0.6756	**Lack of Fit**	3	0.044	1.29	0.3932
Pure Error	4	0.25			**Pure Error**	4	0.034		
Total	16				**Total**	16			

*Note: P < 0.01 (extremely significant, **), P < 0.05 (significant, *);*
Model 1 is variance analysis of fruit removal rate;
Model 2 is variance analysis of damage rate.

Analysis of the effect of experimental factors on fruit removal rate

The response surface of comb distance X_1, combing speed X_2 and comb rod radius X_3 to the fruit removal rate μ is shown in Figs. 8a–8c. When the comb rod radius was 8 mm, the fruit removal rate decreased with the increase in comb distance and combing speed. However, the variation range of the response surface along the comb distance was large indicating that the comb distance had more influence than the combing speed (Fig. 8a). When the combing speed was 300 mm/s, the fruit removal rate decreased with the increase in comb distance. With increased comb rod radius, the fruit removal rate increased initially before decreasing obviously with the increase in comb rod radius, indicating that the comb rod radius had a larger effect on the fruit removal rate than the comb distance (Fig. 8b). When the comb distance was 10 mm, the fruit removal rate initially increased before decreasing, and the effect of combing speed on the fruit removal rate was not obvious (Fig. 8c).

As indicated by the change range of the response value of the experimental factors to the fruit removal rate, the order of influence of the experimental factors on the fruit removal rate was $X_3 > X_1 > X_2$. The overall influence trend was that the comb distance X_1 was small and the comb rod radius was moderate, thereby increasing the fruit removal rate. During combing, *C. humilis* fruits were extruded inward by the comb rod. With the increase in comb distance, the transverse deformation increased, which easily led to fruit leakage. When the comb rod radius was small, the comb rods easily deformed and the comb distance was difficult to guarantee, which indirectly resulted in the increase in comb distance. When the comb rod radius was large, the position of *C. humilis* fruits in the comb rod was 'deep', and fruits easily became stuck in the comb rod clearance. Fruit stuck in clearance played the role of combing other fruits on the branch, and leaked out under the extrusion of the adjacent fruits. The effect of combing speed on the fruit removal rate was not obvious.

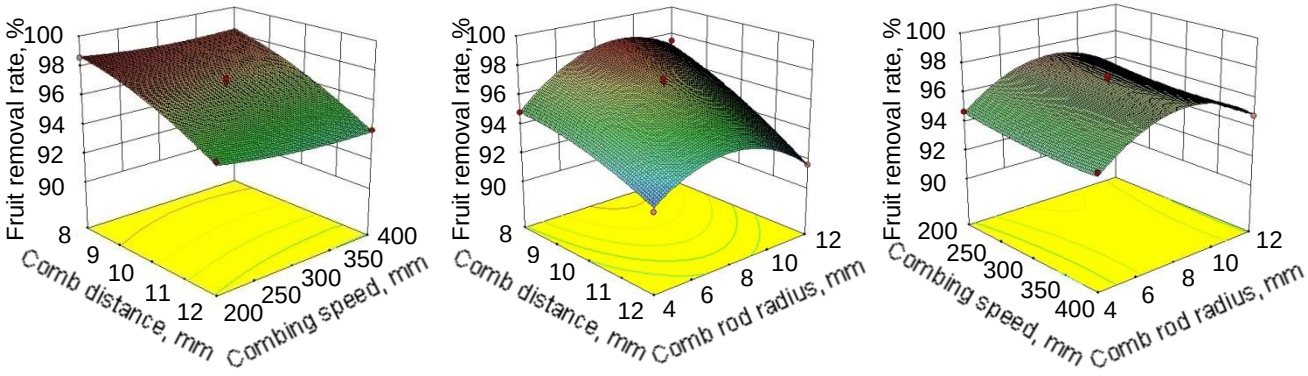

a.μ(X₁,X₂,8) ***b.μ(X₁,300,X₃)*** ***c.μ(10,X₂,X₃)***

Fig. 8 - Response surface of various factors on the fruit removal rate

Analysis of the effect of experimental factors on damage rate

The response surface of comb distance X_1, combing speed X_2 and comb rod radius X_3 to the damage rate η is shown in Figs. 9a–9c. When the comb rod radius was 8 mm, the damage rate decreased first and then increased with the increase in comb distance and increased considerably with the increase in combing speed (Fig. 9a). When the combing speed was 300 mm/s, the damage rate decreased first and then increased with the increase in comb distance and comb rod radius (Fig. 9b). When the comb distance was 10 mm, the damage rate increased with the increase in combing speed, and the damage rate decreased first and then increased with the increase in comb rod radius (Fig. 9c).

As indicated by the change range of the response value of the experimental factors to the damage rate, the order of the experimental factors influence on the damage rate was $X_2 > X_1 > X_3$. The overall influence trend was that the damage rate was low when X_1 and X_3 were moderate and the combing speed was slow. When the comb distance is small, fruit discharge hardly occurs but, blockage of the comb rod may easily occur and increase fruit damage. When the comb distance is large, fruits can easily become stuck in the comb rod clearance, resulting in internal damage of fruit. A high combing speed corresponds to an obvious extrusion effect between fruits, resulting in fruit damage. When the comb rod radius is small, the extrusion stress of comb rod on fruit is large, and the fruit is easily damaged. When the comb rod radius is large, the angle between the extrusion force and horizontal direction decreases, and the transverse deformation of fruit increases, thereby increasing the damage rate.

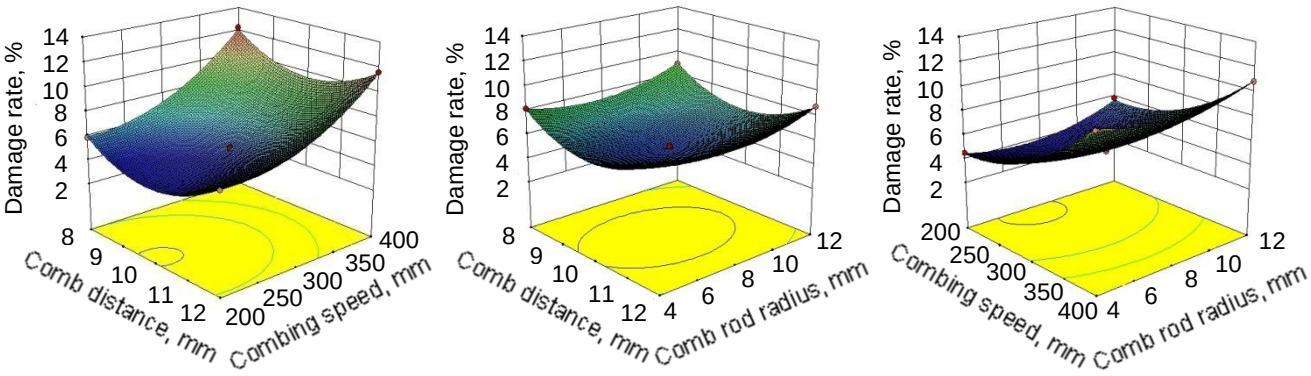

a.η(X₁,X₂,8) ***b.η(X₁,300,X₃)*** ***c.η(10,X₂,X₃)***

Fig. 9 - Response surface of various factors on damage rate

Parameter optimisation and validation

To ensure enhanced performance of the combing parts, this paper aimed to achieve a high fruit removal rate, low damage rate and high efficiency and optimised combing parts. The optimal numerical module in Design Expert software was used to solve the optimisation problem. Its objective function and constraints are as follows:

$$\begin{cases} \max Y_1 \\ \min Y_2 \\ \max X_2 \\ X_1 \in [8\text{mm},12\text{mm}] \\ X_3 \in [4\text{mm},12\text{mm}] \end{cases} \quad (14)$$

After optimisation, the optimum combination of parameters was obtained as follows: comb distance of 9.29 mm, combing speed of 335.4 mm/s, comb rod radius of 8.22 mm. Predicted value of the fruit removal rate was 97.37% and damage rate was 6.71%.

The validation test was carried out on a fruit comb threshing experimental device with parameter combination (the comb distance was 9 mm, the combing speed was 340 mm/s and the comb rod radius was 8 mm). The experiment was repeated five times to obtain the average value. Results showed that the fruit removal rate was 96.89% and the damage rate was 6.36%. These values were consistent with the result of optimisation parameters. Moreover, the regression model was reliable.

CONCLUSIONS

1) The mechanical injury evaluation standard of *C. humilis* was established based on the extrusion deformation energy and fruit storage days. The contact force of *C. humilis* during combing was analysed. The key factors affecting extrusion deformation were comb distance, combing speed and comb rod radius.

2) The results of single-factor experiment showed that the fruit removal rate decreased, and the damage rate first decreased and then increased with the increase in comb distance. The fruit removal rate remained unchanged, and the damage rate gradually increased with the increase in combing speed.

The fruit removal rate first increased and then decreased with the increase in comb rod radius, and the damage rate first decreased and then increased.

3) Response surface analysis demonstrated that the order of influence on the fruit removal rate was comb rod radius > comb distance > combing speed, and the order of influence on the damage rate was combing speed > comb distance > comb rod radius.

4) With high fruit removal rate, low damage rate and high work efficiency as optimisation objectives, the following optimum parameters were obtained: comb distance of 9.29 mm, combing speed of 335.4 mm/s, comb rod radius of 8.22 mm. Predicted value of the fruit removal rate was 97.37% and damage rate was 6.71%. With the optimised parameters (comb distance of 9 mm, combing speed of 340 mm/s and comb rod radius of 8 mm), the validation experiment was carried out. The results showed that the fruit removal rate was 96.89% and the damage rate was 6.36%, which were basically consistent with the optimised parameters, Moreover, the regression model was reliable.

ACKNOWLEDGEMENTS

This research titled 'Parameter optimisation and experiment on the combing of *Cerasus humilis*' was funded by the Key Research and Development Plan of Shanxi Province, China (201703D221029-1). The authors are grateful and honoured to have obtained support from the Laboratory of Key Technology and Equipment for Dry Farming Machinery.

REFERENCES

[1] Bao Y.D., (2017), Collision injury assessment of mechanical harvesting blueberry fruit based on collision deformation energy. *Transactions of the Chinese Society of Agricultural Engineering*, Vol. 33, Issue 16, pp. 283-292;

[2] Chen S.R., (1999), Process simulation on stripping rotor with triangle plate teeth. *Transactions of the Chinese Society of Agricultural Engineering (Transactions of the CSAE)*, Vol.15, Issue 1, pp. 59-62, Beijing/P.R.C;

[3] Chen X.S., (2015), Design and experiment of roots-soil separating device of knotweeds. *Transactions of the Chinese Society for Agricultural Machinery*, Vol. 46, Issue 7, pp. 59-65, Beijing/P.R.C;

[4] Golub G.A., (2018), Research on a boiler furnace module effectiveness working on small fracture wastes. *INMATEH-Agricultural Engineering*, Vol. 55, No.2, pp.9-18, Bucharest/Romania;

[5] Gao Z.C., (2013), Development and test of picking actor in oil-tea camellia fruit picking machine of tooth comb type. *Transactions of the Chinese Society of Agricultural Engineering (Transactions of the CSAE)*, Vol. 29, Issue 10, pp. 19-25, Beijing/P.R.C;

[6] Ji C.Y., (2016), Structure design and experiment of hand-push chrysanthemum morifolium comb-teeth picking machine. *Transactions of the Chinese Society for Agricultural Machinery*, Vol. 47, Issue 7, pp. 143-150, Beijing/P.R.C;

[7] Ji C.Y., (2017), Design and experiment of shear-sucting mountain chrysanthemum picking machine. *Transactions of the Chinese Society for Agricultural Machinery*, Vol. 48, Issue 11,pp. 137-145, Beijing/P.R.C;

[8] Ji M.Y., (2016), Design of rapeseed harvester combined stripping table with cutting table. *Journal of Huazhong Agricultural University*, Vol. 35, Issue 5, pp. 117-124, Beijing/P.R.C;

[9] Li C., (2017). Design and experiment of wine grape trellis travelling stripping platform. *Transactions of the Chinese Society for Agricultural Machinery*, Vol. 48, Issue 2, pp. 98-103, Beijing/P.R.C;

[10] Liu H.F., (2013), Experimental study on technical parameters of Cerasus humilis picking device. *Journal of Shanxi Agricultural University (Natural Science Edition)*, Vol.33, Issue 4, pp. 342-345, Jinzhong/ P.R.C;

[11] Peterson D L., (1997), Fresh market quality blueberry harvester. *Transactions of the ASAE*, Vol. 40, Issue 3, pp.535-540, WA/USA;

[12] Peterson D L., (2003), Fresh-Market Quality Tree Fruit Harvester Part I: Sweet Cherry. *Applied Engineering in Agriculture*, Vol. 19, Issue 5, pp.539-544, WA/USA;

[13] Sun Z.B., (2016), Experiment on physical parameter and biomechanical properties of Cerasus humilis 5. *Agricultural Engineering*, Vol.6, Issue 2, pp. 1-4, Beijing/P.R.C.

[14] Wang Y.C., (2009). Optimization of parameters of blackcurrant harvesting mechanism. *Transactions of the Chinese Society of Agricultural Engineering (Transactions of the CSAE)*, Vol. 25, Issue 3, pp.79-83, Beijing/P.R.C;

[15] Xu L.M., (2018). Design and operating parameter optimization of comb brush vibratory harvesting device for wolfberry. *Transactions of the Chinese Society of Agricultural Engineering (Transactions of the CSAE)*, Vol. 34, Issue 9, pp. 75-82, Beijing/P.R.C;
[16] Yuan J.N., (1998). Researches of the theory for stripping harvester design. *Transactions of the Chinese Society for Agricultural Machinery*, Vol. 29, Issue 2, pp. 37-43, Beijing/P.R.C;
[17] Zhang W., (2018). Simulation analysis and experiment of combing pluck of Cerasus humilis. *Agricultural Engineering*, Vol.8, Issue 5, pp.89-94, Beijing/P.R.C;
[18] Zhang Z.L., (2014). Design and experiment of corn stripping monomer mechanism. *Transactions of the Chinese Society of Agricultural Engineering (Transactions of the CSAE)*, Vol. 30, Issue 20, pp. 1-9, Beijing/P.R.C;

PHYSICAL PROTECTION IN EXPERIMENTAL RASPBERRY PLANTATION
/
ФІЗИЧНИЙ ЗАХИСТ В ЕКСПЕРИМЕНТАЛЬНІЙ ПЛАНТАЦІЇ МАЛИНИ

Szalay K.[1)], Keller B.[1)], Kovács L. [1)], Rák R. [1)], Peterfalvi N.[1)], Sillinger F. [2)], Golub G.[3)], Kukharets S.[*4)], Souček J.[5)], Jung A.[2)]

[1)]NAIK Institute of Agricultural Engineering / Hungary, [2)]Szent István University, Faculty of Horticultural Sciences, Technical Department / Hungary; [3)] National University of Life and Environmental Sciences of Ukraine / Ukraine;
[4)] Zhytomyr National Agroecological University / Ukraine;
[5)] Research Institute of Agricultural Engineering / Czech Republic

Keywords: *shade tunnel, spectroscopy, raspberry production*

ABSTRACT

One of the biggest challenges of raspberry production in Hungary nowadays is the reduction of unfavourable effect of climate changes. The maturation phase of main varieties within the Carpathian Basin falls in a period of extremely high temperature - reaching, or even exceeding, 35-40 °C - and atmospheric drought. This detains the desirable fruit growth. In order to restore or even save the domestic raspberry production and market, introduction of greenhouse or polytunnel solutions is needed. Experimental plantations of three different raspberry varieties were set in two repetitions: covered and uncovered versions. Each cover has characteristic light reflection /absorption/ transmission which should generate devious environmental conditions and also different plant growth. Besides the monitoring of elementary biological indicators a wide range of sensors (temperature, humidity, solar irradiation, spectroradiometer) were used to quantify the difference between cover materials to find the optimal tunnel material for maximal plant productivity.

РЕФЕРАТ

Одним з найбільших викликів виробництва малини в Угорщині сьогодні є зменшення несприятливого впливу змін клімату. Фаза дозрівання основних сортів в межах Карпатського басейну потрапляє в період надзвичайно високих температур та посухи - досягає, або навіть перевищує 35-40°C. Це затримує бажаний ріст плодів. Для того, щоб відновити або навіть зберегти виробництво малини, необхідно впроваджувати парникові або політунельні рішення, щодо її вирощування. Експериментальні плантації трьох різних сортів малини були встановлені в двох повторах: покриті і відкриті способи вирощування. Кожне покриття мало характерне відбиття /поглинання/ світла, яке повинне генерувати умови навколишнього середовища, а також різне зростання рослин. Крім моніторингу елементарних біологічних показників для кількісного визначення різниці між покривними матеріалами для пошуку оптимального тунельного матеріалу для максимальної продуктивності рослин використовувався широкий спектр датчиків (температура, вологість, сонячне опромінення, спектрорадіометр).

INTRODUCTION

At least 80% of the world's raspberry production is covered by leading raspberry producers located in Eastern Europe. Climate change scenarios generate serious threat on raspberry plantations throughout this region. Plant growth, yield and fruit quality are all affected by the increased number of high temperatures, atmospheric drought and sunburn (Figure 1).

Fig. 1 – The symptoms of sunburn

Farmers regularly experience reduction in plant growth, leaf area, yield and fruit quality. Visual signs of heat stress, sunburn are often registered during the summer periods induced by excessive heat and direct radiation causing decreasing photosynthetic activity of plants. Dedicated plant breeding programs have been started to mitigate the effects of climate change *(Dénes, 2016)* but these programs need long time. Fighting alone by using biological ways is not enough. An immediate action is required to save the raspberry production. A physical protection against excessive direct radiation can be considered as the only way to restore the stability and quality of production on short term. Nevertheless, returning the site of raspberry production to the forests (where the species is originated from) or agroforestry systems *(Nagy, 2017)* can be also considered as a solution on middle and long term. Combining solar panels with agriculture *(Hanley, 2017, Hajdú, 2018)* in this particular place can offer an even more reasonable way to solve the question of excessive radiation. An accurately adjusted portion of radiation would be transferred to electricity while the rest can be used by the protected plantation below. In this case, the shading system would produce energy which would possibly offer a more sustainable way of fighting against the effects of climate change *(Szalay K. et al., 2016)* and energy scarcity. Beside the reduction of direct radiation various shading solutions and applied materials are expected to change the spectral characteristic of incident light and so the light utilisation of plants. In order to find a reasonable solution to protect the plants and increase the stability of the production a raspberry plantation with different varieties was established. A sun protective shade tunnel system was erected to create a test site at NARIC - Fruitculture Research Institute (FRI), Fruit Culture Research and Development Institute of Fertőd, Hungary. It provides opportunity to measure and evaluate relevant biological and physical parameters playing an important role in berry production (*Keller et al., 2018*). An additional problem is plant protection. The climate change results in the migration of different pests like Drosophylla Suzukii (Figure 2) which threats the raspberry plantation and can cause 100% yield loss (Figure 3.). Protection against the pest is challenging especially in organic farms where chemical protection is limited. Within the frame of the project the effect of shade materials and possibility to use them against Drosophylla Suzukii was studied.

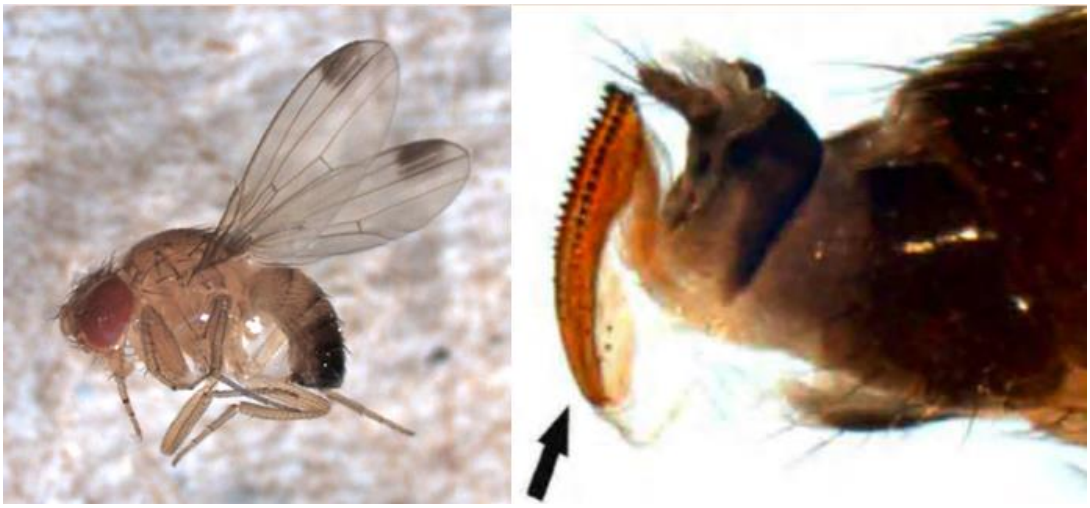

Fig. 2 – Drosophylla suzukii

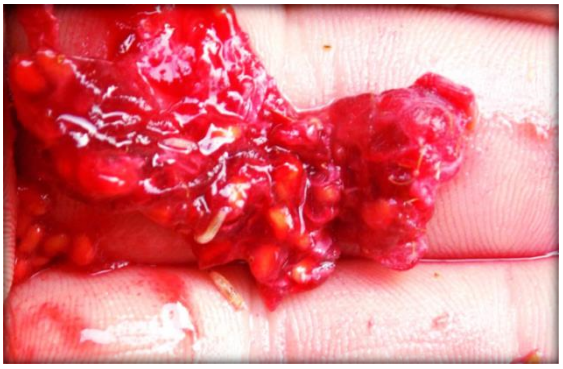

Fig. 3 – Fruit damaged by *Drosophylla suzukii*

Modern remote sensing applications *(Fenyvesi, 2008)* such as portable spectroradiometers can widely be used both in field and under laboratory conditions. It is adequate to carry out independent, fast and precise evaluations in an economic way. ASD FieldSpec 3 MAX portable spectroradiometer *(Csorba et al., 2014, Fekete et al., 2016)* was used to evaluate the incident radiation within the polytunnels and the spectral response of the vegetation. The device extends the range of the detectable visible light *(Lágymányosi and Szabó, 2009, Williams et al., 2010)* to NIR (near infrared) and the SWIR (shortwave infrared) region and covers the range of 350 to 2500 nm *(Szőke et al., 2011)*. The technology provides opportunity to reveal such differences in natural light conditions that are usually unmeasured by traditional weather stations and makes possible to study the correlation between light condition and plant growth in a more complex way.

MATERIALS AND METHODS

Field measurements were carried out in the control area and under two different types of tunnels. Data acquisition was made with ASD FieldSpec 3 MAX portable spectroradiometer. As a reference the full sky irradiation in the control plantation was measured without any cover material above (Figure 4). A reference panel was used as a standard surface that reflects 95% of all incident radiation. Using this etalon the light conditions between treatments (tunnels) could be compared.

Fig. 4 – Tunnels with different cover materials and white reference measurement under open sky

Following this, further measurements were carried out under black and white tunnels. Measurements were carried out in the range of 350 to 2500 nm. In parallel, with in situ meteorological sensors, temperature, humidity and global radiance (400-1100 nm) were measured with Almemo 2890-9 data logger (Figure 5).

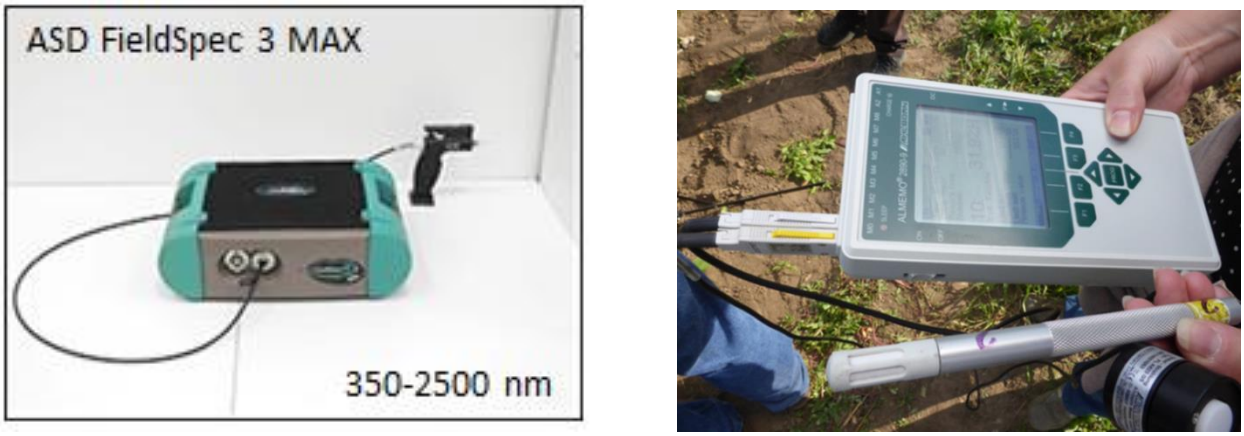

Fig. 5 – ASD FieldSpec3 MAX and Almemo 2890-9 data logger

Beside the above described non-contact data acquisition contact measurements were also carried out. In order to compare the light utilization efficiency, the water and nitrogen management of plants under various circumstances PlantProbe was used to measure the reflectance characteristic of plant leafs within each treatments (Figure 6).

Fig. 6 – Contact reflectance measurement with PlantProbe

From these spectra, photochemical reflectance index (PRI), water index (WBI) and normalizes nitrogen index (NDNI) were calculated with the following equations:

$$PRI = \frac{\rho_{531} - \rho_{570}}{\rho_{531} + \rho_{570}}, \; WBI = \frac{\rho_{970}}{\rho_{900}} \tag{1}$$

$$NDI = \frac{\log\left(\frac{1}{\rho_{1510}}\right) - \log\left(\frac{1}{\rho_{1680}}\right)}{\log\left(\frac{1}{\rho_{1510}}\right) + \log\left(\frac{1}{\rho_{1680}}\right)} \tag{2}$$

Results showed rather high differences within spectra and global radiance but relatively small difference could be detected between other environmental indicators.

RESULTS

While the white tunnel's material absorbed 15 to 30 percent of the light the black material absorbed 40 to 50 [%] of the irradiation. In case of the white material the absorbance level seems more wavelength sensitive than in case of the black material (Figure 7 and Figure 8).

In comparison with the control area, in the tunnel the temperature (Figure 9) was lower, especially in the black tunnel.

The light utilization efficiency was higher under both tunnels than it was in the control area. In case of black tunnel the photochemical index was even higher. In case of water and nitrogen content of leafs no significant difference could be found (Table 1). It means that the soil preparation, nutrient supply and irrigation could create the favourable homogeneity for the plantation. It indicates that the only variable between treatments really is the difference in illumination.

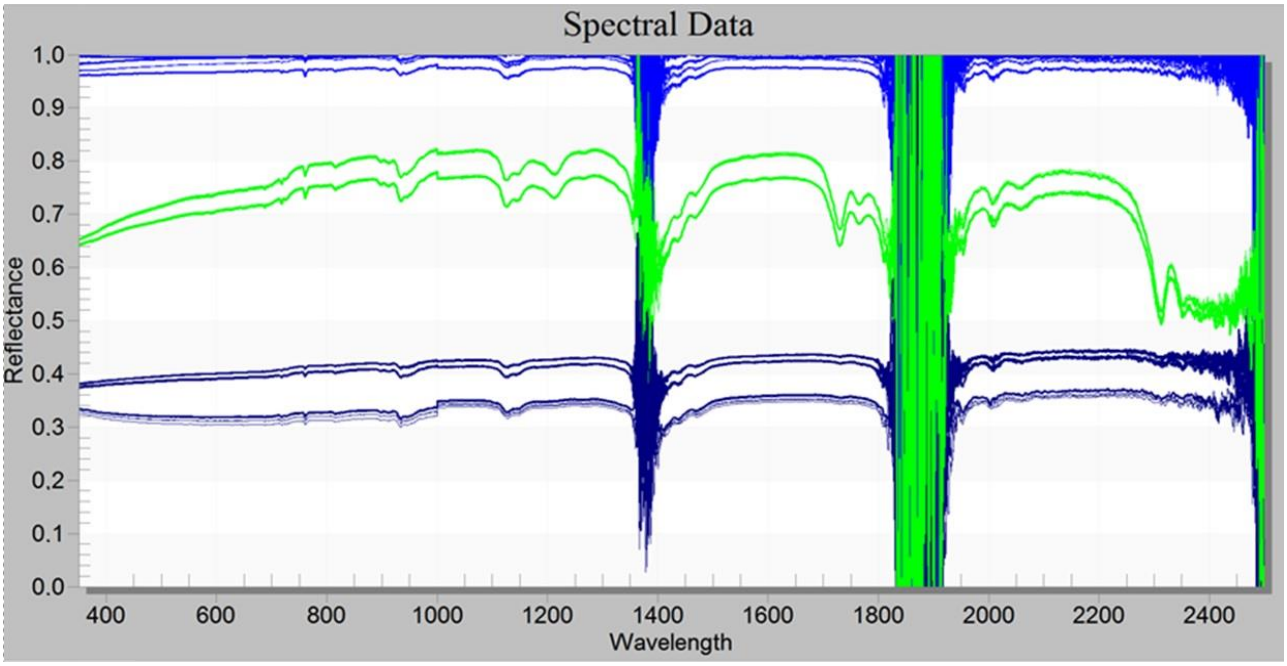

Fig. 7 – Reflectance curves: Full sky (bright blue), black tunnel (dark blue), white tunnel (green)

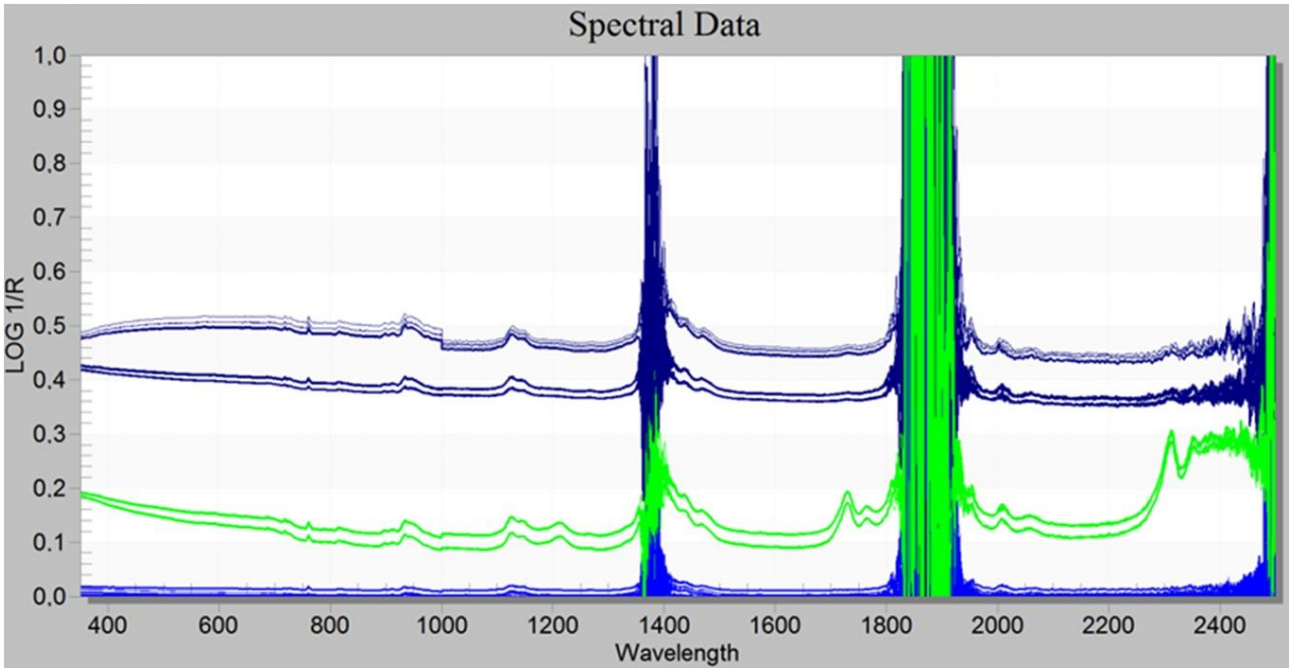

Fig. 8 – Absorbance curves: Full sky (bright blue), black tunnel (dark blue), white tunnel (green)

Table 1

Spectral plant indicators in different treatments

	White tunnel	Black tunnel	Control
Photochemical reflectance index	0.048	0.075	0.044
Water reflectance index	2.946	2.950	2.956
Normalized nitrogen index	0.143	0.139	0.143

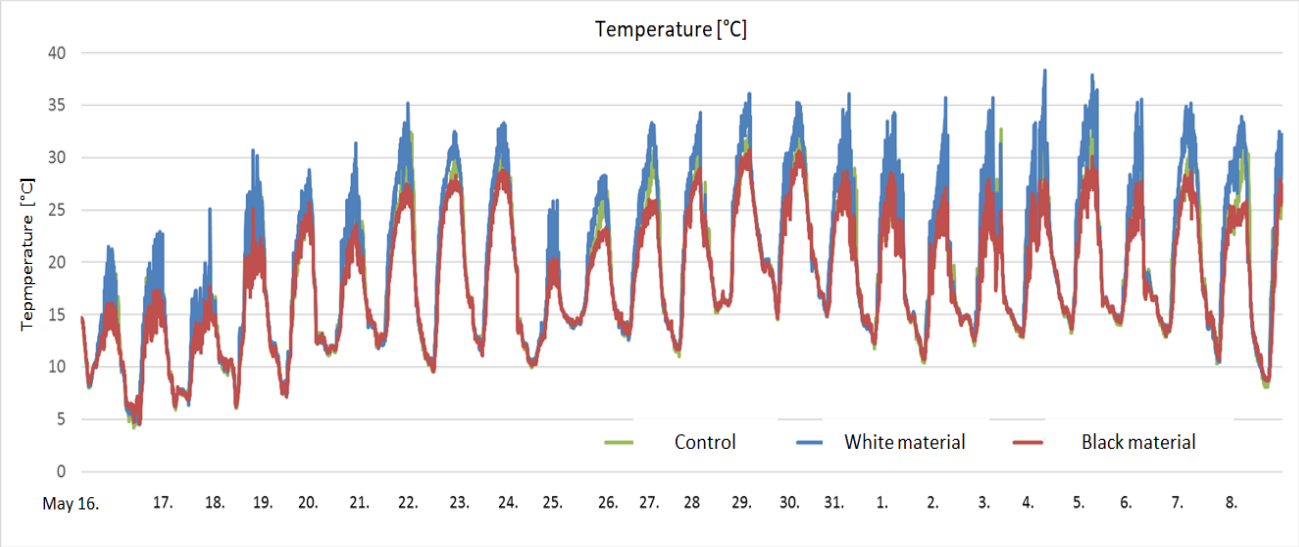

Fig. 9 – Temperature in different treatments

The yield results of year 2016 and 2017 show interesting correlation between different varieties. Results indicate both different effects in total yield and mean berry weight. Certain varieties reacted with higher yield to both types of cover material compared to the control while others did not react significantly to the cover materials (Table 2, Table 3).

Table 2

Yield and berry weight in 2016

Yield 2016				
Name of the variety	**Total yield (g)**	**Ratio**	**Mean berry weight (g)**	**Ratio**
***Julcsi* (covered with white)**	80769	172.2	2.68	90.2
***Julcsi* (control)**	46910	100.0	2.97	100.0
***Julcsi* (covered with black)**	47151	141.8	2.67	96.0
***Julcsi* (control)**	33250	100.0	2.78	100.0
***Fertodi succulent* (covered with white)**	51440	108.2	2.61	103.2
***Fertodi succulent* (control)**	47525	100.0	2.53	100.0
***Fertodi succulent* (covered with black)**	26378	99.1	2.40	99.6
***Fertodi succulent* (control)**	26617	100.0	2.41	100.0
***Eszterhaza productive* (covered with white)**	24057	240.5	1.93	104.6
***Eszterhaza productive* (control)**	10004	100.0	1.84	100.0
***Eszterhaza productive* (covered with black)**	16345	244.3	1.76	97.2
***Eszterhaza productive* (control)**	6691	100.0	1.81	100.0

The analysis of the yield and berry weight in 2016 showed that the ratio of average total yield in a white tunnel to control was 173.6 and in a black tunnel – 161.7. The ratio of mean berry weight in a white tunnel to control was 99.4 and in a black tunnel – 97.6.

The analysis of the yield and berry weight in 2017 showed that the ratio of average total yield in a white tunnel to control was 145.0 and in a black tunnel – 90.8. The ratio of mean berry weight in a white tunnel to control was 111.2 and in a black tunnel – 109.0.

The number of pests collected by traps in the plantation showed minor differences between treatments (Figure 10). The negative effect of the decreasing temperature is visible on the falling number of *Drosophylla suzukii*.

Table 3

Yield and berry weight in 2017

Yield 2017				
Name of the variety	**Total yield (g)**	**Ratio**	**Mean berry weight (g)**	**Ratio**
***Julcsi* (covered with white)**	75092	124.19	2.26	113.57
***Julcsi* (control)**	60465	100.00	1.99	100
***Julcsi* (covered with black)**	69474	98.62	2.15	118.13
***Julcsi* (control)**	70446	100.00	1.82	100
***Fertodi succulent* (covered with white)**	141818	106.58	2.58	83.23
***Fertodi succulent* (control)**	133057	100.00	3.10	100
***Fertodi succulent* (covered with black)**	112024	105.36	2.51	91.94
***Fertodi succulent* (control)**	106326	100.00	2.73	100
***Eszterhaza productive* (covered with white)**	30797	204.24	1.90	136.69
***Eszterhaza productive* (control)**	15079	100.00	1.39	100
***Eszterhaza productive* (covered with black)**	18406	68.27	1.86	116.98
***Eszterhaza productive* (control)**	26960	100.00	1.59	100

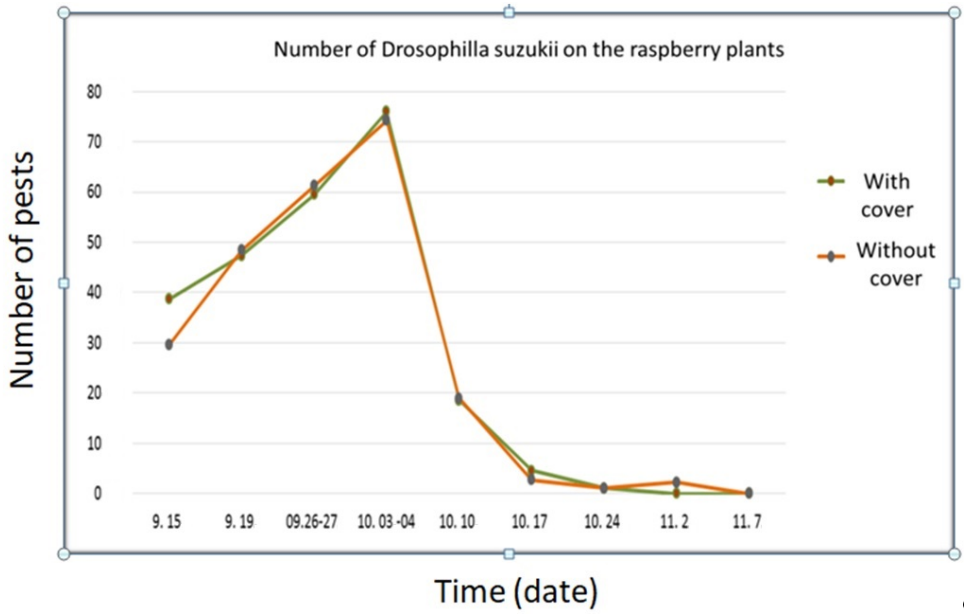

Fig. 10 – The number of pests found in the plantation from September to November

CONCLUSIONS

The preliminary results show significant differences between covered and uncovered plantations. Physical parameters reveal differing characteristics of the two experimental cover materials. It seems there is a strong variety-specific effect. Certain varieties showed no reaction to the covering materials. On the other hand, some varieties increase their yield and average fruit size decisively. The analysis showed that the ratio of average total yield in a white tunnel to control was 159.3 and in a black tunnel – 126.2. The ratio of mean berry weight in a white tunnel to control was 105.3 and in a black tunnel – 103.3.

With an appropriate covering material and shade tunnel solution the latter can provide huge advantage for the farmer on the market. Based on the data obtained, Photochemical Reflectance Index is a good indicator to find optimal light conditions for the plants and the spectroscopy in general proved to be a good solution to find potential cover materials.

An ecological friendly solution to protect the plantation against Drosophylla suzukii is to totally close the plantation. This would increase the positive effects of the shade net by providing closed microclimate for the plants and also a physical, chemical-free protection against the pests.

The biological indicators such as growth, flowering, yield (quantity and quality) are also registered and are still under monitoring. Although the first synthesis show close correlation with the registered physical parameters the continuation, further measurements and analysis are necessary to describe all correlations and identify the best production practice.

ACKNOWLEDGEMENT

Authors would like to express their acknowledgements to the Hungarian Ministry of Agriculture to fund this research project and to colleagues at the NARIC - Fruitculture Research Institute (FRI), Fruit Culture Research and Development Institute of Fertod, Hungary to measure and evaluate relevant biological parameters and for the everyday hard work to maintain and preserve the experimental site. Our special thanks go to Cubert GmbH, Germany, which made it possible to use and test the hyperspectral frame camera. Thanks go to the János Bolyai Research Scholarship of the Hungarian Academy of Sciences to support András Jung's participation in the research project.

REFERENCES

[1] Csorba A., Lang V., Fenyvesi L., Micheli E., (2014), Identification of WRB Soil Classification Units from Vis-Nir Spectral Signatures. *Proceedings of the 20th World Congress of Soil Science In Commemoration of the 90th Anniversary of the IUSS: Soils Embrace Life and Universe*, pp. 539-545, Jeju / South-Korea;

[2] Dénes F., (2016), Strawberry technology and variety experiments in Fertodon (Szamócatechnológia és fajtakísérletek Fertődön), *Kertészet és Szőlészet*, vol. 35, pp. 18-20, Oldal / Hungary; Available: http://magyarmezogazdasag.hu/2016/08/31/szamoca-technologia-es-fajtakiserletek-fertodon, Access on: 12.07.2018;

[3] Fekete Gy., Issa I., Tolner L., Czinkota I., Tolner I. T., (2016), Investigation on the indirect correlation and synergistic effects of soil pH and moisture content detected by remote sensing. *Proceedings of the 5th Alps-Adria Scientific Workshop Növénytermelés*, pp. 203-206, Mali Lošinj / Croatia;

[4] Fenyvesi L., (2008), Characterization of the soil - plant condition with hyperspectral analysis of the leaf and land surface, *Cereal Research Communications,* Vol. 36, pp. 659-662, Stara Lesna / Slovakia;

[5] Hajdú J. (2018), Agro-photovoltaic equipment in agriculture (Agro-Fotovoltaik berendezések a mezőgazdaságban), *Mezőgazdasági Technika*, vol. 49, no. 4, pp. 18-19, Miskolci / Hungary;

[6] Hanley S., (2017), Combining solar panels with agriculture makes land more productive, *Clean Technica*, Available: https://cleantechnica.com/2017/11/24/combining-solar-panels-agriculture-makes-land-productive/, Access on: 12.07.2018;

[7] Szalay K., Dénes F., Szakács A., Nagy R., Katkó T., Rák R., Bablena A., Kovács L., Deákvári J., Gulyás Z., (2016), Preliminary study of various Sun protection solutions in experimental raspberry plantation, *Proceedings of the International Conference on Agricultural Engineering*, pp. 473-474 Aarhus / Denmark;

[8] Keller B.; Jung A., Nagy G. M., Dénes F., Péterfalvi N., Szalay K. D., (2018), Presentation of the applications of hyperspectral remote sensing through an example of a raspberry plantation (Hiperspektrális távérzékelés alkalmazási lehetőségeinek bemutatása egy málna ültetvény példáján keresztül), *NAIK*, pp 63-72, Gödöllő / Hungary;

[9] Lágymányosi A., Szabó I., (2009), Calibration procedure for digital imaging, *Proceedings of the International Symposium "Synergy and Technical Development 2009"*, Gödöllő / Hungary;

[10] Nagy G.M., (2017), Agroforestry – A new start in mixed-use plantations, *Proceedings of the XVII International Conference of Forests of Eurasia*, Kazan / Russia;

[11] Virág I., Szőke Cs., (2011), Filed and laboratory examinations of corn plants by means of hyperspectral imaging, *Növénytermelés*, vol. 60, pp. 69-72, Hungary;

[12] Williams P.C., Manley M., Fox, G. és Geladi, P., (2010), Indirect detection of Fusarium verticillioides in maize (Zea maize L.) kernels by NIR hyperspectral imaging, *Journal of Near Infrared Spectroscopy*, vol. 18, pp. 49-58, Australia.

DETERMINATION OF INTERACTION PARAMETERS AND GRAIN MATERIAL FLOW MOTION ON SCREW CONVEYOR ELASTIC SECTION SURFACE

/

ВИЗНАЧЕННЯ ПАРАМЕТРІВ ВЗАЄМОДІЇ ТА РУХУ ПОТОКУ ЗЕРНОВОГО МАТЕРІАЛУ ПО ПОВЕРХНІ ЕЛАСТИЧНОЇ СЕКЦІЇ ШНЕКА

Prof. DSc. Eng. Hevko R.B.[1)], Ph.D. Eng. Zalutskyi S.Z.[2)], Assoc. Prof. Ph.D. Eng. Hladyo Y.B.[2)], Assoc. Prof. Ph.D. Eng. Tkachenko I.G.[2)], Prof. DSc. Eng. Lyashuk O.L.[2)], Prof. DSc. Econ. Pavlova O.M.[3)], Prof. DSc. Econ. Pohrishchuk B.V.[1)], Assoc. Prof. Ph.D. Eng. Trokhaniak O.M.[4)], Assoc. Prof. Ph.D. Econ. Dobizha N.V.[1)]

[1)]Ternopil National Economical University / Ukraine; [2)]Ternopil Ivan Puluj National Technical University / Ukraine;
[3)]Lesya Ukrainka Eastern European National University / Ukraine;
[4)]National University of Life and Environmental Sciences of Ukraine / Ukraine

Keywords: *sectional screw conveyor, elastic section, interaction parameters, flow motion, grain material*

ABSTRACT

The article presents a new design of a screw conveyor with sectional elastic surface aimed at reducing the grain material damage degree whilst its transportation. Theoretical calculations of a grain-screw conveyor elastic section interaction were made. A dynamic model was developed for determining both the impact of design, kinematic and technological parameters of the elastic screw conveyor on the time and free path of granular material particles whilst their motion between sections and for preventing grain material-screw nonworking surface interaction to reduce the material damage.

РЕЗЮМЕ

У статті представлено нову конструкцію шнека з секційною еластичною поверхнею, яка призначена для зменшення ступеня пошкодження зернового матеріалу при його транспортуванні. Проведено теоретичний розрахунок взаємодії зернини з еластичною секцією шнека. Розроблена динамічна модель для визначення впливу конструктивних, кінематичних і технологічних параметрів еластичного шнека на час та шлях вільного переміщення частинок сипкого матеріалу при їх переміщенні між секціями, а також виключення можливості взаємодії зернового матеріалу з неробочою поверхнею шнекового робочого органу, для зниження його пошкодження.

INTRODUCTION

The problem of reducing the grain materials damage whilst their transportation by screw conveyors hasn't been solved completely despite of a great number of researches dealing with determination of the best parameters of screws. Agricultural materials damage during their transportation can be reduced considerably by using the elastic surfaces of screws the parameters of which minimize the damage and power capacity of the technological process and simultaneously provide the necessary efficiency.

Some papers are dedicated to the solving of above-mentioned problems, namely the development of energy-saving designs of screw conveyors and choosing their most efficient parameters and working modes *(Baranovsky V.M., et.al., 2018; Boyko A.I. and Kulykivskyi V.L., 2011; Haydl H.M., 1986; Hevko B.M., et.al., 2018; Hevko R.B., et.al., 2015; Hevko R.B., et.al., 2016; Hevko R.B., et.al., 2017; Hevko R.B., et.al., 2018; Lech M., 2001; Naveen Tripathi, et.al., 2015;* Owen P.J. and Cleary P.W., 2010*)*.

The results of investigations on grain-working surfaces contact interaction and also the directions of screw conveyors operational life increase are described in some papers *(Loveikin V. and Rogatynska L., 2011; Lyashuk O.L., et.al., 2015; Qi J. et.al., 2017; Roberts Alan W. and Bulk Solids, 2015).*

Some structural concepts aimed at more comprehensive solution of the above-mentioned problems have occurred more and more often in scientific literature and patents for inventions and they mostly deal with elastic elements use on working surfaces. Some theoretical investigation in this direction is described in the papers *(Lyashuk O.L., et.al., 2018; Manjula E.V.P.J., et.al., 2017; Mondal D., 2018; Tian Y. t.al., 2018; Yao Y.P. et.al., 2014; Wang D.-X., 2012)*.

Thus, a new design of screw conveyors with sectional elastic screw surface has been developed to solve the problems dealing with loose materials damage. Some theoretical substantiation on the design,

technological and kinematic parameters impact on loose material flow behaviour has been carried out, which will enable to determine the most efficient parameters and operating modes of screw conveyors suggested design.

MATERIALS AND METHODS

To reduce the degree of grain material damage whilst its transportation by screw conveyors we suggest to fasten some elastic sections to the rigid screw base which would bend when some corns are in a clearance between fixed internal surface of a guiding jacket and rotational peripheral surface of the screw.

For this purpose, an elastic screw conveyor with adjacent elastic sections overlapping has been developed the general view of which is presented in Figure 1. A photo of the spiral conveyor with elastic sections overlapping is given in Figure 2. It consists of a central shaft *1* with rigid base *2* on which elastic sections *3* are fixed by screw bolts with cup heads *4* and screw nuts *5*. Whilst agricultural loose materials transportation in the guiding jacket 6 the elastic sections are bending when some grains are pinched between the jacket fixed surface and rotational surface of the elastic sections. This results in less damage of grain material.

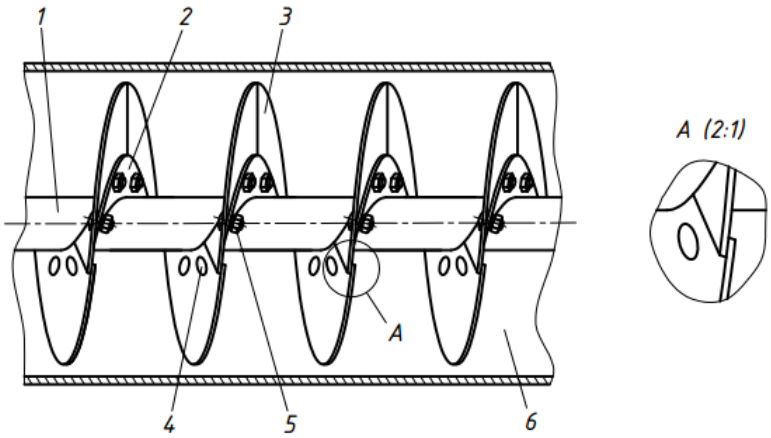

Fig. 1 – General view of the screws with elastic sections overlapping

The transported material while in operation will be rolling off the top edge of the upper section on the lower end of the next section which will have some positive effect on energy consumption of the transportation process and reduce the damage degree of the loose material.

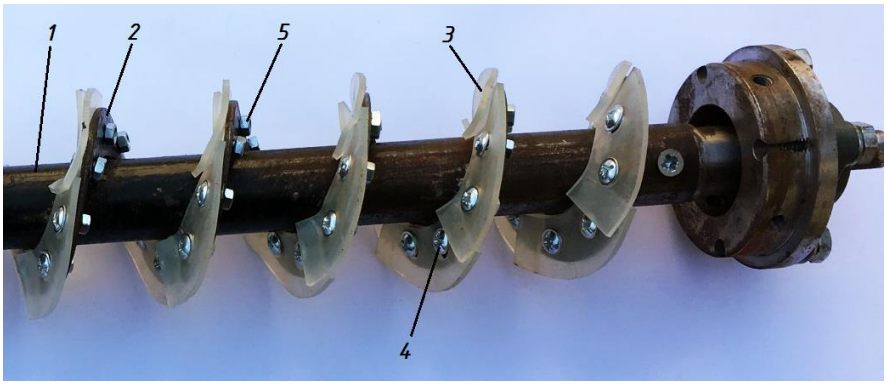

Fig. 2 – Photo of the screw conveyor with elastic sections overlapping

Let's consider a grain of corn with the shape looking like a kind of semi-sphere changing into a cone as grain material *(Hevko R.B., et.al., 2016)* when we determine the force which occur at the direct interaction of the screw elastic edge.

The position of a corn grain which can be the most probably pinched is presented in Figure 3. Let's consider the process of interaction between the screw elastic section and semi-sphere surface of a corn *1* which is pinched between the internal surface of the guiding jacket *2* and the peripheral surface of elastic section *3*.

While pinching, the corn is touching the jacket internal surface with its conical surface but its spherical surface is interacting with the screw elastic surface.

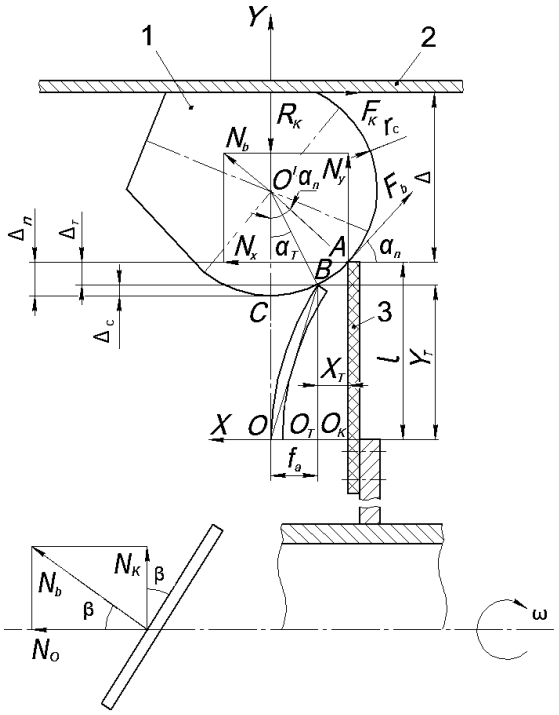

Fig.3 – Schematic diagram of forces, movements and deformations which occur between the screw elastic section and a pinched corn (semi-sphere-cone shape)

The corn pinching takes place in case when the maximum initial angle α_n between normal force of interaction of the screw elastic edge with the corn surface N_b and the plane perpendicular to the screw rotation axis is smaller than the angle of corn friction on the internal surface of the guiding jacket.

With this pinched corn the elastic section is sliding towards it in circumferential and axial directions with a certain deformation. Here the force direction N_b is approaching the axis *OY* and its value is increasing.

The theoretical calculations are aimed at defining such parameters of the corn-elastic section interaction where its damage will be impossible. It means that the screw elastic section will bend towards the pinched corn without its damage.

Let's consider the process of the elastic section movement from the beginning of its contact with the corn (point *A*) which is determined by angle α_T till the certain position (point *B*).

As the elastic section is not completely flexible and its deflection value can be neglected we will take in the first approximation that the chord length *OB* is equal to the overhang length of the elastic section *l*.

First of all, we'll find the height of the elastic section without any deformation Y_T whilst its free end motion from p. *A* to p. *B*, i.e. from the initial contact angle α_n to the current one α_T. Then

$$Y_T = l - \Delta_T \tag{1}$$

where Δ_T – value of the current clearance between the elastic section and the internal surface of the guiding jacket, m;

Value Δ_T is found from the expression

$$\Delta_T = \Delta_n - \Delta_c \tag{2}$$

where Δ_n – value of the initial elastic section overlapping with a corn, m; Δ_c – value of the residual elastic section overlapping with a corn, m.

Values Δ_n and Δ_c are found respectively

$$\Delta_n = r_c - r_c \cos\alpha_n = r_c\left(1-\cos\alpha_n\right) \tag{3}$$

$$\Delta_c = r_c - r_c \cos\alpha_T = r_c\left(1-\cos\alpha_T\right) \tag{4}$$

where r_c – radius of a corn hemispheric surface, m.

By substituting dependences (3) and (4) into (2) we obtain

$$\Delta_T = r_c\left(1-\cos\alpha_n\right)-r_c\left(1-\cos\alpha_T\right)=r_c\left(\cos\alpha_T-\cos\alpha_n\right) \quad (5)$$

By substituting (5) into (1) we obtain

$$Y_T = l - r_c\left(\cos\alpha_T-\cos\alpha_n\right) \quad (6)$$

Then we find the current value of the elastic section bending from the triangle BOO_T

$$f_a^2 = l^2 - Y_T^2,$$

$$f_a = \sqrt{l^2-\left(l-r_c\left[\cos\alpha_T-\cos\alpha_n\right]\right)^2} \quad (7)$$

After some transformations we obtain

$$f_a = \sqrt{r_з\left(\cos\alpha_T-\cos\alpha_n\right)\left(2l-r_з\left[\cos\alpha_T-\cos\alpha_n\right]\right)} \quad (8)$$

According to the known dependencies of strength of materials *(Pysarenko H.S., et.al., 1988)* the motion of loaded end of semi-beam is found as

$$f_a = \frac{Nl^3}{3EI}k \quad (9)$$

where N is a force of elastic section and a corn surface interaction, N; E – elastic modulus of elastic section, Pa; I – inertia moment of elastic section, m^4; k – coefficient calculating the shape of the auger elastic section;

By substituting f_a from the equation (8) into the equation (9), and taking into account inertia moment of elastic section the force N_b appearing between the peripheral elastic section and a corn is found by the dependence

$$N_b = \frac{E\left(b^4-a^4\right)\sqrt{r_c\left(\cos\alpha_T-\cos\alpha_n\right)\left(2l-r_c\left[\cos\alpha_T-\cos\alpha_n\right]\right)}}{16l^2\left(b-a\right)k} \quad (10)$$

In case when the elastic section width is changing by the length l from a to b the coefficient k in the first approximation is equal to $k=1-\frac{b-a}{4l}$.

While analyzing the dependencies (10) we have defined the impact of various interaction parameters on the value N_b as a preliminary.

For this reason, some possible limits of parameters values changing were found.

We assume that elastic section parameters are of trapezium shape and can be made of rubber, low or high pressure polyethylene, and also polypropylene.

According to the data *(Pysarenko H.S., et.al., 1988)* elastic modulus for these materials are: rubber (at small deformation): $E = (0.01…0.1)\cdot10^9$ Pa; low pressure polyethylene: $E = 0.2\cdot10^9$ Pa; high pressure polyethylene: $E = 0.8\cdot10^9$ Pa.

We assume, that we analyse the dependence (10) within the range of values $E = (0.05…0.25)\ 10^9$ Pa, at average value $E = 0.15\cdot10^9$ Pa.

The value of cantilever beam of elastic section was changed within boundaries $l = 0.024…0.032$ m, at average value $l = 0.028$ m.

The width of larger base b and smaller base a of a trapezoid elastic section were assumed within boundaries: $b = 0.020…0.024$ m (mean value $b = 0.022$ m); $a = 0.014…0.018$ m (mean value $a = 0.016$ m).

According to the well-known research *(Tsarenko O.M. et.al., 2003*) a corn length is within boundaries 0.0052…0.014 m; width– 0.005…0.011 m; thickness – 0.003…0.008 m.

Thus, the radius of its hemispheric surface was assumed within $r_c = 0.0015…0.0045$ m (mean value $r_c = 0.003$ m).

The range of corns friction angle change on different kinds of materials and guiding jacket internal surface roughness *(Tsarenko O.M., et.al., 2003)* was assumed within boundaries $\alpha_n = 6°…14°$ (mean value $\alpha_n = 10°$). The current angle α_T is changing from α_n to zero.

Angle β of screw surface inclination of screw elastic edge was assumed within boundaries 10°…30° (mean value β = 20°).

While determining the impact degree of the above-mentioned parameters on the value N_b we assume the boundary value $\alpha_T = 0°$. Thus in the formula (10) the value $\cos \alpha_T = 1$.

Then the dependence (10) is taking the form

$$N_b = \frac{E\left(b^4 - a^4\right)\sqrt{r_c\left(1-\cos\alpha_n\right)\left(2l - r_c\left[1-\cos\alpha_n\right]\right)}}{16l^2\left(b-a\right)k} \tag{11}$$

Force N_b, acting perpendicular to the edge plane is divided into the axial N_o force acting towards the screw axis and centrifugal force $N_к$ acting in its cross-section.

Axial and circumferential forces are taking the form respectively

$$N_o = \frac{E\left(b^4 - a^4\right)\sqrt{r_c\left(1-\cos\alpha_n\right)\left(2l - r_c\left[1-\cos\alpha_n\right]\right)}}{16l^2\left(b-a\right)k}\cos\beta \tag{12}$$

$$N_k = \frac{E\left(b^4 - a^4\right)\sqrt{r_c\left(1-\cos\alpha_n\right)\left(2l - r_c\left[1-\cos\alpha_n\right]\right)}}{16l^2\left(b-a\right)k}\sin\beta \tag{13}$$

To determine the parameters of loose material flow motion between adjacent elastic sections we consider the general view of position of adjacent elastic sections edges which are fixed to the screw rigid base (Figure 4).

Figure 4 specifies: ξ – helix angle of screw surface of auger base; ξ_1 – inclination angle of external section edge.

The size of overlapping between the edges of adjacent elastic sections and the numeric values of above-mentioned angles are defined constructively and can be chosen depending on transportation conditions.

The aim of conducting theoretical investigation is to define the motion path of loose material flow after its leaving the elastic section overhang depending on the design and kinematic parameters of the operating device, and also determining the conditions for the further motion path of loose material flow in case of its landing on the next elastic section *(Zalutskyi S.Z., et.al., 2018*).

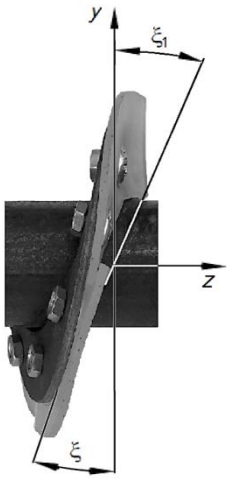

Fig. 4 – General view of position of adjacent elastic sections edges

The research results are necessary to prevent the impact interaction of loose material flow leaving the section edge with the rough base of the further screw turn where some metal joints are located which can cause the increased damage of material.

Let's analyse some loose material flow motion in case there are some overhangs on the screw surface caused by edges overlapping of adjacent elastic sections (Figure 5).

Figure 5 contains the following symbols: h – height of position of external blade edge above the lower blade; $R_к$ – jacket radius; N_1 – screw response on the load; F_1 – friction force caused by reaction N_1; N_2 – jacket response on the load; F_2 – friction force caused by reaction N_2; μ_1 – load friction coefficient on screw surface; μ_2 – load friction coefficient on jacket surface; χ – direction angle of load particle motion against jacket; ψ – angular position of load particle in its rotational motion; z – longitudinal coordinate of the particle along the jacket axis.

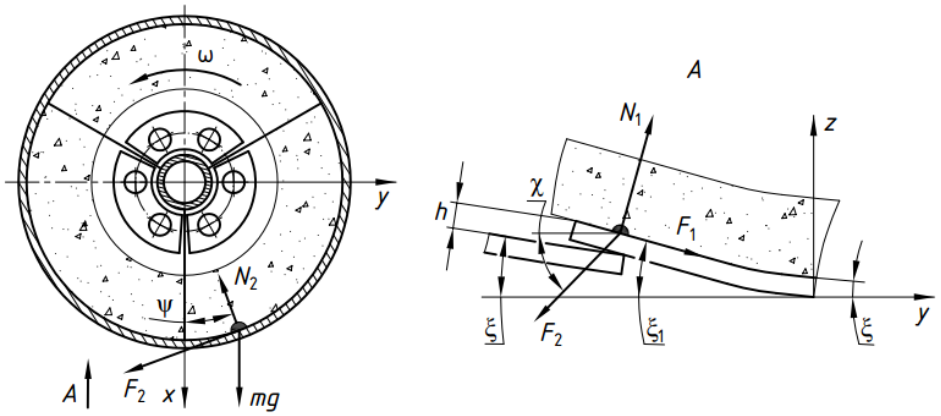

Fig. 5 – Forces acting on an elementary particle of loose cargo flow

We extract an elementary part of loose material which is simultaneously touching the jacket and the screw. Then we define the forces acting on this part and on their basis we set up the equation of its motion. On the jacket side, a reaction is taking place on the elementary particle of the flow which is perpendicular to its surface N_2, and friction force F_2, directed at the side opposite to the direction of particles motion against the jacket. Jacket's reaction is determined by the vector sum of forces obtained from the force of weight of material flow particle and centrifugal force caused by rotation. The particle is also influenced by the screw blade surface N_1 which is perpendicular to the screw surface in the contact point and correspondent force of friction F_1 acting in the direction opposite to the flow motion against the screw conveyor, i.e. tangentially to the screw edge.

The equation of motion of a certain particle of load with mass m transported by horizontal screw conveyor can be written as a system of equations *(Zalutskyi S.Z., et.al., 2018*).

$$m\frac{d^2z}{dt^2} = N_1\cos\xi - F_1\sin\xi - F_2\sin\chi \tag{14}$$

$$mR_к\frac{d^2\theta}{dt^2} = N_1\sin\xi + F_1\cos\xi - F_2\cos\chi \tag{15}$$

$$N_2 = mg\cos\psi + mR_к\left(\frac{d\psi}{dt}\right)^2 \tag{16}$$

$$F_1 = \mu_1 N_1; \tag{17}$$

$$F_2 = \mu_2 N_2 \tag{18}$$

The following geometrical dependences can be written between the directions of particle motion and screw conveyor geometry at its rotation with angular velocity ω

$$\mathrm{tg}\chi = \frac{\dot{z}}{R_к\dot{\psi}} \tag{19}$$

$$\mathrm{tg}\xi = \frac{\dot{z}}{R_к\left(\omega - \dot{\psi}\right)} \tag{20}$$

To solve the system of equations (14) - (20) we use transformations and substitutions to get rid of the unknown force and express all parameters in the terms of angle ψ value. At first, the system looks like

$$m\ddot{z} = N_1\left(\cos\xi - \mu_1\sin\xi\right) - \mu_2\left(mg\cos\psi + mR_\kappa\dot{\psi}^2\right)\sin\chi \tag{21}$$

$$mR_\kappa\ddot{\theta} = N_1\left(\sin\xi + \mu_1\cos\xi\right) - \mu_2\left(mg\cos\psi + mR_\kappa\dot{\psi}^2\right)\cos\chi \tag{22}$$

The differential equation of material particle motion for variable ψ will eventually have the form

$$\ddot{\psi} + \dot{\psi}^2 A + B\cos\psi = 0 \tag{23}$$

In this equation the coefficients *A* and *B* are found by the following dependencies

$$A = \mu_2\left[\cos(\chi+\xi) - \mu_1\sin(\chi+\xi)\right] \tag{24}$$

$$B = \frac{\mu_2 g}{R_\kappa}\left[\cos(\chi+\xi) - \mu_1\sin(\chi+\xi)\right]\cos\xi \tag{25}$$

While some loose material flow is moving it is necessary for the centrifugal force to be bigger than the weight force. Otherwise, the flow particles won't move constantly, and their overflow and mixing will take place, which will spoil badly the whole picture of flow transportation. Thus, this will be obtained under conditions

$$\dot{\psi} > \sqrt{\frac{g}{R_\kappa}} \tag{26}$$

The equation (23) is a second-order nonlinear differential equation the analytical solution of which is impossible and we must use a numerical method of such equations integration, namely Runge-Kutta method.

The important moment of motion is separation of a particle of the material flow from the external blade overhang and free motion of the flow on the jacket surface till the moment of contact with the next screw blade.

Separation of a flow particle from the blade surface is taking place at angle $\xi_1 > \xi$, which is defined by the geometry of adjacent blades relative position (Figure 4). Here, the velocity of material flow against the screw surface due to the negligible change of angle ξ_1 remains steady. The value of linear velocity of relative motion *V* of material flow is found from the kinematic dependence

$$V\sin\xi = \dot{z} \tag{27}$$

Therefore, at angle change of flow descending off the overhang

$$V\sin\xi_1 = \dot{z}_1 \tag{28}$$

Thus, the velocity values of loose material flow motion while descending off the overhang and taking into account the equations (19, 20) and (27, 28), are calculated by the formulae

$$\dot{z}_1 = \dot{z}\frac{\sin\xi_1}{\sin\xi} \tag{29}$$

$$\dot{\psi}_1 = \dot{\psi}\frac{\cos\xi_1}{\cos\xi} + \omega\left(1 - \frac{\cos\xi_1}{\cos\xi}\right) \tag{30}$$

Free motion of particles on the jacket surface in case of separation from the blade is written in the form of two second-order differential equations

$$m\frac{d^2z}{dt^2} = -F_2\sin\chi \tag{31}$$

$$mR_\kappa\frac{d^2\psi}{dt^2} = -F_2\cos\chi - mg\sin\psi \tag{32}$$

with initial conditions at the beginning of loose material leaving the section edge

$$\dot{z}(0) = \dot{z}_1, \quad z(0) = z_1 + h$$

where h – the value of overhang of external section edge above the internal surface

$$\dot{\psi}(0) = \dot{\psi}_1$$

$$\psi(0) = \psi_1 \tag{33}$$

$$\mathrm{tg}\chi = \frac{\dot{z}_1}{R_\kappa \dot{\psi}_1}.$$

After transformation we obtained

$$m\ddot{z} = -\mu_2 \left(mg\cos\psi + mR\dot{\psi}^2 \right)\sin\chi \tag{34}$$

$$mR_\kappa \ddot{\psi} = -\mu_2 \left(mg\cos\psi + mR_\kappa \dot{\psi}^2 \right)\cos\chi - mg\sin\psi \tag{35}$$

Free motion of material flow will take place until the moment of contact with one of the next screw blades. To calculate the moment and place of contact we assume that further part of screw surface is without any overhangs.

The condition of free motion of a flow particle on the screw jacket is described by the inequality

$$R_\kappa \omega t\,\mathrm{tg}\,\xi < z + R_\kappa \psi\,\mathrm{tg}\,\xi \tag{36}$$

where the expression for the screw surface ascending at its rotation is on the right-hand side, integrated motion of the flow particle along the axis z and towards rotational motion is on the left-hand side.

The material particle doesn't touch the screw surface being in free motion when the inequality is satisfied. The values z and ψ are in the solution of the system of equations (34, 35) with correspondent initial conditions.

From the inequality (36) at solving the system of equations of motion at each step the satisfaction of the above-mentioned condition, the time when a particle stops free motion t_2, and also the value of axial movement of a flow particle z_2 are defined.

Therefore, it's necessary to find the value of angle of screw relative turning and flow particle φ_2 till the moment of their next contact in time point t_2. Its value is found by the formula

$$\varphi_2 = \frac{z_2}{R_\kappa\,\mathrm{tg}\,\xi} \tag{37}$$

RESULTS

While defining the impact of any interaction parameter on values N_o and N_k its value was changed within a certain range. The other parameters remained unchangeable, and their average values were substituted in formulae (12) and (13). It was found that the elasticity modulus of elastic section screw surface had the maximal impact on values N_o and N_k, i.e. the properties of material of which the section screw surface was made.

The second in importance after the above-mentioned elasticity modulus regarding impact depth on the value N_o are the initial angle of interaction of elastic section with the grain surface α_n, length of cantilever overhang of screw elastic edge l and inclination angle β of elastic section screw surface.

The increase of a grain radius r_c results in increase both N_o and N_k.

Design parameters of trapezoid elastic section, namely the parameters a and b have minimum impact on values N_o and N_k.

As for the centrifugal force N_k, the inclination angle β of elastic edge screw surface is second in importance after modulus of elasticity regarding the impact power on its value.

Thus, within the boundaries of parameters values range change for the axial force N_o its increase is as follows: for E – 5 times increase; for α_n, – 2.34 times increase; for r_c – 1.79 times increase; for b– 1.42 times increase; for a –1.27 times increase. The decrease of value N_o is as follows: for l – 1.49 times decrease; for β – 1.15 times decrease.

For the centrifugal force N_k its increase is as follows: for E – 5.12 times increase; for β – 2.88 times increase; for α_n – 2.32 times increase; for r_c – 1.79 times increase; for b – 1.4 times increase; for a – 1.32 times increase. The decrease of value N_o is only for l – 1.33 times decrease.

For the given boundaries of interaction parameters values for the central point where plots are met the axial force value N_o is 2.76 times larger than the centrifugal force value N_k.

To analyse the obtained dynamic model (formulae 14 – 37) the program based on the language Delphi was developed. The program helped to determine the numerical characteristics and to plot parameters of the flow free motion versus the change of main coefficients of the mathematical model.

The aim of the analysis was to find the positive effect of mathematical model parameters on free motion of loose material flow. The results of modelling are shown in Figures 6 - 11. Each plot shows the effect of a certain parameter on the x-axis. Here, on y-axis, the plot time t_p and path l_p are shown of material particle free motion till its contact with the next section.

The plot in Figure 6 shows that the increase of helix angle of screw base screw surface ξ results in decrease of distance covered l_p and, correspondingly, time t_p of free motion of particles till the contact with the next section due to the decrease of velocity of loose material flow against the screw surface as exemplified by the analysis of dependency (20). So, the increase of value ξ from 10° to 30° causes the 4.2 times shorter path l_p and 3,1 times less time t_p.

Figure 7 presents plots t_p and l_p versus friction coefficient of loose material on the screw elastic sections μ_1.

Similar to the previous case, increase of value μ_1 results in decreased values t_p and l_p. Thus, the increase of friction coefficient value μ_1 from 0.2 to 0.8 results in 1.6 times shorter path l_p and 1.09 times increase of time t_p.

Figure 8 presents plots t_p and l_p versus friction coefficient of loose material on the jacket internal surface μ_2.

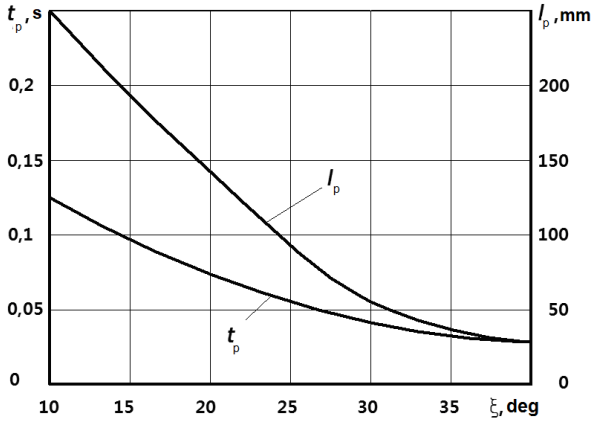

Fig. 6 – Dependencies t_p and l_p versus helix angle ξ of screw base screw surface

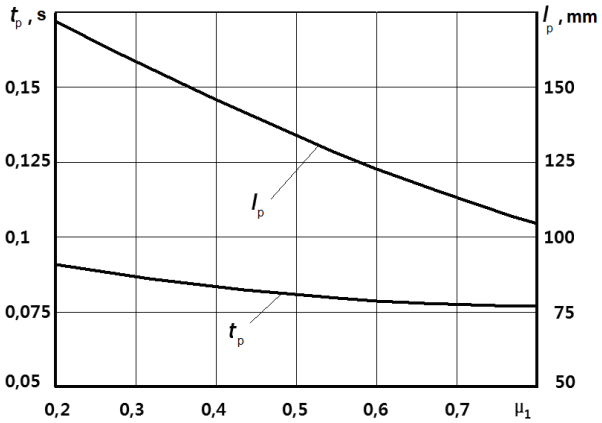

Fig. 7 – Dependencies t_p and l_p versus material friction coefficient μ_1 on screw elastic sections

Analysis of plots data shows that decreasing tendency of values t_p and l_p at increasing friction coefficient μ_2 is the same as in the previous case but the impact force is much bigger. Increase of friction coefficient μ_2 from 0.2 to 0.8 results in 2.1 times decrease of path l_p, and 1.5 times decrease of time t_p.

The following parameters have the opposite effect on the values t_p and l_p behaviour.

Figure 9 presents plots t_p and l_p versus rotation frequency n of screw operating device.

Rotation frequency n increase results in significant increase of value l_p due to the increase of velocity of particle's rolling off the external blade edge.

Thus, increase of value n from 200 to 800 rev/min results in approximately 5 times increase of value l_p.

In this case, time t_p is not changing greatly. It can be explained by the increase of angular velocity of screw rotation in such a way that the next section has approximately the same period of time to approach the flow particles.

Figure 10 presents plots t_p and l_p against height h external blade edge position above the lower blade.

It was found that the given parameter has a little influence on the flow free motion, but the increased value h causes the increase of values t_p and l_p. In fact, time difference is proportional to the time of screw rotation by value h. Thus, increase of value h from 0.5 to 0.35 mm causes the 1.24 times increase of l_p and 1.14 times increase of t_p.

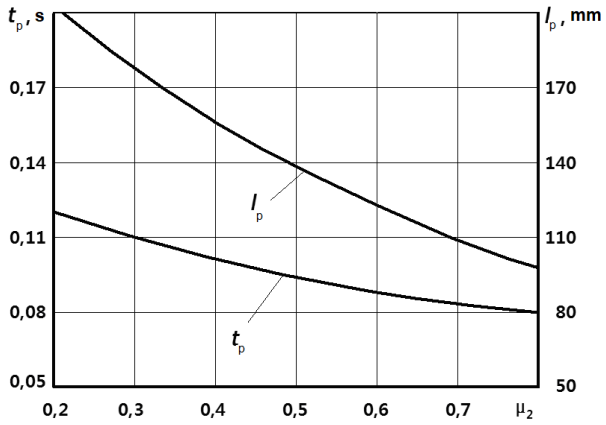

Fig. 8 – Dependencies t_p and l_p versus friction coefficient μ_2 of material on the jacket surface

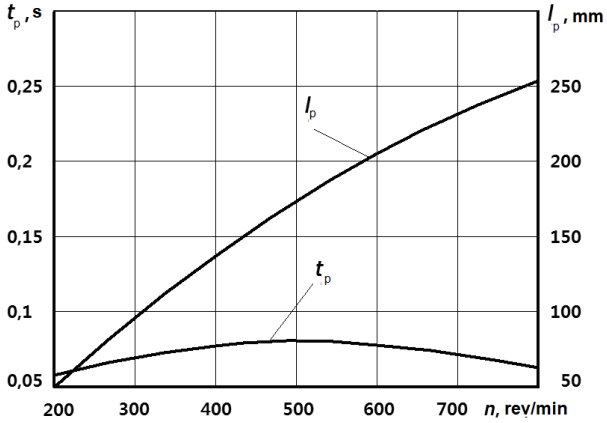

Fig. 9 – Dependencies t_p and l_p versus rotation frequency n of screw operating device

Figure 11 presents plots t_p and l_p versus material convergence angle which is determined by the inclination angle of external section edge ξ_1.

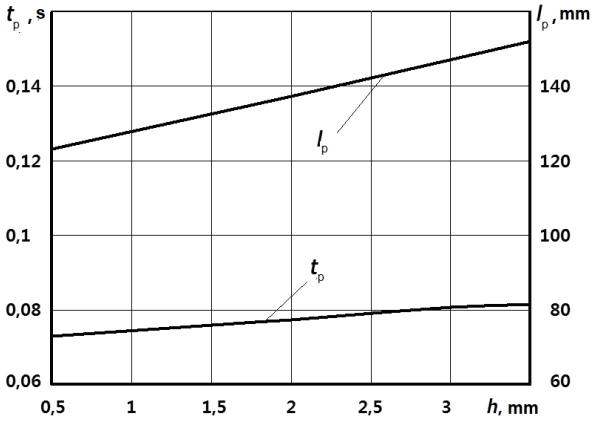

Fig. 10 – Dependencies t_p and l_p versus height h of external blade edge position above the lower blade

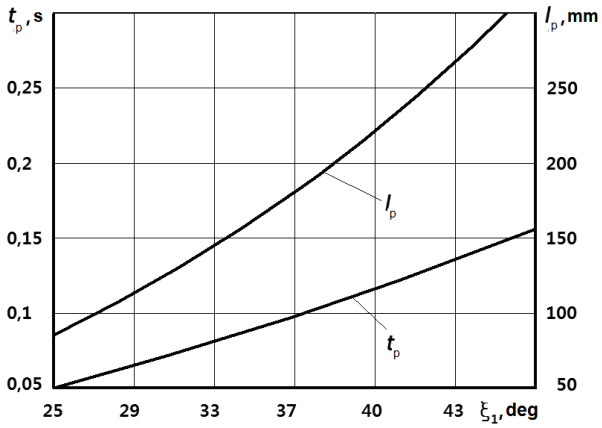

Fig. 11 – Time dependencies t_p and l_p versus inclination angle ξ_1 of external section edge

Unlike the previous case the change of inclination angle ξ_1 of external section edge greatly affects the value t_p and l_p. So, the increase of angle value ξ_1 from 25° to 45° results in 3.53 times longer path l_p and 3.16 times increase of time t_p.

Analysis of diagrams in Figures 6 – 11 allows evaluating the impact of each parameter of the system on the loose material flow behaviour at its passing through the obstacle like a step between the screw plates.

CONCLUSIONS

The most efficient parameters of elastic sections interactions with the grain material of hemisphere-cone shape were substantiated on the basis of obtained analytical dependencies.

The impact depth of interaction parameters of screw elastic section and a corn grain on the values of axial N_o and centrifugal force N_k was determined. It was found that elasticity modulus of screw elastic section has the maximal impact on the values N_o and N_k. The second in importance on the value N_o are the initial angle of interaction of screw elastic edge with grain surface, length of cantilever overhang of screw elastic section and its inclination angle.

As for the centrifugal force N_k, the second in importance after the elasticity modulus regarding impact depth on its value is the inclination angle of elastic section screw surface.

The impact of elastic screw design and kinematic parameters on the loose material flow behaviour in the area between the adjacent sections which are overlapped was determined.

On the basis of obtained analytical dependencies and their analysis we came to the conclusion that the increase of friction forces both on the screw surface μ_1 and jacket surface μ_2 results in decrease of time t_p and path l_p of particles free motion of loose material flow. The increase of friction coefficient value μ_1 from 0.2

to 0.8 causes the 1.6 times shorter path l_p and 1.09 less time t_p. The increase of friction coefficient value μ_2 from 0.2 to 0.8 causes the 2.1 times shorter path l_p and 1.5 less time t_p.

The increase of screw helix angle ξ results in shorter path l_p and time t_p due to the decrease of loose material flow velocity against the screw surface. The increase of screw helix angle ξ from 10° to 30° results in 4,2 times shorter path l_p and 3,1 times more time t_p.

The change of rotation frequency of operating device n from 200 to 800 rev/min causes the 5 times increase of path l_p of particle free motion. In this case, the time of the particle free flight t_p does not change greatly, and it can be explained by the increase of angular velocity of screw rotation, so that the next section is able to approach the flow particles in approximately the same period of time.

It was found that height h of external section free end position over the lower section has a negligible effect on material flow though the increase of value h causes the increase of values of time t_p and path l_p.

The change of departure angle of loose material flow particles which if defined by the inclination angle of external elastic section edge ξ_1 essentially affects the time t_p and path l_p of particles free motion.

Increase of value of inclination angle of external section edge ξ_1 from 25° to 45° results in 3.53 times longer path l_p and 3.16 times more time t_p.

REFERENCES

[1] Baranovsky V.M., Hevko R.B., Dzyura V.O., Klendii O.M., Klendii M.B., Romanovsky R.M., (2018), Justification of rational parameters of a pneumoconveyor screw feeder, *INMATEH - Agricultural engineering*, vol.54, no. 1., pp.15-24, Bucharest/Romania;

[2] Boiko A.I., Kulykivskyi V.L., (2011), Study of grain contact interaction in clearance “turn-jacket” of screw feeder of grain-cleaners (Дослідження контактної взаємодії зерна в зазорі “виток-кожух” шнекових живильників зерноочисних машин), *Scientific bulletin of National University of Life and Environmental Sciences of Ukraine* (Науковий вісник Національного університету біоресурсів і природокористування України), vol.166, pp.267-274, Kiev/Ukraine;

[3] Haydl H.M., (1986), Design aspects of large-diameter tubular conveyor galleries, *Proceedings of the institution of civil engineers, Part 1 – Design and construction,* vol.80, pp. 633-639, London/England;

[4] Hevko B.M., Hevko R.B., Klendii O.M., Buriak M.V., Dzyadykevych Y.V., Rozum R.I., (2018), Improvement of machine safety devices. *Acta Polytechnica, Journal of Advanced Engineering*, Vol.58, no.1, pp.17-25, Prague/Czech Republic;

[5] Hevko R.B., Zalutskyi S.Z., Tkachenko I.G., Klendiy O.M., (2015), Development and investigation of reciprocating screw with flexible helical surface, INMATEH: Agricultural engineering, vol.46, no.2, pp.33-138, Bucharest/Romania;

[6] Hevko R.B. Dzyadykevych Y.V., Tkachenko I.G., Zalutskyi S.Z., (2016), Parameter justification for interworking relationship of elastic screw operating element with grain material, *Bulletin of Ternopil Ivan Puluj National Technical University (Вісник ТНТУ ім. І.Пулюя)*, vol.81, no.1, pp. 77-87, Ternopil/Ukraine;

[7] Hevko R.B., Yazlyuk B.O., Liubin M.V., Tokarchuk O.A., Klendii O.M., Pankiv V.R., (2017), Feasibility study of mixture transportation and stirring process in continuous-flow conveyors, *INMATEH - Agricultural engineering*, vol.51, no.1, pp.49-59, Bucharest/Romania;

[8] Hevko R.B., Liubin M.V., Tokarchuk O.A., Lyashuk O.L., Pohrishchuk B.V., Klendii O.M., (2018), Determination of the parameters of transporting and mixing feed mixtures along the curvilinear paths of tubular conveyors, *INMATEH: Agricultural engineering*, vol.55, no.2, pp.97-104, Bucharest/Romania;

[9] Hevko R.B., Strishenets O.M., Lyashuk O.L., Tkachenko I.G., Klendii O.M., Dzyura V.O., (2018), Development of a pneumatic screw conveyor design and substantiation of its parameters, *INMATEH - Agricultural engineering*, vol.54, no.1, pp.153-160, Bucharest/Romania;

[10] Lech M. (2001) - Mass flow rate measurement in vertical pneumatic conveying of solid, *Powder Technology*, Vol.114, Issues 1–3, pp. 55-58;

[11] Loveikin V., Rogatynska L., (2011), A Model of Loose Material Transportation by Means of High-Speed Conveyers with Elastic Operating Devices (Модель транспортування сипкого вантажу швидкохідними гвинтовими конвеєрами з еластичними робочими органами*)*. *Bulletin of Ternopil Ivan Puluj National Technical University (Вісник ТНТУ ім. І. Пулюя)*, vol.16, pp.66-70, Ternopil/Ukraine;

[12] Lyashuk O.L., Rogatynska O.R., Serilko D.L., (2015), Modelling of the vertical screw conveyer loading*, INMATEH Agricultural Engineering*, vol.45, no.1, pp.87-94, Bucharest/Romania;

[13] Lyashuk O.L., Sokil M.B., Klendiy V.M., Skyba O.P., Tretiakov O.L., Slobodian L.M., Slobodian N.O., (2018), Mathematical model of bending vibrations of a horizontal feeder-mixer along the flow of grain mixture, *INMATEH Agricultural Engineering*, vol.55, no.2, pp.35-44, Bucharest/Romania;

[14] Manjula E.V.P.J., Hiromi W.K. Ariyaratne, Ratnayake Chandana, Morten C. Melaaen, (2017), A review of CFD modelling studies on pneumatic conveying and challenges in modelling offshore drill cuttings transport, *Powder Technology*, Vol.305, pp.782-793;

[15] Mondal D. (2018) - Study on filling factor of short length screw conveyor with flood-feeding condition, *Mater. Today Proc*., vol.5, pp.1286–1291.

[16] Naveen Tripathi, Atul Sharma, S.S. Mallick, P.W. Wypych (2015) - Energy loss at bends in the pneumatic conveying of fly ash, *Particuology*, vol.21, pp. 65-73;

[17] Owen Philip J., Cleary Paul W. (2010) - Screw conveyor performance: comparison of discrete element modelling with laboratory experiments. *Progress in computational fluid dynamics*, vol.10, Issue 5-6, pp.327-333, Geneva/ Switzerland;

[18] Pysarenko H.S., Yakovlev A.P., Matveev V.V. (1988) - Reference on strength of materials (Справочник по сопротивлению материалов), *published by Naukova Dumka (видавництво Наукова думка)*, 736p. Kiev/Ukraine.

[19] Qi J., Meng H., Kan Z., Li C., Li Y. (2017) - Analysis and test of feeding performance of dual-spiral cow feeding device based on EDEM, *Trans. Chin. Soc. Agric. Eng*., vol.33, pp. 65–71.

[20] Tian Y., Yuan P., Yang F., Gu J., Chen M., Tang J., Su Y., Ding T., Zhang K., Cheng Q. (2018) - Research on the Principle of a New Flexible Screw Conveyor and Its Power Consumption, *Applied Sciences*, vol.8, no.7.

[21] Tsarenko O.M., Voityuk L.M., Shvayko M.V. and others (2003) – Mechanical-technological properties of agricultural materials: course-book (Механіко-технологічні властивості сільськогосподарських матеріалів: підручник), *published by Meta (видавництво Мета)*, 448p., Kiev/Ukraine.

[22] Roberts Alan W., Bulk Solids (2015) - Optimizing Screw Conveyors. *Chemical engineering*, vol. 122(2), pp.62-67, New York/USA;

[23] Yao Y.P., Kou Z.M., Meng W.J., Han G. (2014) - Overall Performance Evaluation of Tubular Scraper Conveyors Using a TOPSIS-Based Multiattribute Decision-Making Method, *Scientific World Journal*, New York/USA;

[24] Wang D.-X. (2012) - Research on Numerical Analysis and Optimal Design of the Screw Conveyor, *Univ. Technol*., vol. 27, pp. 32–36.

[25] Zalutskyi S.Z., Hevko R.B., Hladio Y.B., Tkachenko I.H., Klendii O.M. (2018) – Loose material flow motion on surface of screw with overlapping elastic sections, *Kharkiv P. Vasylenko National Technical University of Agriculture (Харківський національний технічний університет сільського господарства імені Петра Василенка)*, vol.11, pp.81-90, Kharkiv/Ukraine.

DETERMINING THE PARAMETERS OF THE DEVICE FOR INERTIAL REMOVAL OF EXCESS SEED
/
ВИЗНАЧЕННЯ ПАРАМЕТРІВ ПРИСТРОЮ ДЛЯ ІНЕРЦІЙНОГО ВИДАЛЕННЯ ЗАЙВОГО НАСІННЯ

Lect. Ph.D. Eng. Vasylkovska K.V.[1)], Prof. Ph.D. Eng. Vasylkovskyi O.M. [1)],
Prof. Dr. Eng. Sc. Sviren M.O. [1)], Lect. Ph.D. Eng. Petrenko D.I. [1)], Prof. Dr. Eng. Sc. Moroz M.M. [2)]
[1)] Central Ukrainian National Technical University / Ukraine;
[2)] Kremenchuk Mykhailo Ostrohradskyi National University / Ukraine
Tel: +380667103625; E-mail: vasilkovskakv@ukr.net

Keywords: *seeds, cell, bending radius, cell disc, seeding machine*

ABSTRACT

The quality of seed dosage to the furrow depends on the uniformity of seeds location on the seed disk. A new design of a seeding machine which provides better sowing was suggested at the Department of Agricultural Machinery of Central Ukrainian National Technical University. The main feature of the new seeding machine is the application of the seed disk with a peripheral arrangement of cells with the blades on its inner surface. The blades are used for the forced seizure of the seeds by the disk in the working chamber and their further transportation to the dropping zone.

In order to determine the rational parameters of the seed cells of the seed disk, an experimental appliance was made and studies were conducted to determine the desired value of the coefficient of filling cells with seeds of different sizes. The experiments were conducted using disks with cell radii of 5.0 mm and 6.0 mm which correspond to their areas of 9.6 mm^2 and 16.3 mm^2, respectively. The vacuum in the vacuum chamber was 0.2 kPa and the peripheral velocity of the cells was 2 m/s.

Taking into account the experiments conducted, it can be stated that in order to ensure the seeding of sugar beet, the radii of the cells' rounding should be within the limits of 5...6 mm which in general is consistent with the results of theoretical studies. According to them the radius of the whole is 5.7 mm.

РЕЗЮМЕ

Якість дозування насіння до борозни залежить, в першу чергу, від рівномірності розташування насінин на висівному диску. На кафедрі сільськогосподарського машинобудування Центральноукраїнського національного університету запропоновано нову конструкцію висівного апарата, який забезпечує більш якісне дозування насіння. Головною особливістю нового висівного апарата є використання висівного диска з периферійним розташуванням комірок, за якими на його внутрішній поверхні розмішені лопатки для примусового захоплення насіння диском в робочій камері та подальшого його транспортування до зони скидання.

З метою визначення раціональних параметрів комірок висівного диска виготовлена експериментальна установка і проведені дослідження по визначенню потрібного значення коефіцієнта заповнення комірок насінням різних розмірів. Досліди проводили, використовуючи диски з радіусами твірних комірок 5.0 мм та 6.0 мм, які відповідають їх площам 9.6 мм^2 та 16.3 мм^2 відповідно. Розрідження у вакуумній камері становило 0.2 кПа, а колова швидкість комірок – 2 м/с.

На підставі проведених дослідів можна стверджувати, що для забезпечення висіву насіння цукрового буряку, радіуси заокруглення твірних комірок повинні знаходитись в межах 5…6 мм, що в цілому узгоджується з результатами теоретичних досліджень, згідно з якими визначений радіус твірної становить 5.7 мм.

INTRODUCTION

The exact seeding - is a necessary condition for obtaining evenly placed on the area of the field of plants, which in this case have the same area plant nutrition and developing well. The quality of seed dosage to the furrow depends on the uniformity of seeds layout on the seeding disc. That is why the approach for selection the form of the holes on the disc is the determinant initial condition for equal dosage (*Sysolin P V., 2004; Vasylkovska K., 2014*).

The main characteristic of the new seeding machine (fig. 1) is the use of the seeding disc with peripheral location of the cells. Behind them, on the disc internal surface, there are blades for the forced taking of the seeds by the disc in the working chamber and their further transportation to the release zone (*Mursec B., 2007; Petrenko M. M., 2011; Petrenko M. M., 2013*).

The main parameter of the cell of the experimental disc is the bending radius of generatrix which influences not only the hole area and seeds' suction process but also the capability of a suctioned seed to leave the cell at release location right in time without any delay or wedging.

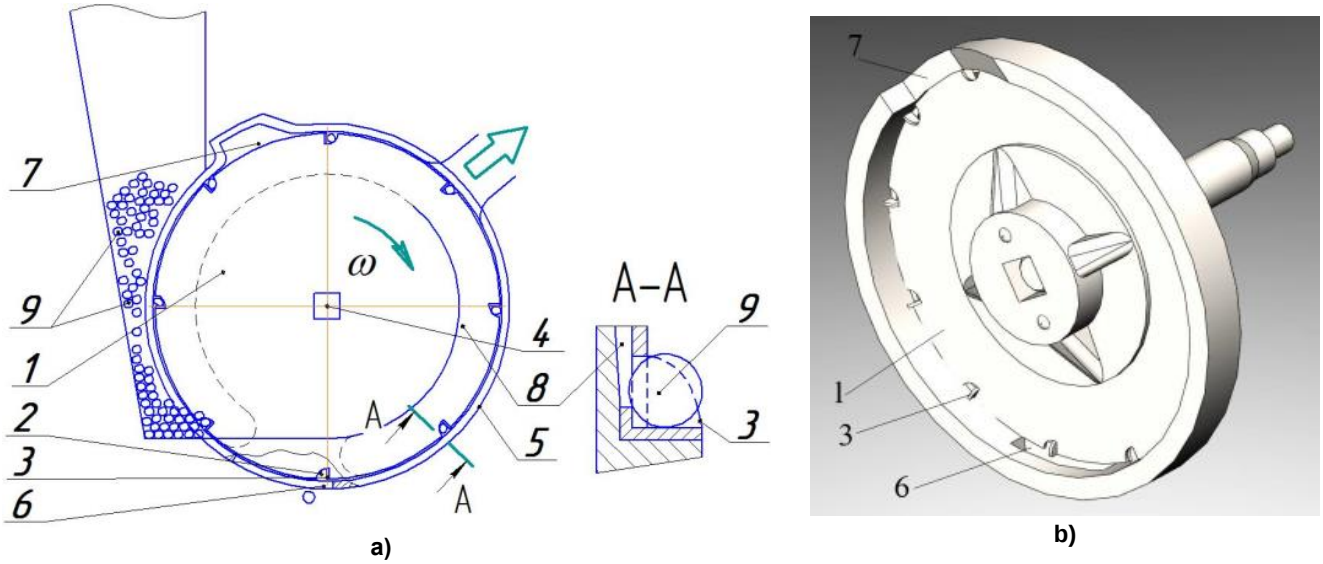

a) **b)**

Fig. 1 - Suggested pneumatic and mechanical sowing apparatus

a) the drawing; b) the three-dimensional model

1 – seeding disc; 2 – cell; 3 – blade; 4 – driving shaft; 5 – housing; 6 – seeds exit; 7 – passive appliance for extracting excessive seeds; 8 – vacuum chamber; 9 – seeds

MATERIALS AND METHODS

The proposed seed disk, due to the presence of blades, allows more securely seize and move of the seeds to the discharge zone at elevated rotational speeds of the cells. However, the question arises of defining their parameters.

To prevent seeds from sticking and moving into the vacuum chamber, we shall use the following formula:

$$S_к < S_s \tag{1}$$

where $S_к$ – is the area of cell suction, [m^2];

S_s is the area of the projection of the seed, [m^2].

Using the well-known formulae proposed by A. Budagov (*Budagov A., 1971*) and V. Chichkin (*Chichkin V., 1984*), we shall write:

$$S_к = 0{,}7 \cdot S_s \tag{2}$$

We shall determine the approximate area of suction of the cell:

$$S_к = \frac{\pi \cdot r_к^2}{4} - S_1 \tag{3}$$

where $r_к$ is the radius of the rounding of the cell, [m];

S_1 is the cross-sectional area of the standout, which is defined as $S_1 = r_к \cdot h$, [m^2];

where h is the height of the rack in the case of the seeding machine between the working chamber and the chamber of dilution, h=0.002 m (fig. 2).

Then:

$$S_к = \frac{\pi \cdot r_к^2}{4} - r_к \cdot h \tag{4}$$

For seeds of sugar beets, the area of the projection of the seed S_s is taken in the form of a circle.

Therefore, taking into account (4), the expression (2) will take the following form:

$$\frac{\pi \cdot r_к^2}{4} - r_к \cdot h = 0{,}7 \cdot \frac{\pi \cdot d_s^2}{4}$$

where d_s is a conditional diameter of the seed, [mm].

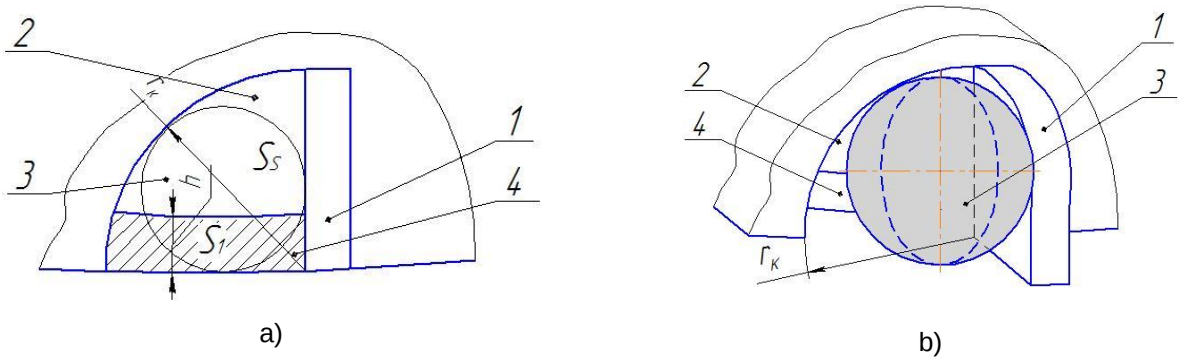

a) b)

Fig. 2 - Scheme for determining the suction area of a peripherally located cell

a) the view of the cell with a seed; b) the three-dimensional model

1 - blade; 2 - cell; 3 - seed; 4 - rack

The radius of a rounding cell will be:

$$r_к = \frac{2 \cdot \left(h + \sqrt{h^2 + \pi \cdot \frac{0{,}7\pi \cdot d_s^2}{4}} \right)}{\pi} \quad (5)$$

The dependence of the cells' area for different types of cultivated crops was obtained (Table 1).

Table 1

Parameters of the cells for different types of cultivated crops

Seeds of perennial crops	Radius of rounding cells $r_к$, mm	Area cell S_h, mm^2
Sugar beets	5.7	14.1
Soybean	7.4	28.2
Sunflower	7.6	30.2
Maize	8.5	39.7
Haricot	9.4	50.6

The dependence of the radius of the seeding disk cell of the experimental pneumatic and seeding machine on the conditional diameter of different types of cultivated crops seeds (Fig. 3) was identified.

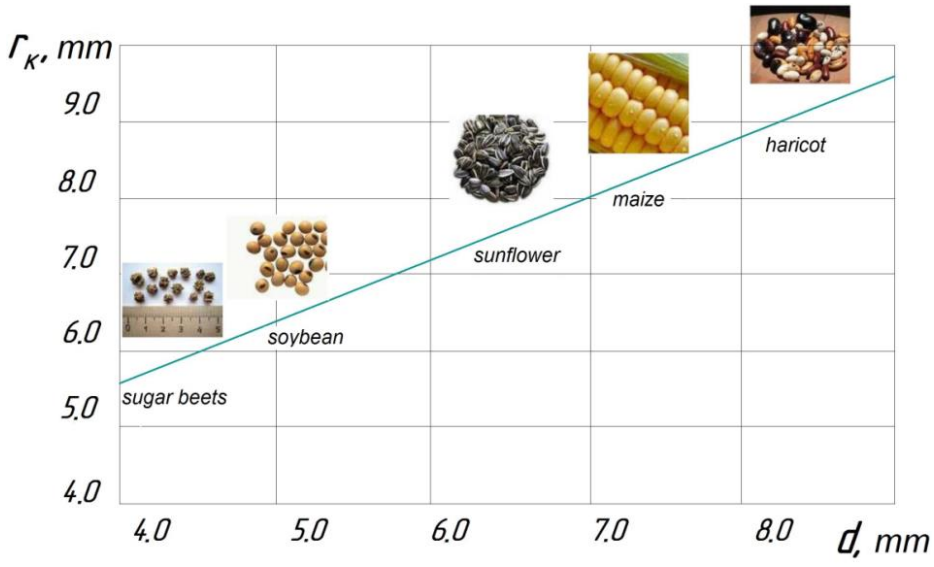

Fig. 3 - Dependence of the radius of the seeding disk cell on the conditional diameter of cultivated crops

The number of cells on the seeding disk is determined by their interval *δ*:

$$z = \frac{2\pi \cdot R}{\delta} \quad 6)$$

By setting the step *δ* of cells location on the disk, the productivity of the seeding machine can be determined by the formula:

$$N = \frac{[V_к]}{\delta} \cdot k \quad (7)$$

where $[V_к]$ is the maximum permissible rotational velocity of the cells.

It is obvious that when *k=const*, the increase in productivity of the seeding machine can be achieved either by increasing the rotational velocity of the cells, or by reducing the interval of their location on the seeding element. (*Rybar R.,1999; Voytyuk D.G., 2017*).

To confirm the theoretical assumptions made by us, experimental research was conducted to determine the optimal size of the seed disk cell for different seed types.

Characterization of rational parameters of seeding disc cells was done through calculation of the necessary coefficient value of filling the cells with seeds of various sizes. For that purpose, the sort seeds of sugar beetroot "Bilotserkivskyy odnonasinnyy 45" were divided into four sub-fractions with the help of sieves with round holes (3.5-4.0 mm; 4.0-4.5 mm; 4.5-5.0 mm; 5.0-5.5 mm) (fig. 4).

Fig. 4 - General view of sub-fractions of sugar beetroot seeds

Dilution ΔP in the vacuum chamber was 0.2 kPa, and peripheral speed of the cells $V_к$ – 2 m/s.

The experiments were carried out using discs with radiuses of tangent cells 5.0 mm and 6.0 mm, which correspond to their areas 9.6 mm 2 and 16.3 mm 2 correspondently (fig. 5).

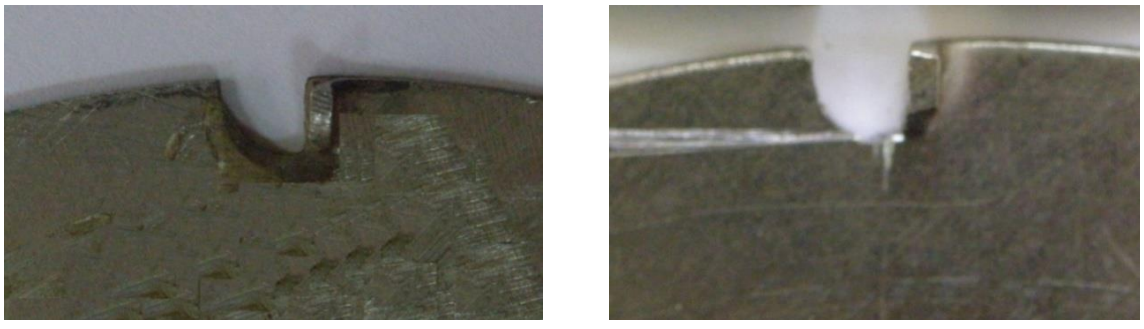

a) ***b)***

Fig. 5 - General view of the cells on the sowing disc

a) the cell with the generatrix radius 5 mm; b) the cell with generatrix radius 6 mm.

RESULTS

The criterion for defining the rational parameters of sowing disc is the coefficient of cells filling by the seeds of corresponding sub-fractions (first – 3.5-4.0 mm; second – 4.0-4.5 mm; third – 4.5-5.0 mm; fourth – 5.0-5.5 mm).

To take into account the influence of the possible presence of twins, video recording of the seeding process was carried out (fig. 6).

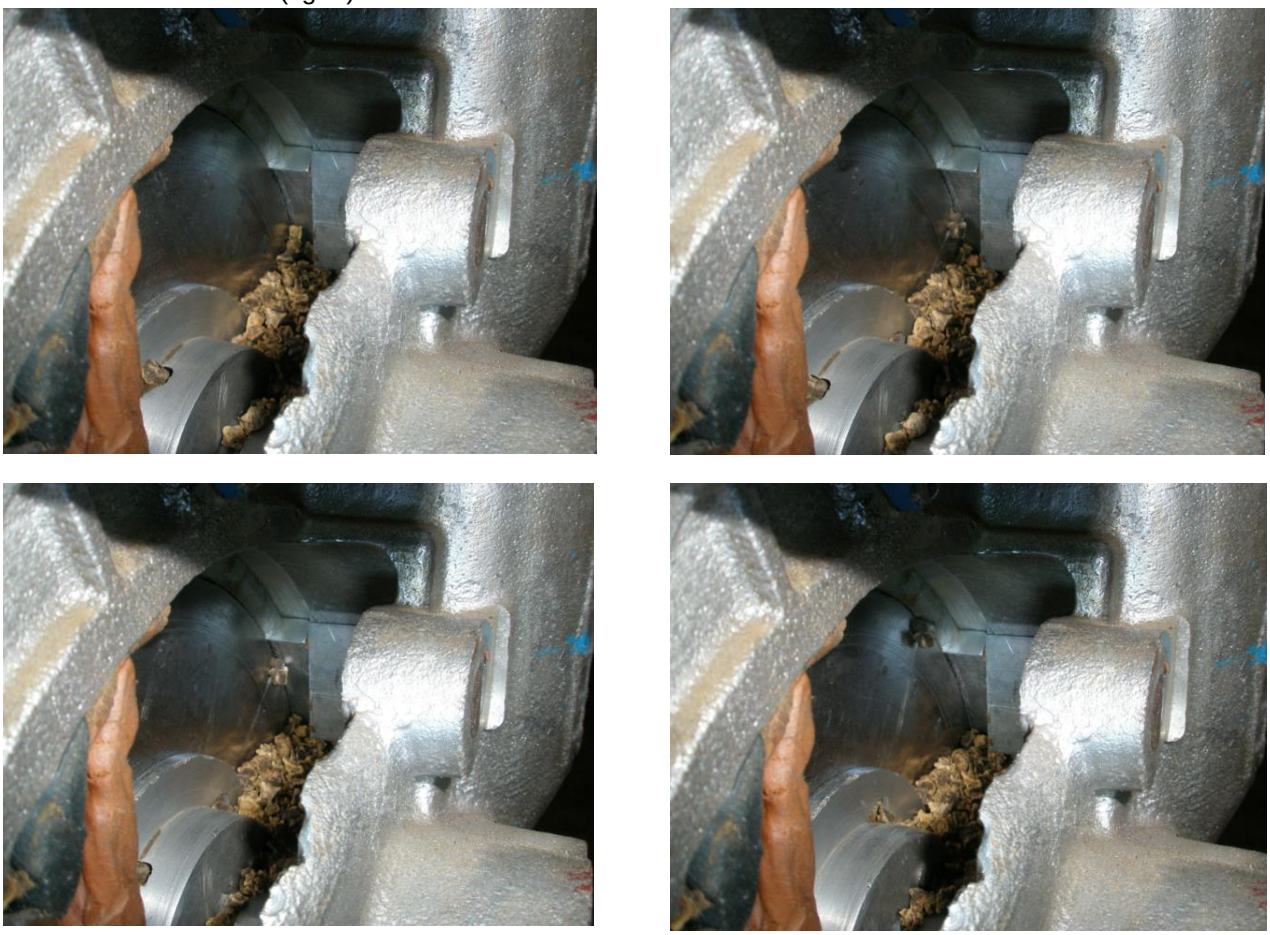

Fig. 6 - A general view of the process of filling the cells

According to the results of the research we got the dependence of the coefficient of cells filling of the sowing disc K for corresponding sub-fractions of sugar beets seeds for discs with radiuses of generatrix cells 5.0 mm and 6.0 mm (fig. 7) (*Borovikov V., 2003; Vukolov E.A., 2008*).

As seen from the diagram of the dependence of the coefficient of cells filling of the dilution in the vacuum chamber with the radius of generatrix cell of 5 mm and 6 mm, both discs are characterised by the presence of duplicates for the first sub-fraction (3.5-4.0 mm).

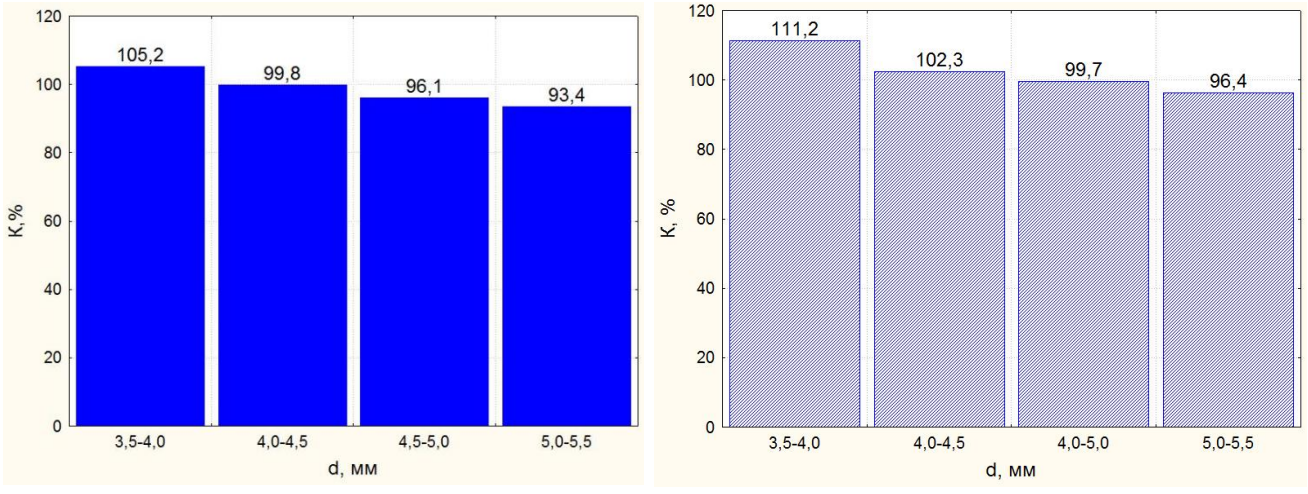

Fig. 7 - Dependences of the coefficient of cells filling for corresponding sub-fractions of sugar beetroots with generatrix of cells as follows:

a) 5.0 mm; b) 6.0 mm

CONCLUSIONS

The disc with the radius of generatrix cell of 5 mm is characterised by nearly 100% of filling cells for the second sub-fraction (4.0-4.5 mm) and decrease of the filling coefficient for the third sub-fraction (4.5-5.0 mm) and the fourth sub-fraction (5.0-5.5 mm). The disc with the radius of generatrix cell of 6 mm is characterized by the presence of duplicates for the second sub-fractions (4.0-4.5 mm), almost 100% of cell filling for the third sub-fraction (4.5-5.0 mm) and the decrease of the filling coefficient for the fourth sub-fraction (5.0-5.5 mm).

Taking into account the experiments it is possible to state that in order to provide sowing of sugar beetroot, the bending radiuses of generatrix cells should be allocated within 5…6 mm, which generally corresponds to the results of theoretical research with the defined generatrix radius of 5.7 mm (*Mostypan M.I., 2017*).

REFERENCES

[1] Borovikov V., (2003), *Statistica. The Art of Data Analysis on a Computer: For Professionals*, 688 p, St. Petersburg / Russia;

[2] Budagov A., (1971), *Precision seeding at high speeds*, 139 p, Krasnodar / USSR;

[3] Chichkin V., (1984), Vegetable seeders and combined aggregates, Chisinau / USSR, 392 p;

[4] Mostypan M.I., Vasylkovska K.V., Andriyenko O.O., Reznichenko V.P., (2017), Modern aspects of tilled crops productivity forecasting. *INMATEH - Agricultural Engineering,* Vol. 53, No. 3*,* pp. 35-40, Bucharest / Romania;

[5] Mursec B., Vindis, P., Janzekovic, M., Cus, F., Brus, M., (2007), Analysis of the quality of sowing by pneumatic sowing machines for sugar beet, *Journal of Achievements in Materials and Manufacturing Engineering*. 22.1: pp. 85-88, Gliwice / Poland;

[6] Petrenko M.M., Vasylkovskyi M. I., Vasylkovska K.V., (2011), Improvement of the pneumo-mechanical seeding machine for precise seeding of cultivated crops' seed, *Bulletin of P. Vasilenko Kharkiv National Technical University of Agriculture. 1. «Mechanization of agricultural production», 107,* pp. 359-363, Kharkov / Ukraine;

[7] Petrenko, M. M., Vasylkovsky, M. I., Vasylkovska, K. V., (2013), Pat. 77191 U Ukraine, IPC A01S 7/04 (2006.01), *Pneumo-mechanical seeding machine,* №201203339, Bul. No. 3;

[8] Rybar R., (1999), Influence of elements of the sowing machine on the yield and developmental dynamics of the grown sugar-beet, *Listy cukrov, 115/3*. pp. 74-76, Prague / Czech Republic;

[9] Sysolin P V., Sviren, M.O., (2004), *Seeding machines of seeders*, 160 p, Kirovohrad /Ukraine;

[10] Vasylkovska K.V., Vasylkovskyy O.M., (2014), Influence of the shape and type of seed cells drive on the quality of dispensing seeds, Eastern European Journal of latest technology, Vol. 6, No. 7 (72), pp. 33-36, Kharkov / Ukraine (DOI: 10.15587/1729-4061.2014.29272);

[11] Voytyuk D.G., Aniskevich L.V., Volyansky M.S., Martyshko V.M., Gumenyuk Yu.O., (2017), *Agricultural machinery: training manual*, 180 p, Kyiv / Ukraine;

[12] Vukolov E.A., (2008), Basics of statistical analysis. Workshop on statistical methods and operations research using Statistica and Excel packages: Tutorial. 464 p, Moscow / Russia.

EXPERIMENTAL STUDIES ON DRYING CONDITIONS OF GRAIN CROPS WITH HIGH MOISTURE CONTENT IN LOW-PRESSURE ENVIRONMENT

/

ЕКСПЕРИМЕНТАЛЬНІ ДОСЛІДЖЕННЯ РЕЖИМІВ СУШІННЯ НАСІННЯ ЗЕРНОВИХ КУЛЬТУР ІЗ ВИСОКОЮ ВОЛОГІСТЮ В СЕРЕДОВИЩІ НИЗЬКОГО ТИСКУ

Prof. Ph.D. Eng. Rogovskii I.L.[1)], Senior lecturer Ph.D. Eng. Titova L.L.[1)],
Senior lecturer Ph.D. Eng. Trokhaniak V.I.[1)], Assoc. Prof. Ph.D. Eng. Solomka O.V.[1)],
Senior lecturer Ph.D. Eng. Popyk P.S.[1)], Ph.D. Eng. Shvidia V.O.[2)], Ph.D. Eng. Stepanenko S.P.[2)]
[1)] National University of Life and Environmental Sciences of Ukraine;
[2)] National Scientific Centre "Institute of Mechanization and Electrification of Agriculture", Ukraine
Tel: +380673513082; E-mail: Trohaniak.v@gmail.com

Keywords: *seed, heating temperature, drying exposure, laboratory germination, thermal damage*

ABSTRACT

During the experimental studies of drying grain crops with high moisture content in a low-pressure environment, the influence of residual pressure in a peri-seed environment and seed heating temperature on drying exposure and laboratory germination have been investigated. These experimental studies have been carried out by means of the experimental facility and its attachments that make it possible to provide residual pressure within the range of 10 – 80 kPa and seed heating temperature of +20 – +40 °C.

Having processed the experimental data, regression equations of drying exposure and laboratory germination of grain crops with high moisture content by the example of corn seeds have been derived. The characteristic curves plotted based on the regression equations show that the minimum drying exposure and, simultaneously, the maximum laboratory germination can be achieved by applying residual pressure of 45 kPa and seed heating temperature of no more than +30 °C.

РЕЗЮМЕ

Під час проведення експериментальних досліджень сушіння насіння зернових культур із високою вологістю в середовищі низького тиску досліджувався вплив залишкового тиску навколонасіннєвого середовища, температури нагріву насіння на експозицію сушіння та лабораторну схожість. Дані експериментальні дослідження були реалізовані на експериментальній установці та пристосуваннях до неї, які дали можливість забезпечити залишковий тиск у діапазоні 10 – 80 кПа, температуру нагріву насіння +20 – +40 °C.

Після оброблення експериментальних даних були побудовані рівняння регресії експозиції сушіння та лабораторної схожості насіння зернових культур високої вологості, в якості якого використовувалося насіння кукурудзи. Графічні залежності, побудовані на основі рівнянь регресії, показують, що найменшої експозиції сушіння та, одночасно, високої лабораторної схожості можливо досягти, застосовуючи залишковий тиск на рівні 45 кПа, температуру нагріву насіння, що не перевищує +30 °C.

INTRODUCTION

In order to dry seeds with high moisture content, convection drying in a fixed, slow-moving and pseudo-fluidized bed is currently used in seed farming and breeding. It is implemented in chamber, conveyer, hopper and column dryers.

In order to stimulate moisture transfer in a seed, heating, which is provided by an air flow at the temperature of no more than 65°C, is used. The upper temperature value is determined by the fact that at this temperature level there is intensive exudation of moisture, but seed proteins are not denaturized. There are mild temperature conditions developed for various crops, which are necessary to follow during seed drying in different convection dryers, in order to reduce the risk of thermal damage.

In spite of the developed measures for reducing thermal damage of seeds during drying, dried seeds have lower germinating ability and germinating power and even less germination compared to the undried ones. It can be explained by the difference in the properties of individual seeds and non-linear behaviour of the temperature conductivity of a seed bed, which results in overheating and under-drying of individual seeds. In order to improve sowing qualities of seeds, it is necessary to decrease their thermal damage

after drying by means of reducing the influence or avoiding a temperature field as well as increasing the uniformity of seed drying.

Investigations *(Kotov B.I. et al., 2018; Kuznetsov Y.A. et al., 2018)* show that drying without seed damage is possible, if seed heating temperature of most grain crops does not exceed 40 – 45°C. At the same time, the change in moisture content does not exceed 5 – 6% in one technological cycle, since, if drying rate is higher, cracks can appear in a seed *(Zahoranová A. et al., 2016)*. In addition, it has been determined that if there is an increase in the initial moisture content of a seed, there is a decrease in the maximum acceptable temperature of seed heating *(Gorobets V.G. et al. 2018; Gorobets V.G. et al. 2018)*. In order to prevent seed damage during drying, the author *(Kuznetsov Y.A. et al. 2017)* suggests using mild drying temperature conditions. However, mild temperature conditions may result in under-drying of seeds. In addition, the existing heat generators do not always provide the required stable temperature conditions *(Dobrin D. et al. 2015)*.

One of the advanced methods of drying seeds is drying in a low-pressure environment *(Kotov B. et al. 2015)*. In this case, seed drying is even more and heating temperature is lower, compared to the one used in a convection method *(Kroulík M. et al. 2016)*.

Research *(Paziuk, V.M. et al. 2018; Bogaert L. et al. 2018)* shows that intensive moist removal can be provided during continued seed heating to the temperature, which is close to the permissible one. Other researchers suggest using a vacuum-pulse method, in order to improve drying rate *(Lukaszuk J. et al. 2008)*. However, the use of these methods may result in seed thermal damage *(Rekas A. et al. 2017)*.

Scientific papers *(Gorji A. et al. 2010)* present the idea that intensive moist removal in a low-pressure medium is possible during cyclic heating, vacuum treatment and blowing under air-pressure through a heat-exchange apparatus *(Gorobets V.G. et al. 2018)*. However, these papers do not consider the influence of operating conditions on the sowing qualities of seeds.

Most of the above-mentioned papers do not consider the influence of the operating conditions of drying in a low-pressure environment both on the sowing qualities of seeds and on their drying exposure simultaneously. That is why, it is necessary to substantiate the parameters, which provide drying in a low-pressure environment with minimum exposure and maximum germinating ability after drying.

MATERIALS AND METHODS

In order to investigate the mutual influence of operating conditions and optimize the number of experiments, a multi-factor experiment procedure *(Paziuk, V.M. et al. 2018; Bogaert L. et al. 2018)* was used. The planning matrix of the experiments was conducted according to D-optimal second-order plans *(Lukaszuk J. et al. 2008)*, based on the theory of joint efficient estimates, which was developed by an American statistician J. Kiefer. At the same time, Box-Behnken design (B–B3) was used for a three-factor experiment.

Drying exposure was determined by measuring the time, during which moisture content of the pre-moistened seed was changed by 6%. Such a change in moisture content was registered by periodic weighing of the seed mass that was used in the experiments. The level of thermal damage was evaluated based on laboratory germination, which was determined according to State Standards of Ukraine 4138-2002.

Regression coefficients, their relevance, adequacy, reproducibility and the homogeneity of the regression equations were determined by means of Wolfram Mathematica 13 software. Graphical interpretation of the regression equations was realized in MathCad 13 software environment.

In order to substantiate drying conditions of seeds in a low-pressure environment with minimum exposure and maximum generating ability after drying, a simple laboratory-scale plant, which is a cylindrical vessel, where residual pressure up to 2 kPa (Fig. 1) can be created inside, was developed. The heating of seeds was performed by means of Rotex RAS15-H infra-red heater with off system of protection from falling outside a drying chamber. Rotex RAS15-H infra-red heater was arranged above a plastic vessel and seed batching lasted for 5 minutes. During seed batch heating by the heater, it was thoroughly mixed to level the temperature. The temperature of seed heating was regulated by the level of infra-red heater arrangement above a seed batch.

Since the seeds of every grain crop have their own individual drying characteristics, the determination of the common patterns of their drying in a low-pressure environment requires a great number of experimental studies. In order to decrease the number of experimental tests, it was decided to use a batch of the variety of corn seeds called Liubava 279 MV weighting 715 g and having 20% initial

moisture content as an example, since, to some approximation, its characteristics can be considered as ones which are typical of the seeds of most grain crops that need drying.

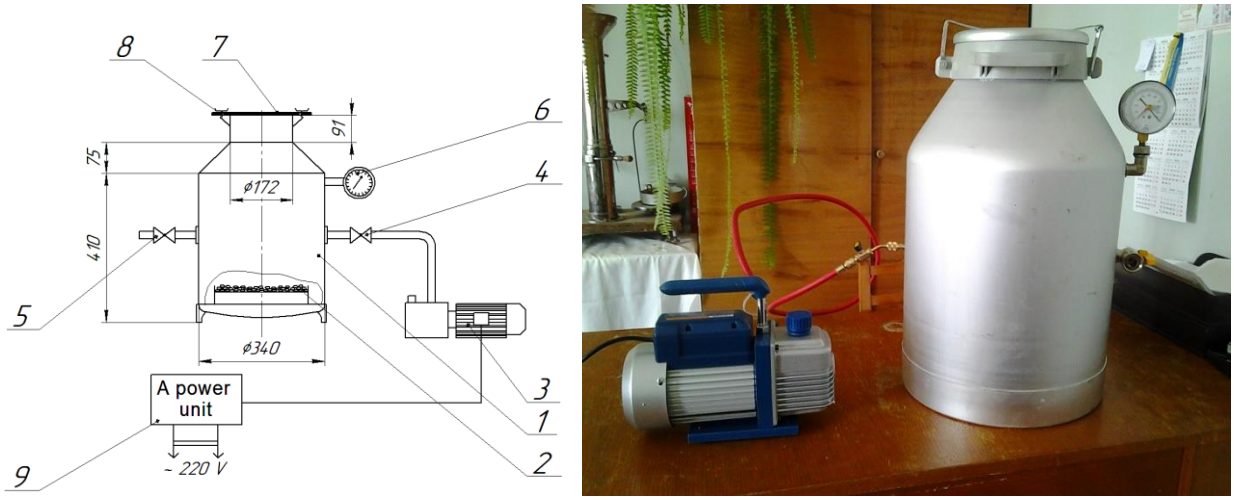

a) b)

Fig. 1 - Laboratory-scale plant design (a) and its general view (b)

1 – a drying chamber; 2 – corn seeds; 3 – a rotary vane-type vacuum low-pressure pump; 4 – a vacuum pressure tap; 5 – a tap for releasing vacuum; 6 – a vacuum meter; 7 – a lid with a seal; 8 – a locking mechanism; 9 – a power unit

The following independent factors, which are the main operating parameters of seed drying in a low-pressure environment, were chosen: *p* – residual pressure in a drying chamber, kPa; *t* – seed heating temperature, °C.

Their values and variability interval are represented in Table 1.

Table 1

Values and coding of independent factors levels during experimental investigation of the operating conditions of drying moist seeds in low-pressure environment

Variability level	Independent factors	
	Residual pressure, *p*, kPa	**Seed heating temperature, *t*, °C**
Low (-1)	10	20
Medium (0)	45	30
High (+1)	80	40
Variability interval	35	10

As mentioned above, a plastic vessel with a batch of corn seeds was heated at regular intervals to the required temperature during 5 min and then it was put into a drying chamber, where it was exposed to low air pressure for 10 min. At the end of each period, sample mass was measured and the amount of the evaporated moisture was determined. The measurement of sample mass and the amount of the evaporated moisture was conducted until the change in moisture content of corn seeds reached 6 %.

RESULTS

Implementation of a D-optimal plan, according to the data presented in Table 1, resulted in the derivation of the regression equations of drying exposure and seed germinating ability. Having conducted the analysis for regression coefficients, their adequacy, reproducibility and correspondence to a certain dependence, the regression equations acquire the following form.

Regression equation of drying exposure, τ_{ex}:

$$\tau_{ex} = 608.151 + 1.06 \cdot p - 13.73 \cdot t \,. \quad (1)$$

Regression equation of laboratory germination of seeds:

$$K_{ger} = 81.37 + 0.12 \cdot p + 0.972 \cdot t - 0.028 \cdot t^2 . \quad (2)$$

In the equations (1) and (2): *p* - residual pressure in a drying chamber, kPa; *t* — heating temperature of a seed batch, °C.

The analysis of the regression equations (1) and (2) shows that drying exposure is greatly affected by heating temperature *t* and laboratory germination is influenced both by seed heating temperature *t* and residual pressure in a drying chamber *p*.

Based on the equation (1), drying exposure τ_{ex} was plotted versus residual pressure *p* without airflow. (Fig. 2).

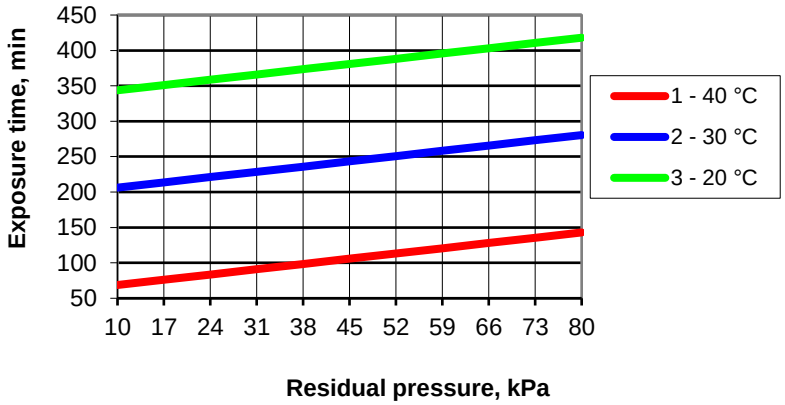

Fig. 2 - Drying exposure-vs-residual pressure characteristic curves at various temperature without airflow:
1 – 40 °C, 2 – 30 °C, 3 – 20 °C

Fig. 3 presents the comparison of laboratory germination-vs-temperature curves at vacuum and convectional drying. According to the characteristic curves presented in Fig. 3, drying exposure τ_{ex} linearly depends on residual pressure *p*. The decrease in residual pressure *p* results in the linear decrease of drying exposure τ_{ex}. If seed heating temperature *t* is reduced, drying exposure τ_{ex} increases. These characteristic curves show that the minimum drying exposure (69.6 min) can be achieved at the lowest level of residual pressure *p* = 10 kPa and the seed heating temperature of *t* = 40°C. The significant influence of seed heating temperature *t* on drying exposure τ_{ex} can be explained by the fact that, during seed drying in a low-pressure environment, it is cooled down due to the evaporation of seed surface moisture with simultaneous decrease of moisture diffusion rate. That is why, seed heating reduces exposure.

In addition, seed heating temperature t is a significant factor that influences laboratory germination and therefore, it affects the level of thermal damage of seeds (equation (2). It is shown in Fig. 3. The dependence of laboratory germination at convectional drying was plotted based on the data *(Kyrpa M.Ya. et al., 2015).*

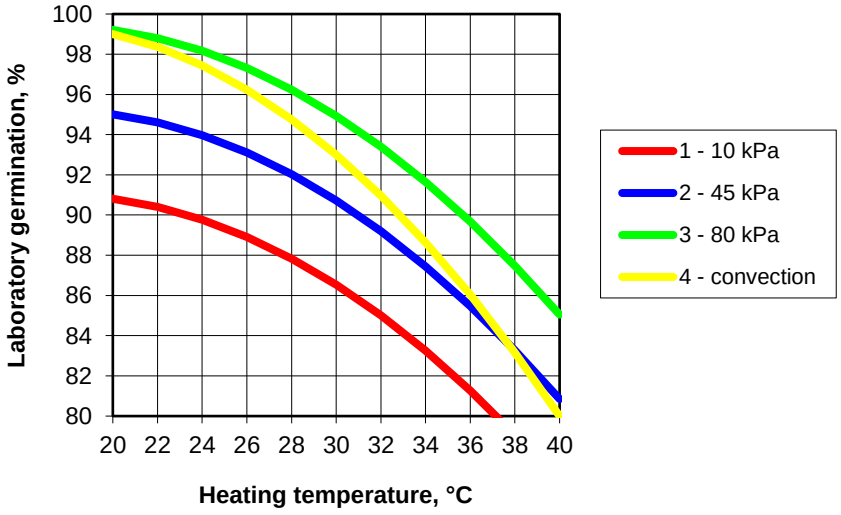

Fig. 3 - Laboratory germination-vs-seed heating temperature curves at various residual pressure and convectional drying
1 – 10 kPa, 2 – 45 kPa, 3 – 80 kPa; 4 – convectional drying

According to the curves presented in Fig. 3, at the same seed heating temperature, vacuum drying makes it possible to dry seeds providing better laboratory germination. It can be explained by the fact that, if drying is performed in a low-pressure environment, the heat supplied to seeds is spent on water evaporation and to only a small extend it is spent on heating seed cells, which reduces thermal influence on seeds.

The increase of seed heating temperature *t* and the decrease of residual pressure *p* result in the reduction of seed laboratory germination Kgerm. This is due to the fact that there is an increase of possible degradation of seed protein structures, if seed heating temperature *t* increases.

The increase of seed heating temperature *t* and the decrease of residual pressure *p* result in the reduction of laboratory germination of seeds Kgerm and simultaneous decrease in drying exposure тех. In order to find rational values of the operating conditions of drying in a low-pressure environment, drying exposure and laboratory germination-vs-seed heating temperature curves at different residual pressure were plotted in one of the graphs (Fig. 4). Their cross point defines the minimum value of drying exposure and the maximum value of the laboratory germination of seeds.

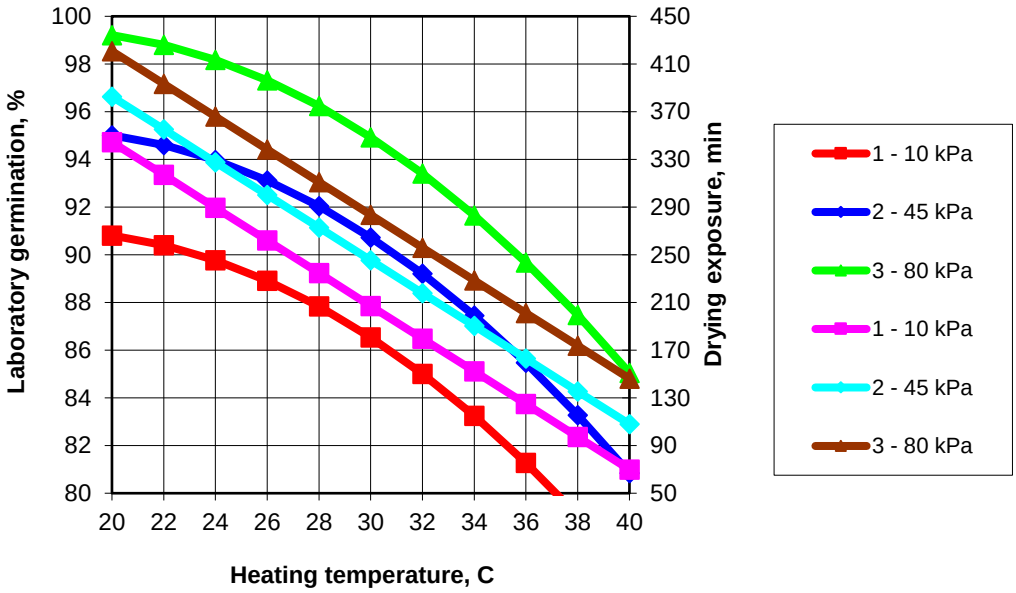

Fig. 4 - Laboratory germination and drying exposure-vs-seed heating temperature curves at various residual pressure:
1 – 10 kPa, 2 – 45 kPa, 3 – 80 kPa

According to the curves presented in Fig. 4, the minimum drying exposure with the lowest level of thermal damage, which is expressed as laboratory germination, can be achieved at seed heating temperature of no more than 30°C and at residual pressure being equal to 45 kPa.

In case of corn seeds with initial moisture content of 20%, the minimum drying exposure is equal to 240 min and laboratory germination is 91.8%. It means that intensive drying in a low-pressure environment can be conducted at the temperature levels, which are 10 – 15°C lower than those used during convection drying, ensuring germinating conditions.

CONCLUSIONS

Experimental research on drying the seeds of grain crops by the example of corn seeds in a low-pressure environment has been conducted. As a result of the conducted experimental investigations, regression equations have been obtained based on which drying exposure-vs-seed laboratory germination curves have been plotted. It has been determined that drying in a low-pressure environment makes it possible to provide high laboratory germination due to the fact that the heat, which is supplied to seeds, is spent on water evaporation mostly and to only a small extend it is spent on heating seed cells. Laboratory germination of 92-95% can be achieved at drying exposure of 200-240 m, at pressure in a peri-seed environment of 30–45 kPa and seed heating temperature of +25–+30 °C during drying.

REFERENCES

[1] Bogaert L., Mathieu H., Mhemdi H., Vorobiev E., (2018), Characterization of oilseeds mechanical expression in an instrumented pilot screw press, *Industrial Crops and Products*, vol. 121, pp.106-113. Wageningen/Netherlands;

[2] Dobrin D., Magureanu M., Mandache N.B., Ionita M.D., (2015), The effect of non-thermal plasma treatment on wheat germination and early growth, *Innovative Food Science & Emerging Technologies*, vol. 29, pp. 255-260, https://doi.org/10.1016/j.ifset.2015.02.006, Seville/Spain;

[3] Gorji A., Rajabipour A., Tavakoli H., (2010), Fracture resistance of wheat grain as a function of moisture content, loading rate and grain orientation, *Australian Journal of Crop Science*, vol. 4, pp. 448–452, Southern Cross/Australia;

[4] Gorobets V.G., Bohdan Yu.O., Trokhaniak V.I., Antypov I.O., (2018), Experimental studies and numerical modelling of heat and mass transfer process in shell-and-tube heat exchangers with compact arrangements of tube bundles, Paper presented at the *MATEC Web of Conferences*, vol. 240, 02006, https://doi.org/10.1051/matecconf/201824002006, Cracow/Poland;

[5] Gorobets V.G., Trokhaniak V.I., Antypov I.O., Bohdan Yu.O., (2018), The numerical simulation of heat and mass transfer processes in tunnelling air ventilation system in poultry houses, *INMATEH: Agricultural Engineering*, vol.55, no.2, pp.87-96, Bucharest/Romania;

[6] Gorobets, V.G., Trokhaniak, V.I., Rogovskii, I.L., Titova, L.L., Lendiel, T.I., Dudnyk, A.O., Masiuk, M.Y., (2018), The numerical simulation of hydrodynamics and mass transfer processes for ventilating system effective location, *INMATEH - Agricultural Engineering*, vol. 56, no 3, pp. 185-192, Bucharest/Romania;

[8] Kotov B., Kalinichenko R., Spirin A., (2015), Mathematical modeling of heat and mass transfer process under heat treatment of grain materials in dense layer, *TEKA, Commission of Motorization and Energetics in Agriculture*, Vol.17, Issue 5, pp.54-57, Lublin/Poland;

[9] Kotov B.I., Spirin A.B., Tverdokhlib I.V., Polyevoda Y.A., Hryshchenko V.O., Kalinichenko R.A., (2018), Theoretical researches of cooling process regularity of the grain material in the layer, *INMATEH - Agricultural Engineering*, vol. 54, no 1, pp. 87-94, Bucharest/Romania;

[10] Kroulík M., Húla J., Rybka A., Honzík I., (2016), Pneumatic conveying characteristics of seeds in a vertical ascending airstream, *Research in Agricultural Engineering*, vol.62, no.2, pp.56-63, Prague/Czech Republic;

[11] Kuznetsov Y.A., Volzhentsev A.V., Kolomeichenko A.V., Kalashnikova L.V., (2017), Grounding of construction parameters of pseudofluidized layer dryer working chamber, *INMATEH - Agricultural Engineering*, vol. 52, no. 2, pp. 33-38, Bucharest/Romania;

[12] Kuznetsov Y.A., Volzhentsev A.V., Kolomeichenko A.V., Kalashnikova L.V., (2018), Influence of technological parameters of pseudofluidized layer grain dryer on the grain drying quality, *INMATEH - Agricultural Engineering*, vol. 54, no.1, pp. 81-86, Bucharest/Romania;

[13] Kyrpa M.Ya., Stiurko M.O., Bondar L.M., Bazilieva Yu.S., (2015), Thermal resistance of the seeds of corn hybrids and peculiarities of their post-harvest processing (Термостійкість насіння гібридів кукурудзи та особливості їх післязбиральної обробки), *Bulletin of Dnipropetrovsk state agrarian and economic university (Вісник Дніпропетровського державного аграрно-економічного університету),* vol. 3, no. 37, pp. 58–63., Dnipropetrovsk/Ukraine;

[14] Lukaszuk J., Molenda M., Horabik J., Szot B., Montross M.D., (2008), Air flow resistance of wheat bedding as influenced by the filling method, *Research in Agricultural Engineering*, vol. 54, no.2, pp.50-57, Prague/Czech Republic;

[16] Paziuk, V.M., Liubin, M.V., Yaropud, V.M., Tokarchuk, O.A., Tokarchuk, D.M., (2018), Research on the rational regimes of wheat seeds drying, *INMATEH - Agricultural Engineering*, vol. 56, no 3, pp. 39-48, Bucharest/Romania;

[17] Rekas A., Scibisz I., Siger A., Wroniak M., (2017), The effect of microwave pre-treatment of seeds on the stability and degradation kinetics of phenolic compounds in rapeseed oil during long-term storage, *Food Chemistry*, vol. 222, pp. 43-52, Leiden/Netherlands;

[19] Zahoranová A., Henselová M., Hudecová D., Kaliňáková B., Kováčik D., Medvecká V., Černák M., (2016), Effect of Cold Atmospheric Pressure Plasma on the Wheat Seedlings Vigour and on the Inactivation of Microorganisms on the Seeds Surface, *Plasma Chemistry and Plasma Processing*, vol. 36, no. 1, pp. 397-414, https://doi.org/10.1007/s11090-015-9684-z, Bern/Switzerland.

IMPROVED REMOTE-CONTROL WIRELESS SENSING SYSTEM OF PLANT GROWTH FACTORS IN GREENHOUSE ENVIRONMENT

/

远程控制型温室环境植物生长要素无线检测系统

Ph.D. Bin Li[1)], Stud. Yuqi Zhang[1)], Ph.D. Ying-Nan Kan[1)], Prof. Yao-Dan Chi[1)], Prof. Xiaotian Yang*[1)], Ph.D. Jianing Wang[2)], Prof. Yiding Wang[2)]

[1)] Institute of Electrical & Computer, Jilin Jianzhu University, Changchun 130012, P.R. China;

[2)] State Key Laboratory on Integrated Optoelectronics, College of Electronic Science and Engineering, Jilin University, Changchun 130012, P.R. China;

Tel: +86-043184566184; E-mail: 870731919@qq.com

Keywords: *greenhouse, remote control, infrared gas sensor, wireless communication*

Abstract

Plant growth factors including carbon dioxide, temperature, humidity and luminance have been detected by using the proposed remote-control wireless sensing system in greenhouse environment. These factors are crucial for photosynthesis and can be detected in real-time by this system. Numerical sensors were adopted and were driven by the developed printed circuit boards. Remote-control and wireless data transmission were also performed and improved by using the developed hardware. In order to satisfy the requirement of remote control, GSM module was integrated in the sensing system. Meanwhile, corresponding software was developed for data storing, wireless transmitting, remote controlling and data analyzing. The proposed system is suitable for precision management of key factors in greenhouse and it also exhibits improved functional performance compared with our previously reported sensing system.

摘要

研制了远程无线检测系统，适用于检测温室中的多种植物生长要素，包括二氧化碳、温度、湿度和光照度。这些植物生长要素是光合作用所必需的，可以通过研制的检测系统进行实时检测。多种传感器在系统中被采用，通过研制的电路板进行驱动。通过使用研制的硬件部分，远程控制和无线数据传输功能均得到实现和改进。为了满足远程控制的需求，系统中采用了 GSM 模块进行远程数据通信。同时，也开发了相应的软件，用于实现数据存储、无线传输、远程控制和数据分析等功能。通过和我们之前研制的系统相比，文中的系统在功能和性能方面得到了提高，该系统适用于温室中多项植物生长要素的精确测控。

INTRODUCTION

Greenhouses have been designed and developed to extend the production season for increasing production and improving crop quality (*Danish et al. 2018; Hwang et al. 2010; Searchinger et al. 2008*). It is a very important type of facilities in the modern agricultural industry around the world and it has been developed and enhanced in recent years. Environmental factors inside greenhouses such as temperature, humidity, gas fertilizer and luminance can be detected and regulated by climate-regulating equipment, sensing devices and control units. These facilities must achieve accurate, convenient, stable and cost-effective goals in order to meet the requirements practically. In this way, the demand of adequate high-tech greenhouse facilities becomes increasingly significant and many research groups have studied in this field in recent years (*Sahbani et al. 2018; You et al. 2017; Jianing et al. 2016*). According to the recent reports (*Erazo-Roads et al. 2018; Sivamani et al. 2018; Bai et al. 2018; Somov et al. 2013*), the growing use of sensing technique, wireless data communicating technique and digitalized data management technique are highlighted for high-precision sensing and dynamic modeling & controlling of climate factors in greenhouse environment.

Sensors have been widely adopted in greenhouses to detect the environmental factors such as temperature, humidity, gas concentration and luminance. These sensors are integrated by using different principles and have been optimized along with the development of sensing techniques (*Yasuda et al. 2012; Suzuki et al. 2018; Lambrecht et al. 2016; Ferrero et al. 2018*). In recent years, optical gas sensors have been studied by researches to replace the traditional chemical sensors.

Optical sensors generally have longer lifespan, quicker response time, larger sensing range and higher sensitivity (*Charles et al. 2014; Kapsalidis et al. 2018; Wei et al. 2014; Fisher et al. 2018; Jiang et al. 2018*). In this way, carbon dioxide (CO_2), which is a key element in the photosynthesis phenomenon, can be detected by using optical sensors as a part of the comprehensive sensing & controlling system in greenhouses.

In recent years, wireless sensor networks (WSNs) have been widely adopted in the agricultural industry especially in modern greenhouses (*Jahnavi et al. 2015; Park et al. 2011*). Data detected by sensors can be transmitted from sensor nodes to network receivers by using wireless systems. This results in two major benefits than using cables including cost-effective construction and convenient deployment of the sensing system especially in large greenhouses that need hundreds of sensor nodes. With the increasing of sensing targets and sensor node numbers, digitalized data management becomes indispensable during the process of data transmission, data storage, signal processing and analyzing. Therefore, effective and reliable data management in quick response time is necessary.

In this paper, an improved remote-control wireless sensing system of plant growth factors in greenhouse is proposed. Compared to our previous work (*Bin et al. 2018*), there are three major improvements. Firstly, the developed wireless sensor node was further integrated with a GSM module. In this way, the sensor node is not only able to connect with the laptop which places in the adjacent control room, but also can send data via the GSM module to a remote PC which is about 20 kilometres away from the greenhouse. Therefore, the detected data can be displayed, stored and analyzed remotely. Secondly, based on the infrared CO_2 sensor and the remote-control mode, adjustable PID algorithm has been applied to sensing system in greenhouse. Finally, a concise and customized web page has been designed and published in this system by using LabVIEW. Therefore, the remotely collected data can be stored and viewed by the developed software for further operation. In the end of this paper, experiments were carried out by using the improved sensing system and results were discussed correspondingly.

MATERIALS AND METHODS

System structure

The improved remote-control sensing system consists of three major parts which are located in the greenhouse, the control room which is close to the greenhouse through a thin wall and a remote control laboratory 20 kilometres away from the greenhouse. The basic schematic diagram of the system is as shown in Figure 1. Firstly, an integrated sensor node is located in the greenhouse to detect numerous analogue signals including temperature, humidity, CO_2 concentration and luminance. Secondly, laptop installed software developed by using LabVIEW is located in the control room of the greenhouse. This sensor node is able to transmit digital data by using the 433 MHz wireless module to the local wireless receiver which is linked to this laptop in the control room. In addition, a GSM module is integrated inside the sensor node for remote signal communication. In this way, the sensor node can also send the detected data to the PCs located in the lab in the university. Thirdly, the computers located in the lab have also installed software developed by using the LabVIEW platform in order to process the received data. The detailed functions of the developed software are shown in the following sections in this paper.

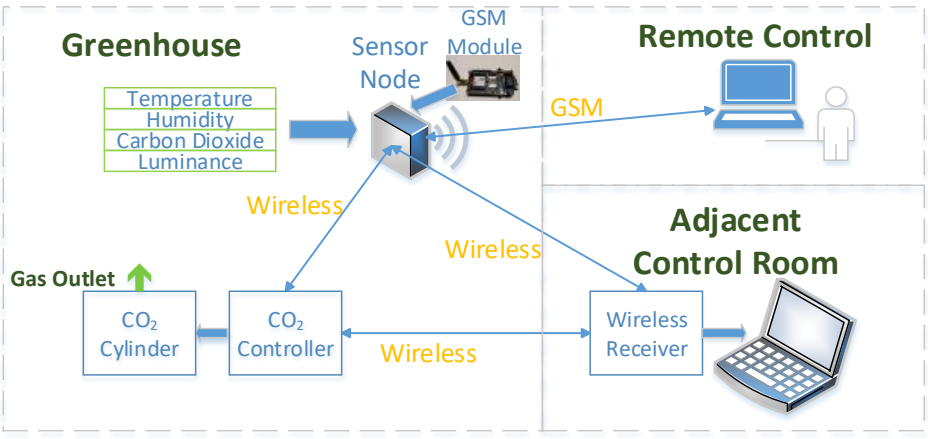

Fig. 1 - Structure diagram of the developed sensing system of plant growth factors

Wireless sensor node and data management

The sensor node was developed to perform sensing and data transmission functions. Ambient factors including temperature, humidity, CO_2 concentration and luminance can be detected by the integrated sensors. The main controller is a 32-bit chip (STM32F103R) with a maximum CPU speed of 72 MHz. The sensor node also consists of wireless modules. One is the 433 MHz local wireless communication module and the other is a GSM module which is responsible for remote-controlled signal transmission. Therefore, the detected greenhouse data can be both transferred to the local laptop which is located in the adjacent control room and the remote-control lab via the GSM module. The developed data management software system consists of three parts of functions. Firstly, data communication and synthesis are performed by this system including display, storage, remote-control and data share etc. Secondly, the fuzzy PID algorithm is adopted and PID characters were adjusted based on analyses and experiments. Thirdly, the software has been developed with good compatibility feature in order to be transplanted to other platform. The detailed structure of the developed software is shown in Figure 2. In this program, the essential characters are firstly initialized and the receiving data is read by using the Serial Communication Interface (SCI). Then, the key modules of the software start to work to perform synchronization of display, database and network. In this way, the further operation can be performed based on the settings to perform PID control, communication adjustment and sensor node status verification etc. In the end of the loop, important data and logs are separately stored and displayed for further operation.

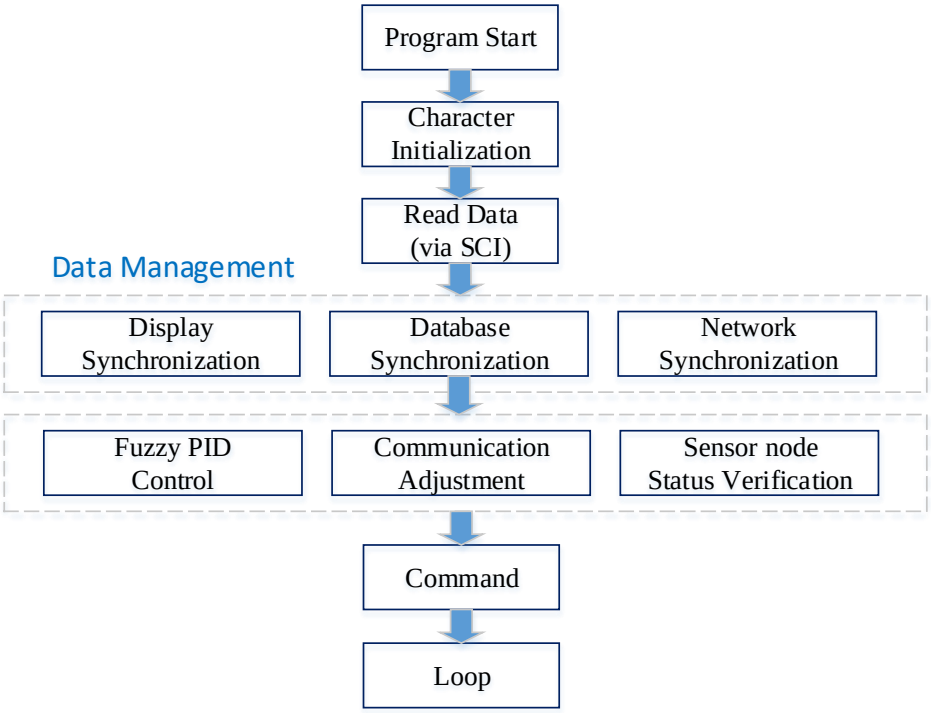

Fig. 2 - Function diagram of the developed data management system

Fuzzy PID control algorithm

Generally, a fuzzy PID control system consists of input & output ports, execution unit, controlled object and fuzzy controller. In the adopted system which is shown in Figure 3, the input & output ports are the communication interfaces of the wireless sensor node, the control laptop and the remote-control computer. The communication includes voltage level switch, communication coding and decoding and other requirements. The execution unit in the system includes an electromagnetic valve, a relay and corresponding driving circuits. The controlled object is CO_2 concentration in greenhouse and the detection unit is the developed sensor node. The fuzzy PID controller is the core of the system. In the developed system, this controller was based on the LabVIEW platform in order to shorten development period.

There are several working steps of the fuzzy PID controller. Firstly, the wireless sensor node detects environmental factors in the greenhouse and sends data to the remote control system. Then, the input variable values are processed to be fuzzy values according to the structure of the adopted fuzzy PID controller. And the fuzzy control values can be obtained based on the fuzzy rule table and corresponding

calculations are performed. Then, precise control value can be obtained in the reverse fuzzy process for the execution unit to perform specific adjustment and modulation. In this way, the CO_2 gas valve can be switched according to the system command based on the measured CO_2 concentration. Therefore, a closed loop of fuzzy PID control process has been established.

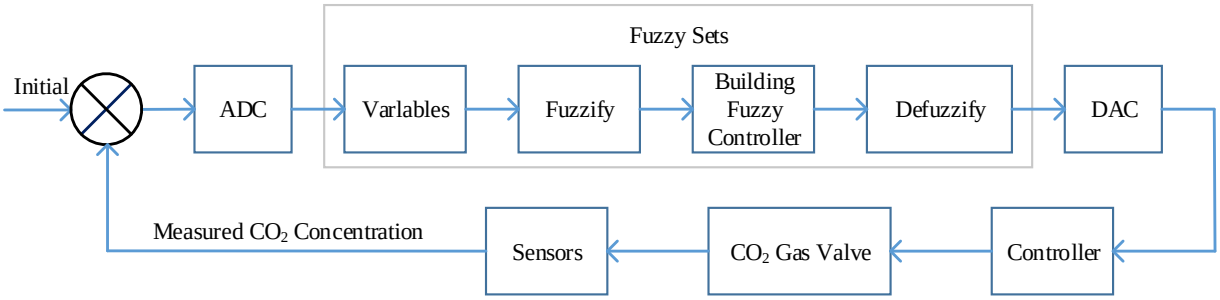

Fig.3 – Function diagram of the adopted control strategy based on fuzzy PID algorithm

In addition, the PID factors are repeatedly adjusted based on LabVIEW which is shown in figure 4 in order to achieve optimized response speed and high stability of the control system.

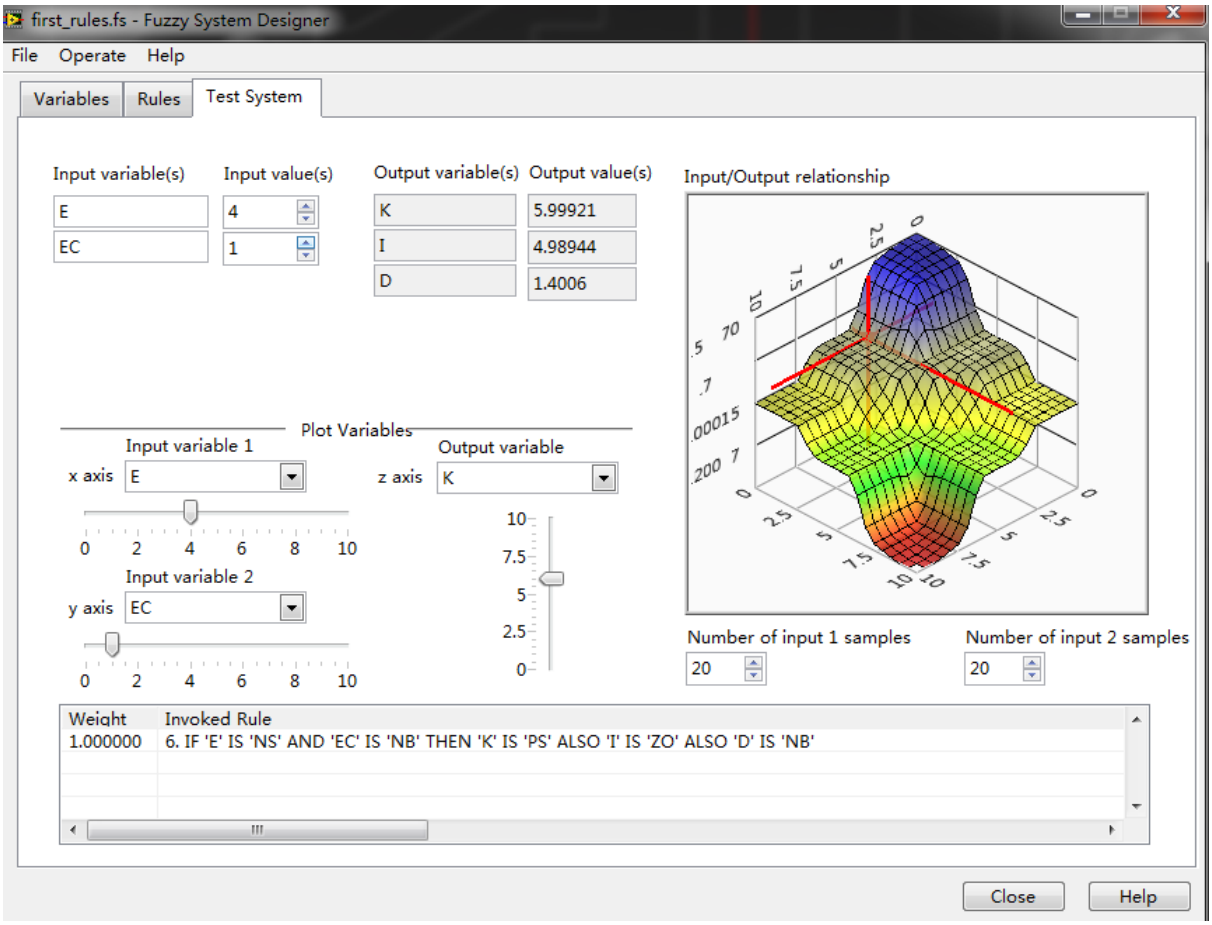

Fig. 4 - Photo of the adjusted PID characters based on LabVIEW platform

Remote-control based on GSM communication

The detected data in the greenhouse can be remotely transmitted to the lab by using the integrated GSM module. Based on the LabVIEW platform, interface of displaying sensing data has been developed as shown in Figure 5. The developed interface supports remotely data synchronism based on dashboard functions in LabVIEW which is shown in Figure 5 (a). This interface can be applied on multiple terminals such as PCs, laptops, iPads and Android devices. In this way, the detected data in greenhouse can be viewed conveniently by using varies devices. In the future, multiple sensor nodes will be applied experimentally and this interface can also be expended to support multiple sets of sensing data.

The program based on LabVIEW has been developed by several steps. Firstly, the developed program was coded according to the requirements and packaged in a project.

Then, there are two options to perform data synchronism which are whole program synchronism and variable values synchronism.

The second option was applied in this project according to the comparison experiments which demonstrated better fluency than the first option.

Therefore, the variable values synchronism option was chosen. In this option, variable values of detected data including temperature, humidity, gas concentration and luminance were named separately for synchronism in both local and remote computers. Meanwhile, service station of DNS (Domain Name System) was established. Then, monitoring interface was developed and was linked to these variable values. Finally, the established DNS was chosen and tested in order to implement the synchronism function of these detected environmental data in greenhouse.

Generally, web pages are designed and developed for viewing in variable devices. In this project, web pages based on LabVIEW platform were also developed to present the detected data and status data. Before publishing the web pages, basic settings including HTTP ports, SSL ports and VI root folder must be determined. Then, remote access authority was permitted and variable values are registered for synchronous access. In this way, the detected data in greenhouse can be monitored by using the developed web pages. The gas valve can be remotely controlled as well by using the interface. The developed interface is shown in Figure 5 (b) including monitoring windows and functional buttons.

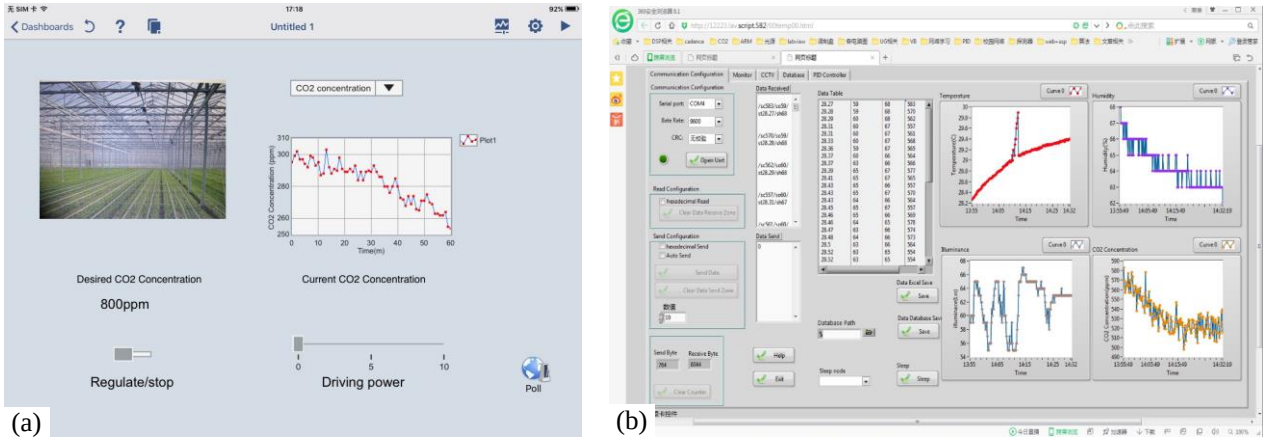

Fig. 5 - Developed remote-control system interface (a) and published web page (b) based on LabVIEW platform

RESULTS

Experiments setup

The developed sensor node was deployed in the greenhouse as shown in Figure 6 (a) to detect environmental factors including temperature, humidity, CO_2 concentration and luminance.

Many small holes have been drilled in the case of the sensor node for air exchanging between the inside and outside of the sensor node. Meanwhile, these holes have been covered with special waterproof film which ensures ventilation. Therefore, the environmental CO_2 concentration can be detected by the integrated gas sensor.

The temperature and humidity sensor is linked with a cable and is able to detect both air and soil temperature and humidity value. The luminance sensor is embedded on the front panel faced to the illumination side in the greenhouse.

The greenhouse, which occupies 640 m^3, is located 20 kilometres away on Google map from the remote-control lab in the university as shown in Figure 6 (b).

The entire zone of the university, the greenhouse and nearby areas are completely covered with 2G, 3G and 4G telecommunication signals. Corresponding base stations have been deployed on masses of

signal towers. In this way, the detected data in the greenhouse can be delivered to the remote-control lab via these facilities with affordable charges.

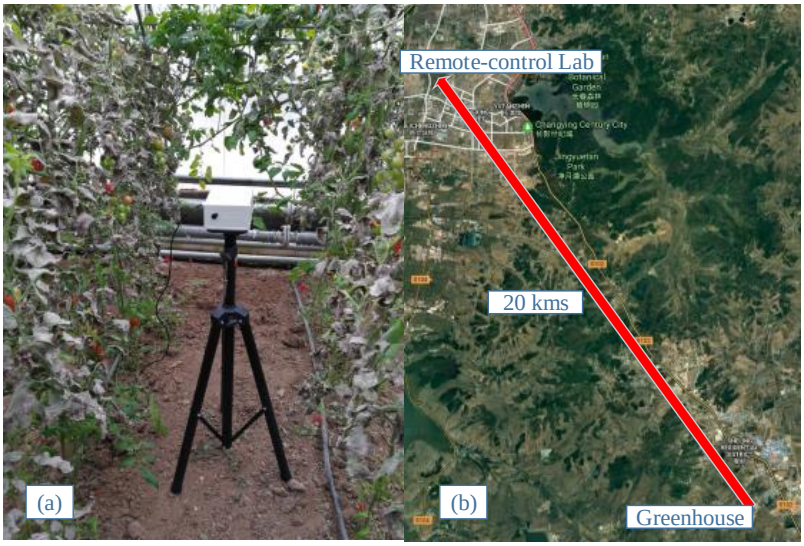

Fig. 6 – Experimental setup of the sensor node in the greenhouse (a) and geography view of the system (b)

Local wireless signal test

The in-situ wireless communication performance can be evaluated by detecting RSSI (Received Signal Strength Indication) in different conditions. There are two significant performance indicators related to RSSI of the antenna which are direction and distance. In this project, the sending and receiving direction of the sensor node is unfixed. In addition, it has been considered that multiple sensor nodes will be adopted in further experiments. Therefore, omnidirectional antenna has been applied in order to achieve good compatibility.

The antenna was placed upward and RSSI value was tested in different distances as shown in Figure 7 (a). The angle of antenna has been changed by using the step of 45 degree and corresponding RSSI was detected and recorded. It can be seen that RSSI value remains stable in different angles of antenna while the distance was fixed. The fluctuation can be considered as the error of detection and operation. Results demonstrate that the impact of antenna direction can be neglected. In this way, the position of the sensor node can be flexible and further experiments involving wireless communication of multiple sensor nodes can be realized efficiently.

The detection error of RSSI was experimentally evaluated while the sending power was set as 20 dBm in a small tomato greenhouse. The greenhouse occupies an area of about 640 square meters with the length of 80 meters. The wireless communication experiments were carried out to evaluate the transmission performance as shown in Figure 7 (b). The detection error was calculated in each distance from 0 to 80 meters. It can be seen that the detection error rises while the transmission distance surpasses 75 meters in the figure. However, considering the length of the greenhouse and reasonable sensing location, the overall detection error of RSSI remains stable in the greenhouse.

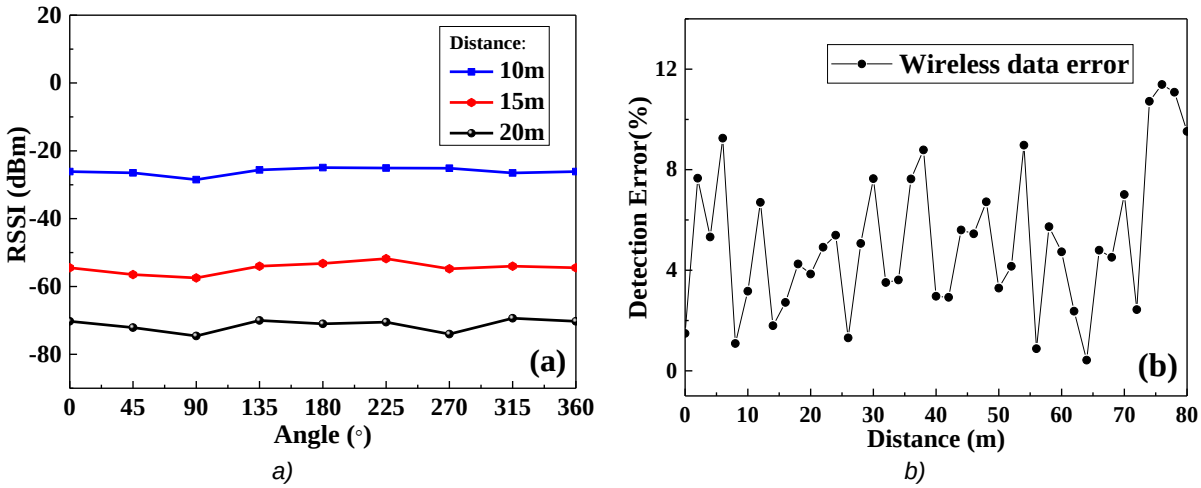

a) *b)*

Fig. 7 - Tests of RSSI value in different angles (a) and detection error in different distances (b) in the greenhouse

Remote-controlled measurements of factors

Remote-controlled measurements of key factors were performed while the preparations were implemented including placement of the sensor node, wireless communication tests and software development. Environmental factors in greenhouse were detected and transmitted to the lab. During a period of 7 hours from 10 a.m. to 5 p.m., CO_2 concentration and luminance were detected and plotted in Figure 8.

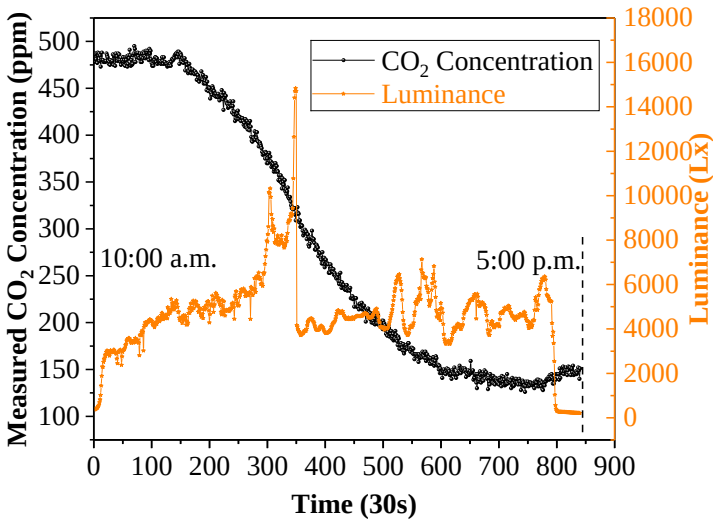

Fig. 8 - Detection of CO_2 concentration and luminance in the greenhouse in 7-hour period

The CO_2 concentration continually decreased from beginning to the end during this period of time. The decrease was caused by the photosynthesis phenomenon. In the sealed greenhouse, ventilation was prevented for warm keeping so the consumed part of CO_2 cannot be supplied by the outside cold air. Then, the roll blind machine started to cover the greenhouse at 4:30 p.m. in order to achieve good heat insulation. In this way, the photosynthesis was terminated because of the lack of sunshine and the decrease of CO_2 concentration stopped as well. The luminance value varied corresponding to the brightness in the greenhouse. It increased from the beginning and mainly maintained in a scope from 3000 – 6000 Lx during the 7 hours. For a short period of time at noon, the luminance reached a peak value at about 15000 Lx and then dramatically decreased to its scope. The peak value of luminance could be caused by the direct ray of light on the sensor. The luminance sharply decreased to zero when the greenhouse was covered with thick light-proof material by the roll blind machine. It can be seen from the figure that the CO_2 concentration and luminance can be effectively detected by using the remotely controlled system. The environmental data can be detected accurately and quickly.

The CO_2 concentration can be controlled to maintain a relative high level. In this way, the photosynthesis process can be ensured because there is sufficient supply of CO_2 in greenhouse. Fuzzy PID is adopted as the control algorithm in the controlling process. Experiment was carried out to evaluate the result as shown in Fig. 9.

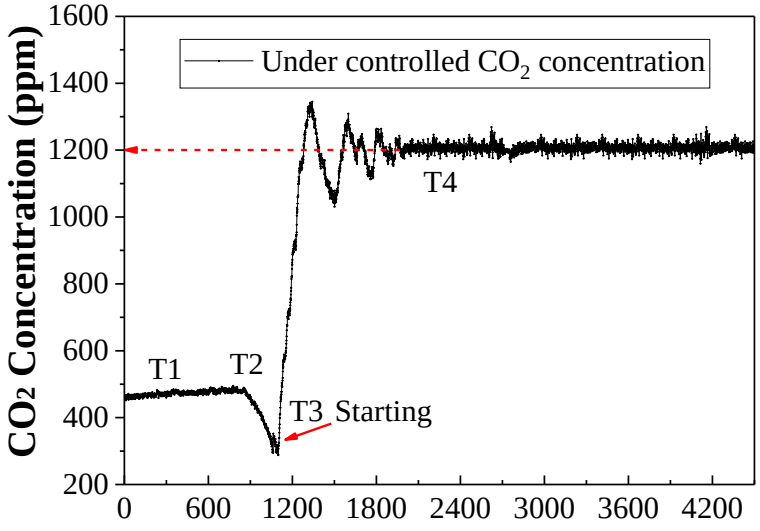

Fig. 9 – Experiment of CO_2 detection under Fuzzy PID control in the greenhouse

During the T1 and T2 period, the CO_2 concentration has been influenced by the environmental factors in the greenhouse without control. The control process starting in the period of T3 and the target value was set as 1200 ppm. As shown in the figure, the concentration of CO_2 has been raised sharply and then has fluctuated. This self-modulation period lasts about 1 hour. Then, in the period of T4, the CO_2 concentration maintains at a relative stable level around 1200 ppm. Therefore, compared with data in Figure 8, the CO_2 concentration can be effectively controlled in the greenhouse by using the fuzzy PID algorithm in order to provide enough gas fertilization for photosynthesis.

Meanwhile, ambient humidity and temperature in the greenhouse were also detected as shown in Fig. 10.

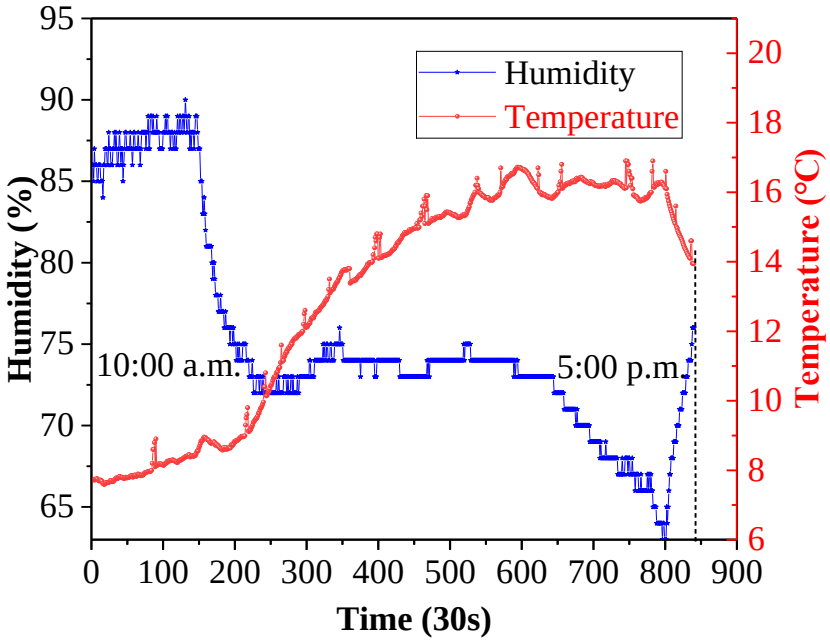

Fig.10 - Detection of humidity and temperature in the greenhouse in a 7-hour period

In figure 10, it can be seen that the humidity and temperature appear opposite trend during the 7 hours. The humidity value fluctuated in the day time from 85% to 60%. This can be also caused by the photosynthesis phenomenon. The deduced part of humidity was absorbed by plants in the photosynthesis process. The temperature value increased from approximately 8°C in the morning and reached its peak value at about 16°C in the afternoon. The temperature value started to decrease at 4:30 when the greenhouse was covered by the roll blind machine. According to our previous 24 hours detection experiments, the temperature maintained over 7°C during the night. Therefore, the plants can be protected from frozen damage in nights. The humidity and temperature value can be detected and transmitted to the lab in real time effectively.

CONCLUSIONS

The proposed remote-control wireless sensing system has been developed for detecting plant growth factors including temperature, CO_2, humidity and luminance in greenhouse environment. The above factors are essential for photosynthesis and can be detected in real-time by this system. The corresponding sensors have been adopted and were driven by the developed printed circuit boards in this system. Remote-control and wireless data transmission were also realized and optimized by using the developed circuits. In order to meet the demand of remote control, GSM module has been integrated in the sensing system. In addition, software has been developed to perform data storing, wireless communication, remote controlling and data analyzing. According to the experiments, the proposed system is suitable for precision management of key factors in greenhouse. It also exhibits optimized functional performance compared with our previously reported sensing system. In the future, based on the remote-control feature, more sensors will be adopted in this system in order to establish a remote-control sensing network in greenhouse environment.

ACKNOWLEDGEMENT

The authors wish to express their gratitude to the National Natural Science Foundation of China (No. 51672103), Jilin Jianzhu University (201810191114, 201810191115, 201810191023), the National Key Technology R&D Program of the Ministry of Science and Technology of China, the Science and Technology Department of Jilin (20180201052SF, 20180201063SF), Province of China and the Education Department of Jilin Province of China (JJKH20180573KJ, JJKH20170240KJ) for the generous support of this work.

REFERENCES

[1] Bai X.Z., Wang Z.D., Zou L. et al., (2018), Collaborative fusion estimation over wireless sensor networks for monitoring CO_2 concentration in a greenhouse, *Information Fusion*, Vol. 42, Elsevier Science BV, 1566-2535, pp.119-126, Amsterdam/Netherlands;

[2] Bin Li, Jitong Wang, Yaodan Chi et al., (2018), Wireless measurement and control system of carbon dioxide using infrared sensor in greenhouse environment, *INMATEH – Agriculture Engineering*, Vol. 54, pp.1583-1019, pp.47-54, Bucharest/Romania;

[3] Danish M, Sheikh, H, (2018), Effect of SiO2 Nanoparticles on the Interaction of Pseudomonas fluorescens and Meloidogyne incognita in Trachyspermum ammi under Greenhouse Conditions, *Phytopathology*, Vol. 108, Amer Phytopathological Soc, 0031-949X, pp.48-48, Boston/U.S.A;

[4] Erazo-Rodas M., Sandoval-Moreno M., Munoz-Romero, et al., (2018), Multiparametric Monitoring in Equatorian Tomato Greenhouses (I): Wireless Sensor Network Benchmarking, *Sensors*, Vol.18, no.8, pp.(2555)1-22, MDPI AG, 1424-8220, Basel/Switzerland;

[5] Ferrero R., Beattie E., Phoenix J., (2018), Sensor City- A Global Innovation Hub for Sensor Technology, *IEEE Instrumentation & Measurement Magazine*, Vol.21, pp.4-16, IEEE-Inst Electrical Electronics Engineers INC, 1094-6969, NJ/U.S.A;

[6] Fisher E.M.D., Benoy T., (2018), Interleaving and Error Concealment to Mitigate the Impact of Packet Loss in Resource-Constrained TDLAS/WMS Data Acquisition, *IEEE Transactions on Instrumentation and Measurement*, Vol.67, pp.439-448, IEEE-Inst Electrical Electronics Engineers INC, 0018-9456, NJ/U.S.A.;

[7] Hwang J., Shin C., Yoe H. (2010), A wireless sensor network-based ubiquitous paprika growth management system, *Sensors*, Vol.10, pp.11566-11589, DPI AG, 1424-8220, Basel/Switzerland;

[8] Jahnavi V.S., Ahamed S.F., (2015), Smart Wireless Sensor Network for Automated Greenhouse, *IETE Journal of Research*, Vol.61, pp.180-185, Taylor & Francis LTD, 0377-2063, Oxon/England;

[9] Jianing Wang, Lingjiao Zheng, Xintao Niu et al., (2016), Mid-infrared absorption-spectroscopy-based carbon dioxide sensor network in greenhouse agriculture: development and deployment, *Applied Optics*, Vol. 55, Issue 25, pp.7029-7036, Optical Soc. Amer, 2155-3165, Washington, D.C./U.S.A.;

[10] Jiang M., Zhou P., Gu X.J., (2018), Ultralong pi-phase shift fibre Bragg grating empowered single-longitudinal mode DFB phosphate fibre laser with low-threshold and high-efficiency, *Scientific Reports*, Vol.8, Nature Publishing Group, 2045-2322, London/England;

[11] Kapsalidis F., Shahmohammadi M., Suess M.J. et al., (2018), Dual-wavelength DFB quantum cascade lasers: sources for multi-species trace gas spectroscopy, *Applied Physics B-Lasers and Optics*, Vol.124, no.6, pp.(107)1-17, Springer, 0946-2171, NY/U.S.A.;

[12] Lambrecht S., Nogueira S.L., Bortole M., et al., (2016), Inertial Sensor Error Reduction through Calibration and Sensor Fusion, *Sensors*, Vol.12, pp1-16, MDPI AG, 1424-8220, Basel/Switzerland;

[13] Park D.H., Park J.W., (2011), Wireless Sensor Network-Based Greenhouse Environment Monitoring and Automatic Control System for Dew Condensation Prevention, *Sensors*, Vol.11, pp.3640-3651, MDPI AG, 1424-8220, Basel/Switzerland;

[14] Sahbani F., Ferjani E., (2018), Identification and Modelling of Drop-By-Drop Irrigation System for Tomato Plants Under Greenhouse Conditions, *Irrigation and Drainage*, Vol. 67, pp.550-558, WILEY, 1531-0353, Hoboken/U.S.A.;

[15] Searchinger T., Heimlich R., Houghton R.A. et al, (2008), Use of US croplands for biofuels increases greenhouse gases through emission from land-use change, *Science*, Vol.319, pp.1238-1240, Amer. Assoc. Advancement Science, 0036-8075, Washington, D.C./U.S.A.;

[16] Somov A., Baranov A., Spirjakin D., et al. (2013), Development and evaluation of a wireless sensor network for methane leak detection, *Sensors and Actuators A*, Vol.202, pp.217-225, Elsevier Science SA, 0924-4247, Lausanne/Switzerland;

[17] Sivamani S., Choi J., Bae K. et al., (2018), A smart service model in greenhouse environment using event-based security based on wireless sensor network, *Concurrency and Computation-Practice & Experience*, Vol. 30, pp.171-184, Wiley, 1531-0353, Hoboken/U.S.A.;
[18] Suzuki K, Oota H., Umeyama T., (2018), Development of Corrosion-Resistant Pressure Sensor with Semiconductor Strain Sensor, *Electrical Engineering in Japan*, Vol.203, pp.58-65, WILEY, 1531-0353, Hoboken/U.S.A.,;
[19] Wei Ren, Wehzhe Jiang, Nancy P. Sanchez, et al., (2014), Hydrogen peroxide detection with quartz-enhanced photo acoustic spectroscopy using a distributed feedback quantum cascade laser, *Applied Physics Letters*, Vol.104, pp.(041117)1-5, Amer. Inst. Physics., 0003-6951, NY/U.S.A., 041117;
[20] Wynn C., Palmacci St., Clark M. et al., (2014), High-sensitivity detection of trace gases using dynamic photo-acoustic spectroscopy, *Optical Engineering*, Vol.53, pp.(021113)1-5, SPIE-SOC Photo-Optical Instrumentation Engineers, 0091-3286, Bellingham/U.S.A., 021103;
[21] Yasuda T., Yonemura S., Tani A., (2012), Comparison of the characteristics of small commercial NDIR CO_2 sensor models and development of a portable CO_2 measurement device, *Sensors*, Vol.12, pp.3641-3655, MDPI AG, 1424-8220, Basel/Switzerland;
[22] You S.M., Tong H.H., Armin H.J. et al., (2017), Techno-economic and greenhouse gas savings assessment of decentralized biomass gasification for electrifying the rural areas of Indonesia, *Applied Energy*, Vol.208, pp.495-510, ELSEVIER SCI LTD, Oxford/England.

RESEARCH OF QUALITY INDICATORS OF WHEAT SEEDS SEPARATED BY PRE-THRESHING DEVICE

/

ДОСЛІДЖЕННЯ ПОКАЗНИКІВ ЯКОСТІ НАСІННЯ ПШЕНИЦІ ВІДДІЛЕНОГО ПРИСТРОЄМ ПОПЕРЕДНЬОГО ОБМОЛОТУ ЗЕРНА

Doctor of technical sciences Sheychenko V.O. [1)], Ph.D. Kuzmych A.Ya. [2)], Postgraduate Shevchuk M.V. [2)], Ph.D. Shevchuk V.V. [3)], Ph.D. Belovod O.I. [1)]

[1)] Poltava State Agrarian Academy / Ukraine; [2)] National Scientific Centre "Institute of Agriculture Engineering and Electrification" / Ukraine; [3)] Uman National University of Horticulture / Ukraine

Tel: +380676892302; E-mail: akuzmich75@gmail.com

Keywords: *combine harvester, header, pre-threshing device, damage of grain, energy of seed germination*

ABSTRACT

The influence on wheat grain quality indices of the preliminary threshing machine parameters of combine harvester header was investigated. The value of the trauma and the germination energy of the grain collected by the combine with the serial and experimental harvester were determined. It was established that as a result of passing the grain through the entire technological chain of the combine, germination energy decreased by 1.13 - 1.15 times. For the proposed options for preliminary threshing of grain, rational throughput values have been established, which correspond to high levels of germination energy. The highest germination energy level of the grain 99% was noted in the header, the drum of which contained four strips, according to the combine throughput 7.5 kg/s. This level was 7% higher than the serial header.

ABSTRACT

Досліджено вплив параметрів пристрою попереднього обмолоту зерна жниварки зернозбирального комбайна на показники якості зерна пшениці. Визначено значення травмування та енергії проростання зерна, зібраного комбайном з серійною та експериментальною жниваркою. Встановлено, що внаслідок проходження зерном усього технологічного ланцюга комбайну відбувається зменшення енергії проростання у 1,13 – 1,15 рази. Для запропонованих варіантів пристроїв попереднього обмолоту зерна встановлено раціональні значення пропускної здатності, яким відповідають найвищі рівні енергії проростання. У жниварки, барабан якої містить чотири планки, за пропускної здатності комбайна 7,5 кг/с зерна, найвищий рівень енергії проростання встановлено на рівні 99%, що на 7% більше ніж у серійної жниварки

INTRODUCTION

Mechanical damage of the grain leads to deterioration of its quality and storage, reduction of baking, technological, sowing qualities, etc *(Puzik L. and Puzik V., 2013).*

The level of seed damage is an integral indicator that allows evaluating the effectiveness of a number of decisions (factors) that are used to implement the technological process. The degree of seeds damage depends on the adjustment of the working units and aggregates of the combine, the biological phase of the plants development, the variety and the type of crops. Harmful are the micro damages in the grain embryo zone, mechanical damage to the germ and endosperm *(Kyrpa M. et al, 2009; Pecen J, 1994)*. A high level of micro damage of seeds is one of the reasons preventing it from promotion to European and world markets.

Low quality of domestic seed is due to significant damage in the conditions of its harvesting and primary processing. As a consequence, there is a discrepancy with the main indicators for seeding. In response to such circumstances, agrarians increase the sowing rate by 20-25% compared to the sowing by conditional seeds *(Harbar I. et al, 2010; Shpokas L. et al, 2016)*.

The research is based on the hypothesis that it is possible to intensify the process of separating cereal seeds from grain-straw mass (GSM) in the transportation phases by the preliminary threshing device of the header before the threshing-separating system (TSS) of the combine. Note that the previously threshed grain settles (concentrates) in the lower part of the process mass flow and is not damaged by the main threshing drum. It passes faster through the concave.

This, as it is known, contributes to reducing the losses of the combine threshing machine. Therefore, it can be concluded that it is expedient grain pre-threshing by the header working units before the cut-off material enters the feeder house conveyor.

The grain threshing process occurs from the moment when the fingers of the header reel begin to interact with the stem. The degree of grain separation from the mass that the header is transporting depends on many factors: the technical and technological characteristics of the harvesting method, the phase of the crop growth, its humidity, maturity, variety, dynamic components of the effect on plants, and others.

Indicators of seed quality depend on many factors *(Fiscus D. et al, 1971; Tarasenko A., 2014)*. They include: 1) the physical and mechanical properties of the technological material, which is processed by threshing, determined by the moisture content of the grain and not the grain part, the ratio of the mass of grain and straw, the shape and structure of the grains, varietal characteristics and other properties; 2) factors associated with the construction of grain harvesting machines and equipment for post-harvest grain processing (types and parameters of working bodies, their arrangement); 3) technological regulations and operating conditions of the main mechanisms of the combine, especially the threshing separating device (drum speed, threshing gaps, feeding); 4) technical condition of the parts (wear of pests, planks, screws, scrapers, etc.).

Present mechanisms used for harvesting grain do not completely prevent seed damage. It should be noted that the level of seed damage depends significantly on humidity *(Zielinski A. and Mos M., 2009)*. Experiments have shown that if the humidity is more than 25%, the injuries are quite significant and can completely damage the germ. With increasing humidity, damage to the seeds increases. For all cereal crops, the optimum moisture for collection is 16-17% *(Derevyanko D., 2011; Shahbazi F. et al, 2012; Szwed G. and Lukaszuk J., 2007).*

It should be noted that the share of grains with macro-damage (crushed, flattened and compressed with damage to the germ or a separate part of the grain) is about 3-5%. The number of grains with micro-damages (damaged shell, hidden internal defects – scratches, dents, cracks, etc.) reaches a level of 50-80% or more (*Baker K. et al, 1986)*. Based on the studies of results of the TSS type influence on the micro-damage of grain, it was established that in an axial-rotor combine, an increase in the rotor speed from 520 rpm to 810 rpm results in a corresponding growth micro-damage of seeds from 25-30% to 45-50%. In the drum-walker combine, the increase in the drum rotation frequency from 700-760 rpm to 820 rpm leads to a corresponding growth of micro-damage of seeds from 37-38% to 41-44%.

MATERIALS AND METHODS

The conducted research aimed to determine the influence of working units, technological operations and technological processes on the indexes of seed quality (micro-damage).

To achieve this purpose, the following tasks were accomplished:

- to determine the quality losses (micro-damages) of wheat seeds separated by the preliminary threshing device in conditions of sequential setting in it of the developed and manufactured: intermediate threshing drum without additional slats (smooth drum) of threshing drum with a rasp bar under the drum; threshing drum with two additional slats (tooth-like profiles with a height of the bar 20 mm, 30 mm and smooth slats) of the intermediate threshing drum with four additional slats (tooth-like profiles with a height of the bar 20 mm, 30 mm and smooth slats) compared to the standard header;
- to determine the level of micro-damages accumulation for the combine's bunker grain as a result of the entire technological cycle of threshing;
- to determine the effect of the throughput of the combine on the quality of grain, separated by a pre-threshing device.

We have developed a preliminary threshing device for grain located in a feeder house of a combine harvester KZS 9-1 "Slavutich". The basis of the device for preliminary threshing of bread mass in the combine harvester was an intermediate thrashing drum and a deck installed below it (Fig. 1). Kherson machine-building plant manufactures the family of KSZ 9-1 "Slavutich" Ukrainian grain harvesters.

Experimental research was carried out on the experimental field of the National Scientific Centre "Institute of Agriculture Engineering and Electrification", sown with winter wheat of Mironovskaya 61, according to standard methods *(Dospehov B., 2014; Vedenyapin G., 1973).* The yield of the field was 5.5 t/ha.

According to the study plan each sample was taken from a combine harvester stone trap which is located in front of the main threshing drum. This mass, which accumulated there, was a mixture of grain separated from the ear, uncoated grain into a spikelet, chaff and straw. Accumulated mass in a stone trap was placed in specially prepared packages beforehand by signing them.

Experimental research was carried out on the preliminary threshing device of a grain combine KZS 9-1. The research program was designed to test an intermediate cylindrical beater with pull-out pins (serial header) in comparison with the following developed and manufactured designs of a preliminary thresher device (a 330 mm cylindrical toothed-blade drum) of an experimental header. These are: a header with a threshing drum without additional slats (smooth drum); a header with an intermediate threshing drum and a rasp bar under it; header with an intermediate threshing drum with two additional slats (tooth-like profiles of a 20 mm, 30 mm slat height and a smooth bar); header with an intermediate threshing drum with four additional (tooth-like profiles of a 20 mm, 30 mm height and a smooth bar). A steel corner (measuring 45 x 45) was used as the slats, one side of which was attached to the side surface of the drum. On the other side of the corner, a tooth-shaped profile was cut in the form of equilateral triangles 20 mm high and 30 mm high.

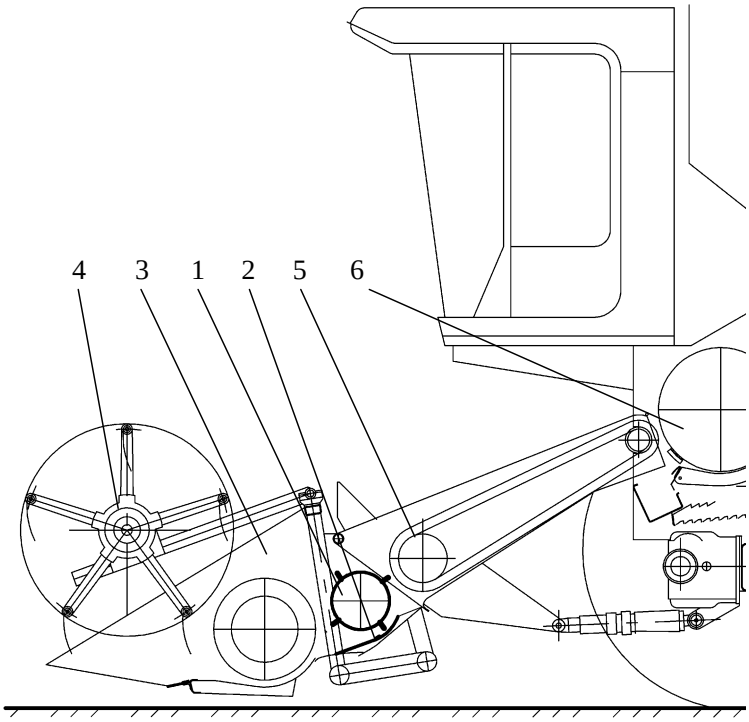

Fig. 1 - General view scheme of a combine harvester header with a device for preliminary grain threshing:
1 − a tooth and spatulate shaped thrashing drum; 2 − a deck; 3 − a header; 4 − a reel; 5 – an inclined chamber conveyor; 6 – threshing-separation system of combine harvester

The methodology of the research included the selection of a site with a uniform and aligned stand of grain. Studies were conducted at four speeds of movement of the combine in three replications. The speed of the combine varied within 0.56-1.67 m/s.

When conducting experiments, we determined the length and area of the experimental plot, the time it took for the combine to pass through the experimental plot, the speed of the combine.

Processing of research results was carried out under laboratory conditions. The mass of the separated grain, the mass of not separated grain and the total mass of the grain in the GSM were determined in the laboratory according to the results of the disassembly of samples taken in the field.

Throughput was determined according to dependencies (1), (2):

$$q = \frac{B \cdot v \cdot Q}{360}, \quad (1)$$

$$Q = Q_G + Q_G \cdot \beta \quad (2)$$

q is the throughput, [kg/s];

B – width of the header, [m];
v – speed of the combine, [km/h]
Q – yield of grain and straw, [t/ha];
Q_G – grain yield, [kg/ha];
β – proportion of straw by weight relative to grain yield.

Estimation of germination and germination energy was carried out according to the ISTA technique *(ISTA Documents, 2011)* and methods of national standard. To determine the germination energy and seed germination, 4 samples of 100 seeds were formed from each sample tested. After that, the seeds were put on 3 layers of moistened filter paper with special vessels (cup of Koch, Petri), which were placed in a dark place. The germination energy was determined by the number of similar seeds 3 days after the germination began, the seed germination was determined after 7 days.

After the term of germination and the end of all calculations, all identified seedlings are divided into three groups according to the quality of germination: a) normally germinated; b) not germinated; c) not sprouting.

The germination and germination energy was determined in percent. Based on the results of the analysis, the arithmetic mean of the results of determining the similarity of all four analyzed samples was taken. Investigation of the germination and germination energy was also carried out for wheat seeds, which were seized in different places of the combine harvester after passing through the whole threshing cycle. The main goal of these studies is to determine the influence of working units, technological operations and technological processes on the indicators of seed quality.

Grain damage at threshing, separation and transportation was determined in accordance with methods for seeds testing. During the research, the amount of damaged wheat seeds in the total mass was assessed, which affects the technological properties of the seeds as a raw material for further processing.

The micro-injury investigation was carried out for wheat seeds taken from different locations of the combine harvester as a result of the threshing cycle.

The processing of experimental results was carried out taking into account the methods of regression analysis. The approximation of the experimental dependencies by the mathematical model was performed using the least squares method using the statistical software package STATISTIKA-6.5. Checking the adequacy of mathematical models was carried out using the elements of variance analysis using the Fisher criterion at a confidence level of 0.95.

RESULTS

There were taken samples of grain from the grain harvester hopper to assess the impact level on seeds of the working units of the entire threshing technological cycle (experimental header).

Based on the results of the conducted investigations, it was established that the arithmetic mean value of the germination energy of the grain harvested by the serial header, as well as the experimental samples (header with a rasp bar under the drum, a header with a smooth drum, a header with a drum that contains two slats, a header with a drum with four slats) was in the range of 88-98% (Figure 2). It should be noted that the speed of the combine harvester did not significantly affect grain quality indicators. This is due to the fact that the experiments were carried out under conditions of a sufficiently high grain yield (5.5 tons/ha) and the grain harvester capacity was 8-10 kg/s.

Micro-damages were assessed according to the following indices: damage to the grain shell; damage to the germ; whole seed.

The average index of damage to the grain shell in the serial header was 10.5%, in the experimental header with a rasp bar under the drum – 9.5%, in header with two additional slats on the drum – 7.25%, header with 4 additional slats on the drum – 10.25%; header without bars on the drum – 11.25%. The highest level of damage to the shell of the grain is installed in the header, without slats on the drum – 11.25% (Figure 3). This is due to the fact that, because of the lack of slats on the drum (smooth drum), the duration of the interaction of the free grain separated from the GSM with the moving layer of mass fed will be greater. Grain-straw mass will slide over the layer of separated grain. Note that in the absence of slats on the drum, the residence time and thickness of the grain layer will be higher than in the designs with slats. This causes a multiple dynamic effect of the GSM (fluctuations in the thickness of the layer, both GSM and separated grain) on the layer of separated grain, which leads to an increase in the index of damage to the grain shell.

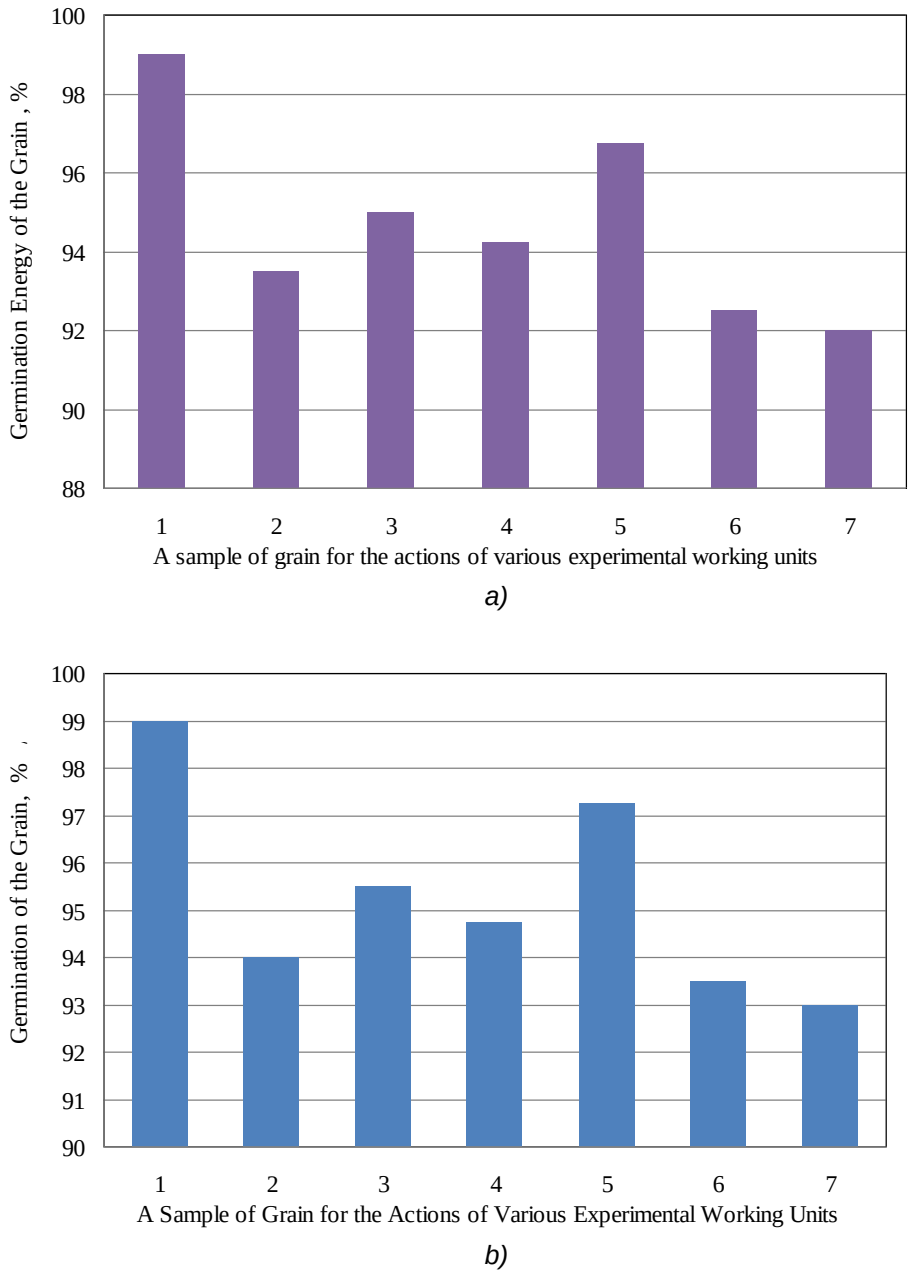

Fig. 2 - Research results diagram of the germination energy *(a)* and the wheat grain germination *(b)* separated by the preliminary threshing device under the conditions of successive setting of experimental working units:

1 - non-threshed grain; 2 - the establishment of rasp bar under the drum; 3 - smooth drum; 4 - a drum with two slats; 5 - a drum with four slats; 6 - grain from the feeder house of the serial header; 7 - grain from the combine's hopper

The least indicator of damage to the grain shell is installed in the header with two additional slats on the drum – 7.25%. The value of the average grain damage factor in the serial and experimental header with 4 additional slats on the drum was approximately the same. The results for determining the level of damage to the grain shell are shown in Fig. 3.

It should be noted that there was certain deterioration in the transport function of the feeder house in the course of the research on experimental samples of the header (header with a rasp bar under the drum, a header with a smooth drum, a header with a drum that contains two slats). It was caused by the fact that experiments at the planned high levels of combine speeds were not realized, because the increase in speed led to the formation of mass that was ejected from the feeder house and accumulated from the outside. Due to this, the operator reduced the speed of the harvester's movement in order to stabilize the transportation function and ensure that the mass formed above the camera enters the feeder house.

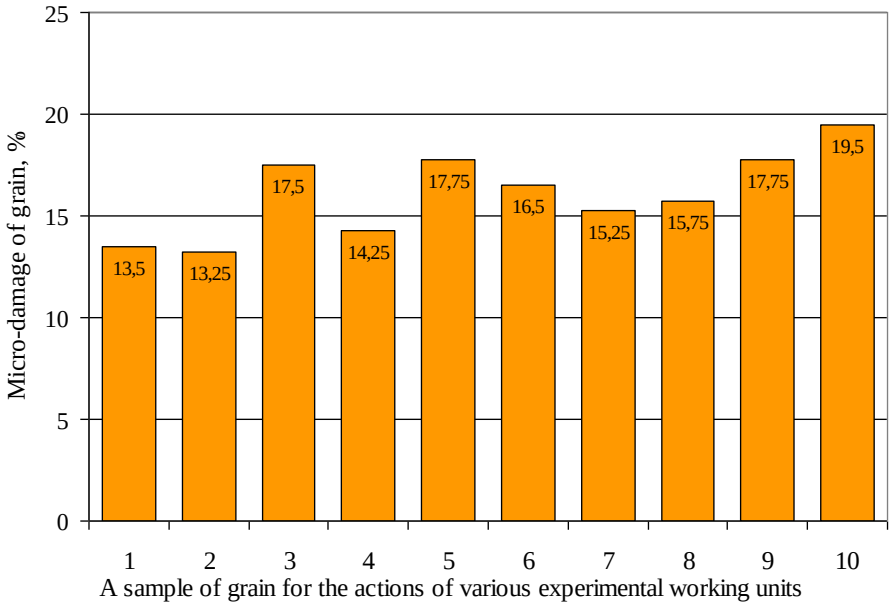

Fig. 3 - Research results diagram of the grain micro-damage of wheat grain separated by the preliminary threshing device under the conditions of successive setting of experimental working units:

1 - grain from the feeder house of the serial header; 2 - the establishment of rasp bar under the drum; 3 - smooth drum; 4 - a drum with two slats and 30mm tooth height; 5 - a drum with two slats and 20mm tooth height; 6 - a drum with two smooth slats; 7 - a drum with four slats and 30mm tooth height; 8 - a drum with four slats and 20mm tooth height; 9 - a drum with four smooth slats; 10 - grain from the combine's hopper

The effect of the combine throughput on wheat seeds quality indicators was determined in order to establish the most rational operation modes of the combine with the header, containing the proposed design of the preliminary threshing device.

It was established that each of the considered devices of the previous grain threshing is characterized by a different value of the throughput level, according to which the injury of the grain will be minimal (Fig. 4).

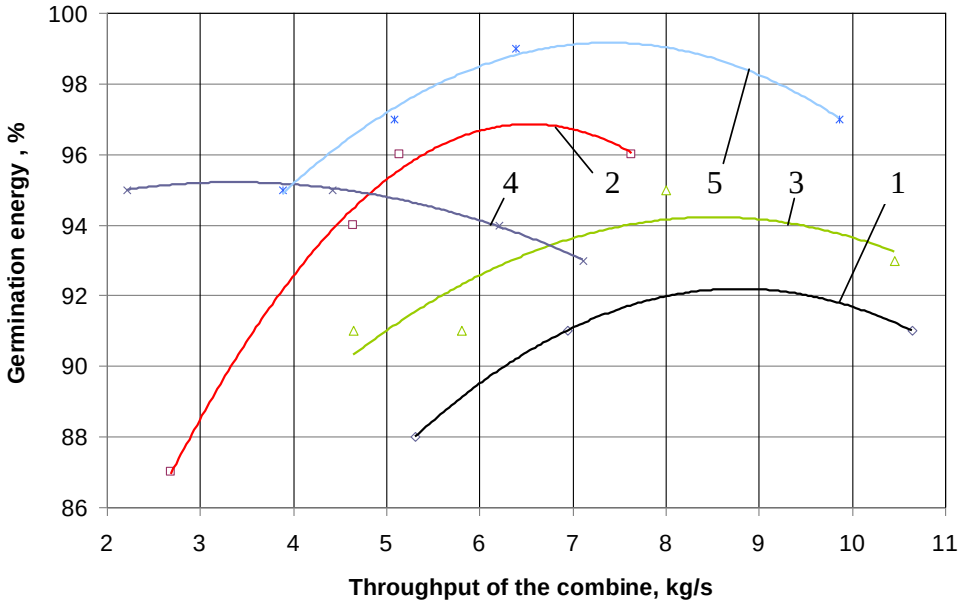

Fig. 4 - Experimental dependencies of grain germination energy on the combine throughput:

1 - serial harvester; 2 - a header with an intermediate threshing drum, which contains a bar under the drum; 3 - header with a smooth drum; 4- header with an intermediate threshing drum, which contains two additional strips; 5 - headers with an intermediate threshing drum, which contains four additional strips

According to the results of the conducted research, the highest germination energy level of the harvested grain was determined by a reaper, the drum of which contains four strips - 99% for loading the combine thresher at 7.5 kg/s.

Values of grain germination for all samples were studied and did not significantly differ from the arithmetic mean values of germination energy.

CONCLUSIONS

According to the results of the conducted investigation it was established that the arithmetic mean value of the germination energy of grain harvested by the serial header was 91-95%, for the header, which contains a rasp bar under the drum was 88-96%, for header with a smooth drum was 93-96%, for the header, the drum of which contains two bars was 93-95% and four bars was 95-98%. The arithmetic mean value of the germination energy of the non-threshed grain (from the sheaf) was 99%, and the grain from the combine harvester hopper was 92%.

The highest values of the grain germination energy are recorded in the header the drum of which contains four slats (95-98%). It was established that as a result of passing the grain through the entire technological chain of the combine, germination energy decreased by 1.13 - 1.15 times.

The values of the grain germination indices for all the samples investigated did not differ significantly from the arithmetic mean values of the germination energy indices.

It was found that the value of the indicator of the unharmed seed in header with a rasp bar under the drum was 86.75%. It was 86,5% for the serial header, 85.75% for the header with two additional slats on the drum (tooth profile, tooth height 30 mm), 83.75% for the header with four additional slats on the drum (tooth-shaped profile, tooth height 30 mm) and 82.5% for the header with no slats on the drum.

According to the integral index of micro-damage, the grain from the grain harvester's hopper had the most highest indicators - 19.5% (14% shell damage and 5.5% germ damage), which is 6.25% worse than in the header with a rasp bar under the drum, 6% more than in the serial header, 5.25% more than in the header with two additional slats on the drum (tooth profile, tooth height 30 mm) and 4.25% more than in the experimental header with four additional slats on the drum (tooth profile, height tooth 30 mm).

For the proposed options for preliminary threshing of grain, rational throughput values had been established, which corresponded to high levels of germination energy.

The highest germination energy level of the grain 99% was noted in the header, the drum of which contained four strips, according to the combine throughput 7.5 kg/s. The high level of grain germination energy for a serial header of 92% was noted at a combine throughput 8.5-9.5 kg/s. The maximum values of the grain germination energy were observed: for the header with a pre-threshing device with a bar under the drum at a throughput 6-7 kg/s; for a header with a smooth drum – 8-9 kg/s.

The level of the germination energy of the grain, which was collected after an experimental header with a pre-threshing drum with four slats, was 7% higher than grain in the serial header. A small decrease (1.0-1.5 kg/s) of the throughput of the combine was noted during the study.

REFERENCES

[1] Baker K.D., Stroshine R.L., Magee K.J., Foster G.H., Jacko R.B., (1986), Grain damage and dust generation in a pressure pneumatic conveying system. *Transactions of the ASAE*, Vol.29, Issue 2, ISSN 0001-2351, pp. 840-847, St. Joseph / U.S.A.;

[2] Derevyanko D.A., (2011), Influence of grain moisture during threshing and post-harvest completion of a grain heap of winter wheat on its injuries and seed quality (Вплив вологості зерна при обмолоті та післязбиральній доробці зернового вороху озимої пшениці на її травмування і насіннєві якості), *Machinery in agricultural production, industrial engineering, automation (Техніка в сільськогосподарському виробництві, галузеве машинобудування, автоматизація)*, Vol.24, Issue 1, ISSN 2409-9392, pp. 181-184, Kirovohrad/Ukraine;

[3] Dospehov B.A., (2014), *Methodology of field experience with the basics of statistical processing of research results (Методика полевого опыта с основами статистической обработки результатов исследований)*, Alyans, ISBN 978-5-903034-96-3, p. 352, Moscow/Russia;

[4] Fiscus D.E., Foster G.H., Raufman H.H., (1971), Physical Damage of Grain Caused by Various Handling Techniques, *Transactions of the ASAE*, Vol.14, Issue 3, ISSN 0001-2351, pp. 480-485, St. Joseph / U.S.A.;

[5] Harbar I.H., Derevyanko D.A., Heruk S.M., (2010), Influence of threshing on grain yield of wheat, rye, and other grains (Вплив обмолоту на посівні якості зерна пшениці, жита, та інших зернових), *Design, manufacture and operation of agricultural machines (Конструювання, виробництво та експлуатація сільськогосподарських машин)* Vol.40, Issue 1, ISSN 2414-3820, pp. 6-9, Kirovohrad/Ukraine;

[6] ISTA Documents, (2011), International Rules for Seed Testing, *International Seed Testing Association,* Edition 2011, p. 97, Bassersdorf/Switzerland;

[7] Kyrpa M.Ya., Pashchenko N.A., Bazilyeva, Yu.S., (2009), Nature of seed damage and methods of its determination (Природа травмування насіння та методи його визначення), S*election and seed-growing (Селекція і насінництво)*, Vol.97, ISSN 0582-507, pp. 196-201, Kharkiv/Ukraine;

[8] Pecen J., (1994) Internal damage identification of seeds, *International Agrophysics*, Vol.8, Issue 2, ISSN: 0236-8722, pp. 289-293, Lublin/Poland;

[9] Puzik L.M., Puzik V.K., (2013), *Technology of storage and processing of grain (Технологія зберігання і переробки зерна)*, Kharkiv National Agrarian University, p. 312, ISBN 978-617-669-113-6, Kharkiv/Ukraine;

[10] Shahbazi F., Valizadeh S., Dowlatshah A., (2012), Mechanical damage to wheat and triticale seeds related to moisture content and impact energy, *Agricultural Engineering International: CIGR Journal*, Vol.14, Issue 4, ISSN 1682-1130, pp.150-155, Kyoto/Japan;

[11] Shpokas L., Adamchuk V., Bulgakov V., Nozdrovicky L., (2016), The experimental research of combine harvesters, *Research in Agricultural Engineering*, Vol.62, ISSN 1212-9151, pp. 106-112, Prague/ Czech Republic;

[12] Szwed G., Lukaszuk J., (2007), Effect of rapeseed and wheat kernel moisture on impact damage, *International Agrophysics*, Vol.21, Issue 3, ISSN: 0236-8722, pp. 299-304, Lublin/Poland;

[13] Tarasenko A.P., Orobinskiy V.I., Georgievskiy A.M., Merchalova M.E., (2014), *Improvement of mechanization of grain crops seed production (Совершенствование механизации производства семян зерновых культур)*, "Rosinformagrotekh", p. 60, ISBN 978-5-7367-1022-5, Moscow/Russia;

[14] Vedenyapin G.V., (1973), General procedure for experimental research and processing of experimental data (Общая методика экспериментального исследования и обработки опытных даннях), Kolos, p. 199, Moscow/Russia;

[15] Zielinski A., Mos M., (2009), Effects of seed moisture and the rotary speed of a drum on the germination and vigour of naked and husked oat cultivars, *Cereal Research Communications*, Vol.37, Issue 2, ISSN: 0133-3720, pp.277-286, Szeged/Hungary.

DESIGN AND CONSTRUCTION OF CHOPPER MACHINE AE02-TYPE FOR OIL PALM FROND
/
RANCANG BANGUN DAN KONSTRUKSI MESIN PENCACAH TIPE-AE02 UNTUK PELEPAH SAWIT

Ph.D. Eng. Ramayanty Bulan[1)], Ph.D. Eng. Safrizal[1)], Ph.D. Eng. Muhammad Yasar[1)], M.Eng. Yudi Nata[2)], M.Sc. Agustami Sitorus[2)*]

[1)]Department of Agriculture Engineering, Faculty of Agriculture, Syiah Kuala University / Indonesia

[2)]Department of Mechanical Engineering, Faculty of Engineering, Nusa Putra University / Indonesia

E-mail: agustami@nusaputra.ac.id

Keywords: *oil palm frond, chopper, appropriate technology, small-scale chopper machine*

ABSTRACT

A low-cost and a small-scale chopper machine for oil palm frond (OPF) was locally designed, manufactured and simply evaluated. It's called chopper machine AE02-type. This type of machine is designed so that it can be of appropriate technology and affordable for smallholders of palm oil in Indonesia. The effect of chopper machine AE02-type operating conditions (three different blade rotation speeds: 800 rpm, 1200 rpm and, 1600 rpm; and three branches of fresh OPF with leaves was cut into ±2.0 m length at three different sections: initial, middle, and edge were investigated. The performance of the developed machinery was evaluated regarding (i) machine capacity, (ii) size of chopped OPF, (iii) percentage of chopped OPF, and (iv) chopper machine efficiency. The chopper machine AE02-type essentially consists of the hopper, mainframe, diesel engine, outlet and chopping blade. It was powered by an 8.5 hp diesel engine and the blade of a chopper is powered through a V-belt connection. Results revealed that the increase of the rotations speed was found to increase the machine capacity and chopping of OPF percentage at all OPF sections. On the other hand, it also results in smaller chopping dimensions. However, it caused a decrease in the mean values of chopping efficiency.

ABSTRAK

Sebuah mesin pencacah daun kelapa sawit berbiaya rendah dan skala kecil telah dirancang, dimanufaktur, dan diuji secara sederhana. Mesin jenis ini dirancang sedemikian rupa sehingga dapat memiliki teknologi tepat guna dan terjangkau bagi petani kecil kelapa sawit di Indonesia. Mesin ini disebut mesin pencacah tipe AE02. Pengaruh dari kondisi kerja mesin pencacah tipe AE02 (putaran pisau: 800 rpm, 1200 rpm, 1600 rpm; dan bagian pelepah sawit dengan dengan panjang ±2,0 m: bagian pangkal, bagian tengah, bagian ujung) telah diselidiki. Parameter kinerja mesin yang diamati diantaranya adalah (i) kapasitas mesin pencacah, (ii) ukuran cacahan pelepah, (iii) persentase pelepah tercacah, dan (iv) efisiensi mesin pencacah. Mesin pencacah tipe AE02 terdiri dari saluran pengumpanan, rangka, mesin penggerak, saluran pengeluaran, dan pisau potong. Mesin penggerak menggunakan diesel berdaya 8,5 hp dan sistem transmisi menggunakan sabuk V-belt. Hasil penelitian menunjukkan bahwa peningkatan kecepatan putar mesin pencacah akan meningkatkan kapasitas mesin dan persentase pelepah yang tercacah pada semua bagian pelepah sawit. Di sisi lain, peningkatan kecepatan putar menghasilkan dimensi cacahan yang lebih kecil. Namun, hal ini menyebabkan penurunan efisiensi mesin pencacah.

Nomenclature			
n_1	Speed of driving motor, rpm	W_{OC}	Weight of OPF chopper, g
n_2	Speed of the blade shaft, rpm	W_{NOC}	Weight of OPF losses, g
d_1	Diameter of driving pulley, m	π	Constant
d_2	Diameter of the driven pulley, m	T	Time, s
W_t	Total weight of OPF put into the machine, g	Cc	Capacity of the chopper machine, kg·h^{-1}
T	Torque, Nm	M_S	Mass of the shaft, kg
F_1	Tight side, N	τ	Torque generated, N·m
F_2	Slack side, N	M_P	Mass of the pulley, kg
c	Centre to centre distance of driving and the driven pulleys, m	M	Total mass of the material contain in blade, kg
M_B	Mass of chopping blade, kg	d	Diameter of shaft, mm
M_b	Maximum bending moment, Nm	M_{OPF}	Mass of OPF, kg
ω	Angular speed of blade, rpm	Mt	Moment of torsion, N·m
K_b	Combined shock and fatigue factor applied to bending moment	Kt	Combined shock and fatigue factor applied to the moment of torsion
n	Revolution per minute of blade, rpm	P	Power required by the machine, W
S_s	Allowable shear stress, Mpa	μ	Coefficient of friction
η_c	Chopper efficiency, %	r_d	Radius of the blade, m
η_{oc}	Percentage of chopped OPF, %	F	Total force, N

INTRODUCTION

The most abundant biomass from oil palm plantation is not oil palm empty fruit bunch (OPEFB) (*Raju and Sitorus, 2017)* or oil palm trunk (OPT) (*Zahari et al., 2012)*. The most generated oil palm biomass is oil palm frond (OPF), which amounted to 83 million tonnes (wet weight) annually (*MPOC, 2011*). OPF is obtained during pruning for harvesting fresh fruit bunch (FFB), therefore it is available daily. OPF is currently under-utilized as the plantation owners believe that all the OPF are necessary for nutrient recycling and soil conservation (*Hassan et al., 1994*, *Bulan et al., 2017*).

Hence, pruned fronds are just left in the plantation. OPF are left natural rotting between the rows of palm trees, mainly for soil conservation, erosion control and ultimately the long-term benefit of nutrient recycling. However, according to researchers (*Bulan et al., 2017*, *Bulan et al., 2015*) natural rotting takes a long time for an OPF. The large quantity of fronds produced by a plantation each year makes them a very promising source of raw material for compost (*Hassan et al., 1994*). However, Study from researcher (*Zahari et al., 2012*) shows that OPF does not contain high metal contents as widely thought, but it contains high carbohydrates in the form of simple sugars. Therefore, part of the OPF can be utilized for other purpose without affecting the nutrient recycling process.

One of the OPF left on the plantation can be processed into compost. The composting process requires a size reduction process called chopping. A chopper machine for OPF with AE01-type (Figure 1) has been designed and tested in terms of performance (*Bulan et al., 2017*; *Bulan et al., 2015*; *Bulan et al., 2016*).

This machine has dimensions of length, height and width respectively 1964 mm, 1902 mm and 1567 mm. This machine also has a weight and capacity of 500 kg and 1966 kg·h^{-1}, respectively.

However, the design of the AE01-type OPF counter still has the disadvantage of being too large and not practical/portable to be transported to the plantation or field. Also, the AE01-type chopper machine cannot be categorized as appropriate, affordable and inexpensive technology to be obtained by smallholders of palm oil in Indonesia. Therefore, it is important to develop a type AE01 chopper machine for OPF that can overcome these disadvantages. The results of the development of the chopper machine are called AE02-type (second generation of AE01-type). The advantages of this designed machine are a low-cost and a small-scale chopper machine.

Therefore, the purpose of this study is to design, manufacture and evaluate the performance of an AE02-type OPF machine.

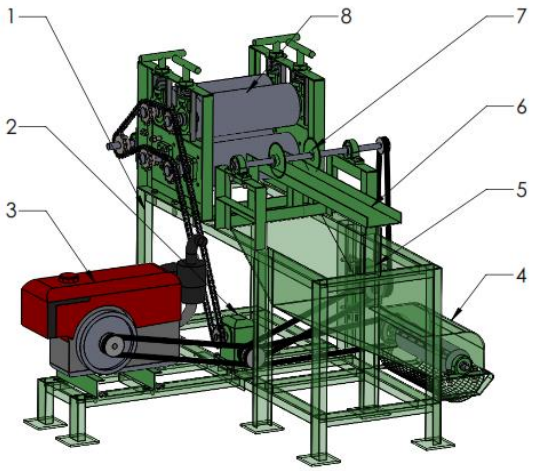

Fig. 1 - Integrated chopper machine AE01-type

1-Frame/stands; 2-Gear box system (1:30); 3-Diesel engine; 4-Chopper unit; 5-Gear box system (1:10); 6-feed channel; 7-Cutter for leaves OPF; 8-Compression unit for OPF

MATERIALS AND METHODS

Machine descriptions and design consideration

As shown in Figure 2-3, The chopper machine for OPF consists of the following major parts: hopper, mainframe, 8.5 hp diesel engine, outlet and chopping blade. The chopping knife consists of 30 blades and 4 fan plates. The total of chopping blade is 30 pieces with 3 pieces per circle and 10 rows. The distance between the blades is 183 mm. The total length of the shaft is 790 mm. The thickness of the blade is 0.5 mm. In operation, OPF will be fed from the hopper to enter the chopping knife. The chopper will chop and distribute the OPF for 550 mm. Furthermore, the OPF that arrives at the end of the chopping knife will be pushed by the fan plate out through the outlet. Materials used for fabrication of this machine are locally available at have affordable costs.

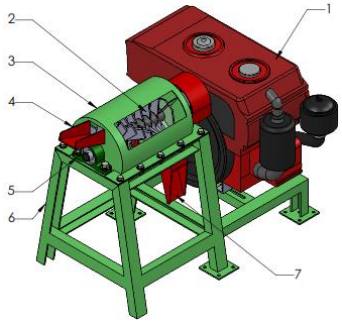

Fig. 2 - Isometric view of the machine

1-Diesel engine; 2- Chopper blade; 3-Top cover for chopper blade; 4-Hopper 5-Bearing; 6-Frame/stands; 7-Outer

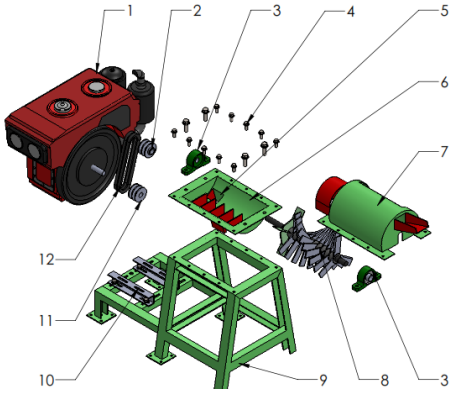

Fig. 3 - Exploded view of the machine

1-Diesel engine; 2-Pulley of the blade shaft; 3-Bearing; 4-Nut-bolt; 5-Outer; 6-Bottom cover for chopper blade; 7-Top cover for chopper blade; 8-Chopper blade; 9-Frame/stands; 10-Frame for diesel engine; 11-Pulley of driving motor; 12-V-belt

Factors considered in the design of this machine were construction cost, the materials availability, machine components strength, construction materials simplicity, ease of operation, maintenance, easy inspection, serviceability, maintenance of the machine and energy requirement. Also, the necessary properties of agricultural materials considered were: the physical and mechanical properties of the oil palm frond (OPF).

Design of chopper machine elements

Power Requirement

The machine power requirement is a function of force upon materials inside the blending chamber such as the weight of the blending blade, the shaft and machine pulley. It is given by below equations (1-5) as reported by researcher (*Khurmi and Gupta, 2005; Sitorus and Sartika, 2017; Sitorus et al., 2017*).

$$P = \frac{2 \times \pi \times n \times \tau}{60} \quad (1)$$

$$\tau = F \times r_d \quad (2)$$

$$F = M \times r_d \times \omega^2 \quad (3)$$

$$\omega = \frac{2 \times \pi \times n}{60} \quad (4)$$

$$M = M_{OPF} + M_B + M_S + M_P \quad (5)$$

Belt design

The shaft speed was determined using equation (6) and length of belt was calculated by equation (7) (*Khurmi and Gupta, 2005*). A standard V-belt C522 size having top width of 9.5 mm, bottom width of 4 mm and 8 mm thicknesses was used. The V-belt was chosen to minimize slippage during motion transfer.

$$\frac{n_1}{n_2} = \frac{d_2}{d_1} \quad (6)$$

$$L = 2c + \frac{\pi(d_2 + d_1)}{2} + \frac{(d_2 - d_1)^2}{4c} \quad (7)$$

Belt forces

The forces on the belt were calculated according to researchers (*Schmid et al., 2014; Kilanko, 2017*) by equation (8-9).

$$T = \frac{(F_1 - F_2) \times d_1}{2} \quad (8)$$

$$\frac{F_1}{F_2} = e^{\mu\left(180 - 2\left(\sin^{-1}\left(\frac{d_1 - d_2}{2c}\right)\right)\right)\left(\frac{\pi}{180}\right)} \quad 9)$$

Shaft diameter

Based on the design, the machine used a vertical shaft with a large part of its stress caused by bending and torsion load. It has little or no load to cause buckling. Hence, the diameter of the shaft was calculated using equation (10) (*Khurmi and Gupta, 2005; Kolawole and Ndrika, 2012; Olughu and Simonayan, 2017*).

$$d^3 = \frac{16}{\pi \times S_s} \sqrt{(K_b \times M_b)^2 + (K_t \times M_t)^2} \quad (10)$$

Design of chopper machine elements

In order to study, composition and distribution in the petiole of the OPF, several branches of fresh OPF with leaves were cut into ± 2.0 m length at three different sections; initial, middle and edge as shown in Fig. 4. Three levels of blade rotation speeds (800 rpm, 1200 rpm, and 1600 rpm calculated using the method by researcher (*Ogunsina and Bamgboye, 2014*) were used for three branches of fresh OPF. The parameters determined during the machine evaluation were machine capacity, size of chopped OPF, percentage of chopped OPF and chopper machine efficiency.

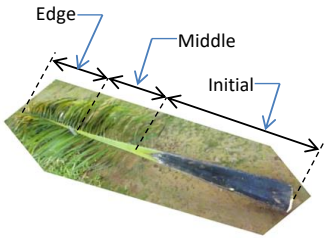

Fig. 4 - Schematic diagram of fresh oil palm frond (OPF) with leaves

The machine was evaluated based on two indices that include percentage of chopped OPF (η_{oc}) and chopping efficiency (η_e) was done by researcher (*Kolawole and Ndrika, 2012; Ojolo et al., 2010; Adekanye and Adelakun, 2018; Drees et al., 2018*). These were calculated respectively by using equations (11-12).

$$\eta_c = \frac{W_{oc} + W_{noc}}{W_t} \times 100\% \quad (11)$$

$$\eta_{oc} = \frac{W_{oc}}{W_t} \times 100\% \quad (12)$$

This is also referred to as the rate of chopping. The capacity of the machine was evaluated as the quantity of the OPF the machine could process within a recorded time (*Fadele and Aremu, 2016; Aremu and Fadele, 2011*). In this case, OPF was introduced into the machine while the time for the chopping operation to complete was recorded. This was calculated using equation (13).

$$C_c = \frac{3.6 \times 10^6 \times W_t}{T} \quad (13)$$

RESULTS

Size of chopped OPF

The average values of the size of chopped OPF at different rotation speeds (800 rpm, 1200 rpm, and 1600 rpm) and sections of OPF (initial, middle and edge) are plotted in Figure 5. It can be observed that, at given rotation speeds and sections of OPF, the size of chopped OPF decreased with the increase of the rotation speeds. The largest and smallest chopped sizes are respectively the edge sections and middle sections. The smallest size of chopped OPF from this research is 1.66 cm.

Machine capacity

The machine capacity versus rotations speed is demonstrated in Figure 6. It could be noticed that increasing the rotations speed resulted in increasing the machine capacity at other parameters used in this study. These results may attribute to increasing rotations speed from the blade. The results of this study also show that chopped on the initial sections OPF gives a larger capacity of the machine than the others. This is due to the initial sections OPF having harder structural characteristics than the others (*Yusri et al., 1995; Shafawati and Siddiquee, 2013; Bulan et al., 2017; Anyaoha et al., 2018*). It makes the chopping process easier to do with the blade. The highest machine capacity from this study is 116.98 kg·h^{-1}.

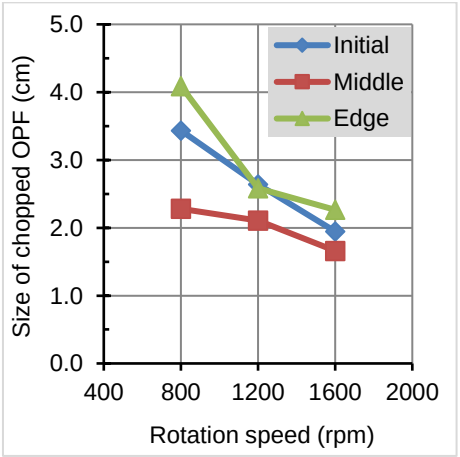

Fig. 5 - Effect of blade rotation speeds and sections of OPF on the size of chopped material

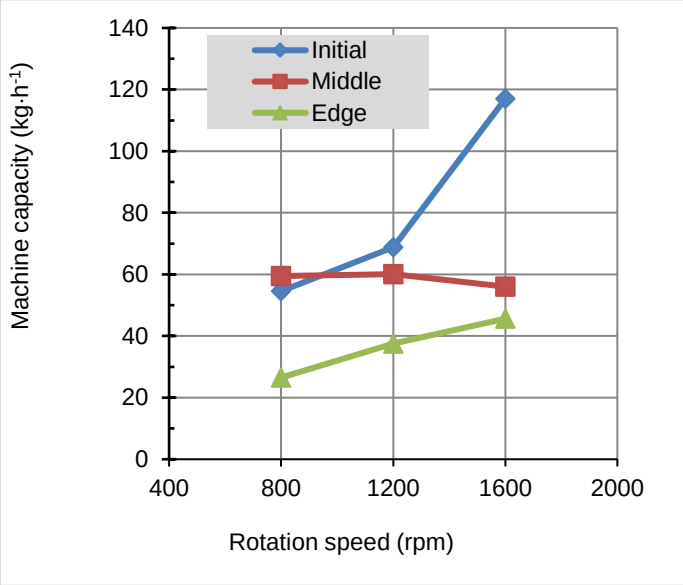

Fig. 6 - Effect of blade rotation speeds and sections of OPF on the machine capacity

OPF chopping percentage

Data of the OPF chopping percentage as influenced by the different operation variables considered in this study is shown in Figure 7. At given rotation speeds and sections of OPF, the OPF chopping percentage was observed to decrease with increasing the rotation speed. For example, an increase in the rotation speed from 800 rpm to 1600 rpm caused the OPF chopping percentage increase from 66.98% to 87.59% in the initial sections.

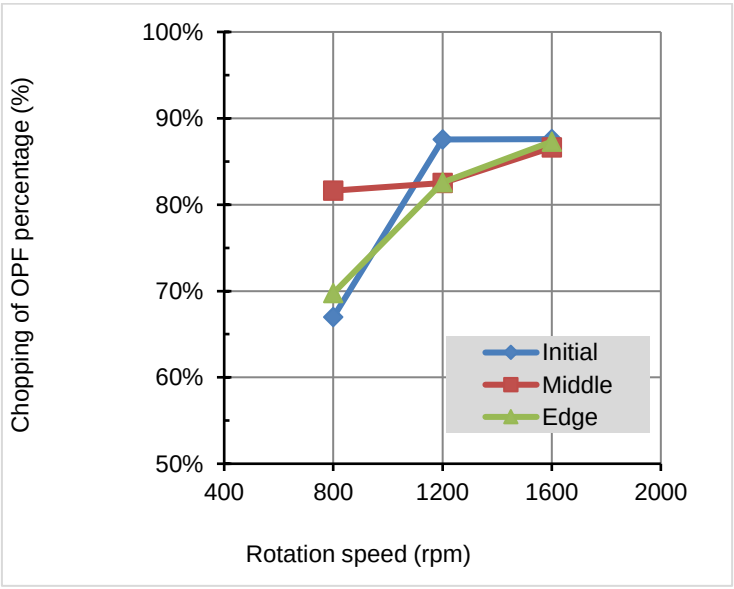

Fig. 7 - Effect of blade rotation speeds and sections of OPF on the chopping percentage

Chopping Efficiency

The average values of the chopping efficiency at rotation speeds levels and sections of OPF are plotted in Figure 8. It shows that increasing rotation speeds from 800 rpm to 1200 rpm can be increasing chopping efficiency in all treatments. However, increasing rotation speeds from 1200 rpm to 1600 rpm can be decreasing chopping efficiency in all treatments.

These results may be due to increasing rotation speeds causing a short time to carry out OPF chopping by the knife so that the OPF becomes non-chopped.

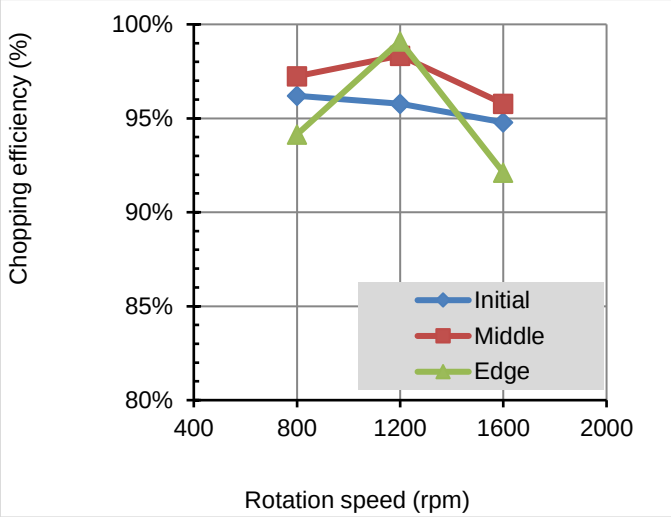

Fig. 8 - Effect of blade rotation speeds and sections of OPF on the chopping efficiency

CONCLUSIONS

A low-cost and a small-scale chopper machine for oil palm frond (OPF) locally was designed and manufactured. The performance of the developed machine was evaluated at three rotation speeds and three sections of OPF. The increasing of the rotations speed was found to increase the mean value of the machine capacity and chopping of OPF percentage at all OPF sections. It also results in smaller chopping dimensions. However, it caused a decrease in the mean values of chopping efficiency.

ACKNOWLEDGEMENT

The authors acknowledge the financial support from The Ministry of Research, Technology and Higher Education (RISTEKDIKTI), through LPPM Syiah Kuala University. We would like to express their appreciation to the journal reviewers for their benevolent and professional suggestions during consideration of the manuscript for publication.

REFERENCES

[1] Adekanye TA, JO Adelakun, (2018), Evaluation of a portable watermelon juice extracting machine, *Agricultural Engineering International: CIGR Journal,* Vol.19(4), pp.219-223;

[2] Anyaoha KE, R Sakrabani, K Patchigolla, AM Mouazen, (2018), Critical evaluation of oil palm fresh fruit bunch solid wastes as soil amendments: Prospects and challenges, *Resources, Conservation and Recycling,* Vol.136(1), pp.399-409;

[3] Aremu A, O Fadele, (2011), Study of some properties of doum palm fruit (Hyphaene thebaica Mart.) in relation to moisture content, *African Journal of Agricultural Research,* Vol.6(15), pp.3597-3602;

[4] Bulan R, T Mandang, W Hermawan, Desrial, (2016), Utilization of Palm Oil Leaf Waste as Compost Fertilizer Raw Material (Pemanfaatan Limbah Daun Kelapa Sawit sebagai Bahan Baku Pupuk Kompos), *Rona Teknik Pertanian,* Vol.9(2), pp.135-146;

[5] Bulan R, Safrizal, TS Bahri, (2015), Physical and Mechanical Properties of Palm Frond for the Development of Palm Oil Waste Chopper and Pressing Machine Design, *International Journal of Scientific & Engineering Research (IJSER),* Vol.6(2), pp.117-120;

[6] Bulan R, Safrizal, TS Bahri, (2017), Conceptual Design Portable Chopper Machine for Palm Oil Frond: Laws of Classical Mechanics and CAD Approach, *International Journal of Scientific & Engineering Research (IJSER),* Vol.8(7), pp.760-765;

[7] Drees AM, MM Ibrahim, MA Aboegela, (2018), Design, construction and performance evaluation of an almond kernel extraction machine, *Agricultural Engineering International: CIGR Journal,* Vol.19(4), pp.133-144;

[8] Fadele O, A Aremu, (2016), Design, construction and performance evaluation of a Moringa oleifera seed shelling machine, *Engineering in Agriculture, Environment and Food,* Vol.9(3), pp.250-256;

[9] Hassan OA, Ishida M, Shukri IM, Tajuddin ZA, (1994), Oil-palm fronds as a roughage feed source for ruminants in Malaysia, *Livestock Research Division, Malaysian Agriculture Research and Development Institute (MARDI),* Kuala Lumpur, Malaysia, pp.1-8;
[10] Khurmi R, J Gupta, (2005), *Theory of machines* (Eurasia publishing house);
[11] Kilanko O, (2017), Design and performance evaluation of centrifugal cashew nut sheller, *Agricultural Engineering International: CIGR Journal,* Vol.19(1), pp.162-170;
[12] Kolawole SS, V Ndrika, (2012), Development and performance tests of a melon (egusi) seed shelling machine, *Agricultural Engineering International: CIGR Journal,* Vol.14(1), pp.157-164;
[13] MPOC PO, (2011), "A Success Story in Green Technology Innovations." In.
[14] Ogunsina BS, AI Bamgboye, (2014), Pre-shelling parameters and conditions that influence the whole kernel out-turn of steam-boiled cashew nuts, *Journal of the Saudi Society of Agricultural Sciences,* Vol.13(1), pp.29-34;
[15] Ojolo S, O Damisa, J Orisaleye, C Ogbonnaya, (2010), Design and development of cashew nut shelling machine, *Journal of Engineering, Design and Technology,* Vol.8(2), pp.146-157;
[16] Olughu O, KJ Simonayan, (2017), Design and construction of a motorized ginger juice expression machine, *Agricultural Engineering International: CIGR Journal,* Vol.19(3), pp.163-169;
[17] Raju, A Sitorus, (2017), Measurement of pyrolysis gases on palm oil shell and empty fruit bunch, *2017 International Conference on Computing, Engineering, and Design (ICCED),* 1-4;
[18] Schmid SR, BJ Hamrock, BO Jacobson, (2014), *Fundamentals of machine elements: SI version* (CRC Press);
[19] Shafawati SN, S Siddiquee, (2013), Composting of oil palm fibres and Trichoderma spp. as the biological control agent: A review, *International Biodeterioration & Biodegradation,* Vol.85(1), pp.243-253;
[20] Sitorus A, W Hermawan, RPA Setiawan, (2017), Design and performance of combine corn transplanter powered by hand tractor, *2017 International Conference on Computing, Engineering, and Design (ICCED),* 1-5;
[21] Sitorus A, TD Sartika, (2017), Analysis of design combine transplanter power by hand tractor: Transmission system and furrow opener, *2017 International Conference on Computing, Engineering, and Design (ICCED),* 1-6;
[22] Yusri A, AM Rasol, O Mohammed, H Azizah, T Kume, S Hashimoto, (1995), Biodegradation of oil palm empty fruit bunch into compost by composite micro-organisms, *Proceedings of the EU-ASEAN Conference Combustion of Solids and Treated Product, Hua-Hin,* 16-17;
[23] Zahari MAKM, MR Zakaria, H Ariffin, MN Mokhtar, J Salihon, Y Shirai, MA Hassan, (2012), Renewable sugars from oil palm frond juice as an alternative novel fermentation feedstock for value-added products, *Bioresource technology,* Vol.110(1), pp.566-571.

EXPERIMENTAL RESEARCH OF MISCANTHUS PLANTING TECHNOLOGICAL PROCESS BY MEANS OF UPGRADED POTATO PLANTER

/

ЕКСПЕРИМЕНТАЛЬНЕ ДОСЛІДЖЕННЯ ТЕХНОЛОГІЧНОГО ПРОЦЕСУ САДІННЯ МІСКАНТУСА ЗА ДОПОМОГОЮ КАРТОПЛЕСАДЖАЛКИ

Prof.PhD. Adamchuk V.[1)], Prof.PhD. Bulgakov V.[2)], PhD. Ivanovs S.[3)], PhD. Prysyazhnyi V.[1)], PhD. Borys A.[1)]

[1)] National Scientific Centre "Institute for Agricultural Engineering and Electrification" NAAS of Ukraine,

[2)] National University of Life and Environmental Sciences of Ukraine,

[3)] Latvia University of Life Sciences and Technologies / Latvia

Tel.+37129403708, e-mail: semjons@apollo.lv

Keywords: *Miscanthus, upgrading, planting, rhizomes, the planting apparatus.*

ABSTRACT

Miscanthus is a promising energy crop. There are no inexpensive and efficient planting machines in practice as yet for planting on small areas up to 10-20 hectares. In order to plant the Miscanthus rhizomes on such areas, it is appropriate to use potato planters equipped with special replaceable spoons. Research has been carried out to optimize the parameters of a planting machine spoons and the length of the planting material (rhizomes), as well as to test mechanised planting under economic conditions by means of a potato planter equipped with a an upgraded planting apparatus.

АНОТАЦІЯ

Міскантус є перспективною енергетичною культурою. Поки що в практиці немає дешевих машин для його садіння на невеликих площах до 10…20 га. Для садіння ризом міскантуса на таких площах доцільно використовувати картоплесаджалки, які оснащені спеціальними змінними ложечками, які є в наявності в господарствах, що вирощують картоплю. Проведенні експериментальні дослідження по оптимізації параметрів ложечек садильного апарату для садіння та довжини садильного матеріалу (ризом), а також проведена перевірка механізованого садіння в господарчих умовах з використанням модернізованого садильного апарату.

INTRODUCTION

The production and use of the plant biomass for energy is an important branch of agriculture in the developed countries *(Arnoult et al., 2015; Richter et al., 2016).* One of the promising energy crops in the areas with limited moisture is Miscanthus *(Bellamy et al., 2007; Quinn et al., 2010; Kalinina et al., 2017).* In a number of Western European countries there takes *place active growing of this crop as an energy plant (for the production of fuel briquettes) (Heaton et al., 2008; Rakhmetov et al., 2015).* Miscanthus is a drought-resistant herbaceous plant that grows up to 4 m tall and produces a large amount of biomass (in Ukraine up to 6.76 t·ha^{-1}), the roots spreading deep into the soil up to 2.5 m *(Kharytonov et al., 2017; Xue et al., 2017).* Such a root system contributes to a very good consumption of the elements and water. The yield of Miscanthus can be harvested up to 30 years; it does not deplete the soil and can grow even in low-productive soils. For the Miscanthus propagation there is applied a method of dividing the rootstock into separate pieces with subsequent planting. Planting of the Miscanthus rhizomes is carried out at a depth of 8...10 cm with a density of 14...8 thousand rhizomes per ha, with an inter-row spacing of 0.7 m and a planting interval (in-the-row spacing) of 0.9 m *(Kurilo et al., 2002).* On the large Miscanthus growing areas, of 50…400 hectares and more, laying of plantations is carried out with the help of special machines. However, on smaller areas the use of these machines is entailed with a high cost, and therefore it is not economical.

Sometimes, when no special equipment is available, the crushed remnants of the Miscanthus rhizomes are scattered by machines for the application of organic fertilizers, followed by ploughing and rolling down with smooth rollers. This way of planting has many shortcomings due to the random scattering of the planting material, low yield and inconvenience of harvesting.

For mechanised planting of the Miscanthus rhizomes a semi-mechanised special machine may also be used, the planting apparatus of which is a vertically installed planting tube through which the planting material is manually fed and supplied to the coulters, covering it with a layer of soil *(Gumentic et al. 2016).*

The disadvantage of this method is low productivity, which is limited by the low speed of manual feeding of the planting material into the planting tube.

For planting of the Miscanthus rhizomes on small areas (up to 10…20 ha) it is economically appropriate to use a potato planter. This method combines the high productivity of a potato planter without manual feeding of the planting material, eliminating the need to purchase a special machine. In this case it is necessary to upgrade the planting apparatus of the potato planter by replacing the spoons for planting potatoes with the corresponding special spoons for planting the Miscanthus rhizomes. The rhizomes must be regular or close to this form and it is purposeful to divide them into pieces with the length of 40…60 mm.

The previously conducted research showed that, under the conditions in Ukraine, planting the Miscanthus rhizomes, 40…60 mm long, with an inter-row spacing of 0.7 m and with increased density of Miscanthus rhizomes in the row (the average planting interval (in-the-row spacing) 0.20…0.3 m), ensures a maximum yield of the stem mass and the output of a quality planting material *(Gumentic et al., 2015).* The purpose of the work is to investigate a possibility to perform the technological process of planting the Miscanthus rhizomes by means of a machine based on a potato planter, to substantiate rational parameters of a spoon of the planting apparatus and to determine the optimum length of the Miscanthus rhizomes corresponding to these spoons length.

MATERIALS AND METHODS

First of all, researches and optimisation of the parameters of the planting apparatus spoon were conducted under laboratory conditions and then an economic testing of its performance was done under field conditions. Processing of the experimental data was carried out by mathematical-statistical methods using standard methods by means of the Matlab program *(Adler, 1971).*

For the research and design upgrading of 4-row potato planter “Hassia”, the most common potato planter in Ukraine, was used with a 2-row arrangement of spoons on the carrier band (there were 4 bands on the planter).

The quality of the planting apparatus work is mainly determined by the size of the gaps (that is, those that have not reached the intended planting points) and the preset distribution uniformity of the rhizomes by length.

To determine the necessary parameters of the spoons, it is necessary to know the basic parameters of the rhizomes – the average thickness and their length.

The average thickness of the Miscanthus rhizomes was determined with a calliper at the place of their greatest thickening. The number of rhizomes was 50 pcs (Fig. 1).

Fig. 1 – Typical forms of Miscanthus rhizomes

The average planting interval (in-the-row spacing) – 24 cm was determined as the arithmetic average of 100 measurements of the distance between the centres of the rhizomes in a row (Fig. 8). The efficiency of planting the Miscanthus rhizomes in the field by an upgraded machine was determined according to a standard methodology *(Kurilo et al., 2002).* The length of the rhizomes is formed during the cutting process and is limited by the need to have no less than 4-5 potential buds on one rhizome. It has been established that to these requirements correspond rhizomes which are more than 40 mm long. The length of the rhizomes more than 100 mm is not practiced.

Accordingly, a planting material was prepared for the experiments from the Miscanthus rhizomes with the length from 40 mm to 100 mm with a 10 mm increment (Fig. 2).

Fig. 2 – The Miscanthus rhizomes and their parts, prepared for planting:
4, 5,...,10 – the length of the Miscanthus rhizomes and their parts – 40, 50,...,100 mm

The rhizomes were divided into parts manually by means of clippers and a ruler. They were selected rectilinear or close to this form. The deviation from the rectilinearity was up to 10%. According to the methodological recommendations *(Kucenko et al., 2002),* such rhizomes are more optimal than the curvilinear ones.

In order to conduct laboratory studies to determine the number of gaps, depending on the length of the rootstock (rhizoma, rhizome) and its parts, the potato planter was installed on a special support (stand). The spoons of the planting apparatus were also able to capture rhizomes, longer than 60 mm. In this case, the rhizomes were placed at an angle to the spoon (one part of the rootstock (rhizoma, rhizome) rested upon the bottom of the spoon, the other on the side wall).

The rhizomes of each typical size (Fig. 3) were alternately filled into the hopper of the potato planter; the planting apparatus was manually turned at the respective working speed by means of a drive wheel until 100 spoons had passed through the top point of the planting apparatus. In order to determine the number of gaps, the number of empty spoons (not occupied by the rhizomes) out of one hundred spoons was calculated. As a result, there was taken as the percentage ratio of the number of identified empty spoons to all the calculated ones. There was triple replication of experiments.

Fig. 3 – Field experiments of the Miscanthus plantations

Practical studies of the operating capacity of mechanised Miscanthus plantation by an upgraded planting apparatus were carried out at the experimental site of the institute in Vasilkovsky District, Kiev region. Before the research, an experimental plot was prepared: ploughing to a depth of 30...32 cm, cultivation to a depth of 14...16 cm. The plantation scheme was with a row spacing of 0.7 m and an increased density of the Miscanthus rhizomes and their parts in the row (with a preset planting interval (in-the-row spacing) of 0.24 m). The planting material was poured into the hopper of the planter and mechanised planting was performed.

The planting interval (in-the-row spacing) was determined by measuring with a tape the distances between the centres of the rhizomes in the row. Triple replication. The work was performed in accordance with the methodological recommendations for conducting research of potatoes *(Standart GOST 28306-2018).*

RESULTS

The measurements of the thickness of the planting material (the common Omega variety) showed that it is 14.1 mm with a root-mean-square deviation 1.1 mm. According to the agro-demands, 40…100 mm long rhizomes with a 10 mm planting interval (in-the-row spacing) were used.

On the other hand, the length of the spoon *d* on the band (with a double-row arrangement of the spoons on the band) is limited to 60 mm. In accordance with these initial requirements, a structural scheme of the spoon for planting the Miscanthus rhizomes has been developed (Fig. 4).

The potato planter was upgraded; special spoons of an appropriate size were made and installed – Fig. 5. The maximum width of the spoon in the modernized design may be 60 mm. Taking into account the fact that the average thickness of the Miscanthus rhizomes is 14 mm, the width of the spoon bottom is 15 mm (by 11 mm more than the average thickness of the rootstock (rhizoma, rhizome)), the height of the front wall is *b* = 15 mm, the width of the upper part of the spoon is 20 mm.

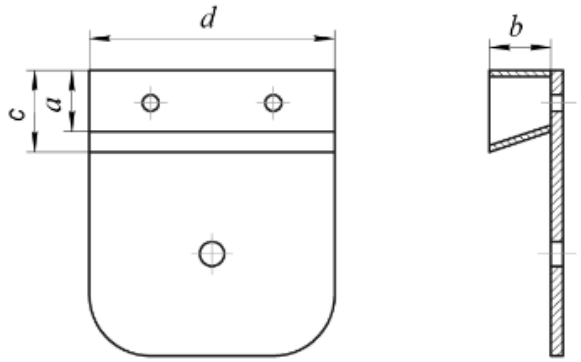

Fig. 4 – The structural scheme of a spoon for planting the Miscanthus rhizomes
a – the width of the spoon bottom; *b – the height of the front wall of the spoon; c – the width of the top of the spoon; d – the length of the spoon*

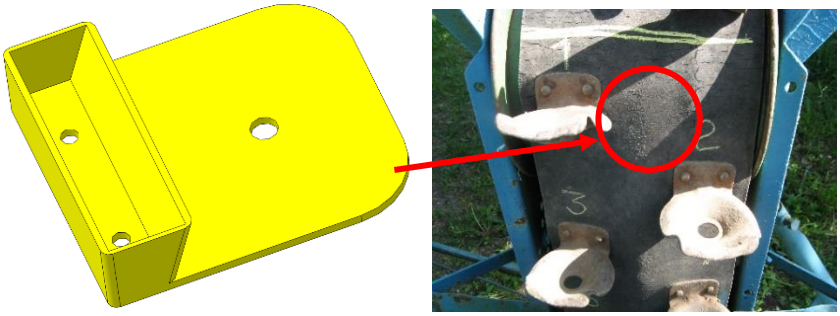

Fig. 5 – An upgraded planting apparatus of the potato planter

In order to determine the optimal length of the work pieces used for planting by means of the spoon with the selected parameters, laboratory experiments were conducted. Dependence (Fig. 6) of the number of the gaps between the Miscanthus rhizomes upon the length of the previously prepared planting material was obtained. It is obvious from the obtained dependence that for mechanised Miscanthus planting by a potato planter the optimum length of the rhizomes and their parts should be 40...60 mm. In this case the number of gaps is from 0.6 to 9%. When the length of the rhizomes is more than 70 mm, the number of gaps increases sharply and reaches 50% and more. According to the agro-requirements the number of gaps is 2%. As a result of field research (Fig. 7) on Miscanthus rhizomes mechanised planting, it was found that the existing number of gaps was generally compensated by twins (that is, it is ensured the required number of plants per fruit). The number of twins, when planting the Miscanthus, rhyzomes 40…60 mm in size, is up to 19% (according to the agrodemands, twins are allowed if the length of the Miscanthus rhyzome is less than 10 cm).

Compared to the gaps, the presence of twins (when the spoon picks up two rootstocks (rhyzomas, rhyzomes) and plants them side by side into the soil) is not a significant shortcoming and, according to the agrodemands, it is allowed if the length of the rhyzome is less than 10 cm. The negative effect of twins presence is mainly only the increased consumption of the planting material.

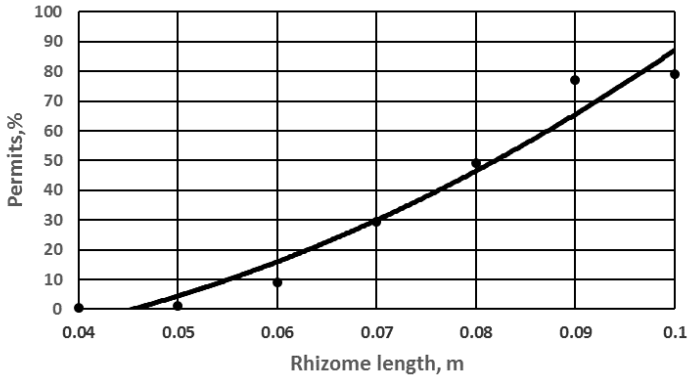

Fig. 6. – Dependence of the number of gaps upon the length of the rhizomes

The maximum distance between the rhizomes in one row is not more than 0.7 m (according to agro-requirements, the maximum distance between the rhizomes in one row is 0.5...0.7 m). The average planting depth was 50…80 mm. Germination of the rhizomes of the size 40…60 mm was 93%.

Fig. 7 – Plantations of Miscanthus rhizomes

According to the testing results of Miscanthus rhizomes mechanised planting by means of a modernized planting apparatus, an average planting interval (in-the-row spacing) was determined – 24 cm with a root-mean-square deviation 3.6 cm (Fig. 8), which was obtained as the arithmetic average of 100 measurements of the distance between the centres of the rhizomes in a row. As it is known *(Gumentic, 2016),* planting of Miscanthus rhizomes and of their parts with their increased density in the row ensures an increase in the yield of the stem mass and output of a high-quality planting material.

Fig. 8 – Determination of the planting interval (in-the-row spacing) of the Miscanthus rhizomes by means of an upgraded planting apparatus of the potato planter

The efficiency of the 4-row potato planter in the experiments was 1.5 ha·h^{-1}, refitting of the planting apparatus of a 4-row potato planter – 300…320 Euro. The cost of a new 4-row potato planter "Hassia" is about 6,000 Euros (it depends on the basic configuration). However, these planters are already on the farms, and the schedule of their use allows one to use them for planting Miscanthus. Therefore no capital investments for the purchase of a special machine are required, and the refitting cost is low. In this case, refitment payback is achieved already in the first year of operation when an area of 5…8 hectares was planted.

CONCLUSIONS

1. For planting the Miscanthus rhizomes on small areas (up to 10 ha) it is economically appropriate to use an upgraded potato planter.

2. The geometrical dimensions of the spoon of the planting apparatus of the Miscanthus rhizomes are substantiated: the width of the spoon bottom – 15 mm, the height of the front wall – 15 mm, the width of the top of the spoon – 20 mm, the length of the planting apparatus spoon – 60 mm.

3. The optimal length of the Miscanthus rhizomes for planting by the proposed spoons is 40…60 mm.

4. The efficiency of the 4-row planter in the experiments was 1.5 ha·h^{-1}.

REFERENCES

[1] Adler J., (1971), *Planning of an experiment when searching for optimal conditions*. Nauka, Moscow / Russia, 283 p.;

[2] Arnoult S., Brancourt-Hulmel M., (2015), A Review on Miscanthus biomass production and composition for bioenergy use: Genotypic and environmental variability and implications for breeding, *Bioenerg. Res.,* Vol. 8, pp. 502-526;

[3] Gumentic M., Kvak V., Zamojsky O., Morozova E., (2015), Impact of the elements of a mechanised technology upon the yield of the Miscanthus biomass. *Collection of scientific papers of the Dnepropetrovsk State Agrarian-Economic Institute*, Vol. 38 (4), Dnepropetrovsk / Ukraine, pp. 50-54;

[4] Gumentic M., (2016), Technology of growing the giant Miscanthus as a raw material for the production of solid biofuel. *Proceedings of the International Scientific and Practical Conference, attached to the 95th Institute of Bioenergetics Crops and Sugar Bee*t. Vinnica / Ukraine, pp.262-265.

[5] Heaton, E.A., Dohleman, F.G., Long, S.P., (2008), Meeting the United States biofuel goals with less land: the potential of Miscanthus. *Global Change Biology Bioenergy* 14, pp. 2000-2014;

[6] Kalinina O., Nunn Ch., Sanderson R., Hastings A.F.S., Weijde T. et al., (2017), Extending Miscanthus cultivation with Novel Germplasm at six contrasting sites. *Frontiers in Plant Science*, Vol. 8, pp. 1-15;

[7] Kharytonov M, Martynova N., Sitnyk S., Naumenko M., Pidlisnuk V., Stefanovska T., (2017), A productive potential estimation of five genotypes of the Miscanthus Anderss genus in the Ukrainian steppe zones conditions. *INMATEH – Agricultural Engineering.* Vol.52, Issue 2, pp. 129-136;

[8] Kucenko V., Osipchuk A., Podgaetsky A., Kononuchenko V., (2002), Methodological recommendations on conducting the research on potatoes. *Institute of Potatoes of the National Academy of Agrarian Sciences of Ukraine*, Nemashaevo, Ukraine, 182 p.;

[9] Kurilo V., Ganzhenko O., Gumentic M., Kvak V., (2002), Methodological recommendations on the pre-plant soil tillage and planting the Miscanthus rhizomes, *Institute of Bioenergy Crops and Sugar Beet*; Kyiv / Ukraine. 56 p.;

[10] Quinn, L.D., D.J. Allen, and R. Stewart. (2010). Invasive potential of Miscanthus sinensis: implications for bioenergy production in the United States. *Global Change Biology Bioenergy* 2, pp.310–320;

[11] Rakhmetov D.B, Shcherbakova T.O, Rakhmetov S.D., (2015), Miscanthus in Ukraine: introduction, biology, bioenergetics (Міскантус в Україні: інтродукція, біологія, біоенергетика), Kiev: *Phytosociocenter*, pp. 158-162;

[12] Richter G. M., Agostini F., Barker A., Costomoris D., Qi A., (2016), Assessment on-farm productivity of Miscanthus crops by combining soil mapping, yield modelling and remote sensing. *Biomass and Bioenergy*, Vol. 85, pp. 252-261;

[13] Standart GOST *28306-2018, (2018), Agricultural machinery*. *Machines for planting potatoes. Test methods*. 28 p. Moscow / Russia;

[14] Xue S., Lewandowski I., Kalinina O., (2017), Miscanthus establishment and management on permanent grassland in southwest Germany. *Industrial Crops and Products,* Vol. 108, pp. 572-582;

[15] Adamchuk V., Bulgakov V., (2016), *Small-size agricultural machinery (design, theory and calculation): monograph*. Kyiv: Agrar. Nauka, 2916. 292 p.

SUBSTANTIATION OF MOTION PARAMETERS OF THE SUBSTRATE PARTICLES IN THE ROTATING DIGESTERS

/

ОБҐРУНТУВАННЯ ПАРАМЕТРІВ РУХУ ЧАСТИНОК СУБСТРАТУ В МЕТАНТЕНКАХ, ЩО ОБЕРТАЮТЬСЯ

Prof., Doctor of Engineering Golub G.A.[1)], Prof. Doctor of Economics Skydan O.V.[2)],.
Doctor of Engineering Kukharets S.M.[2)], Ph.D. Eng. Marus O.A.[1)]
[1)]National University of Life and Environmental Sciences of Ukraine / Ukraine,
[2)] Zhytomyr National Agroecological University / Ukraine
Tel: +380676653548, E-mail: saveliy_76@ukr.net

Keywords: *biogas, mineral particles, organic particles, velocity, displacement, trajectory*

ABSTRACT

To prevent inhomogeneity of the substrate, it is proposed to mix the substrate in a rotating digester. To determine the intensity of substrate components mixing, we have found the trajectory and speed of substrate mineral components movement and substrate organic components in the rotating digester. It was found that the uniform mixing and maximum interpenetration of organic and mineral components of the substrate is provided for the rational values of the digester angular velocity from 0.04 to 0.1 rad/s and the digester blades length from 75 to 80% of its internal radius.

АБСТРАКТ

Для уникнення розшарування субстрату пропонуються виконувати перемішування субстрату в обертовому метантенку. Для визначення рівномірності перемішування компонентів субстрату знайдено траєкторію і швидкість руху мінеральних компонентів та органічних компонентів субстрату в обертовому метантенку. Встановлено що рівномірне перемішування та взаємопроникнення органічних та мінеральних складових субстрату забезпечується за раціональних значень кутової швидкості метантенка від 0,04 до 0,1 rad/s та довжині лопаток метантенка від 75 до 80 % його внутрішнього радіуса.

INTRODUCTION

An important direction in renewable energy is the production of biogas *(Golub et al 2017a).* Biogas plants can use a wide variety of raw materials. In particular, biogas production from both plant biomass (*Shah et al, 2018*) and animal husbandry wastes *(Meyer et al, 2018)* has become widespread.

The efficiency of biogas production depends on the characteristics of biomass (density, dry matter content, dry matter particle size) and the characteristics of the digester (mixing intensity, geometric dimensions, the nature of the placement of blades, mixers and partitions inside the digester) *(Adouani et al, 2016; Carrerea et al, 2015)*. The efficiency of operation also depends on the control of energy consumed by the biogas plant (*Ogbonna et al, 2013*).

One of the main problems in the biogas production is the inhomogeneity of the substrate biomass inside the digester *(Golub et al, 2017b)*. The inhomogeneity of the substrate causes a violation of the availability of organic elements for the supply of methane-forming bacteria (*Theuerl et al, 2019*). Methane-producing bacteria have a density greater than the average density of the substrate in the biogas reactor and therefore, together with mineral particles, are accumulated in the lower part of the digester. And the bacteria food elements (the organic component of the substrate), having a density lower than the average density for the substrate, are accumulated in the upper part of the digester. Therefore, for effective interaction of anaerobic bacteria with biomass, substrate mixing is necessary *(Zhai et al, 2018*). However, too much mixing can disrupt the necessary contact between organic elements and methane-forming bacteria *(Uçkun et al, 2016)*. To solve this problem, it is proposed to use slow or periodic rotation of mixers (*Satjaritanuna et al, 2016)*. However, when using mechanical mixers, it is impossible to completely eliminate the inhomogeneity of biomass in the digester. Such mixing does not essentially eliminate stratification into mineral sediment and organic floating biomass (*Golub et al, 2017b; Theuerl et al, 2019)*.

To eliminate biomass stratification, it is proposed to use rotating digester (*Golub et al, 2017b*; *Uvarov et al, 2017)*. In rotating digesters, substrate mixing is performed by raising the mineral component of biomass and methane-forming bacteria accumulating in the lower part of the digester and immersing the organic component of biomass accumulating in the upper part of the digester. Such mixing is effective due to energy consumption *(Golub et al, 2017b)*. However, there are no studies on the intensity of mixing of substrate components necessary to ensure uniform placement of biomass components in the methane tank. To determine the intensity of the substrate components mixing, it is necessary to find the trajectory and movement speed of mineral components (together with methane-forming bacteria) and organic components of the substrate in the rotating digester.

MATERIALS AND METHODS

It is proposed to perform mixing of the substrate in a rotating digester. The body of the digester is made in the form of a horizontal cylinder (fig. 1) which rotates around the horizontal axis. There are flat blades in the digester body. The digester rotates in the liquid, which is located in the outer casing. This design creates lift for the rotating digester by unloading the support bearings. The friction force in the bearings is reduced and, accordingly, the energy spent on the digester rotation and substrate mixing is reduced. The design of the digester eliminates the possibility of the formation of a floating organic part and submerged mineral sediment.

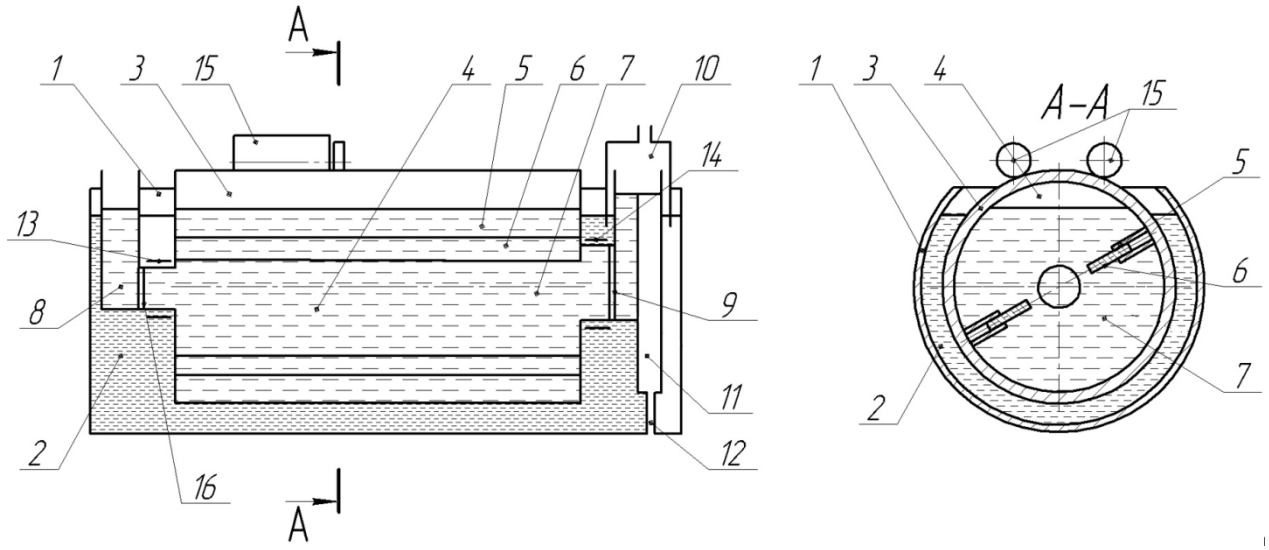

a)

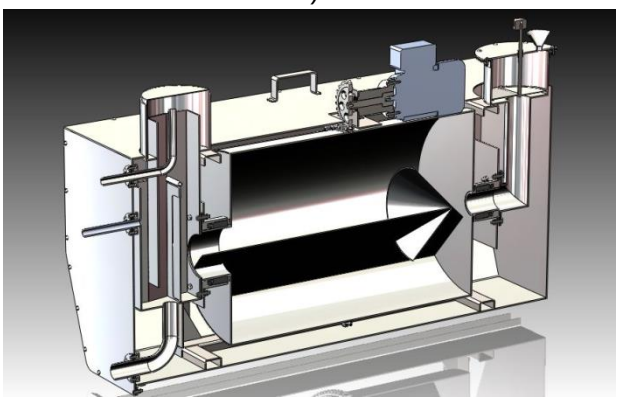

b)

Fig. 1 - Biogas plant

a – scheme, b – model: 1 – horizontal outer housing; 2 – liquid; 3 – rotating digester; 4 – fermentation chamber; 5 – partition; 6 – movable plates; 7 – organic mass; 8, 12 – sockets; 9, 16 – interpolator 10 – gas collector; 11 – the discharge chamber; 13, 14 – bearing joints; 15 – external drive.

To determine the relative velocity and establish the trajectory of the biomass particles, it is necessary to take into account the forces acting on the particles of the substrate mineral component (together with methane-producing bacteria) and on the particles of the substrate organic component. These forces are shown in the cross section image of the digester (fig. 2).

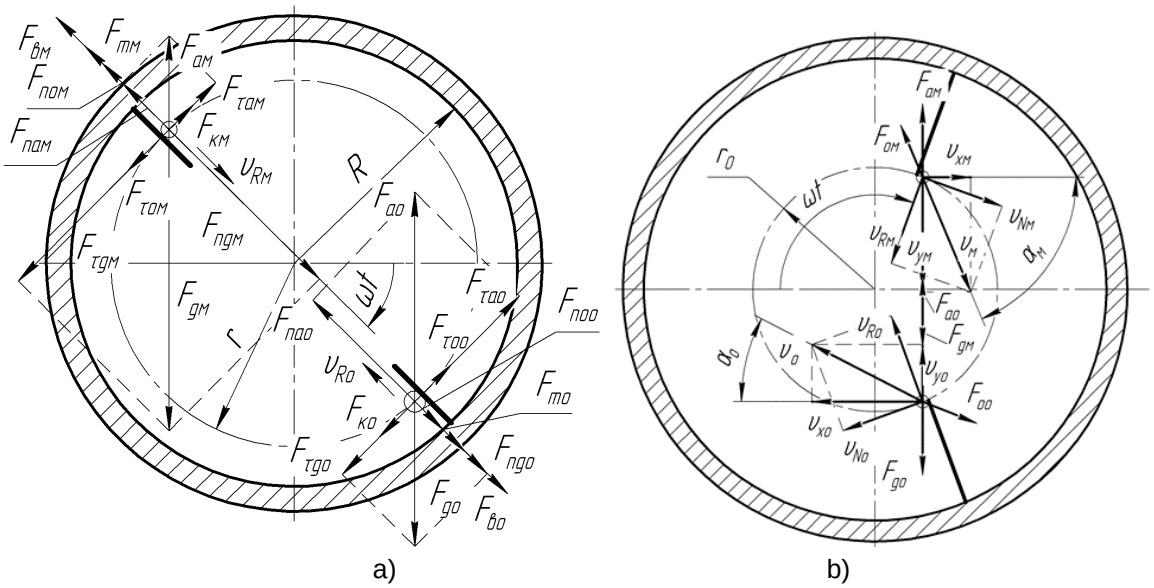

Fig. 2 - Scheme of action of forces on mineral (*M*) and organic (*O*) substrate particles

a) – when interacting with the blades; b) – in free movement

F_g – gravitation force, N; F_a – Archimedes' force, N; F_m – friction force, N; $F_к$ – compound centrifugal force, N; $F_в$ – centrifugal force of inertia, N; F_o – the resistance of the substrate, N; $F_{тg}$, $F_{тa}$, $F_{то}$ – the components of the forces of gravity, Archimedes and the resistance of the substrate, perpendicular to the blade, N; F_{ng}, F_{na}, F_{no} – the components of the forces of gravity, Archimedes and the resistance of the substrate along the blades, N; r – the current radius of the substrate particle position, m; R – the inner radius of the reactor, m; r_0 – the radius at which the blades end, m; υ – absolute particle velocity, m/s; $υ_R$ – relative particle velocity, m/s; $υ_N$ – the normal speed of the particle during the descent off the blade, m/s; $υ_x$ – the projection of the absolute velocity of a particle on the axis x, m/s; $υ_y$ – the projection of the absolute velocity of a particle on the axis y, m/s; α – the angle between the absolute velocity and its projection on the axis x, rad; ωt – the angle of the reactor rotation, rad

The substrate particles moving on the blades of the digester during its rotation are influenced by friction force, resistance force of the medium, centrifugal force, Archimedes' force and compound centrifugal force.

The friction force is determined by the forces which press the particles to the blade or tear them off the blade:

$$F_m = f\left(F_{\tau o} \pm F_{\tau g} \mp F_{\tau a} - F_к\right), \quad (1)$$

where:

$F_{то}$ – component resistance force of the substrate is directed perpendicular to the blade, [N];

$F_{тg}$ – the component of the particle's gravity force is directed perpendicular to the blade, [N];

$F_{та}$ – the component of Archimedes' force for a particle directed perpendicular to the blade, [N];

$F_к$ – compound centrifugal force of the particle, [N];

f – friction coefficient of the substrate over the reactor blade material, [rel. un.].

It is also well-known that:

$$F_в = mr\omega^2;\ F_g = mg;\ F_a = \rho_c gV;\ F_к = 2m\omega\frac{dr}{dt};\ F_{no} = mk_1\frac{dr}{dt};\ F_{\tau o} = mk_1 r\omega, \quad (2)$$

where: m – particle weight, [kg];

ω – the angular velocity of the reactor rotation, [rad/s];

r – the current radius of the substrate particle position, [m];

g – acceleration of gravity, [m/s^2];

V – the volume of the particle, [m^3];

k_1 – coefficient of proportionality in laminar flow of the substrate around the particles, [s^{-1}]; $k_1=18\eta/(\rho_c d_E^2)$;

k_2 – the ratio of the density of the substrate and the particle, $k_2=\rho_c/\rho$; ρ_c – substrate density, [kg/m^3];

ρ– particle density, [kg/m^3];

η – dynamic viscosity of the substrate, [Pa s];

d_E – equivalent particle diameter, [m].

The substrate particles, moving inside the reactor after descent off the blades, are influenced by the friction force, Archimedes' force and the force of the medium resistance:

$$F_g = mg;\ F_a = mk_2 g;\ F_o = mk_1 \upsilon . \quad (3)$$

To establish the trajectory of the biomass particles, differential equations of substrate particles motion over the digester blade and after the decent of the blades inside the rotating digester are composed.

A research facility has been designed in order to provide evidence to the theoretical research (fig.3).

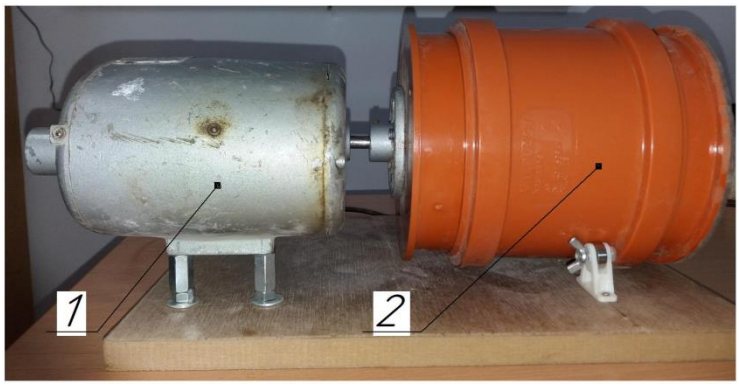

Fig. 3 - Research plant

1 – electric drive, 2 –the body of the plant (horizontal cylinder)

The body of the research plant is made in the form of a horizontal cylinder which rotates around the horizontal axis. There are two flat blades in the body of the plant. The inside radius of the body is 0.2 m and the blade length is 0.15 m. The electric drive can change the plant's rotation frequency.

For this research plant were chosen the substrate components which provide the average substrate density in the range of 1020-1050 kg/m^3, the density of the mineral substrate part in the range of 1150-1250 kg/m^3 and the density of the organic substrate part in the range of 800-900 kg/m^3. The content of the organic substrate part is 8% of the whole substrate volume, the content of mineral substrate part is 5% of the whole substrate volume.

RESULTS

The differential equation of the substrate particle motion in the form of a material point over the rotating reactor blade will have the following form:

$$m\frac{d\vec{\upsilon}_R}{dt} = \vec{F}_{na} + \vec{F}_{в} + \vec{F}_m + \vec{F}_{no} + \vec{F}_{ng}, \quad (4)$$

where $F_в$ – centrifugal force of the particle inertia, [N]; F_m – particle friction force, [N]; F_{na} – the component of Archimedes' force directed along the blade, [N]; F_{no} – component force of the substrate resistance directed along the blade, [N]; F_{ng} – the component of the particle's gravity directed along the blade, [N]; u_R – relative velocity of the particle while moving along the blade, [m/s].

Subject to Eq. (1) and Eq. (2), Eq. (4), the differential equation of a substrate particle motion over the surface of the rotating reactor blade, can be written as follows:

$$\frac{d^2 r}{dt^2} + \left(2f\omega + k_1\right)\frac{dr}{dt} - \left(\omega^2 - fk_1\omega\right)r = -g\left[\, f\left(1-k_2\right)\cos\left(\omega t\right) + \left(1-k_2\right)\sin\left(\omega t\right)\right] \quad (5)$$

This equation is a second-order linear equation with constant coefficients and the right-hand side as a trigonometric polynomial.

The complete solution of the differential equation of motion has the form:

$$r = C_1 \exp\left(\lambda_1 t\right) + C_2 \exp\left(\lambda_2 t\right) + \frac{g\left(1-k_2\right)}{\omega\sqrt{4\omega^2 + k_1^2}}\sin\left(\operatorname{arctg}\frac{4f\omega + k_1\left(1-f^2\right)}{2\left[\,\omega\left(1-f^2\right) - fk_1\right]} + \omega t\right), \quad (6)$$

where:

$$\lambda_1 = -\left(f\omega + \frac{k_1}{2}\right) + \sqrt{\omega^2\left(1+f^2\right) + \frac{k_1^2}{4}};\ \lambda_2 = -\left(f\omega + \frac{k_1}{2}\right) - \sqrt{\omega^2\left(1+f^2\right) + \frac{k_1^2}{4}}.$$

In this case, the relative velocity of the substrate particle while moving over the blade will be:

$$\upsilon_R = \frac{dr}{dt} = \lambda_1 C_1 \exp(\lambda_1 t) + \lambda_2 C_2 \exp(\lambda_2 t) + \\ + \frac{g(1-k_2)}{\sqrt{4\omega^2 + k_1^2}} \cos\left(\operatorname{arctg} \frac{4f\omega + k_1(1-f^2)}{2\left[\omega(1-f^2) - fk_1\right]} + \omega t \right). \quad (7)$$

Considering the initial conditions: t=0, r=R (where R – the inner radius of the reactor), u_R=0, stable integration can be defined by the expressions:

$$C_1 = \frac{\lambda_2}{\lambda_2 - \lambda_1}\left[R - \frac{g(1-k_2)}{\omega\sqrt{(4\omega^2 + k_1^2)}} \sqrt{1 + \frac{\omega^2}{\lambda_2^2}} \sin\left(\operatorname{arctg} \frac{4f\omega + k_1(1-f^2)}{2\left[\omega(1-f^2) - fk_1\right]} - \operatorname{arctg} \frac{\omega}{\lambda_2} \right) \right], \\ C_2 = \frac{\lambda_1}{\lambda_2 - \lambda_1}\left[\frac{g(1-k_2)}{\omega\sqrt{(4\omega^2 + k_1^2)}} \sqrt{1 + \frac{\omega^2}{\lambda_1^2}} \sin\left(\operatorname{arctg} \frac{4f\omega + k_1(1-f^2)}{2\left[\omega(1-f^2) - fk_1\right]} - \operatorname{arctg} \frac{\omega}{\lambda_1} \right) - R \right]. \quad (8)$$

Using the obtained solutions of the differential equation of particle motion it is possible to find the distance (movement) covered by the biomass particles and the speed of its movement for a set period of time.

For example, the calculated displacements and velocity of a mineral particle (together with methane-producing bacteria) for an angular velocity of 0.1 rad/s of a digester with an internal radius of 2 dm are shown in fig. 4.

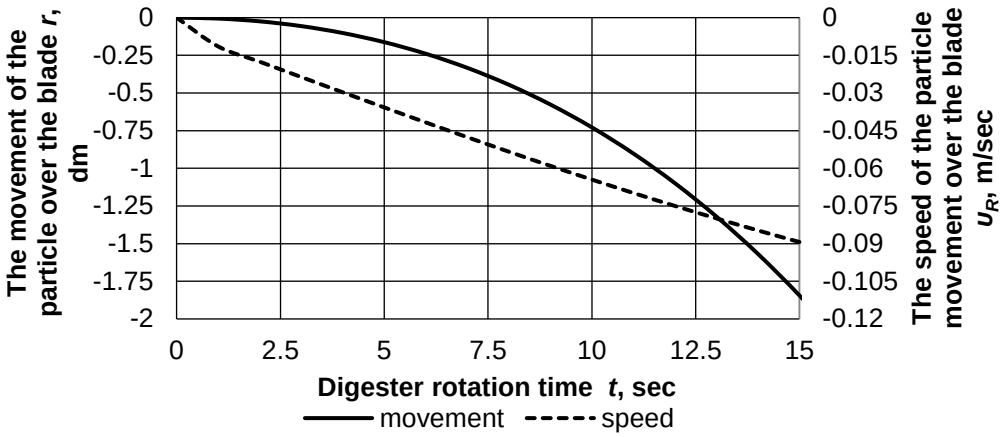

Fig. 4 - The dependence of the movement over the digester blade and the speed of the mineral particle on the rotation time (angular velocity of the digester rotation ω=0.1 rad/s, **inner radius *R*=2 dm)**

The minus sign on the charts indicates that the mineral particle relative to the digester blade is moving to its centre, that is, the current radius of the substrate particle position is decreasing.

The displacement and velocity of the organic particle for the digester rotation angular velocity of 1 rad/s with an internal radius of 2 dm are shown in fig. 5.

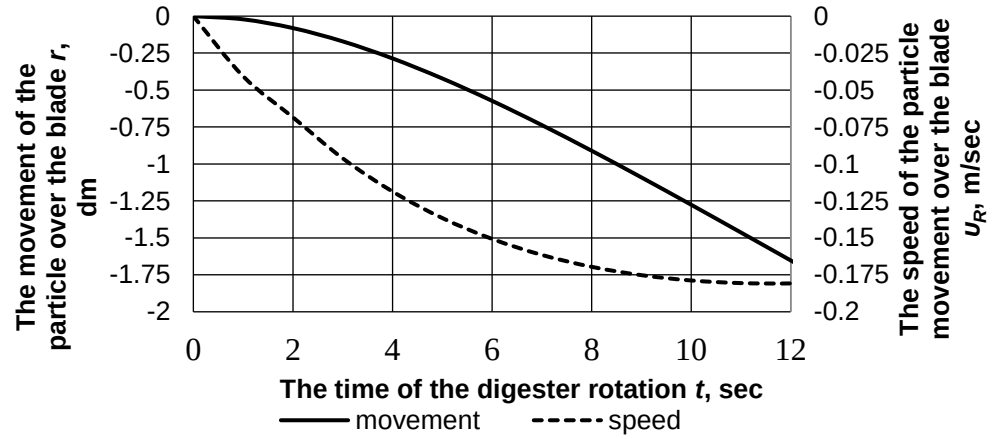

Fig. 5 - The dependence of the movement over the digester blade and the speed of the organic particle on the rotation time (angular velocity of the digester rotation ω=0.1 rad/s, inner radius *R*=2 dm)

A minus sign on the graph indicates that the organic particle relative to the digester blade is also moving to its centre, that is, the current radius of the substrate organic particle position is decreasing.

The calculated scheme of the effect of forces on the substrate mineral and organic particles, which are in free motion in the rotating reactor volume is shown in fig. 2, b.

According To Eq. (3) and taking into account that the mineral particle will sink and the organic one will float, it was composed the equation of motion of such particles mass centre:

$$\begin{cases} \dfrac{d^2x}{dt^2} = \mp k_1 \upsilon \cos\alpha, \\ \dfrac{d^2y}{dt^2} = g\left(k_2 - 1\right) \pm k_1 \upsilon \sin\alpha, \end{cases} \tag{9}$$

where:

x – the movement of the particle along the abscissa axis, [m];

y – the movement of the particles along the axis of ordinates, [m];

t – the time of particle movement after descent off the reactor blade, [s].

To determine the trajectories of mineral and organic particles after the descent off the reactor blades, it was used the method of sequential differentiation, which gives approximate solutions of the systems Eq. (9) in the form of Taylor series.

Considering the initial conditions corresponding to the absolute velocity at the time of the biomass particle descent off the blade $\upsilon=\upsilon_0$, the angle between the absolute velocity and its projection on the axis at this moment is $\alpha=\alpha_0$, and $x_0=0$, $y_0=0$, it can be written:

$$\begin{cases} x = \dfrac{\upsilon_0 \cos\alpha_0}{k_1}\left[\pm 1 \mp \exp\left(-k_1 t\right)\right] \\ y = \dfrac{\upsilon_0 \sin\alpha_0}{k_1}\left[\pm \exp\left(-k_1 t\right) \mp 1\right] \pm \dfrac{g\left(1-k_2\right)}{k_1^2}\left[1 - k_1 t - \exp\left(-k_1 t\right)\right] \end{cases} \tag{10}$$

The first equation of the system (10) allows determining the time of particle motion:

$$t = \frac{1}{k_1} \ln\left(\pm 1 \mp \frac{x k_1}{\upsilon_0 \cos\alpha_0}\right) \tag{11}$$

After substituting Eq. (11) in the second equation of the system (10) we obtain the equation of the particles trajectory after their descent off the digester blades:

$$y = x tg\alpha_0 + \frac{g\left(1-k_2\right)x}{k_1 \upsilon_0 \cos\alpha_0} + \frac{g\left(1-k_2\right)}{k_1^2} \ln\left(\pm 1 \mp \frac{x k_1}{\upsilon_0 \cos\alpha_0}\right) \tag{12}$$

where

α_0 – the angle between the absolute velocity of the mineral particle and its projection on the abscissa axis at the moment of particle decent of the digester blade, [rad];

υ_0 – absolute speed of the mineral particle at the moment of the decent of the digester blade, [m/s];

x – moving of the mineral particle along the axis of abscissa, [m];

y – moving of the mineral particle along the axis of ordinates, [m].

According to Eq. 12, the trajectory of the components particles after the decent of the blade can be found.

In the rational values range of the digester rotation angular velocity and its internal (working) radius based on the equations of motion of substrate components mineral and organic particles over the digester blades and after the descent off the blades, the trajectory of particles inside the digester was found (fig. 6 and fig. 7).

Based on the theoretical obtained solutions of the equations, it is established that at the average density of the substrate ρ_c = 1025-1050 kg/m^3, the mineral part of the substrate ρ_M=1150-1250 kg/m^3 and the organic part of the substrate ρ_o = 800-900 kg/m^3 the rational values of the digester angular velocity are ω=0.04-0.1 rad/s. The length l of the digester blade: $l=(0.75\text{-}0.8)R$.

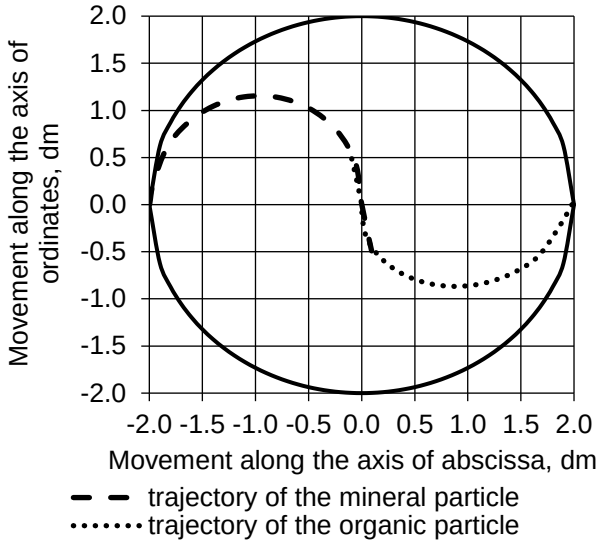

a)

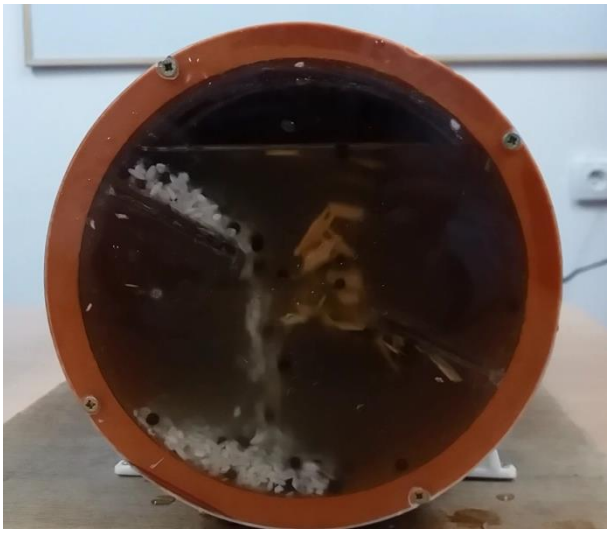

b)

Fig. 6 - An example of the trajectory of the movement of the substrate particles (angular velocity of the digester rotation less than 0.04 rad/s, inner radius 2 dm)

a) – theoretical results; b)– experimental results

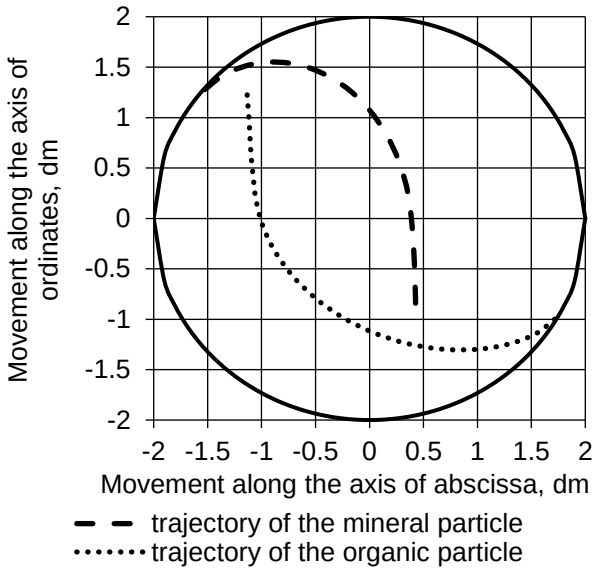

a)

b)

Fig. 7.- An example of the trajectory of substrate particles movement (angular velocity of the digester rotation 0.1 rad/s, inner radius 2 dm)

a) – theoretical results; b) – experimental results

It has been experimentally proved that the angular velocity of 0.1 rad/s will provide uniform mixing and interpenetration of the substrate components. Under the rotary speed of less than 0.04 rad/s the mixing is not sufficient.

CONCLUSIONS

It is proposed to perform mixing of the substrate in a rotating digester. The body of the digester is made in the form of a horizontal cylinder that rotates around a horizontal axis. Inside the digester, there are flat blades. The digester rotates in the liquid, which is located in the outer casing. This design creates lift for the rotating digester by unloading the support bearings. The friction force in the bearings is reduced and, accordingly, the energy spent on the digester rotation and substrate mixing is reduced. The design of the digester eliminates the possibility of creating a floating organic part and submerged mineral sediment.

It was found that the uniform mixing and interpenetration of organic and mineral components of the substrate is provided for the rational values of the angular velocity of the digester from 0.04 to 0.1 rad/s and the length of the reactor blades from 75 to 80 % of its internal radius.

At these values of the angular velocity and blade length, the mineral particles (together with methane-producing bacteria) will rise to the upper part of the digester, after which the particles will separate from the blade and move downwards, and the substrate organic particles will sink into the lower part of the digester, after which they will be separated from the blade and move upwards, thereby ensuring uniform mixing and interpenetration of the substrate components.

REFERENCES

[1] Adouani N., Pons M.-N., Hreiz R., Pacaud S., (2016), Dynamic modelling of an anaerobic digester for wastes at the territory level. *11th IFAC Symposium on Dynamics and Control of Process Systems Including Biosystems DYCOPS-CAB 2016*. Vol. 49, Issue. 7, pp. 1169–1174, Trondheim/Norway;

[2] Carrerea H., Antonopoulou G., Affes R., et al., (2015), Review of feedstock pre-treatment strategies for improved anaerobic digestion: From lab-scale research to full-scale application, *Bioresource Technology*. Vol. 199, pp. 386–397, Netherlands;

[3] Golub G.A., Kukharets S.M., Yarosh Y.D, Kukharets V.V., (2017a), Integrated use of bioenergy conversion technologies in agroecosystems, *INMATEH – Agricultural Engineering*. Vol.51, Issue 1, pp.93–100, Bucharest/Romania;

[4] Golub G., Szalay K., Kukharets S., Marus O., (2017b), Energy efficiency of rotary digesters, *Progress in Agricultural Engineering Sciences*. Vol. 13, Issue 1, pp. 35-49, Budapest/Hungary;

[5] Meyer A.K.P., Ehimen E.A., Holm-Nielsen J.B., (2017), Future European biogas: Animal manure, straw and grass potentials for a sustainable European biogas production, *Biomass and Bioenergy*. Vol. 111, pp. 154-164, Manchester/England;

[6] Ogbonna E. C., Ali R., Pissanidis G., (2013) Simulation model for mesophilic anaerobic digestion heating system, *2013 International Conference on Renewable Energy Research and Applications* (ICRERA), pp. 505-510, Madrid/Spain;

[7] Satjaritanuna P., Khunatorna Y., Vorayosa N. et al., (2016), Numerical analysis of the mixing characteristic for napier grass in the continuous stirring tank reactor for biogas production, *Biomass and Bioenergy*. Vol. 86, pp. 53–64, Manchester/England;

[8] Shah T.A., Ali S., Afzal A., Tabassum R., (2018), Effect of Alkali Pretreatment on Lignocellulosic Waste Biomass for Biogas Production, *International Journal of Renewable Energy Research*. Vol.8, Issue.3, pp. 1318-1326, Ankara/Turkey;

[9] Theuerl S., Klang J., Prochnow A., (2019), Process Disturbances in Agricultural Biogas Production—Causes, Mechanisms and Effects on the Biogas Microbiome: A Review, *Energies.* Vol. 12, Issue 3, pp. 365-385, Basel/Switzerland;

[10] Uçkun K. E., Stamatelatou K., Antonopoulou G.,. Lyberatos G, (2016), Production of biogas via anaerobic digestion, *Handbook of Biofuels Production*, *Processes and Technologies*, National Technical University of Athens, pp. 259–301, Athens/Greece;

[11] Uvarov R., Briukhanov A., Spesivtsev A., Spesivtsev V., (2017), Mathematical model and operation modes of drum-type biofermenter, *16th International Scientific Conference "Engineering for rural development*", pp. 1006-1011, Jelgava/Latvia;

[12] Zhai X., Denka Kariyama I., Wu B., (2018), Investigation of the effect of intermittent minimal mixing intensity on methane production during anaerobic digestion of dairy manure, *Computers and Electronics in Agriculture*. Vol. 155, pp. 121-129, Netherlands.

THE EFFECT OF MASS FLOW RATE OF WHEAT SOLID PARTICLES ON CHARACTERISTICS OF ACOUSTIC SIGNALS IN PNEUMATIC CONVEYING

/

اثر دبی جرمی ذرات جامد گندم در انتقال نیوماتیکی بر ویژگی‌های سیگنال‌های صوتی

Ph.D. Stud. Mehdi Samadi[1)], As Prof. Vahid Rostampour*[1)], Prof. Shamsoallah Abdollahpour[2)]

[1)] Urmia University, Department of Mechanical Engineering, Iran

[2)] Tabriz University, Department of Mechanical Engineering, Iran

Tel: 00984432779558; E-mail: v.rostampour@urmia.ac.ir

Keywords: *Acoustic, Mass Flow Rate, Pneumatic Convey, Wheat*

ABSTRACT

In the industry, the pneumatic conveying of wheat grains has attracted a lot of attention due to benefits such as enclosed transfer and flexibility in routing. Measuring the mass flow of wheat grains is important to avoid problems such as wear of the transmission pipes, pipeline clog due to dense phase and fracture of the seeds. In this research, the acoustic signal analysis method was used to detect the mass flow rate of wheat grains at three levels of 1.5, 3 and 4.5 kg/min in the pneumatic conveying. The signals decomposition was done in time-frequency domain (wavelet transform) with 9 levels. The properties of Sum, Mean, Variance (VAR), Root Mean Square (RMS), Skewness, Kurtosis, and Moment were compared. The results showed that the first (d_1), second (d_2), fifth (d_5), sixth (d_6) and seventh (d_7) detail *sub-signals have the highest ability and priority to detect mass flow levels, respectively. Also among the studied properties, sum, mean, VAR, RMS, and moment, are prioritized for detecting mass flow levels with probability level of 1%, respectively. The values of all these properties increased with increasing mass flow rate. The acoustic signal analysis technique has a good potential for detecting the different mass flow levels of conveyed wheat grains.*

چکیده

انتقال نیوماتیکی دانه‌های گندم به دلیل مزایایی از قبیل انتقال به شکل محصور و قابلیت انعطاف‌پذیری در مسیریابی در صنعت مورد توجه زیادی قرار گرفته است. اندازه گیری دبی جرمی دانه های گندم به منظور جلوگیری از بروز مشکلاتی مانند سایش لوله های انتقال، گرفتگی لوله در اثر فاز غلیظ و شکستگی دانه‌ها حائز اهمیت میباشد. در این تحقیق، برای تشخیص میزان دبی جرمی عبوری دانه های گندم در سه سطح 1/5، 3 و 4/5 کیلوگرم در دقیقه از روش آنالیز سیگنالهای صوتی در حوزه زمان-فرکانس (تبدیل ویولت) استفاده گردید. تجزیه سیگنالها در 9 سطح انجام شد و ویژگیهای Sum، Mean، VAR، RMS، Skewness، Kurtosis، و Moment مورد مقایسه قرار گرفتند. نتایج نشان داد که زیرسیگنالهای دیتلز اول، دوم، پنجم، ششم و هفتم به ترتیب دارای بیشترین توانایی و اولویت برای تشخیص سطوح مختلف دبی های جرمی از یکدیگر می باشند. در بین ویژگی های بررسی شده به ترتیب ویژگی های Sum، Mean، VAR، RMS و Moment برای تشخیص دبی های جرمی با سطح احتمال 1% دارای اولویت هستند. مقادیر همه این ویژگی ها با افزایش دبی جرمی افزایش یافت. تکنیک صوت دارای پتانسیل خوبی جهت تشخیص سطوح مختلف دبی جرمی دانه های گندم در حال انتقال بود.

INTRODUCTION

The pneumatic conveying encompasses transmission of wide range of powdered and granular solids in gas stream (*Klinzing et al., 2009*). Pneumatic conveying has been popular in the industry for many decades because of advantages such as enclosed conveying of products and its flexibility in routing (*Mills, 2013*). Some of the industries that convey materials in pneumatic way include agriculture, chemistry, pharmaceuticals, mine, food, steel, plastic and rubber. Today, this method is used in flour mills to transport wheat from trailers and trucks to storage silos and vice versa, as well as the transfer of raw material from silos toward the flour milling process. The transfer of materials to the wheat silos due to its high height and volume is complicated and various methods are used for this purpose. The pneumatic conveying due to its high speed of material transfer in proportion to its volume, low cost of service and maintenance, least number of needed users and the controllability of the system in different working conditions, has been welcomed.

The mass flow control of solid particles in the pneumatic conveying system is very important *(Zheng and Liu, 2011*) .One of the visible problems in transfer of wheat grains is the wear of the transfer pipes, which

is caused by frequent contact with the pipe walls. The other problem is the fracture of the seeds during the transfer, which is very important because it reduces the seed vigor and causes a disorder in the quality of the produced flour. One of the causes of seed fractures is the non-controlling material flow rate inside the pipe and the contact of the wheat grains with each other, as well as in the walls, especially in the knees. Also, the maximum utilization of energy in the pneumatic conveying system has barriers such as pipe clogging due to massive material mass concentration in the bottom of the pipes which, if not eliminated, will result in considerable energy losses and consequently increase the increased costs.

Different methods are used to measure the mass flow rate of solids in gas-solid medium in pneumatic transmission. Capacitive sensor is used to measure the mass flow rate of solid particles. These sensors has not been welcomed because of its sensitivity to moisture, size and heterogeneity and the chemical composition of solid particles (*Yan, 1996*). In radiometric measurement systems, ionization radiation is used in the form of gamma and x-rays to measure the mass flow rate of solids *(Van et al., 1993*). This system is not suitable for online measurement due to its high cost and safety constraints. One of the most widely used sensors is the optical sensor. In these sensors, the intensity of light passing through the diluted solid gas mixture depends on the volume concentration of solid matter. The major problem of optical sensors is the presence of a contaminated window and its asymmetry when entering and leaving, which can respond false signals and data. Tomography methods are powerful tools for measuring the volume concentration of solid particles moving in pneumatic transition pipe. Among the tomographic measurement systems, two methods of electrical capacity tomography (ECT) and electrical optical tomography (EOT) are used due to their high development. In general, in tomography, the definition level is poor and the sensitivity is very low. Also, using this method, strong dust is generated inside the pipe. The use of digital imaging because of the limited programming capability for dense and concentrated environments cannot be a suitable method for measuring mass flow rate. The flow meter based on the coriolis force (coriolis meter) has measurement limitations due to its difficult installation and the development of strong dust in the tube. Thermal gas flow meters are faced with reduced accuracy with the presence of different compositions of gas and show weak repeatability. Electrostatic sensors are sensitive to moisture, particle size, chemical composition and heterogeneity of particles, and also have high error levels of about 15%. Zheng and Lee provided a review of these methods (*Zheng and Liu, 2011*). Among the available techniques, the acoustic analysis method is attractive because of its advantages such as the relevance of the optimum frequency with particle size, the simplicity of the method, the robustness against difficult conditions, easy installation, online display, equipment costs and low maintenance (*Fuchs et al., 2008*). In this method, a microphone is used to record the sound produced by the materials flow (*Dhoriyani et al., 2006*). Based on the analysis of the density of the power spectrum and wave transfer, a theory on the relationship between the propagation of sound propagation and the mass flow rate of solid particles in the pneumatic convey could be established (*He et al., 2014*). The effect of the locating and positioning of acoustic sensors in the transmission pipe and the verification of their measurement in developing regions, especially after the 90 degree bends, has been investigated (*Tallon et al., 2000*). A new measurement system was developed for the detection of wood components in pneumatic conveying using vibration and sound sensors (*Sun et al., 2014*). Their results showed that both vibration and sound sensors can be used to detect the collisions between particles and the pipe wall. Also, the sound signal, if used with obstruction, has a higher SNR (Signal to-Noise Ratio) than the vibration signal, which is an advantage. A new method based on the passive sound propagation technique was established for the analysis of the particle-wall collision and friction (*He et al., 2014*). Wavelet conversion was used to extract information from particles and walls, as well as friction. According to these analyzes, a theoretical relationship was developed to establish a relationship between the AE (Acoustic Emission) signals and the ratio of solid loading in the vertical pneumatic convey pipe. The error obtained for the mass flow rate of solids using this model was less than 6.62%.

In the present study, a microphone with a high frequency range was used to record audio signals from wheat grains in the transfer pipes. The comparison of the signals in the time-frequency domain was performed and the Sum, Mean, Variance (VAR), Root Mean Square (RMS), Skewness, Kurtosis and Moment properties were used to detect different mass flow levels.

MATERIALS AND METHODS

The research process, used equipment and a detailed description of acoustic signals processing are presented.

- **Research process and preparation of samples**

The acoustic signal analysis method was used to detect the mass flow rate of wheat grains at three levels of 1.5, 3 and 4.5 kg/min in the pneumatic conveying. The Bahar wheat cultivar as one of the most popular cultivars in Iran was used in the research. Wheat samples were prepared and transferred to the post-harvest laboratory to determine the physical and aerodynamic properties. Table 1 shows the physical and mechanical properties of the sample used.

Table1

The physical and mechanical properties of the wheat

Physical and mechanical properties	Size
True density [kg/m^3]	1325
Bulk density [kg/m^3]	815
Sphericity coefficient [%]	55.06
Geometric grain diameter [m]	4.35×10^{-3}
Limit speed [m/s]	12.41
Saltation velocity [m/s]	11.71
Air required speed to prevent sedimentation [m/s]	17.56

- **Equipment**

To pneumatic conveying the wheat grains in a solid-gas two-phase environment, a semi-industrial conveying system with a capacity of 1 ton/h was designed and constructed (Figure 1). In this system, a 0.5-hp centrifugal fan with working speed of 42 m/s, volumetric rate of 2.75 m^3/h and outlet diameter of 4.8 cm was used to supply the air needed for the convey. The feeder has 8 blades and the working capacity of 1 ton/h. The diameter of the transfer pipe is 4.8 cm and the length is 1.30 cm. The cyclone is centrifugal type with a cross sectional area of 78.5 cm^2.

In order to record the acoustic signals generated by the conveying the wheat grains in the pipe, the SENNHEISER (ew100 ENG G3 series) which includes a microphone (ME2 model), a receiver (EC 100 G3 model) and a portable transmitter (SK 100 G3), was used. This set has a frequency response of 25 to 18000 Hz, which is very suitable for fast dynamic responses. In order to record the acoustic signals of wheat grains in the pneumatic conveying, the microphone was mounted on the transmission pipe (Fig. 1). To remove the noise of the environment, the microphone was placed inside the foam and completely covered by the glass wool. Also, to reduce the sound produced by the cyclone separator, its outer part was completely covered by glass wool. Acoustic signals stored online through the oscilloscope section of the Matlab software.

Fig 1 - Schematic of wheat grains conveying system and acoustic signals recording system

- **Signal processing**

The received acoustic signals from wheat grains (at three mass flow rate levels of 1.5, 3 and 4.5 kg/min) were processed in time-frequency domain using wavelet transform. In wavelet transformation, the signal is passed through a series of upstream and downstream filters. Signal is divided in two parts; the section, which passes from a high-pass filter, contains high frequency data i.e. noise. It is called details. The second section, which passes from a low–pass filter, contains low frequency data and includes features of signals and is called approximations. In general, if x(t) is the main signal and using the wavelet is decomposed into n levels, the first signal can be achieved from the sum of approximation signals at the last level and sum of the detail functions at different levels and calculated from equation below (*Soman, 2010; Zanardelli et al., 2005*):

$$x(n) = a_n(n) + \sum_{n=1}^{N} d_n(n) \quad (1)$$

Decomposition operations can be continued until there is no significant data in approximations. So, the first signal can be rebuilt using details signals without losing any necessary data. Selection of function type is different for various problems in wavelet transformation. The Daubechi function (DB3) has been used at the most of studies. The efficiency of Daubechi function is acknowledged. Hence, the mentioned function is used in this research to decompose the acoustic signals. So, Daubechi function with nine decomposition levels was selected after try and error. Therefore, the signal can be written as Equation (2), (d_1- d_9 are details and a_9 is approximation):

$$x[n] = a_9 + d_9 + d_8 + d_7 + d_6 + d_5 + d_4 + d_3 + d_2 + d_1 \quad (2)$$

Where x[n] is the main signal and indices are related to the decomposition level of signal.

In order to detect signals pertaining to several different mass flow levels and finally to differentiate these levels, the characteristic vector of the sub-signals should be selected and according to the changes in these vectors, the mass flow levels can be differentiated. In this study, Sum, Mean, Variance, Root Mean Square (RMS), Skewness, Kurtosis and Moment were used to compare the output signals of different mass flow levels.

SUM

The sum is the total amplitude of acoustic signal data points that can indicate the intensity of the acoustic signal and is defined mathematically as below (*Lei et al., 2008*):

$$Sum = \sum_{n=1}^{N} x(n) \quad (3)$$

Where, $x(n)$ is the amplitude of data points.

AVERAGE (MEAN)

As much as the average value becomes closer to zero, symmetry of the signal of the system increases. Because the vibrational and acoustic signals are in wave forms, the signal value is usually zero. So, to use this factor, the absolute function is used. Its mathematical equation is as below (*Lei et al., 2008*):

$$Mean(abs) = \frac{\sum_{n=1}^{N} abs(x(n))}{N} \quad (4)$$

VARIANCE (VAR)

This factor usually indicates the dispersion of the signal. Whatever the magnitude of the variance, the signal is more uniform and more aggressive. In other words, the received sound is more turbulent and inconsistent (*Lei et al., 2008*).

$$Var(x(n)) = \frac{\sum_{n=1}^{N} (x(n) - mean(x(n)))^2}{N-1} \quad (5)$$

ROOT MEAN SQUARE (RMS)

One of the most commonly used value in acoustic signals analysis, is the Root Mean Squared (RMS). Because the most important property of an acoustic signal is the content of its energy. The energy is proportional to the signal amplitude, and a second-power average will better than the power of the acoustic signal. RMS is calculated as equation 6 *(Mohammed et al., 2013*):

$$RMS = \left[\frac{\sum_{n=1}^{N} (x(n))^2}{N} \right]^{1/2} \quad (6)$$

In which $x(n)$ is the amplitude of data point and *N* is the number of signal data point.

SKEWNESS

This parameter shows the elongation of the signal to one side (*Khazaee et al., 2013*).

$$Skewness = \frac{\frac{1}{n}\sum_{n=1}^{N} \left(x(n) - mean(x(n))\right)^3}{\left(\frac{1}{n}\sum_{n=1}^{N} \left(x(n) - mean(x(n))\right)^2\right)^{3/2}} \quad (7)$$

KURTOSIS

Kurtosis indicates the magnitude and sharpness of the extremes of signals. In fact, the larger Kurtosis indicates that the pulses of the larger system have a bigger, sharper and wider sequence. Kurtosis is used to detect the defects of microstructures. The existence of fine flaws in a structure will increase the distortion of the signal and increase the amount of Kurtosis signal. The value of Kurtosis for random and digital signals x (n) with the number of N data, is calculated as equation 8 *(Mohammed et al., 2013*):

$$kurtosis = \frac{\frac{1}{N}\sum_{n=1}^{N} x(n)^4}{\left[\frac{1}{N}\sum_{n=1}^{N} x(n)^2\right]^2} \quad (8)$$

MOMENTUM (MOMENT)

This factor represents the normalized value of the signal relative to the mean, and is an appropriate factor for checking the signal's impact status (*Khazaee et al., 2013*):

$$Moment(4) = \frac{\sum_{n=1}^{N} \left(x(n) - Mean(x(n))\right)^4}{N} \quad (9)$$

- **Statistical analysis**

The test was performed for each rate with 30 repetitions, and a total of 90 signals were obtained. Signal processing was performed using the MTLAB software. The Duncan method was used to compare the averages at 1% and 5% probability. SAS9.1 software was used for statistical analyzes.

RESULTS

In Fig. 2, the signals related to three mass flow levels of 1.5 kg/min, 3 kg/min and 4.5 kg/min are shown.

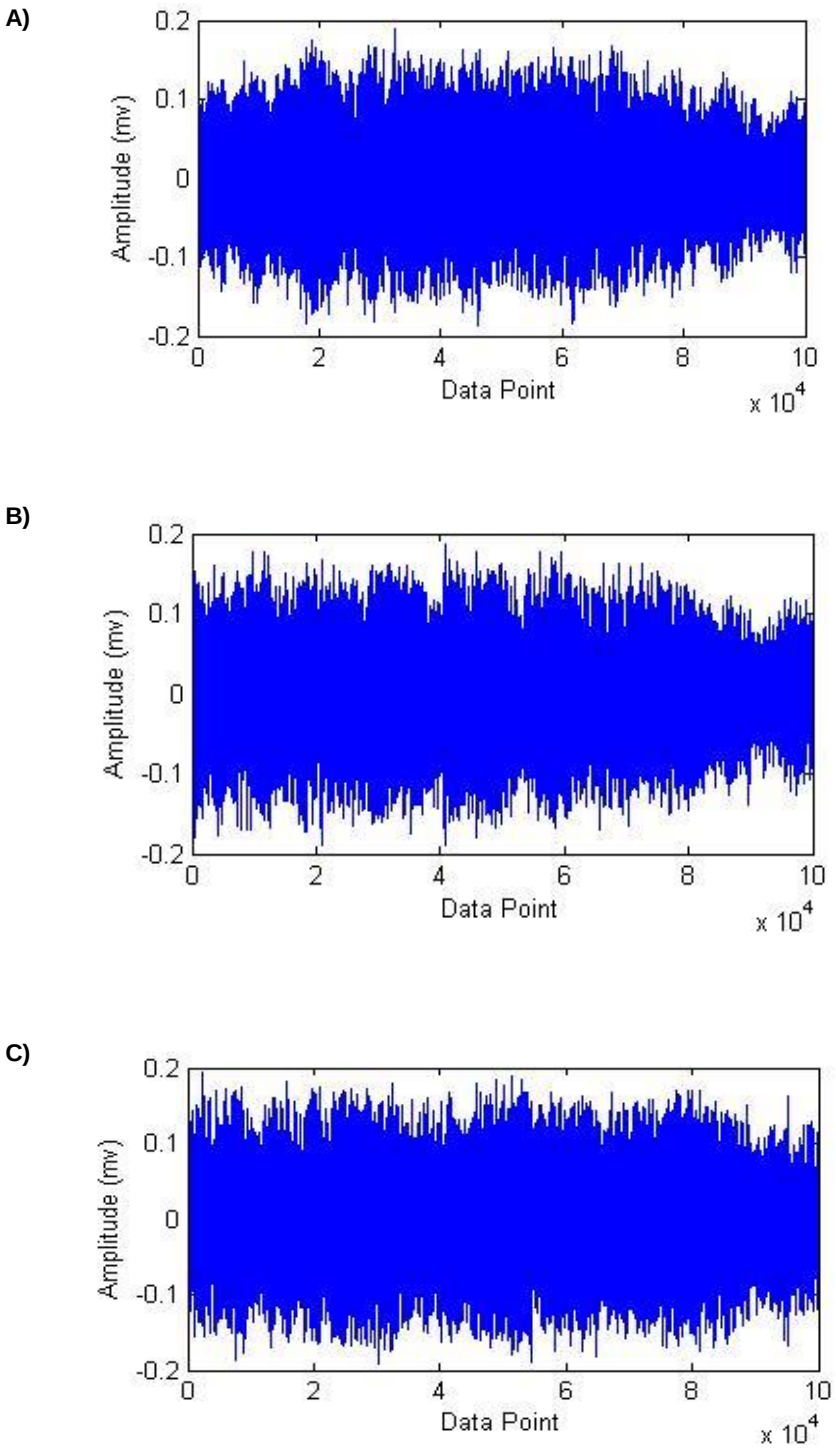

Fig. 2 - Acoustic signals related to different mass flow levels
A) *1.5 kg/min* B) *3 kg/min* and C) *4.5 kg/min*

As shown in fig. 2, the signals related to the three different mass flow levels are similar and separation of mass flow levels is not possible. Therefore, the signals received from different mass flow levels were decomposed using the wavelet transform to the detail sub-signals of 1 to 9 (d_1 to d_9) and 9th approximate (a_9) to allow detection of mass flow levels from each other.

Fig.3 and fig. 4 show the decomposed signals for each mass flow levels.

A)

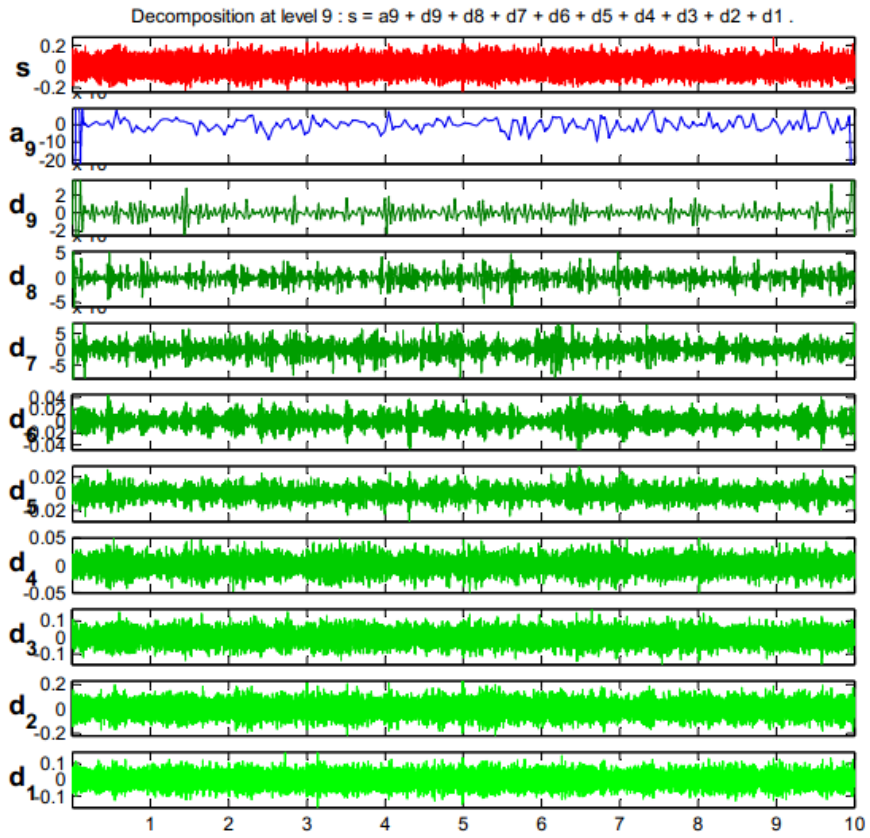

B)

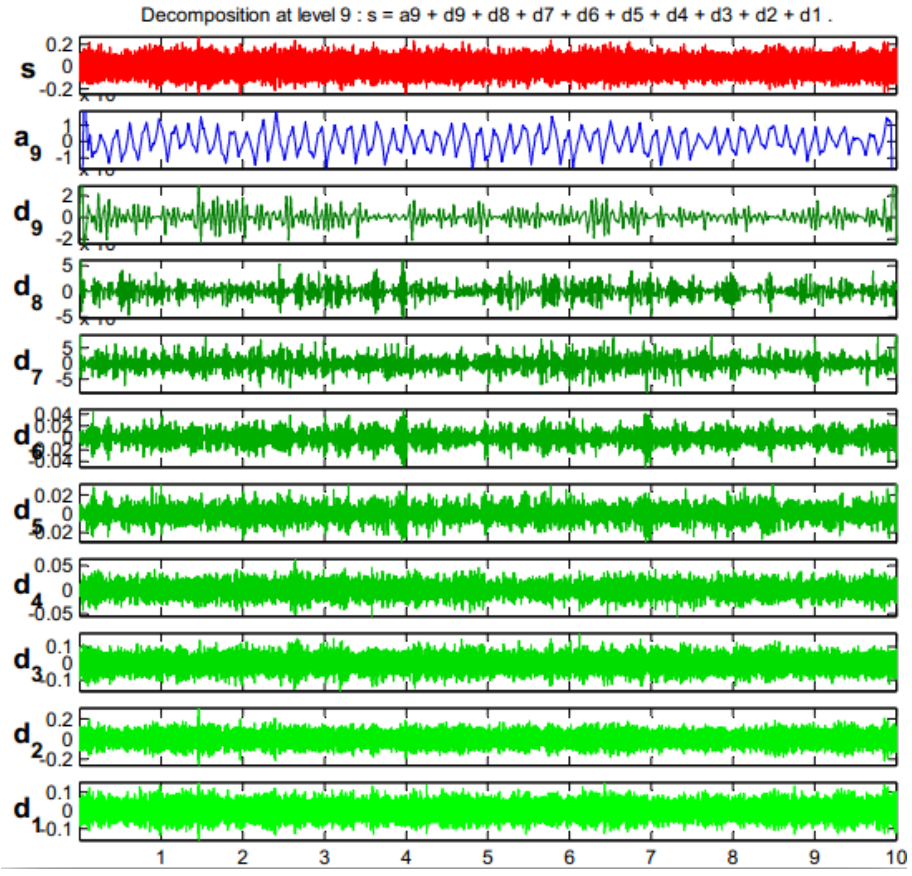

Fig. 3- Decomposing the main signals to detail and approximate sub-signals, A) 1.5 kg/min and B) 3 kg/min

C)

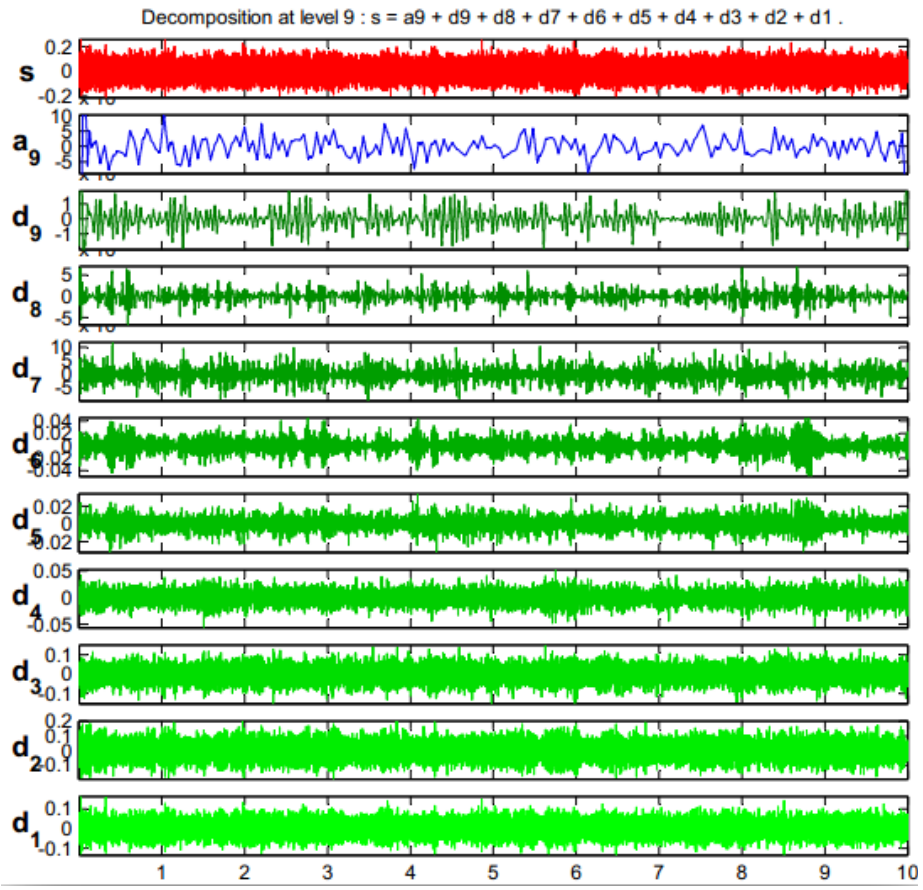

Fig. 4- Decomposing the main signals to detail and approximate sub-signals C) 4.5 kg/min

In order to detect the difference in mass flow levels signals using sub-signals, seven characteristics of Sum, Mean, Variance (VAR), RMS, Skewness, Kurtosis and Moment were used. Comparison of these characteristics at the probability level of 1% and 5% for d_1 to d_9 and a_9 are presented in Tables 2 to 10, respectively.

Table 2

Characteristics of the first detail (d_1) sub-signal

Mass flow rate [kg/min]	Signal properties						
	Sum	Mean	VAR	RMS	Skewness	Kurtosis	Moment
1.5	613^{a}	0.0076^{a}	9.97E-05^{a}	0.0100^{a}	-0.0193$^{a'}$	3.51$^{a'}$	3.5E-08^{a}
3	684^{b}	0.0085^{b}	0.000123^{b}	0.0111^{b}	-0.0185$^{a'}$	3.37$^{b'}$	5.1E-08^{b}
4.5	754^{c}	0.0094^{c}	0.000149^{c}	0.0122^{c}	-0.0135$^{a'}$	3.29$^{c'}$	7.3E-08^{c}

Different superscript indicates significant differences at the level of 1% (normal) and 5% (with Prim).

Table 3

Characteristics of the second detail (d_2) sub-signal

Mass flow rate [kg/min]	Signal properties						
	Sum	Mean	VAR	RMS	Skewness	Kurtosis	Moment
1.5	1292^{a}	0.0161^{a}	0.00044^{a}	0.0209^{a}	-0.0140$^{a'}$	3.50$^{a'}$	6.75E-07^{a}
3	1383^{b}	0.0173^{b}	0.00050^{b}	0.0223^{b}	-0.0091$^{a'}$	3.41$^{a'}$	8.5E-07^{b}
4.5	1494^{c}	0.0187^{c}	0.00057^{c}	0.0240^{c}	-0.0115$^{a'}$	3.27$^{b'}$	1.1E-06^{c}

Table 4

Characteristics of the third detail (d_3) sub-signal

Mass flow rate [kg/min]	Signal properties						
	Sum	Mean	VAR	RMS	Skewness	Kurtosis	Moment
1.5	2552$^{a'}$	0.0319$^{a'}$	0.00176$^{a'}$	0.0420$^{a'}$	-0.00053$^{a'b'}$	4.13$^{a'}$	1.29E-05$^{a'}$
3	2537$^{a'}$	0.0317$^{a'}$	0.00175$^{a'}$	0.0417$^{a'}$	-0.00978$^{a'}$	4.08$^{a'}$	1.26E-05$^{a'}$
4.5	2656$^{a'}$	0.0332$^{a'}$	0.00192$^{a'}$	0.0438$^{a'}$	0.00433$^{b'}$	4.11$^{a'}$	1.52E-05$^{a'}$

Table 5

Characteristics of the fourth detail (d_4) sub-signal

Mass flow rate [kg/min]	Signal properties						
	Sum	Mean	VAR	RMS	Skewness	Kurtosis	Moment
1.5	1213$^{a'}$	0.0151$^{a'}$	0.000434$^{a'}$	0.0208$^{a'}$	0.0056$^{a'}$	5.059$^{a'}$	9.52E-07$^{a'}$
3	1189$^{a'}$	0.0148$^{a'}$	0.000422$^{a'}$	0.0205$^{a'}$	0.0037$^{a'}$	5.108$^{a'}$	9.17E-07$^{a'}$
4.5	1283$^{a'}$	0.0160$^{a'}$	0.000488$^{a'}$	0.0221$^{a'}$	-0.0076$^{a'}$	5.143$^{a'}$	1.23E-06$^{a'}$

Table 6

Characteristics of the fifth detail (d_5) sub-signal

Mass flow rate [kg/min]	Signal properties						
	Sum	Mean	VAR	RMS	Skewness	Kurtosis	Moment
1.5	495^{a}	0.0062^{a}	7.43E-05^{a}	0.0086^{a}	0.0035$^{a'}$	5.827$^{a'}$	3.20E-08$^{a'}$
3	576^{b}	0.0072^{b}	9.8E-05^{b}	0.0099^{b}	0.0492$^{a'}$	5.508$^{a'b'}$	5.31E-08$^{b'}$
4.5	686^{c}	0.0086^{c}	0.00013^{c}	0.0116^{c}	0.0084$^{a'}$	5.069$^{b'}$	9.25E-08$^{c'}$

Table 7

Characteristics of the sixth detail (d_6) sub-signal

Mass flow rate [kg/min]	Signal properties						
	Sum	Mean	VAR	RMS	Skewness	Kurtosis	Moment
1.5	405^{a}	0.0051^{a}	4.83E-05^{a}	0.0069^{a}	-0.0091$^{a'}$	5.28$^{a'}$	1.24E-08$^{a'}$
3	487^{b}	0.0061^{b}	6.83E-05^{b}	0.0082^{b}	0.0059$^{a'}$	5.19$^{a'}$	2.41E-08$^{b'}$
4.5	579^{c}	0.0072^{c}	9.56E-05^{c}	0.0098^{c}	-0.0193$^{a'}$	4.80$^{a'}$	4.40E-08$^{c'}$

Table 8

Characteristics of the seventh detail (d_7) sub-signal

Mass flow rate [kg/min]	Signal properties						
	Sum	Mean	VAR	RMS	Skewness	Kurtosis	Moment
1.5	375$^{a'}$	0.0047$^{a'}$	4.03E-05$^{a'}$	0.0063$^{a'}$	0.116$^{a'}$	5.28$^{a'}$	8.54E-09$^{a'}$
3	430$^{b'}$	0.0054$^{b'}$	5.24E-05$^{b'}$	0.0072$^{b'}$	0.068$^{a'}$	4.98$^{a'b'}$	1.39E-08$^{a'b'}$
4.5	483$^{c'}$	0.0060$^{c'}$	6.55E-05$^{c'}$	0.0081$^{c'}$	-0.041$^{b'}$	4.62$^{b'}$	2.00E-08$^{b'}$

Table 9

Characteristics of the eighth detail (d_8) sub-signal

Mass flow rate [kg/min]	Signal properties						
	Sum	Mean	VAR	RMS	Skewness	Kurtosis	Moment
1.5	330$^{a'}$	0.00412$^{a'}$	2.99E-05$^{a'}$	0.0054$^{a'}$	-0.0262$^{a'}$	4.29$^{a'}$	3.92E-09$^{a'}$
3	361$^{a'}$	0.00451$^{a'}$	3.72E-05$^{a'}$	0.0061$^{b'}$	-0.0054$^{a'}$	4.56$^{a'}$	6.30E-09$^{a'b'}$
4.5	399$^{b'}$	0.00499$^{b'}$	4.48E-05$^{b'}$	0.0067$^{b'}$	-0.0341$^{a'}$	4.51$^{a'}$	9.24E-09$^{b'}$

Table 10

Characteristics of the ninth detail (d_9) sub-signal

Mass flow rate [kg/min]	Signal properties						
	Sum	Mean	VAR	RMS	Skewness	Kurtosis	Moment
1.5	169$^{a'}$	0.0021$^{a'}$	8.30E-06$^{a'}$	0.00287$^{a'}$	0.174$^{a'}$	4.59$^{a'}$	3.4E-10$^{a'}$
3	183$^{a'}$	0.0023$^{a'}$	9.48E-06$^{a'}$	0.00308$^{a'}$	0.037$^{a'}$	4.83$^{a'}$	4.4E-10$^{a'}$
4.5	220$^{b'}$	0.0027$^{b'}$	1.35E-05$^{b'}$	0.00368$^{b'}$	0.014$^{a'}$	4.79$^{a'}$	8.8E-10$^{b'}$

Table 11

Characteristics of the ninth detail (a_9) signal

Mass flow rate [kg/min]	Signal properties						
	Sum	Mean	VAR	RMS	Skewness	Kurtosis	Moment
1.5	119$^{a'}$	0.00149$^{a'}$	3.87E-06$^{a'}$	0.00198$^{a'}$	0.1307$^{a'}$	4.29$^{a'}$	6.57E-11$^{a'}$
3	144$^{b'}$	0.00179$^{b'}$	5.52E-06$^{b'}$	0.00234$^{b'}$	-0.0845$^{a'}$	3.89$^{a'}$	1.18E-10$^{a'}$
4.5	154$^{b'}$	0.00192$^{b'}$	6.53E-06$^{b'}$	0.00256$^{b'}$	0.019$^{a'}$	4.29$^{a'}$	1.83E-10$^{b'}$

In Table 2, the first detail (d_1) sub-signal at the probability of 1% and using the Sum, Mean, VAR, RMS and Moment can detect various mass flow levels as well as the Kurtosis at the probability of 5%. According to the Table 3, the second detail (d_2) sub-signal at 1% probability has the same behavior as the first detail sub-signal (d_1) and with the four characteristics of Sum, Mean, VAR, RMS and Moment can differentiate the mass flow levels. According to the results of Tables 4 and 5, the third and fourth details (d_3 & d_4) sub-signals are unable to detect different mass levels with any of the characteristics. As can be seen in Table 6, in the fifth detail (d_5) sub-signals, the difference between the values of Sum, Mean, VAR, RMS at the probability level of 1% and Moment at a probability level of 5% and at different mass flow levels, is significant and these sub-signals can differentiate mass flow levels. The results of the sixth detail (d_6) in Table 7 show that the conditions of this sub-signal are exactly the same as the fifth detail sub-signals and will have the differentiation capability by using the four properties of Sum, Mean, VAR, RMS at the probability level of 1% and using the moment property at probability level 5 %. As shown in Table 8, the seventh detail (d_7) sub-signal has the ability to detect mass flow levels in each of the four properties of Sum, Mean, VAR, RMS at a 5% probability level. According to Tables 9 and 10, the eighth and ninth details (d_8 & d_9) sub-signal are not capable of detecting and differentiating the different levels of mass flow levels by using any of the properties. Also, according to Table 11, the ninth approximate (a_9) will not be able to detect different levels of mass flow levels from each other. Table 12 shows the prioritization of the first to ninth (d_1 to d_9) sub-signals and the ninth approximate (a_9) according to the probability levels of 1% and 5%.

Table 12

Prioritization of mass flow detection by sub-signals and characteristics

Sub-signals	Probability Level	Characteristics
d_1	1%	Sum, Mean, VAR, RMS and Moment
	5%	Kurtosis
d_2	1%	Sum, Mean, VAR, RMS and Moment
d_5 & d_6	1%	Sum, Mean, VAR, RMS
	5%	Moment
d_7	5%	Sum, Mean, VAR, RMS
d_3 & d_4 & d_8 & d_9 & a_9	*Non-significant*	-

According to Table 12, the first (d_1), second (d_2), fifth (d_5), sixth (d_6) and seventh (d_7) detail sub signals, can be used to determine the different mass flow levels according to priority. On the other hand, the third (d_3), fourth (d_4), seventh (d_7), eighth (d_8), and the ninth (a_9) approximate sub signals, will not be able to detect. The cause of the sub-signals of the separable details in the characteristics of the effective signal is

that the frequency of disturbing sound signals, such as the centrifugal fan and the cyclone, is not present in these details, resulting in lower noise disturbance and the ability to separate them in the details.

CONCLUSIONS

In this study, the acoustic signal analysis technique potential was evaluated to determine the mass flow rate of wheat grains in pneumatic conveying. The acoustic signals of three levels of mass flow rate includes: 1.5 kg/min, 3 kg/min and 4.5 kg/min were measured by a microphone that located in elbow section of pipe. To more detailed research, signals were decomposed using wavelet transform into 9 sub-signals and 7 characteristics of sub-signals including: Sum, Mean, VAR, RMS, Kurtosis, Skewness and Moment were compared. The main results of the present work can be summarized as following:

(1) Among sub-signals, maximum effect of mass flow rate variation was related to d_1, d_2, d_3 and d_4 sub-signals, respectively and these sub-signals have more potential to recognize the various mass flow rate levels.

(2) Among characteristics, the effect of mass flow rate variation on characteristics (Sum, Mean, VAR and RMS) in all 4 sub-signals (d_1, d_2, d_3 and d_4) was significant at probability levels of 1%. So, these characteristics, in mentioned sub-signals have more potential to recognize the various mass flow rate levels. Also, the effect of mass flow rate variation on the characteristic of Moment in d_1 and d_2 sub-signals was significant at probability levels of 1% and in d_5 and d_6 sub-signals was significant at probability levels of 5%.

(3) All of these characteristics were increased by increasing mass flow rate levels, which is due to the amplification of the acoustic signal frequencies and increase in sound received by the microphone.

Over the years, various sensing techniques have been developed and proposed to measure the particle mass flow rate. Among them, the most promising methods are electrostatic, microwave and tomographic methods. These methods are limited in their industrial application, because they are either sensitive to the change of environment, expensive and time-consuming. But, the acoustic signals analysis is attractive because of its advantages such as the relevance of the optimum frequency with particle size, the simplicity of the method, the robustness against difficult conditions, easy installation, online display, equipment costs and low maintenance. Moreover, the results of this study were showed the performance of this technique. Thus, the acoustic signal analysis technique holds a great potential to recognize the particle mass flow rate in pneumatic conveying and other particulate processes.

REFRENCES

[1] Dhoriyani M.L., Mukesh L., Jonnalagad d., Kranthi K., Kandikatla R.K., Rao K., (2006), Silo music: sound emission during the flow of granular materials through tubes. *Powder Technology,* Vol.167, Issue 2, pp. 55-71, India;

[2] Fuchs A., Zangl H., (2008), Measuring flow parameters of particulate and powdery solids in industrial transportation processes. *International journal on smart sensing and systems*, Vol.1, Issue 2, pp. 388-402, Austria;

[3] He L., Zhou Y., Huang Z., Wang J., Lungu M., Yang Y., (2014), Acoustic analysis of particle–wall interaction and detection of particle mass flow rate in vertical pneumatic conveying, *Industrial & Engineering Chemistry Research*, Vol.53, Issue 23, pp. 9938-9948, China;

[4] Khazaee M., Ahmadi H., Omid M., Banakar A., Moosavian A., (2013), Feature-level fusion based on wavelet transform and artificial neural network for fault diagnosis of planetary gearbox using acoustic and vibration signals, *Insight-NonDestructive Testing and Condition Monitoring*, Vol.55, Issue 6, pp. 323-330, Iran;

[5] Klinzing D.C., Madoff L.C., Puopolo K.M., (2009), Genomic analysis identifies a transcription-factor binding motif regulating expression of the alpha C protein in Group B Streptococcus. *Microb Pathog*, Vol.46, Issue 6, pp. 315-20, American;

[6] Lei U., He Z., Zi Y., (2008), A new approach to intelligent fault diagnosis of rotating machinery, *Expert Systems with Applications*, Vol.35, pp. 1593-1600, China;

[7] Mills D., (2013), *Pneumatic conveying design guide*, chapter 1, Butterworth-Heinemann, ISBN 0 7506 5471 6, Chennai/India;

[8] Mohammed O.D., Rantatalo M., Aidanpää J.O., Kumar U., (2013), Vibration signal analysis for gear fault diagnosis with various crack progression scenarios, *Mechanical Systems and Signal Processing*, vol.41, pp. 176-195, Sweden;

[9] Soman K.P., (2010), *Insight into wavelets:* Front Cover. K. P. Soman. PHI Learning Pvt. Ltd., 2010 - Wavelets (Mathematics), 447 p.;

[10] Sun D., Yan Y., Carter R.M., Gao L., Lu G., Riley G., Wood M., (2014), On-line nonintrusive detection of wood pellets in pneumatic conveying pipelines using vibration and acoustic sensors, *IEEE Transactions on Instrumentation and Measurement,* Vol.63, Issue 5, pp. 993-1001, UK;

[11] Tallon S.J., Davies C.E., (2000), The effect of pipeline location on acoustic measurement of gas–solid pipeline flow. *Flow Measurement and Instrumentation*, Vol.11, Issue 3, pp. 165-169, New Zealand;

[12] Van Y., Byrne B., Coulthard J., (1993), Radiation attenuation of pulverised fuel in pneumatic conveying systems, *Transactions of the Institute of Measurement and Control,* Vol.15, Issue 3, pp. 98-103, California;

[13] Yan Y., (1996), Mass flow measurement of bulk solids in pneumatic pipelines, *Measurement Science and Technology,* Vol.7, Issue 12, pp. 1687-1706, UK;

[14] Zanardelli W.G., Strangas E., Khalil H.K., Miller J.M., (2005), Wavelet-based methods for the prognosis of mechanical and electrical failures in electric motors. *Mechanical Systems and Processing*, Signal, Vol.19, Issue 2, pp. 411-426, USA;

[15] Zheng Y., Liu Q., (2011), Review of techniques for the mass flow rate measurement of pneumatically conveyed solids. *Measurement,* Vol.44, Issue 4, pp. 589-604, PR China.

NECESSITY AND POSSIBLE APPROACHES TO APPLYING DEEP LOOSENING WHEN CULTIVATING RICE

/

НЕОБХІДНІСТЬ ТА МОЖЛИВІ ПІДХОДИ ДО ЗАСТОСУВАННЯ ГЛИБОКОГО РОЗПУШЕННЯ ПРИ ВИРОЩУВАННІ РИСУ

Ph.D. Eng. Lukianchuk O.P. [*1)], Prof. Ph.D. Eng. Turcheniuk V.O. [1)], Ph.D. Eng. Prykhodko N.V. [1)], Ph.D. Eng., Volk P.P. [1)], Prof. Ph.D. Eng. Rokochinskiy A.M. [1)],
[1)] National University of Water and Environmental Engineering, Rivne / Ukraine
E-mail: o.p.lukyanchuk@nuwm.edu.ua

Keywords: *deep loosening, rice cultivation, soil density, filtration.*

ABSTRACT

It is ascertained that the issue of ecological rational use of water and land resources in the cultivation of rice determines the need for differentiation of the degree of soil drainage, which involves the direction and intensity of soil processes. It is substantiated that one of the expedient measures is the deep loosening of rice field's soils. Possible approaches to improving, constructing and implementing effective deep loosening tools are suggested. Research and production research was carried out on the basis of Liskovsky rice irrigation system in the Odessa region (Ukraine), the soil conditions of which are typical for most of the Danube rice irrigation systems. It is substantiated that a most effective measure in the cultivation of rice is the implementation of a continuous deep loosening by a long-range deep-thrower of a new type, the application of which reduces the density and increases the permeability of the soil, respectively, by 1.26 and 4.45 times. Due to the corresponding structure of loose soil, this leads to a significant improvement of the water-physical properties of the soils, increasing their filtration capacity throughout the area of fields in grown rice, increasing the accumulation capacity of the aeration zone for the accompanying crops.

РЕЗЮМЕ

Визначено, що питання екологічного раціонального використання водних і земельних ресурсів при вирощуванні рису визначає необхідність диференціації ступеня дренованості ґрунту, з яким пов'язана направленість і інтенсивність ґрунтових процесів. Визначено, що одним з доцільних заходів при цьому є глибоке розпушення ґрунтів рисових чеків. Запропоновано можливі підходи щодо удосконалення та застосування ефективних засобів глибокого розпушення. Дослідно-виробничі дослідження було виконано на базі Лісковської рисової зрошувальної системи в Одеській області (Україна), ґрунтові умови якої є характерними для більшості Придунайських рисових зрошувальних систем. Обґрунтовано, що найбільш ефективним заходом при вирощуванні рису є здійснення суцільного глибокого розпушення ярусним глибокорозпушувачем нового типу, застосування якого через зменшення щільності та збільшення водопроникності ґрунту, відповідно, в 1,26 і 4,45 рази, за рахунок відповідної структури розпушеного ґрунту, призводить до суттєвого покращення водно-фізичних властивостей ґрунтів, підвищення їх фільтраційної здатності за всією площею чеків при вирощувані рису, підвищення акумулюючої здатності зони аерації для супутніх культур.

INTRODUCTION

In the modern world, environmental problems are becoming increasingly acute due to intensive man-made use of water and land resources (*Hamzaa M.A., Anderson W.K., 2005, Iglesias A., Garrote L., 2015, Ward P.R., Flower K.C., Cordingley N. and others, 2012*). In particular, this applies to the environmentally sound use of water and land resources of rice irrigation systems (RIS).

The ecological-improvement state of RIS is determined by a number of factors, the main ones being natural (climatic) and technological. The most significant influence on the ecological and improvement state of the RIS is carried out by groundwater, the regime of which in rice systems is determined by the intensity and direction of filtration processes occurring in the course of prolonged excessive moisture of soils and leads to a decrease in their fertility. (*Shunsaku Nishiuchi, Takaki Yamauchi and others, 2012, Stashuk V.A., Rokochynskyi A.M. and others, 2016, Ward P.R., Flower K.C., Cordingley N and others, 2012*).

With modern changes in climatic conditions, in particular, with changes in the number and timing of precipitation, temperature conditions, it is necessary to modify the implementation of existing technologies of water regeneration of fertile soils RIS (*Iglesias A., Garrote L., 2015, Shunsaku Nishiuchi, Takaki Yamauchi and others, 2012*).

The study and analysis of research data at the Danube RIS in the Odessa region during the 50 years since the 60s of the last century enabled to identify some technological disadvantages in the rice cultivation. Studies have shown that the most favourable salt, temperature and water-air regime is created only along drainage and discharge canals. In a 50 m wide strip along irrigation channels of different order, there is an outflow of groundwater, the temperature of which is lower, and the mineralization is much higher than the irrigation water. This leads to a deterioration of the temperature and salt regime of the upper horizons of soils and, consequently, to a decrease by 5 ... 10%, and in saline lands up to 30% of rice yield as the leading crop. Similar conditions are created in a strip of 30 m wide in the lower field, if the field mark next to it is higher by 0.3 ... 0.6 m. The yield of rice in this strip is 10 ... 30% lower than the average one by field (Fig. 1) (*Stashuk V.A., Rokochynskyi A.M. and others, 2016*).

Active filtering when flooding a field takes place only on the smaller part of the area (about 1/3), which adjoins directly to the drainage and discharge canal. The size of the groundwater outflow zone is about 10-15 m, the active filtration zone is 20 ... 30 m, the rest of the rice field (60 ... 160 m) is a stagnant zone. The yield of rice in a strip with a small filtration is 25 ... 35% lower than the average on a field (Fig. 2) (*Stashuk V.A., Rokochynskyi A.M. and others, 2016*).

This necessitates the improvement of its design in order to increase drainage capacity over the area of the rice field and the soil profile.

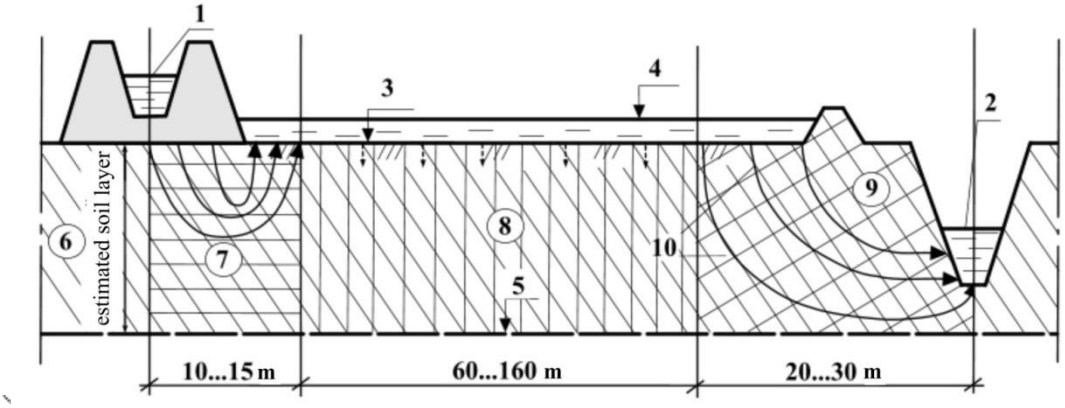

Fig. 1. Scheme of forming characteristic filtration zones on the profile of a rice field**:**

1 – field's irrigation canal; 2 – field's drainage and discharge canal; 3 − soil surface; 4 − water surface; 5 − boundary of the estimated soil layer; 6 − estimated soil layer; 7 − zone of groundwater outflow; 8 − stagnant zone; 9 − active filtration zone; 10 − filtration streams movement direction lines.

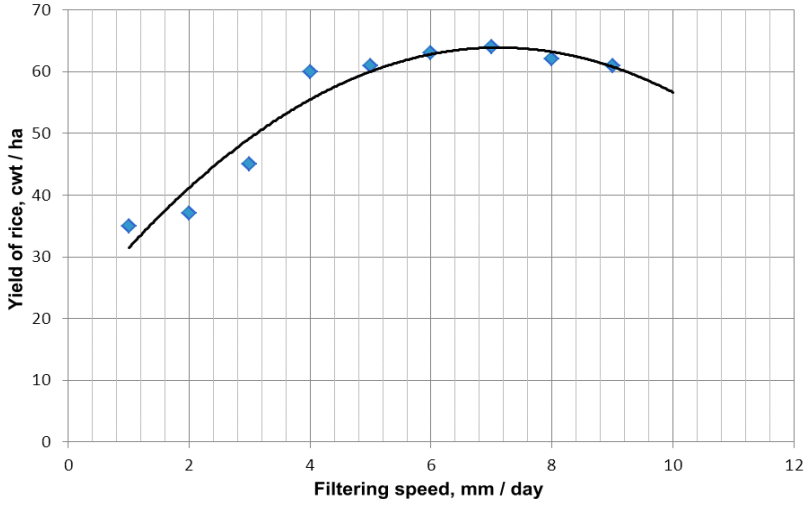

Fig. 2 - Dependence of the rice yield on the rate of filtration from the field's surface during the vegetative season

In conditions of rice systems, increasing the filtering of rice fields may be achieved by arranging a systematic internal closed drainage. This measure is quite effective, but its implementation requires significant investments. Therefore, taking into account the current market conditions, there is a need to find alternative and more economical ways of solving this issue.

One of the most effective measures to increase drainage on the RIS can be the deep loosening of the soil of rice fields.

Execution of deep loosening of the cover layer of soil, which in the conditions of RIS is practically water resistance (*Hamzaa M.A., Anderson W.K., 2005*), will affect the change of its water and physical characteristics, will increase its water permeability, the uniformity of filtration in the area of the field, the accumulation of moisture in the cultivation of related crops.

The technology of deep loosening can be slit, striped and solid. Depending on the principle of action and design features, deep-rippers are divided into two groups: active and passive working equipment (*Pyvovar V., 2011*).

In practice, widespread passive deep-rippers were acquired. They are reliable, simple in design and in operation, but require more powerful tractors (*Kravets S.V., Skobluk M.P. and others, 2018, Mikchail Laziuta, Bajan Kabulova, Chalit Gasanov, 2013*).

In many countries, tools that are very simple in design and reliable in operation, including a frame on the support wheels with several ripping or slit-cutting working elements installed on it are used for deep loosening. The working element of the deep loosening device consists of a straight or curved support, on which a flat or shaped chisel is attached. To increase the loosening area, additional expanders are fixed on the supports (*Kravets S.V., Skobluk M.P. and others, 2018, Gavrysh V.S., Tkachuk V.F. and others, 2013*).

The traditional support pattern deep loosening devices (of type RU-45, RG-0.8A, RNT 0.8A, and others) and their contemporary counterparts do not fully meet the quality criteria for loosening without applying additional soil cultivation due to their design features. The main disadvantage of such deep loosening means is the lack of the guided differentiation of the soil loosening quality in depth, which is very important for obtaining a favourable water-physical state of the soil (*Rokochynskyi A.M. Lukyanchuk O.P. and others, 2017; Rokochynskyi A.M., Lukyanchuk O.P., Volk P.P., 2017, Rokochynskyi A.M., Stashuk V.A. and others, 2011*).

A more progressive in this regard is the construction of a multistage loosening device of a new type (*Tkachuk V.F., Lukyanchuk O.P., Ryzhyi O.P., 2011; Lukyanchuk O.P., Ryzhyi O.P., Ihnatiuk R.M., 2017*) (Fig. 4). This technical solution enables to purposefully influence the structure of the soil in each developed horizon and differentiate the degree of its loosening in depth (*Tkachuk V.F., Lukianchuk O.P., Ryzhyi O.P., 2011*).

It is necessary to determine the rational type of deep loosening and technical means of its implementation due to their influence on the filtration and physical characteristics of the soil RIS.

MATERIAL AND METHODS

Research and production research was carried out on the basis of Liskovsky RIS in the Odessa region (Ukraine). Soil conditions are characteristic of most of the Danube RIS (Table 1).

Table 1

The averaged water-physical properties of the soils of Liskovsky RIS

Soil layer, m	Density, t /m^3	Porosity, %	Water permeability, m/day
0…0.2	**1.42**	**46.8**	**0.13**
0.2…0.4	**1.45**	**45.3**	**0.03**
0.4…0.6	**1.34**	**50.9**	**0.16**
0.6…0.8	**1.58**	**43.8**	**0.12**

The permeability of the cover layer of soils (0 ... 60 cm) is quite low and ranges from 0.008 to 0.02 m / day. The top layer, 0.4 ... 0.6 m thick, is the most dense, represented by loams, and below it is a thin (0.3 ... 0.4 m) layer of sandstone. Still below is the sand, which includes a significant amount of dusty fractions, ranging from 1 to 2 m. The sand gradually becomes sandy loam, under which there is a dusty loam which is waterproof.

Study of various technologies and means of deep loosening on water-physical properties of soils and land improvement status and operation of the existing drainage system in general, conducted to the following options:

1 - slit loosening to a depth of 0.6 m with two-tier deep-ripper type RU -45;
2 - strip loosening to a depth of 0.6 m three-tier deep-ripper of a new type with one riser in each tier (Fig. 3);
3 - solid loosening to a depth of 0.6 m two-tier deep-ripper of a new type with three risers in each tier (Fig. 3);
4 - control version without loosening.

The experimental sites were placed in the form of a "Latin square".

The operational equipment of a new type of deep-thrower consists of a frame with variable risers (1 ... 3 pcs in each tier), on which the loosening elements are fixed in the form of the conjugation of the horizontal knife (cutter) with the concave symmetric surface of the variable curvature (Tkachuk V.F., Lukianchuk O.P., 2014). Due to the shape and parameters of this surface, the required deformation together with the degree of stress are assigned, and, consequently, the crushing of the developed layer of soil (Fig. 3) (*Kravets S.V, Kovan'ko V.V., Lukianchuk O.P., 2015; Lukianchuk O.P., Ryzhyi O.P., Ihnatiuk R.M., 2017*).

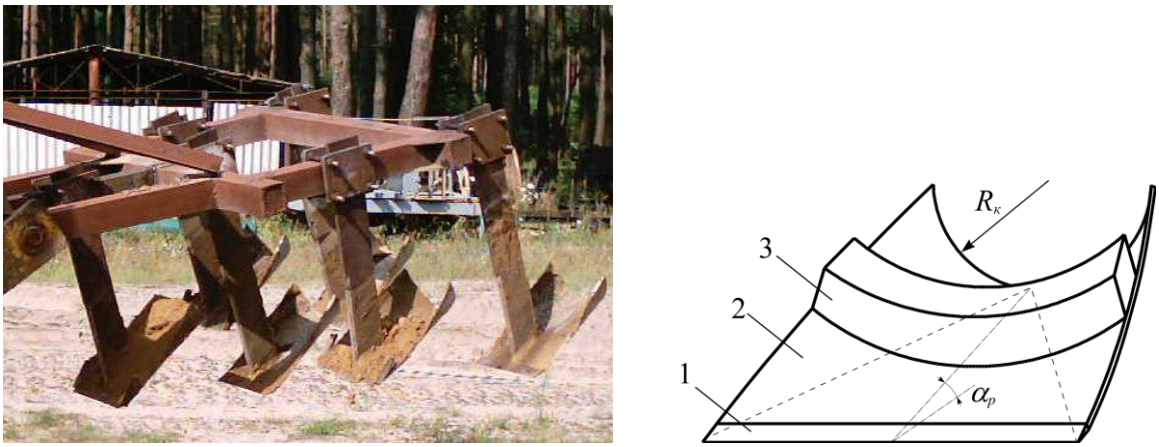

a) b)

Fig. 3. Multi-level deep-ripper for strip and continuous loosening:
a) − a two-tier working equipment; b) − the soil loosening surface: 1 - horizontal knife (cutter), 2 - soil loosening surface, 3 - element of soil chips, $R_к$ − the radius of the end surface curvature, α_p − installation angle.

The choice of a multi-tier deep-ripper of a new type is due to the following. As the practice and acquired agricultural production experience show, the vertical soil profile of the farmland should have an anti-erosion top layer (0 ... 0.05 m), a roots-like layer (0.05 ... 0.4 m) and a lower filtration layer (> 0.4 ... 0.6 m). At the same time, the structure of the soil (percentages by weight of groups of "valuable" and other sizes) of each of these layers should be optimal in accordance with the purpose of each of them (*Gavrysh V.S., Tkachuk V.F. and others, 2013*).

After having been loosened by such a working element, the soil structure is determined by a number of the soil mass grinding stages on the soil loosening surface, and their number, in turn, depends on the value of the surface curvature of each tier (*Tkachuk V.F., Lukianchuk O.P., Melnyk A.V., 2008, Tkachuk V.F., Lukianchuk O.P., Ryzhyi O.P., 2011*). Therefore, it is advisable to make the working equipment of the deep-ripper of 2 ... 4-tier.

In order to determine the working parameters of the new type of deep-throwing loose elements through analytical research, the differentiation and composition of the soil structure in each developed layer was determined and evaluated based on the averaged soil aggregate of loose soil and multiplicity of crushing.

RESULTS

The soil extraction elements with different working parameters have different values of the average soil aggregate and the multiplicity of soil crushing (Table 2, Fig. 4).

Surfaces with various defining parameters have different values of the averaged soil aggregate and the grinding multiplicity of the soil mass. If the value of the averaged soil aggregate has a nearly proportional dependence on the depth of development in the layer and the end radius, then the magnitude of the grinding multiplicity has a rather complex dependence. This difference is due to the fact that the magnitude of the crushing multiplicity is influenced by the width of the soil loosening surface, the value of which, in the

calculation, is variable. It does not affect the magnitude of the formed aggregates. The most effective soil crushing, taking into account the size of the averaged soil aggregate, occurs at a depth of 150 mm and an end radius of 150 mm, and the least effective − at a development depth of 150 mm and an end radius of 200 mm.

Table 3

Results of the soil grinding structure analytical study

Initial parameters		Structure of loosened soil, $l_к$							Grinding multiplicity of the soil initial volume
Tier height, $h_к$, mm	End radius of the surface, $R_к$, mm	Dimensions of formed soil aggregates	<5 mm	5–10 mm	10–25 mm	25–50 mm	>50 mm	Averaged soil aggregate, mm	
100	150	Pcs,%	41.07	24.85	24.12	7.37	2.59	4.92	973
		Capacity,%	2.59	4.28	18.76	33.30	41.07		
	200	Pcs,%	23.37	32.31	31.37	9.59	3.37	5.58	1009
		Capacity,%	1.47	4.33	18.98	33.68	41.54		
	250	Pcs,%	0.00	42.16	40.94	12.51	4.39	6.33	981
		Capacity,%	0.00	4.39	19.26	34.19	42.16		
150	150	Pcs,%	40.44	32.79	15.43	7.26	4.09	5.74	1072
		Capacity,%	1.54	4.39	9.33	19.83	64.90		
	200	Pcs,%	0.00	55.05	25.90	12.19	6.87	7.38	865
		Capacity,%	0.00	4.46	9.48	20.14	65.92		
	250	Pcs,%	0.00	55.05	25.90	12.19	6.87	7.38	1081
		Capacity,%	0.00	4.46	9.48	20.14	65.92		
200	150	Pcs,%	40.23	32.62	15.35	7.22	4.59	6.75	1034
		Capacity,%	1.19	3.40	7.22	15.35	72.84		
	200	Pcs,%	22.75	42.15	19.83	9.33	5.93	7.65	1072
		Capacity,%	0.67	3.42	7.26	15.43	73.23		
	250	Pcs,%	0.00	54.57	25.67	12.08	7.68	8.68	1043
		Capacity,%	0.00	3.44	7.31	15.53	73.72		

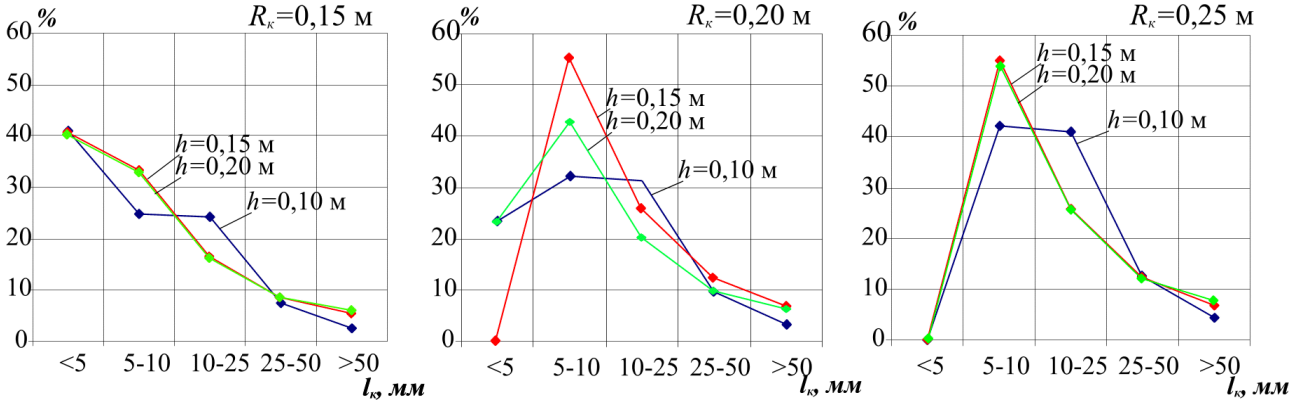

Fig. 4. The structure of loose soil by the number of soil aggregates

$h_к$ - tier height, mm; $R_к$ - the radius of the end surface curvature, mm; $l_к$ - soil aggregates, mm

From fig. 4, it results that in order to loosen the anti-erosion top layer (0 ... 0.05 m), it is expedient to use working surfaces with a finite radius of about 200 mm, for a roots-containing layer (0.05 ... 0.4 m) with a finite radius of about 150 mm, for the lower filtration layers (> 0.4 ... 0.6 m) with a finite radius of about 250 mm.

A generalized comparative characteristic of the main indicators values of water and physical properties in a 0.6 m layer of rice systems irrigated soils depending on different types and variants of their loosening and averaged in time (after the effect term) and space (by the soil profile) are given in Table 3.

Table 3

Comparative characteristic of water and physical properties of 0.6 m soil layer in terms of loosening variants

Indicators / Variants of loosening	Density, t /m³			Porosity, %			Water permeability, m/day		
	abs value	Deviation from control		abs value.	Deviation from control		abs value.	Deviation from control	
		t /m³	%		t /m³	%		t /m³	%
Without loosening (control)	1.45	–	–	42.2	–	–	0.12	–	–
Slit loosening	1.41	0.04	2.9	46.1	3.9	9.2	0.25	0.13	206
Strip loosening	1.32	0.13	8.9	47.3	5.1	12	0.36	0.24	296
Continuous loosening	1.15	0.30	21	54.9	12.7	30	0.53	0.41	443

For all types of loosening there was decreased density and increased permeability. The most effective in this regard was the continuous loosening, with density and permeability changed by 1.26 and 4.45 times respectively.

The results of the experiment were introduced into previously obtained mathematical models of crop yield dependence on ground conditions characteristics (*Stashuk V.A., Rokochynskyi A.M. and others, 2016*). By means of machine experiment, predicted values of crop yields of rice crop rotation for several years with different variants of deep loosening are shown in Table 4.

Table 4

Estimated crop yields of rice crop rotation in terms of loosening variants

No b/o	Loosening variants	Crops	Crop yields in estimated years,%					Predicted crop yields, cwt/ha
			10	30	50	70	90	
1	Without loosening (control)	Rice	32.0	34.0	36.0	38.0	40.0	35.9
		Perennial grasses	240.0	220.0	210.0	180.0	160.0	203.0
		Winter cereals	38.0	36.0	32.0	28.0	26.0	31.9
		Rape	20.0	28.0	34.0	36.0	38.0	32.0
		Vegetables	280.0	300.0	340.0	360.0	400.0	339.0
2	Slit loosening	Rice	40.0	52.0	58.0	62.0	64.0	56.0
		Perennial grasses	270.0	250.0	260.0	210.0	190.0	233.0
		Winter cereals	43.5	41.5	37.5	33.5	31.5	36.5
		Rape	24.0	32.0	38.0	40.0	42.0	36.0
		Vegetables	320.0	340.0	380.0	400.0	440.0	379.0
3	Strip loosening	Rice	45.0	57.0	63.0	67.0	69.0	61.0
		Perennial grasses	280.0	260.0	270.0	220.0	200.0	243.0
		Winter cereals	47.5	45.5	41.5	37.5	35.5	40.5
		Rape	29.0	37.0	43.0	45.0	47.0	41.0
		Vegetables	360.0	380.0	420.0	440.0	480.0	419.0
4	Continuous loosening	Rice	49.0	61.0	67.0	71.0	73.0	65.0
		Perennial grasses	295.0	275.0	285.0	235.0	215.0	243.0
		Winter cereals	50.5	48.5	44.5	40.5	38.5	43.5
		Rape	33.0	40.0	47.0	49.0	51.0	45.0
		Vegetables	390.0	420.0	450.0	470.0	510.0	449.0

According to the results presented, the application of deep loosening provides the following increase in crop yields: slit − 5...10%; strip − 10…20%; continuous − 20...40%.

The results presented in relation to the predicted values of rice crop rotation, crop yields adequately reflect the achieved degree of improving conditions of plants cultivation in terms of the variants of rice systems soils deep loosening.

The obtained results and their dynamics are in good agreement with the results obtained earlier from similar 3-year studies of field trials for various technologies and means of deep loosening on the reclaimed lands of the experimental sites "Uyizdtsi" and "Pechalivka" in the Rivne region (Ukraine) (Gavrysh V.S., Tkachuk V.F. and others, 2013, Rokochynskyi A.M., Lukianchuk O.P. and others, 2017).

CONCLUSIONS

Deep loosening is one of the expedient alternative measures for increasing the efficiency of RIS. It has a positive effect on the increase in yield due to improving the water-physical properties of irrigated soils, increasing their overall moisture content by increasing the accumulation capacity of loose soil.

In the rice field, deep loosening provides the required uniformity and intensity of filtration, ensures uniform filtration by area and profile, and enhances the drainage of the rice field as a whole.

In periods of overflow, deep loosening contributes to accelerated release of the arable layer from excess moisture during rice cultivation, accelerating its movement in the lower layers, and in the dry season deep loosening contributes to the accumulation of moisture due to the high accumulation capacity of loosened soil.

The effectiveness of the drainage system improves and the opportunity to increase the distance between the drains increases, which in turn enables to reduce the specific investments in the RIS construction and reconstruction projects.

The investigated technologies and deep loosening means of rice systems irrigated soils mainly have a positive effect on the change of soil water-physical properties, moisture content during vegetation periods and crop depending on the type of cultivated crops.

In general, the most effective measure for rice cultivation is the implementation of a continuous deep loosening by a new type of deep-ripper, the use of which, due to a decrease in the density and increase in permeability of the soil, respectively, by 1.26 and 4.45 times, due to the corresponding structure of loose soil, leads to significant improvement of soil water-physical properties, increase their filtration ability throughout the area of fields in grown rice, increase the accumulation capacity of the aeration zone for the accompanying crops.

REFERENCES

[1] Hamzaa M.A., Anderson W.K., (2005), Soil compaction in cropping systems: A review of the nature, causes and possible solutions. *Soil and Tillage Research*. Volume 82, Issue 2,, pp. 121-145. Netherlands;

[2] Iglesias A., Garrote L., (2015), Adaptation strategies for agricultural water management under climate change in Europe, *Agricultural Water Management*, Volume 155, pp. 113-124. Netherlands;

[3] Gavrysh V.S., Tkachuk V.F. and others, (2013), *Scientific and methodical recommendations for applying deep loosening on drained mineral soils of the Western Polissia of Ukraine* (*Науково-методичні рекомендації до застосування глибокого розпушення на осушуваних мінеральних ґрунтах Західного Полісся України*), 46 p., Rivne/Ukraine;

[4] Kravets S.V, Kovan'ko V.V., Lukianchuk O.P., (2015), *Scientific bases of creation of earth-tiered cars and underground-moving devices*, NUWMNRU (НУВГП), 322 p., Rivne/Ukraine;

[5] Kravets S.V., Skobluk M.P. and others, (2018), *Critical-pitched two-level soil rippers (scientific basis of creation)*: Monograph, According to the general edition of S.V. Kravets - Rivne: NUWEE, 235 p. ISBN 978-966-327-384-6., Rivne/Ukraine;

[6] Laziuta M., Kabulova B, Gasanov C, (2013), Research of soil tillage by advanced design slit ripper. Agricultural Engineering. *Research papers*, , Vol. 45, No.2. Policy, Vol. 59, pp.152-164. United States;

[7] Lukianchuk O.P., Ryzhyi O.P., Ihnatiuk R.M., (2017), Design of a tiered operating unit for deep differentiated tillage. *Scientific Bulletin of the National Mining University*, Issue 4, pp.43-48, Dnipro/Ukraine;

[8] Pyvovar V., (2011), Deep rippers. Information and analytical newspaper Agrobusiness today. Mechanization of AIC, *http://agro-business.com.ua/agro/mekhanizatsiia-apk/ item/847-hlybokorozpushuvachi.html, Ukraine*;

[9] Rokochynskyi A.M., Lukianchuk O.P. and others, (2017), Restoration of the ecological potential of the drained lands on the basis of the use of an agro-ameliorative multi-tier deep loosener, *Collection of works of the first international ecological forum "Healthy Environment - the Basis for Regional Security*", Volume II, - pp. 262-268., Ryazan/Russian Federation;

[10] Shunsaku Nishiuchi, Takaki Yamauchi and others, (2012), Mechanism for coping with submergence and waterlogging in rice. Rice (N Y); 5 (1): 2. Published online on Feb. 27, *doi: 10.1186/1939-8433-5-2*, New York/United States;

[11] Stashuk V.A., Rokochynskyi A.M. and others, (2016), Rice of the Danube area: collective monograph. Gryn' D.S. 638 p., Kherson/Ukraine;

[12] Tkachuk V.F., Lukianchuk O.P., (2014), *Working element of the loosener-soil structurer (Робочий орган розпушувача-оструктурювача)*, Patent 104774 Ukraine;

[13] Tkachuk V.F., Lukianchuk O.P., Melnyk A.V., (2008), Model of grinding chunks of soil on the soil surface curvature working ripper, *Reporter of National University of Water Management and Nature Resource Use. Collection of Scientific Works. Technical sciences*, Issue 2 (42), Part 1, ISSN 2306-5475, pp. 374-380, Rivne/Ukraine;

[14] Tkachuk V.F., Lukianchuk O.P., Ryzhyi O.P., (2011), *Agro-ameliorative multilayered deep loosening means*, NUWMNRU (НУВГП), −190 p., Rivne/Ukraine;

[15] Ward P.R., Flower K.C., Cordingley N and others, (2012), Soil water balance with cover crops and conservation agriculture in a Mediterranean climate. *Field Crops Research.* Volume 132, 14 June 2012, pp 33-39. Netherlands.

INNOVATIVE TECHNOLOGIES OF OILSEED FLAX STRAW MECHANICAL PROCESSING AND QUALITY OF OBTAINED FIBERS

/

ІННОВАЦІЙНІ ТЕХНОЛОГІЇ МЕХАНІЧНОЇ ПЕРЕРОБКИ СТЕБЕЛ ЛЬОНУ ОЛІЙНОГО ТА ЯКІСТЬ ОДЕРЖАНИХ ВОЛОКОН

Prof. Ph.D. Eng. Chursina L. [1], Prof. Ph.D. Eng. Tikhosova H.[1], Ph.D. Assoc. prof. Holovenko T. [2], PhD. Assoc. prof. Shovkomud O. [2], PhD. deputy director Kniaziev O. [3], Ph.D., Assoc. prof Yanyuk T.[4]

[1] Kherson National Technical University, Faculty of Integrated Technologies, Kherson / Ukraine;

[2]Lutsk National Technical University, Faculty of Biotechnical Systems Engineering, Lutsk / Ukraine;

[3] State enterprise «Research farm «Askaniisky» Askaniyskaya state agricultural research station of the Institute of Irrigated Agriculture of the National Academy of Agrarian Sciences of Ukraine, Kherson / Ukraine;

[4] National University of Food Technologies, Educational and Scientific Institute of Food Technologies, Kiev / Ukraine

Tel: +38 (050) 85-534-80; E-mail: tanyushkagolovenko@ukr.net

Keywords: *oilseed flax, straw, mechanical processing, tow-preparation, combers, technical specifications.*

ABSTRACT

The article presents scientific and practical achievements in creating innovative mechanical technologies for oilseed flax straw processing. As a result of systematic research by scientists of Kherson National Technical University, the technology and equipment for mechanical processing of oilseed flax retted straw based on modernization of existing equipment is proposed. As a result, at certain stages of mechanical processing of the retted straw, oil flax fibre with different physical and mechanical characteristics was obtained, which is suitable for use in various industries.

Due to the absence of standards for products of oilseed flax straw in Ukraine and in the world, the technical specifications TU U 01.1-2303511525 - 001:2016 "Oilseed flax straw. Specifications" and TU U 01.1-05480298 - 001:2017 "Oilseed flax retted straw. Specifications" were developed and registered in the State enterprise "Khersonstandardmetrology". This will allow analyzing this industrial raw material, determining the feasibility of mechanical processing and the quality level of fibre as finished product.

РЕЗЮМЕ

У статті представлені наукові та практичні досягнення в створенні інноваційної технології механічної переробки стебел льону олійного. В результаті систематичних досліджень вченими Херсонського національного технічного університету було запропоновано технології і устаткування для поглибленої механічної обробки трести льону олійного на основі модернізації існуючого обладнання. В результаті чого, на певних стадіях механічної обробки трести, одержується волокно льону олійного з різними фізико-механічними характеристиками, яке придатне для використання в різних галузях промисловості.

У зв'язку з відсутністю як в Україні, так і в світі в цілому стандартів на продукцію зі стебел льону олійного були розроблені і зареєстровані в державному підприємстві "Херсонстандартметрологія" технічні умови ТУ У 01.1- 2303511525 – 001:2016 «Солома льону олійного. Технічні умови» та ТУ У 01.1-05480298-001: 2017 «Треста льону олійного. Технічні умови». Це дозволити оцінювати дану промислову сировину, визначати доцільність її механічної переробки та рівень якості готової продукції - волокон.

INTRODUCTION

According to the analysts of Oil World the largest cropped areas of oilseed flax are concentrated in Canada (about 2 million hectares), Argentina (101 thousand hectares), China (570 thousand hectares), India (930 thousand hectares), Great Britain (101 thousand hectares), the USA (135,17 thousand hectares), Germany (110,048 thousand hectares). Such countries as Finland, Poland, France, Belgium and Belarus (2.5 thousand hectares) have begun to cultivate this crop recently (Saskatchewan Flax Development Commission, 2015). Ukraine is not an exception. If in 2008, the crop sown area in Ukraine amounted to 19.3 thousand hectares (State Statistics Service of Ukraine, 2016), in 2016 it amounted to 66.8 hectares and in 2018 to 32.1 hectares (fig.1).

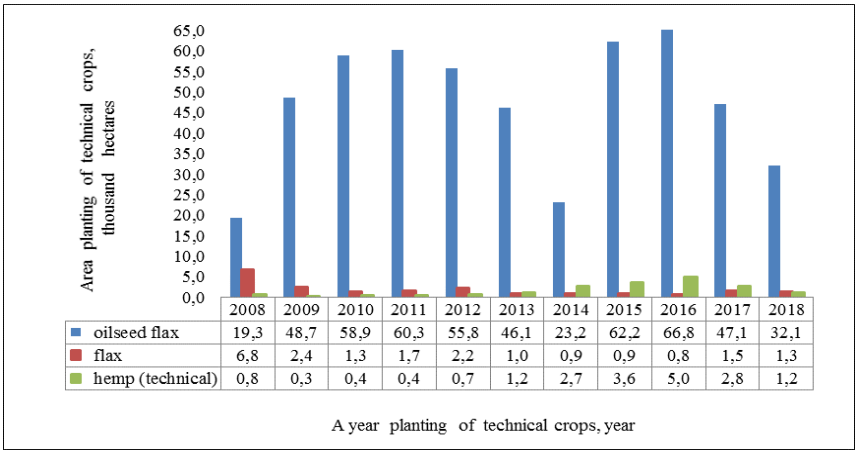

	2008	2009	2010	2011	2012	2013	2014	2015	2016	2017	2018
oilseed flax	19,3	48,7	58,9	60,3	55,8	46,1	23,2	62,2	66,8	47,1	32,1
flax	6,8	2,4	1,3	1,7	2,2	1,0	0,9	0,9	0,8	1,5	1,3
hemp (technical)	0,8	0,3	0,4	0,4	0,7	1,2	2,7	3,6	5,0	2,8	1,2

Fig. 1 - Dynamics of cropped areas of technical crops grown on the territory of Ukraine from 2008 to 2018 (State Statistics Service of Ukraine, 2016)

The rapid increase in this crop acreage is explained by the fact that flax seeds, which contain 48% of oil, is of great demand in the world nowadays. It is widely used in food, pharmaceutical and paint industries. The cost of flax seeds for super elite is $4 000-3 500 per ton and that of commodity seeds is $800-500 per ton.

World experience in using oilseed flax straw shows that it has a wide range of applications. It is due to the fact that oilseed flax stems, as well as the common flax stems, contain cellulose fibres in bast part *(Zhyvetyn V.V. et al., 2000)*. However, oilseed flax straw is not used in Ukraine. Every year a large amount oilseed flax straw, namely about 64,000 tons is burned after harvesting flax seeds causing great harm to the environment and being accompanied by large penalties for farms that grow oilseed flax. However almost 25 600 tons of fibre and 19,200 tons of cellulose for textile, pulp and paper production in Ukraine are wasted. With this amount of straw 38,400 tons of shives for producing biofuel, fireplace wood and building materials can be obtained *(Tihosova A.A. et al., 2010)*.

In the world practice, flax straw burning becomes history and oilseed flax is regarded not only as a seed production crop, but also as a cost-effective supplementary textile raw material. In Ukraine, oilseed flax is the only domestic raw material, which can be an alternative to imported cotton and flax fibre for use in the textile, pulp and paper industries and the production of reinforced composite materials. Not rational use of oilseed flax stems in Ukraine is primarily connected with the lack of technological process of mechanical processing of oilseed flax retted straw.

Oilseed flax retted straw as opposed to linen retted straw suitable for obtaining long fibre, is a matted and differently directed mass of fibres with shives, among which there are a lot of whole stems no longer than 40 cm. Combination of short stems and fibres of different length in the oilseed flax retted straw defines a similar processing of it with unconditioned low-grade retted straw of common flax for using traditional technology for processing on tow-preparation aggregates of known brands: TPAL (Tow-Preparation Aggregates of Linen fibre), ASLF-1 (Aggregate of Short Linen Fibre), ASLF-1-01 (Aggregate of Short Linen Fibre) and their foreign counterpart firms "Charle", "Laroche", "Temafa", etc.

On the basis of the study of physical and mechanical properties of oilseed flax straw stems and their change after combine harvesting we can conclude that mechanical technology of processing oilseed flax retted straw should be similar to the technology of getting the single type linen fibre and unconditioned low-grade retted straw of common flax, taking into account morphological features and anatomical structure of oilseed flax stems.

MATERIALS AND METHODS

At present, the theoretical foundations of mechanical processing of unconditioned low-grade retted straw of common flax are developed by Ipatov A. *(Ipatov A., 1989)*. The technology of getting single type linen fibres was introduced by the Central Research Institute of bast fibres by Derbenev A. *(Derbenev A., 1983)* and the Institute of bast crops of the National Academy of Agrarian Sciences of Ukraine by Hilyazetdinov R. *(Helyazetdinov R., 2009)*.

According to the technology of the Institute of bast crops of NAAS of Ukraine, unlike existing tow-preparation aggregates a new construction of the breaker rollers stripping type is proposed and instead of the stripping part the construction of the stripping-combing aggregate is developed. Under the new technological scheme the pre-production model of the aggregate for getting the single type fibre of common flax is manufactured (figure 2).

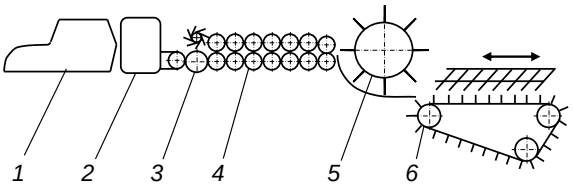

Fig. 2 - The basic technological scheme of the aggregate for selecting the single type flax fibres

1 - machine for unwinding rolls, 2 - drying machine, 3 – layer-forming machine, 4 – breaking part, 5 - stripping part, 6 – tow-shaking part (Helyazetdinov R., 2009)

Despite the fact that these developments would be important to determine the technologies and equipment for processing the oilseed flax stems, now there is no serial production of such equipment. Furthermore, the fibre obtained by this technology is chaffy (it contains 37-40% unseparated and bulk wood), which limits the scope of its use.

Well-known works on purification and separation of oilseed flax fibre is performed by Rome Research Centre (Istituto Poligrafico e Zecca dello Stato) in Italy *(Assirelli A. et al., 1997)*. Figure 3 shows the scheme of oilseed flax stems processing according to the technology developed by IPZS.

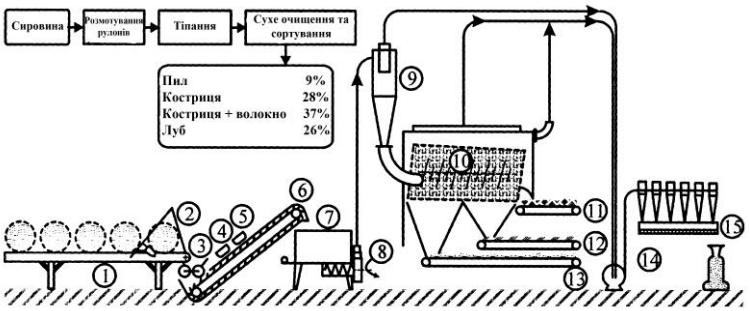

Fig. 3 - Scheme of oilseed flax stems processing to obtain cellulose

1 – round bales conveyor, 2 – "Gemelli" blades, 3 – cylinder press, 4 - metal detector, 5-metal extractor, 6-transporter, 7 - vertical stripping machine, 8 - fan with dryer, 9-cyclone, 10-cylinder separator, 11 - conveyor for bast fibre, 12 - conveyor for shives and bast, 13 - conveyor for shives, 14 - a fan with heating, 15 - transport of dust (Assirelli A. et al., 1997)

Under this scheme, stems are processed on a vertical stripping machine (7) and purified in the cylinder separators (10). Yet, buying this line in Italy would cause large additional foreign exchange costs.

In the works of scientists of Kostroma State Technological University (Russia), *Pashin E.* and *Fedosova N.*, there are only schemes of processing of oilseed flax straw stems, but the mechanism of separating shives is not developed, which is a major technological operation of mechanical processing *(Pashin E. et al., 2003)*. Thus, the question on what equipment can be used for mechanical processing of oilseed flax retted straw, its parameters and operation modes remains open. Therefore, in this paper, the technology of processing unconditioned low-grade retted straw of common flax, which may be analogous to the new technology for the processing of oilseed flax, was analyzed.

Usually, unconditioned low-grade retted straw of common flax, which is similar to the oilseed flax stem is processed at the typical tow-preparation aggregate TPAL (*Ipatov A., 1989*). The technological scheme is shown in figure 4.

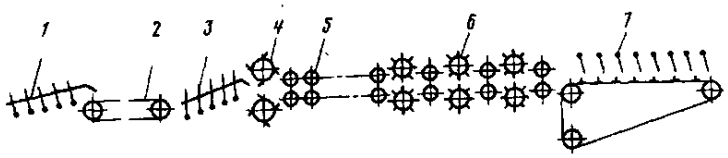

Fig. 4 - Technological scheme of processing unconditioned low-grade retted straw of common flax

1,3,7 – tow-shaking machines, 2 - drying machine, 4 - layer-forming machine, 5 - breaking machine, 6 - stripping machine (*Ipatov A., 1989*)

According to scheme 3, the technology of getting linen fibre consists of primary enrichment of tows on the first tow-shaking machine (1), drying in a drying machine (2), shaking on the second tow-shaking machine (3), forming a layer in layer-forming mechanism (4), breaking in a breaking machine (5), stripping in a stripping machine (6), and final cleaning on the third tow-shaking machine (7).

Systematic research of Kherson National Technical University revealed significant differences of physical and mechanical properties of oilseed flax stems *(Tikhosova H. et al., 2010)*. As a result, it outlined significant heterogeneity of stems:

- in thickness: the ratio of diameters of basal and vertex parts of stems varies between 1.3-4.1 mm.;
- content and hardness of wood: basal and middle parts have a strong connection between the shives and fibre, and the vertex of the stalk, which has a small diameter of a thinner and flexible wood.

Such heterogeneity of stems, connected with difficulties in separation of shives from fibres, causes a significant impact on the results of stem processing, particularly the degree of purity of the obtained fibre product.

Harvesting of oilseed flax is known to be carried out by combine harvester. By this technology stems of the flax group are mowed at a height of 5 cm over the ground, as a result of which, as mentioned before, they have an average length of stems of not more than 40 cm. In addition, approximately 30% of this length is an inflorescence with large amount of thin branches. Therefore, middle and vertex parts of the stems are entered to the processing. These stems are not able to get in the stripping machines clamp conveyors in the first and second sections of breaking-stripping aggregates BSA. Therefore, the relevant task today is to create a new technological line for processing oilseed flax stems.

- **Experimental part**

Scientists of Kherson National Technical University proposed the technology and equipment for mechanical processing of oilseed flax retted straw on the basis of modernization of existing equipment. For this purpose, on the experimental technological line of TPAL, the stripping part was replaced by two sections of stripping machines "Charle". This was done considering the peculiarities of technological properties of oilseed flax stems to prevent the formation of fibres winds on stripping drums, fibre breakage, which will increase the intensity of fibre cleaning from shives. General view of the modernized tow-preparation aggregate is shown in figure 5.

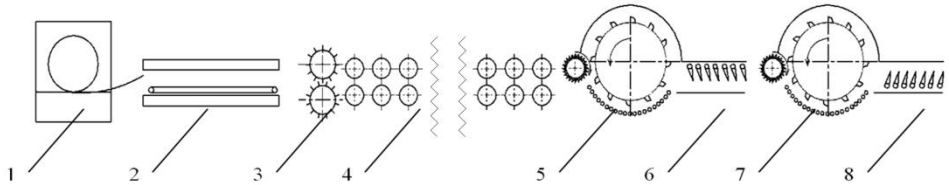

Fig. 5 - Technological scheme of modernized tow-preparation aggregate

1 - machine for unwinding rolls, 2 - drying machine, 3 - nourishing rollers, 4 - breaking machine; 5 - stripping sections of machine «Charle»; 6 – tow-shaking machine with upper ridge field, 7 - stripping sections of machine «Charle»; 8 - tow-shaking machine with the lower ridge field (the author's development)

By the proposed technology of the technological process in comparison with traditional technology (figure 3) tow-shaking machine (1) is excluded. Oilseed flax retted straw after unwinding rolls on the machine for unwinding rolls (1) is sent to a drying machine DCS-10TU1 (Drying Conveyor Steam - 10 Tow Unified) (2). This operation is necessary to increase the distinction of rigidity between fibre and wood, which is achieved by previous drying of oilseed flax retted straw from the moisture of 12-13% to technological moisture of 6-8%. Thus, by changing the moisture in this range, the flexibility and strength of the fibre are slightly decreased and stiffness of shives dramatically increases fact that raises the effectiveness of breaking and stripping impact.

Further, to destroy the connection between fibre and wood in those stems in which it was not broken during laying by nourishing rollers (3), retted straw will be supplied to the breaking machine of tow-preparation aggregate (4), with 19 pairs of breaking rollers that provide a deep breaking of the oilseed flax stems.

Broken flax is fed with the help of feed rollers to stripping sections of machine "Charle" (5), then after the first stripping, fibre is supplied to tow-shaking machine of tow-preparation aggregate with upper ridge field (6) and then to the second stripping sections of machine "Charle" (7).

The process of this raw material stripping as an unconditioned low-grade retted straw of common flax, is designed for intensive separating of shives. The most intensive process of stripping the oilseed flax fibre after breaking is made by using stripping sections of the machine "Charle", in which stripping drum has a diameter of 120 cm, with 12 beating planks. Depending on the fibres quality, with the help of leverage the gaps between the knives and beating planks of stripping drum are controlled.

Final operation on the modernized tow-preparation aggregate is on the tow-shaking machine with the lower ridge field (8), which is used for final cleaning of fibre from shives.

Despite the possibility of regulating the process of tow-preparation, obtained by this technology, fibre contains a large amount of shives, over 28-31%, so this fibre is not suitable for using in textile, pharmaceutical, paper industries and for production of composite materials. After all, for the use in the paper industry, it is required that the fibre has chaffiness of 0.2%, in textile industry the chaffiness should not exceed 1.5%, in the pharmaceutical industry - 0.5%, and for the production of composite materials it must be 0%. At the same time, previous studies show that oilseed flax fibre contains 70% cellulose by fibre length and the form of elementary fibres on the microscopic sections, it is close to cotton. Thus, in case of proper processing it is possible to use it instead of cotton fibres, in its blends and to obtain cellulose *(Tihosova A.A. et al., 2010).*

Therefore, to expand the scope of applications of the oilseed flax fibre it is proposed to use the following technological line and equipment for deep mechanical processing of the oilseed flax retted straw (figure 6).

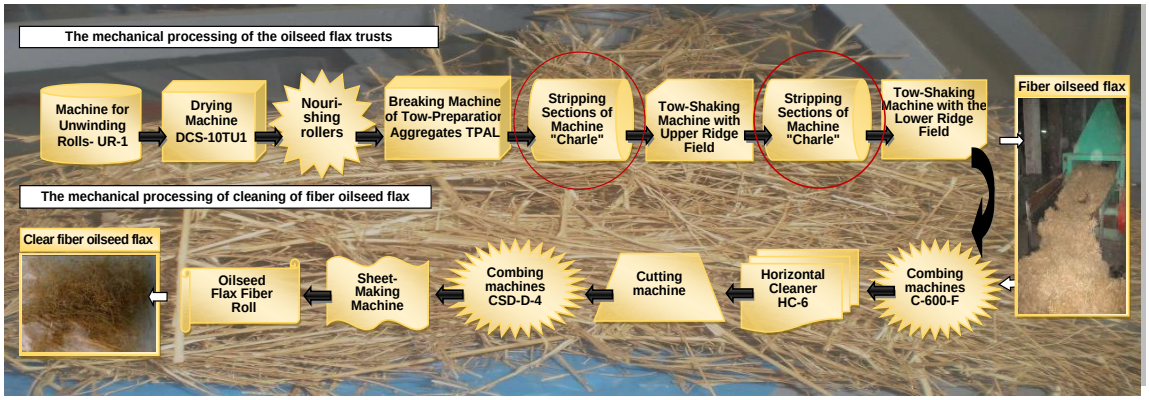

Fig. 6 - Technological line for obtaining the cleaned fibre from the oilseed flax retted straw (the author's development)

For a complete cleaning of oilseed flax fibre the major technological operation is the process of carding on combers of hard and fine carding such as brand C-600-F (Comberss-600-Flax) and CSD-D-4 (Comberss Smallest Double-Drum-4). Optimal operation modes of individual components of this aggregate were identified in the works by Lytvyn Z., Valko N., Kobyakov S. and Meshkov Yu. *(Lytvyn Z., 2000; Valko N. 2002; Kobyakov S., 1993; Mieshkov Yu., 2007)*. Therefore, optimization of technological operation modes of modernized tow-preparation aggregate was not performed.

RESULTS

As a result of processing the oilseed flax retted straw by all technological transitions, according to the technology, presented in figure 5, after a double combing, the fibre was obtained. Fibre distribution according to length is shown in figure 7 and in the form of diagram (figure 8).

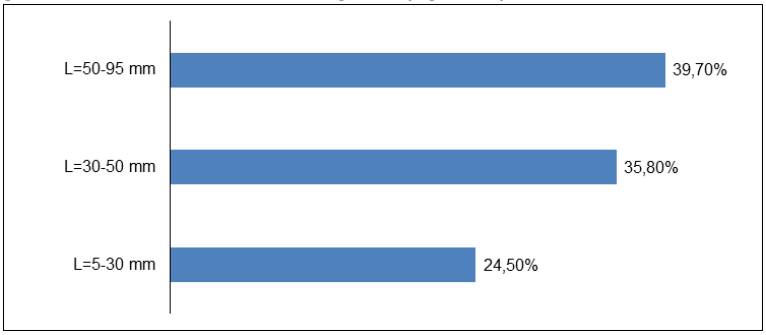

Fig. 7 - Percentage of distribution of oilseed flax fibres by length after processing within all technological cycles

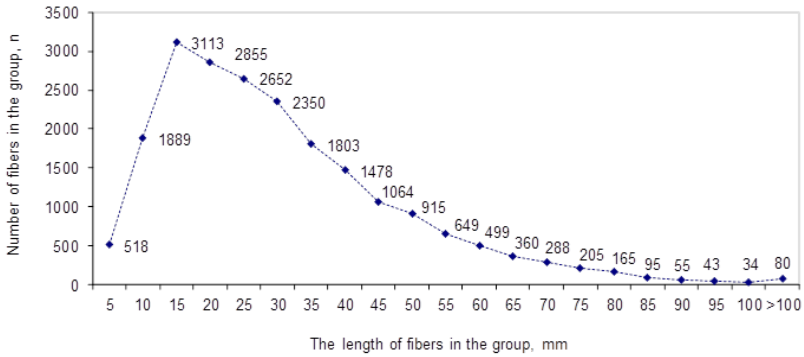

Fig. 8 - Distribution of oilseed flax fibre by length in each group

The results show that the fibre content suitable for processing in conditions of cotton textile production is 35.80 %, in which the length of fibres is from 30 to 50 mm, and the percentage of fibres suitable for processing in cellulose production, where fibre length is in from 5 to 30 mm, is 24.49%. The share of fibres, suitable for wool processing, is 39.71%, with the length of fibres ranging from 50 to 80 mm. The result of production tests of the shives content in fibre, obtained after each cycle of treatment, was analyzed. The shives content after processing on tow-preparation aggregate equals 23.0 – 25.5%. The shives content after processing on combers C-600-F equals 7.5 – 8.6% and after processing on the machines of fine carding CSD-D-4 after the double combing, the shives content was 0.05-1.0%.

As a result of analysis of the fibre quality it was found that processing of oilseed flax retted straw by the developed technological process of the mechanical processing, according to figure 5, allows obtaining fibres with high technological characteristics that can be recommended to be used in various fields of industrial production. Under manufacturing and laboratory conditions, the samples of innovative products from oilseed flax have been obtained. Namely, it is the mixed yarn: oilseed flax-cotton, oilseed flax-polyethylene terephthalate (lavsan), oilseed flax-wool, oilseed flax-capron (LLC "Boguslaw Textile", Kiev region) *(Boiko G., 2014)*, composites (SE "Plastmass" LLC "TD Plastmass-Priluki", Chernihiv region.) semi-finished cellulose materials, non-woven fabrics (JSC "Flax processing mill Starosamborskyi», Lviv region.) *(Holovenko T., 2014)* and filter paper (LLP "Tsyurupinsk pulp and paper mill", Kherson region.) *(Putintseva S., 2015)*. Schematic representation of laboratory samples of innovative products is given in figure 9.

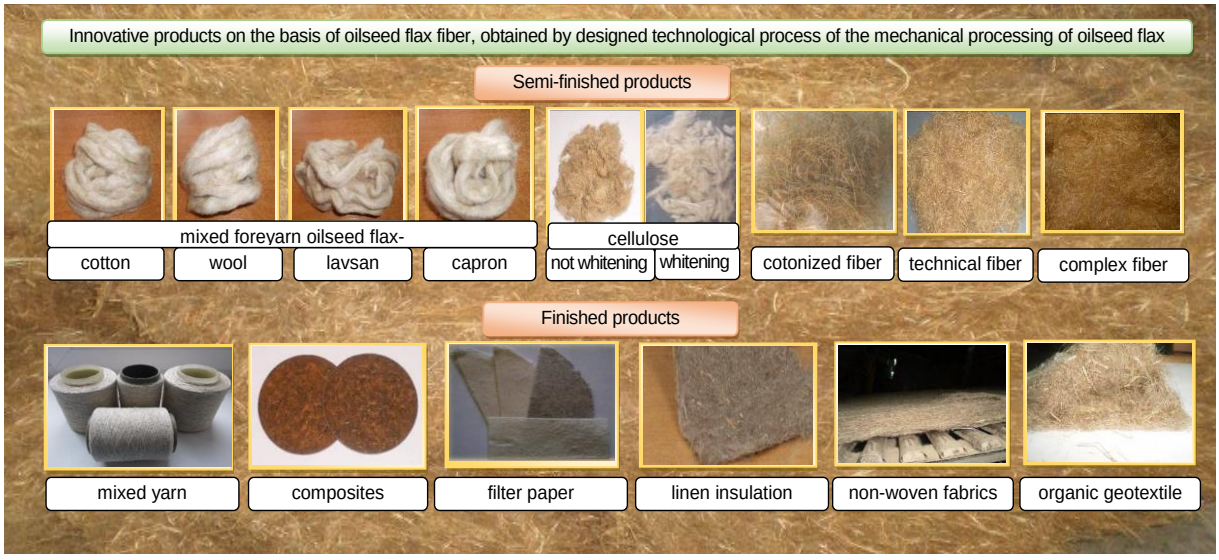

Fig. 9 - Innovative products on the basis of oilseed flax fibre

This product is of great economic importance, environmentally friendly, meets modern consumer needs, can compete with imported products, but above all, there are domestic raw materials for its production. Organization of the industrial complex for processing oilseed flax straw in Ukraine will provide domestic textile enterprises with cellulose-containing raw material, which is of strategic importance in conditions of complete import dependence of our country.

However, large-scale manufacturing of innovative products for the purpose of domestic and international marketing opportunities is only possible upon condition of their standardization. In developing regulations for assessing quality of oilseed flax straw stems and fibres obtained in order to determine the scope of industrial application, it is necessary to take into account their specific anatomical, physical and mechanical properties.

The analysis of standardization of straw and oilseed flax products indicates the absence of regulations determining their quality, the development of such regulations is a crucial issue. At present, there is no clear classification of fibres and physical and mechanical properties that would characterize the scope of their industrial application. Thus, scientists have developed and registered in the state enterprise "Khersonstandardmetrology" the technical specifications TU U 01.1-2303511525 - 001: 2016 "Oilseed flax straw. Specifications" and TU U 01.1-05480298 - 001: 2017 "Oilseed flax retted straw. Specifications". This will allow analyzing this industrial raw material, determining the feasibility of mechanical processing and the quality level of fibre as finished product.

CONCLUSIONS

World practice shows that oilseed flax is annually renewable “biological raw material” of new generation. In Ukraine, oilseed flax is the only domestic raw material, which can be an alternative to imported cotton and flax fibre for using in the textile, pulp and paper industries and the production of reinforced composite materials.

For complex processing of oilseed flax straw stems in Kherson National Technical University systematic research was carried out. As a result, it was found that their physical and mechanical properties, morphological, anatomical structure and distribution of fibres length of oilseed flax straw stems are significantly different in all technological parameters compared to common flax. Therefore, it is not appropriate to carry out mechanical processing of oilseed flax stems according to the schemes used for common flax processing.

Thus, to use oilseed flax fibres in various fields of industries based on the results obtained, the technology and equipment for mechanical processing of oilseed flax retted straw based on modernization of existing equipment is proposed.

So far, in Ukraine and in the world there are no normative documents for standardization of oilseed flax straw and retted straw. Thus, scientists have developed and registered in the state enterprise "Khersonstandardmetrology" the technical specifications TU U 01.1-2303511525 - 001: 2016 "Oilseed flax straw. Specifications" and TU U 01.1-05480298 - 001: 2017 "Oilseed flax retted straw. Specifications". This will allow analyzing this industrial raw material, determining the feasibility of mechanical processing and the quality level of fibre as finished product.

REFERENCES

[1] Boiko G., (2014), *Merchandizing analysis of mixed yarn with fibres of oilseed flax for knitted products (Товарознавча оцінка змішаної пряжі з волокнами льону олійного для трикотажних виробів):* diss. Candidate of Technical Sciences, 215 p., Lutsk/Ukraine;

[2] Assirelli A., Bentini M., Cappelletto P., Pasini P., (1997), Fibre valorisation of oilseed flax. In: *Proceeding of the flax and other bast plants symposium*. Institute of Natural Fibres Poznan, Poland, 30. Sept.-1. Oct. 1997. p. 150-151;

[3] Derbenev A., (1983)*, Development of the technology for the obtaining the single type fibre in the form of band from oilseed flax retted straw (Разработка технологи получения из льняной тресты однотипного ориентированного волокна в ленте):* diss. Candidate of Technical Sciences. 186 p., Russia: Kostroma;

[4] Ipatov A., (1989), *Theoretical basis of the mechanical processing of fibre crops stems. Russia (Теоретические основы механической обработки стеблей лубяных культур)*: 143 p., Moscow;

[5] Helyazetdinov R., (2009), *Development of the scientific basis of high technologies formation for initial processing of bast crop (Розвиток наукових основ створення інноваційних технологій первинної переробки луб’яних культур)*: diss. Doctor of Technical Sciences. 255 p., Kherson / Ukraine;

[6] Holovenko T., Chursina L., Tikhosova H., Mieniailo-Basysta I., (2014), *Innovative technologies for the production of nonwoven and cellulosic materials from oilseed flax (Інноваційні технології одержання нетканих та целюлозовмісних матеріалів з льону олійного)*/ Monograph. – Kherson National Technical University: Grin D.S., 304 p., Kherson / Ukraine;

[7] Kobyakov S., (1993), *Improvement of technology of making flax on retted straw by biological methods (Удосконалення технології приготування тресті льону біологічними способами)*: synopsis. diss. for obtaining science degree Candidate of Agricultural Sciences, 144 p., Kiev / Ukraine;

[8] Lytvyn Z., (2000), *Development of resource-saving technology of low-grade short flax fibre (Розробка ресурсозберігаючої технології переробки низькосортного короткого льняного волокна)*: diss. Candidate of Technical Sciences, 186 p., Kherson / Ukraine;

[9] Mieshkov Yu., (2007), *Development of technological process of obtaining high quality short flax fibre (Розробка технологічного процесу одержання короткого лляного волокна підвищеної якості):* diss. Candidate of Technical Sciences, 304 p., Kherson / Ukraine;

[10] Putintseva S., (2015), *Properties of filter paper based on cellulose from oilseed flax (Властивості фільтрувального паперу на основі целюлози з волокон льону олійного)*: author's abstract of the Thesis for obtaining the Degree of Candidate of Technical Sciences: field of study 05.18.08 / S. Putintseva, 20 p., Lutsk / Ukraine;

[11] Pashin E., Fedosova N., (2003), Technological quality and processing of flax-mezheumok (Технологическое качество и переработка льна-межеумка). *RSRIBC* (*All-Russian Scientific Research Institute of Bast Crops*), 85 p., Kostroma / Russia;

[12] Tikhosova H., Holovenko T., (2010), Motivation of efficiency of oilseed flax stems processing. Khmelnytsky National University Bulletin, № 4, pp. 268–274, Khmelnitsky / Ukraine;

[13] Tikhosova H., Nadieieva T. (Holovenko T.), Knyazev A., (2010), The current state of standardization of oilseed flax stems*. Scientific works of the Odessa National Academy of Food Technologies*, Issue 38. Volume 1, pp.93-95, Odessa/Ukraine;

[14] Tikhosova H., Nadieieva T. (Holovenko T.), Knyazev A., (2010), Theoretical prerequisites for development of high technologies of oilseed flax stems, *Light industry*, № 2, pp.27-28, Kyiv/Ukraine;

[15] Valko N., (2002), *Scientific bases of technological processes of modified flax fibre (Наукові основи технологічних процесів одержання модифікованого лляного волокна)*: dis. Doctor of Technical Sciences, 347 p., Kherson / Ukraine;

[16] Zhivetin V., Ginsburg L., (2000), Oilseed flax and its integrated development (Масляничный лён и его комплексное развитие), *CSRIBC* (*Central Scientific Research Institute of Bast Crops*), 389 p., Moscow/Russia;

[17] ***Saskatchewan Flax Development Commission, (2015), URL: http://www.saskflax.com;

[18] ***State Statistics Service of Ukraine, (2018), URL: http://www.ukrstat.gov.ua.

FOREST GLOBAL POSITIONING METHOD AND EXPERIMENT BASED ON AGRICULTURAL MACHINERY

/

基于农业机械的林木全球定位方法与试验

As. PG. Stud Shuo Li [1), 2)], A.P. Ruili Song [3)], Prof. Feng Kang *[1), 2)], Dr. Yaxiong Wang [1), 2)]

[1)] School of Technology, Beijing Forestry University, Beijing / China;

[2)] Key Lab of State Forestry and Grassland Administration on Forestry Equipment and Automation, School of Technology, Beijing Forestry University, Beijing / China;

[3)] Computer Science Department, Hebei Professional College of Political Science and Law, Shijiazhuang, Hebe / China

Tel: 15956263218; E-mail: ejtsuo@163.com

Keywords: *agricultural intelligent vehicle, tree trunk, laser scanner, global positioning*

ABSTRACT

To overcome the occlusion of satellite signals by dense canopy that invalidates the use of global positioning systems with agricultural machinery, the paper proposed a global positioning method to establish the global positions of forest trees. First, the domain division method of Euclidean distance and a geometric tangent algorithm are used. Then, three-dimensional data consisting of the centre points of tree trunks in the WGS-84 coordinate system are obtained by performing a spatial coordinate transformation. Subsequently, the laser scanned the newly detected trunks at a time t, and the scanning area was determined. Finally, the global positioning of trees by agricultural machinery was completed under a dense canopy. The results of field experiments showed that the standard deviation of the positioning error of the per plant tree trunk in the X, Y and Z directions of the space rectangular coordinate in the WGS-84 world coordinate system are 0.03 m, 0.04 m and 0.03 m.

摘要

卫星信号被密集的树冠遮挡,这使得使农业机械全球定位系统的应用失效，为了克服这一问题，本文提出了一种确定林木全局位置的全球定位方法。首先,利用欧几里得距离的域划分方法和几何切线算法。然后,对 WGS-84 坐标系中树干的中心点进行空间坐标变换,得到三维数据。紧接着,在 t 时, 激光扫描仪对新探测到的树干进行扫描,确定了扫描面积。最后在密集的树冠下完成树木的全球定位。现场试验结果表明, 在 WGS-84 世界坐标系中空间矩形坐标的 x、y 和 z 方向上,每个植物树干的定位误差的标准偏差为 0.03m、0.04m 和 0.03m。

INTRODUCTION

The distribution of trees in a forest is an important information in forests mapping *(Spriggs et al, 2015)*, for precision pesticides application *(Kang et al, 2014)*, and estimating the growth and harvesting of forests *(Kang et al, 2012)*; the tree distribution also serves as a guide for forest management. However, traditional manual contact mapping methods are time consuming and inefficient. Currently, many domestic and foreign scholars and researchers use an airborne mapping system to ascertain the actual locations of tree growth. Nevertheless, while this method is highly efficient, the measurement accuracy is not high, and it is impossible to obtain more detailed information, such as the size and position of a tree trunk, under the canopy. Therefore, vehicle mapping system based on advanced sensor technology was developed, but such systems suffer from a common primary problem: the positioning of the mobile platform. To resolve this issue, several solutions are currently employed. The dead reckoning (DR) method uses odometer information to achieve a higher short-term positioning accuracy. However, the DR method suffers from cumulative errors that gradually approach infinity when estimating the vehicle direction angle. The vision-based positioning method is another option, but it is considerably influenced by optical fibres; moreover, this technique requires a considerable environmental configuration and suffers from a highly complex algorithm with a poor reliability (*Xue et al, 2018*). Alternatively, the Global Positioning System *(Junying et al, 2014)* (GPS) has a high positioning accuracy and fast calculation speed; however, it is easy to lose the signal due to canopy occlusion, thereby limiting its applications on mobile platforms. In contrast, laser scanners *(Bargoti et al, 2015; Xuehua et al, 2013)* are much less influenced by the working environment and lighting conditions and can thus provide larger quantities of accurate distance information at a higher frequency; hence, they can reliably provide the orientations of surrounding objects and better positioning with a mobile platform.

Currently, scholars all over the world value the ability to position mobile platforms based on laser scanners. For instance, Barawid Jr O C et al. used two-dimensional laser scanners as navigation sensors for agricultural navigation *(Barawid et al, 2007)*; he applied the Hough transform to detect rows of trees and applied return to launch-based GPS (RTL-GPS) to determine the direction, thereby achieving the straight line moving of a mobile platform between forest rows, and he produced a positioning result with a lateral deviation of 0.11 m and a navigation deviation of 1.5°. Unfortunately, this method is suitable only for the straight-line walking of vehicles and does not involve the positioning of surrounding objects. Libby et al. used a laser scanner sensor to measure the relative position between an agricultural vehicle and a landmark to correct the predicted path of the vehicle based on a wheel encoder. The test results revealed an average error of approximately 20 cm and a maximum error of 1.2 m. Nevertheless, this method is applicable only to road sign measurements in the relatively flat environment of a road surface, and relatively large corrections are needed for vehicle positioning in hilly or mountainous areas *(Libby and Kantor, 2010)*. Freitas et al. used different kinds of Kalman filtering algorithms to study the positioning of mobile platforms; however, this algorithm is mainly suitable for forest trees in the form of "tree walls" *(Freitas et al, 2012)*. In China, Xue Jinlin used laser scanner sensors to obtain the positioning information of tree rows and studied the navigation performance of an agricultural mobile platform between tree rows with a defined plant spacing and between tree rows without equidistant plant spacing *(Jinlin and Shunshun, 2014)*. In the experiment with an equidistant plant spacing, the lateral maximum deviation of their mobile platform was 17.5 cm, and the longitudinal maximum deviation was 28 cm. However, the deviations measured by their method are within the two-dimensional plane only, while the deviation of the pitch axis is not considered. Zhou Jun et al. proposed a method for positioning a mobile platform between densely planted orchards in combination with global navigation satellite system (GNSS) or artificial identification location information *(Zhou and Hu, 2015; Chen et al, 2018)*. Their experiment showed that the standard deviations of the positioning errors of a mobile platform in the *X* and *Y* directions for a world coordinate system are approximately 0.08 m; however, this method considers only the positioning of a mobile platform between rows of trees and does not currently involve the global positioning information of the orchard.

In this paper, a laser scanner is used as the scanning device, and the position information of the vehicle provided by real-time kinematic differential GPS (RTK-DGPS) in conjunction with an altitude and heading reference system (AHRS) is used to extract the position information of forest trees in real time. Even when the working vehicle is not operating properly and the GPS has no signal, this method can still achieve a centimetre-level positioning accuracy and obtain global positioning information of forest trees.

MATERIALS AND METHODS

- **Principles and method for the global positioning of forest trees**

The mobile platform walks between the forest trees; simultaneously, the laser scanner scans the trunks on both sides and identifies and extracts relevant parameters according to the point cloud data acquired from the scans. The laser scanning field of view can be divided into three regions: 1) the clear region, which comprises the reliable centre positions of established tree trunks; 2) the fuzzy region, i.e., the laser scanner is able to scan the trunks, but there are large errors in the determined positions of the centre points of those trunks; and 3) the invisible region, in which the laser scanner cannot scan the trunks on both sides. Among these regions, the laser scanner divides the data from one frame composed of original scanning points into several clusters, where per plant tree is represented by a cluster of points. The division of clear and fuzzy regions is determined according to the number of minimum scanning points returned by the same cluster of laser scanning points.

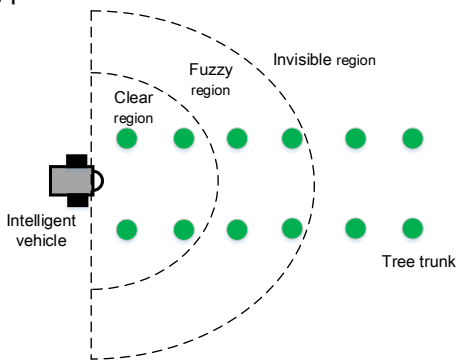

Fig. 1 - Visual field of vehicle laser scanner

- **Trunk feature extraction**

When the laser scanner performs non-contact scanning on the trunk of a forest tree, the tree trunk can be approximated as a cylinder, and thus, a two-dimensional scanning point cloud of an approximately arcuate shape can be formed *(Yu et al, 2015; Wang et al, 2015; Xiao et al, 2016)*. According to the point cloud data acquired by the laser scanner, the data set is divided into different clusters by using the domain division method of Euclidean distance, after which the clustered data are fitted to extract the effective positioning information of the trunk *(Ferrara et al, 2018; Maalek et al, 2018)*.

First, the data are clustered by analysing one frame of raw data acquired with the laser scanner by using the domain division method of Euclidean distance *(Nguyen et al, 2007)*. Assume that the laser scanner collects n discrete information data points in one scanning cycle; the purpose of the region segmentation technique is to divide these discrete data points into regions that are not connected to each other according to the distance between two adjacent points.

Second, the tangent method is used in the geometric class algorithm, as shown in Fig. 2, to standard circle fitting of clustered point-clusters. The principle of this fitting process is as follows: the lines connecting the first and last points of the point cloud cluster belonging to a certain trunk to the centre of the laser cluster are strictly tangential to the cross-sectional circle representing the trunk. The formula for the diameter of this circle is as follows:

$$d = 2l_{\min}\frac{\sin\frac{\Delta\theta}{2}}{1-\sin\frac{\Delta\theta}{2}} \tag{1}$$

In formula (1), $\Delta\theta$ is the laser scanning angle of the same cluster data, and $l_{\min}$ is the shortest distance between the scanning point for the same data cluster and the centre of the laser.

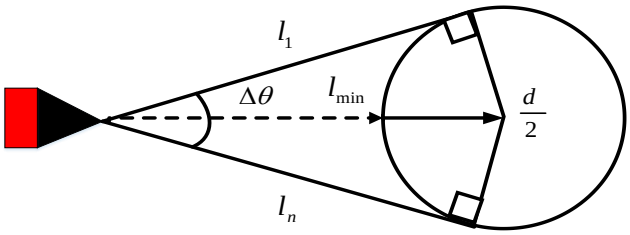

Fig. 2 - Principle diagram of calculating the diameter for the tangent method

- **The trunk centre position in the world coordinate system**

To determine the position of the mobile platform between two rows of trees, it is necessary to convert and record the positions of the centre points of trunks in the working space detected by the laser scanner to the world coordinate system. Since the mobile platform is located at the beginning at the starting point of movement and has not yet entered the forest area, the occlusion of the satellite signal by the canopy is not serious. At this time, GPS can be used to output the longitude, latitude and altitude of the mobile platform in the WGS-84 world coordinate system. The AHRS outputs the pitch angle φ, the roll angle ω, and the yaw angle κ under the local horizontal reference system. The system then uses a four-step coordinate transformation to derive the spatial rectangular space coordinates of the centre points of trunks in the WGS-84 world coordinate system fitted by the laser scanner point cloud data.

This coordinate conversion process uses four coordinate systems, the laser scanner reference coordinate system O-$x_Ly_Lz_L$, the attitude and heading reference coordinate system O-$x_Iy_Iz_I$, the local horizontal reference coordinate system O-$x_Gy_Gz_G$, and the WGS-84 world coordinate system O-$x_{84}y_{84}z_{84}$.

$$Q_{84} = O_{GPS} + R_W\left[R_N\left[O_{LI} + R_M Q_L - O_{IG}\right]\right] \tag{2}$$

Q_L is the coordinates of the trunk centre point Q in the laser scanner coordinate system. O_{LI} denotes the offset between the coordinate origin of the laser scanner coordinate system and the coordinate origin of the AHRS coordinate system, and R_M is the rotation matrix between the laser scanner coordinate system and the AHRS coordinate system. O_{IG} denotes the offset between the GPS antenna phase centre and the AHRS centre, and R_N is the rotation matrix between the AHRS coordinate system and the local horizontal

reference frame. R_W represents the rotation matrix from the local horizontal reference system to the WGS-84 world coordinate system, and O_{GPS} is the position of the GPS phase centre in the WGS-84 coordinate system. Q_{84} is the position of the trunk centre in the WGS-84 world coordinate system.

Based on the above formula, Q_L can be obtained from the output data from the laser scanner, O_{LI} and O_{IG} can be obtained with more accurate data through static measurements, R_N can be obtained from the ARHS, R_W and O_{GPS} can be calculated by the GPS-measured latitude, longitude and altitude.

Therefore, the centre point of the trunk in the working space detected by the mobile platform at its initial position can be expressed as the following collection:

$$B = \{(x_1, y_1, z_1), (x_2, y_2, z_2), L(x_i, y_i, z_i)\} \quad (3)$$

In formula (3), i denotes the centre point sequence number of the detected trunk, and *(x,y,z)* (x, y, z) represents the rectangular space coordinates of the centre point of the trunk in the WGS-84 world coordinate system.

When performing standard circle fitting on a laser scanning point cluster, the number of scanning points within the same data cluster should be greater than M_{min}, which determines the scanning range of the laser scanner. Therefore, during any subsequent movement of the mobile platform between the forest trees, the set is updated only when the mobile platform scans a trunk and the number of scanning points in the data cluster exceeds M_{min}. This method can reduce the number of calculations as well as the accuracy of fitting the standard circle of the trunk section area.

- **Mobile platform inter-row positioning method**

In the inter-row positioning scheme, a threshold T needs to be established to match the coordinates of the centre point of the trunk detected at time t acquired from the mobile platform during its movement between the trees with the data stored in set B consisting of the initial centre point of the trunk. When the mobile platform is within the position coordinate difference $d_{ij}<T$ of the trunk centre position in the laser scanner coordinate system during the two scans at times t_i and t_j, t_i and t_j are any two moments in the course of driving. this position is considered the same tree in both scans; otherwise, a new tree is considered to have appeared.

$$d_{ij} = \sqrt{(x_i - x_j)^2 + (y_i - y_j)^2 + (z_i - z_j)^2} \quad (4)$$

In formula (4), (x_i, y_i, z_i) denotes the centre point coordinates of trunk i detected at time t_i, and $(x_j, y_j z_j)$ represents the centre point coordinates of trunk j detected at time t_j.

After the trunk centre point is matched, the trunk centre points of 3 trees in set B are randomly selected. The rectangular space coordinates $A=(x_A, y_A, z_A)$, $B=(x_B, y_B, z_B)$ and $C=(x_C, y_C, z_C)$ in the WGS-84 world coordinate system are used to calculate the spatial rectangular space coordinates $D=(x_C, y_C, z_C)$ of mobile platform at time t in the WGS-84 world coordinate system, as shown in Fig. 3.

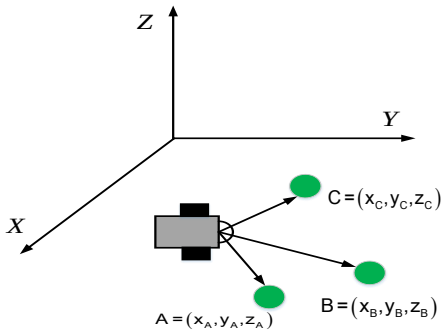

Fig. 3 - Mobile platform position prediction model

- **Test system**

This experiment uses a forest precise positioning mobile platform that was independently developed by Beijing Forestry University for data collection. The system uses a crawler-type mobile platform with a laser detection module and a portable computer on the platform, as shown in Fig. 4.

The laser detection module consists of a laser scanner and an AHRS. The laser scanner uses a LMS511-20100 PRO laser scanning radar produced by SICK. The scanning range of the laser scanning radar is -5°~185°, the angular resolution is set to 0.333°, the corresponding scanning frequency is 50 Hz, the maximum detection distance is set according to the number of scanning points M_{min} within the same data cluster, and the power supply is a 24 V DC lithium battery. The AHRS is fixed onto the vehicle body in a tight and stable manner. The lightweight 9-axis altitude-sensor LPMS-CU has a resolution of 0.06°. The data update frequency is 50 Hz for measuring the pitch angle, roll angle and yaw angle of the laser scanner during the movement of the platform in real time.

Fig. 4 - The structure of forest precise positioning mobile platform
Laser scanner; Attitude and heading reference system;
Portable computer

The three arc-shaped logs at each distance were distributed in the range of 30°~150° in front of the laser scanning radar, and each distance was measured 11 times, as shown in Fig. 5. The three logs (A, B, and C) were each 5 m away from the centre of the laser scanner; the resulting log radius were 92.8, 89.9, and 91.8 mm, respectively. By comparing the radius and distance measurements obtained by scanning the trunks using the laser scanner with the corresponding real values, we analysed the error precision and determined the number of scanning points M_{min} within the same data cluster.

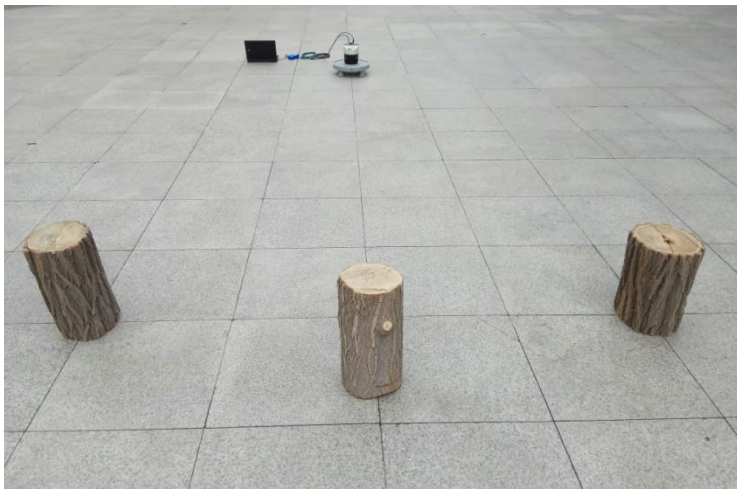

Fig. 5 - Photo of the scene for the verification experiment

- **Forest dynamic positioning test**

A trial was conducted in Beijing Dongsheng Eight Country Park, as shown in Fig. 6. Among the two rows of trees in the scene, the left and right sides are both composed of poplar trees, the trunks of which have different thicknesses, and the ground undulates. Whether from trunk features, trunk alignment, or ground effects, it can be used to test the effectiveness of the proposed algorithm.

Fig. 6 - Experimental scene and the intelligent mobile platform

RESULTS

Fig. 7 shows the average standard deviation in the log radius and placement distance after acquiring 11 measurements at five different placement distances. The average standard deviation measurement unit is mm, the resulting log radius were 92.8, 89.9, and 91.8 mm.Therefore, when performing standard circle fitting of the laser spot cluster in subsequent tree trunk positioning experiments, the number of scanning points within the same data cluster should be greater than 4 to determine the scanning range of the laser scanner.

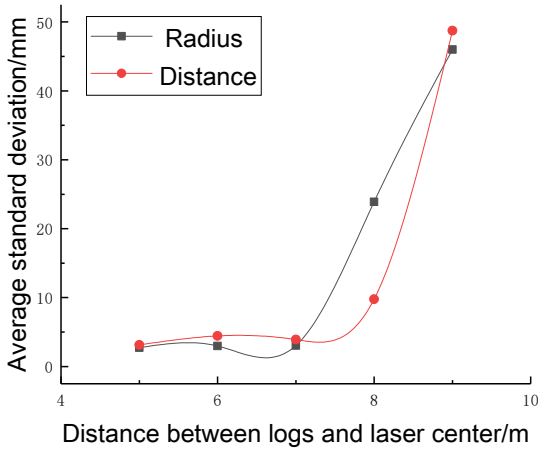

Fig. 7 - Average standard deviation at different placement distances

The actual values in the X, Y, and Z directions were subtracted from the corresponding measured values of the positioning method to obtain the positioning errors in the three directions. Figs. 8, 9, and 10 illustrate the positioning errors in the X, Y and Z directions for the first test. As shown in these figures, the positioning errors in the X, Y and Z directions increased slowly with an increase in the moving distance. An analysis revealed that the positioning results of the mobile platform derived from the tree trunk positioning results in the clear region caused a cumulative error during the movement of the mobile platform. This finding is an important reason for the slow rise in the trunk positioning error in the fuzzy and invisible regions.

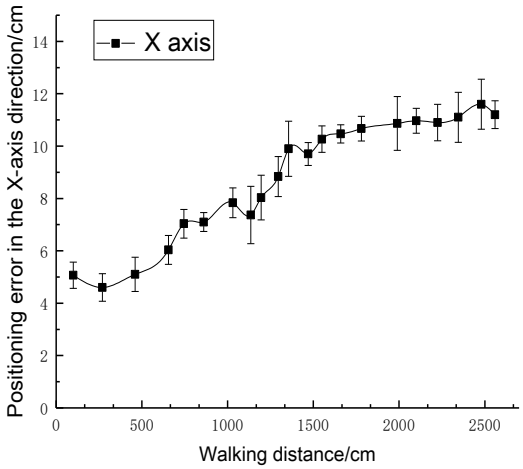

Fig. 8 - Localization errors of the 1st experiment in the X direction

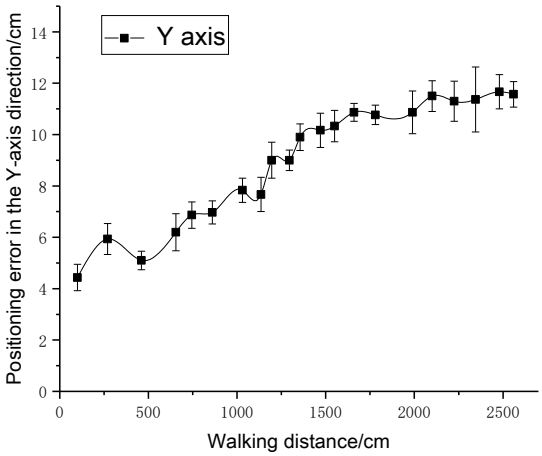

Fig. 9 - Localization errors of the 1st experiment in the Y direction

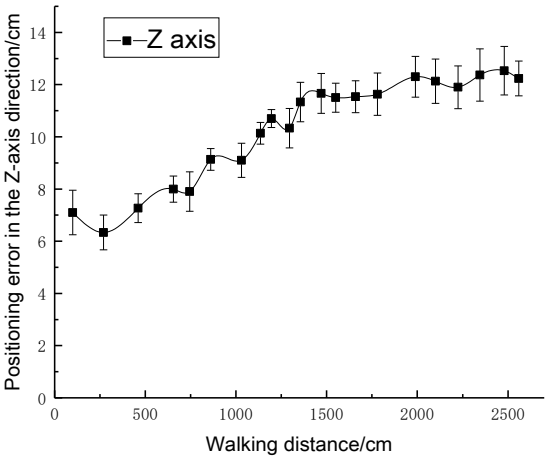

Fig. 10 - Localization errors of the 1st experiment in the Z direction

The statistical results obtained from 11 replicated experiments are shown in Tables 1, 2 and 3. From these 11 experiments, the average value of the maximum error in the X-axis direction was 0.13 m, and the average standard deviation of the positioning error was 0.03 m. The average value of the maximum positioning error in the Y-axis direction was 0.12 m, and the average standard deviation of the positioning error was 0.04 m. The average value of the maximum positioning error in the Z-axis direction was 0.13 m, and the average standard deviation of the positioning error was 0.03 m. These data show that the system boasts a certain controllability and accuracy; furthermore, the maximum error was 0.14 m, which meets the requirements of forest management applications.

Table 1

Localization errors in the X direction (m)

Experiment	Maximum error	Average error	Standard error
1	0.12	0.09	0.02
2	0.12	0.07	0.03
3	0.13	0.09	0.04
4	0.13	0.08	0.03
5	0.14	0.07	0.03
6	0.13	0.08	0.03
7	0.13	0.09	0.03
8	0.12	0.08	0.04
9	0.13	0.08	0.03
10	0.14	0.08	0.03
11	0.13	0.07	0.04
Average	0.13	0.08	0.03

Table 2

Localization errors in the Y direction (m)

Experiment	Maximum error	Average error	Standard error
1	0.12	0.09	0.02
2	0.12	0.08	0.04
3	0.11	0.08	0.04
4	0.11	0.08	0.04
5	0.10	0.09	0.03
6	0.14	0.07	0.04
7	0.13	0.08	0.03
8	0.13	0.08	0.03
9	0.12	0.09	0.05
10	0.12	0.07	0.04
11	0.13	0.08	0.05
Average	0.12	0.08	0.04

Table 3

Localization errors in the Z direction (m)

Experiment	Maximum error	Average error	Standard error
1	0.13	0.09	0.02
2	0.12	0.08	0.04
3	0.13	0.09	0.03
4	0.12	0.09	0.03
5	0.12	0.09	0.03
6	0.13	0.09	0.03
7	0.12	0.08	0.04
8	0.13	0.09	0.03

Experiment	Maximum error	Average error	Standard error
9	0.14	0.09	0.04
10	0.12	0.09	0.03
11	0.13	0.10	0.03
Average	0.13	0.09	0.03

CONCLUSION

Canopy occlusion attributable to forest trees will affect the GPS positioning accuracy in agricultural machinery; hence, we propose the use of RTK-DGPS to locate mobile platforms in the initial position. Then, we combine the altitude information of an AHRS with laser scanner detection information, which are outputted in real time during the movement of the mobile platform. The platform directly calculates the three-dimensional data consisting of the centre points of tree trunks in the WGS-84 world coordinate system by a spatial coordinate transformation. The proposed positioning method is complementary to the RTK-DGPS positioning information, which overcomes the influence of canopy occlusion on GPS signals in agricultural machinery, and overcomes the influence of irregularities in forest planting on the positioning accuracy of forest trees.

ACKNOWLEDGEMENT

This research was funded by the Fundamental Research Funds for the Central Universities (No. 2015ZCQ-GX-01).

REFERENCES

[1] Barawid Jr.O.C., Mizushima A., Ishii K. et al., (2007), Development of an autonomous navigation system using a two-dimensional laser scanner in an orchard application, *Biosystems Engineering*, Vol. 96, Issue 2, pp.139-149;

[2] Bargoti S., Underwood J.P., Nieto J.I. et al., (2015), A pipeline for trunk localization using LIDAR in trellis structured orchards, *Field and Service Robotics: results of the 8th International Conference*, Issue 2015, pp.455-468;

[3] Chen X., Wang S.A., Zhang B, Luo L., (2018). Multi-feature fusion tree trunk detection and orchard mobile robot localization using camera/ultrasonic sensors, *Computers and Electronics in Agriculture*, Issue 147, pp.91-108;

[4] Freitas G., Zhang J., Hamner B. et al., (2012), A low-cost, practical localization system for agricultural vehicles, *Intelligent Robotics and Applications: 5th International Conference*, ICIRA, Issue 2012, pp.365-375;

[5] Ferrara R., Virdis S.G., Ventura A., Ghisu T., Duce P., Pellizzaro G., (2018), An automated approach for wood-leaf separation from terrestrial LIDAR point clouds using the density based clustering algorithm DBSCAN, *Agricultural and Forest Meteorology*, Issue 262, pp.434-444;

[6] Jinlin Xue, Shunshun Zhang, (2014), Navigation of an agricultural robot based on laser radar, *Transactions of the CSAM*, Vol. 45, Issue 9, pp.55-60;

[7] Kang F., Li W.B., Pierce F.J. et al., (2014), Investigation and improvement of targeted barrier application for cutworm control in vineyards, *Transactions of the ASABE*, Vol. 57, Issue 2, pp.381-389;

[8] Kang F., Pierce F.J., Walsh D.B. et al., (2012), An automated trailer sprayer system for targeted control of cutworm in vineyards, *Transactions of the ASABE*, Vol. 55, Issue 5, pp.2007-2014;

[9] Maalek R., Lichti D., Ruwanpura J., (2018), Robust Segmentation of Planar and Linear Features of Terrestrial Laser Scanner Point Clouds Acquired from Construction Sites, *Sensors*, Vol. 18, Issue 3, pp.819;

[10] Nguyen V., Gchter S., Martinelli A. et al., (2007), A comparison of line extraction algorithms using 2D range data for indoor mobile robotics, *Autonomous Robots*, Vol. 23, Issue 2, pp.97-111;

[11] Spriggs R.A., Vanderwel M.C., Jones T.A. et al., (2015), A simple area-based model for predicting airborne LiDAR first returns from stem radius distributions: an example study in an uneven-aged, mixed temperate forest, *Canadian Journal of Forest Research*, Vol. 45, Issue 10, pp.1338-1350;

[12] Wang H., Luo H., Wen C., Cheng J., Li P., Chen Y., Li J., (2015), Road boundaries detection based on local normal saliency from mobile laser scanning data, *IEEE Geoscience and remote sensing letters*, Vol. 12, Issue 10, pp.2085-2089;
[13] Wilson J.N., (2000), Guidance of agricultural vehicles-a historical perspective. *Computers and Electronics in Agriculturs*, Vol. 25, Issue 1-2, pp.3-9;
[14] Xiao W., Vallet B., Schindler K., Paparoditis N., (2016), Street-side vehicle detection, classification and change detection using mobile laser scanning data, *ISPRS Journal of Photogrammetry and Remote Sensing*, Issue 114, pp.166-178;
[15] Xue J, Zhang L, Grift T.E., (2012), Variable field-of-view machine vision based row guidance of an agricultural robot, *Computers and Electronics in Agriculture*, Vol. 84, pp.85-91;
[16] Xue J., Fan B., Yan J., Dong S., Ding Q., (2018), Trunk detection based on laser radar and vision data fusion, *International Journal of Agricultural and Biological Engineering*, Vol.11, Issue 6, pp.20-26;
[17] Xuehua Wei, Yongguo Wang, Jun Zheng et al., (2013), Tree crown volume calculation based on 3-d laser scanning point clouds data, *Transactions of the CSAM*, Vol. 44, Issue 7, pp.235-240;
[18] Yu Y., Li J., Guan H., Wang C., Yu J., (2015), Semiautomated extraction of street light poles from mobile LiDAR point-clouds, *IEEE Transactions on Geoscience and Remote Sensing*, Vol. 53, Issue 3, pp.1374-1386;
[19] Zhou Jun, Hu Chen, (2015), Inter-row Localization Method for Agricultural Robot Working in Close Planting Orchard, *Transactions of the CSAM*, Vol. 46, Issue 11, pp.22-28.

3D SURFACE DEFECTS RECOGNITION OF LUMBER AND STRAW-BASED PANELS BASED ON STRUCTURE LASER SENSOR SCANNING TECHNOLOGY

/

基于结构激光传感器扫描技术的木材和秸秆人造板三维表面缺陷识别

As. Ph.D. Stud Jianhua Yang [1), 2)], Master Stud Xinyu Zheng [1)],
Master Stud Jianping Yao [1)] Prof. Ph.D Jiang Xiao *[1)], Associate Prof. Ph.D Lei Yan [1)]
[1)] Beijing Forestry University, Beijing, 100083 / China;
[2)] Beijing Forestry Machinery Research Institute of the National Forestry and Grassland Administration, Beijing / China
Tel: 18201112198; E-mail: xiaojiang56@126.com

Keywords: *structure laser, deep learning, 3D surface defect, recognition, intelligent algorithm*

ABSTRACT

The surface defects, especially the insects holes and dents, seriously affect the quality and value of lumber and agri-crop straw-based panels. In this study, two kinds of surface defects, insects holes and dents, were selected as the object of system detection. A surface defect recognition system based on Gocator 3D (3 Dimensional) structure laser sensor was built. An image processing method based on deep learning was designed using HALCON. While the shape features (6-dimensional) and gray-scale texture features (7-dimensions) of the image are extracted, the principal components analysis method is used to reduce the dimensions of the eigenvector. The SVM (Support Vector Machine), GMM (Gaussian Mixture Model) and KNN (K-Nearest Neighbor) are used to classify and identify the defects on the surface of the lumber and agri-crop straw-based panels, and the final classification accuracy is up to 94.67%. The experimental results show that the system can quickly and accurately identify the insects holes and dents through intelligent algorithm. The research results show that the quality evaluation of agricultural and forestry products based on image processing technology is feasible. Structure laser sensor scanning technology can be used in 3D surface defects detect and recognition of lumber and straw-based panels.

摘要

木材和农作物秸秆人造板表面缺陷，特别是孔洞和凹痕，严重影响产品的质量和价值。在本文研究中，选择孔洞和凹痕这两种表面缺陷作为检测对象。建立了基于三维结构激光传感器的表面缺陷识别系统。使用 HALCON 设计了基于深度学习的图像处理算法。在提取图像的形状特征(6 维)和灰度纹理特征(7 维)的同时，使用主成分分析方法来减小特征向量的维数。应用 SVM，GMM 和 KNN 三种方法来进行木材和农作物秸秆人造板表面的缺陷的分类和识别, 最终分类精度高达 94.67％。实验结果表明，该系统能够通过智能算法快速准确地识别孔洞和凹痕。研究结果表明基于图像处理技术的农林产品质量评价是可行的。结构激光传感器扫描技术可用于木材和农作物秸秆人造板表面三维缺陷的检测和识别。

INTRODUCTION

The low quality of forest resources, deficiency amount, uneven distribution, inadequate utilization and poor management of the status quo for the forestry has brought great challenges. One of the keys to solve the above problems is to improve the level of lumber production and processing. Another one is the strategic shifting of raw material resources supply must he properly solved (*Zhou D., 2016*). Wood has been the major source of raw material particleboards and fibreboards, but recently, rice-wheat straw(RWS) has gained more attention of researchers to be used as an alternative of wood (*Muhammad Y., Abdul W., Aqeel A. et al. 2010; Qian X. 2010*). Efficient use of crop straw resources is an important indicator of a country's agricultural modernization level (*Ying C., 2015*). The utilization of rice straw for the production of high quality biocomposite products, will add economic value, help to reduce the environmental impact of waste disposal and, most importantly, provide a potentially inexpensive alternative to the existing commercial artificial wood‐panels (*Altaf H., Houssni E., Vivian F., 2013; Wang H., Wang F., Sun R., 2016*). The detection of surface defects is an important way to improve the level of production and processing (*Liu J., Liang J., Liang X., et al., 2010*).

Lumber and wood-based panel surface defects have various kinds and varied shapes, generally divided into sections, insects holes, dents, cracks and discoloration. Traditional method of surface defect detection is mainly through human identification and screening.

However, this method has the problems of low efficiency, low accuracy and high labor cost. With the development of science and technology, the agricultural and forestry manufacturing industry has begun to move toward industrial automation. Surface defects detection can be industrialized through machine vision and image processing. Machine vision is using the machine instead of the human eye to measure and determine *(Zhao P., Zhao Y., Chen G., 2017)*. At present, most of the machine vision systems are based on X-Y 2D (2 Dimensional) plane detection, mainly operating on grayscale of the target object. However, the traditional 2D inspection of machine vision could not meet the demand when information on the Z axis needs to be detected. 3D (3 Dimensional) structure laser sensor scanning technology based on Intelligent algorithm can automatically and accurately scan full range of target, in order to obtain the target's grayscale, height and other information through deep learning.

MATERIALS AND METHODS

Through the 3D structure laser sensor scanning technology to automatically and accurately scan the target image, which including grayscale, height and other information. The highly restored height map and grayscale images using otus method and dynamic threshold method for image segmentation. After extracting defects of the lumber shape and texture eigenvectors, three pattern recognition methods were used to classify the lumber surface defects.

Hardware platform

The system consists of Gocator 3D (3 Dimensional) smart sensor, Gocator data cable, I / O cable, HF150W-S-48 converter, host computer and DH-POL-PY300 experimental platform. System physical map is shown in the Figure 1. The Gocator 3D smart sensor is LMI company's 3D megapixel sensor that combines a line scan camera with a laser emitter. The Gocator 3D smart sensor is manufactured on an industrial design basis, based on the harsh production demanding of the workshop. It has the advantages of high precision, stable performance, good real-time. Therefore, the Gocator 3D smart sensor is suitable for non-contact online real-time detection. The system uses a Gocator2330. Laser Emitter emits structured light for laser molding. Camera observes laser reflected on the target surface, I/O (Input / Out) put Connector accepts incoming and outgoing digital signals, Power / LAN (Local Area Network) Connector turns on power and laser safety signals, and connects to Gigabit Ethernet *(Thies M., Pfeifer N., Winterhalder D., et al., 2004)*. In addition Gocator also includes Camera measurement status indicator, laser status indicator and power status indicator. The principle of Gocator2330 collection of target height data is the triangulation method. The intervals of laser line direction (X axis) and height (Z axis) are calibrated at the factory shipment, and the motion acquisition direction (Y axis) needs to be adjusted to correspond to the actual physical distance. Sensor movement acquisition has two ways: First, the time interval motion acquisition; Second, the encoder motion acquisition, the pulse trigger acquisition. The system uses the encoder motion acquisition, because in the acquisition frequency the acquisition effect will not be distorted for movement speed.

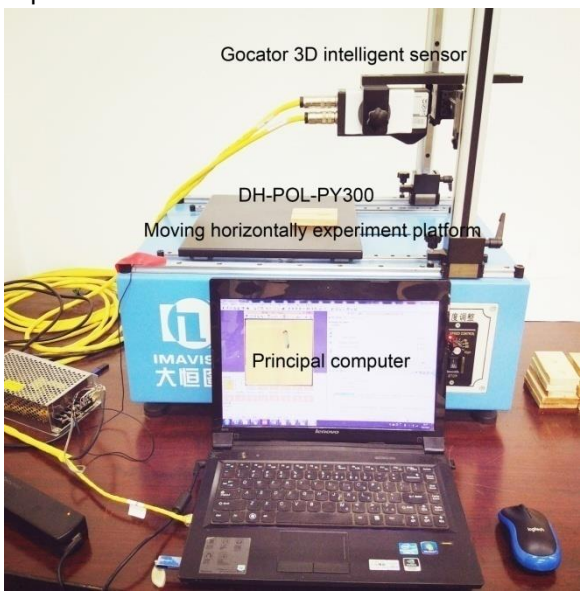

Fig. 1 - Hardware platform physical map

The essence of Gocator2330 is a line scan camera which needs to cooperate with the sports platform to achieve the purpose of acquiring the height information of the target object. DH-POL-PY300 experimental platform includes a rotary encoder to capture images with the Gocator2330. When the target object on the DH-POL-PY300's translation platform starts to reciprocate, the built-in rotary encoder sends a pulse signal synchronized with the platform motion to the Gocator2330. Gocator2330 emits laser beams at the same time capturing imagery multiple messages.

Image acquisition and segmentation

Gocator2330 provides GenTL driver interface, allowing external software to directly control the Gocator2330 to capture the target's 3D point cloud data and grayscale data for processing. The system uses HALCON image processing. HALCON is a software with a widely used machine vision integrated development environment. HALCON provides interfaces to a wide variety of image-captured devices to ensure hardware independence. The system sets GenTL driver to output RGB images of sixteen and input to HALCON for processing, simultaneously sets the acquisition mode for asynchronous loop acquisition. The programming statement of HALCON connecting Gocator2330 and capturing the image is:

open_framegrabber ('GenICamTL', 0,0,0,0,0,0,0 'progressive', 16, 'rgb', -1, 'false', 'default', '192.168.1.10', 0, -1, AcqHandle)

grab_image_start (AcqHandle, -1)

grab_image_async (Image, AcqHandle, -1)

Among them, 'GenICamTL' represents the name of the 3D sensor, 'rgb' represents a color image, and '192.168.1.99' represents a camera IP address. In the Gocator2330 collected sixteen RGB images, R, G, B three channels were saved image height information, grayscale information and parameters. The image is split using Go2GenTL_ParseData (Image1, HeightMap, Intensity, frameCount, timestamp, encoderPosition, encoderIndex, inputs, xOffset, xResolution, yOffset, yResolution, zOffset, zResolution, width, height, hasIntensity) operators to get the grayscale and height map. HeightMap represents the height map, Intensity represents the grayscale, zOffset represents the Z-axis offset, and zResolution represents the Z-axis resolution. Image split effect is depicted in the Figure 2.

Make use of stretching transformation on the slip height map to obtain the actual height value of the sample. Formula (1) was used to stretch and transform height map.

$$H^{\Lambda'} = H^{*} zResolution + zOffset \quad (1)$$

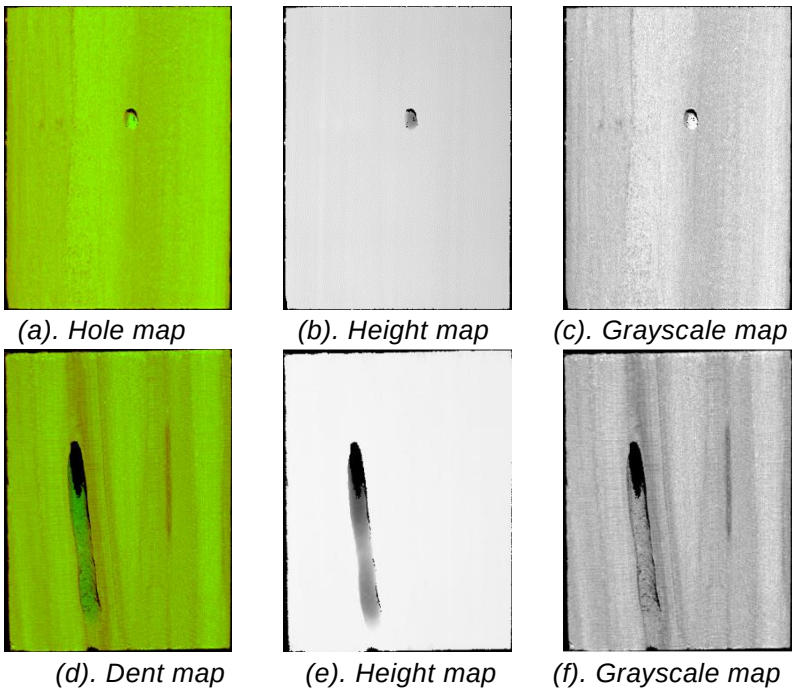

(a). Hole map *(b). Height map* *(c). Grayscale map*

(d). Dent map *(e). Height map* *(f). Grayscale map*

Fig. 2 - Sample image split map

The highly restored height map and grayscale images using otus method and dynamic threshold method for image segmentation, segmentation results are shown in the Figure 3. It can be seen from the comparison chart of the two groups in the Figure 3. That there is no over-segmentation based on the segmentation of the height map of the sample, and the segmentation of the defect obtained by the dynamic threshold method is complete. The image segmentation part of the research is divided into three steps: The height of the image is highly stretched and transformed; Processing the height map to obtain the defect area through the dynamic threshold method; the defect area is superimposed on the grayscale, so as to obtain texture features of defective area.

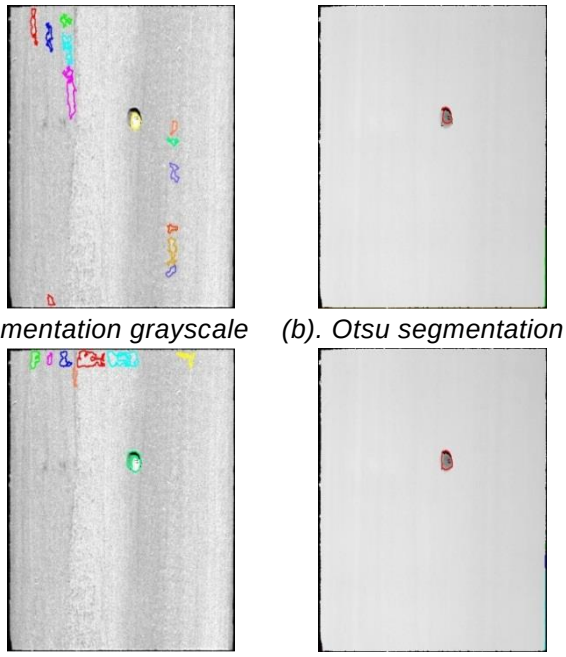

(a). Otsu segmentation grayscale *(b). Otsu segmentation height map*

(c). Dynamic threshold segmentation grayscale (d). Dynamic threshold segmentation height map

Fig. 3 - Segmentation effect comparison chart

Part of the system's image acquisition and segmentation are shown in the Figure 4.

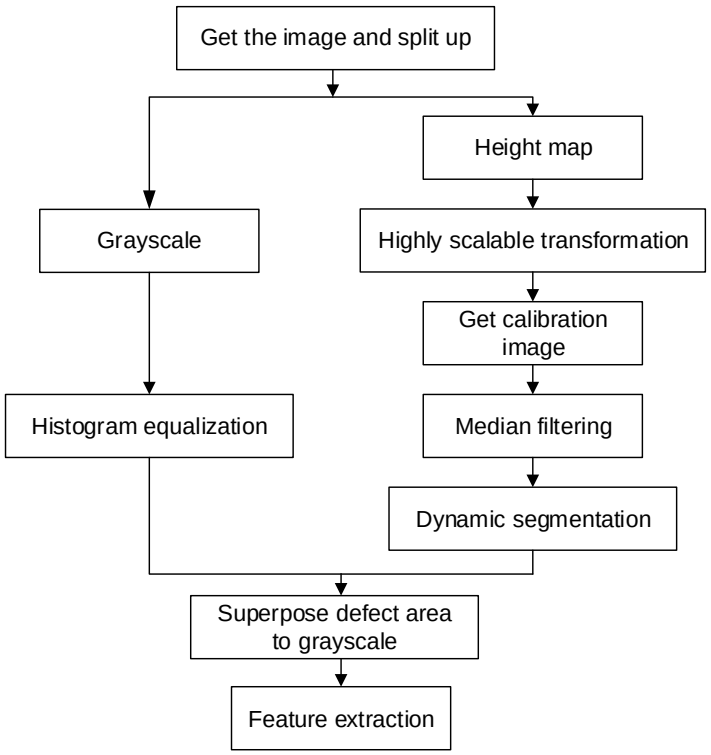

Fig. 4 - Image processing flow chart

RESULTS

Feature extraction

Before recognizing defects, the key step of lumber surface defect recognition system is to recognize and extract the defect eigenvectors. Good eigenvectors should have four characteristics: Reliability: The characteristics of the same category should be as similar as possible; Divisibility: There should be significant differences between features of different categories, and the greater differences, the better. Independence: Eigenvalues should be unrelated to each other and should not interfere with each other. Especially when two eigenvalues are the same, they are not suitable for simultaneous use. Small quantity: In principle the higher the amount of features, the better the recognition and classification, but at the same time it will increase the recognition complexity of the image and the computational complexity of the algorithm and reduce the efficiency and effect of image recognition *(Jiang Q., Liu H., 2004)*.

The system selected a total of six defects of the lumber shape eigenvectors and seven texture eigenvectors. Shape eigenvectors are: circumference, area, circularity, Rectangularity, tightness, eccentricity. The texture eigenvectors are the mean gray-scale value, the variance of gray-scale value and five characteristic parameters selected from the gray-level co-occurrence matrix, which are: Energy, Contrast, Correlation, Entropy, Inverse difference moment *(Bai X., Zou L., 2007)*.

The above thirteen kinds of eigenvectors reflect the differences in the geometric shapes and texture features of the defective areas. Eigenvector information extracted from different defects, such as dents and insects holes, is shown in the Table 1 and Table 2. Because of the high dimension of the eigenvector, the classification speed of the classifier will be slowed down, so it needs to be dimensionally reduced. There are some common feature selection methods: Principal Component Analysis (PCA) (Principal Component Analysis), Linear Discriminant Analysis (LDA) (Linear Discriminant Analysis) and Independent Component Analysis (ICA) (Independent Component Analysis). Because PCA (Principal Component Analysis) has the advantages of simple and no parameter limitation, the system uses PCA (Principal Component Analysis) method to reduce the dimension of the original eigenvectors, and pick out the effective features from it to establish the eigenvector of lumber surface defect recognition *(Zhang X., Zhang C., 2016)*.

Table 1

Eigenvectors of The shape features

Type	Number	Perimeter	Area	Circularity	Rectangularity	Tightness	Eccentricity
Dents	1	473	10675	0.6104	0.7436	1.6379	0.3985
	2	461	14487	0.8621	0.8139	1.1603	1.8275
	3	903	28254	0.4392	0.7573	2.2773	0.9827
Insects holes	1	582	7276	0.1341	0.8538	3.7096	8.4058
	2	789	34779	0.3935	0.8145	2.4438	6.6044
	3	257	2312	0.4127	0.8163	2.2764	3.7724

Table 2

Eigenvectors of the texture features

Type	Number	The mean gray-scale value	the variance of gray-scale value	Energy	Contrast	Inverse different moment	Entropy	Correlation
Dents	1	91.25	37.16	50391	339.207	0.089	12.283	0.00074
	2	121.37	26.34	153125	235.408	0.137	11.780	0.00092
	3	105.63	32.41	5486	700.953	0.059	11.250	0.00067
Insects hole	1	107.55	63.81	249656	268.842	0.312	6.4538	0.00086
	2	110.56	90.57	618996	257.502	0.110	12.018	0.00141
	3	132.39	58.35	320679	272.290	0.103	12.464	0.00095

Principal Component Analysis (PCA) (Principal Component Analysis) is a mathematical analysis method that can transform original data into a set of linearly independent data in every dimension through mathematical transformation. PCA (Principal Component Analysis) can extract the main features of the data to achieve the purpose of data dimension reduction, the essence of which is the optimal orthogonal transform (K-L transform) *(Zhang Y., Zhao Y., Liu Y., et al., 2016)*. The principle of PCA is as follows:

Assuming that the initial eigenvector are $x_1, x_2, ..., x_p$, the linearly independent vector after dimensionality reduction of PCA are $z_1, z_2, \cdots, z_m (m < p)$, the relationship between the two can be expressed as formula (2).

$$\begin{cases} z_1 = l_{11}x_1 + l_{12}x_2 + \cdots + l_{1p}x_p \\ z_2 = l_{21}x_1 + l_{22}x_2 + \cdots + l_{2p}x_p \\ \vdots \\ z_m = l_{m1}x_1 + l_{m2}x_2 + \cdots + l_{mp}x_p \end{cases} \quad (2)$$

In the formula, $z_1, z_2, \cdots, z_m$ which are called the principal components are the linear combination of $x_1, x_2, \cdots, x_p$ called the initial eigenvectors, $l_{11}, l_{12}, \cdots, l_{mp}$ are called the correlation coefficient matrix, which reflects the linear relationship between the principal components and the initial eigenvectors. The dimension of the eigenvector is reduced from the P dimension to the m dimension through the correlation coefficient matrix. Because of the different dimensions and orders of magnitude of the eigenvectors selected by this system, the system first normalizes the eigenvectors by Gauss method and then reduces the dimension. The initial thirteen-dimensional eigenvector is dimensionally reduced by PCA to obtain a nine-dimensional eigenvector.

Defect recognition

After obtaining a sufficient number of lumber samples and extracting the corresponding eigenvectors of the defects, three pattern recognition methods were used to classify the lumber surface defects. The three methods are SVM (Support Vector Machine), GMM (Gaussian Mixture Model) and KNN (K-Nearest Neighbor) respectively. SVM (Support Vector Machine) is a support vector machine (SVM) (Support Vector Machine), which is a learning algorithm that can transform low-dimensional linear inseparable samples through kernel function transform into high-dimensional space making these samples linearly separable. SVM (Support Vector Machine) is a supervised learning model whose classification effect is superior to the traditional method of pattern recognition in small sample. It is based on the theory of structural risk minimization, which builds the optimal hyperplane in high-dimensional space and makes the global optimization of machine learning *(Jia L., Achuan W., Xinran M., 2014)*. GMM (Gaussian Mixture Model) is a Gaussian mixture model, through establishing the estimation model of the sample probability density distribution (the estimation model is generally a weighted sum of several Gaussian models, each of which represents a class), the sample data are respectively projected on these models, so as to select the type having the largest probability of various types as a result of the decision *(Abolghasemi V., Ahmadyfard A., 2009)*. KNN (K-Nearest Neighbor) algorithm is also called K-nearest neighbor classification algorithm, which can achieve classification by measuring the distance between eigenvectors. The advantage of KNN (K-Nearest Neighbor) is easy to implement, no parameter estimation and suitable for incremental learning. The disadvantage is that once a sample size of a certain type of defect is too large, the sample easily lead to the new input type are misclassified *(Akbari A., Fard A., Chegini A., 2006)*.

A total of 200 lumber images are contained in the sample database of the system, 50 samples are selected as training samples and the remaining 100 samples are used as test samples. After extracting the corresponding eigenvectors of the defects of samples, three pattern recognition methods, SVM (Support Vector Machine), GMM (Gaussian Mixture Model) and KNN (K-Nearest Neighbor), were used to classify experiment of the surface defects.

The algorithm time of SVM (Support Vector Machine) classification under different kernel functions is basically the same, but the highest recognition accuracy was used the kernel function Gaussian radial base.

The recognition accuracy, using GMM (Gaussian Mixture Model) classification under different covariance matrices and KNN (K-Nearest Neighbor) classification at different K values, were not so good, and which need more time. The classification accuracy of the three recognition methods shown in the Tables 3, 4 and 5.

Table 3

SVM (Support Vector Machine) classification under different kernel functions

Kernel function	Recognition accuracy	Algorithm time(ms)
Polynomial	86%	265
Gaussian radial base	94%	256
Sigmoid	92%	243

Table 4

GMM (Gaussian Mixture Model) classification under different covariance matrices

Covariance matrix	Recognition accuracy	Algorithm time(ms)
Spherical	84%	323
Diag	80%	317
Full	88%	295

Table 5

KNN (K-Nearest Neighbor) classification at different K values

K value	Recognition accuracy	Algorithm time (ms)
1	84%	134
3	82%	207
5	88%	288
7	86%	385

From the Table 3, the comparison of the average recognition rate shows that the SVM (Support Vector Machine) classifier based on Gaussian radial basis function has the highest classification accuracy of 94%.

CONCLUSION

In this study, a hardware system of grayscale and height image acquisition based on Gocator 3D structure laser sensor was set up, and a series of image processing algorithms based on HAICON were designed, such as image resolution, height recovery, segmentation and recognition. Through the experimental test of dents and insects holes of the sample, the feasibility of the scheme is verified. After comparing the experimental data of table three, table four, and table five, the SVM classification algorithm based on the Gauss radial basis function is selected to classify the experimental samples. The recognition accuracy of the SVM (Support Vector Machine) classification algorithm based on the Gauss radial basis function is the highest among the ten classification algorithms adopted by this experiment, but its recognition rate is relatively slow. The following research should improve the recognition rate as far as possible while keeping the recognition accuracy unchanged.

The experimental results show that the wood image acquisition system based on 3D structure and the Halcon based wood defect classification and recognition algorithm based on this study can accurately and quickly identify the wormholes and indentations on the wood surface. Therefore, this study can be used to detect the surface defects in the agricultural and forestry processing industry, so as to improve the level of production and processing, improve the utilization of resources, and make the relevant processing industry move towards industrial automation.

The experimental comparison shows that this system can precisely segment the impact dents and insects holes on the surface and recognize them accurately with a recognition rate of 94%. The results show that the Gocator 3D structured laser based surface defect recognition system has good feasibility and high precision, and which may be used for the quality evaluation of agricultural and forestry products, such as straw-based panels, potato, lumber and veneer.

REFERENCES

[1] Abolghasemi V., Ahmadyfard A., (2009), An edge-based color-aided method for license plate detection, *Image and Vision Computing*, Vol. 27, Issue 8, pp.1134-1142;

[2] Altaf H., Houssni E., Vivian F., (2013), Performance of rice straw-based composites using environmentally friendly polyalcoholic polymers-based adhesive system, *Pigment & Resin Technology*, Vol. 42 Issue 1, pp.24-33;

[3] Akbari A., Fard A., Chegini A., (2006), An effective image based surface roughness estimation approach using neural network. *2006 World Automation Congress*, *IEEE*, pp.1-6;

[4] Jia L., Achuan W., Xinran M., (2014), Fast Recognition for Wood Surface Defect Image Based on the Multi-model Fusion, *Journal of Northeast Forestry University*, Issue 12, pg.25;

[5] Jiang Q., Liu H., (2004), Extracting TM image information using texture analysis, *Journal of Remote Sensing-Beijing*, Vol. 8, Issue 5, pp.458-464;

[6] Liu J., Liang J., Liang X., et al., (2010), Industrial vision measuring system for large dimension work-pieces, *Optics and Precision Engineering*, Issue 1, pp.126-134;

[7] Muhammad Y., Abdul W., Aqeel A. et al., (2010), Efficient Utilization of Rice-wheat Straw to Produce Value-added Composite Products, *International Journal of Chemical and Environmental Engineering*, Vol. 1 Issue 2, pp.136-143;

[8] Qian X.,(2010), Straw-based Panel Will Take a Significant Share in the Panel Market in the Future, *China Wood-Based Panels*, Issue 12, pp.1-5;

[9] Thies M., Pfeifer N., Winterhalder D, et al., (2004), Three-dimensional reconstruction of stems for assessment of taper, sweep and lean based on laser scanning of standing trees, *Scandinavian Journal of Forest Research*, Vol. 19, Issue 6, pp.571-581;

[10] Wang H., Wang F., Sun R., et al., (2016), Policies and regulations of crop straw utilization of foreign countries and its experience and inspiration for China, *Transactions of the Chinese Society of Agricultural Engineering*, Vol. 32 Issue 16, pp.216-222;

[11] Bai X., Zou L., (2007), Segmentation method of lumber surface defects based on gray level-gradient co-occurrence matrix, *Journal of Forest Engineering*, Issue 2, pp.16-18;

[12] Ying C., (2015), Innovate the concept and ways of crop straw utilization to promote farmers' income increase and emission reduction, *Rural work communication*, Issue 7, pp.7-9;

[13] Zhang Y., Zhao Y., Liu Y., et al., (2016), Identification of wood defects based on LBP features. *2016 35th Chinese Control Conference (CCC)*, *IEEE*, pp.4202-4205;

[14] Zhang X., Zhang C., (2016), Wood Surface Defect Image Segmentation Method based on Canny Operator and GGAC Model of Reaction Diffusion Equation, *International Journal of Signal Processing*, *Image Processing and Pattern Recognition*, Vol. 9, Issue 10, pp.57-68;

[15] Zhou D., (2016), Rapidly Rising and Transcending of the Straw-based Panel Industry in China, *China Forest Products Industry,* Vol. 43 Issue 1, pp.3-8;

[16] Zhao P., Zhao Y., Chen G., (2017), Quantitative analysis of wood defects based on 3D Scanning technology, *Journal of Transactions of the Chinese Society of Agricultural Engineering*, Vol. 33, Issue 7, pp.171-176.

RESEARCH ON SUNFLOWER SEEDS DRYING PROCESS IN A MONOLAYER TRAY VIBRATION DRYER BASED ON INFRARED RADIATION

/

ДОСЛІДЖЕННЯ ПРОЦЕСУ СУШІННЯ ЗЕРНА СОНЯШНИКУ У МОНОШАРОВІЙ ЛОТКОВІЙ ВІБРОСУШАРЦІ НА ОСНОВІ ІНФРАЧЕРВОНОГО ОПРОМІНЕННЯ

Prof. PhD. Bandura V., Lect. Ph.D. Mazur V., Lect. Ph.D. Yaroshenko L., Lect. Ph.D. Rubanenko O.
Vinnytsia National Agrarian University/Ukraine;
Tel: +380977480285; E-mail: olenarubanenko@ukr.net

***Keywords**: drying, sunflower, infrared radiation, vibrotray drying.*

ABSTRACT

Currently, drying of food materials by infrared radiation (IR) becomes widespread. The technology of dehydration of products and materials is far ahead of the theoretical drying conditions. Not only classical literature on problems of drying, but also special literature does not give concrete recommendations for the design of installations with electromagnetic energy supply. Therefore, the only reliable way of their study is an experiment. Despite the great scientific amount of literature on drying, including IR-installations, practical issues of designing infrared dryers have not been worked out. Well-known studies are exclusively private.

The technological features of drying sunflower seeds by means of infrared energy supply are described in this paper and the prospects of vibration monolayer drying of sunflower seeds are grounded. The specific energy costs are determined for the process of infrared drying of the product.

РЕЗЮМЕ

В даний час набуває широкого поширення сушіння харчових матеріалів інфрачервоним (ІЧ) випромінюванням. Техніка зневоднення продуктів і матеріалів значно випереджає теоретичні положення сушіння. Не тільки класична література з проблем сушіння, але і спеціальна не дають конкретних рекомендацій з проектування установок з електромагнітним підведенням енергії. Тому поки єдиним надійним шляхом їх дослідження є експеримент. Незважаючи на велику наукову літературу по сушінню, в тому числі і по ІЧ-установкам, практичні питання проектування ІЧ-сушарок не опрацьовані. Відомі дослідження носять виключно приватний характер.

В роботі описані технологічні особливості сушіння зерна соняшнику за допомогою інфрачервоного підведення енергії, та обґрунтовано перспективність вібраційного моношарного сушіння насіння соняшнику. Визначені питомі затрати енергії на процес інфрачервоного сушіння продукту.

INTRODUCTION

In the system of processing operations after sunflower harvesting, the most important place belongs to drying. Quality of drying not only ensures the storage of the harvested crop, prevents its loss, but in some cases also improves the quality of the finished product.

The freshly harvested sunflower seeds have low resistance to storage, especially at high humidity, temperature and debris. When storing seeds, chemical changes have primarily fats, and then protein substances.

High-polluted sunflower seeds are safely stored if their humidity does not exceed 7% and the temperature is lower than 10°C. At high humidity and temperatures between 20 ... 25°C, in the pile seed begins a rapid development of microorganisms, intensive hydrolytic and oxidative processes occur. Such processes lead to a rapid deterioration of sunflower seeds quality. Even a few hours of storage of freshly collected high-oiled sunflower seeds with a moisture above the critical one leads to massive self-heating and spoilage, which makes it impossible to produce high-grade oils (*Stankevich, G.M., 2003*).

At the present stage, with the emergence of farm and rental companies, new requirements have been created for the technology used for post-harvest treatment and, in particular, the drying of cereals and oilseeds. Farmers tend not only to grow a good harvest, but also to bring it to a state suitable for implementation or long-term storage. The grain should have the necessary moisture, maintain its nutritional properties and seed quality. The cost and timing of drying services on elevators do not suit the farmers.

Special problems arise when drying elite seed grain, which is produced in relatively small batches and requires a strict savings mode of drying and does not allow mixing with other varieties.

To solve this problem dryers with infrared energy supply differ from the known ones by high efficiency and speed of drying, simplicity of structure and operation, work quality and flexibility of technological process of drying control. However, the drying process itself, and the machines that provide it, require further research, in order to control their rational parameters. When, in a farm, there are grain crops from 100 to 300 hectares, the presence of such a dryer will increase the efficiency of the technological process after grain harvesting. The proposed type of grain dryer can also be used effectively in grain mills.

The prospects of using infrared drying of freshly harvested sunflower seeds are due to the fact that this drying method is of quite high intensity, economical and allows you to maintain seed nutrient and quality. In addition, there is no need to use air as a thermal agent, which significantly reduces the energy consumption of the drying process. Promising in this sense is a combination of infrared heat conduction and active contact of seeds with unheated air, which provides, for example, a vibro-boiling layer. The use of infrared heat removal for sunflower seeds drying is also facilitated by the black husk colour and the relatively small thickness of sunflower seeds, which, under certain regime parameters, can provide infrared rays penetration into the central layers of the nucleus.

MATERIALS AND METHODS

Infrared (IR) drying has become one of the potential applications to the general drying method because of its advantages such as the simplicity of the required equipment, the easy placement of IR drying with conductive convective and microwave methods, higher heat transfer rate, energy saving and fast transient response (*Boudhrioua et al., 2009; Basman and Yalcin, 2011*).

Infrared drying implies irradiation of a moist material in the range of wavelengths of 0.8-1000 μm of electromagnetic radiation (*Das et al., 2009*). Many researchers have been studying IR drying as a potential method for obtaining high quality dried fruits, vegetables and grains (*Ruiz Celma et al., 2009a; Khir et al., 2011*). Numerous studies have been conducted to improve the efficiency of heating and obtaining high quality dry food products (*Wang and Sheng, 2006; Zhu et al., 2010; Dondee et al., 2011*)

When using infrared radiation to dry the moist materials, the rays pass through the material, penetrate into it, and the radiation energy is converted into heat (*Pan et al., 2008*).

The energy efficiency of infrared dryers is directly related to the absorption characteristics of the material, which determines the economic feasibility of the dryer (*Pawar and Thorat, 2011*). Infrared drying is a method of dehydration that has high-energy efficiency. This means that the energy savings of an IR dryer are greater than that of convection and other drying methods. Given the distance between the heating source and the material, the air flow rate and temperature, as well as the material speed (if it's a continuous IR dryer) can have a significant effect on energy efficiency.

The transmission of infrared energy is carried out without heating the ambient air so there is no need for a heating medium between the source of energy and the material in IR dryers. Because of the rapid and uniform heating, the infrared radiation penetrates directly into the inner layer of the material without heating the surrounding air, and the energy consumption of infrared drying is lower than other methods (*Swasdisevi et al., 2009; Arsoy, 2008*). Summing up and analysing the experiments of other researchers, we can conclude that an increase in the power level of infrared radiation leads to a reduction in the drying time, while an increase in air velocity leads to an increase in drying time and energy consumption. By increasing the air speed, the surface layer becomes cool and requires longer drying time. Thus, the air velocity must be adjusted to provide better results. The power level of infrared radiation should also be adjusted, since increasing power can lead to loss of quality. In addition, there are other factors that were not considered by the researchers such as the effect of vibration on the drying process in IR dryers.

The work of *Das et al., (2009*), studied the drying characteristics of three varieties of high-volatile rice varieties (slenderness, shankar and basmati) using serial vibration infrared dryer with a radiation intensity of 3100 and 4290 W / m^2 and a depth of 12 and 16 mm grain layer. They found that the drying rate depends on the intensity of the radiation, the drying occurred during the fall and the period of constant velocity was not observed. At a given temperature of air for drying (40°C), the increase in the intensity of infrared radiation reduced the drying time in both fixed and vibration modes.

Researchers in the work of *Nourmohamadi- Moghadamiet al., (2017*), also emphasized that one of the methods of grain rapid and uniform drying is vibration.

In the work of *Bandura et al., (2018*), the processes of radiation-convective heat and mass transfer between all the defining objects inside the vibration dryer with IR-power supply are theoretically substantiated. On the basis of thermal and material balances, the equations that describe the main dynamic characteristics of the drying conditions of oily grain material in a continuously operating IR dryer are determined. Due to the fact that the exact analytical solution of the presented mathematical model in the form of a system of differential equations in partial derivatives does not exist, the proposed solution allows identifying dependencies of temperature distribution and moisture content of grain and oil-bearing material on the length of the dryer at any time.

The work of *Burdo et al., (2017*), proposed technologies of targeted energy delivery for the intensification of heat and mass transfer during the processing of food raw materials. The basis of the proposed hypotheses is the wave technologies of the combined electromagnetic and vibrational action. Mechanisms, effects and mathematical models of barodiffusion and actions of vibration fields are grounded. The numbers of wave similarity are proposed, based on which the bases of experimental data on drying are summarized.

In spite of the fact that air in IR-drying is not a coolant, it has a significant impact on the efficiency of heat exchange radiation. The lower the temperature difference between the air and the irradiated surface, the lower the temperature gradient in the material and its uniform heating. A large temperature gradient inside the drying body (seeds, grains) often causes its destruction - the appearance of cracks, deformations, and the like. Therefore, as a rule, in installations for radiation drying the temperature difference between the air and the material to be dried should be limited.

We conducted our research on a "vibration thermo radiation" monolayer "oscillating" heating dryer. According to laboratory studies, it is possible to achieve lower specific energy consumption in comparison with traditional dryers by about 1.5-2 times (*Rogov and Nekrutumman, 1976*). In order to reduce the humidity of products by 6-8%, with its one-time heating, in the chamber over the thermal tray, it is necessary to create sufficiently high temperatures (up to 200-250^{o}C), while the particles of products are warmed up to a temperature of 140-180^{o}C, which is unacceptable for many kinds of grain products, especially for seed grain. Therefore, in further studies, for the reduction of the product particles heating temperature, with the least decrease in its moisture content, it was proposed (*Yaroshenko, 2002; Goncharevich, 1972*) to use "oscillating" heating with infrared rays. In this case the heating periods alternate with the periods of cooling by cold air, and an electromechanical unbalanced vibration drive is used to excite oscillations.

The purpose of the work is to study the kinetics of the technological process of drying sunflower seeds by infrared irradiation in a vibrotray mono dryer.

Experimental-industrial sample of a vibration machine (fig. 1) for drying sunflower seeds, designed and manufactured in the laboratory of technological processes automation of Vinnytsia National Agrarian University, allows a wide range of drying temperature control (from 20 to 180^{o}C), the air velocity varies within 0, 5 ... 2.5 m / s and the oscillation amplitude of the vibrotray varies from 0.5 to 6 mm.

Technical characteristics of laboratory vibration dryer:	
Productivity, kg/h	110;
Power of the electric machine, kW	5.0;
Power vibration drive of the lot, kW	0.5;
Amplitude of vibrotray oscillations, mm	0-6;
Rotation frequency of the driving electric motor, rpm	910;
Temperature in the thermocouple, ^{o}C	20-180;
Weight, kg	230;
Overall dimensions, mm	1400x600x3000

The basic scheme of such a drying machine is shown in Fig. 1. The machine consists of a closed shell housing *1*, on the basic platforms *2* of which, with the help of elastic elements *3*, are installed two solid heating *4* and two perforated grate vibrotrays *5*.

The work path of the thermal tray *4* is made of heat-resistant steel sheet. The working path of the grate tray is formed by longitudinal vertical strips *7* welded to the brackets *8* so that there is a longitudinal clearance δ = 1.5 ... 2 mm between them. Inside of each tray, there are mounted vibration drives, containing two centrifugal vibro-exciters mounted by the sides of the tray.

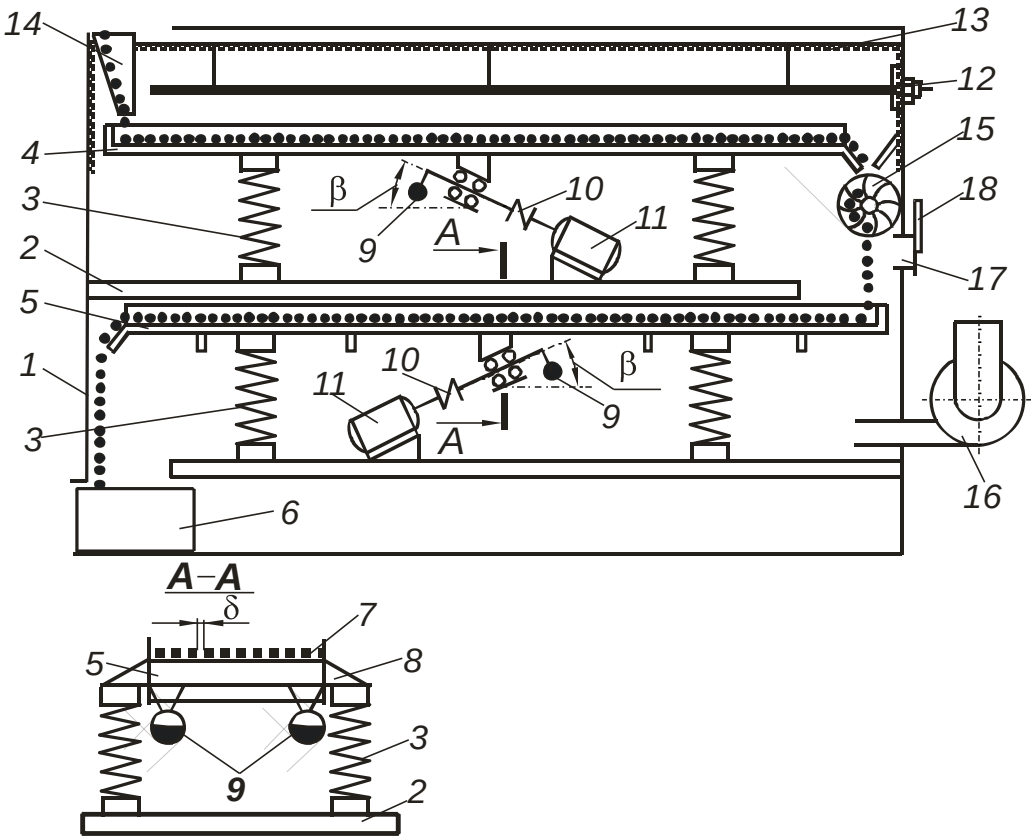

Fig. 1 - Scheme of laboratory infrared monochrome vibration dryer

1 - body; 2 - platform; 3 - elastic elements; 4 – heating tray 5 - grain tray 6 - receiving tank; 7 - longitudinal vertical stripes; 8 - bracket; 9 - unbalance load; 10 - elastic coupling; 11 - electric motor; 12 – thermo-generators; 13 - thermal insulation; 14 - feeding throat; 15 - impeller; 16 - fan; 17 - outlet pipes; 18 - shutters.

Each centrifugal vibrator has a shaft with unbalanced loads *9* which, by means of an elastic muffle *10*, is connected to an actuating asynchronous electric motor *11*. Moreover, in each vibration drive, the electric motors *11* are connected in such a way that, when connected to the network, their rotors are rotated toward each other. Shafts with unbalanced loads *9* are installed on the bearings parallel to each other at an angle *β* to the planes of the trays work tracks. Above the surfaces of the thermal trays *4* are fixed heat generators *12* (infrared emitters). At the top and on the sides, the thermal tray *4* is covered with thermal insulation *13*. Above the start of the thermal tray *4*, the feeding throat *14* is fixed, and at the end of the impeller *15*, at the beginning of the grate tray *5*, there is a discharge nozzle of the fan *16*, and above the grate tray *5*, the outlet pipe *17* with the adjusting shutter *18*. The receiving tank *6* was installed at the end of the grate tray *5*.

The machine works in the following way. When activating electric motors *11*, their rotors start to rotate towards each other in each vibration drive, which leads to a dynamic synchronization of their rotation and the emergence of a directed forcing power. Therefore, the reciprocating vibrations of the trays *4* and *5* are formed at an angle *β* to the planes of their work paths (in the direction of the forcing power). Bulk products are fed through the feed throat to the surface of the trays, where the vibration is distributed by a mono layer. Under the influence of trays vibrations between their surfaces and particles of bulk products there is an asymmetry of frictional forces, which leads to the directed movement of particles of bulk products (vibration transport) along the surface of the trays. At the same time, the points of the trays surface fluctuate relative to some centre without directed motion in general for the period of one oscillation. By changing the static moments of the unbalanced cargoes *9* relative to the rotation axis, a vibration transport mode is established with the continuous dumping of the particles of bulk products during their movement along the trays. Continuous pouring of product particles leads to their chaotic whirlabout when moving along thermal trays *4* above which there are thermo-generators *12* and contributes to their uniform irradiation on all sides with infrared rays, which leads to intense, rapid and uniform heating of sunflower seeds.

Fig. 2 - Photo of experimental vibrotray infrared dryer
(impeller, outlet pipes, regulating sider on the photo not shown)

After passing the thermal lot, the sunflower seeds are fed through the drum impeller *15* to the grate lot *5*, which is blown by the atmospheric air from the fan *16*. In this case, the continuous chaotic throwing and turning of the product particles also improves the uniformity of blowing them with air. It leads to disturbance of the equilibrium state of moisture in product particles, when the pressure of water vapour in them becomes greater than the partial pressure of water vapour in the air, as a result of which moisture begins to intensively evaporate (*Yaroshenko, 2002; Goncharevich, 1972*). The processed seeds are fed into the receiving tank *19*. The drum impeller *15* prevents access of the cold air from the fan *16* to the high temperature chamber over the heating tray *4* and at the same time allows the product to be moved from the heating tray *4* to the grate *5*. The airflow intensity is controlled by a shutter *18*. The speed of vibration transport of loose products, and therefore the time it is located on the surface of the trays, is regulated. The regulation is carried out by changing the static moments of the unbalance loads *9* relative to the axis of rotation, or the angle of the oscillation direction of the vibrating trays *β*. Since the infrared radiation of the thermo-generator *12* can create a very intense heat flow, which facilitates the rapid heating of the product particles, and the process of evaporation requires more time, the speed of vibration transport on the grate tray *5* is set higher and it is made with wider work paths.

The infrared heater consisted of 20 infrared lamps of 250 W (OSRAM, Slovakia), located in the drier in a chess manner. The distance between the lamps, at which the maximum uniformity of the energy irradiance of the dried material surface is achieved, is 0.12 m. The lamps are powered by a 220 V power supply. The infrared lamps can be located 5 ... 15 cm away from the surface of the tray.

Humidity of sunflower seeds is determined by drying the samples to a constant mass. Samples were taken before and after infrared irradiation and blowing by air.

The product loading tank is equipped with a gateway that regulates the thickness of the product monolayer on the lot within the range of 7 ... 22 mm, depending on the size of the grain and the speed of its movement on the tray.

The intensity of the infrared radiation varied as the distance between the lamps and the reception surface changed. Also, to achieve the required uniform levels of intensity of infrared radiation, the before mentioned distance was regulated manually, changing the height of the suspension of the lamp body. To ensure the uniformity of infrared radiation over sunflower, preliminary measurements were made prior to the main tests.

The weight of the grain was determined by the electronic weights TWE-0.21-0.01. The temperature of the product was measured remotely by the Laserliner pyrometer. The change in the mass of grains before and after drying determined the mass of the evaporated liquid.

The experiments recorded the length of the process, the temperature and mass of sunflower in the beginning and at the end of the treatment. Specific mass of material (g) ranged from 4.11 to 8.22 kg/m^2, shows the product weight (m) per unit processing surface (F) and specific power from 2.0 to 5.0 kW/m^2 – IR-

energy consumed per 1 m^2 of treated surface. Experiments were conducted at room temperature of 20°C, relative humidity of 65% in the room. The influence of the IR-power on the average speed of the drying process was studied. Experiments were carried out at a rate of grain movement per lot 0.025 m/s, and a specific load of 4.11 kg/m^2. The amount of moisture was determined by the initial and final humidity of sunflower. The drying rate was calculated based on the amount of moisture and the time during which sunflower was affected by infrared radiation.

Table 1

Range of the process of IR - drying study

Raw material	Specific power IR [kW/m^2]	Temperature, T [°C]	Download, *g* [kg/m^2]	Duration process t [min]
Sunflower seeds	2.0…5.0	33…43	4.11…8.22	30…60

The mass flow rate of the inlet air was provided by the fan and controlled by an electric inverter (N50-007SF, Korea). Air velocity for all experiments was measured using TESTO Anemometer 425 (Germany) with an accuracy of ± 0.03 m / s. The speed of air varies within 0.5 ... 2.5 m/s by adjusting the fan engine speeds.

The initial moisture content of sunflower seeds was 17±0.5%. In total, 34 experiments were performed on combinations of three levels of infrared radiation (2000, 3000, 5000 W/m^2) and vibration (24 Hz)). To measure the change in humidity during drying, the vibrotray dryer was stopped and samples were taken at a time interval of 7 minutes.

RESULTS

Any modernization of the dryer can be considered quite effective if the reduction of specific energy consumption (with the obligatory preservation of product quality) is achieved.

The parameters of IR-drying for sunflower seeds recommended by OSRAM lamps on the basis of experimental studies are: height of hanging infrared emitter during drying of grain h = 0.1 m; t_{min} = 35°C to t_{max} = 43°C. With an increase in specific power by 2.5 times (Fig. 3), the drying process decreases in proportion.

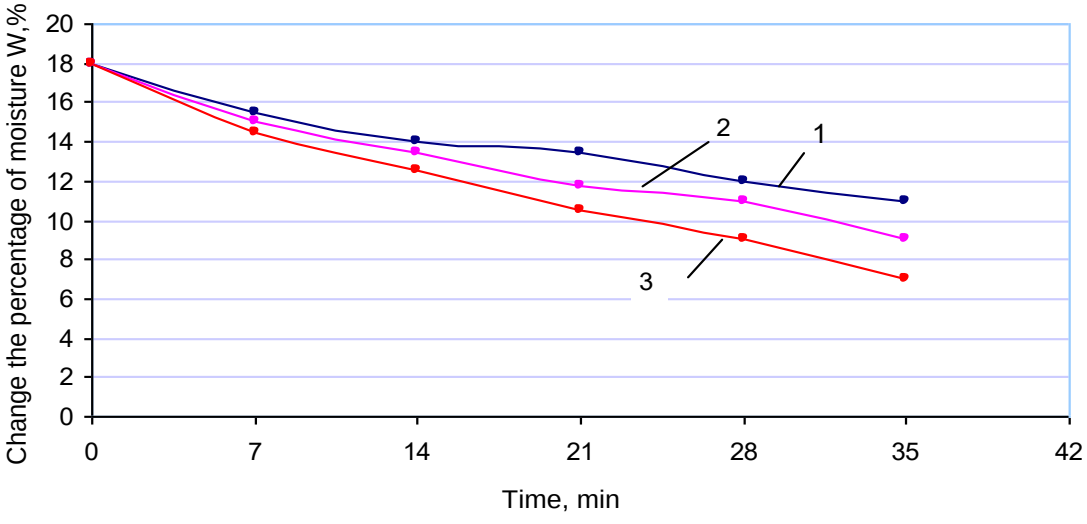

Fig. 3 - Effect of specific power on kinetics of drying

1 - N = 2000 W / m^2; 2 - N = 3000 W /m^2; 3 - N = 5000W / m^2.

The conducted analysis and experimental research suggest that the use of infrared irradiation for drying oilseed raw materials has significant prospects. It is shown that with an increase in the specific power of infrared radiation, the removal of moisture from the product increases over the same period of time.

The drying time to reach the relative humidity of the product of 6-7% takes 35 ... 60 minutes. The data (fig. 3) determined the values of the drying rate (Fig. 4).

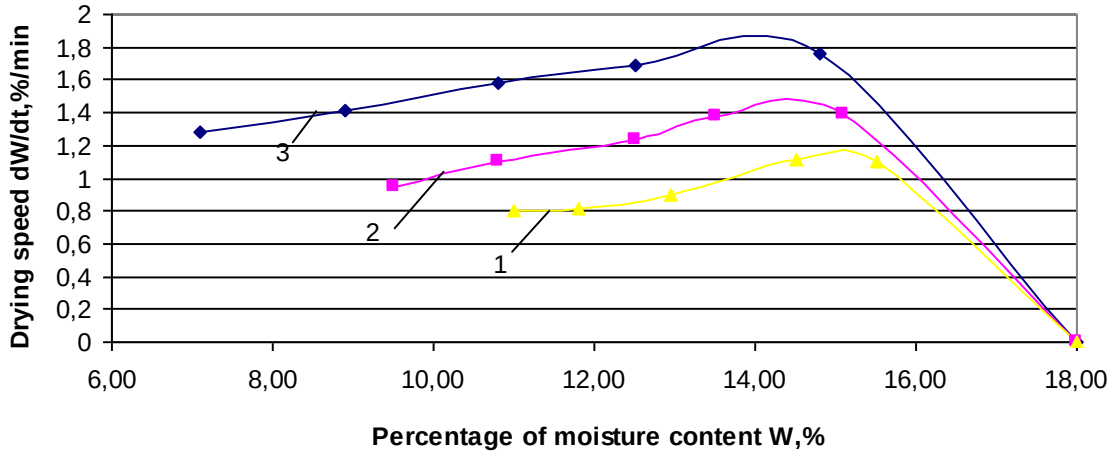

Fig. 4 - Effect of specific power on the drying speed
1 - N = 2000 W / m²; 2 - N = 3000 W / m²; 3 - N = 5000 W / m².

It can be seen (Fig. 4) that, when the amount of IR-power is increased by 2.5 times, the drying rate increases by 50%. The drying rate varies within 1 ... 2.15% / min. The productivity of the installation in a loading mode of 4.11 kg/m² at a rate of grain movement per tray 0.016 ... 0.025 m/s was 80 ... 110 kg/h of dry grain with a moisture content of 6.5%. At the same time, for an increase of power of 2.5 times the increase in the temperature of sunflower seeds at the outlet does not exceed 43°C (Fig. 5), which is very important in the process of drying sunflower seeds.

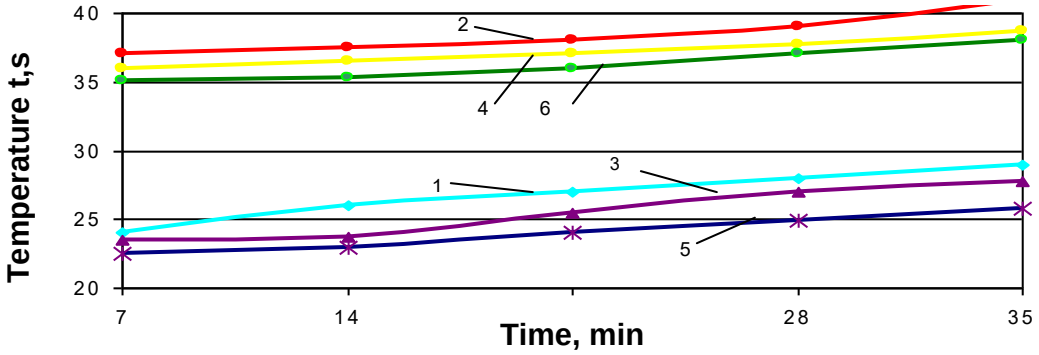

Fig. 5 - Effect of specific power on product temperature
1 - the product temperature at the input to the dryer at N - 5000 W / m²;
2 - the product temperature at the outlet of the dryer at N -5000 W / m²;
3 - the product temperature at the entrance to the dryer at N -3000 W / m²;
4 - the product temperature at the outlet of the dryer at N-3000 W / m²;
5 - the product temperature at the input to the dryer at N -2000 W / m²;
6 - the product temperature at the outlet of the dryer at N -2000 W / m²;

On the basis of the conducted researches the principal scheme of the vibrotray monolayer dryer of intermediate infra-red heating is proposed in Fig. 6. The machine consists of a closed shell housing *1*, on the basic platforms *2* of which, with the help of elastic elements *3*, are installed two (or more) solid thermal *4* and two (or more) perforated grate lots *5.*

The trays are installed under each other, so that the thermal trays *4* alternate with the tray, with the top (first) tray heating and the bottom cooling. The working tracks of the heating trays *4* are made of heat-resistant sheet of steel. The working tracks of the grate strips are formed by longitudinal vertical strips *7* welded to the brackets *8*, in order to have a longitudinal clearance d = 1.5 ... 2 mm between them. In the middle of each tray is mounted the vibration drive, containing two centrifugal vibro-accelerators mounted on the sides of the tray. Each centrifugal vibrator has a shaft with unbalance loads *9,* which, by means of an

elastic coupling *10*, is connected to a driving asynchronous motor *11*. Moreover, in each vibration drive, the electric motors *11* are connected in such a way that, when connected to the network, their rotors are rotated towards each other. Shafts with unbalance loads *9* are installed on the bearings parallel to each other at an angle *β* with the planes of the work tracks of the trays. Above the surfaces of the thermal trays, *4* there are thermo-generators fixed.*12*. On top and on the sides, the thermal trays *4* are covered with thermal insulation *13*. Over the first of the thermal trays *4*, there are feeders *14* fixed, and at the end of the drum − impellers *15*. Below the surfaces of the grate bar *5* are located the nozzles of the fans *16* and above the surface of the grate bars *5* - the outlet pipes *17* with the adjusting shutters *18*. At the end of the lower grate tray *5,* the receiving tank *19* is installed.

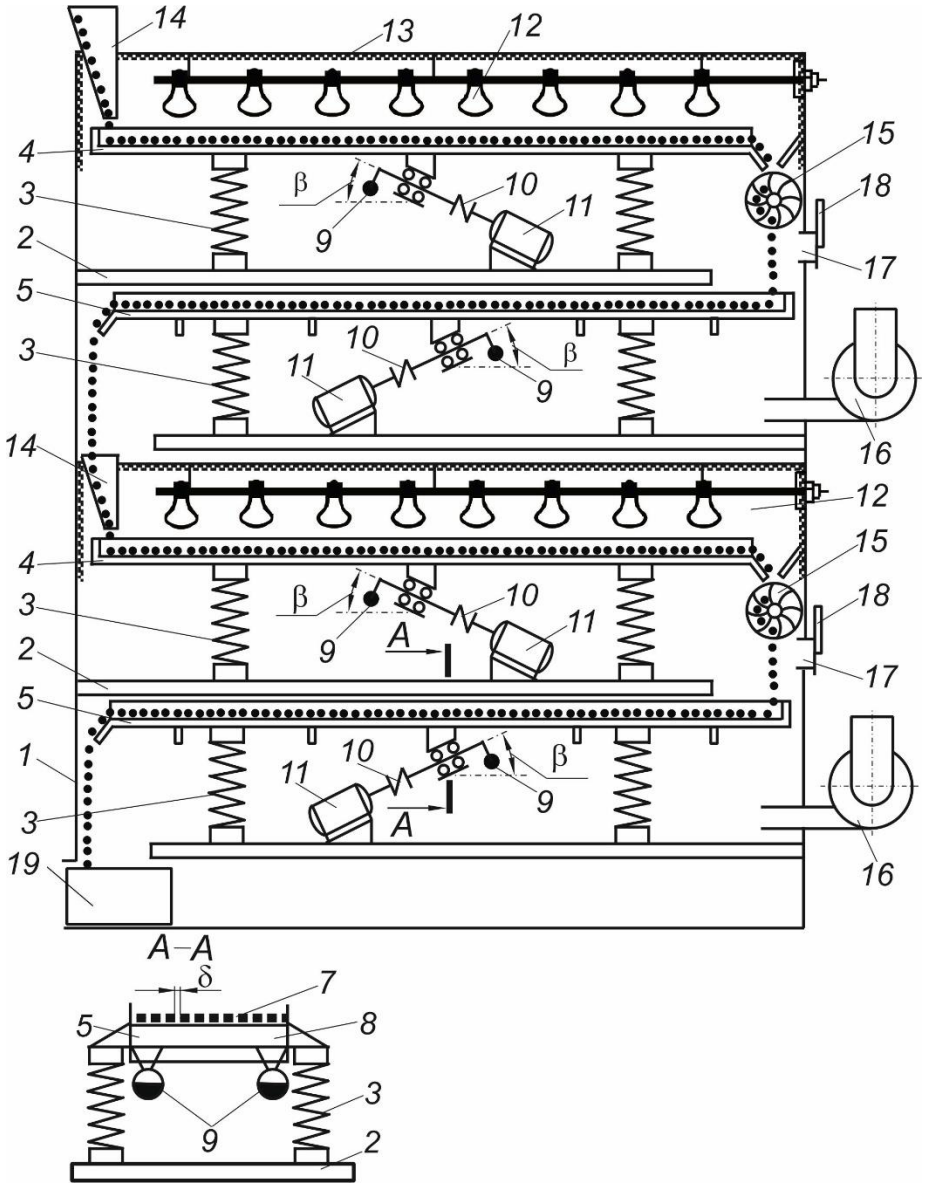

Fig. 6 - Principal scheme of vibration monolayer lot dryer

1 - body; 2 - basic platforms; 3 - springs; 4 - the solid tray; 5 - a grate tray; 7 - strip; 8 - bracket; 9 - shaft with unbalance loads; 10 - elastic coupling; 11 - actuating electric motors; 12 - ICZ lamp; 13 - thermal insulation; 14 - feeding throat; 15 - drum impeller; 16 - electric fan; 17 - branch pipe; 18 - shutters; 19 - the receiving tank.

When the rotors of the activated electric motors *11* start to rotate towards each other in each vibration drive, it leads to a dynamic synchronization of their rotation and results in the translational vibrations of trays *4* and *5* at an angle *β* to the planes of their work paths. Bulk products are fed through the filling throat to the surface of the trays, where the vibrations are distributed by a monolayer.

Under the influence of the vibrations of trays between their surfaces and particles of bulk products there is an asymmetry of frictional forces, which leads to the directed movement of particles of bulk products (vibration transport) along the surface of the trays. At the same time, the points of the surface of the trays fluctuate relative to some centre without directed motion in general for the period of one oscillation. By changing the static moments of the unbalanced cargoes *9* relative to the rotation axis, a vibration transport mode is established with the continuous dumping of the particles of bulk products during their movement along the trays. Continuous throwing of product particles leads to their chaotic whirlabout when moving along thermal trays *4*, over which there are IR heaters *12* and contributes to their uniform irradiation on all sides with infrared rays, which leads to intensive, rapid and uniform heating of sunflower seeds. A reflecting screen is placed on the heater to create a directed beam of radiation from infrared heaters over a layer of grain.

After passing the thermal trays, the heated bulk product is fed through the drum impeller *15* to the grate *5*, which is blown by the atmospheric air from the fans *16*. In this case, the continuous chaotic throwing and turning of the product particles also improves the uniformity of their airflow. It results in a disturbance of the equilibrium state moisture in product particles, when the pressure of water vapour in them becomes greater than the partial pressure of water vapour in the air, as a result of which moisture begins to intensively evaporate. Bulk products alternately pass through several thermal trays *4* and accordingly through several grate stones *5*, which leads to periodic heating and cooling of its particles, and therefore to create optimal conditions for evaporation of moisture, at a low maximum temperature of heating particles of products.

Infrared heaters are installed over a conveyor on which a layer of sunflower seeds (2-3 grains) is placed parallel to the outer surface. A reflective display is placed on the heat layer and the side walls to create a directed beam of radiation from infrared heaters on a layer of grain. Transportation of grain along infrared emitters is accompanied by the mixing of grains normally to the surface of the conveyor, respectively, and before irradiation.

Since the infrared radiation of the thermo-generator *12* can create a very intense heat flux, which facilitates the rapid heating of the particles of products, and the process of evaporation from them requires more time, the speed of vibration transport on the grate bins *5* is set higher, and they are made with wider work paths.

The drying machine described above reduces the specific energy consumption by approximately 1.5-2 times compared with convection shaft driers, retains all the advantages of the laboratory infrared monochrome vibration dryer described above. At the same time, the maximum temperature of products particles heating is 1.5 - 2 times less with larger limits of their humidity. This allows higher quality production of products at lower heat costs.

However, since the output moisture content of loose products may fluctuate within very wide limits, in order to regulate the speed of vibration transport of bulk products along the vibrotrays, and therefore the time of their processing on each tray, it is necessary to adjust the parameters of the lot vibrations by changing the magnitude and frequency of force oscillations to provide energy saving resonance mode of vibration drying. To solve this problem, it is possible to use *(Yaroshenko et al. 2018*) or an unbalance controlled vibration drive with an adjustable magnitude of static imbalance, or an unbalance vibration drive in which a wide-pulse frequency governor of a three-phase alternating current is used for feeding the electric motors. It allows you to adjust the angular speed of the drive motors (and therefore, to maintain the resonant frequency of vibrotrays oscillations and to adjust the magnitude of the vibro-exciter force).

CONCLUSIONS

- Complex experimental research was performed in the vibration laboratory infrared monolayer dryer to discover the influence of regime parameters (specific load and power) on the kinetics of sunflower seeds IR drying.
- With an increase in specific power of up to 2.5 times, the drying process decreases in proportion. The drying time to the relative humidity of the product at 6-7% takes 30...60 minutes. The average temperature of the product was within 35-43ºC. There was no cracking of the husk.
- Vibration monolayer dry intermittent infrared heating allows reducing the specific energy consumption approximately of up to 1.5-2 times, in comparison with the convection dryer, which retains all the advantages of laboratory infrared monochrome vibration dryer. At the same time, the maximum temperature of products particles heating is 1.5 - 2 times less with larger limits of their humidity. This allows for higher quality production of products at lower heat costs.

REFERENCES

[1] Arsoy S. (2008), Temperature-controlled infrared drying characteristics of soils. *Drying Technology*, Vol. 26 (12), pp.1477-1483;

[2] Bandura V.; Kalinichenko, R.; Kotov, B.; Spirin, A. (2018), Theoretical rationale and identification of heat and mass transfer processes in vibration dryers with IR-power supply*, Eastern European Journal of Enterprise Technologies*, Vol.4/8 (94), pp.50-58, Ukraine;

[3] Basman A., Yalcin S., (2011), Quickboiling noodle production by using infrared drying. *Journal of Food Engineering,* Vol.106, pp.245-252;

[4] Boudhrioua N., Bahloul N., Slimen I. B., Kechaou N., (2009), Comparison of the total phenol content and the colour of fresh and infrared dried olive leaves*. Industrial crops and products*, 29, 412-419;

[5] Burdo O., Bandura V., Zykov A., Zozulyak I., Levtrinskaya J., Marenchenko E., (2017), Development of wave technologies to intensify heat and mass transfer processes, *EA-Western European Journal of Enterprise Technologies,* Vol.4/11 (88), pp.34-42;

[6] Das I., Das S.K., Bal S., (2009), Drying kinetics of high moisture paddy undergoing vibration-assisted infrared (IR) drying. *Journal of Food Engineering*, Vol.95, pp.166-171;

[7] Dondee S., Meeso N., Soponronnarit S., Siriamornpun S., (2011), Reducing cracking and breakage of soybean grains under combined infrared radiation and fluidized-bed drying. *Journal of Food Engineering*, Vol.104, pp.6-13;

[8] Goncharevich I.F., (1972), *Dynamics of vibrational transportation*. Moscow: Nauka, 212p. Moscow / Russia;

[9] Khir R., Pan Z., Salim A., Hartsough B. R., Mohamed S., (2011), Moisture diffusion of rough rice under infrared radiation drying. LW T, *Food Science and Technology*, Vol. 44, p. 1126-1132;

[10] Nourmohamadi-Moghadami A, Rahmanian-Koushkaki H, Zare D, Karimi G., (2017), Experimental and theoretical investigation of hot air-infrared thin layer drying of corn in a fixed and vibratory bed dryer, Engineering in Agriculture, *Environment and food*, doi: 10.1016 / j.eaef. 2017.01.004;

[11] Pan Z., Shih C., McHugh T.H., Hirschberg E., (2008), Study of banana dehydration using sequential infrared radiation heating and freeze-drying. *LWT - Food Science and Technology*, Vol.41, pp.1944-1951;

[12] Pawar S.B.; Thorat B.N., (2011), Infrared drying of alumina-silicate mineral cake. *Drying Technology, Vol.29 (7),* pp.819-824*;*

[13] Rogov I.A., (1976), *Ultra frequency and infrared heating of food products (Сверхчастотный и инфракрасный нагрев пищевых продуктов)*, Publishing house "Food industry", 210 p. Moscow / Russia.

[14] Ruiz Celma A., Cuadros F., López Rodríguez F., (2009a), Characterization of industrial tomato by-products from the infrared drying process. *Food and Bioproducts Processing*, Vol. 87, pp. 282-291;

[15] Stankevich G.M., (2003), Modern drying of sunflower seeds is a guarantee of their quality and safety (Современная сушка семян подсолнечника–залог их качества и сохранности). *Olive-fat complex*, Vol.2, pp.25-28/, Kiev / Ukraine;

[16] Swasdisevi T., Devahastin S., Sa-Adchom P., Soponronnar S., (2009), Mathematical modeling of a combination of far-infrared and vacuum drying banana slice. *Journal of Food Engineering*, Vol. 92 (1), pp.100-106;

[17] Wang J., Sheng K., (2006), Far-infrared and microwave drying of peaches. *Food Science and Technology,* Vol.39 (3), pp.247-255;

[18] Yaroshenko L.V., (2002), *Method of vibro-moistened drying*. Patent No. № 45431, Ukraine;

[19] Yaroshenko L.V., Chubik R.V., Bandura V.M., Tomchuk V.V., Shiver N.M., (2016) *Controlled vibration drive of directional action with paired balance.* Patent No. 116418, C2 Ukraine;

[20] Zhu Y., Pan Z., McHugh T.H., Barrett D.M., (2010), Processing and quality characteristics of apple slices processed under simultaneous infrared dry-blanching and dehydration with intermittent heating. *Journal of Food Engineering,* Vol.97, pp. 8-16.

DESIGN AND EXPERIMENTAL OPTIMIZATION OF CLEANING SYSTEM FOR PEANUT HARVESTER

/

捡拾花生收获机清选系统的设计与试验优化

Ph.D. Eng. Wang Shengsheng[1,2)], Prof. Ph.D. Eng. Ji Jiangtao[1,2*)], Prof. Ph.D. Eng.Jin Xin[1,2)], Prof. Ph.D. Eng.Geng Lingxin [1)]

[1)] Henan University of Science and Technology, College of Agricultural Equipment Engineering / China;

[2)] Collaborative Innovation Centre of Machinery Equipment Advanced Manufacturing of Henan Province / China

Tel:+86-379-64877837; E-mail: jjt0907@163.com

Keywords: *Peanut harvester, Cleaning system, Design analysis, Experimental optimization*

ABSTRACT

The new cleaning system, mainly composed of light impurities cleaning device and stems separating device was designed. The former used cross-flow fan to clean light impurities, and the latter used the differences of radial geometry size between peanut pods and stems to separate stems from peanut pods. By means of theoretical calculation and graphic analysis, the structure motion parameters of the main working parts were determined and the performance experiments were carried out. According to the experimental results, the influence law of the structure motion parameters of peanut cleaning system on cleaning performance was analyzed and optimal combination of parameters was obtained. When the rotation speed of cross-flow fan was 920 r/min, the distance between sliding screen and fan impeller was 100mm, and the width of discharging exit was 50 mm, the clearance of separation rollers was 2mm, the rotation speed of separation roller was 300 r/min, and the angle between separating device and horizontal plane was 35°, the impurity content was 0.89%, and the cleaning loss rate was 0.62%, which met the requirement of peanut harvester.

摘要

设计了一种主要由轻杂物清理装置和断杆分离装置组成的花生清选系统，前者采用横流风机以吸气方式清理待清选物料中的轻杂物，后者根据荚果与断杆的径向几何尺寸差异将断杆分离出去。利用解析作图法对断杆分离装置进行受力和运动分析，得出了断杆顺利分离满足的力学关系，并通过理论计算得出了分离辊的结构参数。进行室内参数清选试验，研究了各结构运动参数对花生清选损失率和含杂率的影响，结果表明：当横流风机转速为 920r/min、滑板到风机叶轮的距离为 100㎜、落料口宽度为 50㎜、分离辊间隙为 2㎜、分离辊转速为 300 r/min、分离装置与水平面呈 35°倾角时，清选系统的性能指标：含杂率为 0.89%，清选损失率为 0.62%。

INTRODUCTION

Peanut is one of the important oil and economic crops which has a long cultivation history in China, accounting for about 20% of the total planting areas of the world. Peanut harvesting machinery in foreign countries starts earlier and its technology is relatively mature, while the domestic mechanical harvesting technology level is relatively low *(Colvin B.C. et al,2018; Reddy K.M. et al, 2013; Lim J. et al, 2016; Zhou Dehuan et al, 2017; Shang Shuqi et al, 2005; Ortiz B V et al, 2013)*. As an important part of peanut harvesting machinery, the working performance of cleaning system directly affects the quality of the whole machine. The existing peanut harvesters generally adopt simple air separation or air-screen combination, which has the problems of high impurity rate and high loss rate, seriously restricting the further development of peanut industry *(Tang Bei et al, 2016; Wang Dongwei et al, 2013; Guan Meng et al, 2014; Liang Zhenwei et al, 2018)*. Lots of researches have been done by scholars at home and abroad. Wang Bo and others have designed a new experimental platform of cleaning device for peanut combine harvester *(Wang Bo et al, 2015)*. Zhang Rihong and others have used SolidWoks to simulate and analyse the structure and motion parameters of the vibrating screen and obtained the main factors affecting the screening rate *(Zhang Rihong et al, 2010)*. Tang Bei and others have optimized the fan-vibration sieve cleaning device of 4HBL-2 type peanut combine harvester based on the cleaning characteristics of peanut trashed materials and carried out experiments in the field *(Tang Bei et al, 2015)*.

Based on the differences of radial geometry size between peanuts pods and stems, this study designed a new peanut harvester cleaning system. While the influence law of the structure motion parameters of peanut cleaning system on cleaning performance was studied through test in the laboratory and the optimal combination of parameters was obtained. It could solve the difficulties of cleaning problem in the working process of peanut harvesting mechanization preliminarily.

MATERIALS AND METHODS

- **Structure and principle of peanut cleaning system**

The structure diagram of peanut harvester cleaning system test-bed is shown in Fig.1. It was mainly composed of conveyor belt, cleaning device and collection device and the cleaning device was composed of the light impurities cleaning device and stems separating device. The former consisted of feeding hopper, sliding screen and cross-flow fan, etc.; and the later consisted of a number of separation rollers that rotated oppositely, guide plates, gear transmission mechanism and thread adjusting rod, etc.

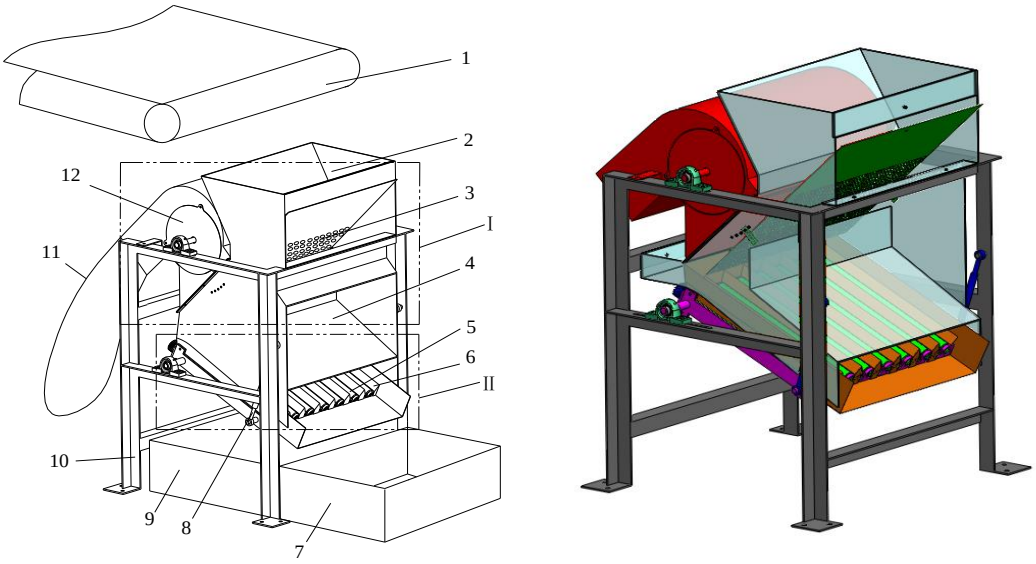

Fig. 1 - Structure diagram of peanut harvester cleaning system test-bed

Ⅰ-Light impurities cleaning device Ⅱ-Stems separating device

1-Conveyor belt; 2-Feeding hopper; 3-Sliding screen; 4-Housing;5-Separation roller; 6- Guide plates; 7-Pods box; 8-Thread adjusting rod; 9-Stems box; 10-Rack; 11-Mesh bag;12-Cross-flow fan

Peanut harvester cleaning device adopted the working principle of air-suction and separation double rollers. Peanut trashed materials were fed stably by conveyor belt to the cleaning device feeding hopper and then slid down along slant sliding screen. Because the sliding screen was full of vents, impurities and short stems were inhaled into cross-flow fan by high speed air through the vents of sliding screen and fan inlet in the slipping process of trashed materials; they were discharged into the mesh bag from the outlet of cross-flow fan. Thus, impurities and short stalks separation from peanut pods was realized. The rest of trashed materials were falling to stems separating device through the discharging exit at sliding screen bottom, and stems were took by opposite rotating separation rollers and sent into stems box. Peanut pods cleaned over stems separating device were falling to pods box. Finally, it completed cleaning work of peanut trashed materials.

- **Design of main working parts of clearing system**

Design of sliding screen

Sliding screen was composed of two different screens, one large, the other small, and the size (length×width) of two different screens were respectively 600mm×580mm, 600mm×200mm. There were many vents in the two screens and cross-flow fan could be provided with air by virtue of vents. In addition, according to the experimental need, the length, position and inclined angle of sliding screen all could be adjusted, changing the width of discharging exit, the distance between sliding screen and fan impeller, the speed of materials sliding along sliding screen and other related parameters.

According to the friction and movement characteristics of peanut pods, we determined the angle of sliding screen as 40° based on experiment of test-bed under the condition that material is not congested during the decline of materials.

Design of cross-flow fan

Due to the unique structure and working principle, the cross-flow fan has many advantages which are lacking in the other kinds of fans, such as high characteristic coefficient, distributing the wind evenly along the fan shaft, self-cleaning ability and so on. All of these advantages of cross-flow fan make the suction part possible *(Marian and Pawel, 2012; Liu Shiduo et al, 1998)*.

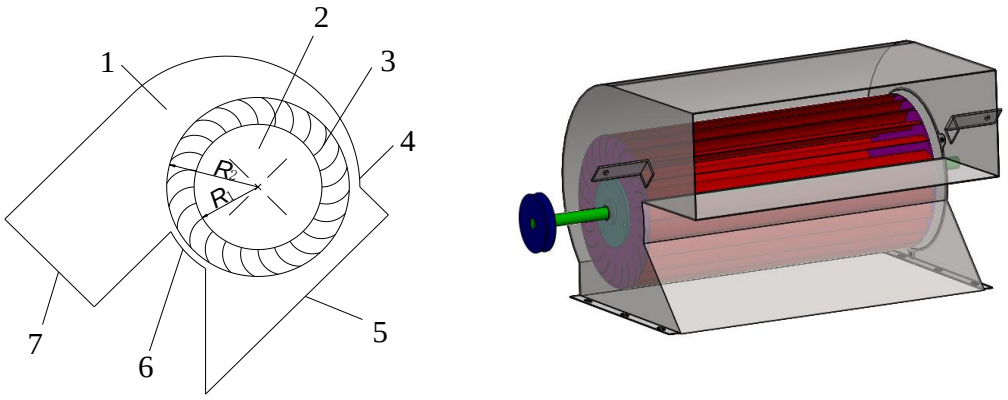

Fig. 2- Structure diagram of cross-flow fan

1-Fan shell; 2- Impeller; 3-Blade; 4-Back shell; 5-Air inlet; 6-Volute tongue; 7-Air outlet

The cross-flow fan designed is shown in Fig. 2; it was mainly composed of fan shell and impeller. The impeller blade is tilted forward and the fan shell adopted eccentric circular approximation scheme design. The main design parameters of cross-flow fan are presented in Table 1.

Table 1

Main design parameters of cross-flow fan

Parameters	Values
Impeller internal diameter [mm]	182
Impeller outer diameter [mm]	260
Blade number	24
Installation angle of blade inlet [°]	90
Installation angle of blade outlet [°]	25
Clearance of impeller outer diameter & volute [mm]	15
Clearance of impeller outer diameter & volute tongue [mm]	10

We imputed the above data in Table 1 into calculating formula (1) and calculated blade curvature radius of 36.58mm.

$$R = \frac{R_2^2 - R_1^2}{2(R_2 \cos\beta_2 - R_1 \cos\beta_1)} \quad (1)$$

where, R is mean curvature radius of blade, mm; R_1 is impeller internal diameter, mm; R_2 is impeller outer diameter, mm; β_1 is installation angle of blade inlet, °; β_2 is installation angle of blade outlet, °.

Design of stems separating device

Stems separating device was one of the core parts of peanut cleaning system, which had direct influence on the working performance of the system. If the separation of stems and pods is achieved, the clearance and diameter of separation rollers must also be considered.

Stems separation device were installed on the rack in a certain angle with the horizontal surface, and the angle could be adjusted in a certain range through the screw adjusting lever to change the speed of the material's decline. Each pair of separation rollers rotated in double opposite directions and adopted the method of gear meshing to transmit power. When stems and pods fell to separating device from sliding screen, they were going down along the axis of the separation roller under the gravity action; meanwhile they were led into the grooves which are formed by each pair of separation rollers rotating oppositely by guide

plates. In order to facilitate the analysis, it was assumed that both stem and pod were cylindrical in the rule. When stem and pod were captured by separation rollers, they were respectively subjected to the reacting force of N, Ng and the grasping force of T, Tg of separation rollers. Force analysis is shown in Fig. 3.

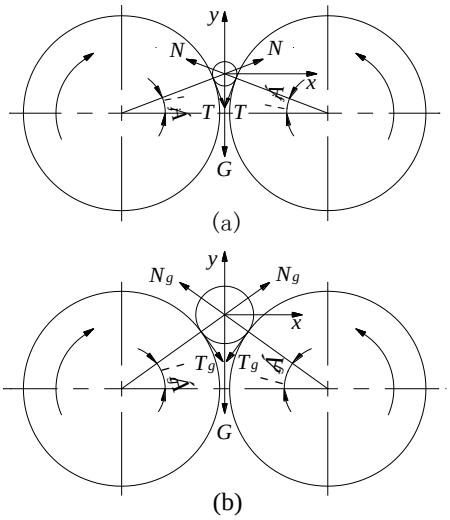

Fig. 3 - Diagram of force analysis

(a) - Stem force analysis; (b) - Peanut pod force analysis

The requirement of separation roller working normally should be that it can grasp stems but not grasp peanut pods. In the case of ignoring the influence of gravity, the requirement of separation rollers grabbing stems was that the resultant force on the Y-axis should be in the negative direction.

$$T\cos\alpha_{\mathrm{j}} - N\sin\alpha_{\mathrm{j}} > 0 \tag{2}$$

Due to $T = N\mu_{\mathrm{j}}$, plugging it into the equation (2), we could get the equation as follows:

$$\tan\alpha_{\mathrm{j}} < \mu_{\mathrm{j}}$$

where, μ_{j} is friction coefficient of stems and nylon; α_{j} is the starting angle of separation rollers grasping stems, °.

Similarly, the following conditions must be satisfied for the pods not to be crushed by the separation roller:

$$\tan\alpha_{\mathrm{g}} > \mu_{\mathrm{g}}$$

where μ_{g} is friction coefficient of pods and nylon; α_{g} - starting angle of separation rollers grasping pods, °.

Given all that, the conditions are as follows: the tangent value of starting angle of separation rollers grasping stems should be less than the friction coefficient of stems and nylon; the tangent value of starting angle of separation rollers grasping peanut pods should be greater than the friction coefficient of pods and nylon.

Design of separation roller

The parameters of separation roller mainly include the material of separation roller, diameter, length, clearance, rotational speed, etc. All of the parameters above decide the separation performance of stems separating device directly; meanwhile the separation roller should have less energy consumption and long service life under the condition of ensuring the separation performance.

The separation rollers were made of nylon rod and both two ends of separation roller were inlaid with steel shaft. According to the normal working conditions of the separation roller mentioned above, that is the tangent value of starting angle of separation rollers grasping stems should be less than the friction coefficient of stems and nylon and the tangent value of starting angle of separation rollers grasping peanut pods should be greater than the friction coefficient of pods and nylon, we could deduce the range of separation roller diameter as follow.

$$\frac{d_{\mathrm{g}} - h\sqrt{1+\mu_{\mathrm{g}}^2}}{\sqrt{1+\mu_{\mathrm{g}}^2}-1} \geq D \geq \frac{d_{\mathrm{j}} - h\sqrt{1+\mu_{\mathrm{j}}^2}}{\sqrt{1+\mu_{\mathrm{j}}^2}-1} \tag{3}$$

Where, D is the diameter of separation roller, mm; d_g is the diameter of peanut pod, mm; d_j is the diameter of stem, mm; h is the gap of double separation rollers, mm.

The clearance of separation rollers had a direct impact on separation performance. When the clearance was too small, separation roller could not grab stems or separation performance was poorer; when it was too large, it could damage peanut pods and even cause loss of pods. Therefore, the clearance of separation rollers was designed as 2mm~4mm.

We found that the width and thickness of peanut pods were extremely similar by measuring multiple groups of samples. The pods can be regarded as a cylinder approximately. The diameter of pod was 8.6~17.5 mm, the diameter of stems was 1.3~5.2 mm and the friction coefficients of pods and stems with separation roller were 0.42 and 0.45 respectively. By substituting data into inequation (3), the range of separation roller diameter was 34~60 mm. In consideration of the logarithm, structural strength and service life of separation roller, the diameter of separation roller was determined as 40mm by the experiment.

The peanut variety “Yuhua 15” was used in the experiment, and the trashed materials separated by peanut picking device were selected as experimental materials. The main components of experimental materials were peanut pods, stems and stalks, light impurities etc., and the materials had an impurity content of 35%. The proportion of stems and stalks was 14%, while the proportion of light impurities was 11%. The moisture content of peanut pod was 18%~20% and the moisture content of stem was 15%~16%. Experimental equipment is homemade peanut cleaning device, as shown in Fig. 4, and the auxiliary equipment included laser velocimeter, moisture meter, electronic balance, computer, frequency conversion motor, converter and so on.

Fig. 4 - Experimental field of peanut cleaning

In order to ensure the stability of the components of the experimental materials, the mixed materials separated from peanut picking device were divided into peanut pods, stems, stalks and light impurities. First of all, according to the length of conveyor belt and feeding time, we could determine the speed of conveyor belt. Then, we could calculate the material quality put on the conveyor belt in each experiment based on feed quantity and length of laying material. Finally, peanut pods, stems and light impurities were mixed evenly and laid on the conveyor belt based on the proportion of trashed materials. Until all parameters of the cleaning system test-bed were adjusted to the requirements of experiment, controlled converter didn’t start the cross-flow fan and stems separation device, and the conveyor belt didn’t start until the test-bed reached a stable working condition. When the materials on the conveyor belt were fed into cleaning device through feeding hopper, light impurities and short stems were sucked into cross-flow fan and discharged into the mesh bag through the fan air outlet, long stems were pulled into stems box by separation roller and clean peanuts fell into pods box through the pods outlet.

Dealing with the materials in the box and mesh bags and weighing and recording the data in the experimental form, the parameters of experimental performance of cleaning system can be obtained by using the following formula.

$$Y_1 = \frac{w_1 - w_2}{w_1} \times 100\% \quad (4)$$

$$Y_2 = \frac{w_3}{w_2 + w_3} \times 100\% \quad (5)$$

Where, Y_1 is the impurities content, %; Y_2 is the cleaning loss rate, %; w_1 is the total quality of material in the pods box, g; w_2 is the quality of pods in the pods box, g; w_3 is the quality of pods in the stems box and mesh bag, g.

RESULTS

The performance experiment of peanut harvester cleaning system could be divided into light impurities cleaning experiment and stems separating experiment. The former aimed to study the influence of the width of discharging exit, the distance between sliding screen and fan impeller and the rotation speed of cross-flow fan on cleaning performance, and obtain the optimal parameters of sliding screen and cross-flow fan. The later mainly studied the influence of the rotation speed of separation roller and the angle between separating device and horizontal plane on the separation performance and the optimal parameters of stems separating device were obtained.

The main factors affecting performance of light impurities cleaning device include feed quantity, the inclined angle of sliding screen, the size of sliding screen vent, the width of discharging exit, the distance between sliding screen and fan impeller and cross-flow fan speed, etc. The width of discharging exit, the distance between sliding screen and fan impeller and the rotation speed of cross-flow fan were selected as experimental factors in orthogonal experiment, while impurities content and loss rate were selected as experimental indexes. The paper carried out orthogonal experiment based on four factors and three levels orthogonal table. Through analyzing the experimental results, the influence laws of three experimental factors on the experimental indexes were obtained and the influence factor sequences and optimal combination of various factors on impurities content and loss rate were ascertained. Theoretical basis for the selection of regression experimental factors was provided. The scheme and results of orthogonal experiment are shown in Table 2.

Table 2

Scheme and results of orthogonal experiment

Test number	A	B	C	Impurities content	Loss rate
	[mm]	[mm]	[r·min-1]	[%]	[%]
1	40	70	550	13.15	0.94
2	40	80	700	8.41	0.44
3	40	90	850	8.08	0.80
4	50	70	850	4.85	0.89
5	50	80	550	14.63	0.47
6	50	90	700	15.9	0.66
7	60	70	700	10.62	0.82
8	60	80	850	5.82	0.78
9	60	90	550	19.18	0.68

A means the width of discharging exit; B means the distance between sliding screen and fan impeller; C means the rotation speed of cross-flow fan. Based on the range analysis of the orthogonal experimental results, the influence factor sequence of three factors on impurities content was C>B>A, and the optimal combination was $A_1B_1C_3$; the influence factor sequence of three factors on loss rate was B>C>A, and the optimal combination was $A_2B_2C_2$. The influence factor sequences and optimal combination of three factors on the experimental indexes was different, so the comprehensive scoring method was used to analyse the orthogonal experimental results. When the weight factors of impurity rate and loss rate factor were 0.4 and 0.6 respectively, the influence factor sequence of three experimental factors on the comprehensive index was C>B>A and the optimal parameter combination is as follows: the width of discharging exit was 50mm, the distance between sliding screen and fan impeller was 80mm, the rotation speed of cross-flow fan was 850 r/min.

The purpose of regression experiment was to establish the relational model of impurities content, loss rate and experimental parameters, and obtain the optimal parameter combination. On the basis of orthogonal experiment, the width of discharging exit was fixed as 50mm in the regression experiment, and the experiment selected the rotation speed of cross-flow fan and the distance between sliding screen and fan impeller as experimental factors, and selected impurities content and loss rate as experimental indexes. The experimental factors and levels are shown in Table 3, and the experimental results are shown in Table 4.

Table 3

Coding of factors and levels

Coding value	Rotation speed of cross-flow fan	Distance between sliding screen and fan impeller
	[r·min-1]	[mm]
-1.414	700	60
-1	744	65.9
0	850	80
1	956	94.1
1.414	1000	100

Table 4

Scheme and results of regression experiment

Test number	X_1	X_2	Impurities content [%]	Loss rate [%]
1	1	1	4.18	0.41
2	1	-1	4.23	1.00
3	-1	1	7.37	0.21
4	-1	-1	4.74	0.65
5	-1.414	0	12.70	0.57
6	1.414	0	4.10	0.95
7	0	-1.414	3.90	0.85
8	0	1.414	10.17	0.36
9	0	0	5.52	0.64
10	0	0	5.37	0.62
11	0	0	5.46	0.67
12	0	0	5.96	0.70
13	0	0	5.33	0.64

Note: X_1 means coding values of the rotation speed of cross-flow fan; X_2 means coding values of the distance between sliding screen and fan impeller

The regression models of impurities content and loss rate were accomplished by MATLAB statistical analysis software based on regression experimental results. The correlation coefficient of regression models of impurities content was 0.8136 and the residual standard deviation was 1.9837.

The correlation coefficient of regression models of loss rate was 0.9619 and the residual standard deviation was 0.0798. The variance analysis of two regression models was carried out and it was found that both the regression models of impurities content and loss rate had good significant level and high fitting degree.

$$Y_1 = 5.52831 - 1.98285X_1 + 1.43094X_2 + 0.78904X_1^2 + 0.10634X_2^2 + 0.67000X_1X_2 \quad (6)$$

$$Y_2 = 0.65401 + 0.13594X_1 - 0.21539X_2 + 0.02425X_1^2 - 0.05328X_2^2 - 0.03750X_1X_2 \quad (7)$$

In order to analyse the effects of the two factors on impurities content and loss rate intuitively and clearly, the response surface of two regression models was drawn by MATLAB, as shown in Fig. 5 and Fig.6.

Fig. 5 shows that both the rotation speed of cross-flow fan and the distance between sliding screen and fan impeller have more significant effect on impurities content. In the test range, with the increase of the rotation speed of Cross-flow fan, the downtrend of impurities content slow down gradually. Because the rotation speed of cross-flow fan determines the airflow velocity at the fan inlet, and when the air-flow velocity at the fan inlet increases gradually, light impurities and short stalks in the trashed materials would be got away continuously by high-speed airflow. Until the end, only the peanut pods and long stalks with high floating velocity are left. While the rotation speed of cross-flow fan is fixed at a certain level, with the increase of the distance between sliding screen and fan impeller, the impurities content shows an upward trend. The reason is that the distance between sliding screen and fan impeller becomes larger and it makes the airflow distribution area below fan inlet enlarge and the suction pressure of sliding screen decrease. So, some flat pods and short stalks could not be sucked away by airflow, which leads to the increase of impurities content.

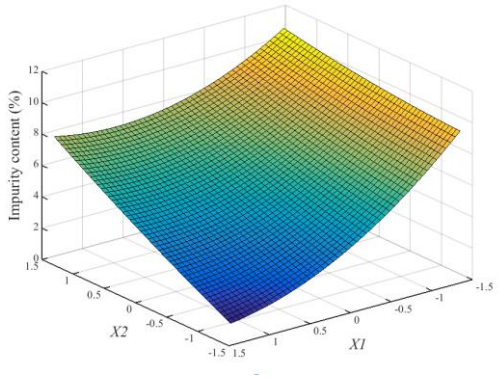

Fig. 5 - Impact of X_1 and X_2 on impurity content

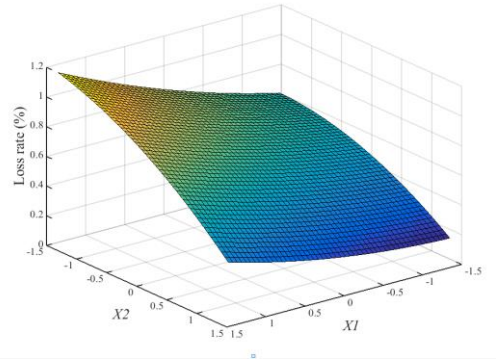

Fig. 6 - Impact of X_1 and X_2 on loss rate

Fig.6 shows that both the rotation speed of cross-flow fan and the distance between sliding screen and fan impeller have more significant effect on loss rate. In the test range, with the increase of the rotation speed of cross-flow fan, the loss rate is increasing. The reason is that the increase of the rotation speed of cross-flow fan causes the airflow velocity of fan inlet to enlarge and some small pods could be sucked away together with impurities. When the rotation speed of cross-flow fan is fixed at a certain level, with the increase of the distance between sliding screen and fan impeller, the downtrend of loss rate accelerates gradually. When the distance between sliding screen and fan impeller is smaller, the airflow distribution area below fan inlet is smaller and the suction pressure of sliding screen is stronger, some pods are sucked away together with impurities by airflow, which causes loss rate to enlarge. When the distance between sliding screen and fan impeller becomes larger, loss rate would decrease gradually.

According to the regression experimental results, it was known that the influence law of two experimental factors on impurity content and loss rate was not consistent. Therefore, the regression equations of impurity content and loss rate were weighted optimization; when the weights of both indexes were 0.4 and 0.6 respectively, we could set up the following objective function:

Objective function: $\min Y(X_1, X_2) = 0.4Y_1 + 0.6Y_2$

Variable constraint:

$$G_1(X) = -X_1 - 1.414 \le 0$$

$$G_2(X) = X_1 - 1.414 \le 0$$

$$G_3(X) = -X_2 - 1.414 \le 0$$

$$G_4(X) = X_2 - 1.414 \le 0$$

By calculating the minimum value of the objective function, we could obtain the optimal combination of parameters that the rotation speed of cross flow fan was 920r/min and the distance between sliding screen and fan impeller was 100mm. The impurity content was 7.42%, and the loss rate was 0.31%. The optimal combination of parameters obtained by optimization was not present in the regression test, so it was necessary to verify the feasibility of optimal parameters. It was indicated that the difference between the theoretical value predicted by regression models and the verification value of the optimal parameters was very small and negligible.

Stems separating experiment was carried out at the end of light impurities cleaning experiment, so we fixed the rotation speed cross-flow fan of 920 r/min, the width of discharging exit of 50mm and the distance between sliding screen and fan impeller of 100mm based on the results of light impurities cleaning experiment. Separation performance of stems separating device was mainly affected by the rotation speed and clearance of separation rollers and the angle between separating device and horizontal plane. So, stems separating experiment mainly studied the influence of three parameters on the separation performance, with impurities content and loss rate as experimental indexes. The scheme and results of orthogonal experiment are shown in Table 5.

By analyzing the orthogonal experimental results, the influence factor sequence of three factors on impurities content was A>C>B and the optimal combination was $A_2B_3C_3$; the influence factor sequence of three factors on loss rate was A>C>B and the optimal combination was $A_1B_3C_2$. The impurities content and loss rate are both two important performance indexes of peanut harvester, so the weights of impurities content and loss rate were selected as 0.5 and 0.5 respectively, and then, analyzing the experimental data by using comprehensive evaluation method the optimal combination was determined. The analyzed results shown that the influence of three experimental factors on the comprehensive index was B>A>C and the optimal parameter combination was $A_2B_3C_1$.

Table 5

Scheme and results of orthogonal experiment

Test number	A	B	C	Impurities content	Loss rate
	[r·min-1]	[°]	[mm]	[%]	[%]
1	200	25	2	3.10	0.51
2	200	30	3	2.28	0.57
3	200	35	4	1.14	0.70
4	300	25	3	1.75	0.69
5	300	30	4	0.91	0.73
6	300	35	2	0.89	0.62
7	400	25	4	0.70	0.79
8	400	30	2	1.34	0.78
9	400	35	3	1.61	0.64

Note: A means the rotation speed of separation rollers; B means the angle between separating device and horizontal plane; C means the clearance of separation rollers.

As it can be seen from Table 5, the optimal parameter combination was exactly the sixth group of the orthogonal experimental scheme; the impurities content was 0.89% and the loss rate was 0.62%. Compared with other peanut harvester cleaning devices, the performance of peanut harvester cleaning system was good, which met the national requirement of peanut harvester.

CONCLUSIONS

A new type of peanut pod cleaning device was designed based on the difference of the clearance characteristics between the different parts of peanut mixture and the structure characteristics and working mechanism of the device were analyzed. In this paper, the indoor bench test was carried out by a self-designed test bed, the influence law of structure motion parameters of the device on cleaning performance was analyzed, the mathematic models between the parameters and the performance indexes were established and the optimal parameter combination of cleaning device was optimized. The conclusions are as follows:

1. On the basis of analyzing the cleaning characteristic parameters of peanut mixture fully, it can be seen that it is an effective method for peanut to remove the light impurities from the selected materials by cross-flow fan and to remove fruit stalks and short stems from the materials by separation rollers.

2. Under the test conditions, the optimal structure motion parameters of light impurities cleaning device are as follows: the width of discharging exit is 50 mm, the distance between sliding screen and fan impeller is 100 mm and the rotational speed of Cross-flow fan is 920 r/min.

3. Under the test conditions, the optimal structure motion parameters of stems separating device are as follows: the angle between separating device and horizontal plane is 35°, the rotation speed of separation roller is 300r/min and the clearance of separation rollers is 2 mm.

4. When the structure motion parameters of peanut pod cleaning device are at the above optimal level, the impurity content and the cleaning loss rate of are 0.89% and 0.62% respectively, which satisfies the performance requirement of peanut combine harvester.

ACKNOWLEDGEMENT

The work was sponsored by the Major Science and Technology Projects of Henan Province (No.171100110100), the University-industry Cooperation Project of Henan Province (No.182107000015), and the Key Scientific Research projects of Henan colleges and universities (No.19B416003).

REFERENCES

[1] Colvin B.C, Tseng Y.C., Tillman B.L. et al, (2018), Consideration of peg strength and disease severity in the decision to harvest peanut in south-eastern USA, *Journal of Crop Improvement*, Vol.*32*, Issue 3, pp.1-18, Florida/USA;

[2] Guan Meng, Shen Yongzhe, Gao Lianxing et al, (2014), Mechanical properties of peanut peg after digging and drying, *Transactions of the CSAE*, Vol. 30, Issue 2, pp.87-93, Shenyang/China;

[3] Lim J, Kim MH, Kim SM et al, (2016), Transport Performance Simulation of Separating System for elf-propelled Peanut Harvester using EDEM Software, *Journal of the Faculty of Agriculture Kyushu University,* Vol.61,Issue 2,pp.361-365, Fukuoka/Japan;

[4] Liang Zhenwei, Li Yaoming, Ma Zheng et al, (2018), Prediction of cleaning performance of air-screen cleaning device based on e-svr, *Journal of Agricultural Mechanization Research*, Vol.40, Issue 4,pp. 26-30, Jiangsu/China;

[5] Liu Shiduo, Zhou Wei, (1998), The Relationship between Inhaling Attribute and Case Parameters of the Cross Flow Fan, *Journal of Luoyang Institute of Technology*, Vol.19, Issue 3, pp.28-32, Luoyang/China;

[6] Marian P, Pawel S, (2012),The Technique and Analysis of the Process of Separation and Cleaning grain materials, *Journal of Food Engineering*, Vol.109, Issue 3,pp. 603-608, Lublin/Poland;

[7] Ortiz B V , Balkcom K.B., Duzy L. et al, (2013), Evaluation of agronomic and economic benefits of using rtk-gps-based auto-steer guidance systems for peanut digging operations, *Precision Agriculture*, Vol.14, Issue 4, pp. 357-375, Auburn/USA;

[8] Reddy K.M., Kumar D.V., Reddy B.R. et al, (2013), Performance evaluation of groundnut thresher for freshly harvested crop, *International Journal of Agricultural Engineering*, Vol.48(1), pp.76-80, India;

[9] Shang Shuqi, Liu Shuguang,Wang Fangyan et al, (2005), Current Situation and Development of Peanut Production Machinery, *Transactions of the Chinese Society for Agricultural Machinery*, Vol.36, Issue 3, pp.143-147, Qingdao/China;

[10] Tang Bei, Lu Zemin, Gong Jun et al, (2016), Experimental Investigation on Cleaning Device of Peanut Combine Harvester, *Journal of Agricultural Mechanization Research*, Vol.38, Issue 3, pp.191-195, Jiangsu/China;

[11] Tang Bei, (2015), Design and Experimental Study of Peanut Combine Harvester Cleaning Device [D] Qing Dao: Qingdao Agricultural University, Jiangsu/China;

[12] Wang Dongwei, Shang Shuqi, Li Xiang et al, (2013), Type-L Cleaning Separation Mechanism of Peanut Combine Harvester, *Transactions of the Chinese Society for Agricultural Machinery*, Vol.44, Issue 2, pp.68-74, Qingdao/China;

[13] Wang Bo, Wang Dongwei, Shang Shuqi et al, (2015),The Development of Peanut Cleaning Test-bed, *Journal of Agricultural Mechanization Research*, Vol.37, Issue 6, pp.109-112, Qingdao/China;

[14] Zhou Dehuan, Hu Zhichao, YU Zhaoyang et al, (2017), Application Situation and Development Route of the Full-feeding Peanut Stripper, *Journal of Agricultural Mechanization Research*, Vol.39(2), pp.246-252, China;

[15] Zhang Rihong, Zhu Lixue,(2010), A kinematics simulation analysis on vibration screen of peanut combine harvester cleaning system, *Journal of Zhongkai University of Agricultural and Engineering*, Vol.23, Issue 24,pp.39-41, Guangdong/China.

STUDY OF FERTILIZER SPREADER CENTRIFUGAL TYPE UNDER FIELD CONDITIONS
/
ДОСЛІДЖЕННЯ РОЗКИДАЧА МІНЕРАЛЬНИХ ДОБРИВ ВІДЦЕНТРОВОГО ТИПУ У ПОЛЬОВИХ УМОВАХ

Prof. Ph.D. Manag. Kobets A.S.[1)], Lect. Ph.D. Eng., Ponomarenko N.A. [1)], Lect.. Ph.D. Eng. Kobets O.M. [1)], Lect.. Ph.D. Eng. Tesliuk H.V. [1)], Prof. Ph.D. Agri.Sci. Kharytonov M.M. [1)], Ass. prof. Ph.D. Eng.,Yaropud V.M. [2)]
[1)]Dnipro State Agrarian and Economics University, Faculty of Agrarian Engineering / Ukraine;
[2)]Vinnitsya National Agrarian University, Faculty of Engineering and Technology/Ukraine;
Tel: +38-097405010; E-mail: envteam@ukr.net

Keywords: *mineral fertilisers, centrifugal spreader, designed disc, machine.*

ABSTRACT
Methods for researching the effect of direction and force of wind on the result of the uniformity and width of mineral fertilizer application have been proposed. Researches on the experimental sample of centrifugal mineral fertiliser spreader in the field conditions have been made. The proposed rotary working body design, structural features of which enable to improve the dispersion evenness of mineral fertilizer, is presented.

РЕЗЮМЕ
Запропоновано методики дослідження впливу сили та напрямку руху вітру на результат рівномірності і ширини внесення мінеральних добрив. Проведено дослідження на експериментальному зразку відцентрового розкидача мінеральних добрив в польових умовах. Запропоновано відцентровий робочий орган, конструкційні особливості якого дозволяють поліпшити рівномірність розсіювання мінеральних добрив.

INTRODUCTION

The most important source of cultivated crops high yields is the mineral fertilizers use (*Lal R., 2008*). It is known that the application of granular fertilizers onto arable lands is mainly performed using centrifugal spreaders (*Biocca et al., 2013; Tijskens et al., 2008; Kobets et al., 2017a; Kobets et al., 2017b*). The effectiveness of mineral fertilizers largely depends on the uniformity of the distribution on the field surface (*Nukeshev et al, 2014*). Unevenness and instability of application reach 20–40% (*Nukeshev et al., 2016*) and leads to loss of grain crops (*Tekin and Sındır, 2014; Ning et al., 2015*). Spinner disc type spreaders simple design and little maintenance requirement made them very popular (*Tekin and Sındır, 2013*). Study of the working process of these devices is important because this knowledge will allow appropriate adjustment and will lead to achieving the desired distribution rules (*Petcu et al., 2015; Dong et al., 2013*). It was shown that flows of particles with a larger mean diameter achieve a higher velocity on the disc, causing the distribution patterns to shift to lower angular positions. It was concluded that a smaller average particle size leads to a higher mass discharge flow rate from the hopper (*Reumers et al., 2003*). Major differences in the quality of the spread pattern deposition can be observed in the field because of difficulties in adjusting the machines (*Vilette et al., 2005; Šima et al., 2013*). Numerous experiments with fertilizers found that the maximum value of the crop yield under certain conditions corresponds to the optimal dose of fertilizer (*Boldea et al., 2015; Andric et al., 2012; Hammad et al., 2012; Nazli et al., 2014*). An increase in the dose above the optimum level leads to a decrease in crop growth per unit of fertilizers, and if it is excessive - to a decrease in yield (*Vetsch and Randall, 2004; Lošák et al., 2011*).

Experimental researches have set the task to study the process of centrifugal mineral fertilizer spreader using an improved working body and compare it with a disc from serial production.

MATERIALS AND METHODS

The program of experimental research was supposed to determine the influence of force and direction of wind on the width of fertilizer spreading and uniformity of distribution over field surface. The fertilizer spreading machines (FSM) were used for tests. FSM - 900, FSM – 0.5 (Ukraine) and JarMet 500 (Poland) were used to compare effectiveness of experimental and serial discs. Machine ROTAFLOW RS-M (Netherlands) was involved separately, for comparison. Field tests were held on fields of three farms, which

are located in the north, east and south of the Dnipropetrovsk region. Experiments were conducted with the following fertilizers: granular superphosphate, sulfuric superphosphate, ammonium nitrate, urea, potassium salt. Quality of mineral fertilizers application was determined in following way. Transverse unevenness and fertilizers separation degree were determined by placing tin sheets (trays) with the size of 0.5 x 0.5 x 0.05 m on the spreading width, 0.5 m apart from each other, in 3 rows, with a 5 m interval between rows. Additional set of trays was arranged to determine the longitudinal unevenness across these three rows, which was equal to half of the spread width (fig.1).

Fig. 1 - Placement of trays on the field to determine the uniformity of fertilizer spreading

Longitudinal and transverse unevenness was determined in 5 passes. Separation degree was estimated in 10 passes of the unit. Variation coefficient during the test was 3-5%. Field tests of JarMet 500 (Poland) with developed working body were held in a motion that was deviated from the progressive movement with the developed working body. Working width and coefficient of heterogeneity were the main indicators of the quality of the machines for applying mineral fertilizers.

The variation characteristic of fertilizer application heterogeneity degree on a centrifugal spreader was obtained before tests. This experiment was held using an upgraded disc (fig. 2).

Fig. 2 - Upgraded centrifugal spreader disc

Variation coefficient of dosing apparatus with an average sample size of 1 kg was 12%. Machine work was performed on equal field areas at the working rate of 250-300 kg/ha. Wind speed on the field was from 1 to 5 m/sec. The research scheme of air flow effect on mineral fertilizers application unevenness is shown in fig. 3. Research methodology of air flow influence allows determining influence of wind speed in laminar mode, which is as close as possible to actual conditions for fertilizer machine. Technological process of mineral fertilizers spreading included the following operations: fertilizers load into spreader, fertilizers

transportation by spreader or by car to a field and fertilizers spreading. Tests were made both on unilateral fertilizers and fertilizer mixtures.

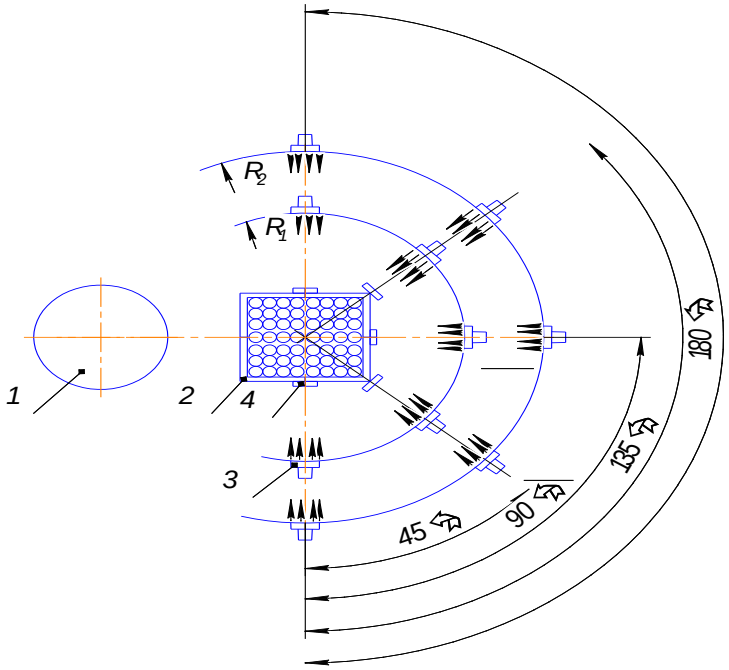

Fig. 3 - Research scheme of air flow effect:
1 – spreader disc; 2 – tray with samplers; 3 – fan; 4 – anemometer

RESULTS

The results of experimental study for centrifugal mineral fertilizer spreader are given in table 1.

Table 1

Parameters of centrifugal mineral fertilizer spreader testing in field experiments

Fertilizer and its humidity		Wind parameters		Rate of application	Delivery of fertilizers,	Effective spreading width,	Hetero geneity coefficient
		Speed	Direction				
		[m / s]	[degree]	[kg / ha]	[kg / s]	[m]	[%]
Granular superphosphate	W = 4.8%	1.0	0	250	0.82	14.5	12.9
	W = 4.8%	2.8	0	300	1.73	15.3	15.5
	W = 4.8%	3.0	0	300	1.96	17.0	16.2
	W = 4.8%	2.1	180	300	1.56	13.8	12.5
	W = 4.8%	2.1	90	300	1.49	13.2	14.25
	W = 4.8%	3.1	45	250	0.76	13.4	18.0
	W = 4.8%	2.2	45	300	1.65	14.6	16.0
	W = 4.8%	2.2	135	300	1.53	13.5	16.25
	W = 4.8%	1.0	180	250	0.68	12.1	12.2
	W = 4.8%	3.0	180	300	1.13	10.0	13.9
Powdered superphosphate, W =16.4%		2.5	0	300	1.79	15.8	-
Ammonium nitrate, W = 1.3%		2.1	0	250	0.92	16.2	-
Urea, W = 0.3%		3.4	0	250	1.03	18.1	-
Potassium salt	W = 2.8%	3.0	0	250	0.77	13.6	-
	W = 2.8%	3.0	0	300	1.58	14.0	-
	W = 2.8%	5.5	0	300	1.76	15.6	-
	W = 2.8%	3.0	90	300	1.27	11.2	-
	W = 2.8%	2.4	180	300	1.46	12.9	-
	W = 2.8%	2.4	45	300	1.24	11.0	-
Mixture of granular superphosphate with ammonium nitrate		2.8	0	300	1.72	15.2	-

It is clear that mineral fertilizer rate does not significantly affect spread width. The most effective width (up to 20 m) is obtained with powdered fertilizer. The effective width reaches 18 m during spreading of granulated and crystalline fertilizers. Less width was fixed when fine crystalline fertilizers were applied. It was found that granular fertilizers with a spreading rate of 10 m/sec were the least affected by the wind. Thus, difference in spreading width with wind, directed at 90° angle to spreading direction (lateral wind) and wind that blows along the spreading direction (passing wind), is more than 12% for granular superphosphate, and 20% - for potassium salt. The increase in the tailwind speed from 1 to 3 m/s contributes to an increase in the effective spreading width of the granular superphosphate by an average of 15%. Results of experimental evaluation of air flow velocity and direction influence on granules distribution are shown in Fig 4.

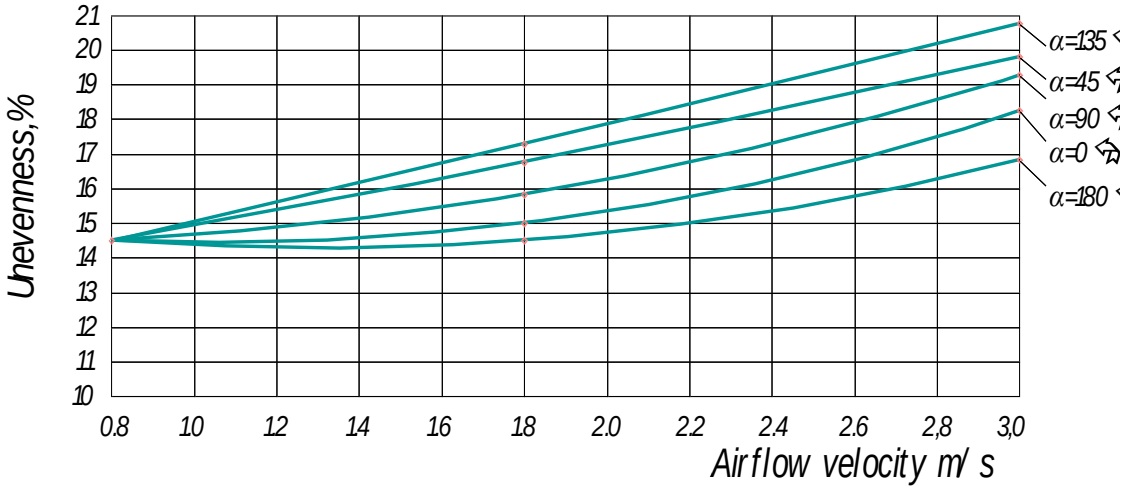

Fig. 4 - Air flow velocity and direction influence on granules distribution

It was established that the wind acting at an angle of 180° to the direction of spreading increases fertilizers separation insignificantly. Side and counter wind, comparing with the action of a passing wind, affects the distribution of particles of fertilizers significantly. Coefficient of heterogeneity increases almost in 2 times. So, fertilizers application at above - mentioned wind directions should be avoided. Fertilizers were applied on an area of 600 hectares during the testing process. Shift productivity reached 55 ha/s (hectare per shift). Quality of fertilizers application met all agrotechnical requirements of the process. Test conditions characteristics: total plot area is 1 ha, field relief is even, microrelief is absent; area inclination - within 2%, type of fertilizer - superphosphate. Presence of wind is up to 2 m/s in opposite direction in relation to machine-tractor unit. Results of determining granules distribution unevenness depending on experimental disc location height above ground level are shown in figure 5.

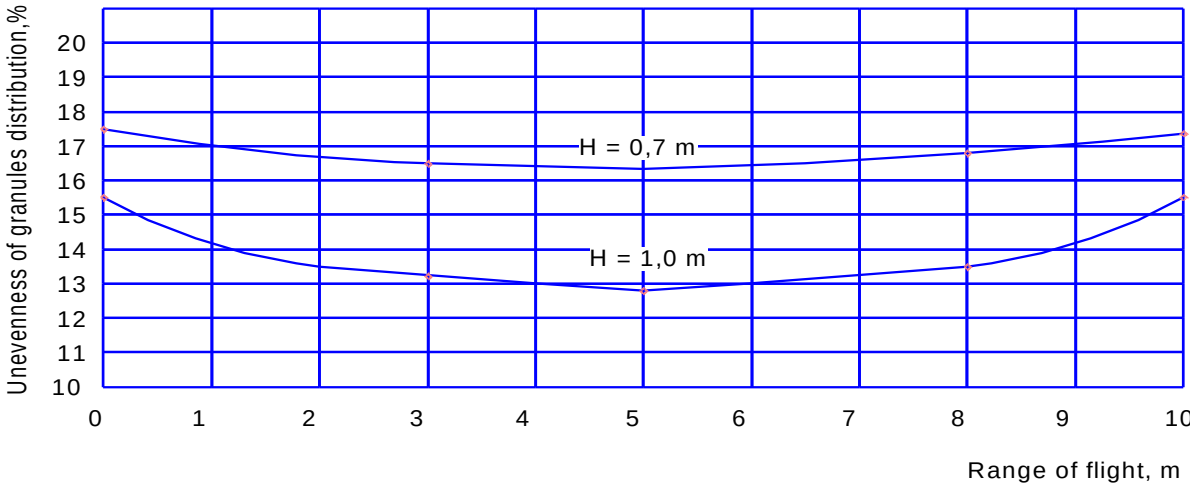

Fig. 5 - Distribution of granules using machine FSM-900 depends on designed disc location height above the ground level and the flight range of granules

The analysis of obtained dependences confirms that uneven distribution of granules is generally satisfactory. It is noteworthy that with the increasing of disc location height above ground level, the unevenness of fertilizer application decreases. This result is due to a longer flight of the particle and, consequently, a longer flow distribution (fig. 6), using machine FSM - 0,5 depending on designed disc location height above the ground level.

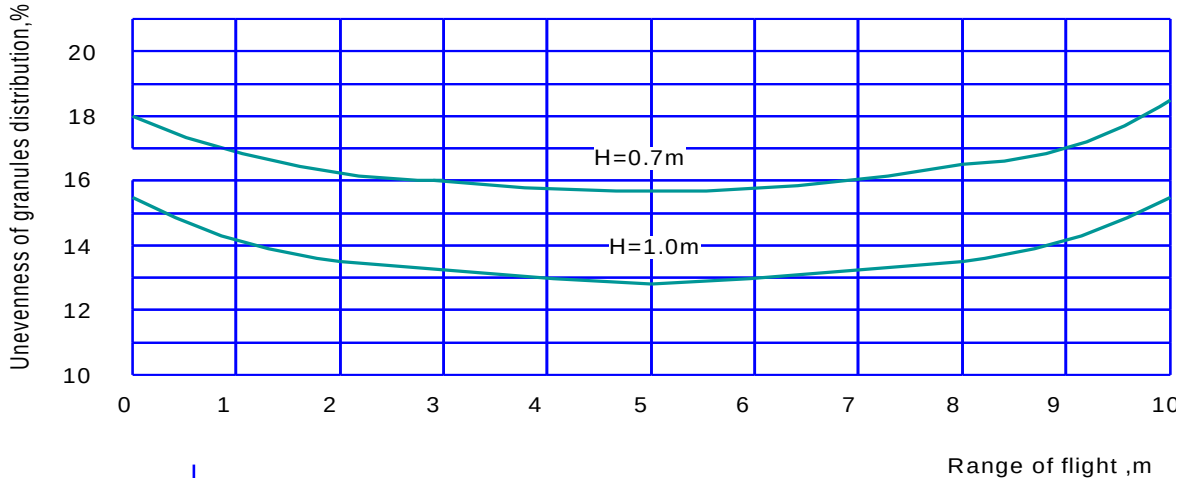

Fig.6 - Distribution of granules depending on designed disc location height above the ground level and the flight range of granules

Results of granules distribution definition for JarMet 500 machine with a designed disc are shown in Fig. 7.

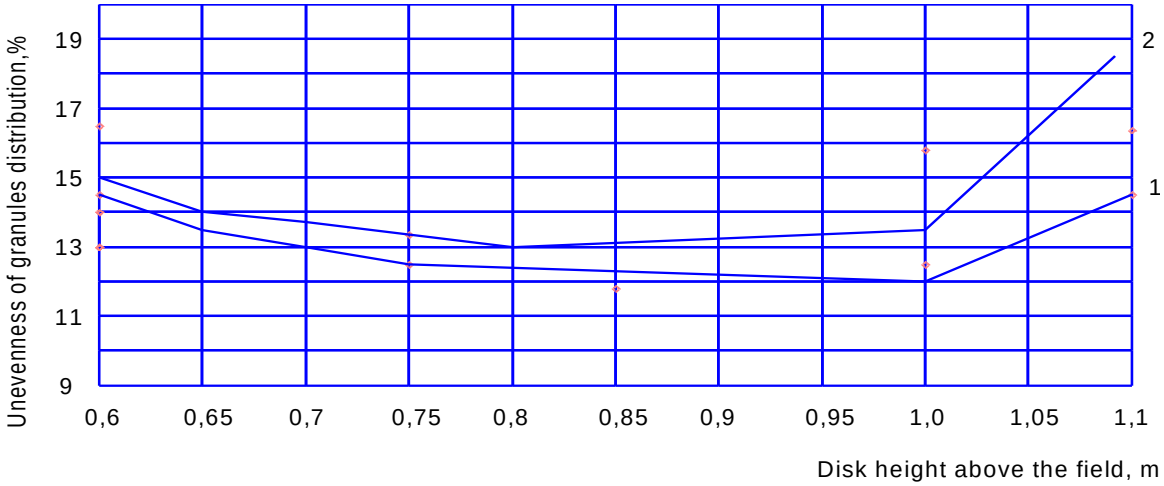

Fig. 7 - Distribution of granules depending on disc height above the field

1 - for steady motion; 2 – deviation from forward motion

After analyzing the obtained dependences, we see that the quality of fertilizer application is influenced by disc location height above ground surface. This applies both to motion deviated from translational with developed working body and steady movement of modernized machine. Thus, fertilizer application uniformity sharply worsens by 5.5 - 6% at the height of 1.1 m. So, optimum disc location height above ground surface level should be considered 1.0 m.

It is obvious that less uniform fertilizer application is observed in single - disc machines FSM-0.5 (Ukraine) and JarMet 500 (Poland). This is due to construction features of the aggregates. Results of determining granules distribution by using the two machines: FSM-0.5 with modernized working body (1) and ROTAFLOW RS-M (2) are shown in Fig. 8.

The machine with serial discs shows unevenness at level of 23-27%, which significantly exceeds indicator of modernized machine, as well as ROTAFLOW RS-M. Uneven distribution with proposed design is less than with the imported one on average by 7-10%.

However, this indicator in ROTAFLOW RS-M is more stable in terms of capture width. Uneven application of mineral fertilizers within limits of agrotechnical requirements does not affect crops harvest and can be considered satisfactory. However, index of a serial machine up to 27% does not meet stated requirements.

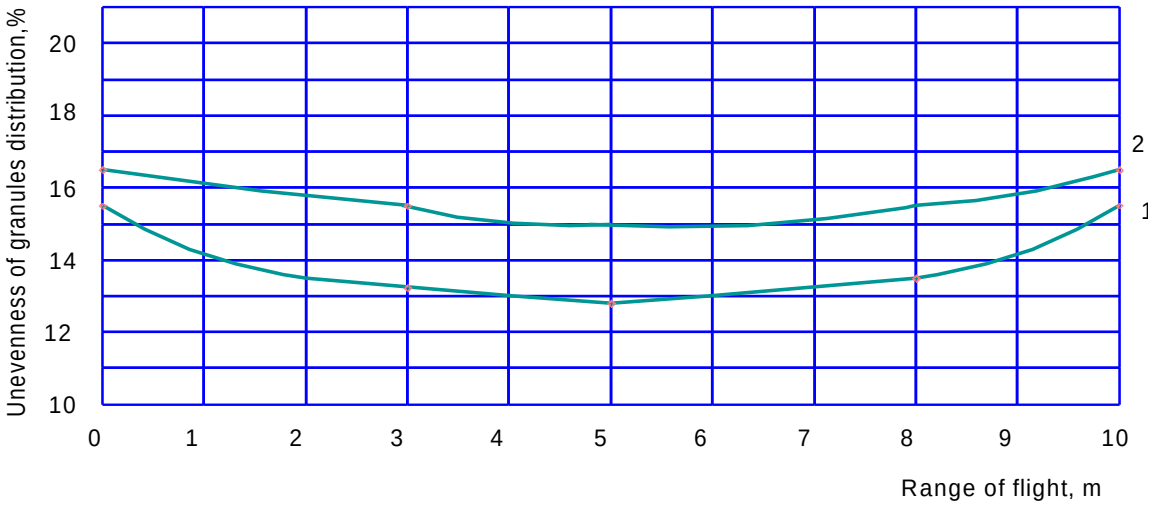

Fig.8. - Distribution of granules depending on designed disc height above the field
1 - for machine FSM - 0,5; 2 –for machine ROTAFLOW RS-M

Experimental research results made it possible to compare work of centrifugal type mineral fertilizer spreader with disc which was designed and serial disc (Table 2). The unit included Ukrainian tractor MTC-82.1 and machine JarMet 500 (Poland).

Table 2

Performance indicators of centrifugal type mineral fertilizer spreader using designed and serial disc of JarMet 500 machine

Indicator	Basic option	Designed option
Field square [ha]	600	600
Productivity per 1 hour work shift, [ha/hour]	12.20	15.96
Number of operating personnel, [people]	1	1
Fuel consumption, [kg / ha]	0.7	0.5
Shift duration, [hour]	7	7
Unevenness of mineral fertilizer application, [%]	20-35	7-12

Thus, as a result of improvements made to the working body, reduction in unevenness of mineral fertilizers application to admissible standards was achieved. When using the designed option of spreader disc compared to base option, productivity of machine - tractor unit increases by 30.8%, and fuel consumption is reduced by 40%.

CONCLUSION

It is proved that air resistance substantially affects final distribution of fertilizer granules along soil surface. This is mainly due to changes in flight range of individual granules. As a result of research it was established that resistance was not proportional to granule velocity. In range of wind velocities up to 0.5 m/s impact of air flow on granule flight distance did not exceed 5%, which corresponded to an increase of uneven distribution by 0.35%. Influence of other factors on unevenness indicator was much higher. It allowed us to not count wind velocity in calculations in the given range. In this case, estimated uneven fertilizer application was 10.02% for indicated constructive and kinematic indicators at accepted granulometric composition of 1-5 mm.

Mechanical and technological properties of fertilizers, which influenced distribution process the most, were experimentally determined. It was established that mineral fertilizers application rate did not affect spreading width significantly. The most effective width (up to 20 m) was obtained during powdered fertilizer spreading, and when granulated and crystalline fertilizers were applied effective width reached 18 m. The width was smaller when applying fine crystalline fertilizers. It was established that the influence of wind was selective. Air flow directed at an angle from 45 to 135 degrees had the greatest impact on fertilizers uneven distribution by surface. At wind velocity more than 2.0 m/s application qualitative indicators were sharply deteriorated. Comparative field tests proved that the proposed design of centrifugal type spreader ensured fulfilment of agrotechnical requirements for uneven spreading (did not exceed 16%). Uneven spreading was 2 times lower than on serial native spreaders on average and by 7-10% lower than on known foreign analogs. Influence of machine oscillations on this indicator ranges from 5% to 8% of overall unevenness. Implementation of developed recommendations will reduce fertilizer consumption, increase unit's productivity and optimize norms of application.

ACKNOWLEDGEMENT

The work has been funded by the Ukrainian Ministry of Education and Science.

REFERENCES

[1] Andric L., Rastija, M., Teklic, T., Kovacevic V., (2012), Response of maize and soybeans to liming. *Turkish Journal of Agriculture and Forestry*, 36, pp.415 – 420, Ankara/Turkey;

[2] Biocca M., Gallo P., Menesatti P., (2013), Aerodynamic properties of six organo-mineral fertiliser particles. *Journal of Agricultural Engineering*; volume XLIV(s2):e83, pp411-41, Milano, Italy;

[3] Boldea M., Sala F., Rawashdeh H, Luchian D,. (2015), Evaluation of agricultural yield in relation to the doses of mineral fertilizers. *Journal of Central European Agriculture*, 16(2), pp.149-161, EU;

[4] Dong X., Song J., Zhang J., Wang J., (2013), Working performance and experiment on granular fertilizer spreader with cone disc in Nongye Gongcheng Xuebao. *Transactions of the Chinese Society of Agricultural Engineering* 29(19), pp.33-40, China;

[5] Hammad H. M., Ahmad A., Abbas F., Farhad W., (2012), Optimizing water and nitrogen use for maize production under semiarid conditions. *Turkish Journal of Agriculture and Forestry*, 36, pp.519-532, Ankara/Turkey;

[6] Kobets A.S., Ponomarenko N.O., Kharytonov M.M.,(2017a), Construction of centrifugal working device for mineral fertilizers spreading. Vol. 51, No. 1. pp.5-14, Bucharest/Romania

[7] Kobets A.S., Naumenko M.M., Ponomarenko N.O., Kharytonov M.M., Velychko O.P., Yaropud V.M. (2017b), Design substantiation of the three-tier centrifugal type mineral fertilizers spreader. INMATEH – Agricultural Engineering. Vol. 53, No. 2, pp.13-20

[8] Lal R., (2008), Soils and world food security. *Soil and Tillage Research* 102, pp.1-4, Ankara/Turkey ;

[9] Lošák T., Hlušek J., Martinec J., Jandák J., Szostková M. et al, (2011), Nitrogen fertilization does not affect micronutrient uptake in grain maize (Zea mays L.). *Acta Agriculturae Scandinavica* Section B: Soil and Plant Science, 61, pp.543-550, Sweden;

[10] Nazli R. I., Kuşvuran A., Inal İ., Demirbaş A., Tansi V., (2014), Effects of different organic materials on forage yield and quality of silage maize (Zea mays L.). *Turkish Journal of Agriculture and Forestry*, 38, pp.23-31, Ankara/Turkey;

[11] Ning S., Taosheng X., Liangtu S., Rujing W., & Yuanyuan, W, (2015), Variable rate fertilization system with adjustable active feed-roll length. *International Journal of Agricultural and Biological Engineering*, Vol. 8, Issue 4, pp.19–26, Beijing/ China ;

[12] Nukeshev S.O., Eskhozhin D., Karaivanov D., Eskhozhin K., (2014), Determination of parameters of the main distributor for fertilizer applying machine. *Bulgarian Journal of Agricultural Science*, 20 (No 6), pp.1513 -1521, Sofia/Bulgaria;

[13] Nukeshev S., Dzhadyger E., Gennady L., Karaivanov D., Zolotukhin E., Syzdykov D., (2016), Theoretical substantiation of the design of a seeding device for differentiated intra soil application of mineral fertilizers. *Acta Universitatis Agriculturae et Silviculturae Mendelianae Brunensis*.V.64, №1, pp.115-122, Brno/Czech Republic;

[14] Petcu A.S., Popa L., Stefan V., Ciuperca R., Nedelcu A., Girleanu I.C., Avramescu A.M., Veringa D., Zaica A., Lazar G., (2015), Theoretical research regarding the working process of the fertilizers managing systems by centrifugation. *Annals of the University of Craiova - Agriculture, Montanology, Cadastre Series.* Vol. XLV, pp.174-184, Craiova/Romania;

[15] Reumers J, Tijskens E., Ramon H., (2003), "Experimental characterization of the tangential and cylindrical fertiliser distribution pattern from a spinning disc: A parameter study," *Biosystems Engineering* 86(3), pp.327-337, U.K.;

[16] Šima T., Nozdrovický L., Krupička J., Dubeňová M., Koloman K., (2013), Granulometric study of dasa 26/13 fertiliser. *MENDELNET*, pp.882-887, Brno, Check Republics;

[17] Tekin A.B., Sındır, K. (2013), Varıable Rate Control System Designed For Spinner Disc Fertilizer Spreader – "PreFer". *Journal of Agricultural Engineering*. No: 2, pp.45 – 53, Milano/Italy;

[18] Tekin A.B., Sındır, K. (2014), Performance assessment of variable rate spinner disc fertilizer spreader – "PreFer". *Agricultural Engineering*. No: 2, pp.43 – 52, Milano/Italy;

[19] Tijskens E., Van Liedekerke P., Piron E., Van Geyte J., Cointault F., Ramon H., (2008), Recent results of experimental and Dem modeling of centrifugal fertilizer spreading. *Granular Matter journal*, Springer Verlag, 10 (4), pp.247 – 255;

[20] Vetsch, J. A., Randall, G. W., (2004), Corn production as affected by nitrogen application timing and tillage. *Agronomy Journal*, 96(2), pp.502-509, USA;

[21] Vilette S., G Cintault F., Piron E., Chopinet B., (2005), Centrifugal spreading an Analytical Model for the Motion of Fertilizer Particles on a spinning disc. *Biosystems Engineering*, 92(2), pp.157-164, U.K.

MODELLING OF SOIL COMPACTION UNDER HEAVY-DUTY TRACTORS
/
MODELAREA COMPACTĂRII SOLULUI SUB ACȚIUNEA TRACTOARELOR DE MARE PUTERE

Prof. Ph.D. Eng. Biriș S.Șt.[1)], Lecturer Ph.D. Eng. Ungureanu N.[*1)], Ph.D. Stud. Eng. Cujbescu D[2)]
[1)]Politehnica University of Bucharest, Faculty of Biotechnical Systems Engineering / Romania;
[2)]INMA Bucharest / Romania
E-mail: nicoletaung@yahoo.com

Keywords: *Compaction, Finite Element Method (FEM), Wheels, Tire pressure*

ABSTRACT

This paper presents a theoretical model for prediction of the stress state in agricultural soil under the agricultural tires of a heavy-duty tractor, using the Finite Element Method. Using an acquisition data system and pressure sensors, the theoretical model was experimentally verified in the laboratory. This study highlights the major advantage of using FEM models, which consists mainly in the spectacular reduction of costs for experimental testing and a considerable reduction in the time needed to analyse the possibility of the occurrence of artificial compaction phenomenon in the agricultural soil under heavy-duty tractors.

REZUMAT

Lucrarea prezintă un model teoretic pentru estimarea stării de tensiune în solul agricol sub acțiunea roților unui tractor de mare putere, utilizând metoda elementelor finite. Cu ajutorul unui sistem de achiziție de date și a senzorilor de presiune, modelul teoretic a fost verificat experimental în laborator. Acest studiu evidențiază avantajul major, în cazul utilizării modelelor FEM, care constă, în principal, în reducerea spectaculoasă a costurilor necesare încercărilor experimentale și a timpului necesar analizării posibilității de apariție a fenomenului de compactare artificială a solului agricol sub acțiunea tractoarelor de mare putere.

INTRODUCTION

At the moment, the heavy-duty tractors are increasingly used in intensive farming and especially where conservative technology for seedbed preparation is applied, because it offers the possibility of working with a minimum number of passes on agricultural soil, thus conserving it and avoiding the risk of artificial soil compaction. The heavy-duty tractors are characterized by the fact that they provide great powers which ensure great traction forces and allow the towing of complex equipment that performs more agricultural works for seedbed preparation in a single-pass. The weight of these tractors is distributed on the two axles (front and rear), respectively the wheels, and transmitted to the soil by means of the footprint, producing soil stress.

Wheel passage on agricultural soil, which for most vehicles is usually of short duration, results in the artificial compaction of soil (*Gill and Vanden Berg, 1968*). The phenomenon of agricultural soil compaction is defined as an increase in soil dry density and the closer packing of solid particles or reduction in porosity (*Kuhwald et al., 2018; McKyes, 1985*), which can result from natural causes including rainfall impact, soaking and internal water stress (*Arvidsson, 1997*). New methods of mechanisation, associated with increasing weight and size of machinery, have the potential to cause undesirable soil compaction to a depth below that of normal tillage operation (*Bennett et al., 2019; Javadi and Spoor, 2006; Martínez-Ramírez et al., 2017; Mohsenimanesh and Laguë, 2017*).

The most important factors that have a significant influence on the artificial compaction of soil are: soil type, soil moisture content, size of external load, area of contact surface between the soil and tire, the shape of contact surface and the number of passages (*Augustin et al., 2019; Cueto et al., 2016; Kuhwald et al., 2018*). Tillage systems influence the physical, chemical and biological characteristics of the soil, which in turn can change the characteristics, growth and development of the roots (*Augustin et al., 2019; Hajabbasi, 2001*).

Since the agricultural soil is not a homogeneous, isotropic and ideal elastic material, the mathematical modelling of the phenomenon of stress distribution is very difficult. Many mathematical models of stress distribution in the soil under various traction devices are based on Boussinesq's equations describing stress distribution below a loaded point (Fig. 1) acting on a homogeneous, isotropic, semi-infinite, and ideal elastic

medium (*Hammel, 1994*). Frohlich has developed equations to take into account stress concentration around the application point of a concentrated load for the semi-space medium subjected to a vertical load (*Koolen and Kuipers, 1983*). The Finite Element Method (FEM) proves to be very promising in modelling this distribution phenomenon (*Cueto et al., 2013*). For agricultural soils, the relations between stresses and deformations are measured on soil samples in the laboratory or directly in the field. The stress-strain relations are given by the constitutive equations (*Gee-Clough et al., 1994; Keller and Lamandé, 2010*). A non-linear finite elements model could be a useful tool in developing a predictive method of soil pressure-sinkage behaviour and can be used to investigate and analyse soil compaction (*Rashidi et al., 2007; Silva et al., 2018*). Other researchers (*Cueto et al., 2013; Khodaei et al., 2016*) developed a three-dimensional model of the soil, and they represented soil properties by an Extended Drucker-Prager material model.

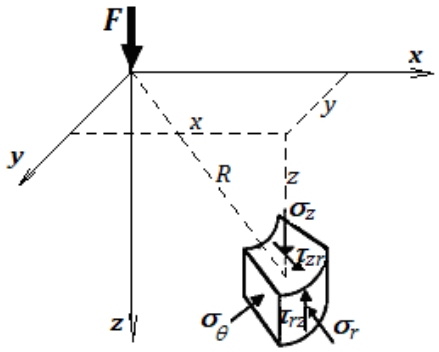

Fig. 1 - Stress state produced by a concentrated vertical load
(*Upadhyaya and Rosa, 1997*)

Validation of the mathematical model of soil stress distribution can be done using special sensors, either in the laboratory - on prepared volumes of soil or in-situ, by comparing the values predicted by the model with those resulting from the measurements. As shown in some studies (*Rashidi et al., 2007*), the statistical analysis of verification confirmed the validity of the FEM model and demonstrated the potential use of FEM in predicting soil pressure-sinkage behaviour. However, experimental verification of the model is required before the model can be recommended for extensive use.

Some researchers (*Loghavi and Khadem, 2006*) developed sensors to detect the location and depth of the hardpans in real time. In their study, a soil compaction profile sensor equipped with four horizontally operating penetrometers was developed and tested, for on-the-go detection and mapping of the site and intensity of the hardpans artificially formed in a soil bin.

Another researcher (*Keller, 2004*) used five stress sensors that were buried in the topsoil at a depth of 0.1 m for measuring of the vertical stress. Each sensor (DS Europe Series BC 302) was attached to an aluminium disc (diameter: 17.5 mm, height: 5.5 mm) embedded in the centre of a larger aluminium disc (diameter: 70 mm, height: 15 mm). The cells were placed on a line perpendicular to the direction of travel below one half of the wheel track.

The main objective of this paper is to find and certify a simulation model for prediction of stress in agricultural soil under the tires of heavy-duty tractors, using the most advanced mathematical tools, such as the Finite Element Method.

MATERIALS AND METHODS

To simulate the behaviour of agricultural soil, the Drucker-Prager plasticity model can be used. The yield criteria can be defined as (*Kushwaha and Shen, 1995*):

$$\mathcal{F} = 3 \cdot \alpha \cdot \sigma_m + \bar{\sigma} - k = 0 \quad (1)$$

where α and k are material constants assumed unchanged during the analysis, σ_m is the mean stress and $\bar{\sigma}$ is the effective stress, α and k are functions of two material parameters (Φ and c) obtained from the experiments, where Φ is the angle of internal friction and c is the material cohesion strength.

Using this material model, the following considerations should be noted: strains are assumed to be small; problems with large displacements can be handled, provided that the assumption of small strains is still valid; the use of NR (Newton-Raphson) iterative method is recommended; material parameters Φ and c must be bounded in the following ranges: $90 \geq \Phi \geq 0$ and $c \geq 0$.

The input parameters required for the constitutive model of wet clay type agricultural soil are (*Gee-Clough et al., 1994*): soil cohesion (*c*): 18.12 kPa; internal friction angle of the soil (φ): 30°; soil density (γ_w): 1270 kg/m^3; Poisson's ratio (υ_s): 0.329; Young's modulus (*E*): 3000 kPa.

The stress levels under a point load, as shown in Fig. 1, are given in cylindrical coordinates as follows (*Upadhyaya and Rosa, 1997*):

$$\sigma_z = \frac{3 \cdot F \cdot z^3}{2 \cdot \pi \cdot R^5} \quad (2)$$

$$\sigma_r = \frac{F \cdot z^3}{2 \cdot \pi} \cdot \left[\frac{3 \cdot z \cdot r^2}{R^5} - \frac{1-2 \cdot \vartheta}{R \cdot (R+z)} \right] \quad (3)$$

$$\sigma_\theta = \frac{F \cdot (1-2 \cdot \vartheta)}{2 \cdot \pi} \cdot \left[\frac{1}{R \cdot (R+z)} - \frac{z}{R^3} \right] \quad (4)$$

$$\tau_{rz} = \frac{3 \cdot F \cdot r \cdot z^2}{2 \cdot \pi \cdot R^5} \quad (5)$$

where *F* –is the point load, ϑ –Poisson's ratio, $\sigma_{z,r,\theta}$ – components of normal stress, and τ_{rz} –shear stress component.

A volume of soil, 2-meter deep, 4.5 meters wide and 6 meters long (Fig. 2) was considered to be under a heavy-duty tractor (Massey Ferguson, range 8700) (Table 1). The nonlinear structural analysis was made on the ideal model, the soil being considered a homogeneous and isotropic material. The QuickFieldTM 6.3 program was used for FEM modelling in planar strain state (Fig. 3).

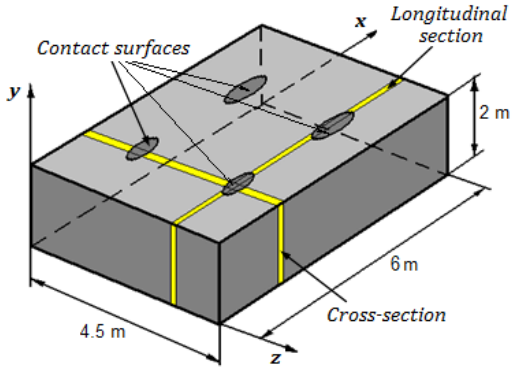

Fig. 2 - Analyzed volume of soil

Table 1

Main characteristics of MF-8700 tractor

Tractor	Soil interaction part	Type of tire	Gauge (mm)	Weight (total / per axle) (kg)	
MF-8700	Front tire	620/75R30	2000	18000	6000
	Rear tire	650/85R42			12000

Fig.3 - Meshed model of soil used to analyze the distribution of stresses and strains in the longitudinal-vertical plane

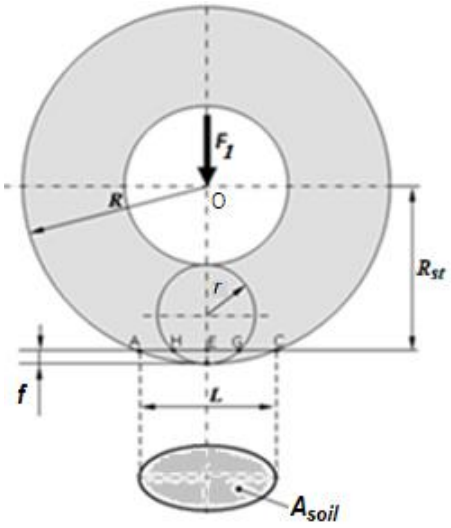

Fig. 4 - Tire deformation under the action of an external load

According to Hedekel's equation, the deformation of the tire in contact with the rolling surface (Fig. 4) is given by the relation (*Koolen and Kuipers, 1983*):

$$f = \frac{F_1}{2 \cdot \pi \cdot p_i \cdot \sqrt{R \cdot r}} \tag{6}$$

where: F_1 – is vertical load on the wheel, (N); p_i – tire inflation pressure, (MPa); R – free radius of the wheel, (mm); r – radius of tire rolling path in cross section, (mm).

Static tire radius is given by:

$$R_{st} = R - f \tag{7}$$

and the length of the contact chord is:

$$L = 2 \cdot \sqrt{R^2 + R_{st}^2} \tag{8}$$

The empirical model for calculating the contact area between soil and agricultural tires (Komandi, 1976) is:

$$A_{soil} = c \cdot F_1^{0.7} \cdot \sqrt{\frac{b}{D}} \cdot p_i^{-0.45} \quad (m^2) \tag{9}$$

where: c –constant; $F1$–wheel load, (kN); b –tire width, (m); D –tire diameter, (m); p_i –inflation pressure, (kPa). Constant c for different substrates has the following values (*Komandi, 1976*): c=0.3-0.32 for rather bearing soil, c=0.36-0.38 for sandy field, and c=0.42-0.44 for loose sand.

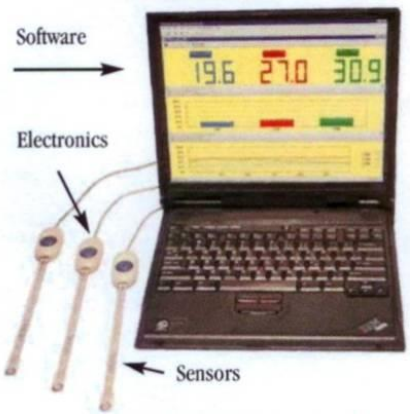

Fig. 5 - Data acquisition system

In order to check the model developed using Finite Element Method (FEM), laboratory tests were conducted using a data acquisition system (Fig. 5) connected to Flexi Force Tekscan W-B201-L force sensors (Fig. 6), vertically mounted in the soil, at 10 cm distance, in a metallic container with 1x1x1 m dimensions (Fig. 7). Fig. 8 shows the testing stand on the Hydropulse installation. The corresponding load on the wheel was applied using the hydraulic cylinder of the Hydropulse.

Fig. 6 - Flexi Force Tekscan W-B201-L force sensor

The soil inside the testing bin is cohesive and has been compacted by compression as the bin has been filled, to reproduce the clayey soil as accurately as possible. By water spraying, soil moisture was brought to the value of 20%, corresponding to the most common case of soil processing, when the contact with the rolling bodies (wheels) of the tractors or agricultural machines occurs.

Fig. 7 - Sensors mounted in the soil bin

Fig. 8 - Test stand in Hydropulse laboratory

On the experimental stand of the Hydropulse installation (Fig. 8) was mounted a wheel from the front axle of MF-8700 tractor, for 3 different tire inflation pressures (0.1 MPa, 0.15 MPa, and 0.2 MPa). With the help of a controlled hydraulic cylinder, the load on wheel was reproduced, according to Table 1, of 3000 kg (30 kN) after a cycle consisting of three distinct phases, namely: 1 second of linear loading up to the maximum value (30 kN), 1 second to maintain this maximum load and 1 second to linear discharge the compression force to the value of 0 N, for each of three different tire inflation pressures. The maximum values of equivalent stress in the soil were recorded by the acquisition system, using the 10 Flexi Force Tekscan W-B201-L pressure sensors disposed vertically in the soil on the symmetry axis of the bin. These experiments are intended to validate the model of soil stress distribution using the Finite Element Method (FEM).

RESULTS

The figures below (Fig. 9, a and b) show the influence of tire inflation pressure on the dimensional characteristics of the MF-8700 tractor wheels (according to Fig. 4), respectively tire deformation *f* (Eq. 6), static radius R_{st} (Eq. 7) and the length of contact chord *L* (Eq. 8), for the front (a) and rear (b) wheel.

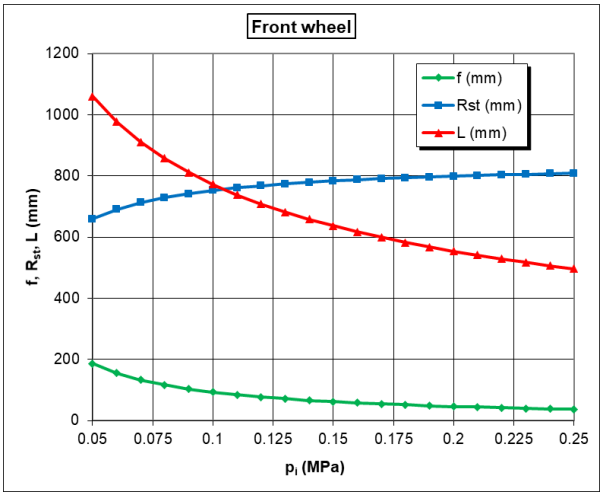

a)

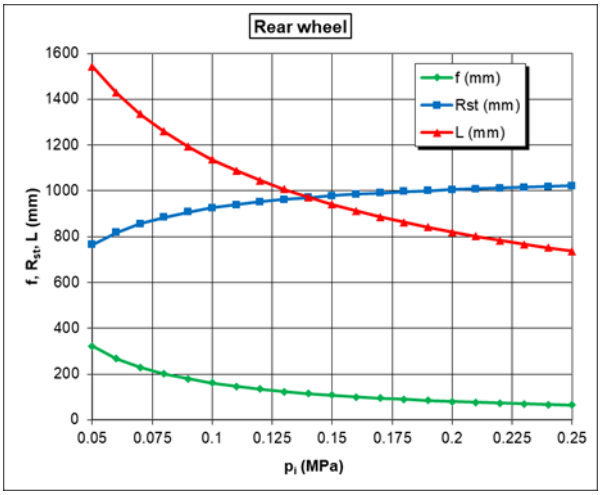

b)

Fig. 9 - Influence of tire inflation pressure on the dimensional characteristics of the wheels (front and rear)

From the two graphs it can be observed the importance of the tire inflation pressure on the dimensional characteristics of the wheel, respectively on the size of tire deformation. Thus, for the front wheel (Fig. 9.a), for the same loading force, tire deformation depending on the value of tire inflation pressure, reaches: 93 mm (for p_i=0.1 MPa), 62 mm (for p_i=0.15 MPa), and 46 mm (for p_i=0.2 MPa). For the rear wheel (Fig. 9.b), for the same loading force, tire deformation depending on the value of tire inflation pressure, reaches: 160 mm (for p_i=0.1 MPa), 107 mm (for p_i=0.15 MPa), and 80 mm (for p_i=0.2 MPa).

The figures below (Fig. 10, a and b) show the variation curves of the contact area A_{soil} (Eq. 9) depending on tire inflation pressure for three different types of substrates, for the front wheel (a) and rear wheel (b) respectively. It can be seen that for both wheels (front and rear), the contact area decreases significantly with increasing tire inflation pressure, regardless of the nature of the rolling surface.

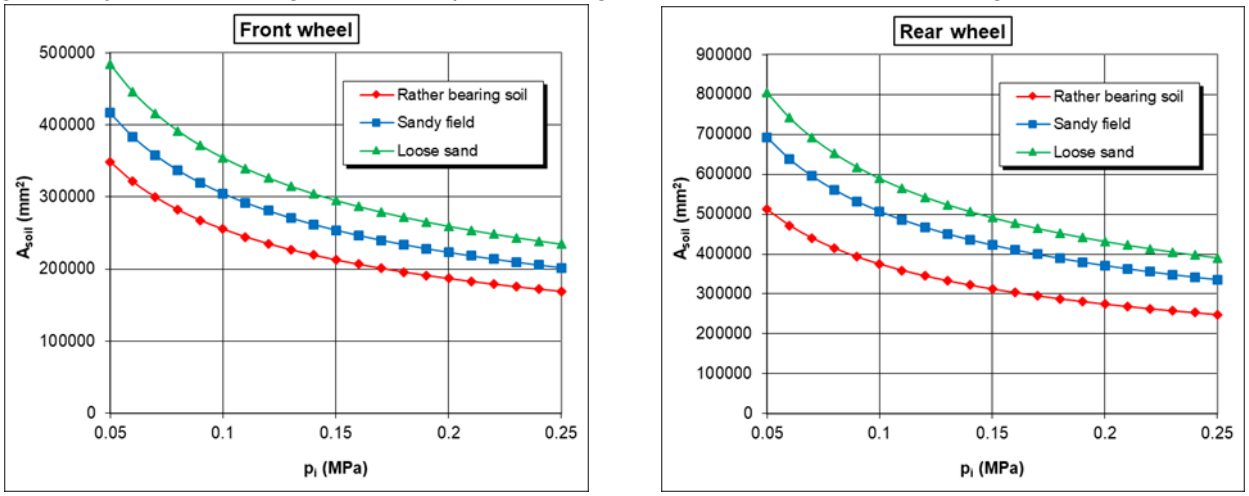

a) b)

Fig. 10 - Influence of tire inflation pressure on the contact area for different substrates of the wheels

The pressure applied by the tractor, through the wheels, on the soil (p), is calculated as the ratio between the vertical load on the wheel (F_1) and the contact area (A_{soil}), for each wheel. This dependency is shown in Fig. 11, for the front and rear wheels of the MF-8700 tractor, in the case of a cohesive soil. As it can be seen, tire inflation pressure influences the tire pressure applied on the soil.

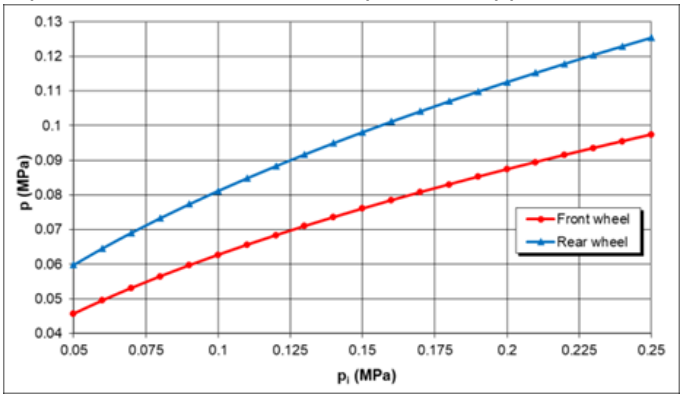

Fig. 11 - Influence of tire inflation on the contact pressure between wheel and soil

By running the simulation model using the Finite Element Method (according to Fig. 3), the results shown in the following figures are obtained. Thus, Fig. 12-a shows the distribution of equivalent stresses in the soil, according to Drucker-Prager yield criteria for the same cohesive soil (clayey), for three different tire inflation pressures (0.1 MPa, 0.15 MPa, 0.2 MPa). It can be observed that the higher the tire inflation pressure, the more the equivalent stresses propagate in the soil at higher depth and they have higher values, especially in the surface (arable) layer. The simulation model allows highlighting the distribution of stresses in the soil and their values, making it possible to highlight situations in which the soil is artificially compacted, usually when the value of equivalent stress exceeds 80 kPa. Analysing Fig. 12-a, it results that if tire inflation pressure is 0.2 MPa, the susceptibility of superficial compaction occurs in the superficial layer, especially in the case of the rear wheel, hence it is recommended to limit the value of this tire inflation pressure to maximum 0.15 MPa.

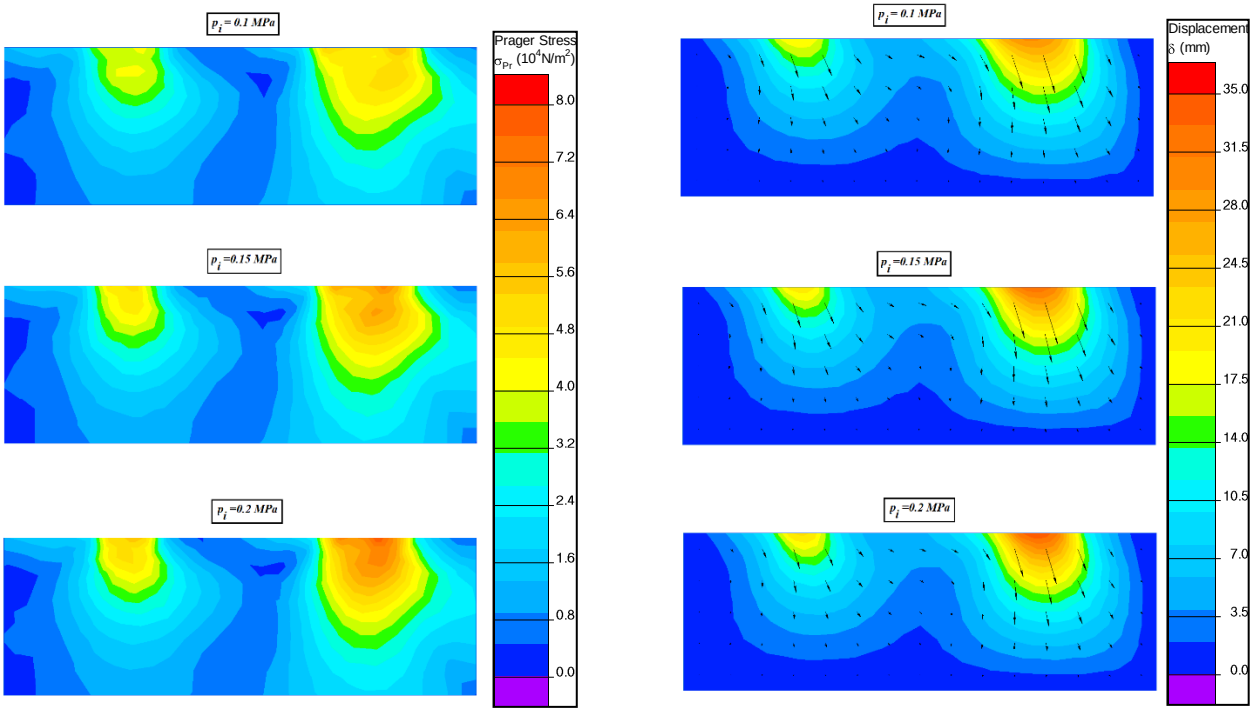

a) b)

Fig. 12 - Distribution of equivalent stresses (a) and of total displacements (b) in the soil for different tire inflation pressures

Fig. 12.b shows the distribution of total displacements in the soil, at the interaction with the wheels of MF-8700 tractor, for the same cohesive soil (clayey) for three different tire inflation pressures (0.1 MPa, 0.15 MPa, 0.2 MPa). It can be observed that the higher the tire inflation pressure, the deformation of agricultural soil increases and the total displacements are distributed in the soil at a higher depth and have higher values, especially in the surface layer (arable).

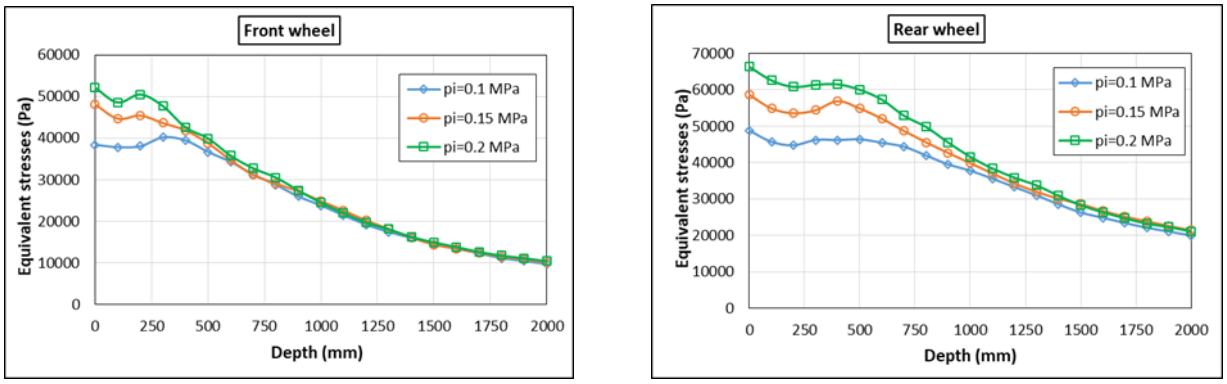

a) b)

Fig. 13 - Variation of the equivalent stress distribution in the soil after vertical-axial direction for different inflation pressures of the front tire (a), and rear tire (b)

In Fig. 13-a and Fig. 13-b there are presented the variation graphs of the distribution of equivalent stresses in the soil after vertical-axial direction, resulting from the numerical simulation, for different inflation pressures (0.1 MPa, 0.15 MPa, 0.2 MPa) of the front tire, respectively rear tire, depending on the depth. Analysing Fig. 13-b in particular, it is observed that if tire inflation pressure is 0.2 MPa, the susceptibility of superficial compaction occurs in the superficial layer, hence it is recommended to limit the value of this tire inflation pressure to a maximum of 0.15 MPa.

Fig. 14 shows the variation graphs of the distribution of vertical displacement in the soil after vertical-axial direction, resulting from the numerical simulation, for different inflation pressures (0.1 MPa, 0.15 MPa, 0.2 MPa) of the front tire, respectively rear tire, depending on soil depth. It can be seen that the largest vertical displacements, respectively the largest deformations, occur in the superficial (arable) layer of soil.

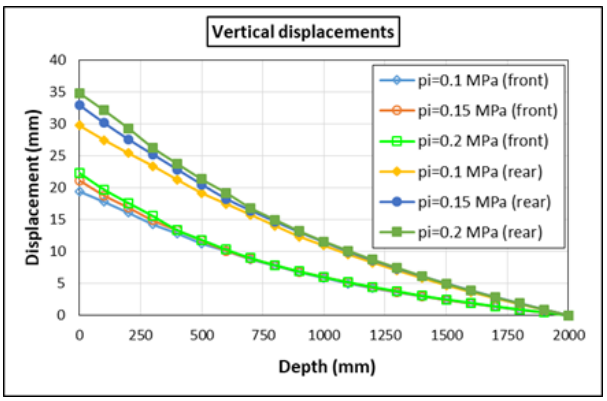

Fig.14 - Variation of distribution of the total displacement in the soil after vertical-axial direction for different inflation pressures of the two tires

In order to validate the model of analysis using the Finite Element Method, Fig. 15 (a, b, and c) presents comparatively the values of the equivalent stresses in the soil after vertical-axial direction in the case of front wheel of the MF-8700, values obtained by numerical simulation using the FEM model developed and those obtained by experimental testing, down to a depth of 1 meter (Fig. 8) for different tire inflation pressures (0.1 MPa, 0.15 MPa, 0.2 MPa).

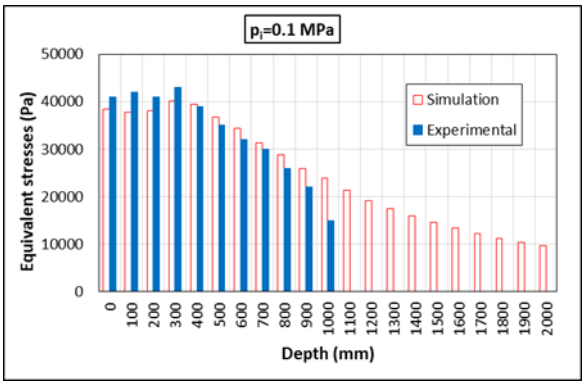

a)

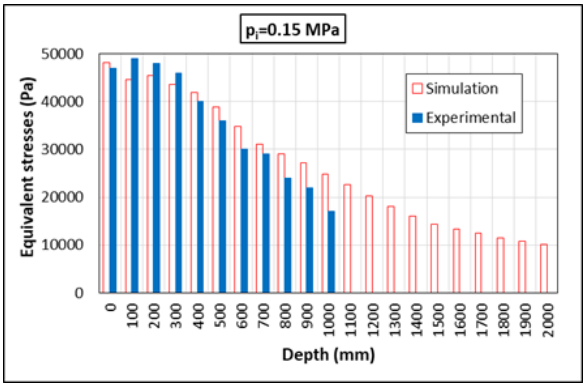

b)

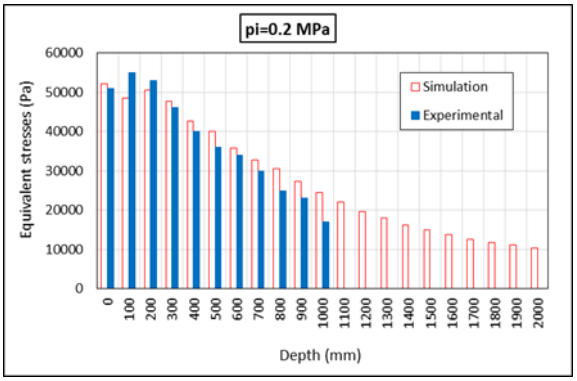

c)

Fig.15 - Equivalent stresses obtained by FEM simulation and experimentally

Comparative statistical calculations were performed for the absolute deviation (ε) of the values of equivalent stress obtained by simulation (S_s) compared to those obtained experimentally (S_e), for the depth of 1 meter of the analysed soil layer, applying the relation:

$$\varepsilon = \frac{\sum_{i=1}^{n} |S_e - S_s|}{\sum_{i=1}^{n} S_e} \cdot 100 \quad (\%) \tag{10}$$

where n is the number of points (10 points) in which experimental values were recorded by means of the Flexi Force Tekscan W-B201-L force sensors placed vertically in the soil in the experimental stand bin (in increments of 10 cm) and of the data acquisition system (Fig. 5).

Following the calculations, the following deviations of the values given by the simulation model from the experimentally obtained values for the front MF-8700 tractor are obtained, for the three different tire inflation pressures: ε=9.23 % (Fig. 15-a), ε=10.31 % (Fig. 15-b) and ε=9.79 % (Fig. 15-c). These relatively small deviations, taking into account the complexity of agricultural soil behaviour at the interaction with the wheels of tractors and agricultural machines, justify us to appreciate that the simulation model using the Finite Element Method can be validated and can be used in assessing the phenomenon of artificial compaction of soil under the action of heavy-duty tractors.

CONCLUSIONS

The Finite Element Method is currently the most advanced mathematical tool that can be used to modelling the process of artificial compaction of soil under the action of rolling bodies of tractors and agricultural machinery. For mathematical modelling, the soil can be considered a homogeneous and isotropic material, and the Drucker-Prager plasticity model can be used to simulate the behaviour of agricultural soil. The simulation model, using the Finite Element Method (Fig. 12-a), allows highlighting the distribution of stresses into the soil and their values, making it possible to highlight situations in which soil is artificially compacted, usually when the value of equivalent stress exceeds 80 kPa.

As it can be seen in Fig. 15, between simulated and experimental results there is a difference of approximately 10% for the front wheel of the MF-8700. These relatively small deviations encourage us to appreciate that the simulation model using the Finite Element Method, developed in the present paper, can be validated and used in assessing the phenomenon of artificial compaction of soil under the action of heavy-duty tractors.

This study highlights the major advantage of using models of stress distribution in the soil by the Finite Element Method (FEM), namely reducing dramatically the costs associated with experimental testing and reducing considerably the time required to analyse the possibility of occurrence of artificial compaction phenomenon of the agricultural soil under the action of heavy-duty tractors. This simulation model can be extremely useful to both manufacturers of tractors and agricultural machinery, but also to those who exploit such machinery and aim to limit the phenomenon of artificial compaction of agricultural soil by properly choosing the rolling bodies and by setting the appropriate tire inflation pressure.

REFERENCES

[1] Arvidsson J., (1997), *Soil compaction in agriculture – from soil stress to plant stress*, Doctoral Thesis, Agraria 41, Swedish University of Agricultural Sciences, Uppsala, Sweden;

[2] Augustin K., Kuhwald M., Brunotte J., Duttmann R., (2019), FiTraM: A model for automated spatial analyses of wheel load, soil stress and wheel pass frequency at field scale. *Biosystems Engineering*, *180*, pp.108-120.

[3] Bennett J. M., Roberton S. D., Marchuk S., Woodhouse N. P., Antille D. L., Jensen T. A., Keller T., (2019), The soil structural cost of traffic from heavy machinery in Vertisols. *Soil and Tillage Research*, 185, pp.85-93.

[4] Cueto O. G., Coronel C. E. I., Morfa C. A. R., Sosa G. U., Gómez L. H. H., Calderón G. U., Suárez M. H., (2013), Three dimensional finite element model of soil compaction caused by agricultural tire traffic. *Computers and electronics in agriculture*, 99, pp.146-152;

[5] Cuet O. G., Coronel C. E. I., Bravo E. L., Morfa C. A. R., Suárez M. H., (2016), Modelling in FEM the soil pressures distribution caused by a tyre on a Rhodic Ferralsol soil. *Journal of Terramechanics*, 63, pp.61-67;

[6] Gee-Clough D., Wang J., Kanok-Nukulchai W., (1994), Deformation and Failure in Wet Clay Soil: Part 3, Finite Element Analysis of Cutting of Wet Clay by Tines, *J. of Agric. Eng. Res.* 58, pp. 121-131;

[7] Gill W.R., Vanden Berg G.E., (1968), *Soil dynamics in tillage and traction*, U.S.A. Department of Agriculture, Handbook 316, USA, Washington D.C.;

[8] Hajabbasi M. A., (2001), Tillage Effects on Soil Compactness and Wheat Root Morphology. J. *Agric. Sci. Technol.* 3, pp.67-77;

[9] Hammel K., (1994), Soil stress distribution under lugged tires, *Soil & Tillage Res.* 32, pp.163-181;

[10] Javadi A., Spoor G., (2006), The Effect of Spacing in Dual Wheel Arrangements on Surface Load Support and Soil Compaction. *J. Agric. Sci. Technol.* 8, pp.119-131;

[11] Keller T., (2004), *Soil compaction and soil tillage - studies in agricultural soil mechanics*, Doctoral Thesis. Agraria 489, Swedish University of Agricultural Sciences, Uppsala, Sweden;
[12] Keller T., Lamandé M., (2010), Challenges in the development of analytical soil compaction models. *Soil and Tillage Research*, 111(1), pp.54-64.
[13] Khodaei M., Fattahi S. F., Navid H., (2016), Evaluation of FEM modelling for stress propagation under pressure wheel of corn planter. *Agricultural Engineering International: CIGR Journal*, *18*(3), pp.14-22.
[14] Komandi G., (1976), The determination of the deflection, contact area, dimensions, and load carrying capacity for driven pneumatic tires operating on concrete pavement. *Journal of Terramechanics*. 13(1), pp.15-20;
[15] Koolen A.J., Kuipers H., (1983), *Agricultural soil mechanics*, Advanced Series in Agricultural Sciences, Vol. 13. Springer, Heidelberg;
[16] Kushwaha R.L., Shen J., (1995), Finite element analysis of the dynamic interaction between soil and tillage tool. *Transaction of the ASAE*, 38 (5), pp.1315-1319;
[17] Kuhwald M., Dörnhöfer K., Oppelt N., Duttmann R., (2018) Spatially Explicit Soil Compaction Risk Assessment of Arable Soils at Regional Scale: The SaSCiA-Model. *Sustainability*, *10*(5), pp.16-18.
[18] Loghavi M., Khadem M. R., (2006), Development of a Soil Bin Compaction Profile Sensor. *J. Agric. Sci. Technol.* 8(1), pp.1-13;
[19] Martínez-Ramírez R., González-Cueto O., Betancourt-Rodríguez Y., Rodríguez-Orozco M., Guillén-Sosa S., (2017), Compaction and variation of the profile of the quarry caused by the CASE IH A8800 harvester in wet soils. *Revista Ingeniería Agrícola*, *7*(3), 30-35.
[20] McKyes E., (1985), *Soil cutting and tillage*, Elsevier, Amsterdam-Oxford-New York-Tokyo;
[21] Mohsenimanesh A., Laguë C., (2017), Impact of load and inflation pressure on traffic-induced soil compaction for two types of flotation tires, *Applied Engineering in Agriculture*, Vol. 33(4), pp.499-507;
[22] Rashidi M., Tabatabaeefar A., Attarnejad R., Keyhani A., (2007), Non-Linear Modeling of Pressure-Sinkage Behaviour in Soils Using the Finite Element Method. J. Agric. Sci. Technol., vol.9, pp.1-13;
[23] Silva R. P., Rolim M. M., Gomes I. F., Pedrosa E. M., Tavares U. E., Santos A. N., (2018), Numerical modeling of soil compaction in a sugarcane crop using the finite element method. *Soil and Tillage Research*, vol.181, pp.1-10.
[24] Upadhyaya S.K., Rosa U.A., (1997), Prediction of traction and soil compaction, *Proceeding of 3rd International Conference on Soil Dynamics (ICSDIII)*. Tiberias, Israel, pp 19-58;

DESIGN OF SMALL MULTIFUNCTION HYDRAULIC CHASSIS FOR HILLY REGIONS OF SOUTHWEST CHINA
/
西南丘陵山区小型多功能全液压底盘的设计

Prof. Ph.D. Eng. Lv Xiaorong*[1)], Prof. Ph.D. Eng. Zhang Lihua[1)], Ph.D. Eng. Lv Xiaolian[2)], M.A. Stud. Eng. Wang Xiao[1)]

[1)] Sichuan Agricultural University, College of Machinery & Electronics/China;
[2)] Ministry of Agriculture, Key Laboratory of Modern Agricultural Equipment/China
Tel: 08352882182; E-mail: lxrxj2008@163.com

Keywords: *small multifunction chassis, intercropping, crawler, hydraulic system, experiment*

ABSTRACT

A small multifunction hydraulic chassis was designed on the basis of the intercropping planting in the hilly regions of southwest China. The overall structure and the design parameters were completed by theoretical calculations and UGNX software. A track-based walking device was studied. It consists of a gauge of 720 mm and a minimum ground clearance of 200 mm. The prototype employs a full hydraulic drive system, effectively solving the steering problems in narrow spaces of intercropping fields. It can also navigate smoothly through a hilly intercropping field, is stable on slopes (<25°) and has good climbing ability.

摘要

针对西南丘陵山区地形及套作种植的特点，设计了小型多功能全液压底盘。通过理论计算及 UG 三维样机技术，完成了整机结构设计和关键部件参数的确定。本文主要研究了小型多功能底盘的行走装置，确定其为履带式，轨距为 720㎜，最小离地间隙为 200㎜；研究了全液压传动系统，此系统有效的解决了套作地头小空间转向问题，实现了原地 360° 转向。性能试验表明机器能够顺利通过丘陵套作田间作业，液压系统设计合理，动力足，能够平稳通过小于 25° 的斜坡，爬坡性能良好。

INTRODUCTION

The hilly southwest region of China (*Lv Xiaorong et al, 2011*) is a typical dry farming area. The region is remote and relatively inaccessible and its terrain is characterized by undulations and slopes, which makes it unsuitable to mechanized crop cultivation. Historically, intercropping has been the predominant method of cultivation in this region. This method involves planting crops in the spaces between narrow rows with intercropping spacing of 1m, where large-scale agricultural machinery cannot be operated. The intercropping pattern currently practiced in the hilly southwest region is that of “wheat/maize/beans.” Its planting is basically a manual and artisanal process, with low productivity and high labour intensity (*Lv Xiaorong et al, 2011*). Hence, the development of miniaturized, lightweight and economical agricultural machinery that is suitable for use in hilly regions is of particular importance.

The “wheat/maize/beans” intercropping pattern employs strip crop rotation (*Lv Xiaorong et al, 2011; Vandeneer J.H., 1989; Fukai S. and Trenbath B.R., 1993; Fang Susu et al, 2017*). This method is implemented in a very narrow space. The undulating ground has a certain gradient and the soil is clayey. As such, the aim of the present study is to design a small multifunction chassis, which uses a self-propelled crawler, with a compact structure, small radius steering and high motor power. Various small-scale agricultural machines can be coupled to the chassis through the suspension support so that various operations such as tillage, seeding, fertilization, spraying of pesticides and irrigation can be carried out.

Most existing small-scale agricultural machinery employ wheel gears for movement. However, such machinery is not suited for use on the cohesive soil found in the southwest region (especially Sichuan). Operation of such machinery on slopes is difficult because of slipping. Moreover, the turning radius of wheeled machinery is large, which decreases manoeuvrability in narrow spaces (*Lv Xiaorong et al, 2011*). A track-based walking structure is proposed with a large ground-contact surface area, high traction, low subsidence and good steering. These features make it suitable for intercropping operations in the hilly region.

MATERIALS AND METHODS

- **Structure and operating principle of machinery**

Structure and Technical Parameters

The overall structure of the small multifunction chassis is shown in Fig. 1.

It consists of moving, control, hydraulic, suspension and transmission. The main technical parameters are listed in Table 1.

Table 1

Main technical parameters

No.	Item	Unit	Parameter
1	Dimensions	mm	2000 × 1100 ×1520
2	Structure weight	kg	540
3	Gauge	mm	720
4	Length of track in contact with the ground	mm	900
5	Minimum ground clearance	mm	200
6	Connection method		suspension
7	Maximum speed	km/h	5
8	Operating speed	km/h	1–2
9	Engine:		
	Rated power	kW	15
	Rated speed	(r/min)	3600
	Maximum torque	(N.m)/(r/min)	47/2600
10	Double pump:		
	Displacement	(CC/r)	12
	Maximum revolutions under idle load	rpm	3600
	System operating pressure	MPa	16

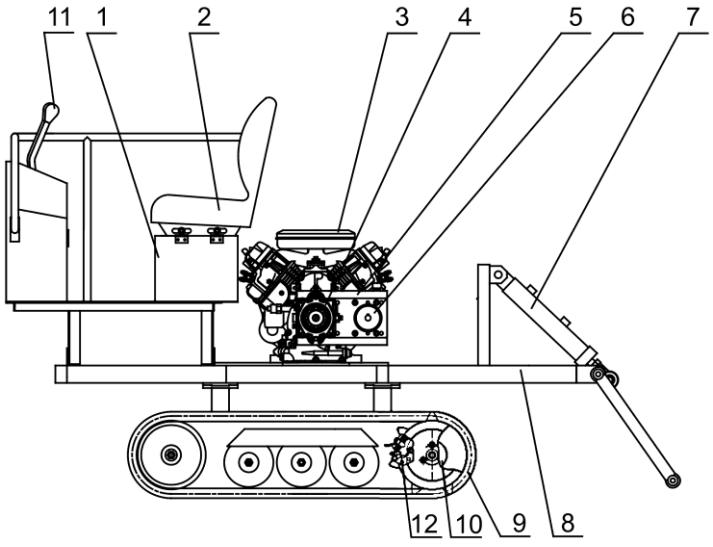

Fig. 1 - Overall structure shown in UGNX

1- Fuel tank; 2- Seat; 3- Engine; 4- Double pump; 5- Transfer case; 6- Gear pump; 7- Hydraulic cylinder; 8- Chassis; 9- Walking system; 10- Motor; 11- Operating system;12- Brake System

Operating Principle

During operation of the multifunction chassis, engine power is transmitted via the transfer case to the hydraulic system, which in turn transfers the power to the moving and suspension systems. This allows the chassis to carry out various moving operations, including forward, backward and turning movements. Planting, cultivation, and other farming operations can be carried out when the chassis is coupled to other agricultural machinery through articulation.

Structural Design of Moving System

The moving system of the proposed multifunction chassis comprises the track, driving, supporting, and steering wheels and the support frame. The left and right tracks wrap around the driving, supporting, and steering wheels and are in direct contact with the ground. The area of the track in contact with the ground is 900 mm long and 180 mm wide, and the gap between the two tracks is 720 mm. The operating principles are as follows: (i) the output power of the motor is transmitted to the driving wheels to drive the tracks; (ii) the steering wheels tighten the tracks, guide their motion, and absorb shocks; (iii) the supporting wheels transfer the entire weight of the machinery to the tracks. The wheels roll along the rails of the tracks to prevent lateral movement.

Determination of Main Parameters

In the design of the walking system, the important parameters include the track support length *L*, track gauge *B*, and width of the track shoe *b*. These must be reasonably matched so that the requirements for ground contact, adhesiveness and turning performance are met. We obtained the following empirical eq. from the agricultural machinery manual (****Agricultural Machinery Design Manual, 2007*):

$$L \approx 107\sqrt[3]{G} \tag{1}$$

$$\frac{L}{B} \approx 1.2\text{-}1.4 \tag{2}$$

$$\frac{b}{L} \approx 0.2 - 0.8 \tag{3}$$

Where：

L —Length of the supporting track, mm;

G—Initial operating weight of the machinery, kg;

B —Track gauge, mm;

b —Width of the track shoe, mm.

The initial weight of the crawler was G = 800 kg. Substituting this value into Formulas (1)–(3) gives:

$$L \approx 107\sqrt[3]{G} = 107\sqrt[3]{800} = 995 \text{ mm}$$

Where：

$L \approx$ 950 mm; B=613-750 mm; b=(0.18-0.22) L=162-198 mm

After comprehensive considerations, the length of the supporting track is 900 mm, the track gauge is 720 mm and the width of the track shoe is 180 mm.

Design of Full Hydraulic System

The chassis includes a complete hydraulic system and it differs from the existing agricultural steering technology, because it uses positive differential system for turning and a unilateral braking system. Here, bilateral reverse differential steering is introduced to micro- and small-scale agricultural machines for the first time. This technique facilitates pivotal turning of the machinery, and effectively reduces its steering radius and hence its weight.

- **OVERALL PROPOSAL**

The hydraulic components of the multifunction chassis comprise a double pump and gear pumps, a driven motor and a hydraulic cylinder. The transmission and principle diagram of the hydraulic system is shown in Fig. 2.

The engine provides power to the double pump and gear pumps through the transfer case. The system is divided into two components. One supplies pressurized oil to the driven motor through the double pump. The dual-direction opening of the two joysticks for the double pump allows the driven motor to turn forward and backward and thus enables the chassis to move forward, move backward, turn, or stop. This results in two closed-loop hydraulic circuits.

The other component supplies pressurized oil through the hydraulic gear pump via an open-loop hydraulic circuit. It is controlled by manipulating a multi-way valve; it can lift and lower various operating systems, as well as operate various mechanical parts. Thus, the component enables seeding, fertilization, irrigation, and other farming operations to be carried out.

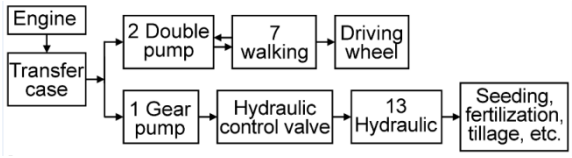

a)

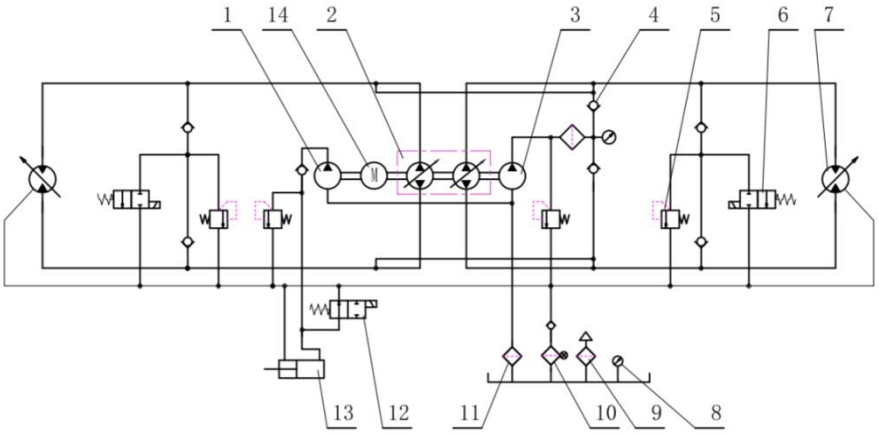

b)

Fig. 2 - Hydraulic system of multifunction chassis

a) Schematic diagram of hydraulic system; b) Principle diagram of hydraulic system

1- Gear pump; 2- Double pump; 3-Charge pump; 4- Check valve; 5- Pressure relief valve; 6- Normally closed unloading valve; 7- Driven motor; 8- Gauge; 9- Air filter; 10- Return filter; 11-Suction filter; 12- Normally opened unloading valve; 13- Hydraulic cylinder; 14- Electric engine

- **DETERMINING PARAMETERS OF MAIN HYDRAULIC COMPONENTS**

The main parameters for the design of a hydraulic system and selection of hydraulic components are the pressure and flow (6). The pressure is determined by the external load, whereas the flow in the hydraulic actuator is determined by the velocity of movement and the structural dimensions.

Selection of driven motor

The hydraulic motor converts hydraulic energy to kinetic energy so that the hydraulic actuator can rotate continuously. The motor torque is calculated as follows (*Merritt H.E., 1967*):

$$T_p = F_T \times r \tag{4}$$

$$\left.\begin{array}{c} F_T = F_q - F_f \\ F_q \le F_\varphi \\ F_f = f \times G_s \end{array}\right\} \Rightarrow F_T \le F_\varphi - fG_s \tag{5}$$

$$\left.\begin{array}{c} F_\varphi = \varphi G_\varphi \\ G_\varphi = G_s \end{array}\right\} \Rightarrow F_\varphi = \varphi G_s \tag{6}$$

Where:

T_p - motor torque (N.m);

r - radius of the driving wheel of the track (mm);

F_T - traction force (N);

F_q - tangential driving force (N);

F_f - Rolling resistance (N);

F_φ - adhesion (N); G_φ - adhesion weight (kg);

G_s - weight used (taken as 800 kg);

f- rolling resistance coefficient (0.06–0.07);

φ - adhesion coefficient (0.9–1.1), from Eqs. (4)–(6).

The following is obtained:

$T_p \le 1223.04 \approx 1223$ N.m

The displacement of the hydraulic motor is:

$$V_{gm} = (\frac{2 \times \pi \times T_g}{\Delta P}) / \eta_{mm} \leq 266.68\, ml/r \quad (7)$$

Where:

V_{gm} - motor displacement;

T_g - single motor torque ($T_p = 2 \times T_g$);

ΔP - pressure differential of motor ($\Delta P = 16 MPa$);

η_m - mechanical efficiency of motor (0.9–0.99).

The following were selected on the basis of theoretical calculations by considering the specific operational requirements: motor model M5-250; torque, 620 N·m; displacement, 250 ml/r.

Selection of double pump

This is mainly based on the maximum operating pressure and flow (*Merritt H.E., 1967*). The maximum operating pressure of the hydraulic pump *Pp* (Pa) of the multifunction chassis is calculated on the basis of the maximum operating pressure of the hydraulic actuator as follows:

$$p_p \geq p_1 + \sum \Delta p = 16.5 \text{ MPa} \quad (8)$$

Where:

p_p - Maximum operating pressure of the hydraulic pump;

p_1 - Maximum operating pressure of the hydraulic motor (16 MPa);

$\sum \Delta p$ - Total piping loss between the outlet of the hydraulic pump and the inlet of the hydraulic motor. A value in the range of 0.2–0.5 MPa was selected on the basis of empirical data.

The flow of the hydraulic pump is determined as follows:

$$q_{vp} \geq K\left(\sum q_{V\max}\right) \quad (9)$$

$$\sum q_{V\max} = \frac{V_{gm} \times n}{1000} = 23\, L/\min \quad (10)$$

Where:

q_{VP} - maximum flow rate of the hydraulic pump;

K - system leakage coefficient (usually in the range of 1.1–1.3);

$\sum q_{V\max}$ - Maximum flow of the hydraulic motor (L/min);

V_{gm} - Motor displacement (250 ml/r);

n -Shaft speed (89 r/min).

From Eqs. (9) and (10), q_{Vmax} is determined as ≥30 L/min.

OYP12 was selected as the model for the double pump. The maximum operating pressure and flow of the pump are 21 MPa and 33.6 L/min, respectively.

- **Design of speed measurement system**

The requirements for crop cultivation vary according to the conditions of the fields. In addition, for various reasons, crop density varies even within the same region. Real-time control and adjustment of the operating speed of the machinery are required.

In this paper, a rotary-driven testing system was designed to facilitate real-time control of the operating speed of the driving wheels. Data processing via a microcontroller is carried out to provide a good understanding of the multifunction chassis operating speed. The structure of the test system is shown in Fig. 3.

Inductive proximity switches (LJ24A3-10-Z/AX, Shanghai Hangrong electric Co., Ltd., Shanghai, China) are used to count wheel rotations. Each wheel has 11 teeth. The sine signal is converted to a square

wave signal by using an optocoupler. The display circuit shows the speeds of the left and right wheels, which produce a periodic signal output for the pulse.

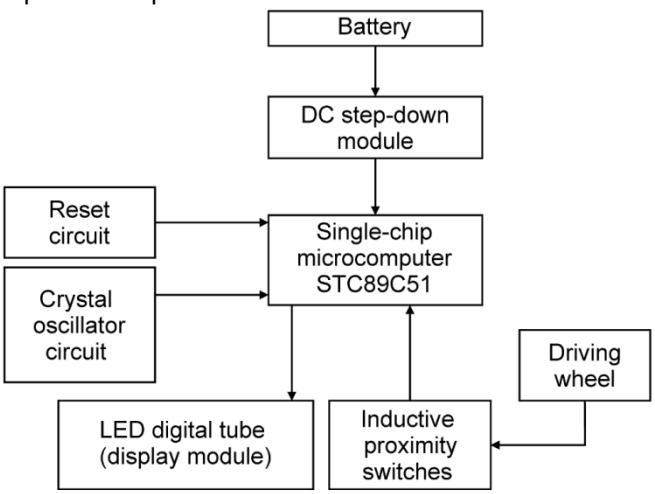

Fig. 3 - Rotary-driven speed test system

The relation between the frequency and pulse speed can be stated as follows:

$$n = \frac{f}{z} \times 60 \tag{11}$$

Where：

n—Speed of the driving wheel (r/min); *f*—Pulse frequency (Hz);

z—Teeth count of the driving wheel (min)

The real-time speeds of the left and right wheels are shown on the display and are adjusted using a control handle according to the actual operational requirements. With real-time monitoring and appropriate adjustments made to the driving speed of the machinery, operational speed is controlled.

- **Design and fabrication of three dimensional prototypes**

The UGNX6.0 three-dimensional software package was used to model and assemble the multifunction chassis as well as to detect the interference of machine components and the centroid of the machinery (*Ma Xinguo, Chen Yuanyuan, 2012; Jayaram S. et al, 1997; Deng Y. M. et al, 1991; Xiaorong Lüet et al, 2013)*. The results show that there is no interference between the various components. Therefore, the structural design of the machinery is acceptable. A prototype of the multifunction chassis was manufactured in Sichuan Agricultural University processing workshops.

- **PERFORMANCE TEST**

Test location

Performance tests of the multifunction chassis were conducted in November 2012 at the Sichuan Agricultural University (SAU) testing base and the nearby hilly region. The plots used for testing were intended for intercropping cultivation. The corn was ripe and had been harvested, leaving only the matured soybeans. Concrete pavements of various gradients (similar in condition to the many existing farm tracks in rural areas) are located in the hills behind the SAU. The steepest slope for pavements is approximately 31°.

RESULTS

Performance tests of the multifunction chassis were carried out in the hilly south-western region in accordance with the relevant provisions stated in Test Methods for Agricultural Wheeled and Crawler Tractors (*Snadu C et al, 2010; Huaifeng YANG et al, 2013; Liang Zhaoxin et al, 2012; Wen Aimin et al, 2014*). The testing criterion was the non-compaction of stems and leaves of the crops located on either side of the multifunction chassis when the machine passed through the intercropping band (Fig.4) at the Sichuan Agricultural University experimental field.

Fig. 4 - Performance testing on intercropping band

The multifunction chassis could smoothly navigate the narrow space within the intercropping band. There was no rolling of the crops on either side, demonstrating that the design parameters of the multifunction chassis could satisfactorily meet the requirements for intercropping cultivation in the hilly southwest region.

(2) Hills with different gradients, located behind the SAU, were also selected for testing (Fig. 5). The prototype was stationed on a straight road that is relatively flat. The machine was started at a slow speed and then accelerated at maximum throttle. It attained a stable speed by the time it reached the base of the slope for testing. It then climbed the slope at a steady speed. This test was performed thrice on each gradient. The test was considered a success if the machine was able to climb the slope at least once.

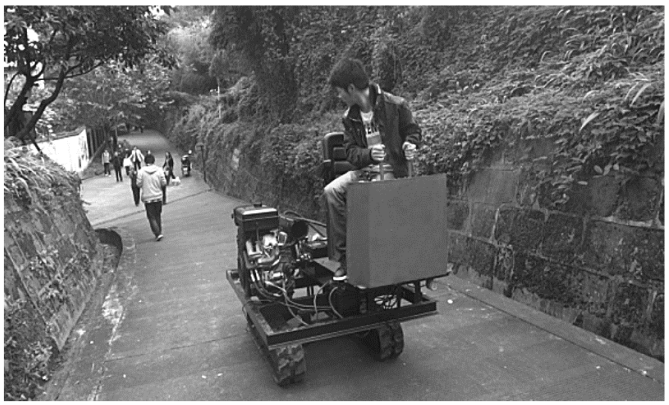

Fig.5 - Test of climbing abilities

During the climbing test, the driving speed for the multifunction chassis was 0.8 km/h. It could successfully climb a gradient with a maximum slope of 31°. The soil and water conservation law stipulates that “the limit of the slope for wasteland cultivation of crops should be <25° (*Nengye Liu, 2012*). The climbing capacity of the prototype is thus sufficient.

(3) The main purpose of steering the multifunction chassis was to observe its suitability for turning in narrow spaces. The turning tests involved observing/measuring bilateral forward and backward speed differentials, unilateral braking and turning radius.

The prototype displayed good steering ability. During a test of the bilateral backward speed differential, it achieved a 360° pivot turn.

CONCLUSIONS

The intercropping field tests, the multifunction chassis stability and smooth navigation through the ups and downs in the field, show that the chassis structure design is reasonable, with excellent traction and good stability performance, suitable for intercropping operations in the hilly region.

(1) The multifunction chassis could smoothly navigate the narrow space within the intercropping band. There was no rolling of the crops on either side, demonstrating that the design parameters such as caterpillar

track 720 mm, the width of 1100 mm and so on, could satisfactorily meet the requirements for intercropping cultivation in the hilly southwest region.

(2) During the turning test, the chassis achieved a 360° pivot turn, showing that design of hydraulic system achieves the function of reverse differential steering, thus solving the difficult problem of turning in narrow spaces.

(3) During the climbing test, the small multi-function chassis at 0.8 km/h speed, could smoothly pass a gradient of 31° slope degree, verifying that the chassis has good climbing abilities and is capable of steadily climbing a slope of <25°. The prototype thus meets the basic operational requirements stipulated for the use of agricultural machinery in the hilly regions of southwest China.

ACKNOWLEDGEMENT

The study was supported by the Key Laboratory of Modern Agricultural Equipment, Ministry of Agriculture, P.R. China (201602002), the National corn industry system project (CARS-02-29) and the National Natural Science Foundation of China (51105261).

REFERENCES

[1] Deng Y.M., Tor S.B., Britton G.A., (1991), Computerized Design Environment for Functional Modelling of Mechanical Products, *Fifth Symposium on Solid Modeling*, Ann Arbor, MI, Association for Computing Machinery, New York/U.S.A.;

[2] Fang Susu, Lu Zhixiong, Wang Zengcai, (2017), Design and prototype performance experiments of steering-by-wire hydraulic pressure system of tractor, *Transactions of the Chinese Society of Agricultural Engineering (Transactions of the CSAE)*, Vol.33, Issue 10, pp.86-93, Beijing/CHN;

[3] Fukai S, Trenbath B.R., (1993), Processes Determining Intercrop Productivity and Yields of Component Crop, *Field Crops Research*, Issue 34, pp.247−271*,* Amsterdam / Holland;

[4] Huaifeng Yang, Xiaorong Lü, (2013), Dynamic Simulation of Small Crawler Chassis Turning Based on RecurDyn, *Advanced Materials Research*, Vol. 774-776, pp.195-198, Zurich/Switzerland;

[5] Jayaram S., Connacher H.I, Lyon K.W., (1997), Virtual Assembly Using Virtual Techniques, *Computer Aided Design*, Vol. 29, Issue 8, pp.575-584, England/U.K.;

[6] Liang Zhaoxin, Huang Hai, Zhang yu feng, (2012), Research on Application of New crawler walking chassis on Rice Combination Harvester, *Agricultural Engineering*, Issue 2, pp.28-31, Beijing/China;

[7] Lv Xiaorong, Liu Lina, Lv Xiaolian, (2011), Prospect of Application of Farm Mechanism Technology in Intercropping Farming, *Journal of Agricultural Mechanization Research*, Issue 12, pp. 245−248, Heilongjiang/CHN;

[8] Ma Xinguo, Chen Yuanyuan, (2012), Based on the multi-body dynamics simulation analysis of the tracked vehicle steering performance, *Mechanical design*, Vol.29, Issue 6, pp.52-56, Tianjin/CHN;

[9] Merritt H.E., (1967), *Hydraulic Control Systems*, John Wiley & Sons Inc., New York/U.S.A.;

[10] Nengye Liu, (2012), People's Republic of China: Water and Soil Conservation Law, *IUCN Academy of Environmental Law e-Journal*, Issue 1, pp.69−74, Maryland/ U.S.A.;

[11] Snadu C, Worlry M E, Morgan J P, (2010), Experimental study on the contact patches pressure and sinkage of a lightweight vehicle on sand, *Journal of Terramechanics*, Vol.47, Issue 5, pp.343-359, England/U.K.;

[12] Vandeneer J.H., (1989), *The Economy of Intercropping*, Cambridge University Press, Cambridge / U.S.A.;

[13] Xiaorong Lü, Weimin Ding, Huaifeng Yang, (2013), Finite element analysis of multi-function chassis underframe, *Advanced Materials Research,* Vol.753-755, pp.1587-1590, Zurich/Switzerland;

[14] Wen Aimin, Lu Zhixiong, Wu Jungan, (2014), Experiment and analysis of full hydraulic steering characteristics, *Journal of Chinese Agricultural Mechanization*, Vol.35, Issue 5, pp.122-127, Nanjing/China;

[15] ***Chinese Academy of AgriculturaL Mechanization Sciences, (2007), Agricultural Machinery Design Manual, *Chinese Agricultural Science and Technology Press*, Beijing/CHN.

PECULIARITIES OF WILLOW PRODUCTIVITY FORMATION IN THE FIRST YEAR OF GROWING UNDER MECHANICAL WEED CONTROL

/

ОСОБЛИВОСТІ ФОРМУВАННЯ ПРОДУКТИВНОСТІ ВЕРБИ ЕНЕРГЕТИЧНОЇ ПЕРШОГО РОКУ ВЕГЕТАЦІЇ ЗА МЕХАНІЧНИХ ПРИЙОМІВ КОНТРОЛЮВАННЯ БУР'ЯНІВ

D. Agri.Sci. Fuchylo Ya. [1], Senior res. Ph.D. Makukh Ya. [1], Senior res. Ph.D. Remeniuk S [1], Senior res. Ph.D. Moshkivska S. [1]., Prof. Ph.D. Agri.Sci. Kharytonov M. [2]

[1]Institute of Bioenergy Crops and Sugar Beet NAAS of Ukraine

[2]Dnipro State Agrarian and Economics University, Faculty of Agrarian Engineering / Ukraine;

Tel: +38-0973456227; E-mail: envteam@ukr.net, S.Yefremova st. 25, Dnipro, Ukraine

Keywords: *willow, weeds, agrotechnical methods, energy yield.*

ABSTRACT

The results of five-year field experiments using various mechanical techniques to protect annual plantings of energy willow from weeds in the central forest-steppe zone of Ukraine were given. The use of inter-row cultivation system (3 treatments every 15 days) reduced the value of forming a weeds mass to 2.9 times; using mounted chain harrow *– 3.1 times, and the use of three consequent harrowing between rows – 3.4 times, compared with the case* without weed treatment *– 3854 g/m². The lowest yield of dry energy willow biomass (1.15 t/ ha) was obtained without weed control, while the highest was obtained after six consequent hand weedings (3.14 t/ha). Successive hoeing of the space between rows ensured, on the average, 2.52 t/ha dry biomass in the first year of growing, while similar harrowing with chain harrow 2.55 t /ha, and cutting of weeds 2.60 t/ha.*

РЕЗЮМЕ

Наведено п'ятирічні результати проведених в Центральному Лісостепу України на чорноземно-лучному ґрунті досліджень ефективності застосування різних механічних прийомів для захисту однорічних посадок верби енергетичної від бур'янів. Використання системи міжрядних культивацій (3 догляди через кожні 15 днів) знижувало величину формування маси бур'янів у 2,9 раз; аналогічної система міжрядних боронувань сітчастими боронами – у 3,1 раз, а при застосуванні трьох послідовних зрізувань сходів у міжряддях – у 3,4 рази, порівняно з варіантом без проведення доглядів – 3854 г/м². Встановлено, що на варіанті забур'яненого контролю рослин верби енергетичної формували мінімальне значення урожайності сухої біомаси – 1,15 т/га, в той же час максимальний рівень урожайності був у варіанті з проведенням шести послідовних ручних просапувань – 3,14 т/га. За проведення системи послідовних міжрядних культивацій отримали середню урожайність верби енергетичної першого року вирощування на рівні 2,52 т/га, за послідовних міжрядних боронувань навісними сітчастими боронами – 2,55 т/га а за системи послідовних зрізувань сходів бур'янів рослини верби сформували 2,60 т/га сухої біомаси.

INTRODUCTION

The first energy willow plantations appeared in Sweden in the late 1980s as a reaction to the volatile fossil fuel market (*Gustafsson et al, 2009; Mola-Yudego B., 2010*). Given the high calorific value of the willow wood, which according to various estimates amounts to 17.0−17.5 MJ·kg^{-1} of absolutely dry matter (*Roik et al., 2015; Fuchylo Ya. D., 2011*) although it can reach 19.8 MJ·kg^{-1} (*Keoleian and Volk, 2005*)), willow biomass is mainly used for the production of chip fuel, pellets and briquettes for combustion in solid fuel boilers.

Dominating in energy-intensive plantations in Sweden were the clones and hybrids of the Salmonidae (Salix viminalis L.) derived from long-term dedicated breeding program for *Salix viminalis* cultivation carried out since 1987 (*Ahman and Larson, 1994*). Simultaneously, breeding was carried out over other species and their hybrids (*Willow Varietal Identification Guide, 2012*). Currently, the varieties of Swedish breeding, due to their high productivity and unpretentiousness to soil conditions, are common in most European countries, including Ukraine. One of the most productive varieties is 'Torah'. In Sweden, this cultivar achieves

productivity up to 22 ton·ha^{-1} year^{-1} (*Volk et al., 2004*) and in the United Kingdom 11.3 ton·ha^{-1} year^{-1} (*Aylott et al., 2008*). In addition to studying general principles of the establishment of energy willow plantations (*Caslin et al., 2010*), much attention in the United Kingdom was being paid to improve the resistance of willow to harmful organisms (*McCracken et al,, 2011; Parfitt and Stott, 1987*).

Various aspects of creation, cultivation, exploitation, economic and ecological efficiency of energy willow plantations are also being explored in the United States *(Caputo et al, 2013; Volk et al., 2006; Volk et al., 2016; Wang et al. 201*5), Finland (*Hytonen J., 1995*), Canada (*Mosseler et al., 2014; Mosseler and Major, 2014; Nissim et al., 2013; Glavonjić, B., 2017*), the Czech Republic (*Weger et al., 2011*) and Ukraine (R*oik et al., 2015; Fuchylo, Ya. D., 2011*). Being a light-demanding plant, energy willow requires weed control in the first years of growing. It was found that weed infestation can reduce willow yield by 50 − 95% in the first years (*Sage R., 1999; Mitchell et al., 1999*). Besides light, weeds compete with willow for nutrients and water (*Weger et al., 2011*). It is clear that the longer the crop remains clear of weeds, the better it grows and forms a larger yield (*Hansen and Netzer, 1985*). Taking into account its low competitiveness, controlling weeds in willow plantations in the early stages of development should include a set of measures for mechanical and chemical weed control carried out, first of all, before the emergence of weeds, as post-emergence control is ineffective (*Davies R. J., 1985*). The most common ways of weed control in small plots include agrotechnical control and hand weeding but large energy willow plantation cannot be maintained without chemical weed control. At the same time, mechanical (agrotechnical) weed control methods also revealed some disadvantages: first of all, the intensive mixing of the upper soil layer when hoeing the space between rows. Such mixing promotes the emergence of the next wave of sprouting weeds. Reducing the level of mixing the soil (using chain harrow), and especially successive cuttings of weeds, reduced the intensity of weed emergence, but did not stop the process completely.

There are a number of registered commercial soil action formulas based on propyzamide, aclonifen, cycloxydim, clopyralid (*Gustafsson et al., 2009),* and glyphosate *(Gustafsson et al., 2009; Gustafsson L., 1987*) in Sweden. The latter is the most common herbicide for willow plantations in Europe and USA. It is introduced annually in the first three years during dormancy period, as glyphosate applied during the growth period suppresses willow plants. Romanian researchers reckon that introduction of herbicides does not inhibit the growth of willow plants (*Kondor et al. 2007*).

Agrotechnical weed control in willow plantations using multi-row cultivators and rotary ploughs was investigated in the early 1990s in different Sweden regions and on different soil types. A common problem of all these methods was to combat weeds between plants in a row, and in the case of using rake for this purpose willow seedlings were significantly damaged (*Albertsson J., 2012*). Three inter-row hoeing in the first half of the growing season practiced for willow in Ukraine almost completely destruct weed sprouts in the space between rows. However, weeds continue their growth in the rows and within buffer (protective) strips. Therefore, hand weeding is necessary for their destruction, which required significant labour costs (Roik *et al*., 2015). According to Polish researchers, the first 4−10 weeks following planting are critical for willow from the herbological point of view (*Sekutowski et al., 2007*); therefore, control of undesirable vegetation at this stage is considered one of the most important components of the growing technology (*Rola et al., 2006; Glavonjić, B., 2017*).

The volatility of energy willow plantations in the first year of vegetation in terms of quantitative and species weed composition usually reflects the weed infestation of the field in the previous years (*Baum et al., 2009*). Therefore it is important to define the groups of dominant and challenging weeds and to timely choose the methods of weed control. It was established that part of the common and challenging weed species survive and compete with willow plants during the first three years even when herbicides are introduced (*Wróbel et al., 2012*). Thus, weed species composition largely depends on the current land use, soil conditions, weed seed stock and other factors.

Consequently, as shown above, willow plants in the first year of vegetation are not very competitive with regard to weeds that spread in the free ecological niches of young energy willow plantations. That is why, the development of weed control practices, especially in the first year of vegetation, is a topical issue and requires a constructive solution.

High sensitivity of young plants to the action of majority of herbicides used against dicotyledonous weeds along with sanitary and environmental restrictions that are associated with planting near water bodies, in water protection and residential areas where the use of pesticides is forbidden, makes it difficult to introduce effective weed control technology for energy willow.

The purpose of the research was to evaluate the effectiveness of the various environmentally friendly mechanical weed control practices for one-year-old energy willow plantations.

MATERIALS AND METHODS

The experiment was carried out from 2012 to 2016 in the fields of the State Enterprise Experimental Farm 'Salyvinky' (Ksaverivka, Vasylkiv district, Kiev region). The weather conditions are typical for the zone of unstable humidification of the Central Forest-Steppe of Ukraine. The soil for the experiment was meadow chernozem or molisols (*Kravchenko et al., 2012*). The experiment was established in energy plantations of *Salix viminalis* in its first growing season according to the following design: (a) without weed treatment; (b) three consequent cultivations between rows at an interval of 15 days; (c) three consequent harrowing between rows using mounted chain harrow at an interval of 15 days; (d) three consequent manual weed cutting (cut height 1.5−3.0 cm at an interval of 15 days); (e) six consequent hand weedings (to total destruction of weeds).

The planting of ligneous cuttings of willow was carried out after the start of field work in early or mid-April. Before planting cuttings continuous tillage was carried out. Pre-planting tillage was made to kill existing sprouts of wintering and early spring weed species such as *Matricaria inodora L., Gallium aparine L., Descurainia Sophia L. Schur., Sisymbrium altissimum L., Thlaspi arvense L., Sinapis arvensis L.* and others. Experimental plot area was 36 m^2 and the registration area was 25 m^2. The plots were randomised with 4-times replication. Weeds observation was carried out using fixed frames measured 1.25 m x 0.20 m = 0.25 m^2 that were permanently set in four places diagonally in each treatment (*Tsyliuryk et al, 2017*). The first and second registration of weeds was made in early May and second decade of August accordingly.

The yield of the above-ground part of plants was determined by the method of cutting the above-ground parts at the experimental sites and expressed in either g/m^2 or t/ha.

RESULTS

The appearance of weed sprouts in the willow plantations occurred simultaneously with the start of opening buds on willow seedlings. The weed composition of energy willow plantation in the first year of vegetation is shown **in f**igure 1.

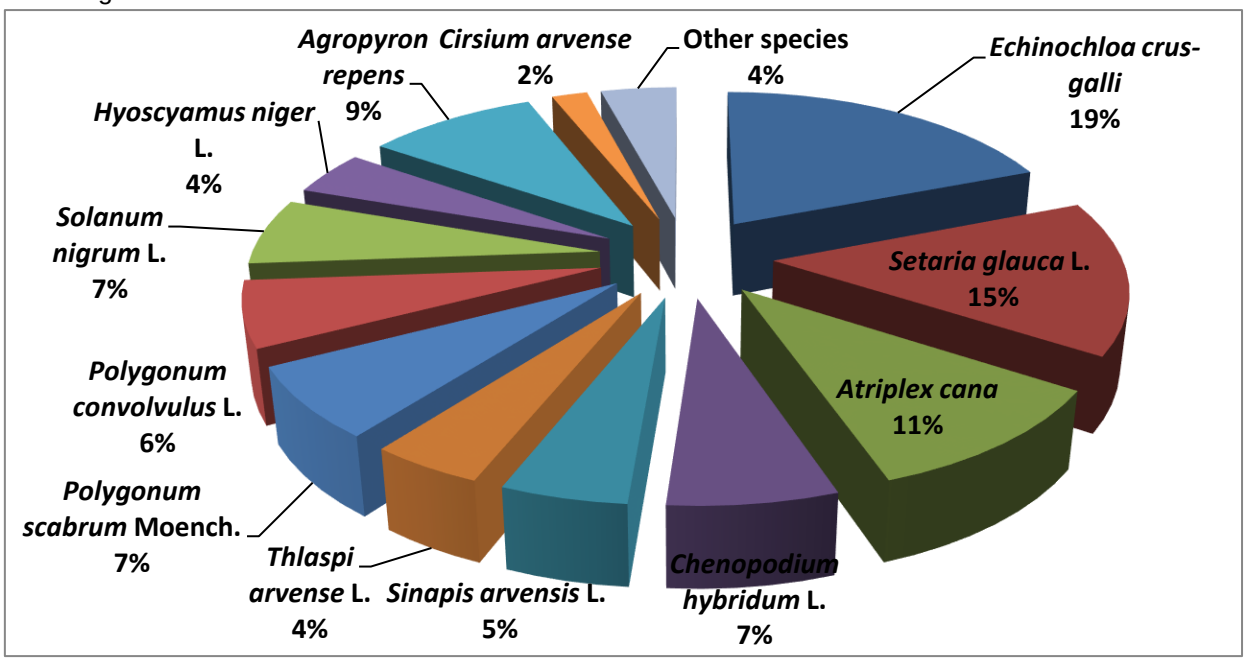

Fig. 1 - Weed composition of energy willow plantation in the first year of vegetation (average of 2012/2016)

Sufficient stock of moisture in soil, available mineral nutrients, a long growing season, access to photosynthetic active radiation (PAR) and favourable temperature regime along with the stock of weed seeds and developed vegetative reproduction organs in the control trial A gave weed plants the opportunity of successful growth, development and formation of the underground mass (Table 1). During five years, the mass of weeds at the second time of the weed observations (mid-August) amounted to an average of 3854 g/m^2. The largest share of the weed species in the willow plantations had Solanum nigrum L. (833 g/m^2 or

21.6%), *Atriplex cana* (18 g/m^2 or 21.2%), *Echinochloa crus-galli* (434 g/m^2 or 11.3%), *Setaria glauca L*. (316 g/m^2 or 8.2%), *Sinapis arvensis L*. (280 g/m^2 or 7.3%) and others. The application of mechanical weed control reduced the ability of weeds for growing and development. The weight of weeds in the trial B amounted to an average of 1312 g/m^2. It was 2.9 times lower than in trial A. The largest share of weed mass after the application of successive hoeing system was formed by *Solanum nigrum L*. (315 g/m^2 or 24.0%), *Atriplex cana* (286 g/m^2 or 21.8%), *Echinochloa crus-galli* (132 g/m^2 or 10.1%), Setaria glauca L. (97 g/m^2 or 7.4%), *Sinapis arvensis L*. (85 g/m^2), and *Polygonum scabrum Moench*. (72 g/m^2 or 5.5%). Plants of such species as *Hyoscyamus niger L*., *Chenopodium hybridum L*., and *Polygonum convolvulus L*., after successive hoeing of the space between rows formed the overweight mass slowly and in small quantities.

Table 1

Effect of mechanical weed control practices on the weed mass accumulation [g/m^2], average of 2012/2016

Weed species	Trials				
	A	B	C	D	E
Echinochloa crus-galli	434	132	106	128	-
Setaria glauca L.	316	97	110	93	-
Atriplex cana	818	286	191	245	-
Chenopodium hybridum L.	102	39	44	36	-
Sinapis arvensis L.	280	85	63	81	-
Thlaspi arvense L.	183	54	37	49	-
Polygonum scabrum Moench.	191	72	86	63	-
Polygonum convolvulus L.	135	38	29	40	-
Solanum nigrum L.	833	315	362	253	-
Hyoscyamus niger L.	108	31	42	35	-
Agropyron repens	109	44	63	26	-
Cirsium arvense	134	52	75	34	-
Other weeds	211	67	36	58	-
Total weeds	3854	1312	1244	1141	-
$LSD_{0.05}$	1.3				-

Successive hoeing of the space between rows (trial C) not only effectively reduced the number of weeds, but also restrained the processes of their mass formation. On average, at the time of the recordings, even taking into account the buffer zones, the mass of weeds was 1244 g/m^2, which made up only 32.3% of the maximum mass of trial A. Among the weed species, the largest share had *Solanum nigrum L*. (362 g/m^2 or 29.1%), *Atriplex cana* (191 g/m^2 or 15.4%), *Setaria glauca L*. (110 g/m^2 or 8.8%), *Echinochloa crus-galli* (106 g/m^2 or 8.5%), *Polygonum scabrum Moench*.(86 g/m^2), and *Cirsium arvense* (75 g/m^2 or 6.0%). Other species formed a smaller mass. In the trial D, to control weeds we used a system of consistent mechanical cutting of above-ground part of weed plants. Partly survived weeds formed a small biomass. The bulk of the mass was formed by young plants that sprouted after successive cuttings. The weight of the weeds in trial D averaged to 1141 g/m^2, which was 3.4 times lower than the maximum accumulation of weeds in trial A. The analysis of the field experiment data proved that all mechanical weed control methods were sufficiently effective. The decrease in the number of weeds during the years of the experiment ranged from 84.3% to 89.1%, i.e. it was close to the level of efficiency adopted for the evaluation of herbicides (above 95%). Noteworthy, application of various options of mechanical weed control in willow plantations in the first year of vegetation significantly influenced the peculiarities of leaf area formation in both willow plants and weeds (Table 2). The leaf area of energy willow plants in the trial A was 5 66 m^2/ha and correlated with the habit of plants of the first year of life. Meantime, the total leaf area of weeds was 106120 m^2/ha. This means that even among the weed plants there was a sharp competitiveness.

The maximum leaf area (m^2/ha) was developed by the following weed species: *Atriplex cana* (28700), *Chenopodium hybridum L*. (17550) and *Thlaspi arvense L*. (1656).

The leaf area of willow plants in the mechanical weed control treatments was 6850−7000 m^2/ha. Meantime maximum values in trial E treatment amounted to 8520 m^2/ha. The largest leaf area of the weed species was developed *for Atriplex cana*, *Chenopodium hybridum L*. and *Thlaspi arvense L*.

The field experiment conducted in 2012/2016 enabled evaluating interaction of weed plants and young willow plants (cuttings) in the first year of vegetation.

Table 2

Effect of mechanical weed control practices on the leaf area of energy willow [1000 m²/ha], average of 2012/2016

Weed species	Trials				
	A	B	C	D	E
Energy willow	5.66	6.85	6.81	7.00	8.52
Echinochloa crus-galli	8.48	0.95	0.57	0.70	-
Setaria glauca L.	6.15	0.70	0.50	0.55	-
Atriplex cana	28.70	2.62	3.77	2.79	-
Chenopodium hybridum L.	17.55	2.30	1.64	1.31	-
Sinapis arvensis L.	1.76	0.24	0.22	0.22	-
Thlaspi arvense L.	16.56	4.14	2.07	1.84	-
Polygonum scabrum Moench.	3.31	0.41	0.35	0.26	-
Polygonum convolvulus L.	3.05	0.32	0.32	0.26	-
Solanum nigrum L.	5.30	0.45	0.55	0.40	-
Hyoscyamus niger L.	3.55	0.40	0.60	0.35	-
Agropyron repens	2.18	0.34	0.24	0.16	-
Cirsium arvense	1.18	0.18	0.15	0.11	-
Other weeds	8.36	1.11	0.86	0.86	-
Total weeds	106.12	14.15	11.84	9.81	-
Leaf area	111.78	21.00	18.65	16.81	8.5
$LSD_{0.05}$	0.02				-

Availability of free ecological niches and favourable conditions for growth and development along with the low competitiveness of young willow plants contributed to the intensive occupation of willow plantation by weed species. On the areas where weeds had the opportunity to grow and develop freely (trial A), they formed the largest above-ground biomass, absorbed significant amounts of mineral nutrients from soil and made willow plants compete for life factors. Intensive vegetation of weeds limited the capacity of young willow plants and reduced their biological potential. Willow plants gradually established and formed shoots. Their annual increment over the years of research amounted to 63 cm (Table 3).

Table 3

Energy willow productivity under different weed control practices (average of 2012/2016)

Indicator	Trials					
	A	B	C	D	E	$LSD_{0.05}$
Shoot length [cm]	63.0	121.8	123.2	125.6	152.0	5.3
Biomass yield [t/ha]	2.08	4.58	4.63	4.72	5.72	0.14
Dry biomass yield [t/ha]	1.15	2.52	2.55	2.60	3.14	0.10
Solid biofuel yield [t/ha]	1.26	2.77	2.80	2.86	3.46	0.11
Energy yield [GJ/ha]	23.3	51.3	51.9	52.9	64.0	1.2

Application of mechanical (agrotechnical) systems of weed control implemented through three successive hoeing of the space between rows provided for the reduction of the biological potential of weed plants that survived in the buffer zones. Weed control measures provided for a more complete implementation of the biological potential of young willow plants. The length of their annual shoots averaged 121.8 cm that exceeded weeded control (trial A) 1.9 times. Application of successive inter-row harrowing with chain harrows showed similar to the previous method efficiency towards weeds and contributed to the formation of annual shoots of willow plants with an average length of 123.2 cm.

Successive cuttings weeds in the space between rows revealed the positive effect of such measures on young willow plants, primarily due to the weakening potential green competitors for life factors. Vegetation of plants was in sufficiently comfortable conditions, therefore, the annual increments of shoots averaged to 125.6 cm, i.e. 2.0 times exceeded the length of shoots of willow plants in control treatment.

The maintenance of willow plantations clear of the negative influence of weeds during the whole vegetation period (trial E) created the most favourable conditions for the growth and development of young plants. Average annual increment of willow shoots made up 152.0 cm over the experiment years.

The research results of many years demonstrated that in the weeded control treatment, the yield of energy willow biomass in the first year of cultivation was the lowest in the experiment and amounted to 2.08 t/ha.

The willow yield was 2.20 times higher after third consecutive hoeing of the space between rows (trial B, compared to trial A).

On the contrary, successive harrowing of the space between rows with chain harrows (trial C) did not differ significantly from trial B with the yield of 4.66 t/ha that exceeded 2.22 times the yield in the trial A.

Successive cutting of weeds in the space between rows improved the yield of willow plants (4.72 t/ha) 2.27 times exceeding the yield in weeded control treatment of the experiment.

The application of mechanical (agrotechnical) weed control methods for protecting plants from weeds by means of three successive hoeing of the space between rows contributed to the dry matter yield of 2.52 t/ha obtained from willow plantation in the first year of growing. The application of successive harrowing of the space between rows with chain harrow ensured the formation of 3.2% more willow biomass. At the same time, in the treatment with successive cutting of weeds in the space between rows, the productivity of willow plants was 2.60 t/ha.

Noteworthy, all the treatment under research did not differ significantly in terms of dry matter yield in the first year of vegetation and their deviations were within the bounds of the experimental error.

In the trial B of mechanical weed control implemented through successive hoeing of the space between rows, on the average of 2012/2016, the yield of solid biofuel was 2.77 t/ha. Successive harrowing of the space between rows resulted in biofuel yield of 2.80 t/ha. Successive cutting of weeds in the space between rows (trial D) ensured biofuel yield of 2.86 t/ha.

Energy yield is a generalizing measure of the efficiency of the technologies we offer for the mechanical weed control in willow stands of the first year of growing.

In the weeded control treatment, on the average over the years of the experiment, the energy yield was 23.3 GJ/ha, while the treatment with three consecutive hoeing of the space between rows ensured twice larger energy yield equalling 51.3 GJ/ha.

On the sites where the system of successive harrowing of the space between rows using chain harrow was applied, energy yield was 51.9 GJ/ha, while the system of successive cutting of weeds ensured 52.9 GJ/ha.

CONCLUSIONS

Mechanical weed control in energy willow stands in the first year of vegetation is quite effective when it was made timely and systematically. Taking into account the weeds in the buffer zones of the rows, the decline in the number of weed vegetation varied from 84.4% (successive hoeing of the space between rows) to 89.1% (successive cutting of weeds in the space between rows).

The accumulation of vegetative mass of weeds in energy willow plantations was affected by the system of mechanical weed control applied. Hoeing the space between rows reduced weed mass 2.9 times, harrowing the space between rows with chain harrow 3.1 times, successive cutting of weeds in the space between rows 3.4 times compared to the highest accumulation value of 3854 g/m^2.

The lowest yield of dry energy willow biomass (1.15 t/ha) was obtained without weed control, while the highest was obtained after six consequent hand weedings (3.14 t/ha).

Successive hoeing of the space between rows ensured, on the average, 2.52 t/ha dry biomass in the first year of growing, while successive harrowing with chain harrow ensured 2.55 t/ha and successive cutting of weeds 2.60 t/ha.

ACKNOWLEDGEMENT

The work has been funded by the Ukrainian National Academy of Agrarian Science.

REFERENCES

[1] Ahman I., Larson S., (1994), Genetic improvement of willow (Salix) as a source of bioenergy. *Norwegian journal of agricultural sciences*. Supplement., *18*, pp.47–56, Norway;

[2] Albertsson J., (2012), Weed problems and their control in Salix for biomass. *Agricultural Science* 2012:5 Swedish University of Agricultural Sciences. 31p. Alnarp/Sweden;

[3] Aylott M. J., Casella, E., Tubby I., Street N. R., Smith P., Taylor, G., (2008), Yield and spatial supply of bioenergy poplar and willow short - rotation coppice in the UK. *New Phytologist*, *178*, pp.358-370. doi: 10.1111/j.1469-8137.2008.02396.x, USA;

[4] Baum S., Weih M., Busch G., Kroiher F., Bolte A., (2009), The impact of short rotation coppice plantations on phytodiversity. *Landbauforschung Volkenrode*, *59*(3), 163 p. Germany;

[5] Caputo J., Balogh S. B., Volk T. A., Johnson L., Puettmann M., Lippke B., Oneil E., (2013), Incorporating uncertainty into a Life Cycle Assessment (LCA) model of short - rotation willow biomass (Salix spp.) crops. *Bioenerg. Res*. Published online: 22 June 2013. doi: 10.1007.s12155-013-9347-y;

[6] Caslin B., Finnan J., McCracken A., (2010), *Short rotation coppice willow best practice guidelines*, 2 Sept.*https://www.teagasc.ie/media/website/publications/2011/Short_Rotation_Coppice_Best_Practice_Guidelines.pdf*;

[7] Davies R. J., (1985), The importance of weed control and the use of tree shelters for establishing broadleaved trees on grass - dominated sites in England. *Forestry,* 58, pp.167–180. London/UK;

[8] Fuchylo Ya D., (2011), Plantation Forestry: Theory, *Practice, Perspectives (Плантаційне лісовирощування: теорія, практика, перспективи)*, 463p. Kyiv / Ukraine;

[9] Glavonjić B., (2017), Status of Using Wood Biomass for Energy Purposes in Serbia, Position paper*:* UNDP Serbia, 39p. Serbia. *http://biomasa.undp.org.rs/wp-content/uploads/2018/11/POSITION-PAPER-Status-of-Using-Wood-Biomass-for-Energy-Purposes-in-Serbia-Final.pdf*

[10] Gustafsson L., (1987), Plant conservation aspects of energy forestry – a new type of land use in Sweden. *Forest ecology and management journal*, *21*, pp.141–161, USA;

[11] Gustafsson J., Larsson S., Nordh, N., (2009), Manual for Salix growers/ Manual för salixodlare/. *Lantmännen Agroenergi*. Available at: *http://www.bioenergiportalen.se/attachments/42/406.pdf*; Sweden;

[12] Hansen E. A., Netzer D. A., (1985), Weed Control Using Herbicides in Short-Rotation *Intensively Cultured Poplar Plantations;* North Central Forest Experiment Station: St. Paul, MN, USA;

[13] Hytönen J., (1995), Effect of fertilizer treatment on the biomass production and nutrient uptake of short-rotation willow on cut-away peatlands. *Silva Fennica*., *29* (1), pp. 21–40. *https://helda.helsinki.fi/handle/1975/9195*;

[14] Keoleian G. A., Volk, T. A., (2005), Renewable Energy from Willow Biomass Crops: Life Cycle Energy, Environmental and Economic Performance. *Critical Reviews in Plant Sciences*, *24*, pp.385–406. doi: 10.1080/07352680500316334;

[15] Kondor A., Lenti I., Szabó B., Vágvölgyi S., (2007), Aspects of energy willow (*Salix viminalis* L.) cultivation. 7th International Multidisciplinary Conference. May 17-18, pp. 343-348; Baia Mare / Romania;

[16] Kravchenko Y ., Rogovska N, Petrenko L,, Zhang X., Song C., Chen Y., (2012), Quality and dynamics of soil organic matter in a typical Chernozem of Ukraine under different long - term tillage systems. In: *Can. J. Soil Sci*.; 92.pp. 429-438, Canada;

[17] McCracken A.R., Walsh L., Moore P.J., Lynch M., Cowan P., Dawson M., Watson S., (2011), Yield of willow (*Salix* spp.) grown in short rotation coppice mixtures in a long - term trial. View issue TOC, *Annals of Applied Biology*, Vol. 159, Issue 2: pp. 229–243. *https://onlinelibrary.wiley.com/doi/pdf/10.1111/j.1744-7348.2011.00488.x;*

[18] Mitchell C. P., Stevens E. A., Watters, M. P., (1999), Short rotation forestry operations, productivity and costs based on experience gained in the UK. *Forest ecology and management journal*, *121*, pp.123–136, USA;

[19] Mola Yudego B., (2010), Regional potential yields of short rotation willow plantations on agricultural land in Northern Europe. *Silva Fennica* 44(1): pp.63–76, *https://www.silvafennica.fi/pdf/article163.pdf*;

[20] Mosseler A., Major J. E., Labrecque M., Larocque G. R., (2014), Allometric relationships in coppice biomass production for two North American willows (Salix spp.) across three different sites. *Forest Ecology and Management*. Vol. 320, 15 May, pp.190–196. *https://www.sciencedirect.com/science/article/pii/S0378112714001224*, USA;

[21] Mosseler A., Major J. E., (2014), Coppice growth responses of two North American willows in acidic clay soils on coal mine overburden. *Can. J. Plant Sci*., *94*, pp. 1269-1279. http://www.bioone.org/doi/abs/10.1139/CJPS-2014-046, Canada;

[22] Nissim W. G., Pitre F. E., Teodorescu T. I., Labrecque M., (2013), Long - term biomass productivity of willow bioenergy plantations maintained in southern Quebec, Canada. *Biomass and Bioenergy*, Vol. 56, pp.361-369;

[23] Parfitt R. I., Stott K. G., (1987). The effect of nitrogen, phosphorus and potassium levels on the productivity of 13 willow clones. R.I. Parfitt, *Biomass Energy and Ind.:* Proc. Int. Conf., Orleans, 11-15 May, 1987. pp.546–550;

[24] Roik M. V., Sinchenko V. M., Fuchylo Ya. D., Pyrkin V.I., Ganzhenko O. M. (2015), *Energy willow: technology of cultivation and use/ Енергетична верба:технологія вирощування і використання*. 338p.. Vinnytsia. Ukraine;

[25] Rola J., Sekutowski T., Rola H., Badowski M., (2006), Problem zachwaszczenia plantacji wierzby krzewiastej – *Salix viminalis*/ The problem of contamination of shrub willow plantations– *Salix viminalis*. *Progress Plant Protection/Post.Ochr.Roślin*, *46* (1): pp.81–87, Poznan;

[26] Sage R., (1999), Weed competition in willow coppice crops: The cause and extent of yield losses. *Weed research journal*, 39, pp.399–411, USA;

[27] Sekutowski T., Rola J., Rola H., Badowski M., (2007), Wykorzystanie niektórych herbicydów do regulacji zachwaszczenia plantacji *Salix viminalis* (L.) / The use of some herbicides to control the weed plantation – *Salix viminalis*. *Progress Plant Protection / Post.Ochr.Roślin*, *47*(4), pp. 379–391. Poznan / Poland;

[28] Tsyliuryk O.I., Shevchenko S.M., Shevchenko O.M., Shvec N.V., Nikulin V.O., Ostapchuk Ya.V. , (2017), Effect of the soil cultivation and fertilization on the abundance and species diversity of weeds in corn farmed ecosystems. *Ukrainian Journal of Ecology*, 7(3), pp.154–159;

[29] Volk T. A., Verwijst Th., Tharakan P. J., Abrahamson L. P., White E. H., (2004), Growing fuel: a sustainability assessment of willow biomass crops. *Front Ecol Environ*, *2*(8), pp.411–418, USA;

[30] Volk T. A. Abrahamson L. P., Nowak C. A., Smart L. B., Tharakan P. J., White E. H., (2006). The development of short-rotation willow in the northeastern United States for bioenergy and bioproducts, agroforestry and phytoremediation. *Biomass and Bioenergy*, 30, pp.715–727;

[31] Volk T. A., Heavey J. P., Eisenbies M.H., (2016), Advances in shrub-willow crops for bioenergy, renewable products and environmental benefits. *Food, Energy and Security,* 5, pp.97–106, USA;

[32] Wang D., Jaiswal D., LeBauer D. S., Wertin T. M., Bollero G. A., Leakey, A. D., Long, S. P., (2015), A physiological and biophysical model of coppice willow (*Salix* spp.) production yields for the contiguous USA in current and future climate scenarios. *Plant Cell and Environment*, *38*, pp.1850–1865, USA;

[33] Weger J., Havlíčková K., Bubeník J., (2011), Results of testing of native willows and poplars for short rotation coppice after three harvests. *Aspects of Applied Biology,* 112, pp.335-340 ref.4. https://www.cabdirect.org/cabdirect/abstract/20123128128;

[34] Willow Varietal Identification Guide, (2012), B. Caslin, J. Finnan, A. McCracken (eds). Crops Research Centre, Carlow & Agri-Food Bioscience Institute. 64p. Carlow/Ireland;

[35] Wróbel M., Gregorczyk A., Wróbel J., (2012), The Effect of Chemical Soil Properties on Weed Infestation Structure in Willow (Salix L.) Short-Rotation Coppice. *Pol. J. Environ. Stud.,* Vol. 21(6), pp.1893–1899, Poland.

THERMODYNAMICS OF ANAEROBIC DIGESTION: MECHANISM OF SUPPRESSION ON BIOGAS PRODUCTION DURING ACIDOGENESIS

TERMODINAMIKA PADA ANAEROBIK DIGESI: MEKANISME PROSES HAMBATAN PADA PRODUKSI BIOGAS SELAMA FASE ACIDOGENESIS

Darwin[1)], Ralf Cord-Ruwisch[2)]
[1)] Department of Agricultural Engineering, Syiah Kuala University, Darussalam, Banda Aceh 23111, Indonesia
[2)] School of Environmental Engineering, Murdoch University, Perth, Western Australia
E-mail: darwin_ae@unsyiah.ac.id; Tel: +62 853 6142 3969

Keywords: *Gibbs free energy, anaerobic digestion, acidogenesis, inhibition*

ABSTRACT
Anaerobic digestion process consists of several stages in which different type of microorganisms are involved. The current study reviews some possible reactions occurred in anaerobic digestion particularly in acidogenesis stage. The paper also reviews the mechanisms of suppression and inhibition of anaerobic digestion in relation to some possible thermodynamic reactions during acidogenesis phase. Results of the study showed that ethanol and lactic acid are intermediate products that could potentially be produced during the anaerobic acid stage fermentation. Thus, those products should be carefully managed due to their acid effects in order to avoid the failure of anaerobic digestion.

ABSTRAK
Anaerobik digesi merupakan proses yang terdiri dari beberapa tahapan yang melibatkan berbagai jenis mikroorganisme pada setiap tahapannya. Studi ini memberikan penjelasan mengenai reaksi yang mungkin terjadi selama proses anaerobik digesi terutama reaksi pada fase acidogenesis. Paper ini juga menjelaskan mekanisme hambatan yang terjadi pada proses anaerobik digesi yang dihubungkan dengan beberapa reaksi termodinamika selama fase acidogenesis. Hasil studi menunjukkan bahwa etanol dan asam laktat merupakan produk menengah yang dapat dihasilkan selama tahapan fermentasi asam. Dengan demikian pembentukan produk tersebut harus dikelola dengan baik untuk menghindari kegagalan pada anaerobik digesi, karena produk tersebut dapat meningkatkan kandungan asam pada kultur anaerobik.

INTRODUCTION

Anaerobic digestion (AD) is a natural process involving a consortium of microorganisms to convert and decompose complex organic materials into simpler chemical molecules, and produces methane gas as the end-product *(Cheng, 2010; Van Lier, 2008)*. Some typical microorganisms involved in anaerobic digestion process include bacteria, yeast, fungi and protozoa *(Ali Shah et al., 2014; Suwannarat and Ritchie, 2015)*. Microorganisms involved in each stage of AD process (i.e acidogenesis and methanogenesis) are quite sensitive to some parameters including temperature, pH, hydraulic/solid retention time (HRT or SRT), solid content and organic loading rate (OLR), hydrogen partial pressure, volatile fatty acids concentration, alkalinity, and the concentration of free ammonia *(McCarty and Mosey, 1991; Appels et al, 2008; Darwin et al., 2016)*.

In anaerobic digestion, during the stage of acidogenesis all dissolved soluble organic compounds generated from hydrolysis process are firstly converted into intermediate products, such as volatile fatty acids (VFAs) and alcohols *(Henze et al., 2008)*, and then the products will be converted into acetate, CO_2 and H_2 in the stage of acetogenesis *(Appels et al., 2008; Cheng, 2010)*. The final stage of the anaerobic digestion is methanogenesis in which the acetate-utilizing methanogenic microorganisms would oxidize the acetate into methane. The methanogenesis would also be carried out by hydrogen-utilizing methanogens in which the microbes would utilize hydrogen as electron donor and carbon dioxide as acceptor to form methane as the end-product *(Appels et al., 2008; Henze et al., 2008).*

The crucial issue for operating anaerobic digestion process is to balance the equilibrium between the acidogenesis and methanogenesis. The rate of methane production would be significantly reduced when acids are accumulated in the digester. If this condition continuously happens, a potential risk in anaerobic

digestion process is inevitable in which the process of anaerobic digestion could stop completely. This occurs as low pH caused by an accumulation of acids could generate acidic condition in the digester *(Yu and Fang, 2003)*.

Not many studies assessed the thermodynamics' reactions during anaerobic digestion process. In this present study, reactions involved during anaerobic digestion were evaluated through thermodynamics point of view in which free Gibbs energy was measured in some possible reactions in order to evaluate the mechanism of suppression in anaerobic digestion and some possible reactions occurred in anaerobic acid stage process.

MATERIALS AND METHODS

Characteristics of anaerobic acidogenesis

In anaerobic acidogenesis phase, all simple and/or soluble organic materials generated from the hydrolysis process, are then fermented into volatile fatty acids, lactic acid and alcohols *(Yu and Fang, 2002; Darwin et al, 2018a)*. In this phase some gases including hydrogen and carbon dioxide were produced *(Borja et al, 2005; Solera et al, 2002)*. As acidogenesis is the second step of the anaerobic digestion process, managing the appropriate operating conditions is important to prevent the failure of anaerobic digestion caused by organic acid build-up *(Darwin et al, 2018b)*.

Some studies revealed that operating conditions such as temperature, pH and HRT could significantly affect the rate of acidification process to produce fermentation end-products, such as VFA and alcohols *(Cha and Noike, 1997; Borja et al, 2005; Zhang et al, 2005)*. Bacterial population and substrate degradation in acidogenesis process are highly dependent on the changes of temperature and HRT especially at low temperature and short HRT. During the process of anaerobic acidogenesis, metabolic pathway could change drastically when pH culture changes. The shift of fermentation pattern may significantly affect the relative numbers of microorganisms present in the reactor *(Cha and Noike, 1997)*.

Some studies showed that the changes of fermentation pathway in acidogenesis are highly influenced by pH *(Thauer et al, 1977; Hwang et al, 2004, Cheong and Hansen, 2006)*. Microbial competition could occur at pH between 5.0 and 6.0, and the competition could involve VFA (e.g. propionate and butyrate) and ethanol producers *(Hwang et al, 2004)*. In anaerobic acidogenesis process, unstable condition may occur when all three types of acidogenic fermentation including butyrate, propionate and alcohol exist in the reactor, and this condition may occur at pH 5.0 *(Ren et al, 2007)*.The operational stability and the overall metabolic rate of the methanogenesis highly depend on the products generated from the acidogenic reactor *(Ren et al, 1997)*.

- *Fermentation end-products from acidogenesis phase*

Although acetate is known as the primary VFA species in anaerobic digestion, it does not always appear as the major VFA in the acidogenesis phase *(Angelidaki et al, 1999)*. The authors mentioned that the distribution of VFA composition produced in acidogenesis is influenced by operating conditions such as pH, temperature and hydrogen partial pressure. Butyrate and propionate were the main fermentation end-products of VFA produced from the anaerobic acidogenesis operated at pH of 5.0 *(Zhang et al, 2005)*. Some other intermediate products that could be directly used by methanogens include H_2/CO_2, formate, methylamine and methanol *(Bhatia et al, 1985; Ren et al, 1997)*.

Study conducted on anaerobic acidogenesis of dairy wastewater at several levels of pH, revealed that when pH increased hydrogen partial pressure decreased with an increase of methane production *(Yu and Fang, 2002)*. At pH 6.5, biogas produced from anaerobic digestion consisted of carbon dioxide and methane, and no hydrogen was detected. Some studies had revealed that propionate was the main fermentation end-product produced from anaerobic acdiogenesis operated at pH lower than 5.0 while acetate and butyrate were the main fermentation end-products produced from the acid stage fermentation operated at pH higher than 5.5 *(Harper and Pohland, 1986; Yu and Fang, 2002; Ren, 1996)*.

$$C_6H_{12}O_6 + 2\ H_20 \rightarrow 2\ C_2H_5OH + 2\ HCO_3^- + 2\ H^+ \quad (1)$$

$$\Delta Go = -225.36\ kJ$$

During the process of anaerobic acidogenesis lactic acid could also be produced as the main fermentation end-products when pH of fermentation culture was too acidic (Darwin et al., 2018b and c). Further, under low pH (< 5.0) lactic acid could be the dominant fermentation end-product of starch

fermentation *(Darwin et al., 2018c)*. Lactic acid tended to be formed when anaerobic digester received shock loading of glucose *(Zoetemeyer et al,1982)* as shown in Equation (2-3).

At this condition, an accumulation of lactate in the digester may occur. As lactate is considered an intermediate product produced during the acidogenesis phase of anaerobic digestion, it could be used as the substrate for the second stage reactor or methanogenic reactor in order to enhance biogas production *(Pipyn and Verstraete, 1981)*.

$$C_6H_{12}O_6 \rightarrow 2CH_3CHOHCOO^- + 2H^+ \quad (2)$$

$\Delta Go = -198.2$ kJ

$$C_6H_{12}O_6 + H_2O \rightarrow CH_3\text{-}CHOH\text{-}COO^- + CH_3\text{-}CH_2OH + HCO_3^- + 2H^+ \quad (3)$$

$\Delta Go = -211.91$ kJ

- *The mechanism of suppression of anaerobic digestion by low pH*

The process of anaerobic digestion is highly affected by pH. An optimum pH in anaerobic digestion for methane production ranges between 6.8 and 7.2 *(Ward et al, 2008; Gontupil et al, 2012)*. The growth of methanogenic bacteria is inhibited at pH lower than 6.6 *(Mosey and Fernandes, 1989; Chen et al, 2008)*. Some studies revealed that the optimum pH for hydrolysis as well as acidogenesis are between 5.5 and 6.5 *(Kim et al, 2004; Yu and Fang, 2002; Ward et al, 2008)*. A lowering in pH may significantly affect the dissociation of VFA and other organic acids by pushing the equilibrium towards the formation of free un-dissociated acids (Equation 4-6).

$$CH_3COO^- + H^+ \rightarrow CH_3COOH \quad (4)$$

$$CH_3\text{-}CH_2\text{-}COO^- + H^+ \rightarrow CH_3\text{-}CH_2\text{-}COOH \quad (5)$$

$$CH_3\text{-}(CH_2)_2\text{-}COO^- + H^+ \rightarrow CH_3\text{-}(CH_2)_2\text{-}COOH \quad (6)$$

RESULTS

Results of the study showed that a lowering in pH also could alter the free energy change of VFA producing and VFA consuming reactions. Oxidation of propionate and butyrate are not only limited by the lack of free energy change but their degradation is also repressed by a drop of pH (Fig. 1). Inhibitory effects generated from propionate and butyrate degradation to acetate may lower pH, and thereby could suppress the activity of methanogens (*Amani et al. 2011*).

When anaerobic digestion is operated under mesophilic condition at 35°C and 10^{-4} atm of hydrogen partial pressure, the conversion of ethanol to acetate is thermodynamically more favorable in comparison to the conversion of propionate and butyrate (Fig. 1). This is due to the fact that the reaction of ethanol degradation is exergonic at low pH. This indicated that the oxidation of ethanol to acetate is also not affected by acidic condition.

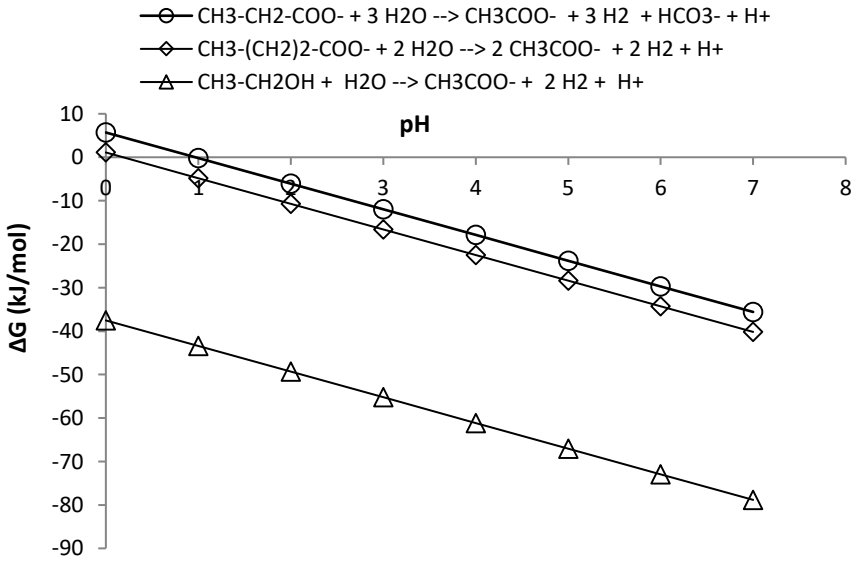

Fig.1 - Free energy change of VFA degradation as a function of pH

- *Problems of propionate accumulation in anaerobic digestion*

Study revealed that propionate was the major substrate affecting the degradation of VFA *(Wang et al, 2009)*. An increase of propionate concentration during anaerobic digestion could lower biogas production as well as methane yield. During anaerobic acidogenesis phase propionate formation should be monitored and prevented otherwise it could stimulate an accumulation of acid in the digester, and thereby could inhibit the growth of methanogens *(Amani et al, 2011)*. Propionate conversion to acetate tends to be more sensitive with hydrogen partial pressure in comparison to other intermediate products such as butyrate, ethanol and lactate in which these products are not too sensitive with hydrogen partial pressure in the reactor*(Ren et al,1997).*

When anaerobic digestion is operated at neutral pH (pH 7) under the temperature of mesophilic condition (35^{o}C), the conversion of propionate to acetate could be inhibited due to high hydrogen partial pressure (Fig. 2). When hydrogen partial pressure is at about 10^{-2} atm, the degradation of propionate is impossible as the reaction is endergonic. Current study revealed that an oxidation of propionate to acetate could generate 1% of hydrogen. However, the conversion of propionate to acetate could be inhibited when the hydrogen produced was at about 1.5 %. The conversion of butyrate acetate would be inhibited at high hydrogen partial pressure in which the butyrate conversion may occur at about 10% of hydrogen produced. The degradation of butyrate into acetate could be inhibited when the hydrogen is produced at about 30%. The current thermodynamical study also revealed that the conversion of ethanol and lactate to acetate would not be inhibited at high hydrogen partial pressure.

As lactate is considered as a precursor of propionate production, it may also be regarded as an undesirable product from the process of acid stage fermentation. Thermodynamically propionate could be produced from the reaction of 1 mole of lactate and 1 mole of hydrogen (Equation 7). Even though lactate is regarded as the precursor of propionate, it also can be considered as a substrate for the second stage process (e.g. acetogenesis and methanogenesis). This is due to the fact that lactate can be converted into acetate and hydrogen *(Van Lier et al, 2008)*, and the reaction involved is thermodynamically possible to occur as shown in Equation 8.

$$CH_3\text{-}CHOH\text{-}COO^- + H_2 \rightarrow CH_3\text{-}CH_2\text{-}COO^- + H_2O \quad (7)$$

$$\Delta Go = -80.448 \text{ kJ}$$

$$CH_3\text{-}CHOH\text{-}COO^- + 2\ H_2O \rightarrow CH_3COO^- + 2\ H_2 + HCO_3^- + H^+ \quad (8)$$

$$\Delta Go = -4.04 \text{ kJ}$$

Some studies mentioned that the production of propionate is more favourable at low pH in comparison to the production of acetate and butyrate *(Yu and Fang, 2003; Hsu and Yang, 1991)*. The production of propionate with hydrogen could occur at pH between 4.0 and 5.0*(Borja et al, 2005)*. Some studies had revealed that propionate considered as undesired end-product of the acidification stage for the subsequent methanogenesis. This is due to the fact that methanogenesis of propionate is slower than other volatile fatty acids such as acetate and butyrate *(Yu and Fang, 2003; Bo et al, 2014; Cohen et al, 1984; Bengtsson et al, 2008).*

This condition may cause accumulated acid in the reactor *(Ren et al, 1997; Bhatia et al, 1985).*Low acetogenic rate of propionate occurred as propionate cannot be utilized directly by methanogens This phenomenon is also in agreement with Equation 9 in which at standard state condition the reaction of propionate conversion to acetate is thermodynamically impossible. The conversion of propionate to acetate may occur when the anaerobic process is operated at pH 7 but the reaction could be inhibited at a higher hydrogen partial pressure (Fig. 1 and 2).

$$CH_3\text{-}CH_2\text{-}COO^- + 3\ H_2O \rightarrow CH_3COO^- + 3\ H_2 + HCO_3^- + H^+ \quad (9)$$

$$\Delta Go = +\ 76.484 \text{ kJ}$$

Research conducted on assessing optimal fermentation type of domestic wastewater added with molasses for the production of hydrogen in continuously-flow acidogenic reactor revealed that propionic acid type fermentation tended to occur at pH 5.5 with high redox potential *(Fukuzaki et al, 1990; Ren et al, 2007).* The attack of propionate producing bacteria could be prevented by maintaining pH level at 4.5 *(Ren et al, 1997)*. *McCarty and Mosey (1991)*revealed that propionate producers were suppressed at pH between 4.5 and 5.0.

An excess of propionic acid in the acidogenic reactor could suppress the process of anaerobic digestion that enable to lower pH. If this condition continuously occurs, the level of non-dissociated acids in the acidogenic reactor may go up. This condition could suppress the growth of methanogens in the conventional single-stage digester, and subsequently could lower methane productivity *(Angelidaki, Ellegaard, and Ahring 1999)*. Research carried out by *Maspolim et al (2014)* revealed that propionate tended to accumulate in the acidogenic reactor when *smithellapropionica* are present in the reactor. The propionate producer is related to the syntrophic propionate oxidizser *S. Propionica*. *Liu et al. (1999)* mentioned that *S. Propionica* may not be able to grow in the acidogenic reactor when pH in the reactor is 6.3.

If anaerobic digestion is operated in the two-stage process, *S. propionica* could be detected in the methanogenic reactor which could consume propionic acid to less than 0.1 mM *(Maspolim et al, 2014).*

- *Speed degradation of intermediate products for methane production*

An increase of methane yield occurs when the concentration of acetate, butyrate and ethanol in the digester increases *(Angelidaki et al, 1999; Ren et al, 2003; Uellendahl and Ahring, 2010; Wang et al, 2009).* However, the growth of acidogenic bacteria may be inhibited when there was an increase of propionate concentration in the digester, and thereby could slower the conversion of VFAs (e.g. butyrate and propionate) and ethanol into acetate. This condition may significantly limit the growth of methanogenic bacteria.

Ren et al. (1997) revealed that several characteristics that should be considered for optimizing methanogenesis include: (1) intermediate products that should be directly used by methanogens, such as acetate; (2) products that should be readily converted into methanogenic substrates by hydrogen-producing acetogens; (3) fermentation products that should contain less propionate. Due to the high rate of hydrogen-producing acetogenesis, the intermediate products including acetate, butyrate and ethanol are regarded as the optimal fermentation products for methanogenesis *(Ren et al, 1997; Hwang et al, 2004)*.

Methane also can be produced from hydrogen and carbon dioxide or bicarbonate as shown in Equation 11. Homoacetogenesis may occur when the formation of acetate as the only end product is derived from the reaction of hydrogen and carbon dioxide or bicarbonate (Equation 12).

Although methane can be produced from hydrogen and carbon dioxide, almost 65-70% of methane formation is derived from acetate *(Thauer et al, 1977)*. Methane formation derived from hydrogen and carbon dioxide has significant impact in the process of anaerobic digestion. This occurs as methanogens consume hydrogen that enables to lower the hydrogen partial pressure in the digester. This condition could support the anaerobic oxidation of VFA (e.g. butyrate and propionate) to acetate and hydrogen, and thereby could prevent acid accumulation in the digester *(Thauer et al, 1977)*.

$$CH3COO- + H2O \rightarrow CH_4 + HCO_3- \quad (10)$$

$$\Delta Go = -31.05 \text{ kJ}$$

$$4\ H_2 + HCO_3- + H+ \rightarrow CH_4 + 3\ H_2O \quad (11)$$

$$\Delta Go = -135.604 \text{ kJ}$$

$$4\ H_2 + 2\ HCO_3- + H+ \rightarrow CH_3COO- + 4\ H_2O \quad (12)$$

$$\Delta Go = -104.552 \text{ kJ}$$

The reactions mentioned in Equation 9 and 10 show that both reactions are thermodynamically not possible to occur as the free energy is positive. The reactions are considered as synthrophic acetogenesis, which involve the oxidation of propionate and butyrate to form acetate and hydrogen. Anaerobic oxidation of both propionate and butyrate tends be inhibited even at a slightly higher hydrogen partial pressure (Fig. 2). The oxidation of propionate and butyrate to acetate can easily proceed when hydrogen is consumed by methanogens to form methane, or it may occur when homoacetogens take hydrogen to form acetate *(Thauer et al, 1977)*. *Amani et al. (2011)* revealed that the anaerobic conversion of propionate is thermodynamically more unfavorable in comparison to butyrate (Fig. 1 and 2). This is due to the fact that propionate formation tends to generate acid accumulation in the anaerobic digester.

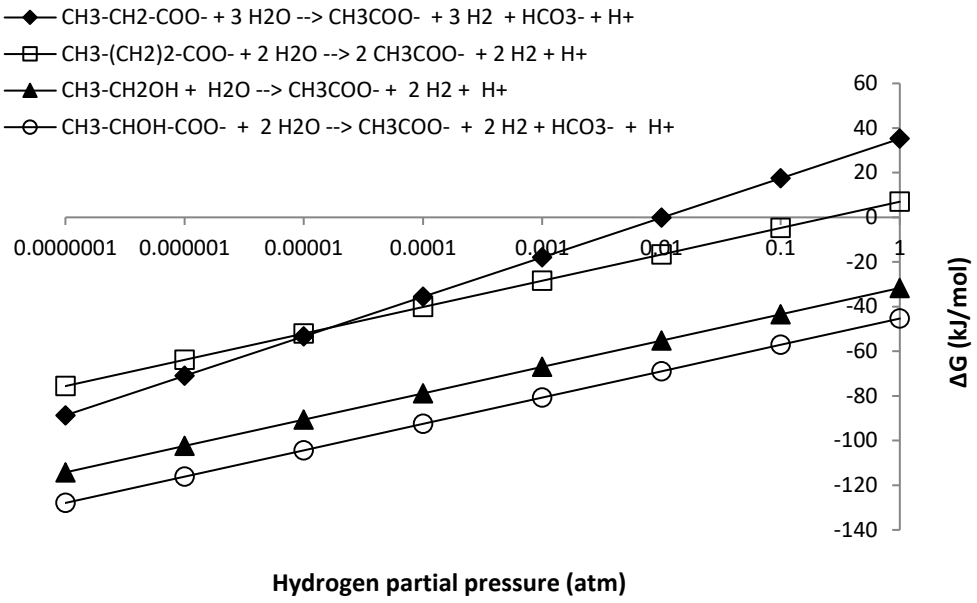

Fig. 2 - Free energy change of VFA degradation as a function of the hydrogen partial pressure

Study conducted by *Amani et al. (2011)* revealed that anaerobic oxidation of acetate to methane may stimulate propionate to be degraded thermodynamically. The study revealed that the maximum conversion of propionate could be accomplished when the concentration of butyrate and acetate in the digester were extremely low.

Even if acetate oxidation may stimulate the degradation of propionate, the presence of acetate in the digester also can contribute to lower pH, and thereby could generate the inhibitory effect on the growth of methanogens as well as acetogens. However, the inhibitory effect generated from acetate is extremely lower in comparison to the inhibitory effect caused by propionate and butyrate *(Amani et al, 2011).*

Although propionate and butyrate to some extent may enhance the formation of methane, they may extremely inhibit the growth of anaerobic microorganisms when their concentration is high in the digester. This condition may lead to the decrease of biogas production. High concentration of propionate and butyrate in the digester may lower pH in the digester, and thereby could significantly suppress the growth of anaerobic microbes, particularly methanogens *(Ahring 1995; Thauer et al, 1977; Kim et al, 2004)*.

Study conducted on the effects of VFA concentrations on methane yield and methanogenic bacteria revealed that ethanol, acetic acid and butyric acid concentrations of 2400, 2400 and 1800 mg L^{-1}, respectively, led to no significant inhibition of the activity of methanogens. However, propionic acid concentration of 900-951 mg/l extremely inhibited the growth of methanogens *(Demirel and Yenigun, 2002; Wang et al, 2009)*.

The studies also revealed that propionic acid concentration of 900-951 mg/l may generate an accumulation of acids due to the decreasing rate of acid degradation.

Study of Gibbs free energy showed that at an extreme low pH the reaction to form acetate and propionate may be shifted by the reaction of ethanol and butyrate (depicted in Fig. 3). Further, during the low pH, the formation of 1 mol of propionate along with 1 mol of acetate as well as 1 mol of hydrogen is possible to occur. The reaction to form propionate is highly dependent on the hydrogen partial pressure in comparison to acetate, butyrate and ethanol (Fig. 3 and 4).

The conversion of propionate to acetate at neutral pH would be inhibited due to high hydrogen partial. Anaerobic conversion of propionate to acetate could generate 1% of hydrogen, and its conversion would be inhibited when the hydrogen produced was at about 1.5 %.

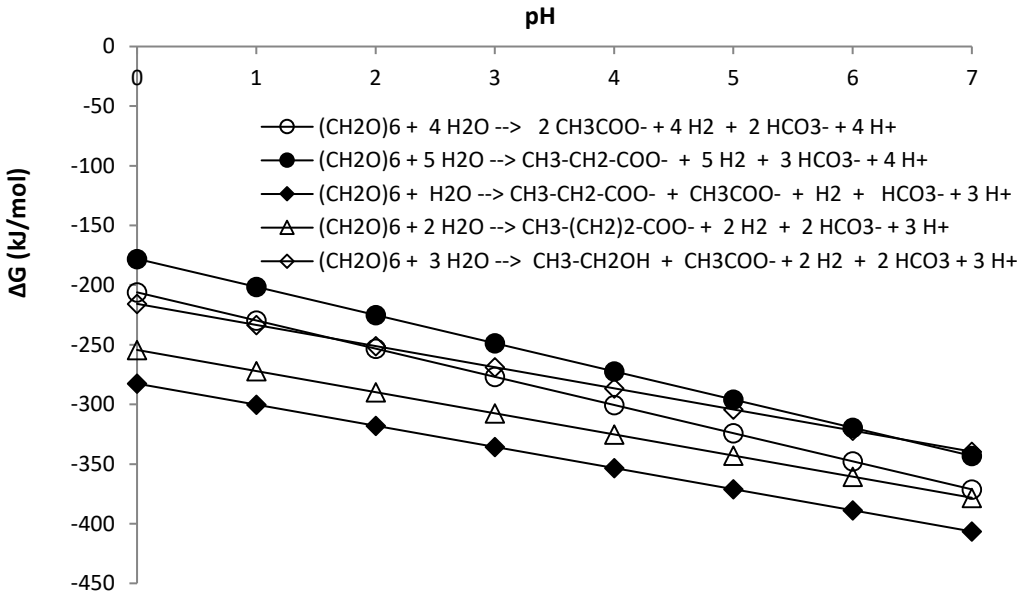

Fig. 3-Free energy change of VFA formation as a function of pH

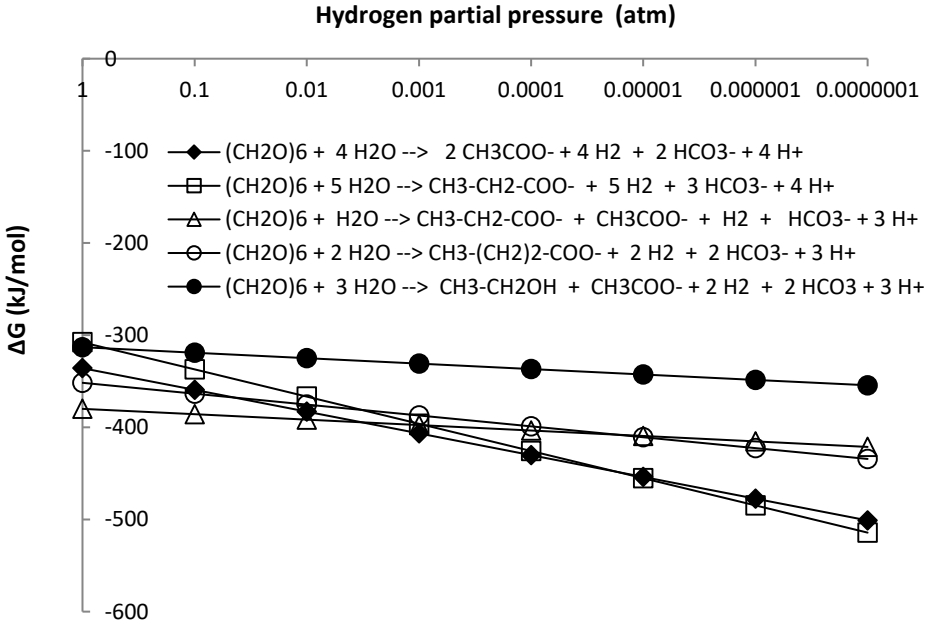

Fig. 4 - Free energy change of VFA formation as a function of the hydrogen partial pressure

CONCLUSIONS

The present study revealed that low pH in anaerobic digester could shift the free energy change in the reactions of both VFA production and VFA utilization. The current result showed that the degradation of VFAs (i.e. propionate and butyrate) during the process of anaerobic digestion is not only caused by the lack of free energy changes but it could also affected by low pH. The VFAs that could not be degraded and oxidized during the anaerobic digestion, would significantly suppress the methanogens' activity due to an increase of proton concentration in the digester caused by acid build-up.

The results of the current study showed that the formation of ethanol as an intermediate product during the stage of acidogenesis is more favorable in comparison to the formation of propionate, lactate and butyrate. This is due to the fact that at the low pH, the reaction of ethanol conversion is thermodynamically spontaneous. This suggested that the oxidation of ethanol to acetate is also not affected by the acidic condition, and thereby could balance and optimize methane production.

This study is significant for enhancing methane production during the process of anaerobic digestion, and also could be useful for developing further research on selectively producing useful fermentation end-products during anaerobic acidogenesis. Further, the study also provided an overview in regards to the intermediate products that potentially accumulated during the phase of acidogenesis.

ACKNOWLEDGEMENT

The authors acknowledge financial support provided by Syiah Kuala University, Banda Aceh, Indonesia through H-index research program coordinated by the Institute for Research and Community Services, UNSYIAH.

REFERENCES

[1] Ahring B.K., (1995), Methanogenesis in thermophilic biogas reactors, *Antonie van Leeuwenhoek*, Vol. 67, pp. 91-102;

[2] Ali Shah F., Mahmood Q., Maroof Shah M., Pervez A., Ahmad Asad S., (2014), Microbial ecology of anaerobic digesters: the key players of anaerobiosis, *The Scientific World Journal*, Vol. 2014, pp. 1-21;

[3] Amani T, Nosrati M., Mousavi, S.M., Kermanshahi R.K., (2011), Study of syntrophic anaerobic digestion of volatile fatty acids using enriched cultures at mesophilic conditions, *International Journal of Environmental Science & Technology*, Vol. 8, pp. 83-96;

[4] Angelidaki I., Ellegaard L., Ahring B.K., (1999), A comprehensive model of anaerobic bioconversion of complex substrates to biogas, *Biotechnology and Bioengineering*, Vol. 63, pp. 363-372;

[5] Appels L., Baeyens J., Degrève J., Dewil R., (2008), Principles and potential of the anaerobic digestion of waste-activated sludge, *Progress in Energy and Combustion Science*, Vol. 34, pp. 755-781;

[6] Bengtsson S., Hallquist J., Werker A., Welander T., (2008), Acidogenic fermentation of industrial wastewaters: effects of chemostat retention time and pH on volatile fatty acids production, *Biochemical Engineering Journal*, Vol. 40, pp. 492-499;

[7] Bhatia D., Vieth W.R., Venkatasubramanian K., (1985), Steady-state and transient behavior in microbial methanification: I. Experimental results, *Biotechnology and Bioengineering*, Vol. 27, pp. 1192-1198;

[8] Bo Z., Zhang B., He P.J., (2014), Performance assessment of two-stage anaerobic digestion of kitchen wastes, *Environmental Technology*, Vol. 35, pp.1277-1285;

[9] Borja R.E., Sánchez B., Rincón F., Raposo M.A., (2005), MartínA. Study and optimisation of the anaerobic acidogenic fermentation of two-phase olive pomace, *Process Biochemistry*, Vol. 40, pp. 281-291;

[10] Cha G.C., Noike T., (1997), Effect of rapid temperature change and HRT on anaerobic acidogenesis, *Water Science and Technology*, Vol. 36, pp. 247-253;

[11] Chen Y., Cheng J.J., Creamer, K.S., (2008), Inhibition of anaerobic digestion process: a review, *Bioresource technology*, Vol. 99, pp. 4044-4064;

[12] Cheng, J.J., (2010), Biomass to Renewable energy process, CRC Press, Boca Raton, Florida/U.S.A.;

[13] Cheong D.Y., Hansen C.L., (2006), Acidogenesis characteristics of natural, mixed anaerobes converting carbohydrate-rich synthetic wastewater to hydrogen, *Process Biochemistry*, Vol. 41, pp. 1736-1745;

[14] Cohen A., Van Gemert J.M., Zoetemeyer R.J., Breure A.M., (1984), Main characteristics and stoichiometric aspects of acidogenesis of soluble carbohydrate containing wastewaters, *Process Biochemistry*, Vol. 19, pp. 228-232;

[15] Darwin Cheng J.J., Gontupil J., Liu Z., (2016), Influence of total solid concentration for methane production of cocoa husk co-digested with digested swine manure, *International Journal of Environment and Waste Management*, Vol. 17, no.1, pp. 71-90;

[16] Darwin, Charles W., Cord-Ruwisch R., (2018a), Concurrent Lactic and Volatile Fatty Acid Analysis of Microbial Fermentation Samples by Gas Chromatography with Heat Pre-treatment, *Journal of Chromatographic Science*, Vol. 56, pp. 1-5;

[17] Darwin, Barnes A, Cord-Ruwisch R., (2018b), In vitro rumen fermentation of soluble and non-soluble polymeric carbohydrates in relation to ruminal acidosis, *Annals of Microbiology*, Vol. 68, pp. 1-8;

[18] Darwin, Cord-Ruwisch R., Charles W., (2018c), Ethanol and Lactic acid Production from Sugar and Starch Wastes by Anaerobic Acidification, *Engineering in Life Science*, Vol. 18, pp. 635-642;

[19] Demirel B., Yenigun O., (2004), Anaerobic acidogenesis of dairy wastewater: the effects of variations in hydraulic retention time with no pH control, *Journal of chemical technology and biotechnology*, Vol. 79, pp. 755-760;
[20] Freitas J.G., Fletcher B., Aravena R., Barker J.F., (2010), Methane production and isotopic fingerprinting in ethanol fuel contaminated sites. Groundwater, Vol. 48, pp. 844-857;
[21] Fukuzaki S., Nishio N., Shobayashi M., Nagai S., (1990), Inhibition of the fermentation of propionate to methane by hydrogen, acetate, and propionate, *Applied and Environmental Microbiology*, Vol. 56, pp. 719-723;.
[22] Gaddy, J. L., Clausen, E.C., (1992), (Patent and Trademark) U.S. Pat. Appl. 5,173,429, 22 Dec 1992, U.S. 76 12221;
[23] Gontupil J., Darwin Z., Liu J.J., Cheng, Chen H., (2012), Anaerobic co-digestion of swine manure and corn stover for biogas production. In: Proceedings from ASABE Annual International Meeting Conference, Dallas, July 29–August 1, 2012, pp. 1342–1347;
[24] Harper S. R., Pohland F.G., (1986), Recent developments in hydrogen management during anaerobic biological wastewater treatment, *Biotechnology and Bioengieering*, Vol. 28, pp. 585-602;
[25] Henze M., van Loosdrecht M.C., Ekama G.A., Brdjanovic D., (2008), *Biological wastewater treatment*. IWA publishing, London/U.K.;
[26] Hsu S.T., Yang S.T., (1991), Propionic acid fermentation of lactose by Propionibacterium acidipropionici: effects of pH, *Biotechnology and Bioengineering*, Vol. 38, pp. 571-578;
[27] Hwang, Moon H., Nam J.J., Hyun S.H., Kim I.S., (2004), Anaerobic bio-hydrogen production from ethanol fermentation: the role of pH, *Journal of Biotechnology*, Vol. 111, pp. 297-309;
[28] Kim I.S., Hwang M.H., Jang N.J., Hyun S.H., Lee S.T., (2004), Effect of low pH on the activity of hydrogen utilizing methanogen in bio-hydrogen process, *International Journal of Hydrogen Energy*, Vol. 29, pp. 1133-1140;
[29] Liu Y., Balkwill D.L., Aldrich H.C., Drake G.R., Boone D.R., (1999), Characterization of the anaerobic propionate-degrading syntrophs Smithella propionica gen. nov., sp. nov. and Syntrophobacter wolinii, *International Journal of Systematic and Evolutionary Microbiology*, Vol. 49, pp. 545-556;
[30] Maspolim, Y., Zhou, Y., Guo, C., Xiao, K., Ng, W.J., (2014), Comparison of single-stage and two-phase anaerobic sludge digestion systems–Performance and microbial community dynamics, *Chemosphere*, Vol. 140, pp. 54-62;
[31] McCarty, P.L., and Mosey, F.E., (1991), Modelling of anaerobic digestion processes (a discussion of concepts), *Water Science & Technology*, Vol. 24, pp. 17-33;
[32] Pipyn P., Verstraete W., (1981), Lactate and ethanol as intermediates in two-phase anaerobic digestion, *Biotechnology and Bioengineering*, Vol. 23, pp. 1145-1154;
[33] Ren N.Q., Chua S.Y., Chan Y.F., Tsang, Y.J., Wang S.N., (2007), Assessing optimal fermentation type for bio-hydrogen production in continuous-flow acidogenic reactors, *Bioresource Technology*, Vol. 98, pp. 1774-80;
[34] Ren N.Q., Wang B., Huang J.C., (1997), Ethanol-type fermentation from carbohydrate in high rate acidogenic reactor, *Biotechnology and Bioengineering*, Vol. 54, pp. 428-433;
[35] Ren N., Wang B., Ma F., (1996), Hydrogen bio-production of carbohydrate fermentation by anaerobic sludge process, *Proc. of 68th Water Environment Federation Conference*, Miami 145;
[36] Solera R., Romero L.I., Sales D., (2002), The evolution of biomass in a two-phase anaerobic treatment process during start-up, *Chemical and biochemical engineering quarterly*, Vol. 16, pp. 25-30;
[37] Suwannarat J., Ritchie R.J., (2015), Anaerobic digestion of food waste using yeast, *Waste management*, Vol. 42, pp. 61-66;
[38] Thauer R.K., Jungermann K., Decker K., (1977), Energy conservation in chemotrophic anaerobic bacteria. *Bacteriological reviews*, Vol. 41, pp. 100;
[39] Uellendahl, H., Ahring, B.K., (2010), Anaerobic digestion as final step of a cellulosic ethanol biorefinery: Biogas production from fermentation effluent in a UASB reactor—pilot-scale results, *Biotechnology and Bioengineering*, Vol. 107, pp. 59-64;
[40] Van Lier J.B., Mahmoud N., Zeeman G., (2008), Anaerobic wastewater treatment. Biological Wastewater Treatment, IWA Publishing, London/U.K.;
[41] Wang Y., Zhang Y., Wang J., Meng L., (2009), Effects of volatile fatty acid concentrations on methane yield and methanogenic bacteria, *Biomass and Bioenergy*, Vol. 33, pp. 848-853;

[42] Ward A.J., Hobbs P.J., Holliman P.J., Jones, D.L., (2008), Optimisation of the anaerobic digestion of agricultural resources, *Bioresource Technology*, Vol. 99, pp. 7928-7940;
[43] Yu H.Q., Fang H.P., (2003), Acidogenesis of gelatin-rich wastewater in an upflow anaerobic reactor: influence of pH and temperature, *Water Research*, Vol. 37, pp. 55-66;
[44] Yu H.G., Fang H.H., (2002), Acidogenesis of dairy wastewater at various pH levels, *Water Science and Technology*, Vol. 45, pp. 201-206;
[45] Zhang B., Zhang S.C., Zhang H.Z., Shi C.W.M., (2005), The influence of pH on hydrolysis and acidogenesis of kitchen wastes in two-phase anaerobic digestion, *Environmental Technology*, Vol. 26, pp. 329-339;
[46] Zoetemeyer R.J., van den Heuvel J.C., Cohen A., (1982), pH influence on acidogenic dissimilation of glucose in an anaerobic digestor, *Water Research*, Vol. 16, pp. 303-311.

WRITING NORMS

Article Types

Three types of manuscripts may be submitted:

1. **Regular articles:** These should describe new and carefully confirmed findings, and experimental procedures should be given in sufficient detail for others to verify the work. The length of a full paper should be the minimum required to describe and interpret the work clearly (max.10 pages, even number);
2. **Short Communications:** A Short Communication is suitable for recording the results of complete small investigations or giving details of new models or hypotheses, innovative methods, techniques or apparatus. The style of main sections has not necessarily to be in accordance with that of full-length papers (max. 6 pages, even number);
3. **Reviews:** Submissions of reviews and perspectives covering topics of current interest are welcome and encouraged (max.10 pages, even number).

Manuscripts should be written in English (American or British usage is accepted, but not a mixture of these) and submitted **electronically** at the following e-mail addresses: ***inmatehjournal@gmail.com***
Please be sure to include your full affiliation and e-mail address (see Sample manuscript)
The authors are responsible for the accuracy of the whole paper and references.
There are allowed 2 papers by each first author.
The text layout should be in single-column format. To avoid unnecessary errors it is strongly advised to use the "spell-check" and "grammar check" functions of your word processor.

Review Process

All manuscripts are reviewed by 2 members of the Scientifically Review Office. Decisions will be made as rapidly as possible and the journal strives to return reviewers' comments to authors in approx.3 weeks.
The editorial board will re-review manuscripts that are accepted pending revision.

NOTE:

Submission of a manuscript implies: that the work described has not been published before (excepting as an abstract or as part of a published lecture or thesis) that it is not under consideration for publication elsewhere.

1. REGULAR ARTICLES

- Manuscripts should be concise, in ***1.15 line spacing***, and should have 2 cm all over margins. The font should be ***Arial 10 pt.*** Ensure that each new paragraph is clearly indicated, using **TAB at 1 cm**.
- Title will be ***Arial 12 pt***. and explicit figures will be ***Arial 9 pt***.
- Text will be written in English.
- Chapters' titles are written by ***Arial 10 pt, Bold, Uppercase*** (e.g. **INTRODUCTION, MATERIALS AND METHODS**), between chapters is left a space for 10 pt. At the beginning of each paragraph, TAB of 1 cm.
- The paper body will be written in ***Arial 10 pt., Justify alignment***.

TITLE ***Arial 12 pt., Uppercase, Bold, Center*** *(in English language)* and ***Bold Italic*** *(in native language).*
Should be a brief phrase describing the contents of the paper. Avoid long titles; a running title of no more than 100 characters is encouraged (without spaces).

AUTHORS ***ARIAL 9, Bold, Centre alignment***
Under the paper's title, after a space (enter) 9 pt., write ***authors' names*** and ***affiliations (Arial 8 pt.-Regular)***
When the paper has more than one author, their name will be followed by a mark (Arabic numeral) as superscript if their affiliation is different. Less than 6 authors.
Corresponding author's name (next row), ***(Arial 8 pt.)***. Should be added also: phone, fax and e-mail information, for the paper corresponding author (***font: 8 pt., Italic***).

KEYWORDS ***(In English)*** about 4 to 7 words that will provide indexing references should be listed (title: ***Arial 10pt, bold italic,*** text ***Arial 10 pt., italic***).

A list of non-standard *Abbreviations* should be added. In general, non-standard abbreviations should be used only when the full term is very long and used often. Each abbreviation should be spelled out and introduced in parentheses the first time it is used in the text. Standard abbreviations (such as ATP and DNA) need not to be defined.
ABSTRACT ***(in English and Native language, Arial 10 pt.)***, the title *bold*; the text of abstract: *italic*) should be informative and completely self-explanatory, briefly present the topic, state the scope of the experiments, indicate significant data, and point out major findings and conclusions. The Abstract should be max.250 words. Complete sentences, active verbs, and the third person should be used, and the abstract should be written in the past tense. Standard nomenclature should be used and abbreviations should be avoided. No literature should be cited.

INTRODUCTION (***Arial 10 pt.)*** should provide a clear statement of the problem, the relevant literature on the subject, and the proposed approach or solution. It should be understandable to colleagues from a broad range of scientific subjects. We should refer to the current stage of researches performed in the field of the paper to be published, by quoting up-to-date specialty studies, preferably published after 2006, excepting certain referential specialty books/studies, especially papers issued in magazines/journals/conferences/ISI quoted symposia or in other international data bases, which are well known and available.

MATERIALS AND METHODS (***Arial 10 pt.)*** should be complete enough to allow experiments to be reproduced. However, only truly new procedures should be described in detail; previously published procedures should be cited, and important modifications of published procedures should be mentioned briefly. Methods in general use need not be described in detail.

RESULTS (***Arial 10 pt.)*** should be clarity presented. The results should be written in the past tense when describing findings in the authors' experiments. Results should be explained, but largely, without referring to the literature. Discussion, speculation and detailed interpretation of data should not be included in the Results, but should be put into the Conclusions section.

CONCLUSIONS (***Arial 10 pt.)*** The main conclusions drawn from results should be presented in a short Conclusions section. Do not include citations in this section.

Formulae, symbols and abbreviations: Formulae will be typeset in Italics (preferable with the Equation Editor of Microsoft Office 2003) and should be written or marked as such in the manuscript, unless they require a different styling. They should be referred to in the text as Equation (4) or e.g. (4). The formulae should be numbered on the right side, between brackets ***(Arial 10 pt.)***:

$$P = F \cdot v \quad (1)$$

Terms of the equation and the unit measure should be explained, e.g.

P is the power, [W];
F – force, [N];
v – speed, [m/s]

SI units must be used throughout.

Tables should be self-explanatory without reference to the text. The details of the methods used in the experiments should preferably be described in the legend instead of in the text. The same data should not be presented both in table and graph form or repeated in the text.
Table's title will be typed***Arial 9 pt, Bold, Centered***
In the table, each row will be written Arial 9 pt, single-spaced throughout, including headings and footnotes.
The table should be numbered on the right side, between brackets ***(Arial 10 pt)***:

Figure (Arial 9 pt., Bold, Center)should be typed in numerical order (Arabic numerals). Graphics should be high resolution (e.g.JPEG).Figure number is followed by what represent the figure or graph e.g.:

Fig.1 – Test stand

Legend: ***Arial 8 pt, Italic, Center,*** e.g.

1 - plansifter compartments; 2- break rolls; 3 – semolina machines; 4 – reduction rolls; 5 – flour

ACKNOWLEDGMENTS (***Arial 10 pt.)*** of people, grants, funds etc should be brief (*if necessarily*).

REFERENCES (***Arial 10 pt.)***

(In alphabetical order, in English and in the original publication language).
Minimum 10 references, last 10 years, minimum 3 references from the last 2 years

References must be from all over the world, not only from the authors' country.
It can be used"*References*" tool from the *Word Editor*.
References should be cited in the text in brackets as in the following examples:

(Babiciu P., Scripnic V., 2000)

All references must be provided in English with a specification of original language in round brackets.
Authors are fully responsible for the accuracy of the references.
References should be alphabetically, with complete details, as follows:
Examples:
Books: Names and initials of authors, year (between brackets), title of the book (Italic), volume number, publisher, place, pages number or chapter, ISSN/ISBN:

[1] Vlădut V., (2009), *Study of threshing process in axial flow apparatus (Studiul procesului de treier la aparatele cu flux axial),* vol.1, ISSN/ISBN ……., "Terra Nostra" Publishing House, Iaşi/Romania;

Journal Article: Names and initials of authors, year (between brackets), full title of the paper, full name of the journal (Italic), volume number, publisher, place, ISSN, page numbers:

[1] Lizhi Wu, Yan Di., (2005), Demonstrational study on the land consolidation and rehabilitation (LCR) project of saline-alkali soil in arid areas: a case study of Lubotan LCR project in Pucheng County, Shaanxi Province(干旱区盐碱化土地整理工程实证研究-以陕西蒲城县卤泊滩土地整理项目为例), *Transactions of the Chinese Society of Agricultural Engineering*,vol.21, no.1, pp.179-182, Madison/Wisconsin;

[2] Leonov I.P., (1973), Basic machine theory for tobacco stringing. Post-harvest care of tobacco and rustic tobacco (Основы теории машин для закрепления табака на шнуры. Послеуборочная обработка табака и махорки), *Collection of scientific articles (сборник научно-исследовательских работ)*, pp.37-45;

Conference or Symposium: Names and initials of authors, year (between brackets), full title of the paper (Regular), full name of the conference/symposium (Italic), volume number, publisher, place, ISSN, page numbers

[1] Bungescu S., Stahli W., Biriş S., Vlăduţ V.,Imbrea F., Petroman C., (2009), Cosmos program used for the strength calculus of the nozzles from the sprayers (Program Cosmos folosit pentru calculul de rezistență la zgomot al aparatelor de distribuție), *Proceedings of the 35 International Symposium on Agricultural Engineering "Actual Tasks on Agricultural Engineering",* pp.177-184, Opatija / Croatia;

Dissertation / Thesis: Names and initials of authors, year (between brackets), full name of the thesis (Italic), specification (PhD Thesis, MSc Thesis), institution, place;

[1] Popa L., (2004), *Research on the influence of structural and functional parameters of the braking system on the braking performance of agricultural trailers (Cercetări privind influența caracteristicilor constructive şi funcționale ale sistemelor de frânare asupra performanțelor de frânare ale remorcilor agricole)*, PhD dissertation, Transylvania University of Braşov, Braşov / Romania.

Patents: Names and initials of authors, year (between brackets), patent title (Italic), patent number, country:

[1] Grant P., (1989), *Device for Elementary Analyses*. Patent, No.123456, USA.

Legal regulations and laws, organizations: Abbreviated name, year (between brackets), full name of the referred text, document title/type (Italic), author, place:

[1] *** EC Directive, (2000), Directive 2000/76/EC of the European Parliament and of the Council of 4 December 2000, on the incineration of waste, Annex V, *Official Journal of the European Communities*, L332/91, 28.12.2000, Brussels.

Web references: The full URL should be given in text as a citation, if no other data are known. If the authors, year, and title of the documents are known and the reference is taken from a website, the URL address has to be mentioned after these data:

The title of the book, journal and conference must be written in Italic, the title of the article, chapter of the book, must be written Regular.

Citation in text

Please ensure that every reference cited in the text is also present in the reference list (and vice versa). Do not cite references in the abstract and conclusions. Unpublished results, personal communications as well as URL addresses are not recommended in the references list.

Making personal quotations (one, at most) should not be allowed, unless the paper proposed to be published is a sequel of the cited paper. Articles in preparation or articles submitted for publication, unpublished, personal communications etc. should not be included in the references list.

Citations style

Text: All citations in the text may be made directly (or parenthetically) and should refer to:

- ***single author:*** the author's name (without initials, unless there is ambiguity) and the year of publication:
  "as previously demonstrated *(Brown, 2010)*".
- ***two authors:*** both authors' names and the year of publication: *(Adam and Brown, 2008; Smith and Hansel, 2006; Stern and Lars, 2009)*
- ***three or more authors:*** first author's name followed by "et al." and the year of publication: "As has recently been shown *(Werner et al., 2005; Kramer et al., 2000)* have recently shown ...."

Citations of groups of references should be listed first alphabetically, then chronologically.

Units, Abbreviations, Acronyms

- Units should be metric, generally SI, and expressed in standard abbreviated form.
- Acronyms may be acceptable, but must be defined at first usage.

Edited by: INMA Bucharest
6 Ion Ionescu de la Brad Blvd., sect. 1, Bucharest, ROMANIA
Tel: +4021.269.32.60; Fax: +4021.269.32.73
http://www.inmateh.eu
e-mail: ***inmatehjournal@gmail.com***